Unclassified **NEA/NSC/DOC(2015)7**

Organisation de Coopération et de Développement Économiques
Organisation for Economic Co-operation and Development **29-Apr-2015**

English text only

NUCLEAR ENERGY AGENCY
NUCLEAR SCIENCE COMMITTEE

Technology and Components of Accelerator-driven Systems
Second International Workshop Proceedings

21-23 May 2013

The document exists only in PDF

simone.massara@oecd.org

JT03375386

Complete document available on OLIS in its original format
This document and any map included herein are without prejudice to the status of or sovereignty over any territory, to the delimitation of international frontiers and boundaries and to the name of any territory, city or area.

NEA/NSC/DOC(2015)7
Unclassified

English text only

Technology and Components of Accelerator-driven Systems

Second International Workshop Proceedings

Nantes, France

21-23 May 2013

© OECD 2015

NUCLEAR ENERGY AGENCY
ORGANISATION FOR ECONOMIC CO-OPERATION AND DEVELOPMENT

ORGANISATION FOR ECONOMIC CO-OPERATION AND DEVELOPMENT

The OECD is a unique forum where the governments of 34 democracies work together to address the economic, social and environmental challenges of globalisation. The OECD is also at the forefront of efforts to understand and to help governments respond to new developments and concerns, such as corporate governance, the information economy and the challenges of an ageing population. The Organisation provides a setting where governments can compare policy experiences, seek answers to common problems, identify good practice and work to co-ordinate domestic and international policies.

The OECD member countries are: Australia, Austria, Belgium, Canada, Chile, the Czech Republic, Denmark, Estonia, Finland, France, Germany, Greece, Hungary, Iceland, Ireland, Israel, Italy, Japan, Luxembourg, Mexico, the Netherlands, New Zealand, Norway, Poland, Portugal, the Republic of Korea, the Slovak Republic, Slovenia, Spain, Sweden, Switzerland, Turkey, the United Kingdom and the United States. The European Commission takes part in the work of the OECD. OECD Publishing disseminates widely the results of the Organisation's statistics gathering and research on economic, social and environmental issues, as well as the conventions, guidelines and standards agreed by its members.

NUCLEAR ENERGY AGENCY

The OECD Nuclear Energy Agency (NEA) was established on 1 February 1958. Current NEA membership consists of 31 OECD member countries: Australia, Austria, Belgium, Canada, the Czech Republic, Denmark, Finland, France, Germany, Greece, Hungary, Iceland, Ireland, Italy, Japan, Luxembourg, Mexico, the Netherlands, Norway, Poland, Portugal, the Republic of Korea, the Russian Federation, the Slovak Republic, Slovenia, Spain, Sweden, Switzerland, Turkey, the United Kingdom and the United States. The European Commission also takes part in the work of the Agency.

The mission of the NEA is:

- to assist its member countries in maintaining and further developing, through international co-operation, the scientific, technological and legal bases required for a safe, environmentally friendly and economical use of nuclear energy for peaceful purposes, as well as
- to provide authoritative assessments and to forge common understandings on key issues, as input to government decisions on nuclear energy policy and to broader OECD policy analyses in areas such as energy and sustainable development.

Specific areas of competence of the NEA include the safety and regulation of nuclear activities, radioactive waste management, radiological protection, nuclear science, economic and technical analyses of the nuclear fuel cycle, nuclear law and liability, and public information.

The NEA Data Bank provides nuclear data and computer program services for participating countries. In these and related tasks, the NEA works in close collaboration with the International Atomic Energy Agency in Vienna, with which it has a Co-operation Agreement, as well as with other international organisations in the nuclear field.

This document and any map included herein are without prejudice to the status of or sovereignty over any territory, to the delimitation of international frontiers and boundaries and to the name of any territory, city or area.

Corrigenda to OECD publications may be found online at:

© OECD 2015

You can copy, download or print OECD content for your own use, and you can include excerpts from OECD publications, databases and multimedia products in your own documents, presentations, blogs, websites and teaching materials, provided that suitable acknowledgment of the OECD as source and copyright owner is given. All requests for public or commercial use and translation rights should be submitted to *rights@oecd.org*. Requests for permission to photocopy portions of this material for public or commercial use shall be addressed directly to the Copyright Clearance Center (CCC) at *info@copyright.com* or the Centre français d'exploitation du droit de copie (CFC) *contact@cfcopies.com*.

Foreword

The accelerator-driven system (ADS) is a potential transmutation system option as part of partitioning and transmutation strategies for radioactive waste in advanced nuclear fuel cycles.

Following the success of the workshop series on the utilisation and reliability of the High Power Proton Accelerators (HPPA), the scope of this new workshop series on Technology and Components of Accelerator-driven Systems has been extended to cover subcritical systems as well as the use of neutron sources.

The second workshop on Technology and Components of Accelerator-driven Systems was organised on 21-24 May 2013 in Nantes, France, and was hosted by the SUBATECH/Ecoles des Mines and co-sponsored by the Institut National de Physique Nucléaire et de Physique de Particules (IN2P3) of Centre National de la Recherche Scientifique (CNRS) France. The workshop organised by the OECD Nuclear Energy Agency provided experts with a forum to present and discuss state-of-the-art developments in the field of ADS and neutron sources.

A total of 40 papers were presented during the oral and poster sessions. Four technical sessions were organised addressing ADS experiments and test facilities, accelerators, simulation, safety, data, neutron sources.

These proceedings include all the papers presented at the workshop. The opinions expressed are those of the authors only, and do not necessarily reflect the views of the NEA, any national authority or any other international organisation.

Acknowledgements

The OECD Nuclear Energy Agency (NEA) gratefully acknowledges the SUBATECH/Ecoles des Mines and the Institut National de Physique Nucléaire et de Physique de Particules (IN2P3) of Centre National de la Recherche Scientifique (CNRS, France) for hosting the second Workshop on Technology and Components of Accelerator-driven Systems.



Table of contents

Executive summary **9**

Opening and Invited Speeches **16**

Chair: Pierre D'Hondt

Alex C. Mueller
CNRS welcome address 17

José Mª Martínez-Val
An ADS perspective on history and physics 18

Didier Haas, Roger Garbil, Michel Hugon
The European activity on ADS: The EURATOM Research Framework Programme 24

S. David[1], S. Massara[2]
Impact of P&T on nuclear scenarios with Generation-IV and ADSs 29

Fabrizio Gabrielli
Fuel for ADS: State-of-the-art, requirements, current and future programmes 37

Session I: Current ADS Experiments and Test Facilities **47**

Chair: K. Tsujimoto

M. Wohlmuther, V. Boutellier, Y. Dai, D. Gavillet, K. Geissmann, S. Hahl, B. Hammer, A. Lagotzki, H. Leu, H.P. Linder, A. Kalt, D. Kuster, J. Neuhausen, D. Schumann, R. Schwarz, H. Schweikert, A. Spahr, P. Suter, S. Teichmann, K. Thomsen, H. Wiese, W. Wagner, U. Zimmermann, Ch. Zumbach
The MEGAPIE PIE sample preparation 48

G.L. Khorasanov, A.I. Blokhin
Neutron spectrum hardening in critical and subcritical reactors cooled with ^{208}Pb 63

Atsushi Sakon[1], Kengo Hashimoto[1], Cheol Ho Pyeon[2]
Power spectral analysis for a thermal accelerator-driven system of the Kyoto University Critical Assembly 68

A. Kochetkov[1], P. Baeten[1], A. Billebaud[2], S. Chabod[2], X.Doligez[3], F.R. Lecolley[4], J.L. Lecouey[4], G. Lehaut[4], N. Marie[4], F. Mellier[5], H.E. Thyébault[2], W. Uyttenhove[1], G. Vittiglio[1], J. Wagemans[1], G. Ban[4], P. Dessagne[6], M. Kerveno[6], L.Mercatali[7]
Current progress and future plans of the FREYA Project 76

N. Marie[1], G. Lehaut[1], J.-L. Lecouey[1], A. Billebaud[2], S. Chabod[2], X. Doligez[3], F.-R. Lecolley[1], A. Kochetkov[4], W. Uyttenhove[4], G. Vittiglio[4], J. Wagemans[4], F. Mellier[5], G. Ban[1], H.-E. Thyébault[2], D. Villamarin[6]
Reactivity monitoring using the area method for the subcritical VENUS-F core within the framework of the FREYA Project 86

S. Chabod[1], X. Doligez[2], G. Lehaut[3], A. Billebaud[1], J.-L. Lecouey[3], F.-R. Lecolley[3], N. Marie[3], A. Kochetkov[4], W. Uyttenhove[4], G. Vittiglio[4], J. Wagemans[4], F. Mellier[5], G. Ban[3], H.-E. Thyébault[1], D. Villamarin[6]
Analysis of prompt decay experiments for ADS reactivity monitoring at VENUS-F Facility 96

Cheol Ho Pyeon, Takahiro Yagi, Yoshiyuki Takahashi, Tadafumi Sano, Hiroshi Shiga
Forthcoming experiments on accelerator-driven systems with 100 MeV protons at the Kyoto University Critical Assembly 107

Yacine Kadi[1,2]
Role of the ADS from the perspective of the International Thorium Energy Committee iThEC 114

Session II: Accelerators 121

Chair: M. Seidel

Yun-long Chi[1], Yuan He[2]
The present status of the Chinese ADS proton accelerator R&D 125

Jean-Luc Biarrotte[1], Didier Uriot[2], Luis Medeiros Romao[3], Dirk Vandeplassche[3]
Beam operation aspects for the MYRRHA linear accelerator* 135

R. Salemme[1*], D. Vandeplassche[1], L. Medeiros Romão[1], J.-P. Carneiro[1], J.-L. Biarrotte[2], M. Baylac[3], D. Uriot[4], H. Podlech[5]
The R&D@UCL Programme in support of the MYRRHA linear accelerator 148

Marouan El Yakoubi[1], Hervé Saugnac[1], Emmanuel Rampenoux[1], Jean Luc Biarrotte[1], Frédéric Bouly[2], Rocco Paparella[3], Paulo Perini[3]
Superconducting RF cavity activities for the Max Project 159

Adrian Pitigoi, Pedro Fernandez
Reliability model of SN linac (spallation neutron source-ORNL) 167

J.-P. Carneiro[1], L. Medeiros-Romão[1], R. Salemme[1], D. Vandeplassche[1], J.-L. Biarotte[2], Frédéric Bouly[2], D. Uriot[3]
Approach of a failure analysis for the MYRRHA linac 175

Tomas Junquera[1], Nicolas R. Chevalier[1], Jean-Pierre Thermeau[2], Luis Medeiros Romão[3], Dirk Vandeplassche[3]
MYRRHA cryogenic system study on performances and reliability requirements * 185

M. Baylac[1], A.Billebaud[1], P.Boge[1], D.Bondoux[1], J.Bouvier[1], T. Cabanel[1], S. Chabod[1], G.Dargaud[1], E.Froidefond[1], M.Heusch[1], A. Kochetkov[2], E. Labussière[1], F.-R. Lecolley[3], J.-L. Lecouey[3], G. Lehaut[3], N. Marie[3], J. Mertens[2], R. Micoud[1], F. Van Gestel[2], C. Van Grieken[2], B. Van Houdt[2], G. Vittiglio[2]
Operation of the accelerator driving the VENUS-F core for the low power ADS experiments GUINEVERE and FREYA at SCK•CEN 197

Session III: Simulation, Safety and Data 207

Chair: Y. Gohar

Enrique M. Gonzalez 208
Nuclear data for safe operation and waste transmutation: ANDES and CHANDA 208

Yousry Gohar, Yan Cao, Roger Kellogg, Elia Merzari
Accelerator-driven system design concept for disposing of spent nuclear fuels 215

Nicolas Thiolliere, Baptiste Mouginot, Arnaud Cadiou, Fanny Courtin, Amélie Pector
A high-power ADS concept 222

Baptiste Mouginot, Nicolas Thiolliere
CLASS: Core Library for Advanced Scenario Simulations 231

Takanori Sugawara, Kenji Nishihara, Kazufumi Tsujimoto
Transient analysis for lead-bismuth-cooled accelerator-driven system proposed by JAEA 241

Session IV: Neutron Sources 253

Chair: B. Grambow

Yousry Gohar[1], Igor Bolshinsky[2], Ivan Karnaukhov[3]
KIPT accelerator-driven system design and performance 254

Karel Samec
A multi-megawatt compact neutron - source for ADS 266

A. Batta, A. Class
Thermal hydraulic numerical investigation of the heavy liquid metal free surface of MYRRHA spallation target experimental 277

Yoann Fusco[1], Masoud Behzad[2], Karel Samec[1], Yacine Kadi[1,2]
A flexible testing facility for high-power targets T-MIF 283

Hironari Obayashi, Hayanori Takei, Hiroki Iwamoto, Toshinobu Sasa
Numerical analysis of the feasibility of a beam window for TEF target 291

Ingrid Proriol Serre, Changqing Ye, Jean-Bernard Vogt
Parameters promoting liquid metal embrittlement of the T91 steel in lead-bismuth eutectic alloy 300

J. R. Fetzer[1*], A. G. Class[1], C. Fazio[2], S. Gordeev[3]
Conceptual design studies for the liquid metal spallation target META:LIC 309

Special Session: In Memoriam Horst Klein 321

Chair: A.C. Mueller

Horst Stoecker[1], A. C. Mueller[2]
Horst Klein - Scientist, Teacher, Leader and Friend 322

O. Kester
The FAIR proton linac 325

Ulrich Ratzinger
Linac strategies for the lower beam energies 329

P. Baeten, D. De Bruyn, R. Fernandez, G. Van den Eynde, H. Aït Abderrahim
Recent developments of the MYRRHA Project 338

Annex 1: Scientific Advisory Committee 347

Annex 2: List of participants 348

Executive summary

Opening and Invited Keynote Speeches

Welcome address

The welcome address was given by A.C. Mueller (CNRS Institut National de Physique Nucléaire et de Physique des Particules, IN2P3, Scientific Deputy Director, Chair of the Workshop), who welcomed the attendees to this second edition of the OECD Nuclear Energy Agency (NEA) International Workshop on Technology and Components of Accelerator-Driven Systems. The first edition of the workshop was held in Karlsruhe in 2010.

A. Mueller noted that the TCADS workshops followed the success of the workshop series on the utilisation and reliability of the High Power Proton Accelerators (HPPA) organised in 1998-2007, with an enlarged scope covering subcritical systems and neutron sources as well.

Following a brief introduction, A. Mueller informed the attendees that, at the end of the workshop, the International Advisory Committee (IAC) of TCADS-2 decided to commemorate Prof. Horst Klein, a Professor Emeritus at the Frankfurt University IAP, a world-renowned accelerator specialist, who passed away in December 2012.

An ADS perspective on history and physics

The history of ADS was briefly retraced in this paper, pointing out the interest of ADS with respect to multiple high-ranking objectives including safety and waste transmutation. The role of the OECD Nuclear Energy Agency in advancing knowledge in this field was also highlighted.

The European activity on ADS: The EURATOM Research Framework Programme

This paper presents the EURATOM programme relating to minor actinide transmutation and accelerator-driven systems (ADS) such as partitioning processes, fuel and material developments, basic neutron data measurements, the support of the MYRRHA project in Belgium through accelerator development, reactor design and safety studies. The paper reviews the background and the status of the European research projects in the field as well as the main conclusion of EC sponsored projects from FP5 to FP7.

Impact of P&T on nuclear scenarios with Generation-IV and ADSs

In its first part, the paper introduces the main principles of the physics of P&T, including a brief comparison of the performance of different strategies with fast reactors (homogeneous vs. heterogeneous recycling, ADS vs. fast breeder reactors, which feature similar performances) and relates the number of ADS in the nuclear fleet with the requirements for the accelerator. The second part provides a brief overview of recent activities carried out in this domain at the OECD Nuclear Energy Agency.

Fuel for ADS: state-of-the-art, requirements, current and future programmes

The paper presents a broad overview of the current state-of-the-art R&D on innovative fuels for ADS systems, mainly focusing on results from the Sixth FP EU EUROTRANS Programme in the following domains: basic properties and design issues, safety requirements, fabrication, reprocessing, behaviour under irradiation. The paper also provides the main experimental results and related safety assessments from in-pile and out-of-pile experiments of Ceramic-Ceramic and Ceramic-Metallic composite fuels and briefly describes the on-going R&D activities in Europe on fuels loaded with large amounts of MAs.

Session I: Current ADS Experiments and Test Facilities

The MEGAPIE PIE sample preparation

The MEGAPIE Project, which aims to demonstrate that a liquid lead-bismuth-eutectic (LBE) spallation target can be licensed, planned, built, operated, dismantled, examined and disposed of, produced samples for post-irradiation examination (PIE) for the analysis of structural material property changes due to the harsh environment of high temperatures, contact with flowing liquid metal (LBE), and proton and neutron irradiation. These samples will be investigated by all partner laboratories (CEA, CNRS, ENEA, KIT, PSI and SCK•CEN). This paper provides an overview of the PIE sample preparation and highlights the first results obtained to-date.

Neutron spectrum hardening in critical and subcritical reactors cooled with ^{208}Pb

This paper deals with neutron spectrum hardening using enriched ^{208}Pb as a coolant. This feature, which can apply both to critical and subcritical reactors and to pure-lead of Pb-Bi coolants, aims to improve the transmutation rate of minor actinides, especially ^{241}Am. The paper addresses the spatial distribution of the neutron mean energy and the fission-to-capture ratio.

Power spectral analysis for a thermal accelerator-driven system at the Kyoto University Critical Assembly

This paper reports on on-going experiments at the Kyoto University and aims to investigate, among others, uncertainties of fission and capture cross-section data for minor actinides, with special emphasis on the power spectral analyses for these experiments.

Current progress and future plans of the FREYA Project

The paper describes the validation of an on-line subcriticality monitoring method, within the framework of the support studies of the transmutation experimental facility MYRRHA/FASTEF, at the zero-power VENUS-F Reactor in Mol (Belgium). The overall structure of the project is discussed for each of the five working packages: ADS on-line reactivity monitoring, subcritical configuration for MYRRHA/FASTEF, critical configuration for MYRRHA/FASTEF, critical configuration for LFR, training and education, and project co-ordination. Major achievements and future activities are highlighted in the paper.

Reactivity monitoring using the area method for the subcritical VENUS-F core within the framework of the FREYA Project

This paper reports on results obtained for pulse neutron source experiment at the VENUS-F Facility in Mol, within the framework of the FREYA Project. Results are analysed using the area method in order to estimate the reactivity of a few subcritical configurations of the VENUS-F reactor. Corrected reactivity values were judged to be compatible and in good agreement with the reference values previously estimated with the MSM method.

Analysis of prompt decay experiments for ADS reactivity monitoring at VENUS-F Facility

This paper describes an innovative analysis method for the ADS reactivity on-line monitoring, which relies on the prompt component of the neutron decay constant and can be applied to shorter beam interruptions (a few tens of microseconds). This method has been applied to the first experimental data taken at SCK•CEN VENUS-F Facility, with promising preliminary results.

Forthcoming experiments on ADS with 100 MeV protons at the Kyoto University Critical Assembly

The paper summarises on-going experiments at the Kyoto University, where a series of uranium-loaded accelerator-driven system (ADS) experiments are planned to be carried out to investigate uncertainties of fission and capture cross-section data for minor actinides. These experiments address different values of subcriticality, external neutron source and neutron spectrum. The paper also analyses other features like the feasibility of the transmutation of ^{237}Np and ^{241}Am by ADS and the transmutation of ^{232}Th into ^{233}U.

Role of the ADS from the perspective of the International Thorium Energy Committee iThEC

The paper focuses on the use of thorium in a subcritical fast reactor configuration driven by an ADS and cooled by natural convection of liquid metal from the perspective of the International Thorium Energy Committee (iThEC).

Session II: Accelerators

Present status of the Chinese ADS proton accelerator R&D

The Chinese ADS Project is progressing in collaboration with several Chinese institutions, such as the Institute of High Energy Physics (IHEP) and the Institute of Modern Physics (IMP), which are responsible for developing the two injectors and the main linac. This paper presents the progress of the key hardware R&D work of the Chinese ADS proton accelerator, including among others: CW RFQ, SC HWR, spoke and elliptical cavities, HP input couplers, SSA RF power sources, SC solenoid magnets, beam diagnostic devices, digital power supplies and cryogenic systems.

Beam operation aspects for the MYRRHA linear accelerator

This paper reports on the current status of the accelerator design for MYRRHA, carried out within the framework of the FP7 MAX Project. For this purpose, several specific aspects linked with beam operation are discussed: beam time structure requirements, beam power control and ramp-up strategies, beam reconfiguration schemes in fault cases, and beam instrumentation needs.

The R&D@UCL programme in support of the MYRRHA linear accelerator

This paper describes the main features of the R&D Programme supporting the development of the MYRRHA linac. An essential part of the engineering activities and the full development cycle of the future MYRRHA injector, this programme addresses engineering design, prototyping, production, tests and in-depth analysis.

Superconducting RF cavity activities for the MAX Project

The paper addresses two tasks related to the design of superconducting accelerator components for the linac facility for MYRRHA: on the one hand, cryogenic tests in a cryomodule configuration carried out with a view to evaluating and improving the reliability of the different components, and on the other hand, a detailed study of the first superconducting linac section cryomodule. The results of the elliptical cavity and the status of the spoke cryomodule design are discussed extensively in the paper.

Reliability model of SNS linac (spallation neutron source-ORNL)

The paper describes a reliability model of SNS linac of MYRRHA. The model, developed using the risk spectrum reliability analysis software, allows carrying out an analysis of the accelerator system's reliability in comparison with the SNS operational data. This analysis aims to identify design weaknesses and provides recommendations to improve the reliability of the MYRRHA linear accelerator.

Approach of a failure analysis for the MYRRHA linac

The paper describes the design strategy aiming at obtaining a very high availability for the MYRRHA linac, which targets less than 10 beam trips longer than three seconds every operating period of three months. The paper focuses on how the three underlying principles in the design of the MYRRHA linac: elements redundancy, elements operation at derated values and the fault tolerance concept, are implemented in a "virtual accelerator", and provide an extensive list of examples of application.

MYRRHA cryogenic system study on performances and reliability requirements

The paper presents a preliminary architecture of the cryogenic system as well as the principles for the cryogenic fluids distribution proposed for the MYRRHA Facility. The paper gives some insights into the reliability of this system and contains a preliminary proposal for the technical buildings, their dimensions, layout and connection with the accelerator tunnel.

Operation of the accelerator driving the VENUS-F core for the low power ADS experiments GUINEVERE and FREYA at SCK•CEN

This paper describes the design and commissioning of the experimental facility of the GUINIVERE Project, which reports on the operation of the GENEPI-3C accelerator coupled with the VENUS-F reactor. On-going analyses of the recorded data set from the accelerator-reactor system show that, in spite of discrepancies of accelerator structures between such a mock-up machine and a high-power proton driver for an ADS demonstrator facility, valuable feedback from the coupled operation can be provided for ADS projects, such as MYRRHA.

Session III: Simulation, Safety and Data

Nuclear data for safe operation and waste transmutation: ANDES and CHANDA

The paper focuses on two projects funded within the Seventh Framework Programme related to nuclear data improvement, summarising the objectives and the main achievements of ANDES and the preparation for CHANDA. ANDES developed new experimental methods, performed new measurements, validations and evaluations of cross-sections and other nuclear data. CHANDA, with a scheduled start in December 2013, will combine similar types of activities with co-ordination of the access of experimental teams to the existing European experimental facilities.

Accelerator-driven system design concept for disposing of spent nuclear fuels

This paper presents the design concept and the system analyses of accelerator-driven systems optimised for TRU transmutation (accelerator with a 1 GeV protons and ~25 MW beam power), providing results on burn-up simulations and preliminary results on mass fluxes and balances.

A high-power ADS concept

The paper presents a large-size Pb-Bi-cooled high-power ADS theoretical concept, based on an annular spallation target irradiated by a rotating proton beam, providing results of a detailed neutronics and thermal-hydraulics study performed with the code MURE (MCNP Utility for Reactor Evolution), based on the Monte-Carlo transport codes MCNP or MCNPX. A complete core and assembly evolution during an irradiation cycle provides mass balance in order to characterise the performance of this system in terms of minor actinide transmutation.

CLASS: Core Library for Advanced Scenario Simulation

The first part of this paper reports on the rationale behind and the basic principles of CLASS, a new simulation code for electronuclear scenarios simulation under development at CNRS-IN2P3. The second part presents an application case based on the French fleet operation during the period 1978-2011.

Transient analysis for lead-bismuth-cooled accelerator-driven system proposed by JAEA

The paper addresses the behaviour of a Pb-Bi-cooled ADS developed at JAEA by means of the transient codes SIMMER-III and RELAP5. The dynamic response is analysed during protected loss of heat sink, protected overcooling and unprotected blockage accident conditions. The protected loss of heat sink does not fulfill the no-damage criteria (fuel

melting after 18-21 hours), requiring the design of a specific safety system, which will be the subject of further studies.

Session IV: Neutron Sources

KIPT accelerator-driven system design and performance

This paper describes the ADS neutron source facility KIPT currently under construction in Ukraine, for a start-up planned for March 2014. The paper focuses on the design of the target assembly, the neutronic design of the subcritical core with the code MCNP-X. This activity is carried out within the framework of a collaboration between KIPT and ANL.

A multi-megawatt compact neutron source for ADS

The paper presents the development of a high-power liquid-metal neutron source in the context of the TIARA FP7 research programme. This innovative design has been developed in Switzerland based on a conical concave thin-gauge beam window optimised for low stress, with multiple barriers to mitigate the consequences of an eventual failure in any component.

Thermal-hydraulic numerical investigation of the heavy liquid metal free surface of MYRRHA spallation target experiment

The paper presents a detailed thermohydraulic analysis of the mock-up of the windowless target for MYRRHA at nominal flow condition, supported by the FP7 Thermal-Hydraulics of the Innovative Nuclear Systems (THINS) Project. The results show that the target has a very stable free surface configuration for the considered flow rate and heat load.

A flexible testing facility for high-power targets T-MIF

An irradiation target is being proposed which should allow significant progress in the field of materials and sensors used in highly irradiated environments. The power is limited to 100 kW in a very compact arrangement in order to obtain the best neutron economy from a moderate beam power, which is more likely to be found in laboratories across Europe. The paper presents the challenges posed by such a compact design and accompanying calculations.

Numerical analysis of the feasibility of a beam window for TEF target

Within the framework of the development of an ADS for P&T application currently underway at JAEA, the feasibility of a beam window of the Transmutation Experimental Facility (TEF) target represents a crucial issue. This paper presents a numerical analysis with a three-dimensional model, performed by considering the current density and shape of the incident beam in the target region, and the thermal-fluid behaviour of LBE around the beam window. The results confirm the feasibility of such a beam window, paving the way for further optimisation to be carried out in future studies.

Parameters promoting liquid metal embrittlement of the T91 steel in lead-bismuth eutectic alloy

This study presents an analysis of the mechanical behaviour of the T91 martensitic steel in liquid lead-bismuth eutectic (LBE) and in inert atmosphere in a Small Punch Test (SPT), aiming to identify which parameters are responsible for liquid embrittlement by LBE, including oxygen content and displacement speed.

Conceptual design studies for the liquid metal spallation target META: LIC

Within the framework of the design studies for the European Spallation Source, this initiative aims to build the world's most powerful spallation neutron source in Sweden. This paper describes the META:LIC target concept, which has LBE (lead-bismuth eutectic) as a spallation material and a primary coolant, with a particular focus on the target module. The paper presents thermo-hydraulic simulations for both options and design measures to mitigate pulsed proton beam induced phenomena.

Special Session: In memoriam Horst Klein

Horst Klein: Scientist, Teacher, Leader and Friend

Professor Horst Klein passed away on 12 December 2012. During his final years as a scientist, H. Klein was a particularly active member of the community performing research and development for the "technology and components of accelerator-driven systems". All his colleagues involved in TCADS-1 (Karlsruhe, 2010) and TCADS-2 benefited from his outstanding expertise. This contribution is to honour his legacy as a scientist, teacher, leader and friend.

In the last ten years, while H. Klein was involved in the FAIR Project and guided many students and collaborators to participate in it, most of his research focused on the development of linear accelerators of the highest possible intensities and reliabilities for nuclear energy applications, both in fusion and in fission for accelerator-driven systems. H. Klein led IAP participation to the relevant EURATOM contracts, such as PDS-XADS (FP5), EUROTRANS (FP6), MAX (FP7). The collaboration for the recently started EURATOM Project MARISA, to which H. Klein's contribution for its preparation was instrumental, will have to continue without its elder statesman.

H. Klein was among the intellectual leaders in heavy ion accelerator science for more than half a century. He shaped this field of science, mentored more than a hundred diploma and PhD students, and will be sorely missed by many.

The FAIR proton linac

FAIR, the Facility for Antiproton and Ion Research in Europe constructed at GSI Helmholtzzentrum für Schwerionenforschung GmbH in Darmstadt, comprises an international centre of heavy ion accelerators that will drive heavy ion and antimatter research. FAIR will provide globally unique accelerator facilities and experimental facilities allowing a large variety of fore-front research in physics and applied science. The main part of the FAIR Facility, a sophisticated accelerator system which delivers beams to different experiments of the FAIR experimental collaborations in parallel, is extensively described in the paper.

Linac strategies for the lower beam energies

Linear accelerator capabilities are improved steadily to fulfill the demands on driver beams for new beam facilities. At high beam energies above 200 AMeV and towards $\beta \rightarrow 1$, well-established concepts exist for both room temperature (r.t.) and superconducting (s.c.) linacs. Concerning low and medium beam energies, different solutions have been developed and realised to meet specifications for individual cases, however, there is still no low and medium energy standard concept for "long" linacs. This paper describes the main limitation of the current technology, namely, field emission already at modest surface fields and, as a result, limited acceleration rate. The paper also discusses current cavity developments and trends.

Recent developments of the MYRRHA Project

This paper presents the most recent developments in the design of the MYRRHA Facility. The challenges related to the design of the accelerator (proton beam with an energy of 600 MeV and an average beam current of 3.2 mA), the core and primary system are described in detail. The MYRRHA design, with the FASTEF version, entered into the Front End Engineering Phase covering the period 2012-2014. MYRRHA is expected to be fully operational by 2024 in both operation modes (subcritical and critical).

Opening and Invited Speeches

Chair: Pierre D'Hondt

CNRS welcome address

Alex C. Mueller
CNRS, France

It is my great honour and delight to welcome you all here to Nantes, the second edition of the OECD/NEA International Workshop on Technology and Components of Accelerator-driven Systems.

Many of you assisted in the first workshop of the series, held in March 2010 in Karlsruhe, which was jointly organised by the OECD/NEA, KIT Karlsruhe and the EURATOM Integrated Project EUROTRANS. Indeed, the public presentation of the final scientific conclusions of EUROTRANS was an important part of a special session.

Thus, it is a pleasure to find you back here in Nantes three years later, and also to warmly welcome new faces. The subject of this workshop will be the continuation of TCDAS-1, overviewing the progress accomplished worldwide in a large number of topics.

The International Advisory Committee (IAC) of TCADS is instituted by the NEA Working Party on Scientific Issues of the Fuel Cycle. I have to thank the IAC for having reviewed all the submitted abstracts and have made a very attractive programme for the next days, as hopefully you will concur.

An outstandingly active person in the IAC has always been Horst Klein, Professor Emeritus at the Frankfurt University IAP, world-renowned accelerator specialist. Horst, "doyen" of the linac community and very active in the application of accelerators in energy technologies, namely in fission and fusion, passed away in December 2012. On the decision of the IAC, we will commemorate Horst in a session specially dedicated to him.

I would like to extend my gratitude to those who have made the organisation of this meeting possible. The workshop is hosted by the SUBATECH laboratory of Ecoles des Mines and the CNRS-IN2P3. Special thanks are due to the staff of SUBATECH, and in particular its director, Bernd Grambow, and to Nicolas Thiollière and Bernard Kubica whose practical aspects have contributed to the organisation of the workshop. The support of the CNRS-IN2P3 and the OECD/NEA, especially its secretary, Simone Massara, is greatly appreciated.

Finally, I wish us all a very interesting and fruitful meeting in Nantes and thank you for your attention.

An ADS perspective on history and physics

José Mª Martínez-Val
Universidad Politécnica de Madrid, Spain

Abstract

Nuclear Physics has been characterised by synergism between nuclear reactions since the very beginning of nuclear research, where two kinds of reactions were easily identified: reactions induced by charge particles that could be accelerated by electric fields, and reactions induced by neutrons, where no acceleration was possible. In contrast, neutron moderation was very effective in producing a type of very reactive particles: the thermal neutrons. The latter led to nuclear reactors, and their history was so successful that current nuclear energy is a consequence of that early success. Charge particles were considered for fusion reactions, but this story is still to be written, because we have been unable so far to build a nuclear fusion reactor.

Going back to the fission field, another important feature is also pending to be achieved: nuclear breeding, which is the mechanism to produce fissile fuels from fertile nuclei. The epitome for that is the conversion from naturally existing ^{238}U into ^{239}Pu. However, the build-up of higher A actinides conveys a degradation of safety features, particularly in the reduction of delayed neutrons fraction, which is essential for reactor control. Moreover, Doppler effect which is the main self-stabilising mechanism in thermal reactors, almost disappears in fast reactors with higher A actinides, making it very difficult, if not impossible, to build and operate a reactor abiding by the essential rules of nuclear safety.

A creative solution for this problem could lie in accelerator-driven systems, where proton-induced spallation reactions contribute to the complementary neutrons to keep a subcritical reactor in a steady state. A subcritical core is needed, but it should be noted that the stabilising and controlling functions can be provided by the accelerator-driven systems, which is a fast reacting device that can adjust its beam intensity to the core state (in reactivity, temperature, etc.).

Introduction

The potential importance of ADS in the future has particular significancein this city, Nantes, birthplace of the famous writer Jules Verne, who invented the journey from the earth to the moon and devised sodium batteries for powering submarines able to travel thousands of miles.

Although science does not share principles with science fiction, the latter helps to break the frontiers of the former, and in this sense, it feels right to pay homage to this famous French writer.

Jules Verne could not anticipate that electricity would become so important for mankind, and even less that 13.5% of word electricity generation would be produced by a special source of energy called nuclear energy (although properly speaking it should be nuclear fission energy). From this point of view of recent history, nuclear energy is a mature commercial field, with all the *pros* and *cons* of big industry with existing interests. At present, the potential for growth is found in Asia, but its development is jeopardised by nuclear accidents by high specific investments and lack of maturity of Generation-III reactors. Moreover, Generation-IV reactors, theoretically considered for long-term solutions are moving at a very low pace. Emphasis has been placed on sodium fast reactors SFR, which inherently present the problem of the positive sodium void coefficient, and therefore does not comply with criterion 11 of Title 10 of the Code of Federal Regulations part 50, Appendix A, which states: “The reactor core and associated coolant systems should be designed so that in the power operating range the net effect of the prompt inherent nuclear feedback characteristics tends to compensate for a rapid increase in reactivity”.

An answer has to be given after analysing the physics of higher A actinides which is a main issue in fully exploiting nuclear energy. First, a short review is presented on the principles of sustainable nuclear energy which is the new framework of reference.

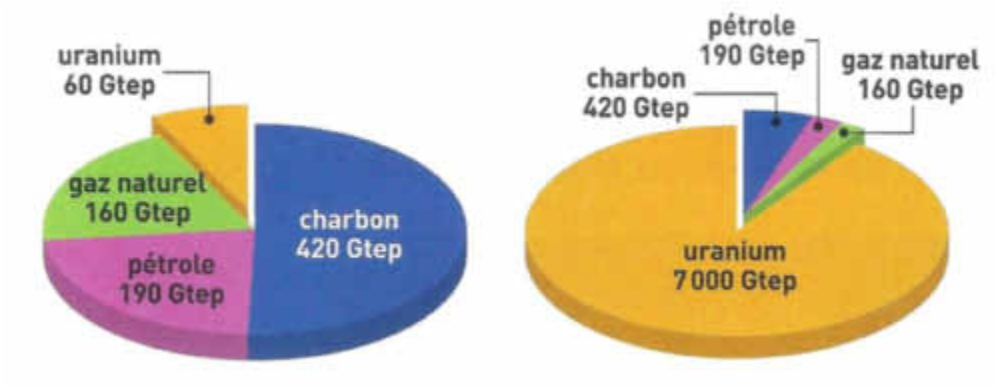
Sustainable development principles for nuclear energy

A set of principles will clearly guide this development. Some of them, such as proliferation resistance are beyond the scope of this paper, which is mainly devoted to technologies enabling nuclear energy renaissance. The principles of this type are as follows:

- Radiological consequences of accidents must be limited to “acceptable values”. For instance, TMI-2 could be accepted, but not Chernobyl.
- Nuclear waste legacy to future generations must be limited in radioactivity and time.
- The technological legacy for properly exploiting the “nuclear fuels” should be improved by orders of magnitude, what is mainly related to the “breeding” issue. Nuclear systems are necessary to fully exploit the natural research of uranium and thorium in a safe and economic way.

The latest point is shown in Figure 1 (taken from CEA "Clefs" n° 61, 2013):

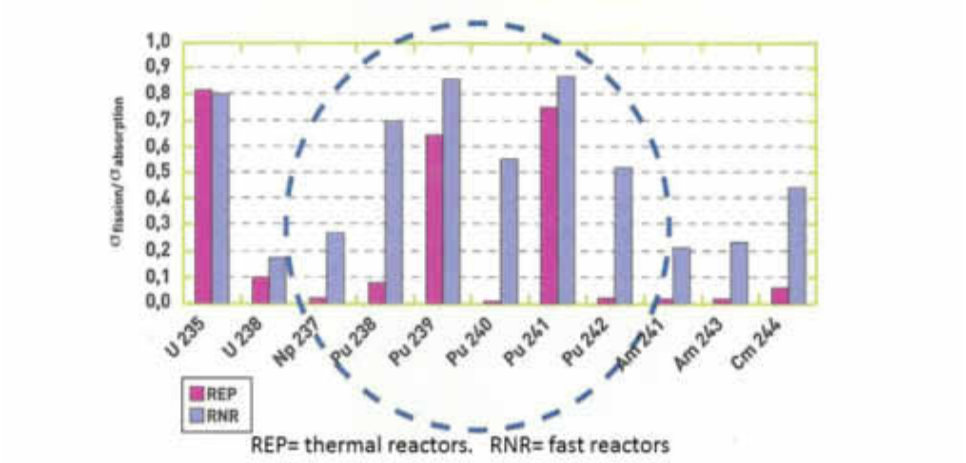
Figure 1. World energy resources



In the cake on the left, uranium is considered burnt in light water reactors, in the current once-through cycle (the number does not change much if Pu is recycled in LWR). In the cake on the right, uranium is burnt in breeder reactors.

The best spectrum for breeding is the fast one (1, 2) for a number of reasons that yield the right value of the neutron chain requisite, expressed as follows: the mean number of secondary neutrons per absorption in the fuel must be higher than two. One out of these two neutrons is for keeping criticality, and another is for replacing the fuel nucleus that has disappeared by absorption. In the following graph, it can be seen that all actinides behave more reactively when they are in a fast neutron environment than in a thermal neutron system (3, 4).

Figure 2. A relevant spectral index to measure the reactivity potential of nuclei is the cross-section ratio between fission and absorption



Some isotopes as ^{240}Pu and ^{242}Pu, which are a burden for the neutron economy in thermal reactors, become fuels in fast neutron environments (from CEA "Clefs" n° 61, 2013).

The nuclear safety of the fission core

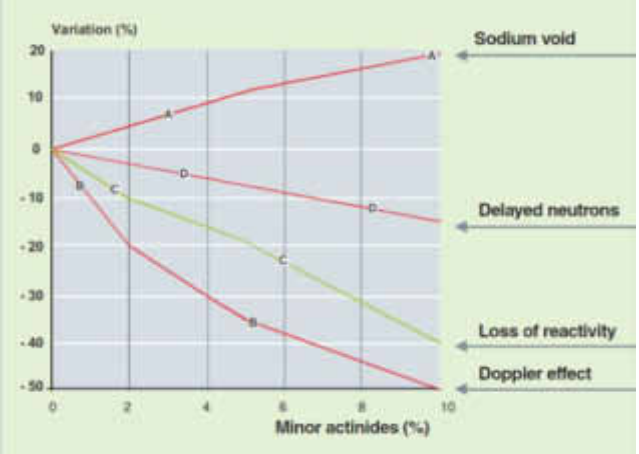
Safety is the most relevant topic in nuclear energy, and it mainly implies two goals: to keep the chain reaction under control, and keep radioactive products within the barriers of the system. The first one went wrong in the Chernobyl accident, and it entailed a tremendous power surge that destroyed all the confinement barriers. The key to that was

the positive feedback established between reactivity and thermal-hydraulics, which was not a common feature of RBMK reactors in regular states; but Chernobyl-4 was at the end of its first and long operating cycle, with a huge content of Pu, and safety parameters were degraded, and the reactor jumped from submoderated state to over-moderated, which conveyed such a positive feedback. RBMK are thermal neutron reactors (5), but positive feedback can occur in fast spectrum reactors as well, and the margin for controlling the reactor is much shorter than in the previous case.

In the case of fast reactors, the following features (6) are particularly bad, as can be seen in the following figure:

- inclusion or internal build-up of higher actinides (HA, also called MA) in the fuel of a fission reactor produces a degradation of its main safety features;
- in fast reactors cooled by molten metals sodium void reactivity coefficient becomes more positive as MA content increases;
- Doppler effect suffers degradation;
- delayed neutron fraction decreases.

Figure 3. Safety features degradation in fast reactors as the content of minor actinides (those which are neither U or Pu nor Th) increases



Build-up of these MAs is inherent to high burn-ups, and it is also associated with waste transmutation.

Going back to the main idea of this section, the best spectrum for breeding is the fast one; but it conveys a series of risks which have to be properly addressed, because not all the systems are equal in capability to counteract these risks.

Roles, *pros* and *cons* of ADS

The first ADS was the experimental set-up devised and operated by Nobel Laureate E. Lawrence during the Manhattan Project, using a proton cyclotron to irradiate samples of natural uranium. One of the main outcomes of that pioneering activity was the identification of plutonium by Glenn Seaborg, who received the Nobel Prize in Chemistry for that work. It should be noted that a plethora of brilliant scientists, as Fermi, Wigner, Teller and other major names, were building the first nuclear reactors to produce ^{239}Pu, identified as a very good fission fuel.

ADS did not advance rapidly, two decades later, a new use of these machines emerged to eliminate the most offending nuclear waste products, in the Accelerator Transmutation of Waste (ATW) Program at Los Alamos National Laboratory US (8).

The interest in ADS for the nuclear energy domain at large received the highest momentum at the very central place of accelerators, the CERN institution, whose director general, Carlo Rubbia, Nobel Prize winner in Physics in 1984, started the "Energy Amplifier" initiative (9) which included a test at large scale (10) for characterising not only the spallation source but also the subcritical multiplication in the surrounding subcritical core, originally placed at Madrid Technical University, in the College of Industrial and Power Engineering, where the author of this paper was Director and Chair Professor of Nuclear Technology. The key person for mobilising all the required resources to launch the project was Juan Antonio Rubio, at that time at CERN in Rubbia's cabinet, and director general of CIEMAT (Spain) some years later.

The importance of ADS can be summarised as follows:

- main role: to keep the neutron chain reaction in a core with degraded safety parameters for: energy generation, fissile breeding and transmutation;
- *pros*: subcriticality margin, simpler control, better use of higher actinides;
- *cons*: additional equipment, system complexity, radiation damage in the source.

Synthesis and conclusion

The history of ADS emphasises the interest of ADS Physics to benefit from the nuclear world. The future of the so-called "strong force" in the structure of matter as a physical potential to be used for the benefits of mankind could depend on the way scientists and engineers deal with this subject:

- Synergism between nuclear mechanisms is well rooted in physics, although it was forgotten because of the success of thermal reactors. New challenges are ahead. Nuclear breeding is absolutely necessary.
- The question arises whether to use critical or subcritical reactors. It depends on the safety-relevant parameters of fuels and cores. Nuclear safety features are indeed very different with new fuels in very fast spectrum. In any case, the famous criterion 11 of 10CFR50 Appendix A must be kept as a fundamental requirement.
- The risk of safety degradation in a critical reactor seems too high to be acceptable when the load of higher actinide becomes significant, and this trend is the one followed naturally by the fuel as burn-up increases.
- An accelerator and its neutron source could be a smart tool to control reactors without inherent capability to self-stabilise reactivity trips or to have time for stopping the chain reaction.

The role of the OECD Nuclear Energy Agency is fundamental in the field of many activities such as the notorious comparison between ADS and fast reactors in advanced nuclear fuel cycles (11).

References

[1] Harms, A. A., Heindler, M (1982), "Nuclear Energy Synergetics", New York.

[2] Martínez-Val, J.M, M.Piera (2007), "Nuclear fission sustainability with hybrid nuclear cycles", Energy Conversion and Management, 48, 1480-90.

[3] Storrer, F. (1973), "Introduction to the physics of fast power reactors", IAEA series No 143, Vienna.

[4] Walter McCarthy, David Okrent (1964), "Fast Reactor Safety", *The technology of nuclear reactor safety,* Beckerley and Thomson The MIT Press.

[5] Martínez-Val JM et al. (1990), "An analysis of the physical causes of the Chernobyl accident", *Nuclear Technology*; 90:371.

[6] CEA (2012), "Research nuclear reactors", DEN Monographs A Nuclear Energy Division Monograph, edited by André Chabre.

[7] Van Atta, C.M., Lee, J.D., Heckrotte, W. (1970), "The Electronuclear Conversion of Fertile to Fissile Material", Lawrence Livermore Laboratory Report UCRL-52144.

[8] Bowman C, Jameson R, Lawrence G. (1992), "Accelerator driven transmutation technology for incinerating radioactive waste and for advanced application to power production", *Nuclear Instruments & Methods B*;68:474.

[9] Rubbia, C. et al. (1995), "Conceptual design of a fast neutron operated high power energy amplifier", CERN/AT/95-44.

[10] Andriamonje, S. et al. (1995), "Experimental determination of the Energy generated in Nuclear Cascades by a high energy beam", *Phys.Lett.B.,* 348, 697.

[11] NEA (2002), "Accelerator-driven systems and fast reactors in advanced nuclear fuel cycles".

The European activity on ADS: The EURATOM Research Framework Programme

Didier Haas, Roger Garbil, Michel Hugon
European Commission, Brussels, Belgium

Abstract

Each European member state is responsible for its nuclear energy policy including the back-end of the cycle. Thus, major R&D programmes are performed on a national level. For this purpose, several research actions are undertaken under the EURATOM Research and Training Framework Programmes. The main emphasis in the EURATOM programme in the fields of minor actinide transmutation and Accelerator-driven Systems (ADS) is placed on partitioning processes, fuel and material developments, basic neutron data measurements, and the support of the MYRRHA project in Belgium through accelerator development, reactor design and safety studies. This article reviews the background and the status of the European research projects in the field.

Introduction

The European Union produces almost one third of its electricity from nuclear energy by fission. It represents an important factor in maintaining European competitiveness and the security of energy supply. After the Fukushima accident in 2011, the main emphasis in terms of the public perception of nuclear energy is now clearly linked to safety aspects. However, due to the long time periods involved in the storage of irradiated materials, and to the potential associated uncertainties, implementing solutions for the treatment and final disposal of nuclear wastes remains an equally important factor for obtaining the public acceptance of the use of this source of energy.

In Europe, two main spent fuel strategies are being implemented, namely fuel reprocessing followed in most cases by the recycling of residual uranium (U) and plutonium (Pu) in light water reactors, and the direct disposal of the irradiated fuel elements. Both strategies, however, need the deep-geological disposal technology for disposing of, either the glass packages issued from the reprocessing, or the fuel elements. Concrete projects are being implemented in several European countries, with the most advanced being in Finland and Sweden.

In order to reach the goals of long-term sustainability in nuclear energy, by using uranium resources in a much more efficient way and by reducing high level waste volumes and hazards, the use of fast neutron reactors (FRs) will be required. To further reduce waste radiotoxicity in the long-term, transmutation by fission of minor actinides (MA) is being developed on a research basis. In such a case, critical FRs and ADS (subcritical fast neutron reactor coupled to a proton accelerator through a neutron spallation target) are proposed.

Fast neutron reactor development

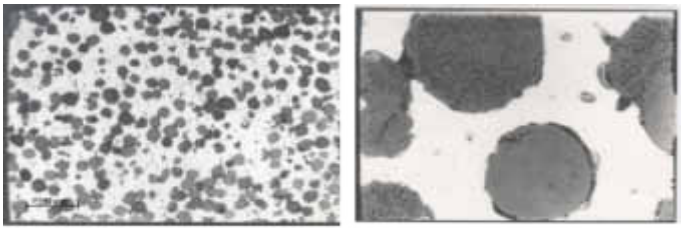
FRs development is the basis for a long-term sustainable nuclear energy policy, as recognised at a European level within the SET (European Strategic Energy Technology) Plan. On the initiative of SNE-TP (Sustainable Nuclear Energy Technology Platform www.snetp.eu), a SET Plan industrial initiative named ESNII (European Sustainable Nuclear Energy Industrial Initiative) has been launched. It gathers the main research and industry players in the field. Three tracks are followed (which are all coherent with the roadmap of the Generation-IV International Forum), namely those cooled with sodium (SFR), lead or lead-bismuth (LFR), and gas (GFR). The ADS is a large part of the lead/lead-bismuth track of ESNII (although not part of GIF). The EURATOM Framework Programmes (cordis.europa.eu), "FP7+2" (2012-2013) and the future HORIZON 2020 (2014-2018) support these initiatives through several projects (in particular for the ADS, MAXSIMA, for example), which are focusing on safety aspects upon the request of the European Council after the Fukushima accident in March 2011. In addition, the Joint Research Centre Institutes (ec.europa.eu/dgs/jrc) contribute to the same programme through safety and material studies (at JRC-IET in Petten), nuclear data (at JRC-IRMM in Geel) or fuel partitioning and transmutation (P&T) experiments (at JRC-ITU in Karlsruhe).

Several demonstration projects are now proposed in Europe. ASTRID (SFR) in France and MYRRHA (lead-bismuth-cooled ADS) in Belgium are the most promising ones, being financially supported by their respective host countries. Besides the demonstration role of these new facilities, it is very important to have an available fast neutron facility in Europe to be able to perform irradiation experiments for fuels and materials and to develop and license the advanced fuels. This will be the second main objective of MYRRHA.

Minor actinide transmutation strategies and ADS R&D programmes

In addition to Pu which will be recycled in FRs, a further reduction of high level waste radiotoxicity and thermal power can be achieved by the extraction from the spent fuel and the transmutation in a reactor of the MAs: americium (Am) and curium (Cm). Today, three ways to achieve transmutation of MAs are considered, namely (i) in a homogeneous way in a critical FR core, (ii) in a heterogeneous way in the blanket of the FR, and (iii) in the core of a subcritical ADS. The reprocessing technologies and the fuel or target designs have to be adapted to the selected option. In this paper, we emphasise the third route, which presents the advantage to enable reaching the highest concentration of MA in the core due to its neutron physics characteristics. The fuels will be composed of Pu (even of second generation, which is already irradiated once in a LWR) and MA in high concentration (up to 40%), embedded in inert matrices (see Figure 1). It will be necessary to develop a new type of reactor (linked to an accelerator), and of very innovative fuels. It should be noted that the fuel partitioning processes will have to be adapted to the fuel type selected.

Figure 1. CERMET Am, Pu oxide in Mo matrix (JRC, Karlsruhe)



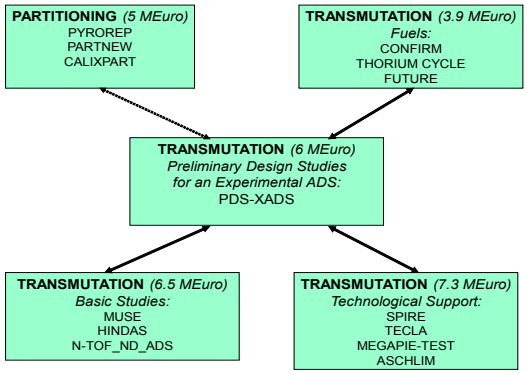
The EURATOM research in support of P&T and ADS development

Since the 1990s, the European Commission has been funding research on nuclear energy through the EURATOM Framework Programmes. In particular, research on advanced systems for the back-end of the fuel cycle (P&T) and for nuclear energy generation (next generation of the nuclear energy systems) was part of the Third to Seventh Framework Programmes. The increased interest for P&T in the EU started in the Fifth Framework Programme (FP5), which was reflected by a strong increase in funding in this area, which then remained constant over the successive EURATOM Framework Programmes.

The objective of the research carried out under these Framework Programmes was to provide a basis for evaluating the practicability, on an industrial scale, of P&T for reducing the amount of long-lived radionuclides to be disposed of. The work on partitioning concerned the experimental investigation of efficient hydro-metallurgical and pyro-chemical processes for the chemical separation of long-lived radionuclides from high-level liquid waste. The work on transmutation was first related to the preliminary design studies of an ADS and acquisition of data, both technology and basic, necessary for its development including the characterisation of fuel and targets for an ADS.

A network called ADOPT (ADvanced Options for Partitioning and Transmutation) was created to co-ordinate the activities of the ADS design project with those of the four clusters of FP5 projects in the area of P&T (see Figure 1). One cluster was on the chemical separation of radionuclides (PARTITION) and there were three on transmutation: (i) Basic studies (BASTRA), (ii) Technological studies (TESTRA) and (iii) Fuel studies (FUETRA).

Figure 2. Structure of the ADOPT thematic network

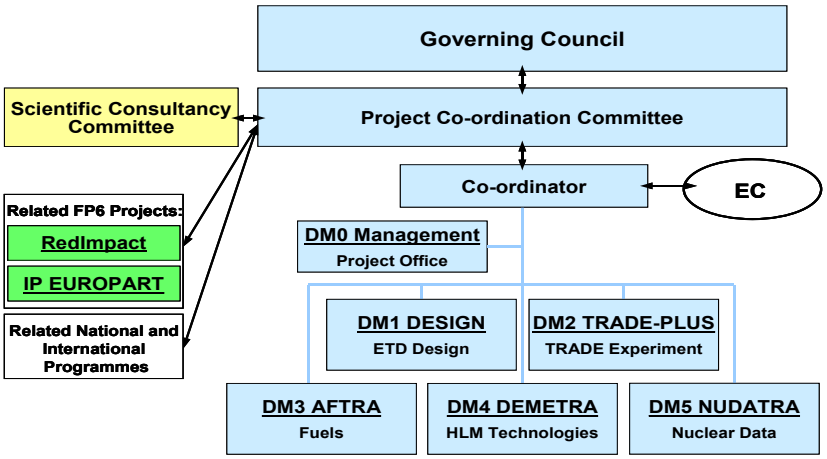


The partners of ADOPT were European research organisations and industries, either co-ordinating the FP5 projects on P&T described below or having a significant role in them. The objectives of ADOPT were: (i) to suggest actions suited to promote consistency between FP5 projects and national programmes, (ii) to review the overall results of the FP5 projects, (iii) to identify gaps in the overall research programme on P&T in Europe, (iv) to provide input to future research proposals and (v) to maintain relations with international organisations and countries outside the EU involved in P&T and ADS development.

Both EC (non-nuclear) and EURATOM Sixth Framework Programmes (FP6) were adopted in 2002 to make the European Research Area (ERA) a reality. Research on advanced systems, both P&T and future nuclear energy systems, were included in the EURATOM FP6. Following a call for proposals, all activities linked to P&T (except for partitioning, which had a separate project called EUROPART) and ADS were gathered in

the very large EUROTRANS Integrated Project which was selected for funding by the Commission (42 M€ total budget with about 50% funding from the EC).

Figure 3. EUROTRANS IP organisation



* TRADE-PLUS has been renamed in ECATS.

Within the EUROTRANS project a consistent design and safety analysis of the two facilities "XT-ADS" and "EFIT" have been made. In that respect, EUROTRANS has been, so far, the only project where a complete assessment of a future MA burner ADS (lead-cooled EFIT) was performed. EFIT, a 400 MWth prototype, was designed to achieve an optimal MA destruction rate of 42 kg per TWh thermal. The fuel firstly selected for this system was the MgO-CERCER. However, an alternative core using the MO-CERMET fuel has also been considered, which presents advantages from the safety behaviour point of view. However, a final selection will only be possible after further experimental results are available. Guidelines for future studies and, in particular, the needs for specific complementary irradiations have been observed in order to complete the validation of a preferred fuel type. On the other hand, the XT-ADS demonstration facility to be developed in the short term has also been defined, based on MOX fuel and lead-bismuth coolant. It has a nominal power of 57 MWth and is mainly intended as an irradiation facility for transmutation fuel validation and as a test bench to demonstrate the technological feasibility of coupling a high power proton accelerator with a subcritical core at an appropriate subcriticality level. All data that have been produced within the five EUROTRANS technological domains in support of design are of paramount importance for the future advancement of ADS systems (including now MYRRHA) and to consolidate their feasibility assessment. In the field of heavy liquid metals, relevant technologies, experimental techniques and range of validation for specific materials have been obtained and documented. Consolidation of the domain of applicability of cladding and component materials need, however, some more experimental work and, also in this field, irradiations have been identified and will play a crucial role.

As for the spallation target, both window and window-less concepts have been assessed. The completion of the MEGAPIE post-irradiation analysis was of high relevance. Physics phenomena in the field of subcriticality measurement and monitoring are now better understood, in particular at zero-power and in power conditions. This allows envisaging multiple controls and monitoring systems that should be tested at low power in the initial start-up procedures of a power system like XT-ADS. The construction and operation of the GUINEVERE zero-power facility at SCK•CEN is a concrete example of a successful development initiated by EUROTRANS.

In FP7, projects are continuing in all areas, but not in the same way. Most of the advanced reactor projects (on fuels, materials, partitioning) became horizontal since the

research was also applicable to critical FRs. As far as reactor design, technologies and safety research are concerned, all projects in the ADS area were oriented towards a support for the Belgian MYRRHA concept. In addition, essential EURATOM efforts on ADS have been placed on the safety assessment studies since 2012. The project named MAXSIMA, for example, will include accidental events studies with a focus on transients potentially leading to pin failures. The project also incorporates validation experiments with MOX fuel for safety computer codes. Fuel-coolant-clad chemical interactions will be studied up to 1700°C.

The role of the Joint Research Centre

Several institutes of the Joint Research Centre of the European Commission are involved in the research on P&T and on future systems. The Institute for Transuranium Elements (ITU) in Karlsruhe is an important player in European efforts on basic actinide research and on the fuel cycle developments. The two most relevant topics are partitioning techniques (aqueous processes and pyro-reprocessing) and fabrication and characterisation of fuels and targets for transmutation. For the latter, a minor actinide laboratory has been in operation since 2003. The fuel irradiation experiments are performed in the High Flux Reactor (HFR) operated by the Dutch company NRG in close co-operation with the Institute for Energy and Transport (IET) in Petten. This Institute is also in charge of structural material studies and reactor safety assessment studies. For the transmutation programme, improved measurements of nuclear data are obtained at various neutron energies in the Institute for Reference Materials and Measurements (IRMM) in Geel.

Conclusion

The main choices and decisions regarding P&T are directly linked to the irradiation scheme. Today, two ways are considered in Europe, namely the critical FR and the ADS. At present, the first cores of such demonstration infrastructure would use U-Pu mixed oxide (MOX) fuel. Design and fabrication experience is large in Europe, since MOX fuel has been used in previous FR programmes in Belgium, France, Germany and in the UK. Its reactor behaviour is quite well known, but should be re-assessed in view of new design parameters, and alternative coolants (lead or lead-bismuth). In parallel, R&D work should be performed both for the MA recovery (partitioning) and for the innovative MA fuel developments. Concerning the ADS development, support will be provided for safety improvements and the creation of a construction consortium.

Acknowledgements

The authors wish to thank all colleagues from the European Commission (Research and Innovation DG and the JRC in particular), and from the organisations of the European member states who are actively involved in programming, financing and managing the research activities described here.

Impact of P&T on nuclear scenarios with Generation-IV and ADSs

S. David[1], S. Massara[2]
[1]CNRS, Orsay, [2]OECD/NEA, France

Nuclear context

Present reactors produce energy through the fission of ^{235}U, which is the only fissile isotope present in nature (0.7% of uranium ore). Many of these reactors use an enriched uranium fuel, up to 4-5%, and are cooled by light water (LWR). The uranium consumption is around 200 tonnes per 1 GWe.y (electrical GW.y). The reserves of uranium ore are estimated today at around 16 millions of tonnes, which represent around 200-400 years of nuclear energy generation at the present consumption rate, taking into account optimisation of LWR technology, as enrichment, plutonium mono-recycling, improvements of thermodynamic yield, etc.

The LWR spent fuel contains essentially non-burned uranium, with around 1% of ^{235}U and 99% of ^{238}U, plutonium (1%), fission products (~4%) and minor actinides as Np, Am and Cm. After a few years of cooling, plutonium dominates the radiotoxicity of the spent fuel, and continues to dominate over geological time-scale. The management of plutonium depends on the chosen strategy; for example, the US and Sweden consider the spent fuel as waste, whereas France has developed a reprocessing strategy, which implies recovering U and Pu from the spent fuel for further use. U can be re-used after a re-enrichment process, and Pu is reprocessed in the MOX fuel (Pu on depleted U as support). These reprocessed fuels allow saving around 20% on natural uranium consumption. The waste coming from reprocessing is handled in glass canisters containing fission products, minor actinides and chemical losses of reprocessed U and Pu. The spent MOX fuel is not reprocessed so far, but it still contains a significant mass of Pu, and is thus considered today as a valuable material for further use (in Gen-IV reactors, for instance).

Breeding and the question of Pu

The real long-term valorisation of Pu requires breeding of it from ^{238}U ($^{238}U + n \rightarrow {}^{239}Pu$). This can be achieved by using fast neutron reactors, like sodium-cooled fast reactors [1]. In a self-breeder reactor, each time a Pu atom undergoes fission, a new Pu nucleus is produced by neutron capture on ^{238}U. Hence, the mass of Pu remains constant and only ^{238}U is consumed, at a rate of around 1t/GWe.y.

The 16 millions of tonnes of natural U available would allow energy generation over several thousands of years. This strategy would be unavoidable in the coming century only if nuclear power grows significantly in the coming decades, to reach at least 3 Gtoe/y, as compared to 0.7 today [2] [3].

Regularly, every 5 years, the fuel must be reprocessed to extract the fission products and replace the consumed U. Self-breeder reactors just need a first load of Pu to be started. Taking into account the irradiation period, but also the necessary cooling and fabrication process to recycle the spent fuel and produce the new one, the order of magnitude of the total mass of Pu needed for 1 GWe breeder reactor is around 20 tonnes. This corresponds – again, as an order of magnitude – to the total mass of Pu produced by

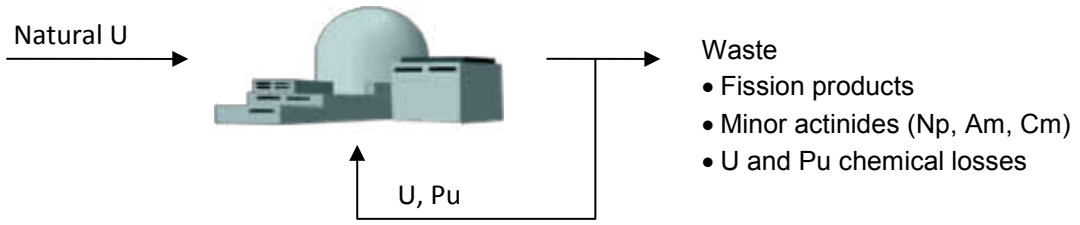
a LWR during its whole life time (~50 years). In a scenario where breeding would be necessary before the end of the century, plutonium must thus be kept and saved, and cannot be considered as waste and buried in an irreversible way. But, in a scenario where nuclear power continues to be used at a low rate, plutonium becomes the main waste to manage [4].

Most of the time (at least in France and Europe), Pu is considered as a valuable material which is reprocessed "somewhere", and transmutation concerns only ultimate waste as fission products and minor actinides. But it should be noted that Pu will remain the main radioactive material to manage (as waste or as a fuel), and it is not necessary to discuss the transmutation of minor actinides without knowing how plutonium is used. In the following, we will consider that plutonium is reprocessed in fast breeder reactors, and we will focus on minor actinide transmutation.

Minor actinide transmutation

Figure 1 presents the reference case for fast breeder cycle. Only the main fertile and fissile materials are reprocessed (respectively U and Pu), and fission products and minor actinides are vitrified together and become the ultimate waste.

Figure 1. Reference cycle for U/Pu breeder reactors without minor actinide transmutation

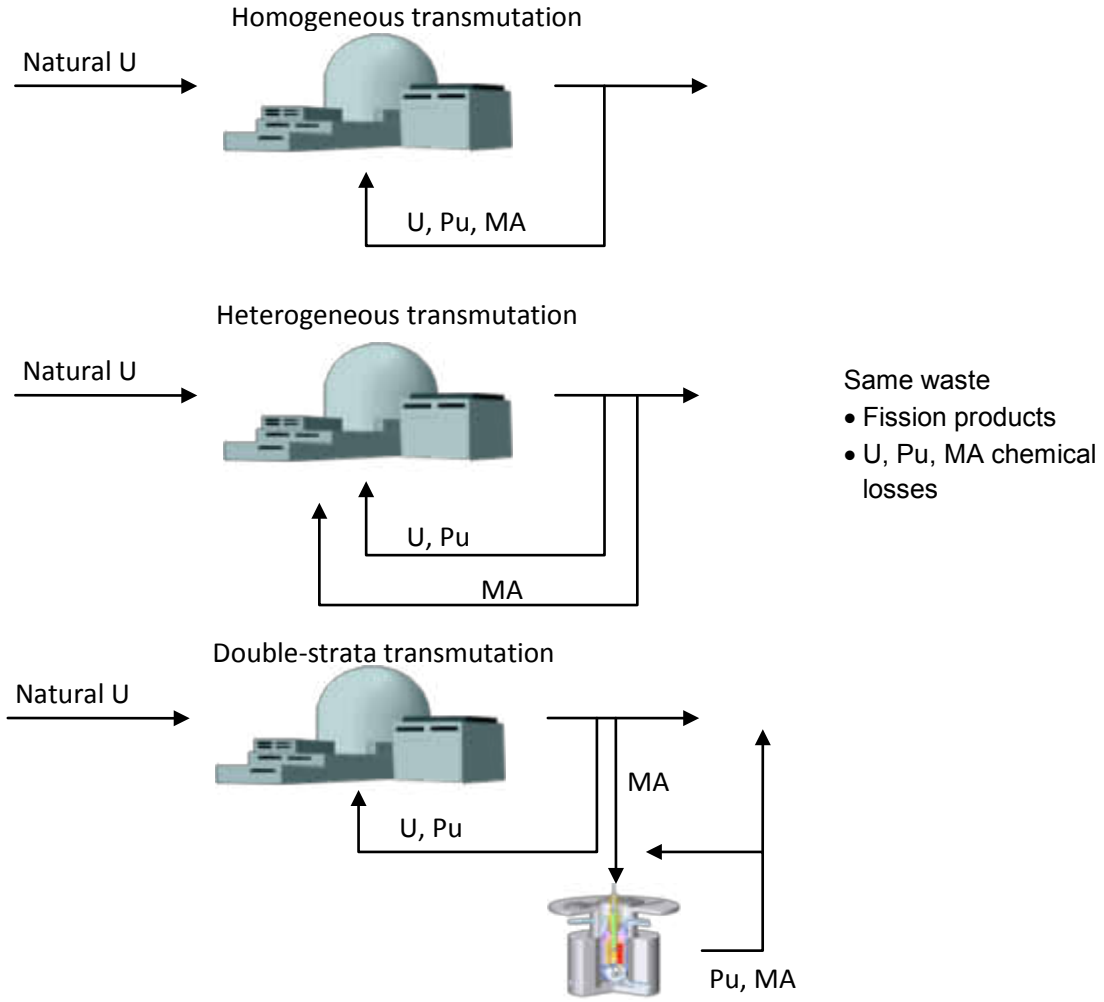


The main minor actinides are the following:

- ^{241}Am, produced by β decay of ^{241}Pu. The ^{241}Am has a period of 433 years and plays a major role in dimensioning the waste geological disposal because of its mid-term residual heat.
- ^{243}Am, produced by neutron capture on ^{242}Pu and immediate β decay of ^{243}Pu. It dominates the mid- and long-term radiotoxicity of waste (period of 7370 years).
- ^{244}Cm, produced by neutron capture on ^{243}Am. ^{244}Cm has a short period (14 years). It plays an important role in short-term radiotoxicity, short-term residual heat and as a spontaneous fission neutron emitter.
- ^{237}Np (2.14 millions of years) produced by (n, 2n) reaction on ^{238}U and immediate β decay of ^{237}U. It does not play an important role in waste except for in specific geological storage where it can migrate and play a role in the long-term residual dose at the surface.

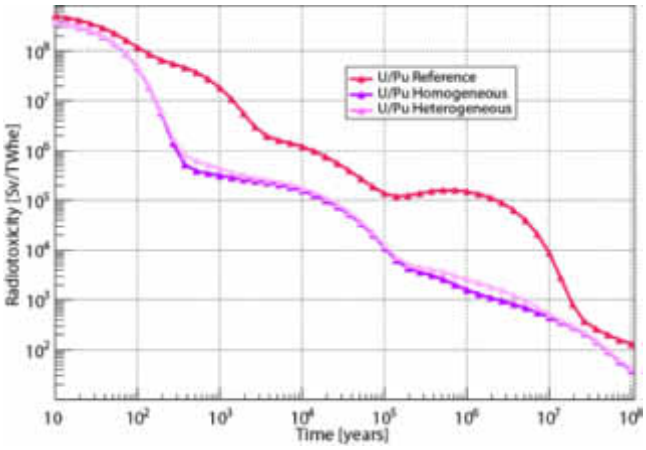
Transmutation consists in separating minor actinides from the waste, and in reprocessing them in a reactor to "burn" (or transmute) them. Different strategies of recycling can be considered. The so-called homogeneous transmutation consists in reprocessing minor actinides together with U and Pu in fast breeder reactors. Heterogeneous transmutation indicates the reprocessing of minor actinides in blankets containing depleted uranium and around 10-20% of minor actinides. Finally, in double-strata strategies minor actinides are transmuted in dedicated reactors, as U and Pu are recycled in the main stratum dedicated to electricity generation (see Figure 2).

Figure 2. Different transmutation strategies for U/Pu cycle



When minor actinides are transmuted, the mid- and long-term radiotoxicity of the ultimate waste are slightly reduced. Figure 3 shows a comparison of waste produced by fast breeder reactors with and without transmutation. Same differences exist on residual heat of waste. Short-term radiotoxicity remains dominated by fission products such as ^{90}Sr and ^{137}Cs (around 30 years of period), but it appears clearly that transmutation of minor actinides helps significantly reduce the mid- and long-term radiotoxicity of vitrified waste, as well as the mid-term (100-1000 years) residual heat which plays a major role in geological disposal dimensioning.

Figure 3. Comparison of waste produced by a fast sodium breeder reactor based on uranium cycle, with and without (U/Pu) transmutation of minor actinides



Homogeneous and heterogeneous transmutation is considered. Actinide chemical losses are 0.1%.

The equilibrium inventory of nuclei to be transmuted needs to be considered. The simplified equation for a transmuted nucleus is:

$$\frac{dN}{dt} = P - (\sigma\phi + \lambda)N$$

where N is the number of nuclei to be transmuted, P the production rate which would be vitrified every year without transmutation, σ the total absorption (capture and fission) cross-section of transmutation of the given nucleus, ϕ the neutron flux of the reactor where the nucleus is transmuted and λ its radioactive period. This equation gives:

$$N(t) = \frac{P}{\sigma\phi + \lambda}(1 - e^{-(\sigma\phi+\lambda)t}$$

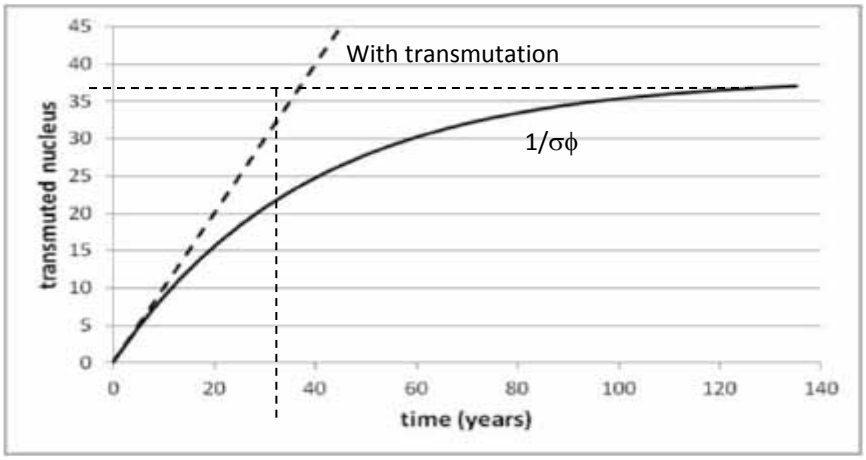
It appears that the transmutation rate $\sigma\phi$ plays two major roles: it fixes the characteristic time $(\frac{1}{\sigma\phi+\lambda})$ the nucleus needs to reach its equilibrium, and also fixes its equilibrium inventory $(\frac{P}{\sigma\phi+\lambda})$. This equilibrium inventory is the "price to pay" to transmute 100% (except chemical losses) of produced minor actinides, and has to be compared with cumulative waste which would be produced without transmutation strategy.

The neutron flux considered should take into account the whole cycle process, including cooling and fuel fabrication. For mid- and long-term radioactive waste, one can neglect the radioactive decay as compared to the transmutation process. Typical values are:

- $\phi_{reactor}$ ~ 2. 10^{15} n/cm^2/s;
- Irradiation time = 5 years;
- Cooling + fabrication = 7 years;
- σ ~0.5 – 1.5 barns (fast spectrum).

A typical characteristic time of evolution is then $\frac{1}{\frac{5}{12}2.10^{15}*1\ 10^{-24}} \sim 40\ y$ and the equilibrium inventory is around 40y*P, where P is a mass produced per year without transmutation. This shows that transmutation needs to be operated over centuries (again, as an order of magnitude) to become really efficient. Indeed, if transmutation lasts for 40 years or less, the total mass of minor actinides to manage will be slightly the same with or without transmutation, with the difference that in the transmutation strategy all the storage issues appear in the end. Figure 4 illustrates these considerations.

Figure 4. Evolution of the inventory of a given nucleus with and without transmutation



The
inventory is normalised to the production per year without transmutation.

Homogeneous transmutation vs double-strata strategies

The double-strata strategy consists in transmuting minor actinides in dedicated reactors, which would represent a small part of the fleet. This immediately implies an increasing complexity of the fuel management in burner reactors allowing a significant reduction of the volume of waste refabricated as a new fuel to feed second stratum reactors. Dedicated fuels would contain a significant amount of minor actinides, which leads to a small value of delayed neutron and bad basic safety parameters such as the Doppler effect or the coolant void effect. This implies that subcritical dedicated reactors show additional safety margin with respect to critical ones and are, practically, the only possible solution for transmuter reactors in the second stratum [6]. Since the chain reaction is not able to keep the power constant, they need an external neutron source to maintain the fission reactions in the core, and the transmutation process. Table 1 indicates the impact on the fuel cycle for both homogeneous and double-strata strategies, as well as material fluxes in the cycle [7].

Transmutation efficiency is mainly governed by the neutron flux, the mean absorption cross-sections and the cycle characteristics such as irradiation, cooling and fabrication times. Scenario studies for double-strata strategy are based on a small power accelerator-driven system (ADS) of 400 MWth, initially designed for ADS industrial demonstration. This leads to severe disadvantages for the double-strata transmutation strategy:

- The small power of the considered ADS leads to a great number of reactors. For example, the transmutation of the total amount of minor actinides produced by a 60 GWe (around 40 reactors) fleet composed of fast breeder reactors would require around 20 reactors of 400 MWth.

- The small size of ADS leads to high neutron leakage, which has to be compensated by adding fissile material (Pu) at every cycle, which degrades the transmutation efficiency since some fissions come from plutonium isotopes (instead of minor actinides).
- Plutonium is not bred during irradiation, and this leads to a decreasing reactivity and limits the irradiation time to 2 or 3 years, as compared to 5 years for FBR.

In these conditions, the results of scenario studies show a larger minor actinide inventory in the whole cycle for the double-strata strategy than for homogeneous recycling and a significant cost increase, due to the high number of ADS needed. These studies clearly show that a main R&D objective in the coming years is to shape the design of a mid-power ADS (around 1500 MWth).

Table 1. Impact on the fuel cycle for both homogeneous and double-strata strategy, as well as material fluxes in the cycle

	MOX (ref)	FBR Pu+AM	FBR Only Pu	ADS
	Reprocessing			
Residual power (W/g/tHM)	1	x 2	x 1	x 70
Neutron source (n/s/tHM)	1	x 2	x 1	x 200
	Fabrication			
Residual power (W/g/tHM)	1	x 2.5	x 0.5	x 90
Neutron source (n/s/tHM)	1	x 150	x 1	x 20000
t/y	820	~400	~400	9

Values are given for the French fleet of 60 GWe and compared to the existing technology for UOX spent fuel reprocessing and MOX fuel fabrication.

Finally, accelerator intensity is directly defined by the subcritical level and the global thermal power of the system. The thermal power produced by an ADS, normalised per the proton beam power gives:

$$\frac{P_{th}}{P_{beamc}} = \frac{N_n \frac{1}{1-k}\frac{k}{\nu}\,\varepsilon_f}{E_p}$$

Where N_n is the number of spallation neutron produced by one impinging proton, k the multiplication factor of the ADS core, ν the number of neutrons produced per fission, ε_f the energy delivered per fission and E_p the kinetic energy of the proton. For typical values (E_p= 1 GeV, N_n= 30, k = 0.95, ν = 3, ε_f=210 MeV), a 1500 MWth ADS thus requires a proton of beam of around 40 MW, which corresponds to a beam intensity of 40 mA@1 GeV. A key point remains radial power distribution which is very heterogeneous in a subcritical core [7].

NEA analysis and comparison of international studies

The OECD Nuclear Energy Agency (NEA) has performed a detailed analysis and a comparison of different international studies [9]. The difficulty of a global comparison and global conclusions is due to the fact that scenario hypotheses can strongly differ from one country to another. In particular, the status of plutonium can differ from waste which has to be burned in standard reactors or dedicated systems to a valuable material multi-recycled in breeder systems. Nevertheless, this work allows clarifying the criteria of comparison and extracting common conclusions on transmutation strategies.

The main comparison criteria concern:

- Radiotoxicity of the ultimate waste. This term is not representative of the real risk associated with geological disposal since it does not take into account the diffusion ability of different elements in the ground. Nevertheless, radiotoxicity represents the source term which is buried, and allows characterising the waste in a more consistent manner than only masses and volumes would allow.
- Decay heat of waste. Decay heat during the first centuries is the main parameter to determine the size of the geological disposal, and thus the number of geological repositories which have to be built and operated for a considered nuclear reactor fleet.
- Peak dose rate. Although the hazard of waste is characterised by radiotoxicity – which is relevant for direct contact with the materials - the effectiveness of the isolation provided by the repository can be evaluated by the estimated peak dose rate to exposed individuals caused by releases from repositories. This depends on the degradation of the containers and transport mechanisms through the ground. A global comparison requires taking into account the multiple geological repositories considered in the specific countries, as argillaceous formations, unsaturated volcanic tuff, crystalline formations, bedded salt and dome salt.
- Costs. Transmutation has an impact on the cost of the electricity produced by the whole fleet, essentially due to the intrinsic difficulties of reprocessing and fabrication plants. On the other hand, transmutation can reduce the cost of ultimate storage by minimising the size of the high-level waste area.

Although the difficulty due to the multiple hypotheses and strategies should be considered, it is nevertheless possible to extract global conclusions concerning the benefits and drawbacks of transmutation:

- Waste radiotoxicity strongly depends on chemical losses of actinides in the reprocessing plants, especially for transmutation strategies.
- Transmutation has a strong impact on the size of the high-level waste disposal. The size of the high-level waste area could be reduced by a factor of 5 to 10 but requires increasing the period of surface intermediate storage before final burying in the geological repository. Taking into account the amount of low and intermediate-level waste, the reduction of the excavated volume of the repository is only reduced by 20-30%.
- Transmutation drastically reduces the radiotoxicity of ultimate waste, by a factor of 10 to 1000, depending on the considered timeframe. This reduction has a strong impact on the safety associated with the geological disposal for different human intrusion scenarios. Nevertheless, these scenarios are often considered non-consistent for safety analysis and are strongly debatable. The role of these intrusion scenarios in the public area constitutes an interesting multi-disciplinary research subject, requiring physical, chemical, geological and sociological analyses.

- The additional cost of transmutation strategies remains low as compared to the global cost of nuclear electricity generation which is dominated by reactor investment costs. Nevertheless, for small ADS (~400 MWth), the number of ADS dedicated to transmutation is high, and the impact on the global cost of electricity is significant (~+20%).

Conclusion

It should be noted that the adoption of a transmutation strategy cannot be realised before a strategy for plutonium is adopted; plutonium can be seen as waste if nuclear power continues at a low level in the world, or as a rare and valuable fuel if nuclear energy increases significantly in the coming decades. In any case, plutonium will represent potential waste, which will dominate long-term radiotoxicity even after centuries of reprocessing. Figure 4 compares the radiotoxicity of the fuel needed to run a 1 GWe fast sodium breeder reactor and the radiotoxicity produced by the same reactor every year. A factor of 1000 means that if nuclear power stops after 1000 years of energy production, the radiotoxicity of the fuel at that moment will be equivalent to the total radiotoxicity of the waste produced during 1000 years. This illustrates the major role played by plutonium for the long-term management of nuclear waste.

Finally, it is to be noted that in those countries (like France) where minor actinides coming from a reprocessed UOX fuel are vitrified in glass canisters, this process is irreversible. Hence, the benefits of the potential deployment of a transmutation strategy will be reduced because of the amount of waste contained in glass canisters (containing minor actinides and fission products) that will have to be disposed of in a geological repository, regardless of the deployment (or not) of a transmutation strategy.

References

[1] GIF SFR System Steering Committee (2007), "System Research Plan".

[2] Bouneau, S. et al. (2010), "Building a World Energy in 2050", *Annales de Physique*, 341–101.

[3] Nifenecker, H. et al. (2003), "Scenarios with an intensive contribution of nuclear energy", Global Energy Issues, Vol. 19, No.1, ISSN 0954-7118.

[4] David, S. (2005), "Future Scenarios for Fission-Based Reactors", *Nuclear Physics* A 751.

[5] Brizi, J. et al. (2009), "Sodium-Cooled Fast Reactors", Void Coefficient and Waste Minimization, Neutronics Studies Using MURE, *Global 2009 Proceedings*.

[6] Nifenecker, H. et al. (2003), "Accelerator-Driven Subcritical Reactors, Series in Fundamental and Applied Nuclear Physics", Series Editors: RR. Betts and W. Greiner.

[7] Garzenne, C. et al. (2006), "La physique de la transmutation", *Revue Générale du Nucléaire*.

[8] Thiollière, N. et al. (2013), "A High power ADS concept. Technology and Components of Accelerator-Driven Systems", *Second International Workshop*, Nantes, France.

[9] NEA (2011), "Potential benefits and Impacts of Advanced Nuclear Fuel Cycles with Actinide Partitioning and Transmutation".

Fuel for ADS: State-of-the-art, requirements, current and future programmes

Fabrizio Gabrielli
Karlsruhe Institute of Technology, Germany

Abstract

Fuels are the cornerstone of R&D of accelerator-driven systems for transmuting minor actinides (MAs). Compared with the fuels for critical reactors, fuels for ADS are generally U-free to improve the transmutation performance and contain high volumetric concentrations (~50%) of MA and Pu compounds. Their specific fabrication, reprocessing, design and safety issues are being currently investigated. This paper provides an overview of the current state-of-the-art of the assessment of these innovative fuels. Emphasis has been placed on the main outcomes of the work performed within the Sixth FP EU EUROTRANS Programme, which provided a decisive step forward in improving knowledge on fabrication, properties, and behaviour under irradiation of these challenging fuels. In EUROTRANS, for the ADS application, the focus was on Ceramic-Ceramic (Pu,MA)O_2+MgO and Ceramic-Metallic (Pu,MA)O_2+^{92}Mo composite fuels, which were recommended for the European Facility for Industrial Transmutation (EFIT). The fuels consist of particles of (Pu,MA)O_2 phases dispersed in a magnesia or molybdenum matrix. Solid nitride (Pu,MA,Zr)O_2 fuels have also been considered as a back-up solution. This paper presents the main experimental results from out-of-pile and in-pile experiments of the Ceramic-Ceramic and Ceramic-Metallic composite fuels as well as related safety assessments. Further, the on-going R&D activities on fuels loaded with large amount of MA will be presented.

Introduction

R&D of fuels for accelerator-driven systems (ADS) for minor actinides (MA) burning has been performed worldwide for many years. In Europe, emphasis has been placed on the oxide route in line with the wide European experience [1]. At JAEA in Japan, focus has been on solid solution nitride fuels with ZrN matrix [2] and in the US metallic fuels are under investigation [3].

Fuel is one of the most challenging components of ADS. Fuels for ADS are generally U-free, to improve transmutation performance, and contain a large volumetric concentration of MAs (45 to 70%) and Pu (30 to 55%) compounds. Therefore, these highly innovative fuels require specific design and safety assessment compared with those employed in critical cores; the high concentration of transuranics (TRU) e.g. results in high gamma and neutron emissions at fabrication and handling stages. To examine their behaviour under irradiation would be necessary because of:

- the significant He production and;
- the deterioration of kinetics and safety parameters (i.e. low Doppler effect and effective delayed neutron fraction ,β_{eff}).

Finally, it is necessary to study the behaviour of a system as a combination of a fuel loaded with large amounts of TRU, an external source-driven system, and a heavy liquid metal coolant. Therefore, the "optimal" fuel results from the evaluation of its thermo-mechanical and chemical properties as well as the neutronics and technological constraints related to ADS.

In Europe, the Sixth EU FP EUROpean Research Programme for the TRANSmutation (EUROTRANS) of High-Level Waste in an Accelerator-driven System [4] represented an important step forward to improve our knowledge of fuels for ADS. The objective of the programme was to improve the design, the development, and the qualification in representative conditions of U-free fuel for the 400 MW_{th} European Facility for Industrial Transmutation (EFIT) [5]. The Domain DM3 (AFTRA) was responsible for the fuel assessment and development for EFIT and the Domain DM1 (DESIGN) aimed to develop the conceptual reference design of the whole plant, including core and target. The outcomes of AFTRA address recommendations about fuel design and performance of the most promising candidate for EFIT, taking into account a number of criteria, ranging from fabrication, reprocessing, via economics to safety [6-8]. The primary candidates are CERamic-CERamic (CERCER) and CERamic-Metallic (CERMET) inert matrix fuels (IMF) consisting of $(Pu,MA)O_{2-x}$ particle dispersed in MgO and Mo inert matrices, respectively, in line with the Fifth EU FP FUTURE programme [9]. The CERMET fuel is ^{92}Mo-enriched in order to reduce the neutronic penalties due to the high ^{95}Mo capture cross-section and prevent the long-lived ^{99}Tc production by $^{98}Mo(n,\gamma)^{99}Tc$ reaction [6, 7]. Nitride- and zirconia- based fuels have been also considered as back-up solutions.

Before the start of the EUROTRANS project, the experience of the fabrication and irradiation of these innovative fuels was limited and little was known about thermo-physical properties. Therefore, a large fuel data base was created by performing in-pile and out-of-pile experiments on CERCER and CERMET fuels. Further, analyses of the performance of TRU-oxide fuel elements and safety analyses of CERCER and CERMET EFIT cores were carried out. Investigations relating to the fabrication of such fuels were conducted at the Institute for Transuranium Elements (ITU) and at CEA-ATALANTE [10-12]. In particular, the fabrication of Am-bearing fuels was demonstrated at lab-scale [13]. In addition, solid solution nitride fuels with ZrN matrix were fabricated at JAEA [2].

This paper provides an overview of the state-of-the-art of R&D on fuels for ADS in Europe. The major outcomes of the AFTRA programme are described concerning irradiation tests, out-of-pile experiments, and fuel safety assessments [14, 15]. The current European programmes on R&D of fuel for ADS will be described and requirements for further investigations will be addressed.

Irradiation tests

Prior to the start of the EUROTRANS project, the irradiation behaviour of TRU-fuels was quite limited because very few irradiation tests of samples containing large amounts of MA were performed in Europe. Nevertheless, Post-Irradiation Examination (PIE) on irradiated targets containing a few per cent of Am showed the significant role played by irradiation conditions, temperature, He production and accumulation, and the material swelling due to structure modifications [16]. Irradiation programmes have been performed to further investigate the irradiation effects on IMF in EFIT representative conditions in the FUTURIX-FTA test (CEA, US-DOE, JRC-ITU) [17] at the Phénix reactor, the He behaviour versus temperature and microstructure in IMF in the HELIOS test [18] at the High Flux Reactor (HFR, Petten) and the He build-up and release mechanisms versus temperature in ^{10}B-doped inert matrices in the BODEX test [19] at HFR. Further, PIE of nitride fuels ($Pu_{0.3}Zr_{0.7}N$) irradiated at HFR within the Fifth EU FP CONFIRM project [20] has been performed.

Table 1 presents the composition and the employed fabrication route of the samples for the FUTURIX-FTA and HELIOS tests. The Am content ranges from 0.2 g/cm^3 to

1.9 g/cm^3 in FUTURIX-FTA pellets and it is about 0.7 g/cm^3 in the HELIOS samples, namely from ADS type fuels to transmutation targets to benefit from the experience gained in the EFFTRA-T4 and EFFTRA-T4bis tests [21, 22]. The samples have been fabricated at ITU and CEA at laboratory scale by using two processes [23]: an oxalic co-precipitation route [11] for CEA, and a combination of external gelation and infiltration methods [12] for ITU. The composite materials have been prepared with conventional powder metallurgy methods [24] and are similar for all the samples, except for the HELIOS CERCER fuel, whose porosity has been tailored to remain open to allow He to escape [1].

Table 1. Composition and fabrication process of the FUTURIX-FTA and HELIOS pellets [1] [7]

FUTURIX-FTA		HELIOS	
Composition	Fabrication	Composition	Fabrication
$Pu_{0.8}Am_{0.2}O_{2-x}$+86 vol% Mo	ITU route	$Am_2Zr_2O_7$+80 vol% MgO	CEA route
$Pu_{0.23}Am_{0.25}Zr_{0.53}O_{2-x}$+60 vol% Mo	ITU route	$Zr_{0.8}Y_{0.13}Am_{0.07}O_{2-x}$	ITU route
$Pu_{0.5}Am_{0.5}O_{1.88}$+80 vol% MgO	CEA route	$Pu_{0.04}Am_{0.07}Zr_{0.76}Y_{0.13}O_{2-x}$	ITU route
$Pu_{0.2}Am_{0.8}O_{1.73}$+75 vol% MgO	CEA route	$Am_{0.22}Zr_{0.67}Y_{0.11}O_{2-x}$+71 vol% Mo	ITU route
		$Pu_{0.8}Am_{0.2}O_{2-x}$+84 vol% Mo	ITU route

The FUTURIX-FTA tests were completed in March 2009 after 235 efpd of irradiation and cumulated neutron fluence for CERMET and CERCER samples of 1.4x10^{23} n/cm^2 and 1.0x10^{23} n/cm^2, respectively [1] [8]. Several non-destructive examinations have been performed at CEI-Phénix Facility [8] and PIE analyses have been performed within the Seventh EU FP FAbrication, Irradiation and Reprocessing of FUELS and targets for transmutation (FAIRFUELS) (CEA, JRC, NRG, Chalmers, KTH, SCK•CEN, CIEMAT, LGi, Imperial College, SERCO) Programme [25] at ITU and LECA-STAR Facility (CEA, Cadarache) [28]. The HELIOS tests were completed in March 2010 after 241 efpd of irradiation. Non-destructive examinations have been performed at NRG [26] and PIE is currently under investigation within the FAIRFUELS project [27] at ITU and NRG.

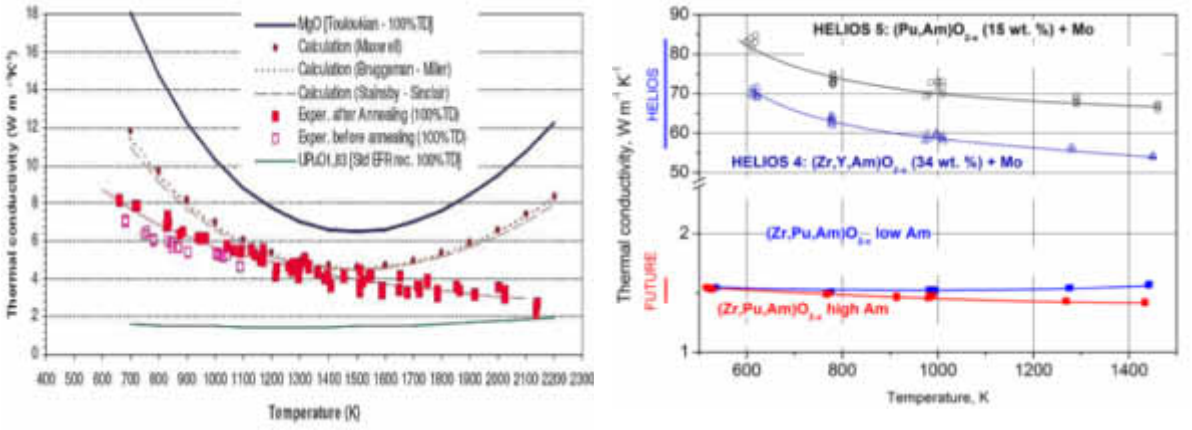
The He-induced swelling behaviour of ^{10}B-doped (1 wt%) MgO and Mo inert matrices was investigated in the BODEX experiment [19] at HFR at 800°C and 1100°C, ^{10}B being used as Am surrogate. A detailed description of the samples and of the investigations performed is given in [7, 19]. ^{10}B-MgO sample at 1100°C is significantly embrittlened and shows 2-3% swelling, about 30% of He release, and no cracks. ^{10}B-Mo sample at 800°C and 1100°C shows cracks, swelling (1.5% and 6%, respectively) and low He-release (6% at 1100°C). Finally, the un-doped Mo sample shows neither cracks nor swelling (<1%).

Out-of-pile experiments

The work of AFTRA allowed creating a large database of thermo-physical properties of IMF and nitride fuels [1] [2] [29-31] as well as of the FUTURIX-FTA and HELIOS samples [30] [31]. Chemical compatibility tests of Pb coolant, T91 clad, and inclusions PuO_2,AmO_2,$(Pu,Am)O_2$ as powders with several fuels and inert matrices MgO and Mo, have been performed [32] [33].

Figure 1 shows the thermal conductivity results of the $Pu_{0.5}Am_{0.5}O_{1.83}$+70 vol% MgO CERCER fuel and of the HELIOS samples. CERCER fuel shows a significant drop at T>1500 K which is not predicted by calculations based on phase mixing models. The thermal conductivity of CERMET fuels is larger and it is about 30 times higher than that of $(Zr,Pu,Am)O_{2-x}$ fuels, as observed for the FUTURIX-FTA CERMET samples.

Figure 1. Thermal conductivity of CERCER [1, 29] and of the HELIOS CERMET fuels [31]



Vapourisation and melting temperature of CERMET and CERCER fuels have been measured at CEA and ITU under vacuum and neutral atmosphere, for closed and open systems [1] [7]. Results are shown in Figure 2. Molybdenum is still detected at T>2300 K (not shown in Figure 2) and shows a higher stability than MgO, whose vapourisation begins at 1750-1800 K and significantly increases at 1800-1900 K. Concerning TRU species, Am is detected as Am and AmO in CERMET (Am signal being larger than AmO) while gaseous Am species are already detected at 1800 K in CERCER, the AmO_2 being the main species up to 2200 K. Detailed analyses can be found in [1] [7].

Concerning chemical compatibility tests, Figure 3 shows the results of the Electron Dispersive X-ray spectroscopy (EDX) analysis at 550°C and 950°C of the T91/MgO contact area [1, 7]. Results show that MgO is compatible with T91 up to 550°C while a slight diffusion of Mg appears at 950°C [1] [7]. No interaction has been observed between T91 and FUTURIX-FTA CERMETs and Mo samples [1] [7]. Detailed analyses of compatibility tests can be found in [1] [7] [32] [33].

Figure 2. Vapourisation rate vs. T of the components of the FUTURIX-FTA ($Pu_{0.8}Am_{0.2}O_{2-x}$+ 86 vol% Mo) CERMET (left) ($Pu_{0.5}Am_{0.5}O_{2-x}$+ 80 vol% MgO) CERCER fuels (right) [1] [7]

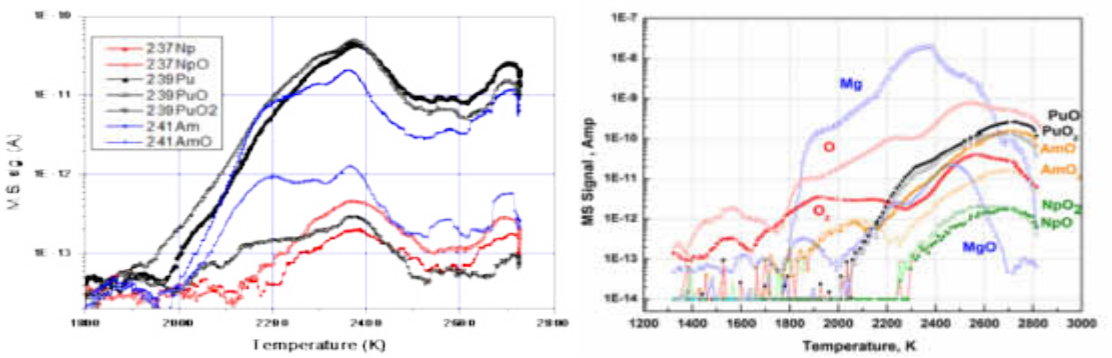


Figure 3. EDX analyses of T91 interface in contact with MgO at 550 °C and 950 °C [1] [7] [33]

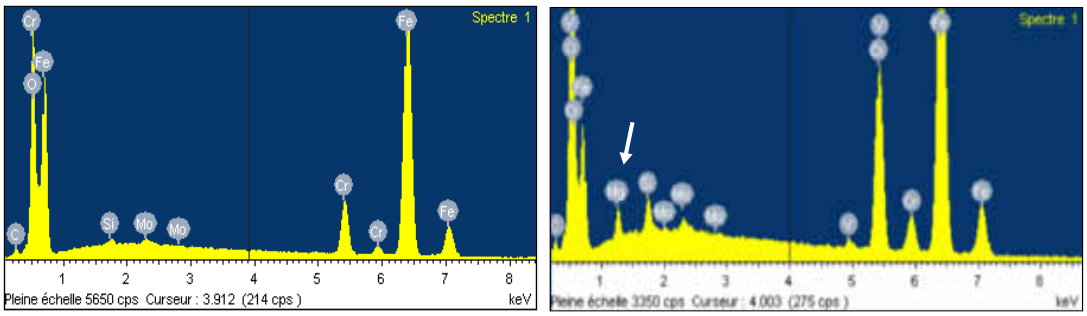
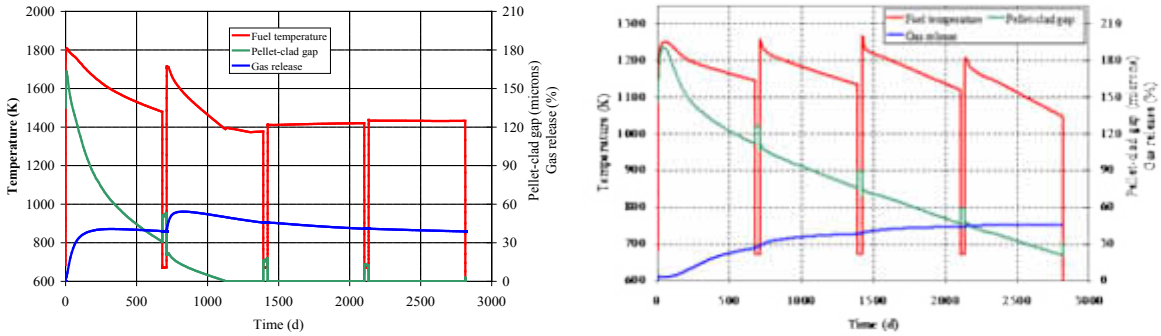


Figure 4. TRAFIC results for fuel temperature and pellet-clad gap size in the CERCER (left) and CERMET (right) fuels [7]



Experimental data have been used to improve the models employed in the simulation tools. As an example, the thermo-mechanical performance of CERCER and CERMET fuels under EFIT conditions (peak linear power ~200 W/cm) have been simulated by means of the MACROS (SCK•CEN) and TRAFIC (SERCO) codes. The maximum CERCER fuel temperature is 1800 K at BOL (300 K below Category 4 [14, 34]), and decreases as the gap closes. Concerning CERMET, the fuel temperature remains more than 1100 K below the failure limits and the gap remains open during the irradiation. Therefore, both CERCER and CERMET fuels fulfill the EFIT design criteria. Nevertheless, results are affected by large uncertainties due to the lack of data on properties of fuel, matrix, and cladding materials under representative conditions. Keeping this in mind, PIE of FUTURIX-FTA and HELIOS samples will provide important information.

Fuel safety assessment in the EFIT CERCER and CERMET cores

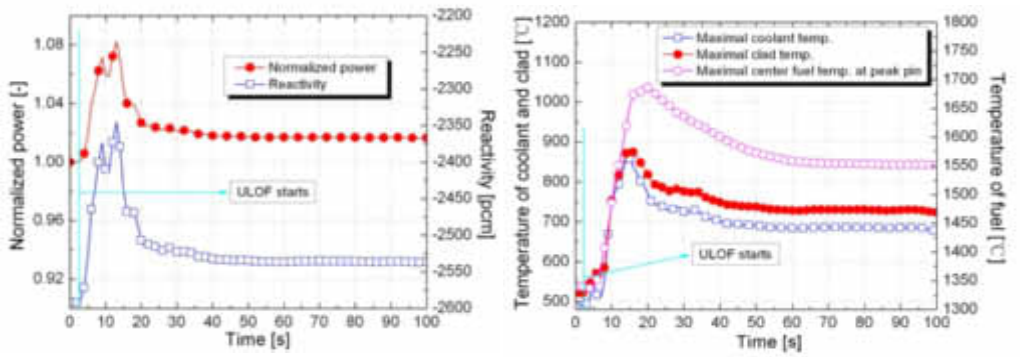
A large amount of work has been performed within EUROTRANS to analyse the safety behaviour of the 400 MW_{th} EFIT MgO-CERCER and Mo-CERMET three-zone lead-cooled cores [14, 15, 34]. The detailed description of the systems is given in [5, 34]. The main safety parameters have been evaluated for both EFIT cores by means of deterministic and stochastic codes [35], namely the Doppler constant (K_D) and the coolant void worth. K_D is equal to -31 pcm (CERCER) and -68 pcm (CERMET). The coolant void worth is ~6600 pcm (CERCER) and ~7300 pcm (CERMET), if the entire EFIT cores are voided. The clad worth potentials are ~2000 pcm. The total reactivity potentials are larger than the assumed subcriticality margin of 3000 pcm. The general impact of U-free fuels on global core dynamics and safety (especially in DEC) is therefore characterised by the lack of a prompt fuel feedback effect and significant positive (delayed) reactivity feedback potentials. As described above, the coolant void worth is high, which is, however, acceptable because of the very low boiling probability of Pb. Nevertheless, even in cases of no-coolant boiling,

local voiding may be triggered by clad failure, e.g. He release, or steam ingress in cases of steam generator tube rupture (SGTR) [14].

The safety objectives indicated in AFTRA are that all reasonably practicable measures are taken to prevent accidents, and to mitigate their consequences [34]. This is achieved based on the defense-in-depth concept. The demonstration of the safety adequacy of design is structured along three different accidental categories; the design basis conditions (DBC–structured in four categories), design extension conditions (DEC–limiting events, complex sequences and severe accidents), and residual risk situations [36]. For innovative reactors such as the ADS, cliff-edge effects should be also identified and excluded. Due to the lack of detailed experimental data on transient fuel and clad conditions and the phenomenological uncertainties in the high-temperature range, both CERCER and CERMET fuels and clad limiting temperature maps are defined for the different defense in-depth categories [14, 34]. To evaluate the results of calculations of severe transients, for CERCER, the Category IV fuel temperature is 1677°C and DEC temperature is 1857°C [14, 34]. For the CERMET, the Category IV temperature is 2127°C and DEC is 2177°C [1, 34]. Besides the fuel limits, clad limits of EFIT are of major interest. Clad creep induced fuel pin failures for unirradiated T91 must be expected at ~1000°C at 5 MPa. The choice of GESA (FeCrAlY coating) treated clad [37] for the EFIT has high relevance for normal operation (no deterioration of clad/coolant heat transfer by oxide layers) and safety, ranging from beam trip (clad surface layer stability) to assumed unprotected transients like e.g. the blockage accident (local corrosion product build-up). Safety analyses have been performed by means of SIMMER-III (KIT), SAS4A (KTH), and SITHER (SCK•CEN). Here, the investigations with the SIMMER-III code [38] are discussed. Several transients have been investigated such as Protected and Unprotected LOss of Flow (P/ULOF), Beam Trip/Interruption (BT/I), Protected and Unprotected Transient Over Power (P/UTOP), Unprotected Transient Over Current (UTOC), Protected and Unprotected Blockage Accident (P/UBA), and STGR accident [14-15, 34].

The SIMMER-III results of the ULOF accident for MgO-CERCER EFIT core are shown in Figure 5. The ULOF is one transient of interest to show the safety potential of the design. The liquid lead has good natural convection properties. After a short undershooting of the coolant mass flow rate in the core and a 30% reversed flow after the pump stop, the coolant mass flow rate in the core is finally stabilised at 30% due to the natural convection. With the 30% remaining coolant heat removing capacity, the fuel and clad peak temperatures are finally at 1500°C and 740°C (Figure 5). For the CERMET, core fuel and clad are leveling out at 900°C (more than 1000°C below the failure limits) and 740°C. The SIMMER-III analyses showed that both CERCER and CERMET fuels for EFIT had good safety performance. The results demonstrate the general high safety potential of EFIT, as neither core violates the safety limits in the most severe conditions. Also, analyses revealed that the most limiting conditions in design and safety are mainly related to the T91 clad and not to the fuels [34]. In order to reduce the uncertainties associated with these analyses and to extend the models, further experimental and theoretical investigations are needed on materials behaviour under irradiation, transients, and high temperature conditions [34].

Figure 5. ULOF results for the MgO-CERCER EFIT core: power, reactivity and temperatures of fuel, clad, and coolant [14]



Current research programmes in Europe

Different projects aiming to improve knowledge of TRU fuels are currently on-going in Europe. The European network EFFTRA (Experimental Feasibility of Targets for Transmutation) (JRC-IE, JRC-ITU, CEA, EdF, KIT, NRG) has been very active for many years. Reference experiments have been performed within EFFTRA like the above mentioned EFFTRA-T4 [21] and EFFTRA-T4bis [22] on Am transmutation. EFFTRA allows a continuous exchange of experimental information among the different partners. In the frame of Seventh EU FP the above mentioned FAIRFUELS [25], the Actinide reCycling by SEParation and Transmutation (ACSEPT) [39], and the Advanced fuelS for Generation-IV reActors: Reprocessing and Dissolution (ASGARD) [40] programmes have been launched. The FAIRFUELS project aims to gather experience on fuels containing MAs from both a theoretical and an experimental point of view. During the project, the PIE analyses of FUTURIX-FTA and HELIOS samples have been performed. The programme, focused on the behaviour of He release, has several objectives; the fabrication of dedicated fuels containing MAs, performing irradiation tests in the HFR, and modelling development and validation against experiments. The ACSEPT collaborative project (34 partners) aims to develop chemical separation processes compatible with fuel fabrication techniques, in view of their future demonstration at the pilot level [39]. One of the final goals is to study the reprocessing aspects of the irradiated actinide targets. The ASGARD project (16 institutions from 9 European countries) examines oxide, nitride, and carbide fuels [40]. Concerning oxide fuels, the focus is on MgO- and Mo-IMF, whose dissolution and separation issues have not been coherently investigated by that time. In fact, it is important to assess the fuel complete cycle, taking into account the behaviour of such fuels in the dissolution and separation processes and verify their compatibility with the future vitrification (impact on the stability of the waste and amount of generated waste). The use of Mo as inert matrix poses additional challenges concerning its redox chemistry, the need of avoiding precipitation or co-precipitation, and the necessity of Mo recover, possibly isotopically to improve the fuel behaviour. Basic studies will be performed on the dissolution of MAs containing high Am and Pu content oxides. A final objective is to address the conversion of the reprocessed solution to suitable precursors for fuel fabrication. Concerning nitride fuels, the project aims to acquire information on the impact of carbon and oxygen impurities on the dissolution rate in nitric acid and improve the performance of the ^{15}N enrichment, fabrication, and recycling routes. Finally, concerning the carbide fuels, the problems of fuel swelling and the issues concerning the reprocessing will be addressed.

Conclusion

Activities are on-going in Europe, Japan, and the United States to improve our knowledge of fuels for ADS. In Europe, the work of the Sixth FP EU EUROTRANS project gave a significant impulse in this direction. The DM3 AFTRA was responsible for the fuel assessment and development for the 400 MWth EFIT machine. The objective of AFTRA work was to rank U-free fuels for EFIT. Emphasis has been placed on ^{enr}Mo-CERMET and MgO-CERCER fuels in line with the previous FUTURE programme. Nitride-based fuels were also investigated as a back-up solution and PIE analyses of the samples from CONFIRM programme were performed. Prior to EUROTRANS, sparse experimental data of such fuels and targets were available and their behaviour under irradiation was quite unknown. Therefore, a large experimental campaign was launched. The fabrication of Am-bearing fuels with Am content up to 36 wt% (1.9 g/cm3) and TRU-oxide fraction up to 40 vol% was demonstrated at lab-scale. Mo-CERMET and MgO-CERCER samples have been fabricated at CEA and ITU with Am content ranging from targets to ADS type fuels. Irradiation tests have been performed and concluded in order to analyse the irradiation effects in EFIT representative conditions (FUTURIX-FTA test, Phénix) and the He behaviour and microstructure (HELIOS test, HFR). The BODEX test has been performed at HFR to study the He build-up and release mechanisms of ^{10}B-doped MgO and Mo inert matrices. The PIE analyses are currently on-going within the Seventh FP EU FAIRFUELS programme. Out-of-pile measurements have been performed on FUTURIX-FTA and HELIOS samples and large amounts of data have been collected on their thermal properties. Further, chemical compatibility tests have been performed between fuel components, between T91 clad and IMF and Mo and MgO inert matrices, and between Pb and CERMET, Mo, and MgO. Simulations have been performed to assess the TRU-oxide fuel element for EFIT and to evaluate the safety behaviour of CERCER and CERMET EFIT cores. A conservative approach has been employed on the fuel limits and the defence-in-depth concept has been used. Safety analyses demonstrated that sufficient margins for both fuels exist (much larger for CERMET) and that the T91 clad failure limits pose the main restriction on safety. Finally, the interest in ^{enr}Mo-CERMET and MgO-CERCER fuels is reinforced. Nevertheless, only PIE results can define the most suitable concept between CERCER and CERMET.

Further investigations are needed on ADS fuels. Reprocessing of the fuels favoured for the EFIT has been confirmed within the Fifth FP EU FUTURE and PYROREP programmes [41]. Still to be tackled, however, (although several possible solutions are existing) is the question how to keep the MgO ceramic or light Mo metal out of fission products stream and re-use them at the fuel fabrication stage in order to avoid large amounts of high-level waste. Keeping this in mind, the investigations performed within the ASGARD project on new process schemes can make progress on this issue. A limited experimental and theoretical knowledge on fuel behaviour under irradiation still exists and the evaluations of the impact on operational conditions, transients, and accidents are affected by large uncertainties, i.e. the microphysics of the fuel should be further investigated and modelled into the codes. In order to accomplish these requirements, facilities for performing transient tests are needed as well as advanced modelling and simulation tools. Finally, the analysis of the impact and of the assessment of the new experimental findings on design, safety, and fuel cycle is pending. In this respect, the outcomes of the current activities in Europe (EFFTRA, FAIRFUELS, ACSEPT, and ASGARD programmes) on fuel R&D for ADS may be very useful.

Acknowledgements

The author wishes to thank F. Delage (CEA), J. Somers (JRC-ITU), W. Maschek (KIT), K. Pasamehmetoglu (INL), K. McCarthy (INL), R. Kennedy (INL), K. Minato (JAEA), and M. Pouchon (PSI) for their support.

References

[1] Delage, F. et. al. (2009), "Advanced Fuel Developments for an Industrial Accelerator Driven System Prototype", *Proc. of Global 2009*, Paris, France, 6-11 September 2009.

[2] Takano, M. et al. (2009), "Thermal expansion of TRU nitride solid solutions as fuel materials for transmutation of minor actinides", *J. Nucl. Mat.*, 389, 89.

[3] Kennedy, J. R. (2012), "The Development of Metallic Fuels for Actinide Transmutation", *Proc. of the 12th IEMPT,* OECD/NEA, Prague, Czech Republic, 24-27 September 2012.

[4] 6th FP EU – IP EUROTRANS, FI6W-CT-2004-516520 (2006).

[5] Artioli, C. et al. (2008), "Minor actinide transmutation in ADS": The EFIT core design, *Proc. of PHYSOR 2008*, Interlaken, Switzerland, 14-19 September 2008.

[6] Delage, F. et al. (2010), "Minor Actinide Transmutation in an Accelerator Driven System Prototype": Results from Fuel Developments within the European Program EUROTRANS, *Proc. of the 11th IEMPT*, San Francisco, CA, USA, 1-4 November 2010.

[7] Delage, F. et al. (2011), "ADS Fuel Developments in Europe": Results from the EUROTRANS Integrated Project, *Energy Procedia*, 7, 303–313.

[8] Delage, F. et al. (2010), "Minor Actinides transmutation in the EFIT: Results from fuel development in domain AFTRA", *Proc. of TCADS*, Karlsruhe, Germany, 15-17 March 2010.

[9] Pillon, S. et al. (2003), "The european FUTURE programme", *Proc. of Global 2003*, ANS/ENS meeting, 16-20 November 2003, New Orleans, LA, USA.

[10] Fernandez, A. et al. (2007), "HELIOS irradiation experiment in HFR", Fabrication of fuel pellets, JRC-ITU-TPW-2007/25, 2007.

[11] Jankoviak, A. et al. (2008), "Preparation and Characterization of $Pu_{0.5}Am_{0.5}O_{2-x}$-MgO Ceramic/Ceramic Composites", *Nucl. Sci. Eng.*, 160, 378-384.

[12] Fernandez, A. (2008), "Advanced Fuel Fabrication Processes for Transmutation", *Proc. of the 10th IEMPT*, Mito, Japan, 6-10 October 6-10 2008, OECD/NEA, (2010).

[13] McGinley, J., Somers, J. (2011), "MA Fuel Fabrication": Recent Advances at ITU, EFTTRA Mtg., Marcoule, France, 11-12 April 2011.

[14] Maschek, W. et al. (2010), "Safety and design concepts of the 400 MW_{th}-class EFIT accelerator driven transmuter and considerations for further developments", *En. Convers. Manage.*, 51, 1764.

[15] P. Liu, et al. (2010), "Transient Analyses of the 400 MWth-Class EFIT Accelerator Driven Transmuter with the Multi-Physics Code: SIMMER-III", *Nucl. Eng. Des.*, 240, 3481.

[16] Béjaoui, S. et al. (2009), "ECRIX-H Experiment": First Post-Irradiation Examinations and Simulations, *Proc. of Global 2009*, Paris, France, 6-11 September 2009.

[17] Jaeky, et al. (2004), "The FUTURIX-FTA Experiment in Phénix", *Proc. of the 8th IEMPT*, Las Vegas, NV, USA, 9-11 November 2004.

[18] D'Agata, E. (2009), "HELIOS: The new design of the irradiation of U-free fuels for Americium transmutation", *Proc. of Global 2009*, Paris, France, 6-11 September 2009.

[19] Den Dexter, M. J. et al. (2006), "Investigation of He-induced swelling behaviour of inert matrices by ^{10}B doping: the BODEX Irradiation Experiment", *Proc. of the 9th IEMPT*, Nîmes, France, 25-29 September 2006.

[20] Wallenius, J. et al. (2001), "Collaboration on Nitride fuel Irradiation and Modelling", *Proc. of AccApp'01*, Reno, NV, USA, 11-15 November 2001.

[21] Konings, R.J.M, et al. (2000), "The EFFTRA-T4 experiment on americium transmutation", *J. Nucl. Mat*, 282, 159-170.

[22] Klaassen, F. et al. (2006), "Post Irradiation Examinations of an Americium Containing Transmutation Target (EFFTRA-T4bis) at High Americium Burn-up", *Workshop IMF-11,* Park City, UT, US, 10-12 October 2006.

[23] Maschek, W. et al. (2008), "Accelerator driven systems for transmutation: Fuel development, design and safety", *Prog. Nuc. Energy*, 50, 333.

[24] Fernandez, A., Konings, R.J.M., Somers, J. (2003), "Design and fabrication of specific ceramic-metallic fuels and targets", *J. Nuc. Mat.*, 319, 44.

[25] http://www.fp7-fairfuels.eu/.

[26] Knol, S. (2011), "HELIOS Non destructive Post Irradiation Examinations", *FAIRFUELS Workshop*, Stockholm, Sweden, 9-10 February 2011.

[27] Knol, S., HELIOS PIE status, ibid.

[28] Delage, F. (2012), "FUTURIX-FTA Progress Status", EFTTRA Mtg., Cadarache, France, 5-6 December 2012.

[29] Ottaviani, J-P., Staicu, D. (2010), "Major outcomes of WP3.4 activities", *2nd Joint Workshop EUROTRANS-JAEA on ADS activities*, Karlsruhe, Germany, 18-19 March 2010.

[30] Fernandez, A. et al. ,DM 3: WP 3.3 Irradiation Tests and Fuel Qualification, ibid.

[31] Staicu, D. et al. (2008), "Thermal properties of cermet fuels for P&T concepts", *Proc. ANS 2008,* Anaheim, CA, USA, 9-12 June 2008.

[32] Belin, R., et al. (2008), "Chemical compatibility tests between Plutonium and Americium oxide fuels and inert matrices for transmutation", *Proc. of ARWIF,* Fukui, Japan, 18-19 February 2008.

[33] Gavilan, E. et al. (2009), "Structural investigations on americium and plutonium mixed oxides/inert matrices systems", *Proc. of Global 2009*, Paris, France, 6-11 September 2009.

[34] Maschek, W. et al. (2008), "Design, Safety and fuel developments for the EFIT accelerator driven system with CERCER and CERMET cores", *Proc. of IEMPT*, Mito, Japan, 6-10 October 2008.

[35] Rineski, A., et al. (2010), "WP3.1: Design, Modelling and Selection of Fuel for MA Transmutation in EFIT (normal operation)", *2nd Joint Workshop EUROTRANS-JAEA on ADS activities*, Karlsruhe, Germany, 18-19 March 2010.

[36] IAEA (1999), Safety series No. 75 – INSAG 3.

[37] Müller, G. et al. (2004), "Behaviour of steels in flowing liquid PbBi eutectic alloy at 420-600 °C after 4000-7200 h", *J. Nucl. Mater.*, 335, 163.

[38] Maschek, W. et al. (2005), "SIMMER-III and SIMMER-IV Safety Code Development for Reactors with Transmutation Capability", *M&C 2005*, Avignon, France, 12-15 September 2005.

[39] http://www.acsept.org/.

[40] http://asgardproject.eu/.

[41] 5th PCRD FP EU, PYROPREP, FIKW-CT-2000-00049, (2003).

Session I: Current ADS Experiments and Test Facilities

Chair: K. Tsujimoto

The MEGAPIE PIE sample preparation

M. Wohlmuther, V. Boutellier, Y. Dai, D. Gavillet, K. Geissmann, S. Hahl, B. Hammer, A. Lagotzki, H. Leu, H.P. Linder, A. Kalt, D. Kuster, J. Neuhausen, D. Schumann, R. Schwarz, H. Schweikert, A. Spahr, P. Suter, S. Teichmann, K. Thomsen, H. Wiese, W. Wagner, U. Zimmermann, Ch. Zumbach
Paul Scherrer Institut, Villigen PSI, Switzerland

Abstract

On the way towards Accelerator-driven Systems (ADS), the MEGAPIE (MegaWatt Pilot Experiment) project is one of the key milestones. The MEGAPIE project aimed to prove that a liquid Lead-Bismuth-Eutectic (LBE) spallation target can be licensed, planned, built, operated, dismantled, examined and disposed. The project has finished the phase of producing the samples for Post-irradiation Examination (PIE). Samples to study structural material property changes due to the harsh environment of high temperatures, contact with flowing liquid metal (LBE), proton and neutron irradiation will be investigated by all partner laboratories (CEA, CNRS, ENEA, KIT, PSI and SCK•CEN).

Introduction

The MEGAPIE initiative was started in autumn 1999 with the aim to design, fabricate, build, cold-test, license, operate, dismantle, dispose and examine a liquid Lead-Bismuth Eutectic (LBE) spallation target [1]. The project is carried out by the international collaboration of several research institutes and organisations, namely: CEA (France), CNRS (France), DOE (US), ENEA (Italy), the European Union, JAEA (Japan), KAERI (Republic of Korea), KIT (Germany), LANL (US), PSI (Switzerland) and SCK•CEN Mol (Belgium). The project is considered as a key milestone towards the building of an ADS system. One of the design goals was to operate the MEGAPIE target at a beam power in the MW regime. Therefore, the high power proton accelerator (HIPA) at PSI [2] was chosen to drive the target, as the proton accelerator complex at PSI is the only facility to deliver a continuous MW proton beam. Currently, the accelerator chain delivers a maximum proton current of 2.4 mA of 590 MeV protons. The MEGAPIE liquid metal target and its ancillary systems were installed in the Swiss Intense Neutron Source (SINQ) [3], one of the user facilities served by HIPA.

In the first half of 2006, the MEGAPIE target was intensely cold tested [4]. Then, in August 2006, the first liquid metal target, operated in the MW range (0.8 MW) - MEGAPIE - came into operation [5]. The LBE target received an integrated current of 2.8 Ah of 575 MeV protons and was operated successfully until 21st December 2006; the neutron flux increased 80% with respect to the SINQ solid target operated in 2004/2005 [6]. In the shutdown following the MEGAPIE operation, the ancillary systems of MEGAPIE were disintegrated. The target was put into the target storage facility of SINQ, waiting to be dismantled and the extensive post irradiation examination (PIE). As no suitable large enough hot cells existed at PSI, it was decided to transport MEGAPIE to the hot cell of the central interim storage facility of the Swiss nuclear power plants (ZWILAG) for a detailed description of the dismantling concept [7, 8]. In 2007 and 2008, several campaigns were

conducted in the hot cell of ZWILAG to test the different devices and machinery for the dismantling of MEGAPIE, as well as to train the involved personnel [9]. In 2009, the target was successfully dismantled into 21 pieces using a band saw. Eleven of the target pieces were directly disposed off, while the ten remaining target sample pieces were shipped to the Hot Laboratory (HL) of PSI for the PIE sample preparation [10].

The PIE sample preparation consisted of nine major work steps. After licensing and clearance from the authorities for all operations planned in the Hot Laboratory of PSI non-destructive tests – a visual inspection, a thickness measurement of the T91 beam entrance window and a γ-mapping of the AlMg3 safety shroud (H10) – were conducted, followed by an LBE sample taking campaign (including the retrieval of absorber foils from the expansion tank of the target). Thereafter, the structural materials of the target (T91 and 316L steel) were separated from the spallation target material, LBE, by means of melting and separating the LBE inside a special oven and its subsequent disposal. The cylindrical and hemi-spherical structural material sample pieces were then raw cut into smaller samples using a diamond disk cutter. Subsequently, the remains of the LBE were mechanically and chemically removed from the structural materials, i.e. T91 and 316L steels. In a next step the raw cut steel pieces were cut with an EDM wire cutter into miniaturised PIE sample groups. Finally, several sample groups were packed into customised containers. At the same time, sample groups have been shipped successfully to KIT, SCK, LANL, CEA, and JAEA. In addition, the remaining waste produced during the PIE sample preparation will be disposed off.

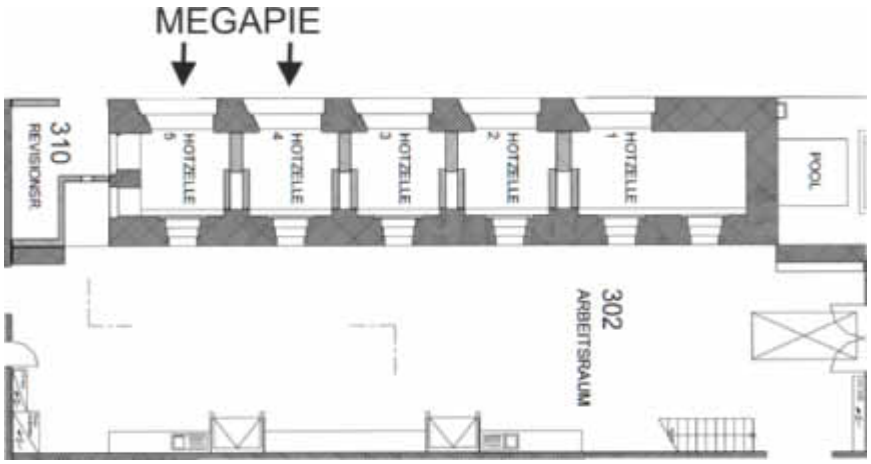
An overview of the PIE sample preparation in the Hot Laboratory of PSI will be reviewed in the next section.

The Hot Laboratory at PSI

All works relating to the PIE sample preparation, except for the analysis of LBE samples, have been performed in the hot cells 4 and 5 of the hot cell chain of the Hot Laboratory (see Figure 1). Before starting any work in the hot cells of the Hot Laboratory, all major working steps had to be licensed by the Swiss Nuclear Safety Inspectorate (ENSI). The remaining subtasks of the PIE sample preparation were as follows:

- non-destructive tests (visual inspection, ultra-sonic thickness measurement of T91 calotte and γ-mapping of AlMg3 beam entrance window);
- LBE sample taking and extraction of the absorber foils from target piece H09;
- LBE melting;
- first disposal of waste;
- raw cutting of steel parts from the pieces H02, H03 and H04;
- cleaning of raw cut sample pieces;
- EDM cutting of sample groups;
- packing of sample groups and transports to the partner laboratories;
- final waste disposal.

Figure 1. Scheme of the hot cells in PSI's Hot Laboratory



Hot cells 4 and 5 were used for the PIE sample preparation.

The MEGAPIE target pieces, brought to PSI in the TC3 transport cask (see Figure 2), as well as the produced samples, have been stored in hot cell 4. All major works have been carried out in hot cell 5, except for the γ-mapping of the AlMg3 beam entrance window. The two hot cells are connected by a movable gate which allowed transferring target or sample pieces. In between two subtasks hot cell 5 was always cleared and cleaned to minimise the risk of cross-contamination and to allow the installation of the specific devices.

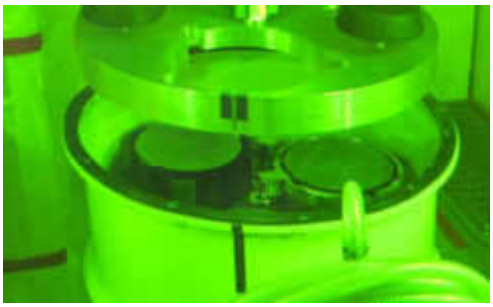
Figure 2. Scheme of the nine stacked target pieces (left) and TC3 transport container (right)



The leak detector and the material piece inside the AlMg3 beam entrance window (see Figure 4) were put on top of the stacked pieces.

A total of 9 target pieces (H02-H10), the leak detector [11] and the piece of black material inside the AlMg3 safety shroud of the MEGAPIE target were packed inside a 200 l drum, which was then placed inside the TC3, see right side of Figure 2. The 200 l drum was transferred into hot cell 5, opened and the AlMg3 beam entrance window was unpacked (see Figure 3).

Figure 3. 200 l drum unpacking with the target sample pieces



The non-destructive tests (NDT)

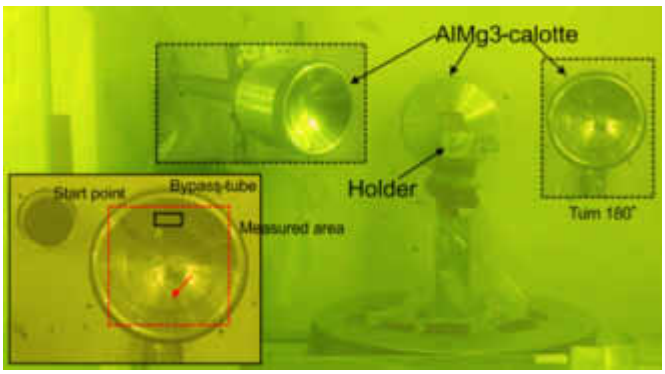
The first non-destructive test was the γ-mapping of the beam entrance window of the aluminium safety shroud. Therefore, the inner wall of the AlMg3 piece (H10) cut in ZWILAG had to be cleaned, because the lower part of the safety shroud showed significant contamination by some unknown materials (see Figure 4).

Figure 4. Contamination on the inside of the beam entrance region of the AlMg3 safety shroud



Besides a solid piece composed of a black material in the centre of the beam entrance region on the inside of the $AlMg_3$ safety container, a similar material was stuck to the inner aluminium side walls as well. To eliminate any distortion of the γ-mapping, a large amount of the material was removed. The cusp-shaped AlMg3 beam entrance window (BEW), (see Figure 5), was positioned on a movable holder inside hot cell 4. The holder could be moved in x- (horizontal) and y-direction (vertical) with a precision better than 0.01 mm and be rotated about its vertical axis. This allowed the positioning of the cusp-shaped BEW in front of a 2×2 mm^2 pin-hole/collimator drilled through the backward shielding of the hot cell. At the exit of the pin-hole, at a distance of 1.41 m from the AlMg3 calotte, a germanium detector was positioned to measure the ^{22}Na activity of a 2×2 mm^2 segment of the calotte. A total of an area of 160×160 mm^2 was investigated, as depicted in the small photo in the lower left corner of Figure 5. Each 2×2 mm^2 segment was measured for 10 minutes.

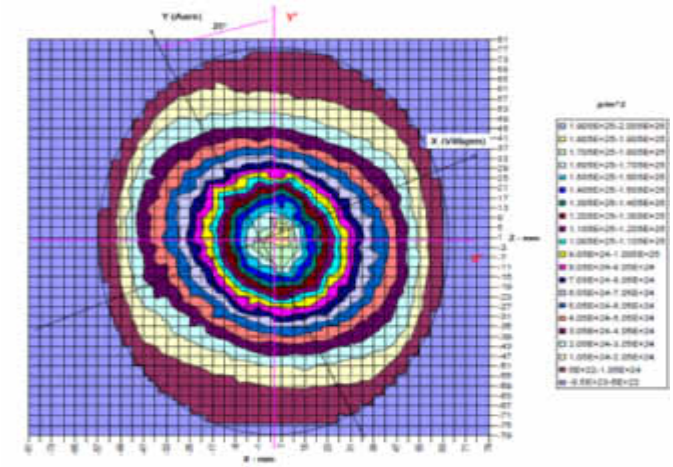
Figure 5: γ-mapping setup inside of hot cell 4



Lower left: Pin-hole through the hot cell shielding and AlMg3 calotte, with indicated starting point and measurement area (160×160 mm^2).

This method allowed for a precise determination of the time-average proton beam profile delivered onto MEGAPIE via the proton induced reaction $^{27}Al(p,X)^{22}Na$. This information was subsequently used in Monte-Carlo calculations to determine the dpa-values in the PIE sample taking regions of H02 (T91 beam entrance window), H03 and H04. The time-averaged proton beam fluence has been shifted by 4.3 mm with respect to the beam entrance window centre (see Figure 6) [12].

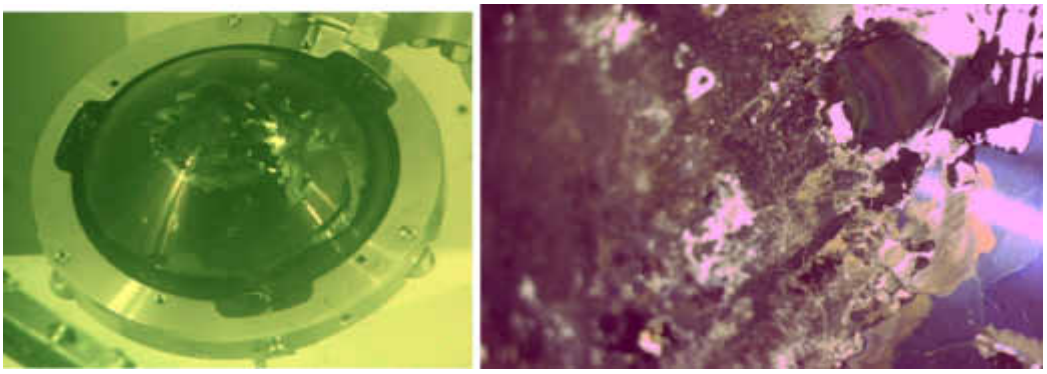
Figure 6. Evaluated time-averaged proton beam fluence in the targets' co-ordinate system (top view)



Following the determination of the time-averaged proton beam profile, a detailed visual inspection of the T91 calotte was performed, using a high resolution video-camera installed in hot cell 5. As already observed in ZWILAG during cutting of the target, the target sample pieces H02, the lower liquid metal container (LLMC) beam entrance window (calotte), and H10, the beam entrance window of the AlMg3 safety shroud suffered severe contamination with a black, sometimes white material of unknown origin (see Figure 7). The layer with a thickness of up to 1 mm was difficult to remove from the T91 and AlMg3. The LLMC (T91) surface showed the highest accumulation of the material in the central region, while the inner surface of H10 was evenly covered everywhere (see Figure 4), with a massive material accumulation in the central region. After samples had been taken from the black and white parts of the covering material, the deposit was removed from the LLMC with a sponge. After extensive "cleaning" with a sponge, the T91 surface could be inspected for visible failures; none were observed. The deposit appeared to have three differently coloured layers (see Figure 8). In a next step, the structure of the

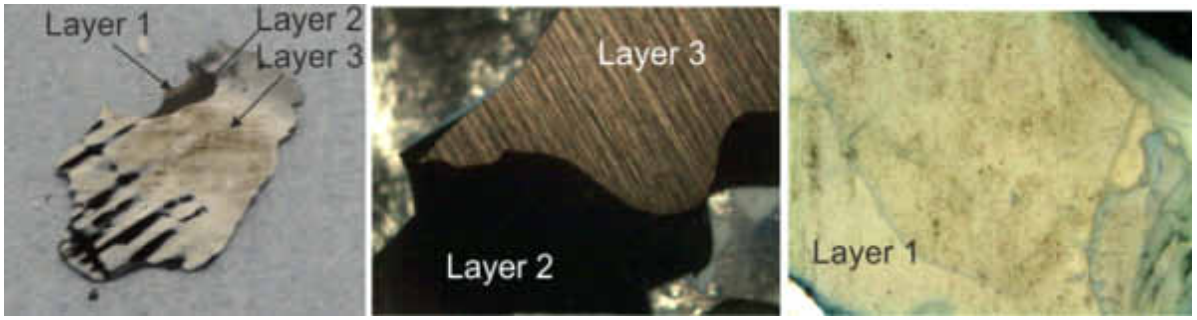
different layers was studied with SEM (see Figures 9 and 10). The black deposit seems rather uniform, while going to Layer 1 and Layer 2. It should be noted that the structure of the deposit became porous and crystalline-like, respectively.

Figure 7. Visual inspection of the T91 calotte ($H0_2$)



Left: Photograph taken through the lead glass window of the hot cell. Right: High-resolution photograph taken by a video camera installed inside the hot cell.

Figure 8. Different layers of the deposit on the T91 LLMC outer surface



Left: High resolution photograph. Middle: Optical microscopy picture of Layers 2 and 3. Right: Optical microscopy picture of Layer 1.

Figure 9. Optical microscopy picture as in Figure 8, SEM picture of the same region and SEM picture with high resolution (from left to right)

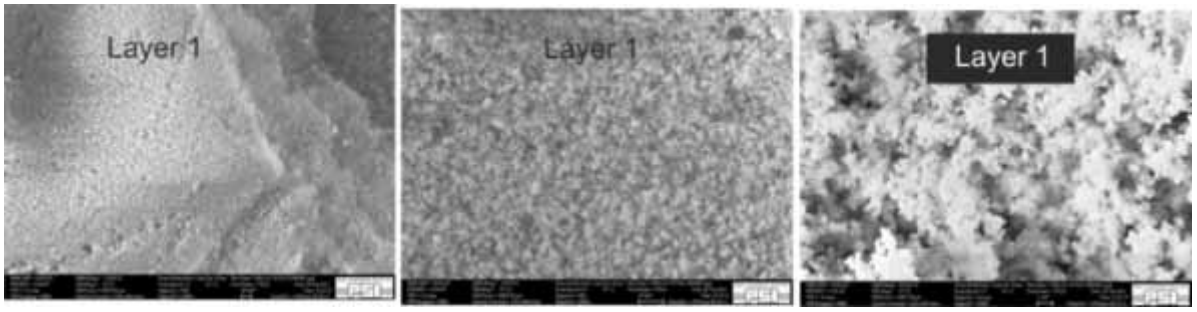
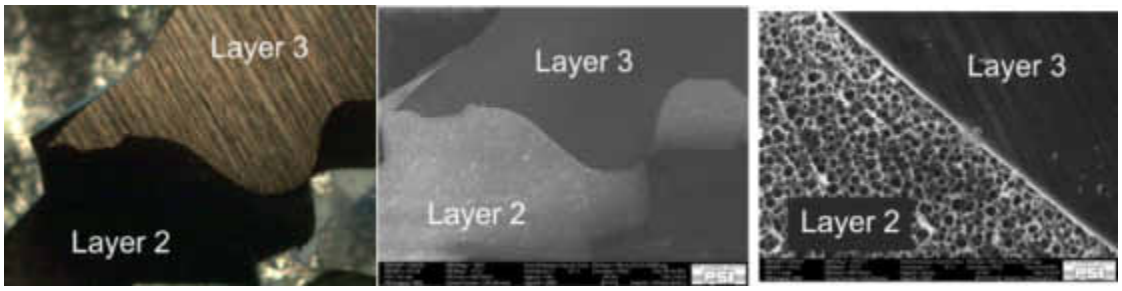


Figure 10. SEM pictures with increasing resolution of Layer 1 (from left to right)



Finally, the composition of the three layers was examined using energy-dispersive X-ray spectroscopy (EDX). The results are given in Table 1. The chemical composition of the black deposit (the dominating species) supports the hypothesis that the contamination has been produced in the harsh radiation environment from oil leaking out of the cooling loop. The oil used in the heat exchanger was Diphyl THT.

Table 1. Elemental composition of the three layers

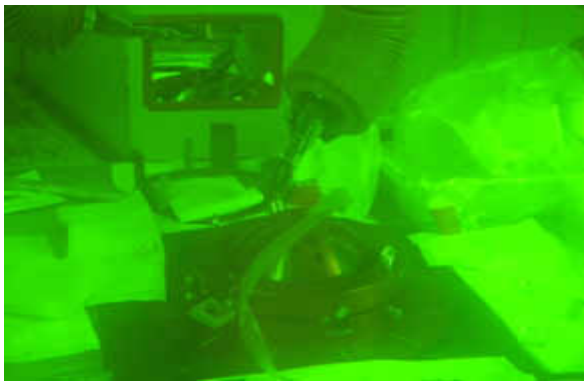
Element	Layer 1 (white deposit)	Layer 2 (gray intermediate layer)	Layer 3 (black deposit)
	Weight% (atom%)	Weight% (atom%)	Weight% (atom%)
C	4.5 (7.1)	76.59 (82.33)	89.26 (91.79)
O	53.2 (63.0)	19.90 (16.06)	10.5 (8.1)
Si	4.1 (4.1)	3.51 (1.61)	0.24 (0.11)
F	38.2 (25.8)		

Left: high resolution photograph, middle: optical microscopy picture of Layers 2 and 3. Right: optical microscopy picture of Layer 1.

The last step of the non-destructive tests was an ultrasonic thickness measurement of the beam entrance window of the T91 LLMC. Prior to the operation of MEGAPIE in SINQ, thickness measurements had been conducted before the target was filled with LBE. As the LBE had been solidified inside the target after irradiation, the determination of thickness changes was performed on the target sample piece H02 still filled with LBE. For this purpose, a special fixture was designed and fabricated, which allowed thickness measurements of the T91 beam entrance window at 102 positions (see Figure 11).

Those measurements were compared to the thicknesses determined before irradiation; within the measurement accuracy of 5 µm, no LBE corrosion induced dimension change was found.

Figure 11. Thickness measurement of the T91 beam entrance window

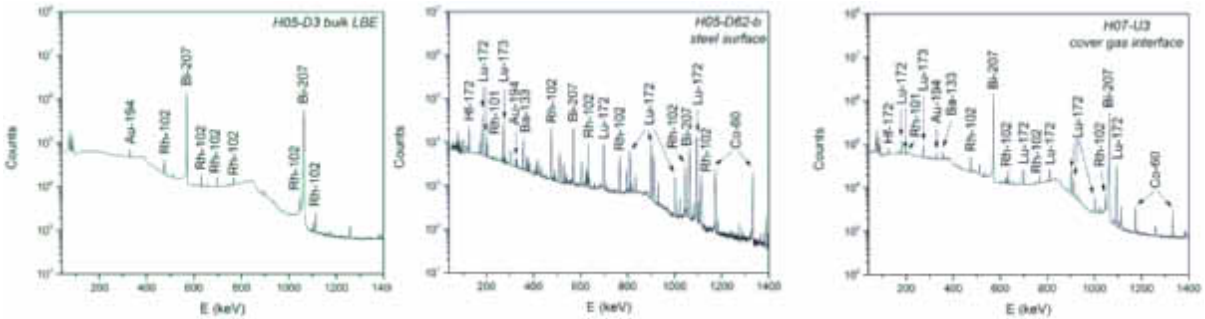


LBE sample taking and analysis

Besides the structural material samples, the target and cooling material, LBE, was also investigated. In total, 79 samples were drilled from the solidified LBE [13]. In order to study the spatial distribution of the produced isotopes, radially distributed samples across the target diameter were also examined for the target pieces H03 and H05. Special emphasis was placed on LBE sampling at interfaces to the structural materials and to the cover gas as previous investigations of a proton-irradiated ISOLDE LBE target at CERN [14] and on neutron-activated LBE, irradiated inside SINQ [15], revealed an enrichment of specific isotopes at such material boundaries. In particular, this behaviour has been observed for polonium, one of the most hazardous species produced in MEGAPIE during operation.

As a first step of the analysis, the gamma spectra of all LBE samples were studied. It was observed that the gamma spectra of bulk LBE did not include isotopes sensitive to oxidation; those elements, like, for instance Lu, were mainly found in samples taken at steel-LBE and cover gas-LBE interfaces (see Figure 12).

Figure 12. Gamma spectra from different LBE samples

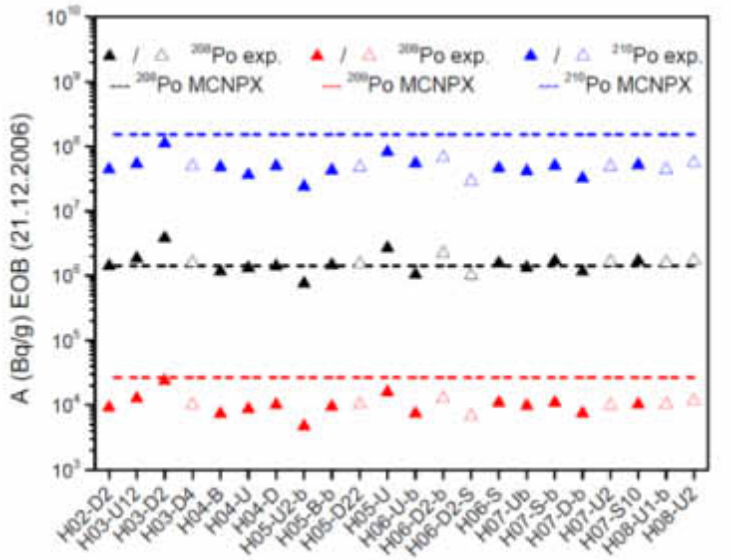


Left: Spectrum of a bulk sample taken from H05. Middle: Spectrum of a steel-LBE interface sample taken from H05. Right: Spectrum from a LBE sample taken from the cover gas-LBE interface (from H07), figure taken from [5].

After the analysis of the gamma spectra, a first chemical separation of polonium from the LBE samples was performed and the activities of the isotopes ^{208}Po, ^{209}Po and ^{210}Po were determined. In contrast with the results obtained from previous investigations of the spatial distribution of polonium in LBE [16], polonium was found to be homogeneously distributed inside the LBE of the MEGAPIE target. Moreover, the prediction of several Monte Carlo particle transport codes agreed well with the measured specific activities for $^{208/209/210}$Po (see Figure 13).

More details on the investigation of the nuclide inventory of the LBE samples are in [17].

Figure 13. Comparison of the specific activities [Bq/g] of $^{208-210}$Po as determined experimentally (symbols) and with the particle transport code MCNPX (dashed lines)



EOB denotes “end of beam”; figure taken from [18].

The segregation of LBE and the structural materials

To prepare PIE samples of the MEGAPIE structural materials (T91 and 316L steel), it was necessary to separate the steels – T91 for the lower liquid metal container and SS316L for the flow guide tube – from the LBE. For this operation, a special furnace was developed which allowed heating the target sample pieces to temperatures above the melting point of LBE. The liquefied LBE was collected in a tank situated directly below the heated part of the oven and was solidified there. To prevent any spread of contamination due to volatiles produced during the melting process, the oven was designed as a closed and tight vessel, equipped with a special filter system that was directly connected to the exhaust of the hot cells. The setup is displayed in Figure 14.

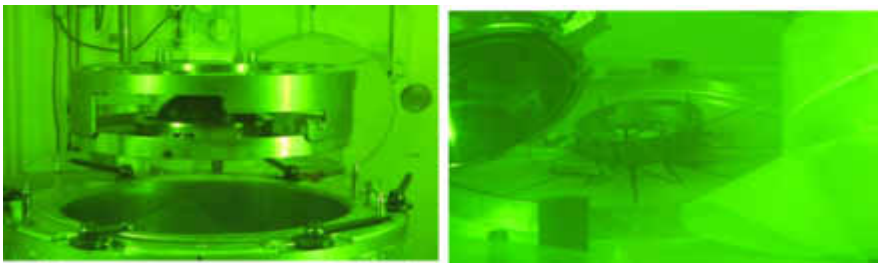
Figure 14. Oven with the upper heated part and the LBE catching volume directly below (left) and filter system of the oven before off-gas went into the exhaust (right)



After a target piece was inserted into the oven from the top, the oven was flushed with argon and a pressure below 100 mbar was established. Then the temperature was gradually increased to 150°C and kept at this temperature until the LBE level detector in

the catching volume indicated an increase in the LBE level. For another 20-30 minutes, the temperature was kept at 150°C and subsequently the heating was switched off. After cool-down, the oven was flushed with argon via the filter system for several times and the structural material pieces were retrieved (see Figure 15).

Figure 15. Retrieving $H0_2$ from the oven after the melting process (left) and calotte beam entrance window and flow guide tube of $H0_2$ (right)



This procedure was repeated for all target pieces which contained LBE – H02 to H07. As shown in Figure 16, sizeable fractions of wetting LBE remained on the structural material parts.

Figure 16. Part of the 316L flow guide tube after melting of the LBE



Raw cutting of sample pieces

After the segregation of the structural materials from the LBE, the structural material sample pieces were available in highly unfavourable dimensions and shapes for the forthcoming handling steps. Therefore, the structural material pieces were cut into smaller segments, which could separately be cleaned from the LBE remains and subsequently EDM machined to sample groups. As shown in Figure 17, this raw cutting was performed within the set-up using a diamond disc saw.

Figure 17. Set-up used for raw cutting

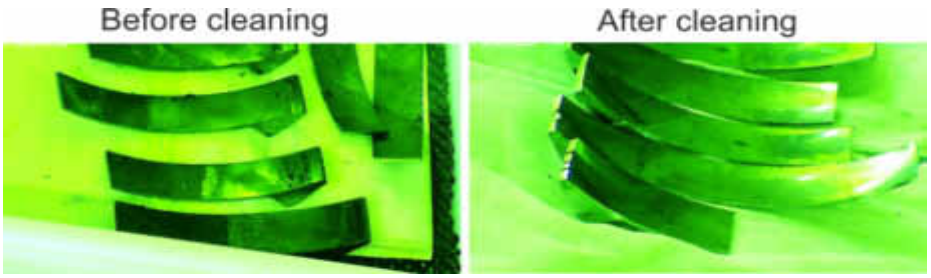


The disc saw was positioned inside a Plexiglas container to minimise the contamination area due to air-borne particles or volatiles produced by the melting of LBE remains. The heat release inside the sample material was minimised due to cuts in the sections. A total of 73 raw cut sample pieces were produced; all but 4 raw cut sample pieces were subsequently cleaned from the LBE remains to finally produce the PIE sample groups via EDM cutting.

Cleaning of the structural material parts

The removal of the LBE remains from structural material samples was performed in a two steps process developed by Y. Dai [19]. First, the structural material samples were put into a hot oil (UCON-HTF) bath at a temperature of 190°C. The LBE liquefied and was wiped off the steel parts with tissue. Then the steel parts were cleaned in an ultrasonic demineralised H_2O bath to remove any oil remains. Only a thin layer of LBE was found after these cleaning steps, which was subsequently removed by placing the steel sample pieces inside 5 molar HNO_3 for a few minutes. After this chemical cleaning, the sample pieces were again cleaned in an ultrasonic demineralised H_2O bath several times.

Figure 18: Examples of raw cut sample pieces before (left) and after (right) completion of the cleaning procedure

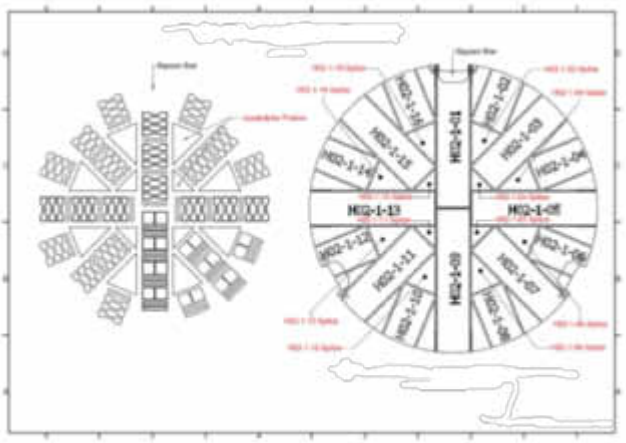


The goal of this “cleaning” procedure was to minimise the alpha contamination due to Po and Gd isotopes produced in LBE on the steel samples so that the produced PIE samples could be accepted by the laboratories at all partner institutes. Moreover, the LBE layer on the steels could have had an effect during the EDM cutting, e.g. producing shortcuts. For that reason, the LBE layer had to be as thin as reasonably achievable. The alpha contamination level could be brought down to a maximum of 1.5 Bq/cm^2, which translates to an LBE thickness of 0.67 nm.

EDM cutting of PIE samples

As shown in Figure 19 (right), the T91 BEW was raw cut with a diamond disk saw into 16 target sample pieces; the EDM cutting scheme is given on the left.

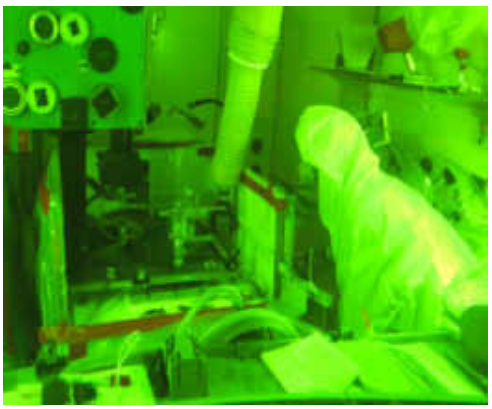
Figure 19. EDM cutting scheme of the BEW target piece $H0_2$ (left) and raw cutting scheme of $H0_2$ (right)



Essentially two sample groups were machined during EDM cutting $H0_2$. The first sample group consisted of 3 tensile and 4 TEM samples (Group I), while Group II was made up of 2 bend bars and 2 OM samples.

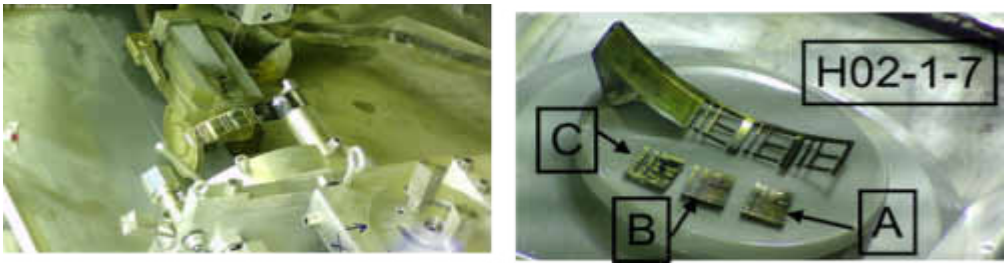
For EDM cutting, an AGIE 250 machine was installed inside hot cell 5 (see Figure 20). The electronics and controls were positioned outside the hot cell.

Figure 20. Installation of the AGIE 250 EDM machine inside the hot cell



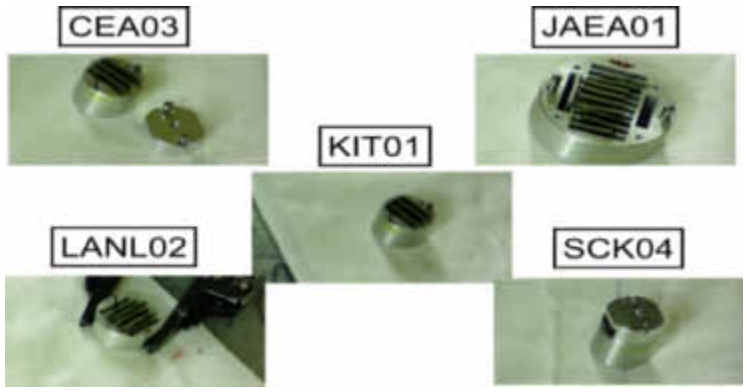
All cutting schemes were cold tested on 1:1 mock-up pieces before the EDM cutting of the active target sample pieces was started. The cutting speed allowed producing 2 or 3 sample groups per day. Figure 21 shows the sample groups produced from H02-1-07.

Figure 21. EDM cutting of H02-1-07 (left) and weighing of the sample groups (right)



All sample groups could be produced as originally planned. Therefore, a total of roughly 750 samples were produced from the target sample pieces H02-1 (BEW, T91), H03-1 (Lower Liquid Metal Container, LLMC, T91), H03-2 (Flow Guide tube, FGT, 316L), H04-1 (LLMC, T91) and H04-2 (FGT, 316L). Each of the sample groups was weighed and dose rates were measured; the maximum dose rates of 316L sample groups were ~ 36 mSv/h in 10 cm distance. No alpha contamination could be detected on analysed samples.

Figure 22. Sample holders dedicated for the different partner institutes



In a last step, the sample groups were packed into special sample holders dedicated for each partner institute (see Figure 22) [20]. The sample holders were then packed into sample containers, which then were inserted into the transport containers. By the end of May 2013, roughly 370 structural material samples had been shipped to the partner institutes in Germany, Belgium, the United States, France and Japan.

The Post-Irradiation Examination (PIE) of the structural material samples can be started.

References

[1] Bauer, G. S., Salvatores, M., Heusener, G. (2001), "MEGAPIE, a 1 MW pilot experiment for a liquid metal spallation target", *J. Nucl. Mat* 296, p. 17.

[2] Seidel, M., Adam, S.R.A., Adelmann, A., Baumgarten, C., Dölling, R., Fitze, H., Fuchs, A., Grillenberger, J., Humbel, M., Kiselev, D.C., Mezger, A.C., Reggiani, D., Schneider, M., Zhang, H. (2010), "Production of a 1.3 MW proton beam at PSI", *Proceedings of IPAC'10,* 23-28 May 2010, Kyoto, Japan, p. 1309 (2010), http://accelconf.web.cern.ch /AccelConf/IPAC10/papers/tuyra03.pdf.

[3] Fischer, W.E. (1997), "SINQ-The Spallation Neutron Source, a new Research Facility at PSI", *Physica B* 234-236, p. 1202.

[4] Fazio, C., Gröschel, F., Wagner, W., Thomsen, K., Smith, B.L., et al. (2008), "The MEGAPIE-TEST project: Supporting research and lessons learned in first-of-a-kind spallation target technology", *Nucl. Sci. Eng.* 238, p.1471.

[5] Wagner, W., Gröschel, F., Thomsen, K., Heyck, H. (2008), "MEGAPIE at SINQ - The first liquid metal target driven by a megawatt class proton beam", *J. Nucl. Mat.* 377, p. 12.

[6] Zanini, L. et al. (2008), "Neutronic and Nuclear Post-Test Analysis of MEGAPIE", PSI Report Nr. 08-04, ISSN 1019-0643.

[7] Strinning, A., Wohlmuther, M. (2007), "Handling, dismantling and disposal concept of the irradiated MEGAPIE liquid metal target", *Proceedings of the Eighth international topical meeting on nuclear applications and utilization of Accelerators (ACCAPP'07)*, Pocatello, Idaho, 29 July-2 August 2007, p. 621.

[8] Ake Strinning, Michael Wohlmuther (2005), "Konzept zur Handhabung, Zerlegung und Konditionierung des aktivierten MEGAPIE Targets", MPS-11-SK85-003/01, MEGAPIE internal report, unpublished.

[9] Wohlmuther, M., Strinning, A., Züllig, J., Geissmann, K., Zumbach, Ch., Suter, P., Thermer, R., Meier, R., Hösli, Ch., Erne, R., Bugmann, F., Binkert, B., Leuzinger, R., Miotti, M., Keller, R., Mossmann, D., Schörck, Ch., Emch, R., Läuchli, O. (2009), "Beschreibung der Kalthandhabungstests von August bis November 2008 zur Zerlegung des MEGAPIE Targets in der ZWILAG, MPR-1-WM85-020/0", MEGAPIE internal report, unpublished.

[10] Wohlmuther, M., Wagner, W. (2012), "PIE preparation of the MEGAPIE target", *J. Nucl. Mat.* 431, p.10.

[11] Thomsen, K. (2008), "Liquid metal leak detection for spallation neutron sources", *Nuclear Instruments and Methods* A, p. 476.

[12] Dai, Y., Wiese, H., Linder, H.P., Lagotzki, A., Hahl, S., Schwarz, R. (2011), "Gamma-Mapping of the AlMg3 Calotte and evaluation of proton fluence distribution of the MEGAPIE target", MPR-11-DY34-003-1, MEGAPIE Report, not published.

[13] Dai, Y., Neuhausen, J., Schumann, D., Zumbach, C., Leu, H., Schweikert, H., Spahr, A. (2011), "Specimen extraction plan for MEGAPIE PIE", MPR-1-DY34-001-3, MEGAPIE Report, not published.

[14] Hammer, B. (2010), "Production and distribution of long-lived radionuclides in a lead-bismuth target from ISOLDE", master thesis, PSI and University of Bern.

[15] Neuhausen, J., von Rohr, F., Schumann, D. (2006), "Segregation of ^{210}Po in eutectic lead-bismuth alloy", Analytics and sample homogenisation, LCH Annual Report, Paul Scherrer Institute Report.

[16] Neuhausen, J., Hammer, B., Schumann, D., Zanini, L., Boutellier, V., Rüthi, M., Eikenberg, J., Noah, E. (2010), Annual Report of the Laboratory of Radio and Environmental Chemistry, Uni Bern & PSI, p. 34.

[17] Hammer, B., Neuhausen, J., Boutellier, V., Linder, H.P., Shcherbina, N., Wohlmuther, M., Türler, A., Schumann, D. (2013), "Analysis of the ^{207}Bi, ^{194}Hg/Au and ^{173}Lu distribution in the irradiated MEGAPIE target", *J. Nucl. Mat.*

[18] Hammer, B., Schumann, D., Neuhausen J., Wohlmuther, M., Türler, A. (2013), "Radiochemical determination of Polonium in Liquid Metal Spallation Targets", *Nuclear Data Sheets*.

[19] Dai, Y. (2011), "Cleaning Lead-Bismuth Eutectic (LBE) on Surfaces of Specimens after Corrosion Test", MPR-11-DY34-002-2, MEGAPIE internal report, unpublished.

[20] Wohlmuther, M. et al., "Final MEGAPIE PIE Sample Distribution and Packing Plan", TM-85-13-02/MPR-1-WM85-052/2, MEGAPIE report, PSI internal report, not published.

Neutron spectrum hardening in critical and subcritical reactors cooled with ^{208}Pb

G.L. Khorasanov, A.I. Blokhin
Institute for Physics and Power Engineering, Russian Federation

Abstract

In nuclear power installations with fast neutrons, ADSs and FRs, the mean energy of core neutrons does not exceed 0.5 MeV, while the mean energy of fission neutrons emitted by ^{235}U is equal to 1.98 MeV. Hard spectrum of neutrons in ADS and FR core is preferable for incineration of minor actinides. Neutron moderation is due to the interaction of neutrons with fuel, structural materials and coolants. In critical and subcritical reactors cooled with lead, a possibility of neutron hardening exists if lead enriched with ^{208}Pb is used. This paper presents that in critical and subcritical reactors cooled with ^{208}Pb the neutron spectrum is hardened at 6.3-6.4% and one-group ^{241}Am fission cross-sections increase by 8-10%.

Introduction

As is generally known, the spent nuclear fuel of light water reactors contains approximately 2% of transuraniums (plutonium, neptunium, americium and curium) and long-lived products of fission (technetium, cesium and others). The spent nuclear fuel contains radio nuclides which have to be isolated from the environment during a period of more than 1000 years [1]. Among these nuclides, the most dangerous from the radiotoxicity point of view are plutonium and ^{241}Am. While plutonium can be used as a fuel for future fast reactors (FRs), low fissile ^{241}Am must be incinerated or transmuted into other short-lived radio nuclides in future accelerator-driven systems (ADSs) or FRs. Long-term isolation of ^{241}Am, over 300 years, in special man made containers is problematic due to its high-level thermal irradiation, about 200 watts/tonne, and its conversion to ^{237}Np, a long-lived radionuclide (T1/2 = 2.14x106 yr) with a relatively high solubility and a tendency for aqueous subsurface transport.

The threshold of ^{241}Am fission in the hard part of neutron spectrum is around 0.1 MeV. In the intermediate and thermal parts of neutron spectra, the ^{241}Am fission cross-sections are great enough but radiation neutron capture is higher with an impact on the transmutation of americium into high order actinides. Usually in ADSs and FRs, the mean energy of core neutrons does not exceed 0.5 MeV, while the mean energy of fission neutrons emitted by ^{235}U, for example, is equal to 1.98 MeV. The investigation of the possibility of the neutron spectra hardening in nuclear power installations with the aim to increase the ^{241}Am fission probability is of practical interest. One of the ways to enhance neutron spectra hardening is to use core materials such as coolants, constructive elements, which have small neutron moderation. The molten lead enriched with lead stable isotope – ^{208}Pb – is proposed as such a coolant [2].

This paper analyses the possibility of neutron spectra hardening with the aim to enhance ^{241}Am fission probability. A blanket of the ADS with a thermal power of 80 MW designed by authors [3], a core and lateral blanket (LB) of the FR RBEC-M with a thermal power of 900 MW designed at the Russian National Centre "Kurchatov Institute" [4] are examined.

Methods of calculations

The neutron spectra of the 80 MW ADS blanket, the reactor RBEC-M core and lateral blanket were calculated and then, on the basis of the spectra obtained, the mean energies of neutrons, one-group ^{241}Am fission and radiation neutron capture cross-sections were found.

Code MCNP5 [5] and input data for RBEC-M were used for determining the corresponding neutron spectra. Mean energies of neutrons were calculated. Expression: $<E_n>=\sum E_n\varphi_n/\sum\varphi_n$, were E_n – is the mean neutron energy in the group g (number of groups g=28) of the ABBN-93 system [6], φ_n – neutron fluxes into the group g, summation $\sum$ was made with respect to all groups where neutron fluxes are higher than zero. Similarly, ^{241}Am one-group fission and radiation neutron capture cross-sections, $<\sigma_{fis}>$ and $<\sigma_c>$, were calculated. The evaluated files of the library ENDF/B-VII.0 were used to determine microscopic cross-sections of ^{241}Am fission and radiation neutron capture.

^{208}Pb is used as a coolant for neutron spectra hardening. In this replacement, all other parameters of 80 MW blanket were kept unchanged. As regards the reactor RBEC-M, the fuel plutonium enrichment was decreased from 13.59% to 13.0% to preserve the criticality K_{eff}=1.01. The data relating to the volume shares of the coolants in subcores-1, -2, -3 and LB of the reactor RBEC-M are shown in [7].

Calculations and discussion

Table 1 gives the mean energies of neutrons and the probability of ^{241}Am fission along the subcritical blanket of the ADS with a thermal power of 80 MW. The blanket was homogeneously supplied with uranium-plutonium nitride fuel, in which the plutonium enrichment was equal to 13.5%. ^{208}Pb and Pb-nat were used as coolants. In replacement of ^{208}Pb with Pb-nat coolant, the effective neutron multiplication factor K_{eff} was decreased to 2% [3].

The annular blanket of 100 cm height and 134 cm outer diameter was divided into 9 local subzones to perform calculations. Table 1 presents the mean energies of neutrons in subzones along the blanket. The mean neutron energy averaged over the blanket is equal to 0.4026 MeV when using ^{208}Pb as a coolant and 0.3787 MeV when using natural lead. Thus, the coolant replacement leads to neutron spectrum hardening at 6.3%. Similarly, the probability of ^{241}Am fission, which is determined as the ratio $Fis=<\sigma_{fis}>/(<\sigma_{fis}>+<\sigma_c>)$, where $<\sigma_{fis}>$ - is one-group fission cross-section and $<\sigma_c>$ - is one-group radiation neutron capture cross-section, increases by 5.8%.

Table 1. Mean energies of neutrons, (En, MeV), and probability of ^{241}Am fission, (Fis, %), in parts (subzones) of the blanket cooled with: ^{208}Pb (bold)/^{nat}Pb (thin)

The blanket height – 100 cm:

	Subzone1 **En=0.4254**/0.4406 **Fis=13.9982**/11.3604	Subzone 2 **En=0.4438**/0.3408 **Fis=13.6897**/9.,8404	Subzone 3 **En=0.3346**/0.2362 **Fis=6.2326**/3.8327
Target-source of neutrons	Subzone 4 **En=0.4820**/0.5576 **Fis=18.9701**/21.5634	Subzone 5 **En=0.5377**/0.4929 **Fis=21.7887**/17.6977	Subzone 6 **En=0.3723**/0.3754 **Fis=9.1580**/11.9034
	Subzone 7 **En=0.3365**/0.2554 **Fis=8.6446**/8.3228	Subzone 8 **En=0.3731**/0.3811 **Fis=11.2360**/12.4424	Subzone 9 **En=0.3182**/0.3285 **Fis=6.0852**/6.7810

0 28 39 51 62

The blanket radius, cm.

The probability of ^{241}Am fission in the central parts of the blanket reaches 22% while at the periphery of the blanket it drops to 6%.

Table 2 presents the one-group ^{241}Am fission cross-sections along the blanket cooled with ^{208}Pb and Pb-nat.

Table 2. One-group ^{241}Am fission cross-sections (barns) along the blanket of 80 MW cooled with: ^{208}Pb (bold) and Pb-nat (thin)

	Subzone 1 **0.2852**/0.3387	Subzone 2 **0.2884**/0.1874	Subzone 3 **0.2198**/0.1170
Target-source of neutrons	Subzone 4 **0.3334**/0.3724	Subzone 5 **0.3686**/0.3333	Subzone 6 **0.2431**/0.2631
	Subzone 7 **0.2217**/0.1706	Subzone 8 **0.2479**/0.2593	Subzone 9 **0.2193**/0.1933

As shown in Table 2, along the ADS blanket of 80 MW, one-group ^{241}Am fission cross-sections are of 0.1170-0.3724 barns while the maximum cross-section is reached at the central parts of the blanket (subzones 4 and 5) and the minimum cross-section drops at the periphery of the blanket (subzones 3 and 9). This dependence is in good correlation with the dependence of mean neutron energy along the blanket.

Table 3 shows the same parameters (mean neutron energy, ^{241}Am one-group fission and radiation neutron capture cross-sections, probability of fission) for subcores and the

lateral blanket of the reactor RBEC-M cooled with its standard lead-bismuth coolant and the coolant from ^{208}Pb.

Table 3. Neutron and physical parameters of subcores and LB of the reactor RBEC-M [4] cooled with: ^{208}Pb (bold) and Pb-Bi (thin)

Parameters	Inner subcore	Middle subcore	Outer subcore	Lateral blanket
Mean energy, $<E_n>$, MeV	**0.4246**/0.3992	**0.4408**/0.4209	**0.4433**/0.4307	**0.2662**/0.2509
Relative increase of $<E_n>$, %	6.3627	4.7280	2.8790	6.0980
Coolant volume share, %	62.5	57.3	44.6	56.5
Fuel volume share,%	23.3	27.6	38.2	-
Fuel plutonium enrichment, %	13.59	13.59	13.59	-
^{241}Am cross-section $<\sigma_{fis}>$, barns	**0.2882**/0.2629	**0.2975**/0.2779	**0.2950**/0.2829	**0.1671**/0.1521
Relative increase of $<\sigma_{fis}>$, %	9.6234	7.0529	4.2771	9.8619
^{241}Am capture cross-section $<\sigma_c>$, barns	**1.5816**/1.5967	**1.5306**/1.5366	**1.5632**/1.5627	**2.4249**/2.4958
Probability of ^{241}Am fission, %	**15.4134**/14.1374	**16.2737**/15.3155	**15.8755**/15.3283	**6.4468**/5.7442

As shown in Table 3, at the RBEC-M reactor, the replacement of its standard lead-bismuth coolant with ^{208}Pb coolant leads to the hardening of the neutron spectra of the subcores and the lateral blanket at 6.4% and 6.1%, respectively. Usually, ^{241}Am is inserted into lateral and top blankets of FRs. It follows from Table 3 that the probability of ^{241}Am fission in the lateral blanket of the reactor RBEC-M does not exceed 5.7-6.4%, which leads to ^{241}Am transmutation into higher actinides due to the large one-group radiation neutron capture cross-section. In the subcores of this reactor, the probability of ^{241}Am fission is dramatically higher, 15-16%, but there are some restrictions on inserting ^{241}Am large quantities into the reactor core.

Conclusion

It can be concluded that the replacement of the lead or lead-bismuth coolant with a ^{208}Pb coolant in installations with fast neutrons leads to neutron spectrum hardening up to 6.3-6.4%. Under these conditions, one-group ^{241}Am fission cross-sections grow at 8-10%. In the ADS annular blanket (H=100 cm, outer D=134 cm), ^{241}Am fission probability reached 22% in the central parts of the blanket while at its periphery it dropped to 6%.

The probability of ^{241}Am fission in the lateral blanket of the fast reactor RBEC-M does not exceed 5.7-6.4%, while in the subcores of this reactor the probability of ^{241}Am fission is dramatically higher, 15-16%.

It should be noted that ^{241}Am fission in relatively hard neutron spectra is more preferable than its transmutation via neutron capture in the intermediate and thermal neutron spectra which leads to accumulation of curium and californium.

Acknowledgements

The study is performed with the financial support of the Russian Fund of Fundamental Research (Project No 08-08-92201-GFEN_a).

References

[1] Sheffield R.L., Pitcher E.J. (2010), "Subcritical minor actinide reduction through transmutation –SMART", *Technology and Components of Accelerator Driven Systems,*

International Workshop, Karlsruhe, Germany, 15-17 March 2010, Book of Abstracts, Published by OECD/NEA, p. 68.

[2] Khorasanov, G.L. (2013), "Application of stable lead isotope Pb-208 in nuclear power engineering and its acquisition techniques", NOVA publishers, 2013, 184 p., (ISBN: 978-1-62417-653-1).

[3] Khorasanov G.L., Korobeynikov, V.V., Ivanov, A.P., Blokhin, A.I. (2009), "Minimization of an initial fast reactor uranium-plutonium load by using enriched lead-208 as a coolant", *Nuclear Engineering and Design*, v. 239, No 9, pp. 1703-1707, (ISSN 0029-5493).

[4] Alekseev P.N., Mikityuk, K.O., Vasiljev, A.V., Fomichenko, P.A., Shchepetina, T.D., Subbotin, S.A. (2004), "Optimization of Conceptual Decisions for the Lead-Bismuth Cooled Fast Reactor RBEC-M", *Atomnaya Energiya*, v. 97, No 2, pp.115-125 (In Russian); http://www.iaea.org/NuclearPower/ SMR/crpi25001 /html/).

[5] MCNP – A General Monte Carlo N-Particle Transport Code, Version 5. X-5 Monte Carlo Team. Los Alamos National Laboratory Report LA-UR-03-1987 (April, 2003).

[6] Manturov G.N., Nikolaev, M.N., Tsiboulia, A.M. (1996), "Group constant system ABBN-93. Part 1: Nuclear constants for calculation of neutron and photon emission fields", *Issues of Atomic Science and Technology, Series: Nuclear Constants*, Issue 1, p. 59 (1996) (in Russian), (ISSN 0207-3668).

[7] Alekseev P.N., Mikityuk, K.O., Vasiljev, A.V., P.A. Fomichenko, Shchepetina, T.D., Subbotin, S.A. (2001), "Optimization of Conceptual Decisions for the Lead-Bismuth Cooled Fast Reactor RBEC-M", Preprint of the Russian National Centre, Kurchatov Institute, IAE-6229/4, 2001, p.38 (In Russian).

Power spectral analysis for a thermal accelerator-driven system of the Kyoto University Critical Assembly

Atsushi Sakon[1], Kengo Hashimoto[1], Cheol Ho Pyeon[2]
[1]Interdisciplinary Graduate School of Science and Engineering, Kinki University, Japan
[2]Nuclear Engineering Science Division, Research Reactor Institute, Kyoto University, Japan

Abstract

A series of power spectral analyses for a thermal subcritical reactor system driven by a pulsed 14 MeV neutron source was carried out at the Kyoto University Critical Assembly (KUCA) to determine the prompt-neutron decay constant of the accelerator-driven systems (ADSs). A cross-power spectral density between the time-sequence signal data of two neutron detectors was composed of a familiar continuous reactor-noise component and many delta-function-like peaks at the integral multiple of pulse repetition frequency. The prompt-neutron decay constant could be inferred from the former reactor noise component and the latter peak-point data, respectively, and these decay constants were consistent with those obtained by a pulsed neutron experiment. Another cross-power spectral density between the time-sequence signal data of a neutron detector and a beam current meter was also measured. In the magnitude of the measured complex cross-power spectral density, we could observe many delta-function-like peaks at the integral multiple of the repetition frequency, while the spectrum, except for these peaks, was almost white and had no information on reactor physics. From the magnitude and phase data of the complex spectral density at the integral multiple of the repetition frequency, respectively, the consistent decay constant could be determined. A furthter power spectral analysis is in progress for pulsed spallation neutrons generated from tungsten or lead-bismuth target. The cross-power spectral density between two neutron detectors has a quite similar feature to that observed in the above 14 MeV source. The prompt-neutron decay constant can be determined from the spectral density measured for these spallation sources.

Introduction

Research and development on accelerator-driven systems (ADSs) has been of great interest in recent years. The subcritical reactivity of the system indicates a safety margin from the viewpoint of nuclear safety and governs a power gain of the system to a source neutron input. Among the several technological subjects for the future ADS, the development of subcriticality monitoring is particularly important. Only stochastic techniques such as reactor noise analysis may be available for the on-line monitoring of subcriticality in the operation of ADS. For the ADS operation, a pulsed-current-mode operation of the accelerator is expected to be feasible. For such a periodic and pulsed neutron source, power spectral analyses in the frequency domain may be suitable.

Recently, the Kyoto University Critical Assembly (KUCA) has been combined with a proton beam accelerator to supply spallation neutrons to its subcritical core [1]. A wide variety of reactor physics experiments on ADS using the pulsed spallation neutrons is now in progress [2] [3]. In the preparatory phase of connecting the proton beam accelerator at KUCA, a series of static and kinetic experiments on ADS with pulsed 14 MeV neutrons has been conducted [4-8]. As a basic study for the on-line monitoring of the subcriticality in the operation of ADS, various power spectral analyses were carried out for a thermal subcritical reactor system driven by the 14 MeV neutron source.

A cross-power spectral density between the time-sequence signal data of the two neutron detectors was measured under various pulsed-current-mode operations of the Cockcroft-Walton-type accelerator [9]. Another cross-power spectral density between the time-sequence signal data of a beam current meter and a neutron detector was also measured. Muñoz-Cobo et al. [10] simulated spectral density by using a Monte Carlo code. However, no experimental study on the cross-power spectral analysis has been reported. This paper presents preliminary results of a further power spectral analysis for the pulsed spallation neutrons, which are generated at tungsten or lead-bismuth target by 100 MeV protons from a fixed field alternating gradient (FFAG) accelerator [11].

Experimental set-ups and condition

Reactor system

The experiments were performed in a solid-moderated and -reflected core, whose effective multiplication factor k_{eff} was about 0.97. The reactor configurations with 14 MeV neutron source and with spallation neutron source are shown in Figures 1 and 2, respectively. The core was composed of 25 fuel assemblies (1/8″P60EU-EU), which were loaded on the grid plate. The fuel and moderator plates of each assembly were set in a 1.5 mm-thick aluminum sheath and the cross-section of these plates within the assembly was the square of 2″. The fuel assembly was composed of 60 unit cells. The unit cell was composed of two (1/16″ thick) uranium plates with Al cladding and one (1/8″ thick) polyethylene plate. The active height of the core, namely 60 unit cells, was about 38 cm. Adjacent to both axial sides of the active region of each fuel assembly, about 55 cm upper and lower polyethylene reflectors were attached. KUCA has six control rods, where three are assigned as safety rods for reactor scram and are referred to as S4, S5 and S6, respectively. Others are rods for the adjustment of reactivity and are referred to as C1, C2 and C3, respectively. As a subcritical rod pattern for this experiment, the shutdown pattern was used, where all control and safety rods were completely inserted.

Figure 1. Top view of a configuration with 14 MeV neutron source

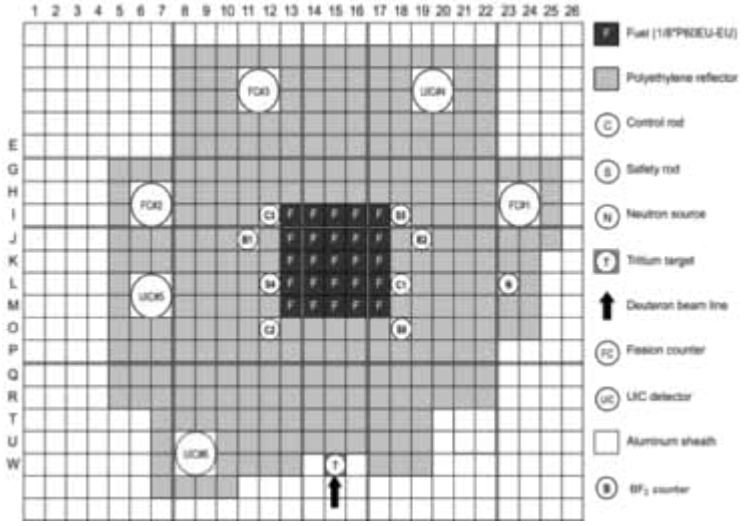
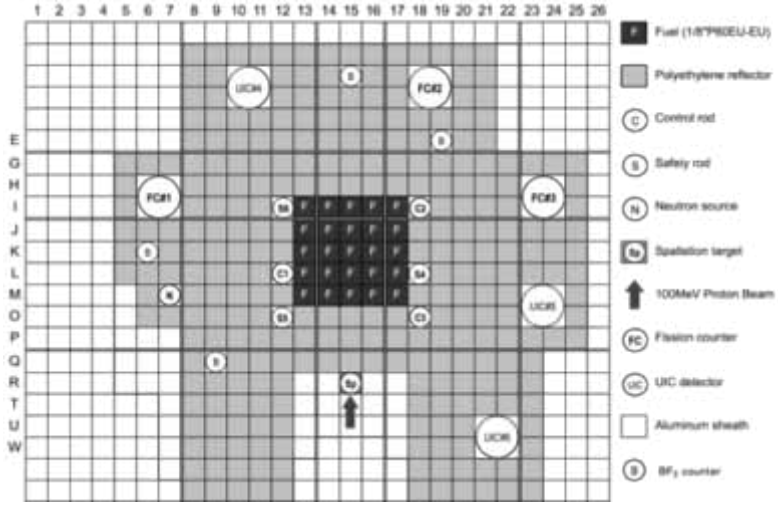


Figure 2. Top view of another configuration with spallation neutron source



Experimental condition and instrumentation system

As reactor start-up channels, three fission counters (FCs) are employed. Three uncompensated ionisation chambers (UICs) are assigned as linear power, logarithmic power and safety power channel, respectively. In addition to the above instrumentation for reactor operation, the reactor with 14 MeV neutron source had two BF_3 proportional counters (1″ dia.) employed as experimental channels. These BF_3 counters are referred to as B1 and B2, respectively, and the location is also shown in Figure 1. The signals from these counters were fed to a fast Fourier transformer to analyse cross-power spectral density and to record the signals as digital data. An analysis range in frequency from 1.25 to 1000 Hz was specified to obtain 800-point spectral data from the transformer. On the other hand, the reactor system with spallation neutron source had no BF_3 counter. The count rate of BF_3 counter was so high that the counter could not be placed near the core. Instead of BF_3 counter, signals from the above fission counters were fed to the Fourier transformer.

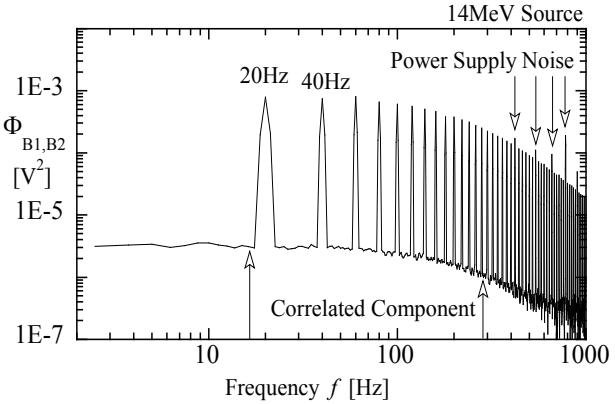
The pulsed 14 MeV neutrons were generated through the D-T reaction by accelerated deuteron beam and tritium in the target metal. The tritium target was placed outside the polyethylene reflector, as shown in Figure 1. The spallation neutrons were generated through the injection of 100 MeV protons onto tungsten or lead-bismuth target. The location of these spallation targets is indicated in Figure 2. As pulse repetition period (frequency) of the present 14 MeV and spallation experiment, 50 ms (20Hz) were employed.

Results and discussion

Cross-power spectral density between two neutron detectors for 14 MeV source

Figure 3 shows measured cross-power spectral densities between the two neutron detector B1 and B2, where the spectral density is real and accordingly only the magnitude of the spectral density is presented. The cross-power spectral density is composed of a continuous reactor-noise component and many delta-function-like peaks at the integral multiple of the repetition frequency 20 Hz. The former correlated reactor-noise components were similar to a familiar reactor noise for a stationary neutron source. The reactor noise component has a flat spectrum in a low frequency range, while above a break frequency (cutoff frequency) the component is attenuated. The break frequency in radians per second corresponds to the prompt-neutron decay constant of the present subcritical system. As can be seen from Figure 3, also, the top point of the delta-function-like peaks has a frequency dependence similar to the above spectrum of the reactor noise component. As a result of this observation, the decay constant may be determinable not only from these correlated reactor-noise components but also from the top points of the uncorrelated peaks. At some frequency of the utility frequency 60 Hz multiplied by odd numbers (3, 5, 7), additional peaks can be seen. These peaks originated from power supply are masked in the present analysis.

Figure 3. Cross-power spectral density between two neutron detectors for 14 MeV neutron source



We derived a formula for this cross-power spectral analysis [9]. Assuming the one-point kinetics model, the correlated reactor-noise component and the top points of the uncorrelated peaks could be respectively described as:

$$\Phi(\omega) = \frac{A_0}{\alpha_0^2 + \omega^2}, \qquad \text{for reactor noise component} \qquad (1)$$

$$\Phi(\omega) = B_0 \sum_{m=1}^{\infty} \frac{\delta(\omega - \omega_m)}{\alpha_0^2 + \omega^2}, \qquad \text{for peak point} \qquad (2)$$

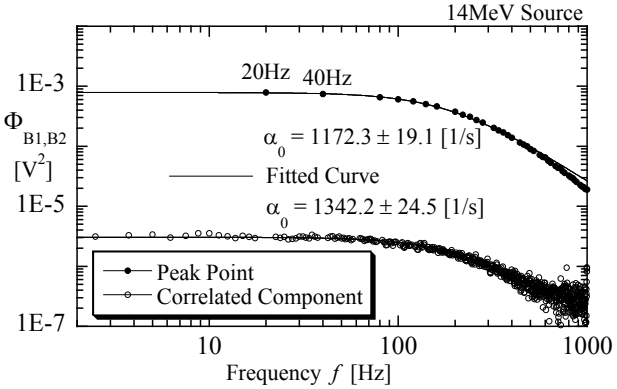
Where:

$$\omega_m = 2\pi m / T_R . \tag{3}$$

In the above equations, ω is angular frequency, α_0 the prompt-neutron decay constant of fundamental mode and T_R pulse repetition period. A_0 and B_0 are constants dependent on detection efficiency, generation time, and accelerator parameters.

Figure 4 shows a least-square fit of Equation (1) to the correlated reactor noise component and another fit of Equation (2) to the uncorrelated peak point. The former fit overestimates the prompt-neutron decay constant, compared with 1226.1±5.3 obtained by a pulsed neutron experiment. The latter fit leads to a slight underestimation of the constant. These over- and under-estimations are expected to result from the contribution of a spatially higher mode to the spectral density data. Considering the contribution, the consistent decay constant 1187.1±28.5 and 1219.7±16.2 could be respectively inferred from the correlated component and the peak point data [9].

Figure 4. Least-square fit to correlated reactor noise component and uncorrelated peak point of cross-power spectral density shown in Figure 3



Cross-power spectral density between beam current meter and neutron detector for 14 MeV source

Magnitude of cross-power spectral density

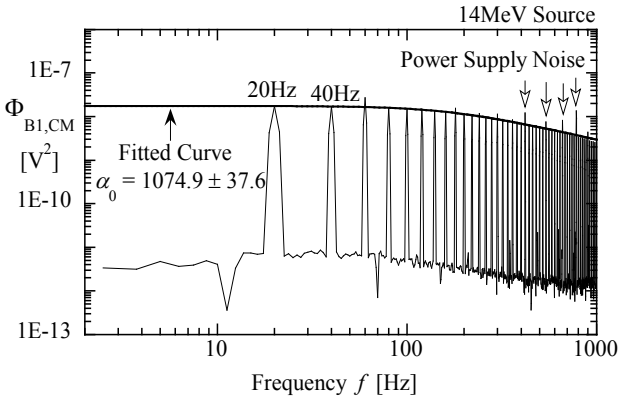
Figure 5 shows the magnitude of measured cross-power spectral densities between signals of the beam current meter and the neutron detector. Several delta-function-like peaks can be observed at the integral multiple of the repetition frequency, while no continuous reactor-noise component can be seen from this figure. A formula was derived for the present cross-power spectral analysis. Assuming the one-point kinetics model, magnitude and phase of the imaginary spectral density can be respectively described as

$$\left|\Phi(\omega)\right| = C_0 \sum_{m=1}^{\infty} \frac{\delta(\omega - \omega_m)}{\sqrt{\alpha_0^2 + \omega^2}}, \tag{4}$$

$$\angle\Phi(\omega_m) = -\tan^{-1}(\omega_m / \alpha_0). \tag{5}$$

A least-square fit of Equation (4) to the peak point leads to the decay constant of 1074.9±37.6. This fit underestimates the prompt-neutron decay constant, compared with 1226.1±5.3 obtained by a pulsed neutron experiment. The underestimation originates from the contribution of the higher mode, and the improvement is now in progress.

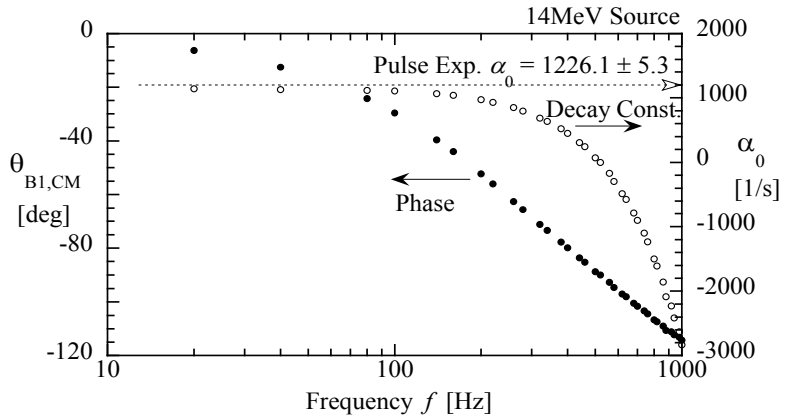
Figure 5. Magnitude of cross-power spectral density between beam current meter and neutron detector for 14 MeV neutron source



Phase of cross-power spectral density

Figure 6 shows the phase of measured cross-power spectral density at the integral multiple of pulse repetition freqency 20 Hz. Equation (5) indicates that the phase lag increases with an increase in frequency and is asymptotic to -90 degrees. However, the measured phase data go beyond -90 degrees in a higher frequency range than 600 Hz. This generates from the lag effect of the higher mode. Substituting the phase data in Equation (5), the prompt-neutron decay constant can be obtained arithmetically. A least-square fit is not necessarily required to obtain the decay constant and this feature is advantageous for the rapid estimation or on-line monitoring of subcriticality. Figure 6 shows the decay constants arithmetically obtained from the phase data. In a lower frequency range, the present decay constant is consistent with that gained by the pulsed neutron experiment. In the frequency range higher than around 200 Hz, however, the decay constant tends to decrease significantly with an increase in frequency. This underestimation is expected to originate from a significant contribution of the higher mode.

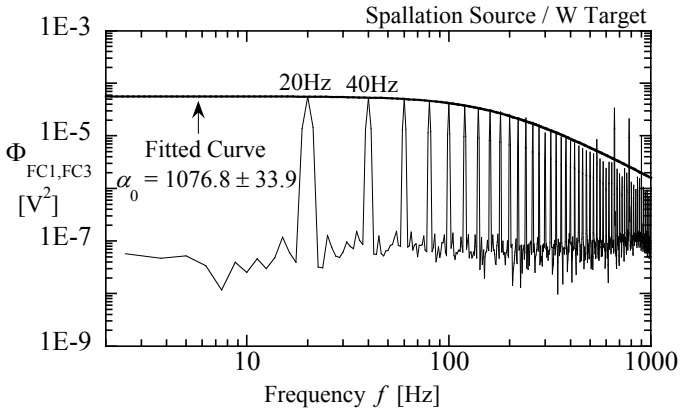
Figure 6. Phase of cross-power spectral density between beam current meter and neutron detector and inferred prompt-neutron decay constant for 14 MeV neutron source



Cross-power spectral density between two neutron detectors for spallation source

Figure 7 shows measured cross-power spectral densities between two fission counters FC1 and FC3, where the subcritical reactor is driven by spallation neutrons from tungsten target. Many delta-function-like peaks can be observed and this feature is similar to that observed in the above 14 MeV source. However, no continuous reactor-noise component can be seen in this figure. This is because these fission counters are located far from the core and consequently the efficiency is extremely low.

Figure 7. Cross-power spectral density between two neutron detectors for spallation neutron source



The least-square fits to the peak point data for tungsten or lead-bismuth target lead to the prompt-neutron decay constants of 1076.8±33.9 and 1060.2±32.5, respectively. These fits underestimate the decay constant, compared with 1226.1±5.3 obtained by a pulsed neutron experiment. The underestimation originates from the contribution of the higher mode, and the improvement is now in progress.

References

[1] Pyeon C.H., Misawa T., Lim J.Y., Unesaki H., Ishi Y., Kuriyama Y., Uesugi T., Mori Y., Inoue M., Nakajima K., Mishima K., Shiroya S. (2009), "First injection of spallation neutrons generated by high-energy protons into the Kyoto University Critical Assembly", *J. Nucl. Sci. Technol*, 46: 1091-1093.

[2] Pyeon C.H., Lim J.Y., Takemoto Y., Yagi T., Azuma T., Kim H., Takahashi Y., Misawa T., Shiroya S. (2011), "Preliminary study on the thorium-loaded accelerator-driven system with 100 MeV protons at the Kyoto University Critical Assembly", *Ann. Nucl. Energy*, 38: 2298-2302.

[3] Pyeon C.H., Azuma T., Takemoto Y., Yagi T., Misawa T. (2013), "Experimental analyses of spallation neutrons generated by 100 MeV protons at the Kyoto University Critical Assembly", *Nucl. Eng. Technol*, 45: 81-88.

[4] Pyeon C.H., Hervault M., Misawa T., Unesaki H., Iwasaki T., Shiroya S. (2008), "Static and kinetic experiments on accelerator-driven system with 14MeV neutrons in the Kyoto University Critical Assembly", *J. Nucl. Sci. Technol*, 45: 1171-1182.

[5] Pyeon C.H., Shiga H., Misawa T., Iwasaki T., Shiroya S. (2009), "Reaction rate analyses for an accelerator-driven system with 14 MeV neutrons in the Kyoto University Critical Assembly", *J. Nucl. Sci. Technol*, 46: 965-972.

[6] Taninaka H., Hashimoto K., Pyeon C.H., Sano T., Misawa T., Ohsawa T. (2010), "Determination of lambda-mode eigenvalue separation of a thermal accelerator-driven system from pulsed neutron experiment", *J. Nucl. Sci. Technol*, 47: 376-383.

[7] Taninaka H., Hashimoto K., Pyeon C.H., Sano T., Misawa T., Unesaki H., Sugiyama W., Ohsawa T. (2011), "Determination of subcritical reactivity of a thermal accelerator-driven system from beam trip and restart experiment", *J. Nucl. Sci. Technol,* 48: 873-879.

[8] Taninaka H., Miyoshi A., Hashimoto K., Pyeon C.H., Sano T., Misawa T., Sugiyama W., Ohsawa T. (2011), "Feynman-α analysis for a thermal subcritical system driven by an unstable 14MeV neutron source", *J. Nucl. Sci. Technol*, 48: 1272-1280.

[9] Sakon A., Hashimoto K., Sugiyama W., Taninaka H., Pyeon C.H., Sano T., Misawa T., Unesaki H., Ohsawa T. (2013), "Power spectral analysis for a thermal subcritical reactor system driven by a pulsed 14 MeV neutron source", *J. Nucl. Sci. Technol*, 50: 481-492.

[10] Muñoz-Cobo J.L., Rugama Y., Valentine T.E., Michalzo J.T., Perez R.B. (2001), "Subcritical reactivity monitoring in accelerator driven systems", *Ann. Nucl. Energy*, 28: 1519-1547.

[11] Yonemura Y., Takagi A., Mori M. et al. (2007), "Development of RF acceleration system for 150MeV FFAG accelerator", *Nucl. Instrum. Methods*, 576:294-300.

Current progress and future plans of the FREYA Project

A. Kochetkov[1], P. Baeten[1], A. Billebaud[2], S. Chabod[2], X.Doligez[3], F.R. Lecolley[4], J.L. Lecouey[4], G. Lehaut[4], N. Marie[4], F. Mellier[5], H.E. Thyébault[2], W. Uyttenhove[1], G. Vittiglio[1], J. Wagemans[1], G. Ban[4], P. Dessagne[6], M. Kerveno[6], L.Mercatali[7]

[1]Studie Centrum voor Kernenergie-Centre d'Etude de l'Energie Nucléaire, Belgium
[2]Laboratoire de Physique Subatomique et de Cosmologie-CNRS-IN2P3/UJF/INPG, France
[3]Institut de Physique Nucléaire d'Orsay, CNRS/IN2P3, Université Paris-Sud, Orsay France
[4]Laboratoire de Physique Corpusculaire de Caen, ENSICAEN/Université de Caen, France
[5]Commissariat à l'Energie Atomique et aux Energies Alternatives, DEN, France
[6]Institut de Physique Hubert Curien-DRS/UdS/CNRS-IN2P3, France
[7]Karlsruhe Institute of Technology, Germany

Abstract

Reactor physics experiments are required for the design of a Fast Spectrum Transmutation Experimental Facility MYRRHA/FASTEF working in subcritical mode and in critical mode. Reactor physics experiments aim to validate a methodology for on-line subcriticality monitoring. For this purpose, building on the former activities accomplished in the previous FP6 project GUINEVERE, investigations on the subcritical VENUS-F (lead/uranium) cores coupled with the GENEPI-3C accelerator will be extended. This activity has been planned in within the framework of the on-going FREYA (Fast Reactor Experiments for hYbrid Applications) FP7 project. This paper presents the current progress of the project and the future plans.

Introduction

Zero-power experiments have always been precursors of the development of a new reactor technology. For accelerator-driven systems (ADSs), such types of experiments were initiated in the FP5 EURATOM project (MUSE programme) [1], where the first coupling of an accelerator to a fast subcritical assembly was studied in more detail. These experiments used a pulsed neutron generator GENEPI-1 that was coupled to a fast sodium core representative of sodium cooled reactors. At the end of the MUSE programme, a first proposal for a methodology for the on-line reactivity monitoring of an ADS was made based on the outcomes of the experimental investigations (a neutron source and a core representative of an ADS). For future experiments, an accelerator working in continuous mode with beam interruptions dedicated to reactivity monitoring will be necessary and the subcritical core should be made of lead instead of sodium, being in this way much more representative for lead-alloy cooled ADSs.

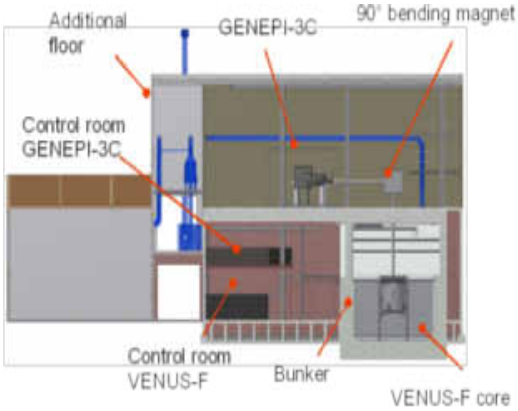
Within the framework of the ECATS (Experimental activities on the Coupling of an Accelerator, a spallation Target and a Subcritical blanket) [2] research domain of the FP6 EUROTRANS integrated project, the GUINEVERE (Generation of Un-interrupted Intense NEutron pulses at the lead VEnus REactor) [3] project was launched in 2006 in line with the conclusions of MUSE. The GUINEVERE project was devoted to the coupling of a flexible GENEPI accelerator, operating in current mode with and without beam interruptions but also in pulsed mode, with a subcritical fast neutron core based on

enriched metal uranium and solid lead. In order to reach this goal, there was a clear need for the construction of a new lead fast zero-power facility as well as for the development of an accelerator with new specifications. The new GENEPI-3C accelerator adds the same specifications as the first GENEPI accelerator in pulsed mode to the possibility of operating in continuous mode with and without interruptions. GENEPI-3C was designed and constructed by a CNRS/IN2P3 collaboration (LPC Caen, IPN Orsay, IPHC Strasbourg and LPSC) and first assembled at LPSC in Grenoble for beam characterisation measurements. It was then disassembled, transferred to SCK•CEN in Mol (Belgium) and finally reassembled in the VENUS reactor built in 2009 to be vertically coupled to the VENUS reactor. The VENUS reactor itself, a zero power, thermal neutron water moderated critical facility up to 2007, was turned into the VENUS-F lead fast reactor. The construction phase of this new facility ended with the completion of the EUROTRANS project (2010). The VENUS-F core was loaded in 2011 after receiving the safety authorisation. The experiments at the critical core (CR0) [4] [5] were carried out and the first subcritical coupling launched the SC1 ($k_{eff} \approx 0.96$) subcritical experiment campaign in October 2011. First, the data obtained for the SC1 reactivity by Pulsed Neutron Source experiments (PNS) were analysed using prompt decay and area analysis methods were compared to the reference reactivity value given by the MSM method [6-8].

Due to the delay of commissioning such a new facility, the GUINEVERE experimental programme could not be completed within the EUROTRANS project and it was achieved within a new project in the FP7. The FREYA (Fast Reactor Experiments for hYbrid Applications) [9] FP7, a five-year project was launched in March 2011 with the following objectives:

- complete the experimental programme for the validation of the methodology for on-line reactivity monitoring initiated within the GUINEVERE project in EUROTRANS;
- conduct the necessary experiments in support of the design and licensing of MYRRHA/FASTEF [10];
- conduct the necessary experiments in support of the design and licensing of lead fast reactors.

Figure 1. VENUS-F reactor coupled to the GENEPI-3C accelerator for the GUINEVERE programme



The investigations concerning the first item will be related to the different subcriticality levels for the nominal operation mode of an ADS. This means that different subcritical configurations with k_{eff} values in the range of 0.95-0.97 will be loaded and investigated with respect to the applicability of the different measurement techniques. Also, specific configurations with a deeper subcritical level of 0.85-0.95 will be investigated to study the determination of the subcriticality level during core loading

operations. In MUSE, the reflector effect has been shown to be of significant influence on specific reactivity monitoring techniques. In order to investigate the robustness of the methodolodgy with regard to the reflector effect, experiments with different reflector materials should be performed. To complete this work, the robustness of the reactivity indicators with regard to the source position, a change of the vertical height of the source target will be investigated to reproduce possible variations of the height of the spallation source in a real ADS. In this way, FREYA will contribute to obtaining a fully validated methodology for on-line reactivity monitoring in an ADS.

On the other hand, given the objectives for MYRRHA/FASTEF to be operated as a subcritical and critical facility, an experimental programme in support of the design and licensing of both these operation modes is needed. Although the experimental programme with regard to the critical mode operation of MYRRHA/FASTEF can generate useful information for the validation of reactor codes for LFR development, a dedicated effort for the validation of reactor codes for LFR developments has been proposed by the LFR community.

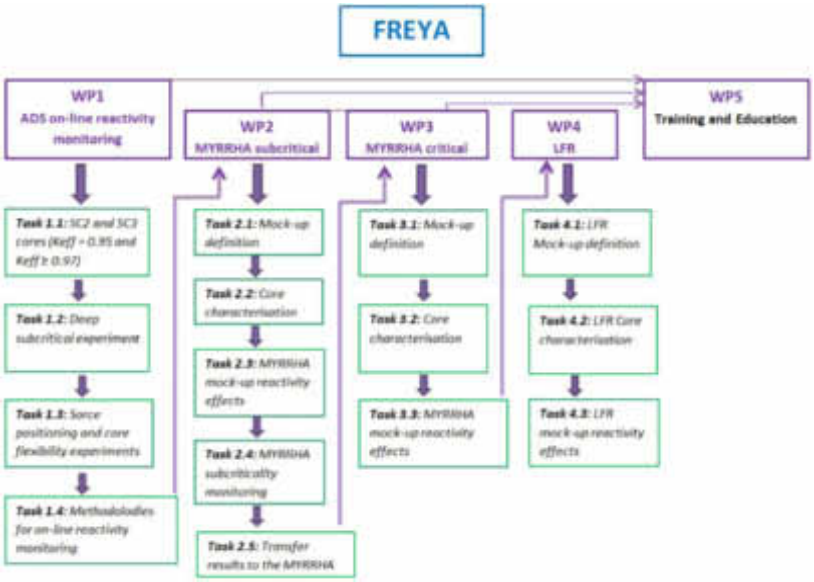
FREYA overall strategy and general description

The FREYA overall work plan includes one co-ordination working package (WP) plus five technical WP's as listed below:

- WP1: ADS on-line reactivity monitoring methodologies;
- WP2: Subcritical configurations for design and licensing of MYRRHA/FASTEF;
- WP3: Critical configurations for design and licensing of MYRRHA/FASTEF;
- WP4: Critical configurations for LFR;
- WP5: Training and education;
- WP6: Co-ordination of the FREYA project.

The working packages and the tasks will be peformed one by one in the same installation with different configurations (see Figure 2).

Figure 2. FREYA working Packages (WP) and tasks



The scope of activity in the technical WPs of the Project is as follows:

WP1: ADS on-line reactivity monitoring methodologies

The purpose of this work package is to extend and finalise the investigations of the subcritical VENUS-F (lead/uranium) core configurations coupled with GENEPI-3C accelerator for the validation of the methodologies for on-line reactivity monitoring of ADS systems. First, besides the SC1 core with k_{eff} = 0.96, foreseen in the GUINEVERE project, two additional configurations (SC2, SC3) for the nominal operation mode of ADS will be investigated with k_{eff} = 0.95 and $k_{eff} \geq 0.97$, respectively. These two variant configurations will be obtained from the SC1 core by changing some fuel assemblies in the peripheral region without other modifications in the reflector or source characteristics. The same type of experiments as in SC1 will be carried out in the SC2 and SC3 cores (MSM, PNS, current-to flux) to obtain a full set of data for the validation of the reactivity monitoring methodology. A study of the alpha-modes theory for the analysis of experiments will be performed to enlarge the possibilities of measurement interpretation. Application of neutron noise methods is also under consideration and a detailed evaluation of such measurements by Monte Carlo simulations is planned.

Moreover, specific configurations with deep subcriticality k_{eff}-values in the range of 0.85-0.95 will be investigated. In these configurations, especially the performance of the PNS area method and the current-to-flux technique will be examined. These situations require further studies to establish the accuracy and methodology of core loading procedures.

Next, this WP1 predicts the investigations of the robustness of measurement techniques with regard to the reflector effect and a change in vertical position of the neutron source. Finally, the results of FREYA WP1 on the ADS reactivity monitoring methods and those obtained during the previous FP5 and FP6 projects (MUSE, EUROTRANS) will be analysed and reviewed and a methodology for on-line reactivity monitoring in ADS with accuracy levels will be obtained.

WP2: Subcritical configuration for the design and licensing of MYRRHA/FASTEFF

Following the objectives for MYRRHA/FASTEF to be operated as a subcritical facility, an experimental programme in support of the design and licensing is necessary.

In this case, a different core configuration other than one of WP1 could be chosen and assembled for the VENUS-F Facility. Within the constraints of available fuels at the VENUS Facility during the FREYA project, this core will be as representative as possible for the MYRRHA/FASTEF core design. The definition and the realisation of this mock-up core at VENUS-F is the first task of WP2.

Then, standard characterisation core measurements will be accomplished. These are axial and radial flux distributions, spectral indices, control rods worth measurements and minor actinide responses by fission chambers. Application of neutron noise methods here is also under consideration and a detailed evaluation of such measurements by Monte Carlo simulations is planned. Different reactivity effects can further be investigated such as void effects, water ingress effects and fuel agglomeration effects. Finally, in this WP, the reactivity effects from the introduction of experimental devices such as in-pile-section (IPS) irradiation equipment, and Na and H_2O loops will be investigated. The IPS has been discussed for the MYRRHA/FASTEF design and will be simulated by the proper materials and then inserted into the proper place of the MYRRHA/FASTEF mock-up subcritical VENUS-F core.

Simulation of all these design peculiarities and the measurement of their reactivity effects on MYRRHA/FASTEF subcritical core will be estimated by recent different calculational tools. C/E comparison will help to reduce the design safety margins and to improve the reliability of the computational tool for the licensing of the design.

Experimental validation of neutronic codes is an essential component in every safety case towards licensing. It can also lead to the optimisation of the core design in an early stage.

WP3: Critical configuration for design and licensing of MYRRHA/FASTEFF

To fulfill the objectives for MYRRHA/FASTEF to be operated as a critical facility, an experimental programme in support of the design and licensing is needed, too. The tasks of this WP3 and the list of experiments required are almost the same as in WP2, but they will be performed in a critical core configuration.

WP4: Critical configuration for LFR

This work package has a strong link with the FP6 project ELSY [11] and the on-going FP7 project LEADER [12] on the development of the lead-cooled fast reactor. A thorough validation of neutronic calculation codes is necessary when constructing and licensing a LFR. The design safety margins should be reduced due to integral validation in zero power mock-ups based on static validation experiments and reactivity effect measurements. The list of experiments needed for the design and licensing support of LFR is almost the same as in WP2 and WP3, but an essential difference in this case will be a different core configuration than in WP1, WP2 and WP3 of the FREYA project, for the VENUS-F Facility.

Within the constraints of available fuels at the VENUS Facility during the FREYA project, this core will be as representative as possible of the LFR core design; fuel/coolant features (volume fraction, fuel enrichment), control rods etc. The description of the LFR core will be resulted from the exchanges of the LEADER project. The definition and the realisation of this mock-up core at VENUS-F is the first task of WP4. Then, standard characterisation core measurements will be accomplished. Different fuel loading patterns will be analysed and characterised according to the different steps in a reloading scheme. The precise determination of flux gradients and subsequent hot temperature points will be of importance.

Different reactivity effects can further be investigated such as void effects, water ingress effects and fuel agglomeration effects.

In the last task of WP4, the results obtained in the other WP4 tasks will be collected and analysed using the same computation tools as for the LFR design. This C/E comparison will help reduce the design safety margins of the LFR and can significantly contribute to the LFR development.

WP5: Training and education

This working package has a strong link with all other FREYA work packages, since it relies on the experience gained during the different WP's for student training and education.

This work package is divided into three separate tasks. The first is devoted to the preparation of the contents of a training session. This laboratory session covers the issues of the experimental methods used for the measurements of the main neutronic parameters for subcritical and critical cores based on the experience gained in WPs 1 to 4 at the VENUS-F Facility in combination with the use of the BR-1 reactor. The second task is dedicated to the implementation of a one-week laboratory session at the SCK•CEN site. The third task is dedicated to the organisation of a dissemination seminar for a wider international audience on the results at the end of the project.

Results achieved

Since the first coupling of VENUS-F to GENEPI-3C (in October 2011) until now, the core configuration has remained the same (SC1, see Figure 3). The authorisation (requiring a royal decree) to change the configuration of the VENUS-F core in order to execute the next tasks of FREYA is expected. But, in spite of this, several subcritical levels of the core were investigated during this period by changing the height of the absorber rods (CRs and SRs).

The following activities were performed:

- installation commissioning phase: from October 2011 to March 2012;
- first FREYA campaign (Task 1.1 of WP1): from April 2012 to June 2012;
- second FREYA campaign (Tasks 1.1 and Task 1.2 of WP1): from September 2012 to December 2012.

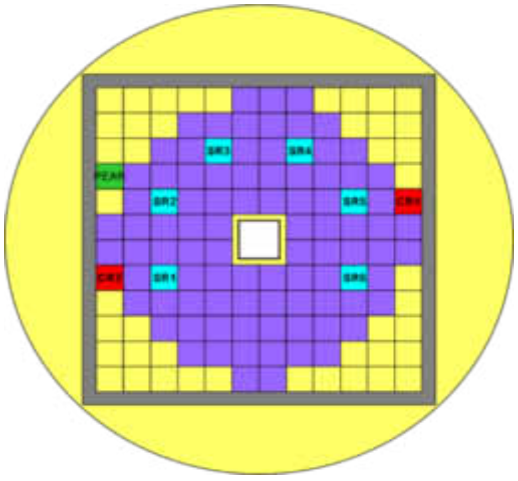
The greater part of the task 1.1 experiments of WP1 were achieved, except for the ones requiring the SC2 and SC3 cores as they could not be changed yet. Essential progress has been made in task 2.1 and task 3.1 (WP2 and WP3, MYRRHA subcritical\critical core definition), by implementing the computational investigations of the MYRRHA representative VENUS-F core and by ordering the proper materials.

The coupling commissioning phase

During the commissioning phase the accelerator worked as:

- a pulsed source to validate the pulsed mode (PM) operation of the GENEPI-3C+VENUS-F coupled system;
- a continuous source to validate the continuous mode (CM) operation and return to power in case of an "unforeseen beam trip" situation (mainly caused by accelerator HV sparks);
- a continuous source with "beam trip" mode (BTM), i.e. with short beam interruptions to commission the BTM piloting module and software of GENEPI-3C.

Figure 3. Cross-section of the SC1 (subcritical) core configuration (93 FA), including safety rods (blue, SR), control rods (red, CR) and accelerator insertion channel (empty central zone)



Legend: violet=FA, yellow=lead, grey=stainless steel.

This commissioning period was necessary to receive the authorisation papers for the facility, for the optimisation and the adjustment of several instrumentation aspects such as:

- beam parameters data acquisition;
- reactor parameters data acquisition;
- efficiency and location of the detectors;
- neutron monitor tunings;
- software (beam current measurement, data acquisition, etc.).

Incidentally, the data recorded during this period were used for preliminary analyses that helped prepare the first FREYA measurement campaign.

The first FREYA campaign

The FREYA experiment programme started on 16 April 2012. The following measurements were fulfilled:

- pulse neutron source (PNS) measurements with optimised detectors;
- control rods worth investigation in CM (by moving the CRs'height step by step);
- source-jerk integral measurements;
- BTM measurements: short beam trip structure (trip duration = 300 µs, repetition rate = 200 Hz).

The second FREYA campaign

The experiments with the same SC1 core were restarted in September 2012:

- long BTM measurements (trip duration = 2 ms, repetition rate = 40 Hz);
- continuous mode measurements;
- current to flux relationship investigation;
- CRs worth investigation (prolongation).

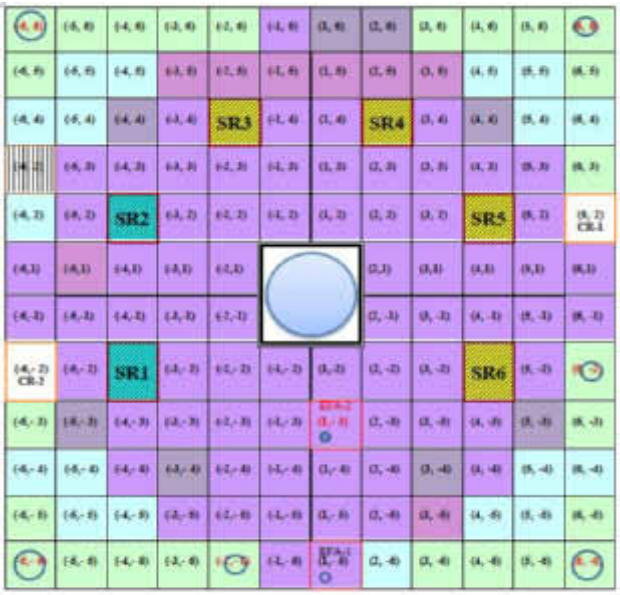
Then, measurements in "deep subcritical" core (task 1.2 of WP1, with k_{eff} around 0.9) were accomplished. Due to a lack of an exploitation license, we had no permission to change the core arrangement. Therefore, we tried to realise the "deep subcritical" core by leaving four safety rods inserted, while the two others were lifted up (Figure 4).

For this deep subcritical core, the following experiments were carried out:

- CM experiments;
- PNS experiments.

These measurements were completed in December 2012 and have recently restarted with the same SC1 configuration until the licence is received.

Figure 4. VENUS-F deep subcritical core with four safety rods inserted



	Amount
- lead assemblies, PbA	43
- FA	87
- standard control rods (CR)	2
- PEAR rod drop IN	1
- safety rods, (SR) OUT	2
- safety rods (SR) IN	4

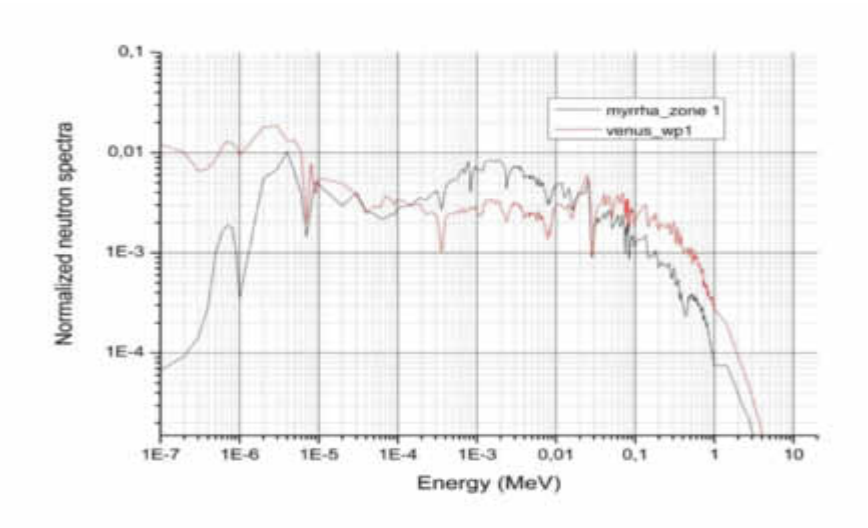
Future work

Task 1.2 (deep subcritical core non-perturbated by SRs with k_{eff} = 0.9) and task 1.3 (source positioning and core flexibility experiments) of the WP1 was expected to be completed in 2013 and then SC2 (k_{eff} =0.95) and SC3 (k_{eff} =0.97) cores were expected to be investigated in 2014. The WP1 programme was scheduled to be completed in March 2014.

The main activities of 2014 were devoted to WP2 experiments (MYRRHA subcritical). For this case, a core configuration different from the one of WP1 will have to be assembled in the VENUS-F Facility. This new core definition, simulating the subcritical configuration of MYRRHA design, planned in task 2.1 of WP2 has already started.

As a metallic U fuel is used in the current VENUS-F core, the neutron energy spectrum is harder than that of MYRRHA with MOX fuel because of the absence of oxygen (see Figure 5). It has been shown that the introduction of oxygen by implementation of Al_2O_3 material in the core, in addition to the use of the available MOX fuel, will make this core configuration closer to the MYRRHA spectrum. In addition, bismuth in combination with lead is expected to be used for the simulation of the MYRRHA coolant (which is settled to be the Pb-Bi euthectic).

Figure 5. MYRRHA neutron spectrum in inner zone compared to that of the present WP1 VENUS-F core



Conclusion

The experimental part of the FREYA project:

- the greater part of the WP1 task 1.1 experiments were completed, except for SC2 and SC3, as the core has not been changed (license expected);
- task 1.2 (deep subcritical) was anticipated to reproduce a deep subcritical core by means of safety rods insertion;
- all experiments requiring a different core (or source) are postponed until after the license is received;
- performing these measurements has allowed valuable experience, so future campaigns will be executed faster;
- a first deliverable (D1.1) containing all the results obtained in the SC1 core (PNS, current-to-flux, source-jerk integral and pulse) was released in January 2013 and an updated version is under preparation;
- a second deliverable (D2.1) concerning the determination of the materials and configuration of the VENUS-F core for simulation of the MYRRHA was released in May 2013.

Acknowledgements

This work was partially supported by the Seventh Framework Programme of the European Commission (EURATOM) through the FREYA contract # 269665. The authors would like to thank the GENEPI-3C accelerator and VENUS reactor technical team for their help and support during the experiment.

References

[1] MUSE collaboration (2005), 5th EURATOM FP-Contract #FIKW-CT-2000-00063. Final Report.

[2] Knebel, J. et al. (2006), "EUROTRANS – European Research programme for the transmutation of high level nuclear waste in an accelerator driven systems", *Proceedings of the International Conference on Research and Training in Reactor Systems (FISA 2006)*, Luxembourg.

[3] Billebaud, A. et al. (2009), "The GUINEVERE Project for Accelerator Driven System Physics," *Proceedings of Global 2009*, Paris, France.

[4] Kochetkov, A., Wagemans, J., Vittiglio, G. (2011), "VENUS-F: a fast lead critical core for benchmarking", *Journal of ASTM International*.

[5] Uyttenhove, W. et al. (2012), "Experimental Results from the VENUS-F Critical Reference State for the GUINEVERE Accelerator Driven System Project", IEEE Transactions on Nuclear Science, 59(6):pp. 3194–3200.

[6] Thyébault, H.E. et al. (2012), "The GUINEVERE Experiment: First PNS Measurements in a Lead Moderated SubCritical Fast Core", *Proceedings of ICAPP '12,* Chicago, USA, 24-28 June, 2012, Paper 12144.

[7] Marie, N. et al. (2013), "Reactivity monitoring using the area method for the subcritical VENUS-F core within the framework of the FREYA project".

[8] Chabod, S. et al. (2013), "Analysis of prompt decay experiments for ADS reactivity monitoring at VENUS-F facility".

[9] Kochetkov, A. (2010), "Fast Reactor Experiments for hYbrid Applications (FREYA)", description European Commission 7th Framework Programme project, technical report.

[10] Abderrahim, H.A. et al. (2008), MYRRHA Technical Description, technical report for the OECD MYRRHA Review Team, SCK•CEN, Belgium.

[11] ELSY Work Program, European Lead Cooled System (ELSY) Project, FP-036439, 6th Framework Program, EURATOM, Management of Radioactive Waste, 2006.

[12] Lead-cooled European Advanced Demonstration Reactor (LEADER) Project, FP-249668, 7th Framework Program, EURATOM, 2010.

Reactivity monitoring using the area method for the subcritical VENUS-F core within the framework of the FREYA Project

N. Marie[1], G. Lehaut[1], J.-L. Lecouey[1], A. Billebaud[2], S. Chabod[2], X. Doligez[3], F.-R. Lecolley[1], A. Kochetkov[4], W. Uyttenhove[4], G. Vittiglio[4], J. Wagemans[4], F. Mellier[5], G. Ban[1], H.-E. Thyébault[2], D. Villamarin[6]

[1]Laboratoire de Physique Corpusculaire de Caen, ENSICAEN/Universite, France
[2]Laboratoire de Physique Subatomique et de Cosmologie, CNRS-IN2P3/UJF/INPG, France
[3]Institut de Physique Nucléaire d'Orsay, CNRS-IN2P3/Universite, Paris Sud, France
[4]Studie Centrum voor Kernenergie-Centre d'Etude de l'Energie Nucléaire, Belgium
[5]Commissariat à l'Energie Atomique et aux Energies Alternatives, France
[6]Centro de Investigationes Energeticas MedioAmbientales y Tecnologicas, Spain

Abstract

Accelerator-driven systems (ADSs) can be employed to incinerate minor actinides and so partly contribute to answering the problem of nuclear waste management. An ADS consists in the coupling of a subcritical fast reactor to a particle accelerator via a heavy material spallation target. The on-line reactivity monitoring of such an ADS is a serious issue regarding its safety.

In order to study the methodology of this monitoring, zero-power experiments were undertaken at the GUINEVERE Facility within the framework of the FP6-IP-EUROTRANS programme. Such experiments have been under completion within the FREYA FP7 project. The GUINEVERE Facility is hosted at the SCK•CEN site in Mol (Belgium). It couples the VENUS-F subcritical fast core with the GENEPI-3C accelerator. The latter delivers a beam of deuterons, which are converted into 14 MeV neutrons via fusion reactions on a tritiated target.

This paper presents one of the investigated methods for ADS on-line reactivity monitoring which has to be validated in the programme of the FREYA project. It describes the results obtained when pulsed neutron source experiments are analysed using the area method in order to estimate the reactivity of a few subcritical configurations of the VENUS-F reactor, around $k_{eff} = 0.96$.

First, the GUINEVERE Facility is described. Then, following general considerations on the area method, the results of its application to the neutron population time decrease spectra measured after a pulse by several fission chambers spread out over the whole reactor are discussed. Finally, the reactivity values extracted are compared with the static reactivity values obtained using the Modified Source Multiplication (MSM) method.

Introduction

Accelerator-driven Systems (ADSs) could be employed to incinerate minor actinides and so partly contribute to answering the problem of nuclear waste management. An ADS consists in the coupling of a subcritical fast reactor to an accelerator whose light ion beam hits a heavy material spallation target immersed inside its lead alloy cooled core in order to provide the extra external neutrons needed to sustain the power delivered by the reactor core. The on-line reactivity monitoring of such an ADS is a serious issue regarding its safety.

In order to study the methodology of this monitoring, zero-power experiments were initiated within the framework of the MUSE programme (FP5) [1] and further developed within the GUINEVERE (Generation of Un-interrupted Intense NEutron pulses at the lead VEnus REactor) project [2] of the FP6-IP-EUROTRANS programme [3]. Such experiments have been under completion within the FP7 FREYA (Fast Reactor Experiments for hYbrid Applications) project [4].

The GUINEVERE Facility is hosted at the SCK•CEN site in Mol (Belgium). It is the result of the coupling of the VENUS-F subcritical fast core, composed of enriched uranium and solid lead, with the GENEPI-3C accelerator delivering a deuteron beam which impinges on a tritium target installed at the reactor core centre. The 14 MeV neutrons produced by the T(d,n) fusion reactions provide the external neutron source. The latter can be operated in a pulsed mode or in a continuous mode with periodic short beam interruptions, referred to as "beam trips".

This paper presents one of the investigated methods for ADS on-line reactivity monitoring which has to be validated in the programme of the FREYA project. It describes the results obtained when pulsed neutron source experiments are analysed using the area method [5] in order to estimate the reactivity of a few subcritical configurations of the VENUS-F reactor, around k_{eff} = 0.96 (a typical configuration among the ones of interest for ADS studies). This technique can be accomplished during core loading and start-up phases of an ADS.

First, the GUINEVERE Facility is described. Then, following general considerations on the area method, the results of its application to the neutron population time decrease spectra measured after a pulse by several fission chambers spread out over the whole reactor are discussed. Finally, the reactivity values extracted are compared to the static reactivity values obtained using the Modified Source Multiplication (MSM) method.

The Guinevere Facility

Initially, the VENUS Facility, located at SCK•CEN, Mol (Belgium), was a critical water-moderated thermal reactor. It was modified to become a fast reactor with highly enriched metal uranium and lead, referred to as VENUS-F (see Figure 1). It can be coupled to an accelerator, GENEPI-3C, which delivers a deuteron beam (at about 220 keV energy), either in a continuous mode (with and without beam interruptions) or in a pulsed mode. The beam impinging on a copper target with a titanium-tritium (TiT) deposit, provides 14 MeV neutrons via T(d,n)^{4}He reactions, right at the centre of the VENUS-F core.

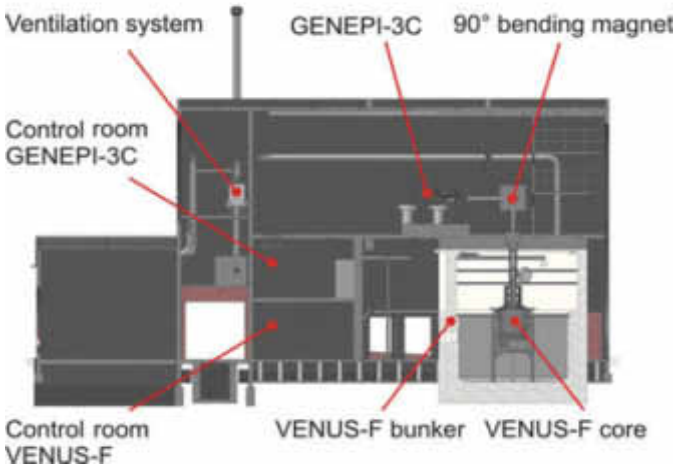
The GENEPI-3C accelerator

In contrast to an industrial ADS, the GUINEVERE neutron source is not provided by high energy spallation reactions but by T(d,n)^{4}He fusion reactions by means of the accelerator GENEPI-3C (GEnérateur de NEutrons Pulsé et Intense) [2]. Built by a collaboration of CNRS-IN2P3 laboratories and first assembled at the Laboratoire de Physique Subatomique et de Cosmologie (Grenoble, France), it accelerates deuteron ions to the energy of 220 keV and guides them onto a tritiated target. In the GUINEVERE Facility, the target is located at the

core mid-plane of the VENUS-F reactor. This source provides a quasi-isotropic field of about 14 MeV neutrons.

This accelerator was designed for the GUINEVERE programme and has dedicated specifications. In pulsed mode, the GENEPI-3C accelerator provides one-microsecond pulses of around 20 mA peak current. The neutron source intensity is around 1-2x10^6 neutrons/pulse in this mode.

Figure 1. Sketch of the GUINEVERE Facility

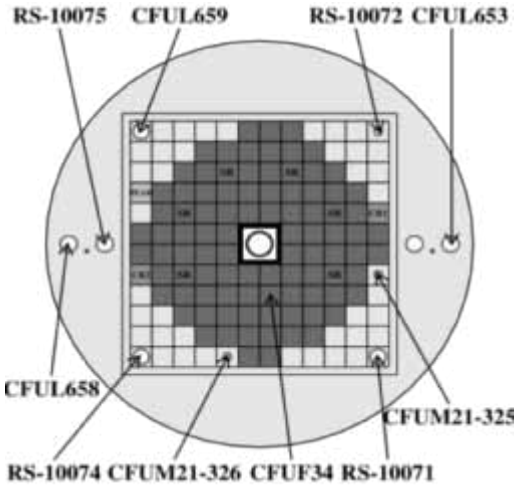


The VENUS-F reactor

The VENUS-F fast zero power reactor is placed in a cylindrical vessel of approximately 80 cm in radius and 140 cm in height. A 12x12 grid surrounded by a 30 mm stainless steel casing can receive up to 144 elements of 8x8 cm^2 in section, which can be fuel assemblies, lead assemblies or specific elements for accommodating detectors or absorbent rods. The remaining room in the vessel is filled with semi-circular lead plates, which act as an outer radial neutron reflector. In addition, the core is reflected by top and bottom 40 cm-thick lead reflectors. Each fuel assembly (FA) consists of a 5x5 pattern filled with 9 fuel rodlets and 16 lead bars surrounded by lead plates. The fuel is 30 wt.% enriched metallic uranium provided by the CEA.

Various configurations of the reactor in terms of reactivity can be studied due to the modular shape of the core. The main configurations of interest are all derived from the SC1 subcritical configuration shown in Figure 2. 93 FAs (dark grey) are arranged in a way to create a pseudo-cylindrical core. Among them, six are actually safety rods (SR) made of boron-carbide with fuel followers with the absorbent part retracted from the core in normal operation. At the core periphery, two boron-carbide control rods (CR, light gray) are used to adjust the reactivity. They can be moved from 0 mm (fully inserted inside the core) to 600 mm (fully retracted). For the SC1 configuration, both CRs are at 479.3 mm. The PEAR (Pellet Absorber Rod) rod (light grey) is used for rod drop experiments. Its reactivity worth is very small (-136±5 pcm [6]) and it can be dropped almost instantaneously (in less than 0.5 second). It is fully inserted when the reactor is in the SC1 configuration. The remaining slots in the 12x12 grid are filled with pure lead assemblies (very light grey).

Figure 2. Cross-sections of the SC1 configuration



SC1 was the first configuration studied in the dynamical reactivity measurement experiments. By moving the two control rods around their initial position, which is 479.3 mm, the other subcritical reactor configurations were obtained. They are named SC1/CR=0 mm and SC1/CR=600 mm.

In order to study the evolution of the neutron population in the reactor after injection of neutron pulses at the core center, ten fission chambers (FC) with ^{235}U deposit were installed in the reactor. Table 1 gathers the detector names and their compositions as well as their deposit masses. For practical issues (presence of the guiding structure of the vertical beam line and, safety and control rod mechanisms) but also owing to experimental requirements (interest for a homogeneous fissile zone without local perturbation) all the detectors except for one were positioned in the reflector, as shown in Figure 2.

Table 1. Detectors used for the PNS experiments

Detector	Deposit	~Mass (mg)
CFUL659	^{235}U (≈92%)	1000
CFUL658	^{235}U (≈92%)	1000
CFUL653	^{235}U (≈92%)	1000
RS-10071	^{235}U (≈90%)	100
RS-10072	^{235}U (≈90%)	100
RS-10074	^{235}U (≈90%)	100
RS-10075	^{235}U (≈90%)	100
CFUF34	^{235}U (≈100%)	1
CFUM21-325	^{235}U (≈90%)	10
CFUM21-326	^{235}U (≈90%)	10

In order to test the performances of the area method for reactivity monitoring, the reactivity of each subcritical configuration was first determined by other experiments using the MSM (Modified Source Multiplication) method [6]. It is a well-established static reactivity measurement technique, which has been extensively and successfully used to

determine large subcriticality levels (up to several dollars). The unknown reactivity is determined by comparing detector count rates driven by an external neutron source in the configuration of interest with those obtained in another subcritical configuration whose reactivity is known [7]. Indeed, SC1 was first obtained from a critical configuration CR0 by removing the four central fuel assemblies (which allow inserting the accelerator beam tube) and by dropping the PEAR rod. A slightly subcritical configuration of known reactivity was created by simply dropping the PEAR rod in the reactor in CR0 configuration. Table 2 shows the results of the MSM experiments. These results will be considered as reference reactivity values and will be used as a benchmark for the area method.

Table 2. Reactivity of the subcritical configurations determined by the MSM method [6]

Configuration	SC1/CR=0mm	SC1	SC1/CR=600mm
Height of control rod 1 (mm)	0	479.3	600
Height of control rod 2 (mm)	0	479.3	600
MSM reactivity ($)	-6.35 ± 0.27	-5.30 ± 0.23	-5.09 ± 0.22

The area method

The principle of the area method

When dealing with Pulsed Neutron Source (PNS) experiments, the area method (also referred to as the Sjöstrand method) [5] allows one to determine in a straightforward way the reactivity (in dollars) of a subcritical nuclear reactor with no input from theoretical calculations, as long as the assumptions of the neutron point kinetics hold in the reactor. This technique is based on the analysis of the time response of detectors placed in the reactor after a source neutron pulse. The evolution of the detector count rates strongly reflects that of the neutron population over time. Indeed, assuming that neutron point kinetics can represent the neutron population evolution over time, the equation of its time decrease after a pulse (considered as a Dirac peak) within the one-delayed neutron group approximation reads:

$$N(t) = N_0\left[\exp\left(\frac{\rho-\beta_{eff}}{\Lambda_{eff}}t\right)+\frac{\bar{\lambda}\Lambda_{eff}\beta_{eff}}{\left(\rho-\beta_{eff}\right)^2}\exp\left(-\frac{\bar{\lambda}\rho}{\rho-\beta_{eff}}t\right)\right] \quad (1)$$

where $\bar{\lambda}$ is the average decay constant obtained by averaging the inverse constants $\frac{1}{\lambda_i}$. In Equation (1), we can distinguish a "fast" component due to prompt neutrons, and a "slow" component, due to delayed neutrons. The integration of the prompt component over time gives the prompt surface A_p:

$$A_p = N_0\frac{\Lambda_{eff}}{-\rho+\beta_{eff}} \quad (2)$$

whereas the integration of the delayed component gives the delayed surface A_d:

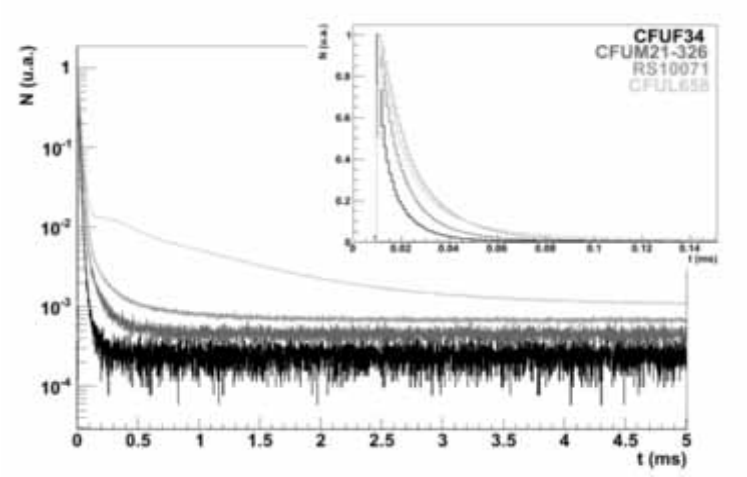
$$A_d = N_0\frac{\beta_{eff}\Lambda_{eff}}{\rho(\rho-\beta_{eff})} \quad (3)$$

Then, the ratio of these two surfaces gives directly the value of the antireactivity in dollars:

$$-\rho_{\$} = \frac{A_p}{A_d} = -\frac{\rho}{\beta_{eff}} \tag{4}$$

Experimentally, for a set of pulses repeated with a fixed frequency, a single Pulsed Neutron Source (PNS) histogram is constructed by summing the fission chamber time responses as a function of the time elapsed after the neutron pulse. The analysis consists in separating in this histogram the prompt neutron contribution from the delayed neutron one. After integrating the time spectrum to get the surfaces Ap and Ad, the antireactivity can be calculated using Equation (4).

Figure 3. Time-dependent PNS histograms obtained with 4 different FCs for the reactor configuration SC1/CR=479.3 mm



Typical PNS histograms

In order to extract the reactivity value of the SC1 and the SC1 variant configurations, the area method was applied to the count rates measured during the PNS experiments by the ten FCs installed in the reactor. When necessary, count rates were corrected for dead time. Figure 3 shows the typical PNS histograms for various detector positions; CFUF34 in the core, CFUM21-326 at the core-reflector interface, RS100-71 in the corner of the 12x12 grid and CFUL658 inside the outer part of the reflector. These histograms were built by adding-up at least one million pulses for a beam frequency of 200 Hz and they are normalised to the same maximum.

Except for the CFUL658, it should be noted that the PNS time spectra have almost the same shapes, which depend on the detector position inside the reactor (they are not homothetic). First, right after the neutron pulse injection, a sharp increase of the fission rates is observed. This delay, before reaching the maximum count rate, is explained by the neutron transport time from the source location all the way to the FC position. Then, the count rates decrease more or less rapidly, depending on the reactor region, within about 1.5 ms. This "fast component" corresponds to the prompt neutron driven decay of the neutron population. It is also observed that the closer to the reflector the FC is, the slower the decay of this fast component. This behaviour might signal the presence of spatial effects, which are not predicted by the point kinetics model. Except for the two detectors located inside the outer lead reflector, beyond 2 ms, a quasi-constant level referred to as the delayed neutron level L_d, is reached. This so-called "slow component" is the sum of the contributions of the delayed neutrons originating from the successive pulses.

Obviously, it should be examined that the neutron precursors have reached equilibrium before analysing the data within the framework of the area method. A study of the delayed neutron level saturation using point kinetics shows that at least 200 000 pulses should be considered. Also, the PNS experiments should not be performed at frequencies larger than about f ≈ 500 Hz. Indeed, above this value, shorter time intervals between pulses would prevent the PNS histogram from reaching the delayed neutron level. As shown in Figure 3, this frequency upper limit becomes lower when a detector farther away from the core is considered.

The constant level of the delayed neutrons L_d is first obtained by calculating the average count rate on a domain ranging from a fixed upper time limit, t_{max}, to a lower time limit, t_{min}. t_{max} is simply the period between two beam pulses. The lower limit t_{min} is chosen in the flat region of the PNS histogram in order to get a good estimate of L_d even for the smaller FC (CFUF34) and in order to maintain the systematic error on L_d around 1% for the FCs having the slowest prompt neutron population decrease. Finally, t_{min} was fixed to $t_{min} = t_{max}$- 0.5 ms. Then:

$$A_d = \int_{t=0}^{t_{max}} L_d dt = \frac{L_d}{f} \tag{5}$$

Introducing A_{tot}, the total number of counts in the PNS histogram, we have:

$$\frac{\rho}{\beta_{eff}} = -\frac{A_p}{A_d} = -\frac{A_{tot} - A_d}{A_d} = 1 - \frac{A_{tot}}{A_d} \tag{6}$$

This relationship is valid only if the neutron intrinsic source originating from the fuel can be neglected. This is the case here, since the fuel is metallic uranium and was never irradiated at high power.

Results

The area method was applied to reaction rates measured by the ten fission chambers during the PNS experiments for the three different subcritical configurations obtained by moving the control rods. Figures 4 and 5 show the results. Reactivity values extracted according to formula (6) are represented by solid dots. The error bars were calculated by taking into account the statistical as well as systematic errors. The horizontal dashed line represents the reactivity of the subcritical configuration as inferred from the MSM method, while the solid horizontal lines show the uncertainty range on the MSM value.

A dispersion of the results seems to depend on the detector location in the reactor. Three groups can be identified. The first one contains only the CFUF34 detector, which is the only one located in the reactor core. It is also the only one from which the reactivity value obtained with the area method is in very good agreement with that of the MSM method. The second group gathers six (RS10074, RS100-71, CFUL659, CFUM326, CFUM325 and RS10072) or even seven (RS10075) detectors, which are located either at the core-reflector interface or in the corners of the 12x12 grid, in the inner part of the reflector. The last detectors (RS10075, CFUL653 and CFUL659) form the third group. They are located rather far away from the core, in the outer part of the reflector, outside the casing. The area method fails to provide the correct value of the reactivity when the FCs are not in the core. The effect seems to be stronger when the detector is farther from the core. In the case of the third group, Figure 3 shows that the neutron population does not decay as predicted by neutron point kinetics. Furthermore, the neutron population does not even reach the delayed neutron level within the time window corresponding to the period between the beam pulses. In these conditions, the area A_d is overestimated, which leads to an underestimation of A_p and the reactivity value extracted is wrong.

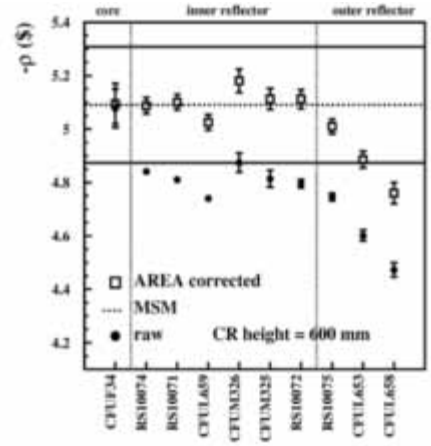
In order to correct for this detector location effect, we now turn to Monte Carlo simulations with MCNP [8]. If the dispersion of the reactivity values given by the area method is due to spatial effects, Monte Carlo simulations of neutron pulses should be used to correct for the dispersion since Monte Carlo simulations transport neutrons without geometric approximations. First, an MCNP input file with a simplified geometry of the VENUS-F reactor was created in order to save computing time and investigate the hypothesis that spatial corrections are not very sensitive to the details of geometry. Second, Monte Carlo correction factors to be applied to the experimental values of reactivity can be calculated for each configuration and each detector location by:

$$f_{area} = \frac{\left(\frac{\rho^c}{\beta^c_{eff}}\right)}{\left(\frac{R^c_p}{R^c_d}\right)} = \left(\frac{\rho^c}{\beta^c_{eff}}\right)\left(\frac{R^c - R^c_p}{R^c_p}\right) \tag{7}$$

where p^c is the reactivity computed with the MCNP model for the considered core configuration of VENUS-F. R^c_d and R^c_p are fission rates at some detector location, due to a Dirac pulse at the core center, associated with delayed neutrons and with prompt neutrons, respectively. Since MCNP cannot calculate the former, the total fission rate R^c is computed and the difference $R^c - R^c_p$ is used instead. β^c_{eff} is the calculated effective delayed neutron fraction associated with the reactor configuration. Since Monte Carlo estimates of β^c_{eff} are very time consuming, this parameter was taken from calculations performed with the deterministic code ERANOS [9] for the same reactor configuration, which gave β^c_{eff} =722 pcm [10]. ρ^c/β^c_{eff} can be regarded as the "true" reactivity value, while R^c_p/R^c_d is the distorted one corresponding to some detector position. If point kinetics would hold everywhere in the VENUS-F reactor, f_{area} would be equal to one. Finally, the corrected reactivity value reads:

$$\rho_{\$} = f_{area} \times \frac{A_p}{A_d} \tag{8}$$

Figure 4. Uncorrected (solid dots) and corrected (open squares) reactivity values extracted from detector counts for the reactor configuration SC1/CR=600 mm



The MSM reference value is the dashed line and its uncertainty range is given by the solid lines.

The corrected values are symbolised by open squares in Figures 4 and 5. For every configuration, as expected, the effect of the correction is negligible for the CFUF34 located inside the core. Except for the fission chambers installed in the outer lead reflector, the corrected values are all compatible with the reactivity given by the MSM method. It is not

surprising that the correction fails for the FCs in the outer reflector, since for these the delayed neutron level could not be reached in the PNS time window given by the 200 Hz frequency of the beam.

Finally, discarding the results obtained for the fission chambers located in the outer part of the reflector, the average corrected value of reactivity was calculated for the three configurations studied. To calculate the uncertainty, it was assumed that the correlations are at maximum between the values given by the detectors. As can be seen in Table 3, the agreement between the MSM reactivity and that given by the area method is remarkable.

Figure 5. Uncorrected (solid dots) and corrected (open squares) reactivity values extracted from detector counts for the reactor configuration SC1/CR=600 mm (case withCR height at 479.3 mm (left) and CR height at 0 mm (right))

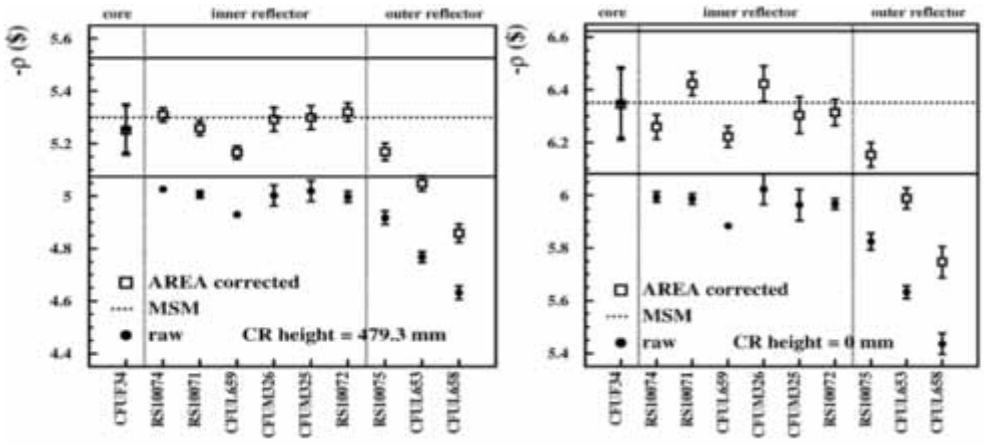


Table 3. Average reactivity value given by the Area method compared with the MSM reference value, for the three reactor configurations studied

CR height (mm)	$\langle\rho\rangle_{\$}^{Area}$	$\langle\rho\rangle_{\$}^{MSM}$
600	-5.09 ± 0.03	-5.09 ± 0.22
479.3	-5.26 ± 0.03	-5.30 ± 0.23
0	-6.31 ± 0.05	-6.35 ± 0.27

Conclusion

This paper presents the reactivity estimates of three different subcritical levels of the VENUS-F reactor extracted from PNS experiments with the area method. First, the technique was applied to count rates measured by ten fission chambers used during PNS experiments driven by the GENEPI-3C deuteron accelerator and performed for three different reactivity levels of the reactor. The dispersion observed among the reactivity estimations inferred from the responses of the detectors spread over the entire reactor volume pointed out that space-energy effects bias the results and that they must be accounted for. Then we exposed the method used to compute, by means of simulations performed with MCNP, correction factors for all the detector positions inside the VENUS-F reactor. Except for two fission chambers located inside the outer lead reflector, all the corrected reactivity values were compatible and in good agreement with the reference values previously estimated with the MSM method.

Acknowledgements

This work was partially supported by the Sixth and Seventh Framework Programmes of the European Commission (EURATOM) through the EUROTRANS-IP contract # FI6W-CT-2005-516520 and FREYA contract # 269665, and the French PACEN programme of CNRS. The authors wish to thank the VENUS reactor and GENEPI-3C accelerator technical team for their help and support during the experiments.

References

[1] MUSE collaboration, 5th EURATOM FP-Contract #FIKW-CT-2000-00063. Final Report (2005).

[2] Billebaud, A. et al. (2009), "The GUINEVERE Project for Accelerator Driven System Physics," *Proceedings of Global 2009*", 6-11 September 2009, Paris, France.

[3] Knebel, J. et al. (2006), "EUROTRANS – European Research programme for the transmutation of high level nuclear waste in an accelerator driven system", *Proceedings of the International Conference on Research and Training in Reactor Systems (FISA 2006)*, Luxembourg.

[4] FREYA, Euratom FP7 contract FP7-269665.

[5] Sjöstrand, N.G. (1956), "Measurement on a subcritical reactor using a pulsed neutron source", Arkiv för fysik, 11, 13.

[6] Lecouey, J.L., in preparation.

[7] Blaise, I.P., F. Mellier, P. Fougeras. (2011), "Application of the Modified Source Multiplication (MSM) Technique to Subcritical Reactivity Worth Measurements in Thermal and Fast Reactor Systems", *IEEE Transactions on Nuclear Science*, 58(3), 1166-1176.

[8] MCNP – A General Monte Carlo N-Particle Code, Version5, LA-ORNL, RSICC LA-UR-03-1987, Los Alamos National Laboratory (2003).

[9] Rimpault, G. (2002), "The ERANOS code and data system for fast neutronic analyses", *PHYSOR 2002*, Seoul, Korea, 7-10 October 2002.

[10] Carta, M. (2011), ENEA, private communication.

Analysis of prompt decay experiments for ADS reactivity monitoring at VENUS-F Facility

S. Chabod[1], X. Doligez[2], G. Lehaut[3], A. Billebaud[1], J.-L. Lecouey[3], F.-R. Lecolley[3], N. Marie[3], A. Kochetkov[4], W. Uyttenhove[4], G. Vittiglio[4], J. Wagemans[4], F. Mellier[5], G. Ban[3], H.-E. Thyébault[1], D. Villamarin[6]

[1]Laboratoire de Physique Subatomique et de Cosmologie, CNRS-IN2P3/UJF/INPG, France
[2]Institut de Physique Nucléaire d'Orsay, CNRS-IN2P3/Universite, Paris Sud, France
[3]Laboratoire de Physique Corpusculaire de Caen, ENSICAEN/Universite de Caen, France
[4]StudieCentrum voor Kernenergie-Centre d'Etude de l'Energie Nucléaire, Belgium
[5]Commissariat à l'Energie Atomique et aux Energies Alternatives, France
[6]Centro de Investigationes Energeticas MedioAmbientales y Tecnologicas, Spain

Abstract

The GUINEVERE (EUROTRANS-IP FP6) and FREYA (FP7) projects address the main issue of ADS reactivity on-line monitoring. The latter aims to validate a methodology that consists in the combination of two approaches: (i) the time monitoring of the reactor power as well as beam intensity (i.e. source intensity), which gives access to the on-line relative fluctuations of the reactivity, p(t), around a reference value; (ii) some calibration measurements, performed regularly, providing an absolute level of p. This absolute level – which may evolve with time too but slower – is used as a reference for on-line relative measurements.

The calibration measurements are based on the analysis of the time decay of the reactor neutron population, N(t), measured during programmed beam interruptions. Different analysis techniques can be applied, but most of them require analysing both prompt and delayed neutron contributions (as the area method, ibid. Marie et al.). Consequently, to give precise results, these techniques require the use of long beam interruptions of several ms durations.

This paper describes the innovative analysis method that relies only on the prompt component of the neutron decay. It can thus be applied to shorter beam interruptions of a few tens of microseconds. The method, called integral k_p method as it allows the determination of the reactor prompt multiplication factor, is applied to the first experimental data taken at SCK•CEN VENUS-F Facility.

Introduction

Research on accelerator-driven systems (ADSs) led to several experimental projects supported by the EURATOM Framework Programmes. One of the main issues investigated is linked to safety. In particular, the property of piloting a reactor due to the accelerator holds only if the core is far enough from criticality. In a powerful core, several phenomena could lead to an increase in reactivity (fuel evolution, Doppler effect). It is then of paramount importance during the operation of an ADS to be able to prove that it remains subcritical in a given margin. The absolute reactivity measurement of a core is, however, not a trivial issue, especially in steady state operation, as the only available observable is the neutron flux (or more exactly fission rates in detectors). Moreover, standard techniques to determine the reactivity of a subcritical core must refer to a critical core, which is not a step foreseen in powerful systems. This issue has been investigated for the last 15 years, which has represented the time scale for preparing and exploiting two fast ADS mock-ups in Europe in dedicated experimental projects. In 2006, the GUINEVERE project joined the EUROTRANS Integrated Project (FP6) to continue with the reactivity monitoring work started in the MUSE project (FP5) at the MASURCA reactor facility (CEA, France). The GUINEVERE (Generator of Uninterrupted Intense NEutron at the lead VEnus REactor) project (2006-2010) consisted first in achieving an innovative lead fast ADS mock-up at the VENUS Facility (SCK•CEN, Belgium), with dedicated neutron source specifications. The exploitation of this mock-up for the reactivity monitoring methodology investigation carries over to the FREYA (Fast Reactor Experiments for hYbrid Applications) project, launched in 2011 in the FP7. The strategy chosen to monitor a subcritical core reactivity combines two approaches: (i) the on-line monitoring of the relative fluctuations of the reactivity $\rho(t)$, due to the measurement of the ratio of the beam intensity to the reactor power; (ii) some calibration measurements, performed regularly, providing an absolute level of ρ. These absolute or calibration measurements are performed during beam interruptions and are based on the analysis of the time decay of the reactor neutron population, $N(t)$. This paper focuses on the prompt decay part of $N(t)$ and presents a method to determine the prompt multiplication factor k_p, from which the k_{eff} can be inferred. The method is applied to Pulsed Neutron Source (PNS) measurements.

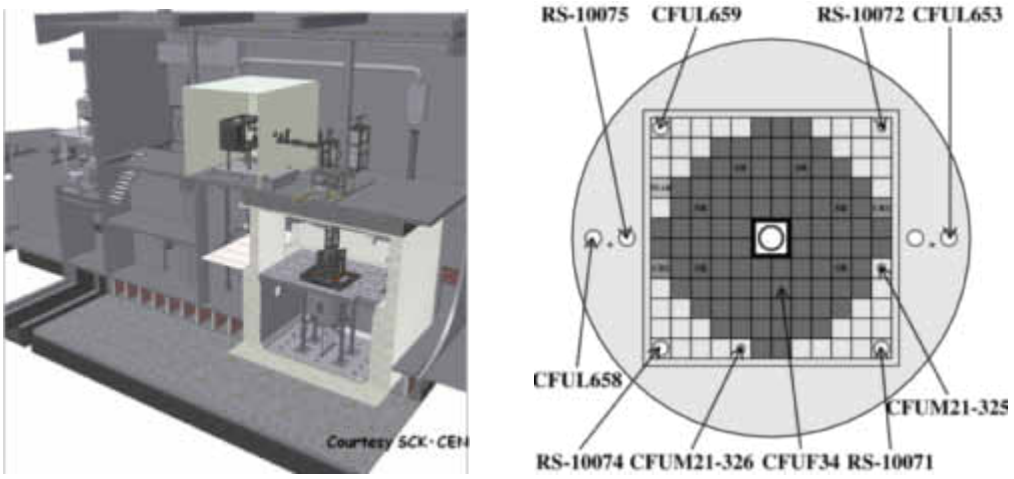
The VENUS-F Facility

The VENUS-F Facility (see Figure 1) is a zero power ADS mock-up and consists in the vertical coupling of the VENUS reactor (SCK•CEN, Mol, Belgium) with a deuteron accelerator GENEPI-3C. The deuteron ions are accelerated (220 keV) onto a tritiated target located at the reactor core centre, creating neutrons by $T(d,n)^4He$ reactions. The time structure of the beam is one of three different modes: the pulsed mode (20 mA peak current over 1 µs, with a repetition rate bounded by 10 Hz and 4 kHz), the continuous mode (with an intensity bounded by 100 µA and 1 mA), and the beam trip mode where beam interruptions (300 µs to a few ms) are made at a low frequency (a few tens to a few hundreds of Hz) in the continuous beam.

For the subcritical experiments in the FEYA project, the VENUS-F reactor is loaded with 93 square fuel assemblies (FA) arranged in a cylindrical geometry, composed of 30% ^{235}U enriched metallic uranium (provided by CEA) and solid lead rodlets that mimic a fast system coolant. The fissile zone is surrounded axially and radially by a lead reflector. For mechanical reasons, the 12x12 assemblies are placed into a square stainless steel casing. The reactor is equipped with six safety rods (SF) with fuel followers, two control rods (CR) and one absorbent rod for rod drop experiments. The ending part of the accelerator is inserted into the core in a central hole corresponding to the size of 4 fuel assemblies. This subcritical configuration, with the CRs at a height of 479.3 mm and the absorbent rod inserted is called “SC1” level. The CRs' height is the one giving a critical core when the four central FAs are added and the absorbent rod is withdrawn. Figure 1 shows the cross-

section view of the SC1 core. More details on the VENUS-F Facility are found in [1]. The reactivity value of the SC1 core was found to be equal to –5.3 ± 0.23 $ by the MSM method [2].

Figure 1. The VENUS-F Facility (SCK•CEN, Mol, B); (left) the subcritical core SC1 (cross-section) with detector locations (right)



Pulsed neutron source measurements

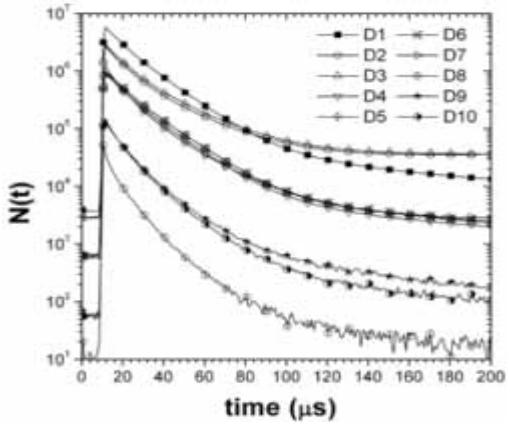
Measurements in the core consist in fission rate measurements performed with ten ^{235}U fission chambers having different efficiencies. Table 1 summarises the different types of detectors and their associated fissile deposits. Most of them are located in the reactor reflector, some of them being inside the casing (inner reflector) and a few of them being outside (outer reflector), as shown in Figure 1 (right). One fission chamber is placed inside the core part composed of FAs. The pulsed neutron source measurements are performed with the accelerator in pulsed mode, at 200 Hz and in the SC1 configuration described above. The neutron source shape is close to a Gaussian with a FWHM of the order of 500 ns.

Table 1. Detector specifications

Name	Type	Location	Deposit (content)	Approximate mass (mg)
D1	CFUL659	Inner reflector	^{235}U (~92%)	1000
D2	CFUL658	Outer reflector	^{235}U (~92%)	1000
D3	CFUL653	Outer reflector	^{235}U (~92%)	1000
D4	RS-10072	Inner reflector	^{235}U (~90%)	100
D5	RS-10071	Inner reflector	^{235}U (~90%)	100
D6	RS-10074	Inner reflector	^{235}U (~90%)	100
D7	RS-10075	Outer reflector	^{235}U (~90%)	100
D8	CFUF34	Fuel	^{235}U (100%)	1
D9	CFUM326	Inner reflector	^{235}U (~90%)	10
D10	CFUM325	Inner reflector	^{235}U (~90%)	10

Fission events are time stamped with a resolution of 20 ns by the GANDDALF data acquisition system designed for this programme. The neutron source intensity is of the order of 10^6 neutrons per pulse. The time spectra obtained for each pulse are added and Figure 2 shows the final time spectra obtained for 8.36×10^6 neutron pulses for the ten detectors. At first glance, the different detector efficiencies can be seen and curve shapes gather as a function of detector locations.

Figure 2. Raw pulsed neutron source measurements obtained at 200 Hz in SC1 configuration



Description of the k_p method

Number of neutrons born at time t into a subcritical reactor

Let us suppose we inject a number, $S(t)$, of source neutrons at time $t \geq 0$ into a subcritical reactor. These neutrons, of generation 0, will propagate throughout the medium and, a fraction of them will induce fissions. The neutrons of generation 1, released by these first fissions, in turn, induce new fissions, initiating a fission chain that ultimately dampens due to system subcriticality. The number, $N_{n+1}(t)$, of neutrons of generation n+1 born at time t in the reactor can be related to the number, $N_n(t)$, of neutrons of generation n through a simple equation:

$$N_{n+1}(t) = k_p (P \otimes N_n)(t) = k_p \int_{\tau=0}^{t} N_n(t-\tau) P(\tau) d\tau, \quad \int_{\tau=0}^{+\infty} P(\tau) d\tau = 1 \cdot \tag{1}$$

In (1), symbol $\otimes$ stands for the convolution product, k_p is the prompt multiplication factor. Function $P(\tau)$ is the intergeneration time distribution, i.e. the probability density that a newly born neutron induces a fission after time τ. This study shows that the distribution $P(\tau)$ is independent of the generation number.

We intend to calculate the number, $N(t)$, of neutrons that are generated in the reactor at time t by fissions. This number is given by the sum of all neutron generations: $N(t) = N_0(t) + N_1(t) + \ldots + N_n(t) +$ etc. Thus, using relation (1) and observing that $N_0(t) = S(t)$, an equation is obtained that governs the time evolution of the neutron population $N(t)$:

$$N(t) = S(t) + k_p (P \otimes N)(t) \cdot \tag{2}$$

In this study, the neutron source pulse $S(t)$ is modelled by a Gaussian. Using Laplace transform, that transforms a convolution product into an algebraic one, we can reformulate (2):

$$L(N) = \frac{L(S)}{1 - k_p L(P)}, \quad L(f) = \int_{t=0}^{+\infty} e^{-pt} f(t) dt, \quad L(f \otimes g) = L(f) L(g). \tag{3}$$

An analytical solution of (3) can be obtained, which reads:

$$N(t) = S(t) + k_p (P \otimes S)(t) + k_p^2 (P \otimes P \otimes S)(t) + k_p^3 (P \otimes P \otimes P \otimes S)(t) + \ldots. \tag{4}$$

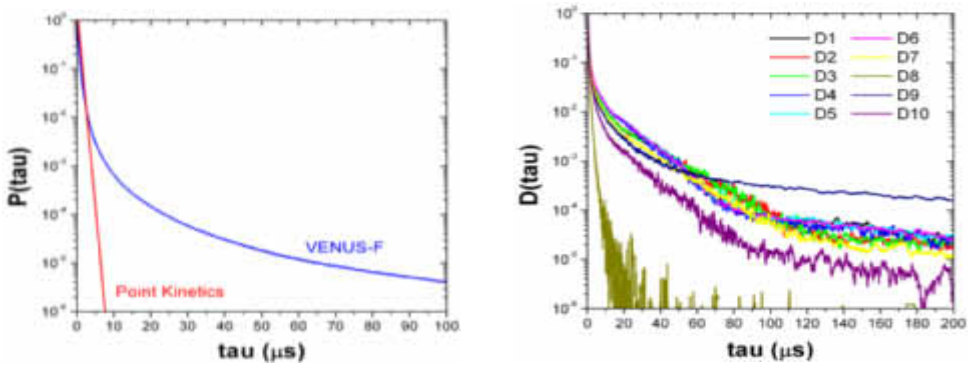
With a good knowledge of the intergeneration time distribution, $P(\tau)$, by using the integral equation (2) it is possible to calculate numerically the time evolution of the number, $N(t)$, of neutrons born at time t in a subcritical reactor.

The intergeneration time distribution P(τ)

The $P(\tau)$ distribution can be computed using the MCNP transport code in a KCODE mode [3]. The results obtained for VENUS-F reactor are presented in Figure 3 (left), alongside with an analytical distribution, $P_{PK}(\tau) = \exp(-\tau/\Lambda)/\Lambda$. The $P_{PK}(\tau)$ curve is the intergeneration time distribution obtained for the point kinetics hypothesis. Number Λ is the mean time elapsed between two fissions, equal to 0.5 μs in VENUS-F. As shown in Figure 3, the point kinetics hypothesis is unable to reproduce the VENUS-F $P(\tau)$ shape, more specifically, its tail at large times. This tail is due to the VENUS-F lead reflector and concrete, which act as pools returning moderated neutrons back to the fissile core after several tens of μs.

For a given reactor, we indicate that the distribution $P(\tau)$ is insensitive to: (i) reasonable changes in reactivity. Indeed, the differences between two $P(\tau)$ curves computed for k_{eff} = 0.964 and 0.994 are negligible; (ii) choice of the nuclear cross-sections database; (iii) reasonable changes in core geometry [4] [5]. The insensitivity of the $P(\tau)$ function to these changes is a cornerstone of the k_p method. Therefore, by computing a single $P(\tau)$ distribution and by folding it using (4), we can simulate the prompt decays occurring in a reactor for a large range of k_p configurations.

Figure 3. Distribution $P(\tau)$ obtained for the VENUS-F reactor compared with the predictions of point kinetics (left) and distributions $D(\tau)$ obtained for the D1 to D10 detectors (right)



Number of events, M(t), detected at time t in a fission chamber

In our experiment, however, the physical observable is not the number $N(t)$ of fissions occurring in the reactor, but the number of counts measured in several fission chambers positioned inside the VENUS-F core and reflector (see Figure 1). The theoretical number of counts, $M_{th}(t)$, recorded at time t in a detector can be related to the neutron population, $N(t)$, by introducing a new distribution called $D(\tau)$. Function $D(\tau)$ is the distribution of times elapsed between a fission occurring in the reactor and a fission occurring in the fissile deposit of the considered detector. Omitting the detector efficiency we have:

$$M_{th}(t) = (D \otimes N)(t). \tag{5}$$

Distribution $D(\tau)$ accounts for the transport of neutrons from the coordinates of fissions to the detector position. As a result: (i) the distribution $D(\tau)$ is more sensitive than the $P(\tau)$ distribution to the reactor geometry and composition; (ii) to obtain $D(\tau)$ with sufficient statistics, more computer resources are required than what is needed to compute $P(\tau)$. For both reasons and according to MUSE conclusions, it is recommended to apply the k_p method preferentially to threshold detectors, such as fission chambers with ^{237}Np or pure ^{238}U deposits. For a threshold detector, the $D(\tau)$ function does reduce to a Dirac, $\delta(\tau)$, since the time needed to transport MeV neutrons along a distance of about 1 m is negligible compared to the prompt decay time. Easing the need for $D(\tau)$ calculation facilitates the comparison of experimental to theoretical data.

Unfortunately, it is very difficult to get threshold fission chambers with an efficiency adapted to a zero power experiment. For these experiments, only conventional ^{235}U fission detectors were used that are sensitive to low-energy neutrons and thus to the details of the neutron trajectories. In turn, the $D(\tau)$ distributions were computed by MCNP [3]. Figure 3 presents the results for the detectors used in VENUS-F reactor.

Extraction of the k_p factor

By computing the distributions $P(\tau)$ and $D(\tau)$, then by using the theoretical background summarised in Equations (2) and (5), it is possible to simulate the time evolutions, $M_{th}(t,k_p)$, of the count rates measured by our detectors, as a function of two parameters: (i) time t; and (ii) the prompt multiplication factor k_p. By comparing this theoretical data with the experimental ones, $M_{exp}(t)$, we can infer the k_p value for the SC1 configuration.

Improvement of the k_p method

New methodology to compare the theoretical and experimental results $M_{th}(t, k_p)$ and $M_{exp}(t)$

As they have neither the same normalisation nor the same starting times, the theoretical and experimental count rates, $M_{th}(t, k_p)$ and $M_{exp}(t)$, cannot be directly compared. In the classical approach of the k_p method, this comparison is undertaken by calculating and then by comparing their logarithmic time derivatives [4] [5]. However, this approach is highly sensitive to the statistical fluctuations occurring in the experimental $M_{exp}(t)$ curves, fluctuations that, in turn, induce large fluctuations on the $M_{exp}(t)$ logarithmic derivatives [6]. To circumvent this issue, we propose a novel estimator, $W(t)$, which relies on the integration of the $M(t)$ curves rather than on their derivation, since an integral is more continuous than a derivative. This estimator is one of the simplest, self-normalised, integral estimators that can be chosen, and is defined by:

$$W(t) = \int_{t'=t_{\min}}^{t} M^2(t')dt' \Bigg/ \left(\int_{t'=t_{\min}}^{t} M(t')dt' \right)^2. \tag{6}$$

In (6), time t_{min} is a cut-off, used to reject the first 10 μs of the theoretical and experimental curves, sensitive to issues such as: (i) the source time shape, which is not perfectly Gaussian; (ii) the dead time effects, corrected in our study, but minor errors can still occur; (iii) the weight of the first generations of neutrons whose intergeneration time distributions are not strictly equal to $P(\tau)$; (iv) numerical transients: as the distribution $P(\tau)$ is given in the form of a histogram, it should be noted that the integral Equation (2), which governs the time evolution of the neutron population is mathematically equivalent to the equation giving the neutron flux in an infinite medium where the moderation is due to elastic collisions. The solution of (2) thus exhibits a short and artificial transient, identical to Placzek's one [7], during the first μs, which must be discarded.

Statistical errors on the theoretical and experimental estimators, $W_{th}(t)$ and $W_{exp}(t)$, respectively coming from: (theory) the MCNP statistical fluctuations on $P(\tau)$ and $D(\tau)$ histograms; (experiment) the statistics of the detector count rates, can be computed using a Monte-Carlo procedure (Gaussian sampling within the error bars). As the W(t) fluctuations were proven to be normally distributed, we can use a χ^2 test to compare the theoretical and experimental data in order to determine the value of the prompt multiplication factor k_p:

$$\left(\chi^2/n\right)\left(k_p\right) = \frac{1}{N-1}\sum_{i=1}^{N}\frac{\left(W_{\exp}\left(t_i\right) - W_{th}\left(t_i, k_p\right)\right)^2}{\varepsilon_{W_{\exp}}\left(t_i\right)^2 + \varepsilon_{W_{th}}\left(t_i, k_p\right)^2} \tag{7}$$

where N is the number of points, t_i, used to compare the $W_{th}(t,k_p)$ and $W_{exp}(t)$ data. Functions $\varepsilon_W(t)$ are the error bars on W(t). We did not have enough time to compute the theoretical errors, $\varepsilon_{Wth}(t,k_p)$, for each $M_{th}(t,k_p)$ curve, since the Monte-Carlo procedure requires large numbers of computer resources. Thus, these should be omitted.

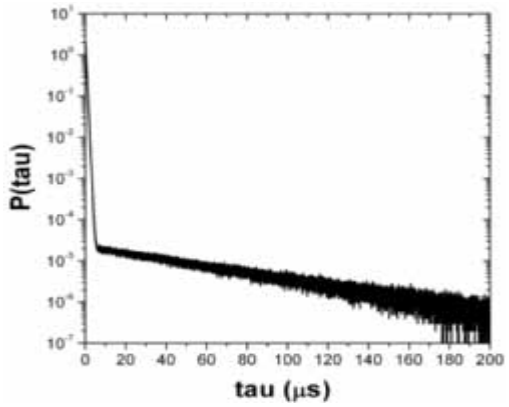
Blind test of the analysis methodology

A blind test was performed to investigate: (i) the precision of the numerical procedure used to solve the integral Equation (2); (ii) the ability of the integral estimator, W(t), to constrain the k_p value at the 100 pcm level. We considered a distribution $P_{test}(\tau)$ given by the sum of two exponentials of different characteristic times: a short one to model a fissile core, a longer one to model the influence of a reflector:

$$P_{test}\left(\tau\right) = Ae^{-\alpha\tau} + Be^{-\beta\tau}, \quad L\left(P_{test}\right) = \frac{A}{p+\alpha} + \frac{B}{p+\beta} \tag{8}$$

with A = 2.4 μs^{-1}, B = 2.2×10^{-5} μs, α = 2.4 μs^{-1}, β = 1.8×10^{-2} μs. Parameters A, B, α, β were chosen: (i) to mimic the long tail of the VENUS-F $P(\tau)$ distribution, (see Figure 3); (ii) to obtain a mean intergeneration time, Λ, similar to the 0.5 μs of VENUS-F; (iii) to preserve the normalisation of $P_{test}(\tau)$. We then transformed the distribution $P_{test}(\tau)$ into a histogram and artificially noised it to mimic the statistical fluctuations observed on MCNP simulations. Figure 4 shows the resulting curve. Finally, we numerically solved the integral Equations (2) and (5), for k_p factors ranging from 0.949 to 0.951 by steps of 10 pcm, to create a set of theoretical count rates, $M_{th}(t,k_p)$, for a threshold detector (reminder: $D(\tau) = \delta(\tau)$ for a threshold detector).

Figure 4. Simplified intergeneration time distribution, $P_{test}(\tau)$, used for the methodology blind test



In a second step, we generated a set of pseudo-experimental data. For an instantaneous source pulse, $S(t) = \delta(t)$, the time evolution of the count rate in a threshold detector obeys:

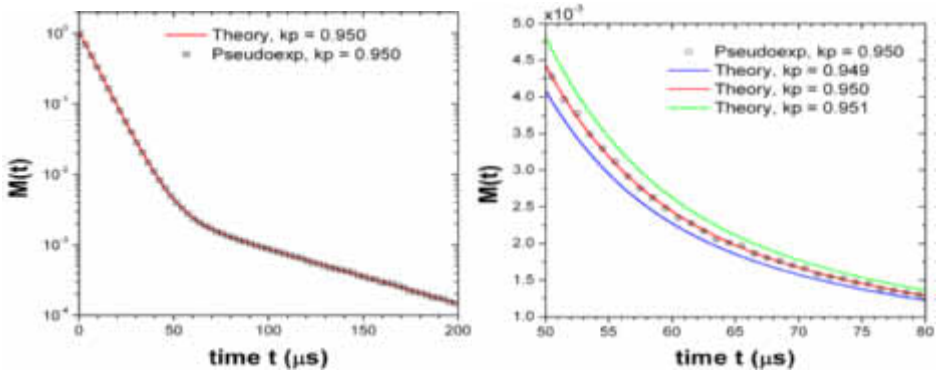
$$L(M) = \frac{L(D)L(S)}{1 - k_p L(P)} = \frac{1}{1 - k_p L(P)} . \tag{9}$$

Using expression (8), transforming the ratio $1/(1–k_pL(P))$ into a sum of partial fractions, then inverting the Laplace transform leads to the detector count rate:

$$\begin{aligned} &M(t) = \delta(t) + K_1 e^{p_1 t} + K_2 e^{p_2 t} \\ &p_1 = \frac{1}{2}\left[k_P(A+B) - (\alpha+\beta) + \gamma\right], \quad p_2 = \frac{1}{2}\left[k_P(A+B) - (\alpha+\beta) - \gamma\right] \\ &K_1 = (p_1+\alpha)(p_1+\beta)/\gamma , \quad K_2 = -(p_2+\alpha)(p_2+\beta)/\gamma \\ &\gamma = \sqrt{(A+B)^2 k_P^2 - 2(A-B)(\alpha-\beta)k_P + (\alpha-\beta)^2} \end{aligned} \tag{10}$$

It should be noted that a double-exponential intergeneration time distribution leads to a neutron population varying as a double-exponential. The computation of the characteristic times, $1/p_1$ and $1/p_2$, as a function of k_p gives interesting results. For instance, $p_1 \to 0$ when $k_p \to 1$; the double-exponential behaviour of $N(t)$ vanishes when the reactor approaches criticality. The set of pseudo-experimental data was thus generated using expression (10) for $k_p = 0.95$. The $M_{exp}(t)$ curve was transformed into a histogram and noised to reproduce the statistical fluctuations observed on VENUS-F detectors. Figure 5 shows the $M_{exp}(t)$ curve along with the theoretical curve $M_{th}(t, k_p = 0.95)$.

Figure 5. Pseudo-experimental count rates (dots), $M_{exp}(t)$, obtained for $k_p = 0.95$, compared to theoretical results (lines), $M_{th}(t, k_p = 0.949–0.951)$, obtained by folding the noised distribution $P_{test}(\tau)$

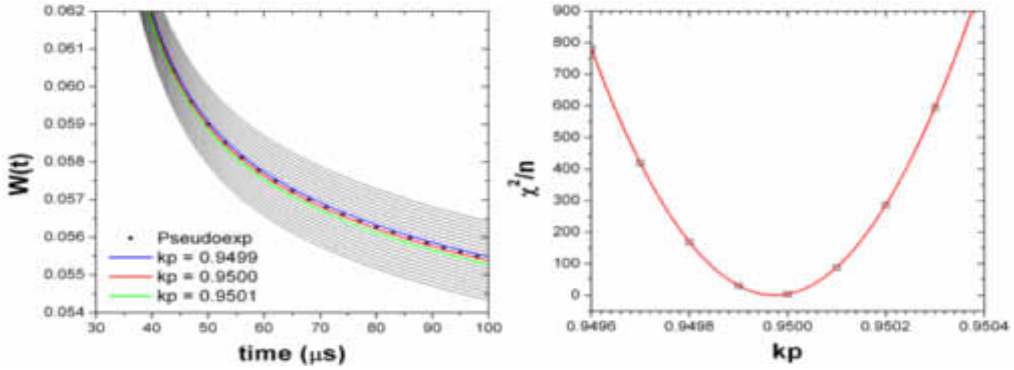


Finally, we computed the theoretical and experimental estimators $W_{th}(t,k_p)$ and $W_{exp}(t)$. The statistical fluctuations on the $P_{test}(\tau)$ and $M_{exp}(t)$ curves were propagated using a Monte-Carlo method (Gaussian sampling within the error bars) to obtain the error bars on W_{th} and W_{exp}. The $W_{th}(t,k_p)$ and $W_{exp}(t)$ curves are shown in Figure 6 (left). We then used a χ^2 test to compare the theoretical and experimental data. The evolution of the reduced χ^2, given in (7), as a function of k_p is shown in Figure 6 (right). Despite the large statistical fluctuations generated on $P_{test}(\tau)$ and $M_{exp}(t)$, the χ^2 analysis leads to a precise value of k_p, equal to 0.949974 ± 1.4 pcm. This result is compatible with the value, $k_p = 0.95$, used to generate the pseudo-experimental set of data.

The blind test thus gives two important results: (i) the numerical errors, resulting from the numerical resolution of equation (2), are responsible for a systematic error on k_p lower than 5 pcm. This is affordable; (ii) even when the $M_{th}(t,k_p)$ and $M_{exp}(t)$ curves are plagued by large statistical fluctuations, the estimator $W(t)$ has a resolution power high

enough to separate k_p values differing from each other by less than 5 pcm. With these conclusions, the analysis methodology is validated.

Figure 6. Experimental estimator $W_{exp}(t)$ (dots) and theoretical estimators $W_{th}(t,k_p)$ (lines) as a function of time (left)



The theoretical curves $W_{th}(t,k_p)$ are calculated for k_p values ranging from 0.949 to 0.951 by 10 pcm steps; (right) evolution of the reduced χ^2 (7) as a function of k_p.

Analysis of VENUS-F experimental data and conclusions

The methodology detailed in this work is applied to the PNS measurements described above. The time spectra are corrected for dead time effects. The delayed neutron component, assumed constant over the few tens of μs after the pulse, is subtracted. The experimental estimators, $W_{exp}(t)$, are compared with arrays of theoretical estimators, $W_{th}(t,k_p)$, computed for k_p values ranging from 0.93 to 0.97 by steps of 50 pcm. The reduced χ^2, (7), are calculated for each detector as a function of the prompt multiplication factor, k_p, and the time, T, elapsed since the neutron pulse injection. Figure 7 shows their contour plots for three representative detectors. For each detector, the k_p value and its error bar are given by the width of the $\chi^2 \leq \chi^2_{min}+1$ area. The k_p to k_{eff} correspondence is performed with the relation $k_{eff} = k_p/(1-\beta_{eff})$, using a β_{eff} value of 722 pcm calculated with ERANOS [8]. Finally, the reactivities ρ obtained for the detectors D1 to D10 are gathered in Table 2 and in Figure 8. Except for D2 and D3 detectors, the preliminary results obtained with the improved k_p method are compatible with the reference MSM value, calculated in [2]. The D2 and D3 detectors are located outside the core casing, in an area that is, to date, not correctly simulated. D2 and D3 mitigated results emphasise the need for threshold fissile deposits when the detectors have to be positioned far away from the core, as they are more sensitive to the modelling of neutron transport.

Figure 7. Contour plots of the reduced χ^2 as a function of k_p and T, time elapsed since the neutron pulse, for three representative detectors: D8 (in fuel), D1 (inner reflector), D2 (outer reflector)

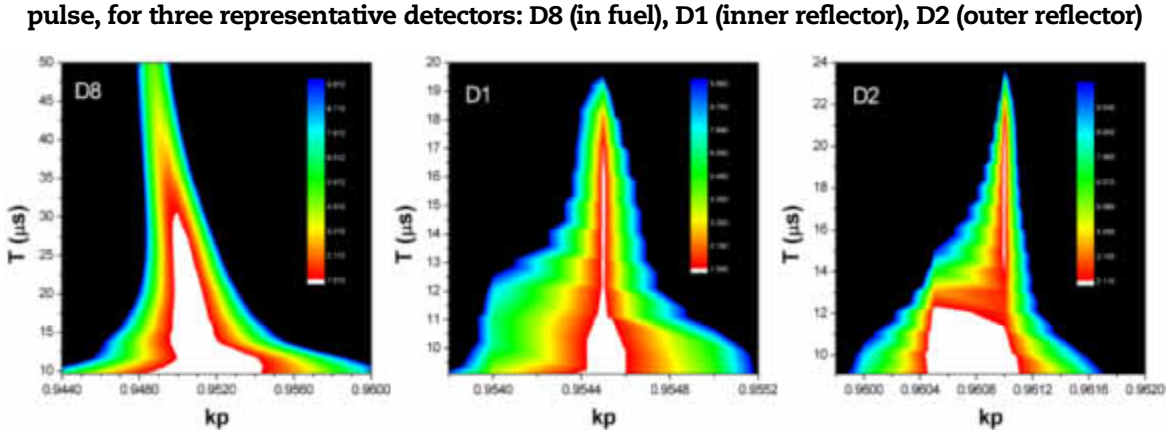
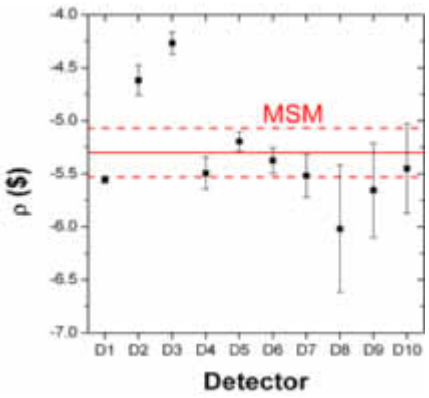


Figure 8. Reactivities obtained with the improved method for the ten detectors used at VENUS-F Facility (squares)



The results are compared with the MSM value (horizontal solid line) and its uncertainty (dashed lines).

Table 2. Preliminary results of the improved k_p method applied to the PNS experiments performed at the VENUS-F reactor

Detector	k_p	k_{eff}	$-\rho$, in $
D1	0.9543 – 0.9547	0.9612 – 0.9616	5.52 – 5.58
D2	0.9598 – 0.9617	0.9668 – 0.9687	4.48 – 4.76
D3	0.9624 – 0.9638	0.9694 – 0.9708	4.16 – 4.37
D4	0.9539 – 0.9559	0.9608 – 0.9629	5.34 – 5.65
D5	0.9563 – 0.9575	0.9633 – 0.9645	5.10 – 5.28
D6	0.9549 – 0.9565	0.9618 – 0.9635	5.25 – 5.49
D7	0.9534 – 0.9561	0.9603 – 0.9631	5.31 – 5.72
D8	0.9475 – 0.9554	0.9544 – 0.9624	5.42 – 6.62
D9	0.9509 – 0.9568	0.9578 – 0.9638	5.21 – 6.10
D10	0.9524 – 0.9580	0.9593 – 0.9650	5.03 – 5.87
MSM			5.30 ± 0.23

The last line gives the reference MSM result [2].

Acknowledgements

This work was partially supported by the Sixth and Seventh Framework Programmes of the European Commission (EURATOM) through the EUROTRANS-IP contract # FI6W-CT-2005-516520 and FREYA contract # 269665, and the French PACEN programme of CNRS. The authors wish to thank the VENUS reactor and GENEPI-3C accelerator technical team for their help and support during the experiments.

References

[1] Billebaud, A. et al. (2009), "The GUINEVERE Project for Accelerator Driven System Physics", *Proceedings of Global 2009*, Paris, France.

[2] Lecouey, J.-L. et al. (2013), IEEE Trans. Nucl. Science 58 3 (2011) 1166-1176.

[3] MCNP - A General Monte Carlo N-Particle Code, Version 5, LA-ORNL, RSICC, LA-UR-03-1987, Los Alamos National Laboratory (2003).

[4] Perdu, F. et al. (2003), *Prog. in Nucl. Energy*, 42 (2003) 107.

[5] Vollaire, J. (2004), "L'expérience MUSE-4: Mesure des paramètres cinétiques d'un système sous-critique", PhD thesis, Grenoble INP.

[6] Thyébault, H.E. et al. (2012), "The GUINEVERE Experiment: first PNS measurements in a lead moderated sub-critical fast core", *Proceedings of International Congress on the Advances in Nuclear Power Plants (ICAPP'12)*, 24-28 June 2012, Chicago, US.

[7] Placzek, G. (1946), *Phys. Rev*. 69. 423.

[8] Carta, M. (2011), ENEA, private communication.

Forthcoming experiments on accelerator-driven systems with 100 MeV protons at the Kyoto University Critical Assembly

Cheol Ho Pyeon, Takahiro Yagi, Yoshiyuki Takahashi, Tadafumi Sano, Hiroshi Shiga
Research Reactor Institute, Kyoto University, Japan

Abstract

At the Kyoto University Critical Assembly, a series of uranium-loaded accelerator-driven system (ADS) experiments are planned to be carried out to conduct the conversion analysis of capture and fission reactions to investigate the uncertainties of cross-section data of minor actinides (MAs) in the case of the variation of the subcriticality, the external neutron source and the neutron spectrum. Then, the uranium-loaded ADS experiments with 100 MeV protons could be conducted using the Pb-Bi-zoned region to examine the feasibility of the nuclear transmutation by ADS, including ^{237}Np and ^{241}Am. Also, another conversion analysis of ^{232}Th capture and ^{233}U fission reactions is expected to investigate the reaction rate characteristics in ADS when subcriticality, neutron spectrum and external neutron source are varied in the subcritical system.

Introduction

The experimental studies on the accelerator-driven systems (ADSs) are being conducted with the combination of the Kyoto University Critical Assembly (KUCA) [1]-[6] and the fixed-field alternating gradient (FFAG) accelerator [7]-[9] at the Kyoto University Research Reactor Institute. The spallation neutrons generated by 100 MeV proton beams from the FFAG accelerator were injected into not only the uranium-loaded core [1] [3] [5] [6] but also the thorium-loaded core [2] [4]. A series of the uranium- and thorium-loaded ADS experiments were carried out by varying an external neutron source (14 MeV neutrons and 100 MeV protons) and neutron spectrum of the core with the combined use of fuel (highly-enriched uranium: HEU, natural uranium: NU and thorium: Th) and moderator (polyethylene: PE, graphite: Gr and beryllium: Be). Then, the reactor physics parameters were obtained successfully, including reaction rate distribution, neutron decay constants, neutron multiplication, and subcriticality.

In forthcoming uranium-loaded ADS experiments, the reactor physics parameters in the subcritical systems could be evaluated successively by the experimental and numerical analyses with the variation of subcriticality, the external neutron source and the neutron spectrum. Among these experiments, the uranium-loaded ADS experiments with 100 MeV protons could be conducted using the Pb-Bi-zoned region to examine the feasibility of the nuclear transmutation by ADS, including minor actinides (MAs: ^{237}Np and ^{241}Am). The conversion analyses of ^{237}Np/^{238}U and ^{241}Am/^{235}U are expected to investigate the uncertainties of MAs cross-section data in the high-energy neutrons when the subcriticality, the neutron spectrum and the external neutron source are varied in the subcritical system. Also, a series of the ADS experiments is planned to be carried out to conduct another conversion analysis of ^{232}Th capture and ^{233}U fission reactions using the capture and fission ratio: ^{232}Th/^{238}U and ^{233}U/^{235}U, respectively. The objective of these experiments is to conduct a feasibility study on ADS through the experiments at the

KUCA Facility combined with the FFAG accelerator for a high-performance transmutation system with a capability to generate power.

KUCA core configuration

Uranium-loaded ADS experiments

The uranium-loaded core (A-core; Figure 1) used in the ADS experiments was composed of the HEU fuel (see Figure 2) and PE-moderator and -reflector rods. In the fuel region, a unit cell is composed of two 93% enriched uranium fuel plates 1/16" thick and a polyethylene plate 1/8" thick. In the ADS experiments, an original target was located not at the centre of the core but outside the critical assembly, as shown in Figure 1. The fuel rod in the thorium-loaded ADS experiments (see Figure 3) was composed of thorium, HEU, PE and Gr plates, as shown in Figure 4.

To obtain the reaction rate in the core, an indium wire was set along the core region in an axial centre position, because the sensitivity of thermal neutron flux can be acquired by $^{115}In(n, \gamma)^{116m}In$ reactions. Another indium foil was set at the target location for monitoring the generation of the spallation neutrons, which can be acquired by $^{115}In(n, n')^{115m}In$ reactions (threshold energy; 0.32 MeV).

Figure 1. Top view of configuration of A-core in the ADS experiments with 100 MeV protons

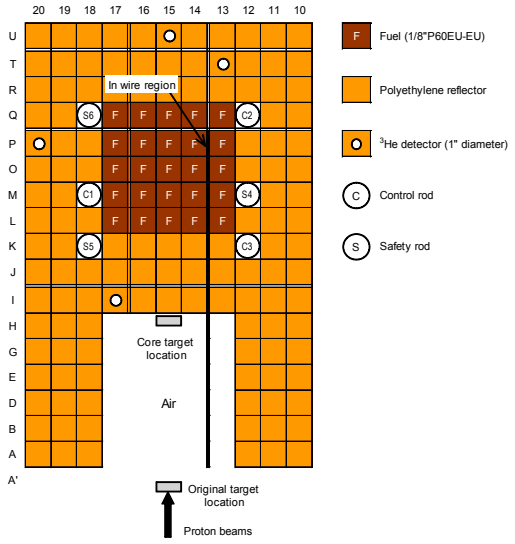


Figure 2. Side view of uranium fuel rod (F, 1/8"P60EUEU) shown in Figure 1

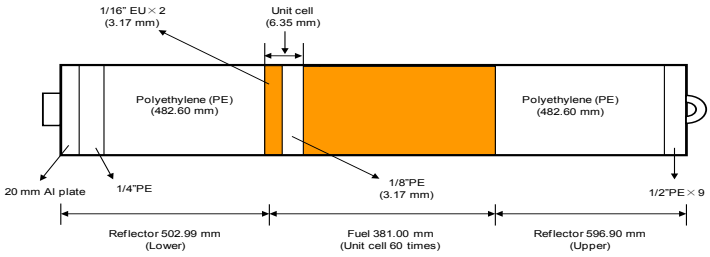


Figure 3. Top view of configuration of thorium-loaded ADS experiments with 100 MeV protons

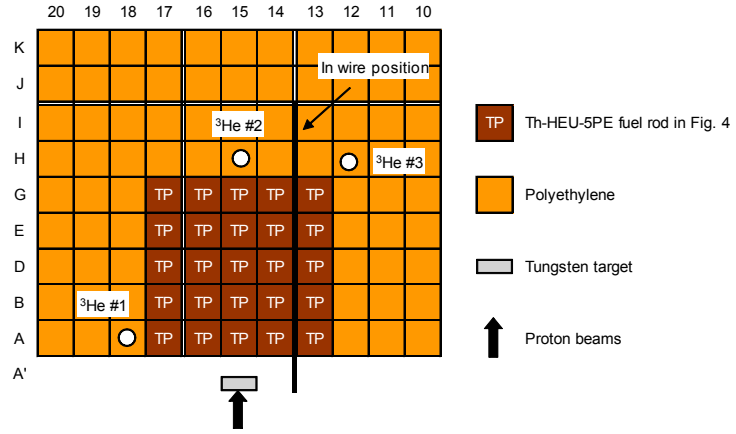
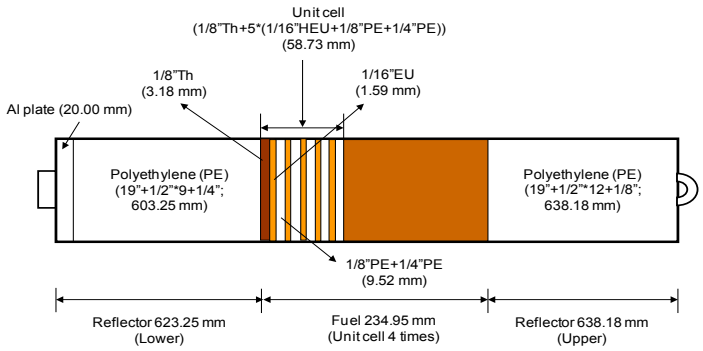


Figure 4. Side view of thorium-uranium fuel rod (TP, Th-HEU-5PE) shown in Figure 3



ADS Experiments with 100 MeV protons

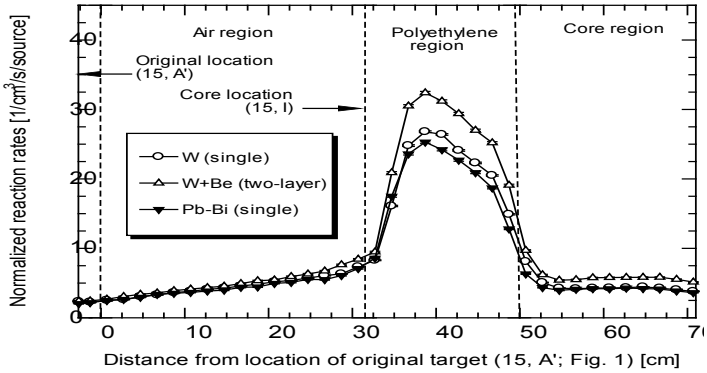
Two-layer-target experiments

The combined use of the heavy- (W, Pb and Bi) and the light-nuclide (Be and Li) was considered useful for the accomplishment of the research objectives related to the neutron spectrum and the neutron yield rather than single-use target. The target characteristics [10] were numerically examined by the MCNPX [11] and SRIM codes [12] with ENDF/B-VII.0 [13] and JENDL/HE-2007 [14] [15] libraries to investigate the neutron spectrum in the high-energy region and to determine the thicknesses of the two-layer-target so that the incident protons could be fully stopped inside the target. The numerical results [5] showed that the neutron spectrum had increased in the high-energy region with the combined use of W and Be. In the design of the two-layer-target, the proton beams could be actually penetrated into the Be target, and inversely stopped inside the W target. The thickness of the W and Be targets was determined by the numerical results of the range of high-energy protons obtained by SRIM. Finally, on the basis of previous studies [3] [5], the dimensions of the W+Be target were determined to be in W (50 mm diameter and 9 mm thick) and Be (50 mm diameter and 6 mm thick), since the spot size of proton beams were in 40 mm diameter and these dimensions could be considered to be covered with the proton beams and to be satisfied sufficiently with the penetration and the full-stopping in the two-layer-target. Also, the thickness of the Pb-Bi target was determined to be 12 mm (50 mm diameter) from the viewpoint of full-stopping inside the

Pb-Bi target. The proton beams in the ADS experiments were as follows: 100 MeV energy, 0.5 nA intensity, 20 Hz repetition, and 100 ns width. In the experiments, the target was located at (15, I; see Figure 1) to aim at neutron multiplication in the core rather than the location of the original target at (15, A'; see Figure 1).

The measured reaction rate distributions of ^{115}In(n, γ)^{116m}In reactions normalised by ^{115}In(n, n')^{115m}In reactions were revealed by varying the type of the target, as shown in Figure 5. The measured reaction rate distributions were observed to be high with the combined use of W and Be, whereas the effect of the Pb-Bi target was relatively low compared with the W target.

Figure 5. Measured results of ^{115}In(n, γ)^{116m}In reaction rate distributions along (14,13–A',P) shown in Figure 1



In a previous study [3], neutron multiplication was proved to have been obtained successfully by the ^{115}In(n, γ)^{116m}In reaction rate distributions in the core region, because the relationship between the reaction rates of ^{115}In(n, γ)^{116m}In and ^{235}U(n, f) in the core region was apparently applicable to the subcritical multiplication analyses through the proportionality of ^{115}In(n, γ)^{116m}In and ^{235}U(n, f) cross-sections in the thermal region.

As shown in Table 1, the neutron multiplication increased by 30% for the two-layer-target (W+Be), compared with the W single-target, whereas the Pb-Bi target decreased by 20%. The change of the location of the core target into that of the original target was considered effective rather than the original target location, as shown in Figure 1. From the experimental results, the effect of the two-layer-target on the neutron multiplication was found at the location (15, I) in the core region.

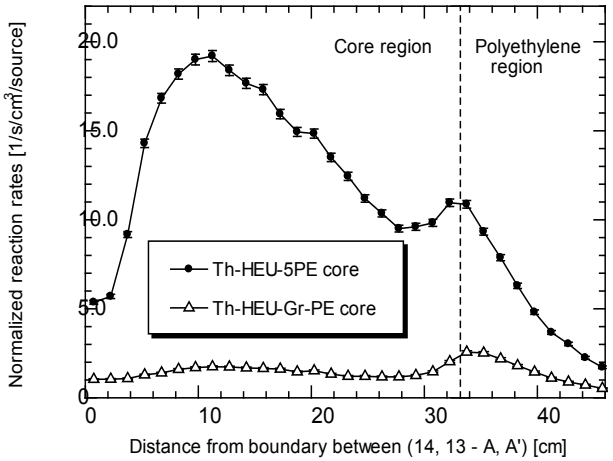
Table 1. Measured results of neutron multiplication M in target characteristic experiments

Target	M
W (single)	103.22 ± 0.14
W+Be (two-layer)	131.14 ± 0.22
Pb-Bi (single)	82.82 ± 0.16

Thorium-uranium-loaded ADS experiments

For an injection of 100 MeV protons into the W target, the neutron spectrum was varied in the core through the change of polyethylene (see Figure 4) into graphite. The bombarding model of 100 MeV protons was conducted using MCNPX and JENDL/HE-2007 at the W target, and the neutronic simulations were executed with the combined use of MCNPX, ENDF/B-VII.0 for transport and JENDL/D-99 [16] for reaction rates. As shown in Figure 6, the reaction rates of ^{115}In(n, γ)^{116m}In reactions normalised by ^{115}In(n, n')^{115m}In reactions in the Th-HEU-5PE (k_{eff} = 0.8512) core were higher than those in the Th-HEU-Gr-PE (k_{eff} = 0.3547) core, demonstrating that the effect of the neutron spectrum on the reaction rates was observed by varying the moderation material. In the future, numerical approaches could additionally be conducted with MCNPX together with other libraries to investigate the accuracy of experimental analyses and the effect of nuclear data libraries.

Figure 6. Measured results of ^{115}In(n, γ)^{116m}In reaction rates along (14, 13-A, A') shown in Figure 3



Forthcoming ADS experiments

At KUCA, forthcoming experiments could be conducted to investigate the neutronic characteristics of ADS coupling with the KUCA core and 100 MeV protons as follows:

- sample worth experiments of Pb and Pb-Bi in the critical state for the investigation of the uncertainties of Pb and Pb-Bi cross-sections, before the ADS experiments;
- mock-up experiments on neutronic characteristics of ADS with 100 MeV protons in the uranium-loaded and Pb-Bi-zoned core;
- MAs integration experiments on reaction rates of ^{237}Np capture and ^{241}Am fission reactions in the ADS with 100 MeV protons;
- conversion analysis of ^{232}Th capture and ^{233}U fission reactions in ADS.

Among the experiments, the uranium-loaded ADS experiments with 100 MeV protons could be conducted in the subcritical core using Pb-Bi-zoned region to examine the feasibility of the nuclear transmutation by ADS, including MAs (^{237}Np and ^{241}Am). The conversion analysis of ^{237}Np/^{238}U and ^{241}Am/^{235}U is expected to be carried out to investigate the uncertainties of MAs cross-section data in the high-energy neutrons when the subcriticality, the neutron spectrum and the external neutron source are varied in the subcritical system. Furthermore, another conversion analysis is planned to be carried out to examine the uncertainties of ^{232}Th capture and ^{233}U fission cross-sections using capture

to fission ratio: ^{232}Th/^{238}U and ^{233}U/^{235}U, respectively in the case of the variation of the subcriticality, external neutron source and neutron spectrum.

Summary

The experimental studies on the accelerator-driven systems (ADSs) are being conducted with the combined use of the KUCA core and the FFAG accelerator. In the ADS experiments with 100 MeV protons, the reactor physics parameters have been successfully obtained, including reaction rate distribution, neutron decay constants, neutron multiplication, and subcriticality to investigate the neutronic characteristics of ADS.

ADS experiments with 100 MeV protons will be carried out using Pb-Bi-zoned region to examine the feasibility of the nuclear transmutation by ADS, including ^{237}Np and ^{241}Am. The conversion analysis of ^{237}Np/^{238}U and ^{241}Am/^{235}U will be conducted to investigate the uncertainties of MAs cross-section data in the high-energy neutrons when the subcriticality, the neutron spectrum and the external neutron source are varied in the subcritical system. Also, another conversion analysis will be conducted to examine the uncertainties of ^{232}Th capture and ^{233}U fission cross-sections using capture to fission ratio: ^{232}Th/^{238}U and ^{233}U/^{235}U, respectively, in cases of the variation of the subcriticality, the external neutron source and the neutron spectrum.

References

[1] Pyeon, C.H., Misawa, T., Lim, J.Y. et al. (2009), "First Injection of Spallation Neutrons Generated by High-Energy Protons into the Kyoto University Critical Assembly," *J. Nucl. Sci. Technol.*, 46, 1091.

[2] Pyeon, C.H., Lim, J.Y., Takemoto, Y. et al. (2011), "Preliminary Study on the Thorium-Loaded Accelerator-Driven System with 100 MeV Protons at the Kyoto University Critical Assembly," *Ann. Nucl. Energy*, 38, 2298.

[3] Lim, J.Y., Pyeon, C.H., Yagi, T. et al. (2012), "Subcritical Multiplication Parameters of the Accelerator-Driven System with 100 MeV Protons at the Kyoto University Critical Assembly," *Sci. Technol. Nucl. Install.*, 2012, ID: 395878, 9 pages.

[4] Pyeon, C.H., Yagi, T., Lim, J.Y. et al. (2012), "Experimental Study on the Thorium-Loaded Accelerator-Driven System at the Kyoto University Critical Assembly," *Proc. Int. Conf. on Advanced in Reactor Physics – Linking Research, Industry, and Education* (PHYSOR2012), Knoxville, Tennessee, 15-20 April 2012, CD-ROM, *American Nuclear Society*.

[5] Takahashi, Y., Azuma, T., Nishio, T. et al. (2013), "Conceptual Design of Multi-Targets for Accelerator-Driven System Experiments with 100 MeV Protons," *Ann. Nucl. Energy*, 54, 162.

[6] Pyeon, C.H., Azuma, T., Takemoto, Y. et al. (2013), "Experimental Analyses of Spallation Neutrons Generated by 100 MeV Protons at the Kyoto University Critical Assembly," *Nucl. Eng. Technol.,* 45, 81.

[7] Planche, T., Yamakawa, E., Uesugi, T. et al. (2010), "Scaling FFAG Rings for Rapid Acceleration of Muon Beams," *Nucl. Instrum. Methods A*, 622, 21.

[8] Planche, T., Lagrange, J.-B., Yamakawa, E. et al. (2011), "Harmonic Number Jump Acceleration of Muon Beams in Zero-Chromatic FFAG Rings," *Nucl. Instrum. Methods A*, 632, 7.

[9] Lagrange, J.-B., Planche, T., Yamakawa, E. et al. (2012), "Straight Scaling FFAG Beam Line," *Nucl. Instrum. Methods A*, 691, 55.

[10] Pyeon, C.H., Yagi, T., Misawa, T. (2012), "Application of Multi-Target to the Accelerator-Driven System Experiments in the Kyoto University Critical Assembly," *Proc. Winter Mtg. of the Am. Nucl. Soc.*, San Diego, California, 11-15 November 2012, CD-ROM, *Trans. Am. Nucl. Soc.*, 107, 1029-1031 (2012), American Nuclear Society.

[11] Pelowitz, D.B. (2005), "MCNPX User's Manual Version 2.5.0," LA-CP-05-0369, Los Alamos National Laboratory.

[12] Ziegler, J.F., Biersack, J.P., Ziegler, M.D. (1985), "The Stopping and Range of Ions in Matter", *Pergamon Press*, New York.

[13] Chadwick, M.B. et al. (2006), "ENDF/B-VII: Next Generation Evaluated Nuclear Data Library for Nuclear Science and Technology," *Nucl. Data Sheets*, 107, 2931.

[14] Fukahori, T. (2002), "JENDL high-energy file," *J. Nucl. Sci. Technol.*, suppl., 2, 25.

[15] Takada, H., Kosaka, K., Fukahori, T. (2009), "Validation of JENDL High-Energy File through Analyses of Spallation Experiments at Incident Proton Energies from 0.5 to 2.83 GeV," *J. Nucl. Sci. Technol.*, 46, 589.

[16] Pyeon, C.H., Shiga, H., Abe, K. et al. (2010), "Reaction Rate Analysis of Nuclear Spallation Reactions Generated by 150, 190 and 235 MeV Protons," *J. Nucl. Sci. Technol.,* 47, 1090.

[17] Kobayashi, K., Iguchi, T., Iwasaki, S et al. (2002), "JENDL Dosimetry File 99 (JENDL/D-99)*", JAERI Report* 1344.

Role of the ADS from the perspective of the International Thorium Energy Committee iThEC

Yacine Kadi[1,2]
[1]iThEC, Geneva, Switzerland,
[2]Sungkyunkwan University, Republic of Korea

Abstract

The international Thorium Energy Committee in Geneva has been established to investigate the ADS fuelled by thorium. The committee, formed by prominent members of the scientific community of CERN under the auspices of Carlo Rubbia, the original inventor of the ADS concept, also comprises business leaders and members acquainted with public relations in an effort aimed at broadening the appeal of the ADS concept.

Nuclear policy today in Europe and more particularly in Switzerland has reached a point where crucial decisions must be made, which affect the security of the electricity supply, the fulfillment of commitments to the Kyoto Protocol to combat climate change while addressing public concerns following the Fukushima accident. Nuclear power has its advantages, yet the perennial problem of what to do with the waste, the perceived risks due to criticality have long been a thorn in the side of nuclear power, preventing it from taking its place as a core technology of the 21st century and beyond. The iThEC committee members are actively pursuing the goal of reversing the current negative trends in Europe by supporting thorium ADS technology by actively engaging in the scientific, political and business leadership.

Introduction

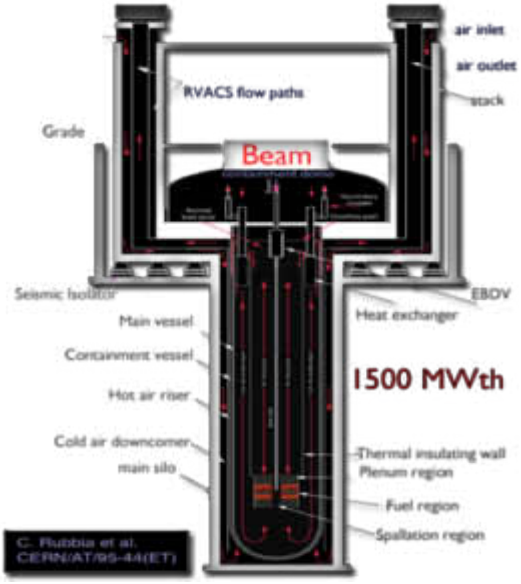
In October 2013, the International Thorium Energy Committee (iThEC) created in 2012 as a non-profit organisation, held at CERN an international conference on a new form of nuclear energy production based on thorium. This committee aims to contribute to the development of a sustainable solution to the world energy problem by promoting the construction of a prototype thorium reactor controlled by a particle accelerator system called an ADS or Accelerator-driven System as proposed by the Nobel laureate in physics; Carlo Rubbia at CERN [1] [2], (see Figure 1).

The benefits of such a proposal can be summarised as follows:

- Demonstrate on an industrial scale that much of the volume and the lifetime of existing nuclear waste can be eliminated, thus reducing the risk of deep disposal, along with the costs and fears that it generates.
- Demonstrate that it is possible to develop a new global energy concept, sufficient to contribute to the harmonious development of the planet without compromising its fragile ecological balance.
- Preserve local know-how and independence in the nuclear field to ensure an effective direct control of existing nuclear power plants including their future

dismantling. The permanence of nuclear expertise is also vital for the future of nuclear medicine.

Figure 1. Carlo Rubbia's energy amplifier concept [1] [2]



The energy problem is a major challenge for our civilisation and the manner in which it will be dealt with, will largely determine the fate of humanity. World energy consumption should be tripled in order to provide the world population at the end of the 21st century with a consumption level comparable to that of today's European population, even when assuming increased energy efficiency.

It would therefore seem unwise not to undertake a systematic piece of research in all modes of energy production, as otherwise the world will be deprived of innovative and sustainable solutions. In some countries such as Switzerland, the parliament decided that the country could manage without its current nuclear power plants until 2050, but prudently also reaffirmed that it would continue to encourage research and development in this field.

Nuclear waste management in Switzerland

Opting out of nuclear energy implies decommissioning existing nuclear power plants but it also still entails dealing with the waste that these plants have produced throughout their useful operational lives as well as finding other realistic environmentally acceptable energy sources. Today, the only considered option for the waste is deep burial, which is a controversial political subject. Projections from the Swiss repository authority NAGRA (Nationale Genossenschaft für die Lagerung Radioaktiver Abfälle) of the cost of burial have given rise to concerns in economic circles. It is significant that a recent vote calling for a faster provision of funds to the nuclear decommissioning fund over 40 years instead of 50 years was overwhelmingly approved by the Swiss parliament. The nuclear decommissioning fund is to accrue 20 billion Swiss Francs in total, of which 13 billion is marked for financing deep burial.

Thorium-ADS

In this context, iThEC undertook to promote research and development in the field of nuclear energy based on the use of thorium. Current nuclear power systems do not offer the best possible use of nuclear fission. Therefore, it seems natural to question whether it would be possible to conceive other methods that would be more acceptable to society. A number of nuclear experts believe that it is indeed possible to develop new nuclear systems without the drawbacks of existing plants, such as accidents, waste management and military proliferation. The work of Nobel-prize laureate Carlo Rubbia has shown that there are many more efficient ways due to the effective coupling of particle accelerators technology with subcritical nuclear reactors and using thorium, a thorium-ADS.

The use of thorium in a subcritical fast reactor configuration driven by an accelerator (ADS) and cooled by natural convection of liquid metal offers significant advantages in terms of resource abundance, security, non-proliferation and drastic reduction of existing and future waste.

High intrinsic safety is ensured by the possibility of immediate shutdown due to the accelerator, while maintaining cooling liquid metals such as lead at a temperature well below boiling. This chemically inert coolant removes the danger of the formation and explosion of hydrogen like in Fukushima, and is naturally safer than liquid sodium envisaged in Gen-IV reactors. Furthermore, the natural circulation is independent of pumps and does not require a power supply.

The risk of military proliferation is greatly reduced because the plutonium production is negligible. The main element is the fissile isotope ^{233}U (produced by neutron capture by thorium: Figure 3), but it is present in an isotopic mixture unfit for military operational use.

The production of long-lived waste (plutonium and minor actinides) is greatly reduced compared to uranium-based fuel. With a thorium-ADS, it is possible to eliminate much of the waste resulting from the operation of existing uranium plants (see Figures 2, 3). This reduces the size and complexity of, or may indeed eliminate the need for long-term nuclear waste storage sites, which is an important issue.

Figure 2. Reduction in activity through transmutation of long-lived nuclear waste [1] [2]

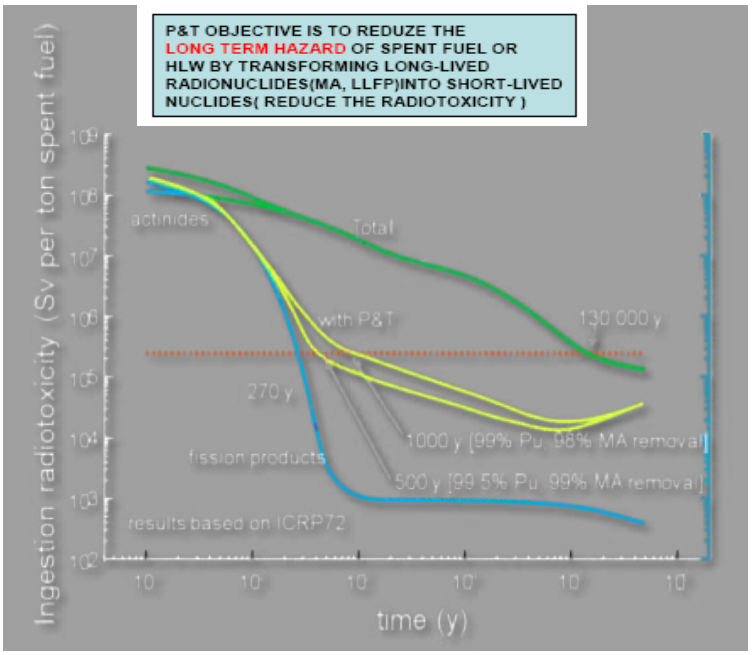
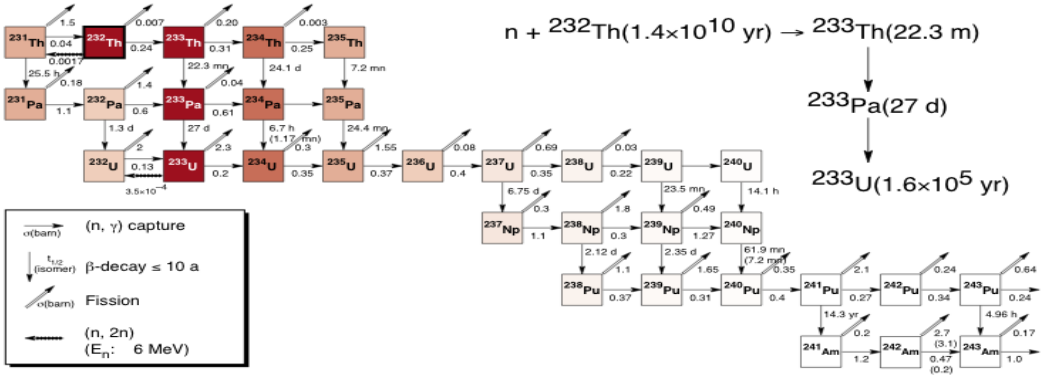


Figure 3. The thorium chain



Thorium

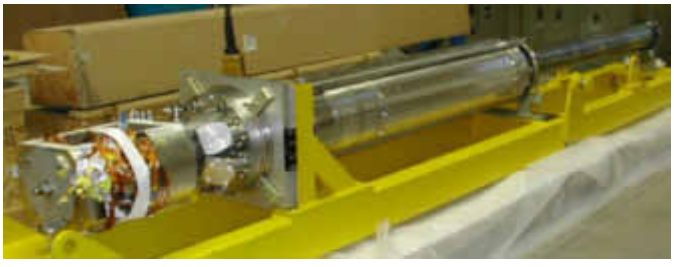
Thorium resources are more abundant than uranium and mainly located in politically stable countries (India, US, Australia, Norway, etc.). They ensure a reliable supply of electric power, independent of weather fluctuations, without releasing greenhouse gas emissions and with minimal impact on the landscape. In addition, used in an ADS, thorium would greatly facilitate a wider use of renewable energy, by ensuring a source of electrical power that can be modulated and is continuously available.

Competitive advantages of Switzerland

The policy of Switzerland, which accounts for only one thousand of the world's population, will have little influence on the energy balance of the entire planet. However, Switzerland, one of the richest and more technologically advanced countries, is in a position to contribute significantly to the development of new solutions to the energy problem by encouraging innovation. The results of the "EU stress test" of the existing Swiss nuclear power plants show the advantage of being ahead of other countries from a technological point of view. The European Parliament took action to implement the required improvements at considerable cost, whereas Switzerland, due to a higher and internationally recognised level of security, is already at the stage of implementing simpler yet adequate measures.

Switzerland has unique strengths in a number of areas directly related to the basic elements of an ADS system for the destruction of nuclear waste. First, the Paul Scherrer Institute (PSI) in Villigen has developed a cyclotron with a proton beam whose characteristics and power have the capacity to drive a nuclear waste incinerator. In January 2007, PSI managed a pioneering experiment with the operation of a high-power neutron spallation source; MEGAPIE [3] (see Figure 4).

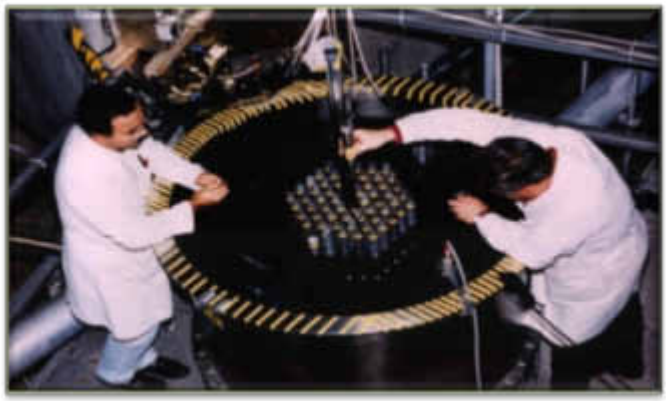
Figure 4. MEGAPIE Target in transport dolly prior to vertical integration at PSI



With a proton beam power in the order of one megawatt, such a neutron source would be sufficient to eliminate about 30 kg of plutonium and minor actinides per year. The PSI also employs many specialists in nuclear safety, which, in the context of the Swiss nuclear withdrawal, could be redeployed, using their expertise for the elimination of the existing waste inventory and for evaluating the safety aspects of the thorium chain.

The presence of CERN in Switzerland is also an important asset because it is at CERN that the founding experiments of an ADS were performed; notably FEAT (see Figure 5) and TARC by Carlo Rubbia and his team. The "n-TOF" installation is also available at CERN for measuring the neutronic characteristics of materials, a knowledge which is necessary for the optimisation of any new nuclear system. Technologies for a new nuclear reactor free from the danger of nuclear accidents, which minimises waste and does not emit CO_2, should be an acceptable choice for the society.

Figure 5. FEAT target at CERN



The iThEC Programme

ADS provides a way of eliminating long-lived waste, mainly in the form of transuranic elements. The method not only transforms these elements into stable waste products but at the same time provides energy, which would finance all or part of the system (see Figure 6). Evidently, such a project must be approached carefully in order to limit the financial risks. iThEC has, therefore, proposed a three-step approach spanning a decade, consisting, first, in an assessment of the costs, followed by a second part for testing the innovative technologies elements of the system and finishing with a third stage which would lead to the construction of a prototype with sufficient capacity to demonstrate the feasibility of a large-scale Thorium-ADS at a power level of several megawatt.

Figure 6. Schematic of a thorium-ADS for energy production and waste elimination

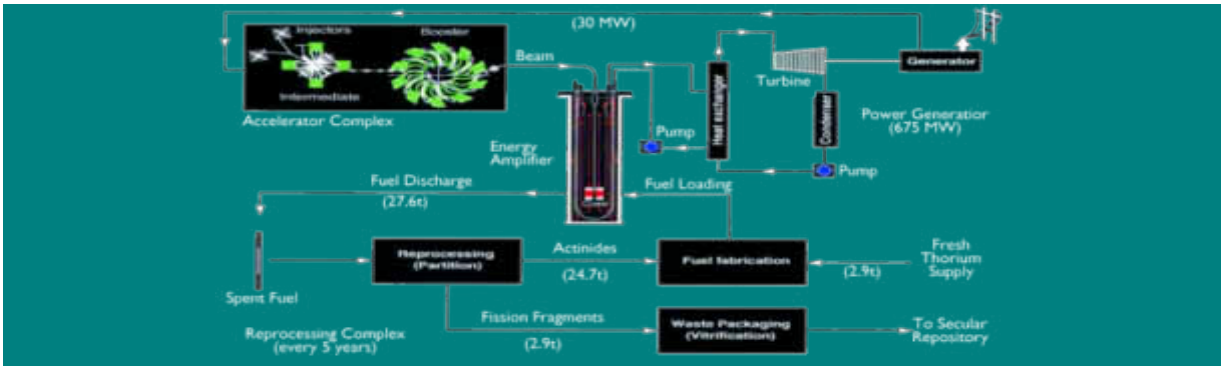


Figure 7. THEC13 conference organised in Geneva by iThEC in October 2013



Conclusion

iThEC [4] proposes that Switzerland undertake, along with other interested parties, a programme on the elimination of nuclear waste through the thorium-ADS concept, taking advantage of synergies with Swiss institutions willing to offer their skills for the rapid implementation of a pilot project. The conference organised by iThEC at CERN in October 2013 will lead global research efforts in thorium-related technologies. This could mark the beginning of a new energy era through international collaboration, an era in which thorium will play a major role along with other new energy sources.

References

[1] Rubbia, C. et al. (1995), "Conceptual design of a fast neutron operated high power energy amplifier", CERN Internal Note CERN-AT-95-44 ET.

[2] Rubbia, C. (1996), "The energy amplifier; a description for the non-specialists", CERN/ET/Internal Note 96-01.

[3] Wagner, W., Groeschel, F., Thomsen, K., Heyck, H. (2008), "MEGAPIE at SINQ – the first liquid metal target driven by a megawatt class proton beam", *J. Nucl. Mater*, Vol 377, pp 12-16.

[4] http://www.ithec.org.

Session II: Accelerators

Chair: M. Seidel

The present status of the Chinese ADS proton accelerator R&D[1]

Yun-long Chi[1], Yuan He[2]
[1]Institute of High Energy Physics, China, [2]Institute of Modern Physics, China

Abstract

Due to the rapid development of nuclear power plants in China, nuclear waste management has become a crucial issue. The roadmap of nuclear transmutation aiming to operate a demonstrator accelerator-driven subcritical systems (ADSs) in 2032 has been set up in China. Supported by the "Strategic Priority Research Programme" of the Chinese Academy of Sciences (CAS), the Chinese ADS project is now on-going based on the collaboration of several Chinese institutions. The proton accelerator of Chinese ADS is a superconducting CW linear accelerator. Its energy is 1.5GeV, with a beam current of 10 mA. The Institute of High Energy Physics (IHEP) and the Institute of Modern Physics (IMP) are responsible for developing the two injectors and IHEP is the leading institute for the development of the main LINAC. This paper presents the progress of the key hardware R&D work of the Chinese ADS proton accelerator.

Introduction

The Chinese ADS project is aimed to solve the nuclear waste problem and the resource problem for nuclear power plants in China. With its long-term planning to last until 2030, the project will be carried out in 3 phases: Phase I: R&D facility, Phase II: Experiment facility and Phase III: Industrial demonstration facility. The proton accelerator for this project is a CW accelerator adopting superconducting technologies, except for RFQ in injectors. Table 1 shows the design specifications for the Chinese ADS proton accelerator.

Table 1. Specifications of the Chinese ADS proton accelerator

Parameters	Value	Units
Energy	1.5	GeV
Current	10	mA
Beam power	15	MW
Frequency	162.5/325/650	MHz
Duty factor	100%	
Beam Loss	<1 (0.3)	W/m
Beam trips/year	<25000 <2500 <25	1s<t<10s 10s<t<5m t>5m

[1] Work supported by CAS "Strategic Priority Research Programme.

The Strategic Priority Research Programme of ADS is financially supported by the central government and administrated by CAS, focusing on the development of key technologies and the construction of a CW proton accelerator of 50 MeV with a maximum beam current of 10 mA.

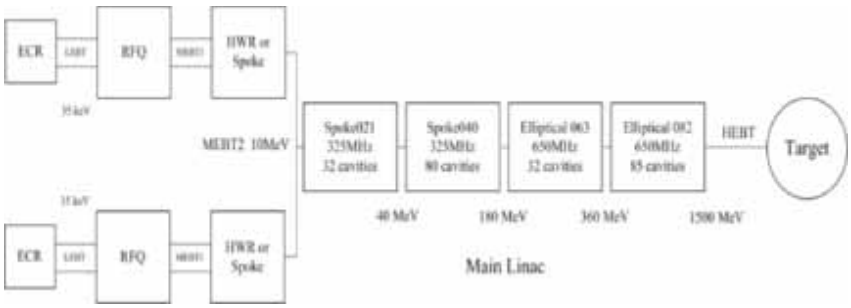
In the past two years, IHEP an IMP have made efforts to improve the Chinese ADS Proton Accelerator, both the accelerator physics design and the key hardware development, including CW RFQ, SC cavities, HP input coupler, SSA RF power source, SC solenoid magnet, CW proton beam diagnostics, digital power supply andcryogenic system.

Accelerator lattice design

The Chinese ADS accelerator (see Figure 1) adopts the design with two identical injectors of 10 MeV, so one can be the hot-spare of the other. At present, two different injector schemes are under development by IHEP and IMP and the final solution will be chosen based on the R&D results. IHEP is developing one injector based on 325 MHz RFQ and beta=0.12 Spoke SC cavity and IMP is developing another injector based on 162.5 MHz RFQ and beta=0.10 HWR SC cavity.

In the main accelerator section, a fully modular superconducting accelerator brings the beam up to the final energy with two types of spoke sections (geometry beta=0.21 and 0.40) and two types of elliptical cavity sections (geometry beta=0.63 and 0.82). The main accelerator is designed to be intrinsically fault tolerant, which means that an individual cavity or focusing element failure can be handled at all stages without introducing significant beam loss along the accelerator by means of local compensation-rematch method. The local compensation-rematch methods for different element failures are studied systematically. This shows that with proper compensation and re-matching, the beam can be accelerated to the final energy without serious beam quality de-rating in the cases of cavity, solenoid and quadrupole failures.

Figure 1. Layout of the Chinese ADS proton accelerator



Key hardware development

Ion source

The Chinese ADS proton accelerator needs very reliable and stable intense CW proton beam sources and is being developed and under testing in IMP. Table 2 shows the design specifications of the Chinese ADS proton accelerator ion source.

Table 2. Specifications of Chinese ADS proton accelerator ion source

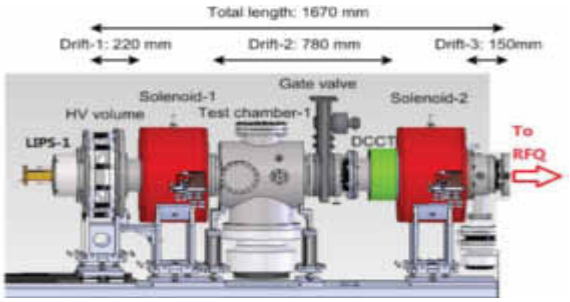
Energy	35	keV
Current	15	mA
Operation mode	CW	
ΔE/E	0.1	%
Stability	<±1	%
α	2.41	
β	7.72	cm/rad
ε (nRMS)	<0.2	π.mm.mrad

Figure 2 shows the sketch plot of the ion source and the LEBT system for the Chinese ADS proton accelerator. Beam intensity and quality have been reached and the critical issue is to minimise the sparking and the source breakdown time.

CW RFQ

The two different frequency CW RFQs are under development in IHEP and IMP for two different injectors. The main parameters of the two RFQ are listed in Table 3.

Figure 2. Chinese ADS ion source and LEBT layout



325 MHz RFQ

The fabrication of the 1st section of the RFQ is completed (see Figure 3) and the RF measurement results show that the design values have been achieved. The fabrication of the whole RFQ structure was completed in 2013. According to RF power requirements, Toshiba E37705 600 kW 325 MHz klystron and 80 kV PSM power supplies have been adopted as the RF power source.

162.5 MHz RFQ

The RFQ is designed by collaboration with LBNL. A demo section has been fabricated and is ready for high-power test (see Figure 4). The whole RFQ structure was completed in 2013. Tube TH781 of Thales is employed for the 200 kW RF amplifier. It has been commissioned with dummy load.

Table 3. Main parameters of RFQs

Frequency	162.5	325	MHz
Injection energy	35	35	keV
Output energy	2.1	3.2	MeV
Beam current	10	10	mA
Beam duty factor	100	100	%
Beam transmission	99.6%	98.7	%
Inter-vane voltage *V*	65	55	kV
Average bore radius r_0	5.731	2.775	mm
Vane tip curvature	4.298	2.775	mm
Maximum surface field	15.7791	28.88	MV/m
Input norm. rms emittance (x,y,z)	0.3/0.3/0	0.2/0.2/0	πmm.mrad
Output norm. rms emittance (x/y/z)	0.31/0.31/0.92	0.2/0.2/0.50	πmm.mrad/keV-ns
Vane length	419.2	467.75	cm
Accelerator length	420.8	469.95	cm

Figure 3. The first section of 325 MHz CW RFQ

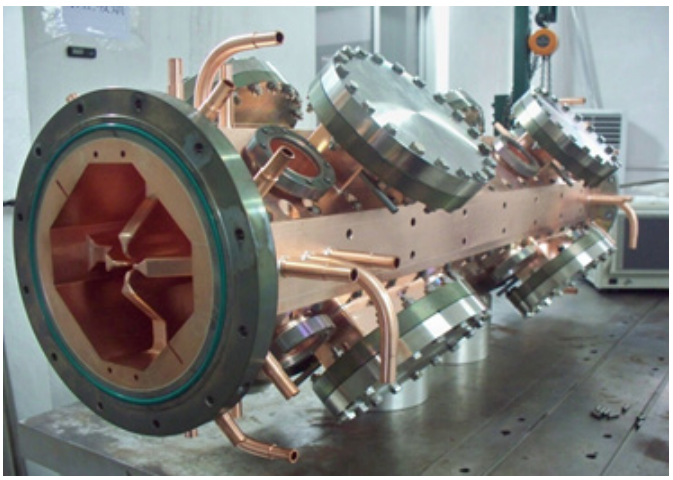
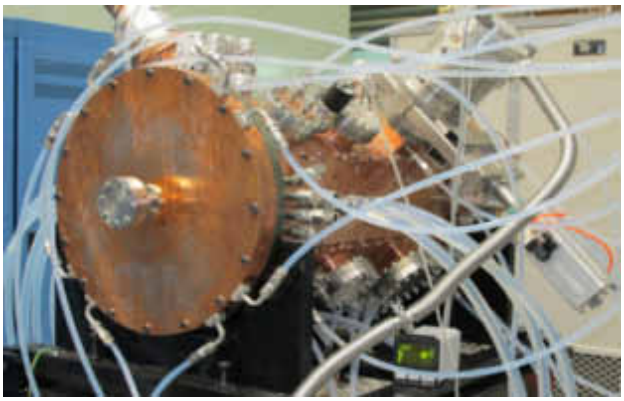


Figure 4. The demo section of 162.5 MHz CW RFQ



Superconducting cavities

Table 4 shows the main parameters of the Chinese ADS proton accelerator SC cavities. The 162.5 MHz half-wave resonator (HWR) has been developed for the injector-II, 325 MHz Spoke cavities and elliptical cavities have been developed for the injector-I and the main accelerator.

Table 4. Main parameters of superconducting cavities

Parameters		Cavities					Units
	HWR010	S012	S021	S040	E063	E082	
Frequency	162.5	325	325	325	650	650	MHz
Epeak/Eacc	5.9	4.5	325	325	2.6	2.12	
Bpeak/Eacc	12.1	6.4	3.78	3.33	4.73	4.05	mT/(MV/m)
R/Q	153	142	8.07	8.93	304	514	Ω
G	28.4	61	193	263	193	235	Ω
Q_0	4.0						E+08

Spoke012 Cavity

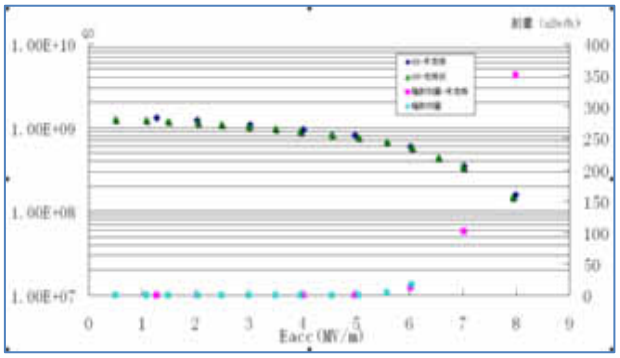
The 325 MHz spoke012 cavity for the 3~10 MeV injector-I is the most challenging one, because of the ambitious technical target and the lack of experience of the whole team. The design and the first two cavities' fabrication of Spoke012 (Figure 5) have been completed by the IHEP-PKU-HIT joint group.

Figure 5. Two fabricated spoke012 prototype cavities



The post-processing and vertical tests of the two prototype cavities were completed in 2012. There are no serious multiplication effects observed and the VT tests results are very promising (see Figure 6).

Figure 6. Vertical test result of Spoke012: Q_0=5.8x10^8@6MV/m, 4K; Q_0=3.4x10^8@7MV/m, 4K



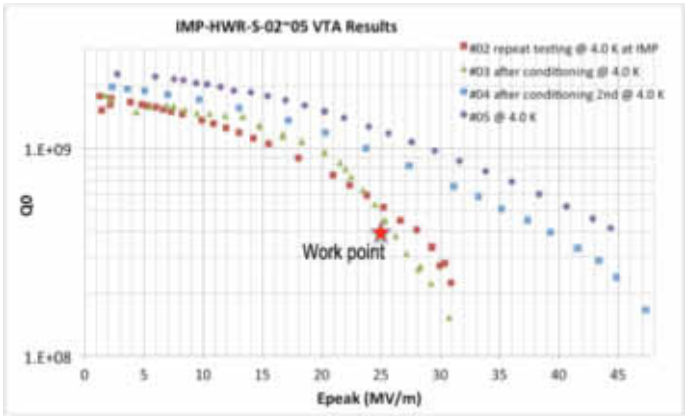
HWR009 Cavity

The 162.5 MHz HWR010 cavity for the 2.1~10 MeV injector-II is being constructed by IMP. HWR is a well-built superconducting cavity, some projects and institutes such as SARAF, IFMIF and FZJ have designed and constructed HWR cavities. Four HWRs have been tested at IMP. Two of them are ready for helium-vessel welding. Figure 7 shows a fabricated HWR cavity and Figure 8 shows vertical test results of HWR010. The horizontal testing was completed in 2013.

Figure 7. HWR010 cavity



Figure 8. Vertical test results of HWR010



Spoke021 Cavity

The 325 MHz spoke021 cavity (see Figure 9) has been designed for the low energy part of the main accelerator, which covers the energy range of 10~40 MeV. A set of moderate parameters have been adopted. Some novel ideas such as simple stiffen ring structure and the last welding seams implanted in the cavity have been developed. They should increase the yields in mass production. The fabrication of the two prototype cavities was completed and a vertical test was carried out in 2013.

Figure 9. The spoke021 cavities parts



Elliptical082 Cavity

The 650 MHz elliptical082 cavity has been designed for the high energy part of the main accelerator, which covers the energy range of 367~1500 MeV. The multiplication effect was examined by Track3P and the results show no hard multiplication barrier in the cavity.

High power input coupler

Three types of high-power input couplers have been fabricated and tested for the 325 MHz RFQ cavity, the Spoke012 cavity and HWR010 cavity. The main parameters of input couplers are listed in Table 5. All the couplers feature a tristan type RF window with one coaxial planar ceramic and choke structures.

Figure 10. 650 MHz elliptical082 cavity parts



Table 5. Main parameters of the HP input couplers

Cavity	Frequency	Power (kW)	Qe
RFQ	325 MHz	80, CW, TW	~5670
Spoke	325 MHz	10, CW, TW	~7.0E+5
HWR	162.5	15, CW, TW	~7.0E+5

Two prototypes of the window and inner conductor assemblies for the RFQ input coupler (see Figure 11a) have been tested up to 100 kW CW RF power in travelling wave mode (TW), two prototypes of the Spoke012 cavity coupler (see Figure 11b) have been tested up to 10 kW CW RF power in TW mode and two prototypes of HWR010 cavity coupler (see Figure 11c) have been tested up to 20 kW CW RF power in TW mode. The HP test of the input coupler prototypes for the Spoke012 cavity and the HWR010 cavities show good performances.

Figure 11. (a) RFQ input coupler; (b) Spoke012 input coupler HP test; (c) HWR010 input coupler



(a) (b) (c)

Solid state amplifier

The variable RF power Solid State Amplifier (SSA) has been adopted as the RF power source for variable accelerating structures except for RFQ. The power requirements of the SSAs are listed in Table 6. Two prototypes have been developed and tested, one 325 MHz 10 kW and the other 162.5 MHz 20 kW SSA (see Table 7 and Figure 12), which are the combination of several ~700 W power modules, have been adopted and tested. The SSA with higher RF power will be manufactured with the same topology.

Table 6. SSA power source for the accelerating structures

ACC. Structure	Frequency (MHz)	Power (kW)
Buncher	325	10
Buncher	162.5	8
Spoke012	325	10
HWR010	162.5	12
Spoke021	325	20
Spoke040	325	40
Elliptical063	650	80
Elliptical082	650	160

Table 7. Main parameters of the SSA prototype

Parameters	Value		Unit
	10 kW	20 kW	
Frequency	325±3	162.5±2	MHz
Output power	≥ 10 CW	≥ 20 CW	kW
Harmonic	≤ -50	≤-30	dBc
Random harmonic	≤ -80	≤-60	dBc
Amplitude stability	≤ ± 1	≤ ±1	%
Phase stability	≤ ± 1	≤±1	°

Figure 12. Prototypes of 325 MHz 10 kW SSA (left) and 162.5 MHz 20 kW SSA (right)



Summary

Most of the key technologies for the Chinese ADS Proton Accelerator key components, such as CW RFQ, SC HWR, Spoke and Elliptical cavities, HP input couplers, SSA RF power sources, SC solenoid magnets, beam diagnostic devices, digital power supplies, cryogenic system are under development at IHEP and IMP. IHEP and IMP constructed two injectors in 2013-2014 and CW beam commissioning started in 2014.

References

[1] Pan, W. et al. (2012), "Chinese ADS project and proton accelerator development", TU1A03, LINAC.

[2] Chi, Y. (2012), "Progress of ADS Linac R&D at IHEP", *TTC meeting*, JLab, 15 November 2012.

[3] He, Y. (2013), "Low beta cavities at IMP", *TTC meeting*, U. Cornell, 12 June 2013.

[4] Li, Z. et al., "Progress on the physics design of the C-ADS injector Scheme-1", THPWO043, IPAC13.

[5] Yue, W. et al. (2012), "R&D OF IMP superconducting HWR for China ADS", TUPB055, LINAC.

[6] Huang, T. et al., "The Development of an RFQ Input Coupler for the CADS", THPWO041, IPAC13.

[7] Liu, Z. et al. "ADS 650MHz beta=0.82 Superconducting cavity research status", WEPWO021, IPAC13.

[8] He, Y. et al. (2012), "Progress of one of 10 MeV superconducting proton linear injectors for C-ADS" THPB027, LINAC.

[9] Zhang, Z.L. et al. (2012), "Design of a four-vane RFQ for China ADS Project", THPB039, LINAC.

Beam operation aspects for the MYRRHA linear accelerator*

Jean-Luc Biarrotte[1], Didier Uriot[2], Luis Medeiros Romao[3], Dirk Vandeplassche[3]
[1]IPN Orsay (CNRS/IN2P3), France
[2]CEA Saclay (IRFU/SACM), France
[3]SCK•CEN, Mol, Belgium

Abstract

The aim of the MYRRHA project is to demonstrate the technical feasibility of transmutation in a 100 MW_{th} accelerator-driven System (ADS) by building a new flexible irradiation complex in Mol (Belgium). The MYRRHA Facility requires a 600 MeV accelerator delivering a maximum proton flux of 4 mA in continuous operation with an additional requirement for exceptional reliability. This paper describes the current status of this ADS accelerator design and focuses on the specific aspects related to beam operation such as beam time structure requirements, beam power control and ramp-up strategies, beam reconfiguration schemes in fault cases and beam instrumentation needs.

* This work is being supported by the European Atomic Energy Community's (EURATOM) Seventh Framework Programme under grant agreement n°269565 (MAX project).

Introduction

MYRRHA ("Multi-purpose Hybrid Research reactor for High-tech Applications") is a new flexible fast spectrum research reactor that is planned to be operational around 2023 in SCK•CEN Mol (Belgium) [1]. Composed of a proton accelerator, a spallation target and a 100 MW_{th} core cooled by liquid lead-bismuth are especially designed to demonstrate the feasibility of the ADS concept in view of high-level waste transmutation. To feed its subcritical core with an external neutron source, the MYRRHA Facility requires a powerful proton accelerator (600 MeV, 4 mA) operating in continuous mode, and above all, featuring a very limited number of unforeseen beam interruptions. The conceptual design of such an ADS-type proton accelerator has been initiated during previous EURATOM Framework Programmes (PDS-XADS and EUROTRANS projects). It is a linac (linear accelerator) based solution, which brings excellent electric efficiency due to the use of superconductivity and high potential for reliability using several redundancy schemes.

R&D on ADS-type accelerators are being developed within the framework of the MAX project [2], supported by EURATOM FP7. This project aims to deliver an updated consolidated reference layout of the MYRRHA linac with sufficient detail and adequate level of confidence in order to initiate, in 2015, its engineering design and subsequent construction phase. To reach this goal, advanced beam simulation activities are being undertaken and a detailed design of the major accelerating components is being carried out, building on several prototyping activities. Emphasis has been placed on all the aspects that pertain to the reliability and availability of this accelerator with the development of a detailed reliability model of the MYRRHA accelerator and with dedicated R&D to experimentally prove the feasibility of the innovative "fault-tolerance" redundancy scheme.

This paper describes the present status of this ADS accelerator design and focuses on specific aspects linked to beam operation such as beam time structure requirements, beam power control and ramp-up strategies, beam reconfiguration schemes in fault cases and beam instrumentation needs.

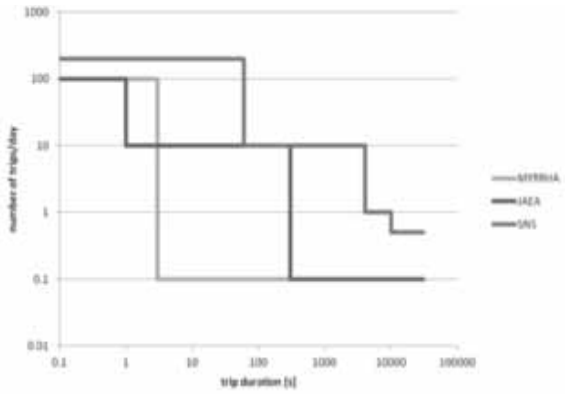
MYRRHA accelerator overview

The energy of the proton beam driving a Pb or Pb-Bi ADS reactor must typically be around 1 GeV. This value is the result of a compromise dictated by different criteria. The proton energy must be high enough to maximise the efficiency of the spallation reaction (and reach a typical yield of 25 to 30 neutrons per incident proton and GeV), but also to limit the energy deposited in the target and its window, thereby facilitating its design and usage constraints. On the other hand, cost optimisation of the accelerator promotes low energy. Therefore, a reference energy of 600 MeV has been chosen for the MYRRHA 100 MW_{th} demonstrator. For the record, this compromise has been set to 800 MeV for the industrial prototype 400 MW_{th} version called EFIT [3].

Once the proton energy is fixed, the beam current necessary to ensure control of the reactor is mainly determined by the thermal power and the level of subcriticality of the core. In the case of MYRRHA (k_{eff} = 0.95), the required nominal average current is 2.5 mA– up to about 4 mA being foreseen for burn-up compensation through the cycle – while for EFIT (k_{eff} = 0.97) it would be about 20 mA, corresponding to a mean beam power of 16 MW. In the current state of technology, the only alternative to producing such a high beam power continuously (and reliably) is the use of a linear accelerator. It is partly for this reason that MYRRHA, as a demonstrator, has also chosen this option at the expense of the cyclotron option, following the recommendations of the 2002 workshop at the NEA [4].

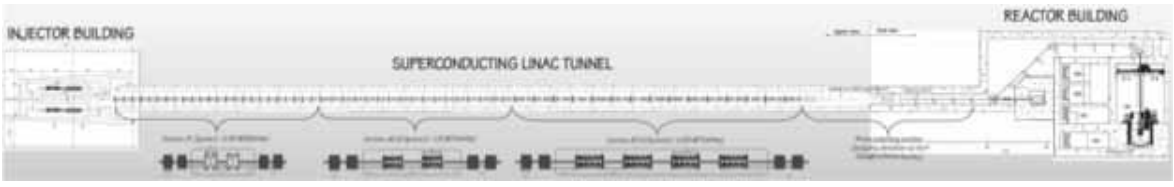
Besides the very high level of mean beam power to be produced by the MYRRHA accelerator (2.4 MW), the main challenge to address for this machine is the level of reliability required, since the number of beam interruptions should be limited to extremely low values: the current maximum limit is set to 10 beam interruptions per a three-month operating cycle, only interruptions of more than three seconds being counted, leading to a global accelerator MTBF (Meant Time Between Failures) of about 250 hours. This extremely strict reliability specification, settled during the EUROTRANS project, is motivated by the fact that beam interruptions longer than a few seconds could, if repeated frequently, lead to unacceptably high thermal stresses on the highly irradiated materials of the target window, on the fuel claddings and more generally on all the reactor structures. In addition, such long beam interruptions will probably be systematically associated with reactor shutdowns that could also significantly affect the availability of the system since the considered restart procedures could typically last about 20 hours [5]. It is, however, to be underlined that other studies in Japan or in the United States [6] are quoting much less severe reliability specifications for similar ADS machines, highlighting that a lot of uncertainties still remain on this theme. However, it should be noted that the reliability target for the MYRRHA ADS accelerator will need to be significantly higher than the actual reliability recorded worldwide on comparable accelerators in operation today, like the SNS, which exhibits a MTBF of a few hours presently at best. This gap to be filled is illustrated in Figure 1 [7], which shows that reliability is indeed the main challenge for the MYRRHA accelerator.

Figure 1. Beam trips frequencies as a function of their duration: Recorded in SNS, allowed by the Japanese ADS (JAEA), accepted for MYRRHA



The conceptual design of the MYRRHA machine has been on-going for several years [8-11] and it should be noted that in order to be able to reach the reliability goal, the linac scheme should consist – apart from the final beam transport lines – of 2 distinct sections (see Figure 2), a low energy part, composed of two redundant compact injectors with fast switching capabilities, followed by a highly modular and acceptant 17-600 MeV superconducting linac based on independently controlled accelerating cavities yielding a strong tolerance to faults, as detailed after.

Figure 2. Schematic overview of the MYRRHA linac (to scale, the SC linac tunnel being ~300 metres long)



Beam time structure and power control

In nominal operation, the proton beam produced by the MYRRHA accelerator must meet the following needs:

- Keep an "as CW as possible" beam time structure by avoiding producing beam interruptions longer than typically 100 ms; this is to eliminate any unnecessary thermal stress source on the reactor structures.
- Periodically produce beam interruptions of at least 200 μs [12] to be able to monitor the subcriticality level of the core on line.
- Feed in parallel and simultaneously an ISOL@MYRRHA Facility [13] by deviating up to 200 μA mean current from the MYRRHA beam by means of a fast kicker.

In order to reconcile these requirements, it is proposed to produce the following beam time structure for the nominal operation of the MYRRHA Facility (see Figure 3), 250 Hz repetition rate with 3.8 ms beam pulses for the reactor needs and 0.19 ms beam pulses for the ISOL facility needs, each pulse being separated at low energy using the chopping system located at the proton source exit. At maximum intensity (4 mA peak current), such a time structure leads to a total available beam power of 2.28 MW for the reactor and of 114 kW for the ISOL facility.

Figure 3. Proposed MYRRHA beam time structure for full power (~2.4 MW) nominal operation: Long 4 mA pulses (2.28 MW) are sent to the reactor while short ones (114 kW) are sent to the ISOL Facility

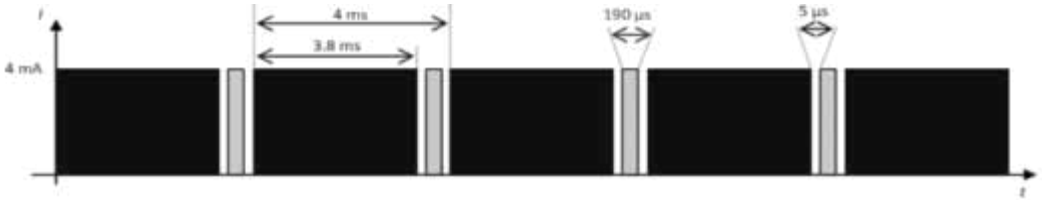
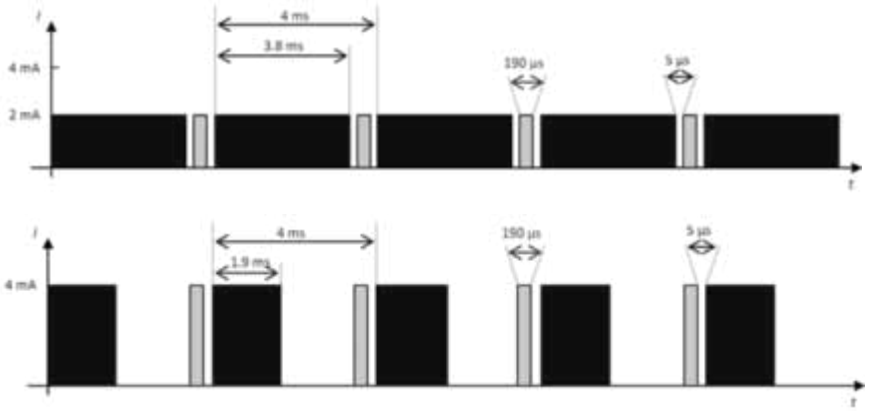


Figure 4. Possible MYRRHA beam time structures for half-power operation: (top) varying the peak current: 1.14 MW to reactor, 57kW to ISOL, (down) varying the duty cycle (preferred solution): 1.14 MW to reactor, 114kW to ISOL



To drive the reactor power, this mean beam power needs to be controlled and varied over a quite large range, from typically 20% to 100% of the maximum power [5]. The most

efficient and simple way to do this is to vary mean beam intensity, keeping the beam energy constant. In practice, this can be performed in two ways: by varying the overall peak current (see Figure 4, top), or by varying the duty cycle at constant peak current (see Figure 4, down). Even if the first option has the advantage of keeping a more "close to CW" time structure, the second method brings two considerable advantages as far as beam operation is concerned.

- The peak beam current is always kept constant (4 mA), meaning that space charge effects and therefore beam dynamics remain exactly the same whatever the required beam power. This is a crucial advantage because in this case, the accelerator elements (especially the low-energy ones actually) do not need to be retuned while changing the beam power, which should bring a lot of simplification and reliability for the whole facility operation. Only the low-energy beam chopper rhythm needs to be changed to cope with a beam power variation demand.
- Moreover, this second method allows varying the beam power sent to the MYRRHA reactor without affecting the beam power sent to the ISOL Facility, leading in a total decoupling of the two applications. Such independence is not feasible using the first option (unless the main beam pulse 250 Hz repetition rate is modified and therefore all the machine synchronisation retuned).

The method using a pulsed beam at constant peak current is therefore to be preferred for beam power control, at least as a baseline approach, especially as it also ensures that beam interruptions seen by the reactor will never (apart from failures) exceed 4 milliseconds during nominal operation. It is nevertheless to be underlined that, due to the pulsed nature of the beam, special attention should be paid to beam transients' management. In particular, the beam space charge compensation rising time, which plays a significant role in low-energy magnetic beam transport lines, will need to be carefully assessed and its effect on beam stability minimised. This physical process, which mainly depends on the gas nature and pressure conditions in the beam line, is complex to model and understand [14-16]. In this regard, dedicated experimental measurements at the UCL MYRRHA injector test stand [17] are expected.

Beam power ramp-up

During the first beam tunings and the commissioning phases of the accelerator and of the whole MYRRHA plant, the duty cycle will need to be extremely low (typically 10^{-4} or lower) for machine protection and safety reasons. This will require the use of a much lower beam repetition rate of typically 1 Hz. From there, the beam duty cycle and repetition rate will then be increased step by step to reach nominal beam operation. A possible scheme for this power ramp-up is as follows:

- Start the first tunings with a "pencil" beam, using for example 100 μs pulses at 1 Hz with 0.1 mA peak current (i.e. a 6 W beam). After this phase, the longitudinal tuning of the linac should work well.
- Increase, step by step, the peak current from 0.1 mA to the nominal 4 mA (i.e. increase the beam power from 6 to 240 W). After this phase, the transverse tuning of the linac should work well.
- Increase, step by step, the repetition frequency from 1 Hz to 250 Hz (i.e. increase the beam power from 240 W to 60 kW). During this phase, attention should be focused on the minimisation of possible beam pulse transients. When reaching 10 Hz (2.4 kW), the 100 ms threshold duration between two pulses is reached and the beam can be sent inside the reactor "careless".
- Increase, step by step, the pulse length from 0.1 ms to the nominal length (i.e. increase beam power from 60 kW to the nominal MW-class power).

Such a procedure will need to be followed in several cases: accelerator first commissioning phase (duration for a full power ramp-up: weeks/months), accelerator restarts after maintenance phases (duration: hours/days), reactor power ramp-up (duration: minutes/hours), fast beam restart after a less than three seconds beam interruption (duration: seconds, see after). The last case underlines that such a procedure will need to be managed by the machine control system in a complete automated way (which is very atypical in existing high power accelerator).

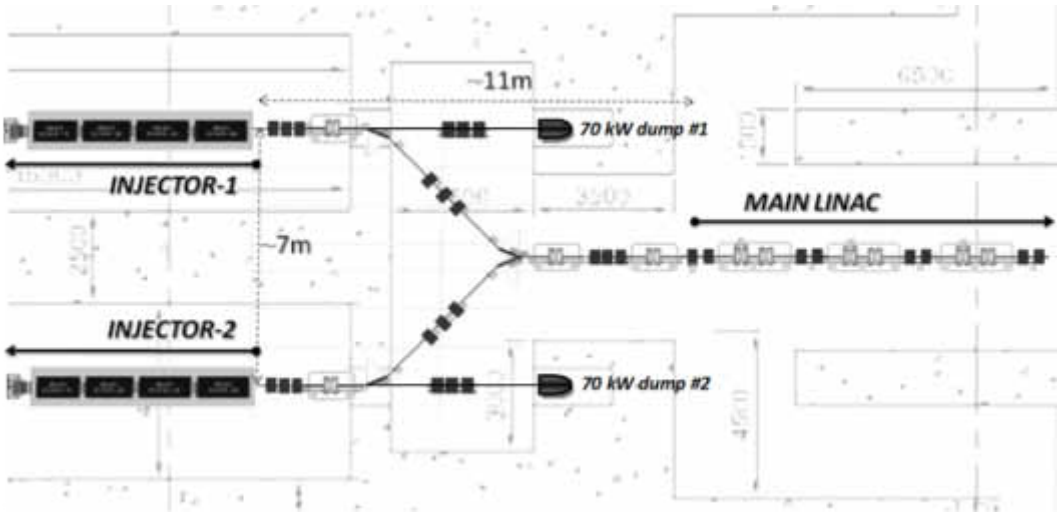
Injector beam reconfiguration in fault cases

The 17 MeV MYRRHA injector line [18] is designed to provide optimal acceleration efficiency with a minimised number of components. It is composed of a 30 kV ECR proton source and its 2-metre long Low Energy Beam Transport (LEBT), a 4-metre long 176 MHz 4-rod RFQ [19], accelerating the beam to 1.5 MeV and operating with very conservative inter-vane voltage (30 kV), followed by a booster – still under fine optimisation within the MAX project – made with several room-temperature and then superconducting multi-cell CH cavities [20].

To increase reliability, the philosophy consists in doubling the whole 17 MeV linac, providing a hot stand-by spare injector able to quickly resume beam operation in case of any failure [8]. The fault-recovery procedure is based on the use of a switching dipole magnet with a laminated steel yoke connecting the two injectors through a "double-branch" Medium Energy Beam Transport (MEBT) line, as shown in Figure 5. In a fault case, the injector beam reconfiguration should last no longer than 3 seconds. The mains steps of the reference scenario are the following:

- In the initial configuration, one of the injectors (e.g. Injector #1) provides a beam for the main linac. The other parallel injector (#2) is also fully operational but the produced beam is sent to a dedicated beam dump and continuously monitored.
- A serious fault is detected during operation and the beam is immediately and automatically stopped at the source exit in both injectors by the machine protection system, by means of the LEBT chopper (as a first step).
- The origin of the fault is analysed and diagnosed by the control system.
- If the fault is indeed localised in Injector #1, the necessary injector retuning procedure is started, and a new beam path is set to be able to feed the main linac using Injector #2; especially, the polarity of the power supply feeding the MEBT switching magnet is changed and Injector #2 45 dipole is switched on.
- Once steady-state is reached in the retuned magnets, the beam is resumed in Injector #2 first with very short pulses to control that the transport reaches the target; the duty cycle is then ramped within a second ("fast commissioning mode") to recover nominal beam operation.
- Once beam operation is resumed, maintenance is started on the failed injector #1, the casemate of which is supposed to be accessible during the operation of Injector #2. If the failure can be fixed, Injector #1 is then re-tuned, the beam is re-commissioned locally on the dedicated beam dump. Injector #1 then stays in "stand-by-mode", ready to relive Injector #2 in case of failure.

Figure 5. General layout of the MYRRHA medium energy beam transport line



Main linac beam reconfiguration in fault cases

The present architecture and main parameters of the MYRRHA main superconducting linac [21] are summarised in Table 1. It is composed of a periodic array of independently-powered superconducting cavities [22] with moderate energy gain per cavity and regular focusing lattices. The linac is designed to increase the tuning flexibility and ensure a very large beam acceptance in order to provide sufficient margins for the implementation of a fault tolerance capability by serial redundancy, where a missing element's functionality can be replaced by retuning other elements with nearly identical functionalities. Such a fault tolerance scheme can typically be applied to the failures of focusing elements or – more crucial because much more common – of RF units. Several beam dynamics studies have already been performed [23] [24], yielding the certainty of the theoretical feasibility of such a fault tolerant scheme. Furthermore, the scheme was verified experimentally in the SNS [25].

Table 1. Main parameters of the MYRRHA main linac

Section #	**#1**	**#2**	**#3**
E_{input} (MeV)	17.0	80.8	184.2
E_{output} (MeV)	80.8	184.2	600.0
Cav. Technology	Spoke	Elliptical	
Cav. freq. (MHz)	352.2	704.4	
Cavity optimal β	0.375	0.510	0.705
Nb of cells / cav.	2	5	5
Focusing type	NC quadrupole doublets		
Nb cav / cryom.	2	2	4
Total nb of cav.	48	34	60
Nominal E_{acc} (MV/m)	6.4	8.2	11.0
Synch. phase (deg)	-40 to -18	-36 to -15	
4 mA beam load / cav. (kW)	1.5 to 8	2 to 17	14 to 32
Nominal Qpole gradients (T/m)	5.1 to 7.7	4.8 to 7.0	5.1 to 6.6
Section length (m)	73.0	63.9	100.8

The present reference scenario for a fault-recovery procedure in the MYRRHA main linac is based on the use of a local compensation method, in which only adjacent elements are used to recover nominal beam operation. This procedure should last no longer than three seconds and is defined as follows:

- In the initial configuration, the main linac is operational with all elements operating with nominal (derated) parameters. The typical needed derating level has been evaluated to be about 30% for cavities (accelerating field), 40% for amplifiers (RF power) and 10% for quadrupoles power supplies.
- A serious fault is detected during operation (abnormal beam loss for example) and the beam is immediately and automatically stopped at the source exit in the operating injector by the machine protection system, by means of the LEBT chopper.
- The origin of the fault is analysed: if it is successfully diagnosed and can be compensated, the fault recovery procedure is initiated (otherwise the beam needs to be stopped permanently). The proposed basic preliminary rules to be fulfilled to make the compensation possible are the following:
  - fault implying a cavity: the 4 nearest neighbouring cavities operating derated (i.e. not already used for compensation) are used for compensation, the maximum allowed number of consecutive failed cavities is 2 (in sections #1 and #2) or 4 (section #3);
  - fault implying a quadrupole: the whole doublet is switched off and the 4 neighboring doublets are used for compensation, the maximum allowed number of consecutive failed doublets is 1.
- The recovery procedure is then processed as follows (example of a cavity fault [26]):
  - The failed cavity RF loop is immediately disabled and the cavity quickly detuned by typically more than 100 bandwidths to avoid the beam loading effect when the beam is resumed (time budget: less than 2 seconds).
  - In parallel, new (voltage/phase) set-point values for compensating cavities are picked in the control system database; these values should have been determined beforehand, from past beam experience if the fault configuration has already been met, or from a predictive calculation using a dedicated beam dynamics simulation code if the fault configuration has not been met. The new set-points are then applied in the corresponding LLRF systems.
- Once steady-state is reached in the retuned cavities (or magnets), the beam is resumed in the linac first with very short pulses to control that the transport reaches the target; the duty cycle is then ramped within a second or so ("fast commissioning mode") to recover nominal beam operation.
- Once beam operation is resumed, maintenance is started i.e. if the faulty element is located outside the tunnel. If the repair is successful, the opposite procedure could be envisaged to return to the initial configuration.

As for the injector fast reconfiguration procedure, several points require further studies on R&D. The switching time of 3 seconds will clearly be a critical issue, with probably huge consequences on the required capabilities of the machine control system (efficient and fast fault diagnostics, fast automated beam restart and consequences). Also, an efficient predictive beam simulation code will need to be developed and benchmarked during the machine commissioning phase in order to be able to efficiently predict the optimal retuning set points in every fault configuration. On the RF cavity side, fast and reliable cold tuning systems and adequate LLRF digital systems also need to be developed. On these aspects, a R&D programme is on-going within the MAX project to experimentally demonstrate the main steps of this recovery procedure.

The proposed local recovery system has the advantage that a minimal number of cavity settings need to be modified, which should optimise reliability. A disadvantage is that a significant cavity voltage increase (up to 30%) is required to be reliably delivered in a short time (100's of msec) after being run at the derated lower voltage for months. This issue needs to be evaluated and the capability of cavities to increase their accelerating field by 30% should be regularly checked at each maintenance period. Another back-up recovery approach could be to adopt a non-local recovery system, in which all cavities are running at maximum gradients while some "back-up" cavities are kept available at the high-energy linac end at full voltage but in a non-accelerating mode (at -90° or 90° synchronous phase). In such a recovery scheme, the phases of all downstream cavities between the failed cavity and the end of the linac are, therefore, retuned, but the accelerating field is kept constant everywhere. This alternative scheme is being analysed within the MAX project, and the first results tend to show that such a global retuning would induce more beam mismatching than a local one, making the compensation of multiple faults more difficult. The final choice of strategy (local Vs global) and of available acceleration margins (30% at present) will be re-assessed in the light of the results of the on-going MYRRHA linac reliability analysis [27], which will give information mainly on the expected maximum number of failed cavities to be compensated simultaneously.

Beam monitoring and protection systems

Beam diagnostics will need to be deployed all along the accelerator in order to monitor the beam properties from place to place and thus be able to tune the first beams, maintain normal operation according to specifications, and protect the beam line equipment in case of malfunctioning. Due to the high beam power in the MYRRHA linac, special attention should be paid to operate with the lowest possible beam loss (below typically 1 W/m) in order to induce a low enough activity for hands-on maintenance.

Table 2 shows a very preliminary part-count of the MYRRHA needs in terms of beam instrumentation. Even if some intrusive sensors will be required for specific measurements (e.g. halo monitors during nominal operation, emittance-meters, wire profilers and bunch length monitors for first beam tunings at low duty cycle), only non-interceptive beam sensors should be used at full power due to the large amount of beam energy deposited. Especially, the beam power directed at the reactor will be constantly monitored by means of a beam current measurement associated with a time of flight energy measurement located in the high-energy transport lines [28]. The obtained power value will be surveyed and will need to stay constant within ±2% (uncontrolled beam trips excluded) on a typical time scale of 100 ms. Any deviation will trigger a (controlled) beam shutdown, if necessary. The beam footprint on the reactor window, which needs to be circular 85 mm diameter within ±10% (with a donut beam distribution profile), will also be constantly monitored using a near-target profile monitor and associated safety collimators. It is to be noted that such a near-target imaging system, which could be similar to the VIMOS system developed at PSI [29] or to the SNS target imaging system [30], will have a crucial role in both the tuning of the line and the monitoring and survey of the beam footprint on target, and will require dedicated R&D to be adapted to the MYRRHA case.

Table 2. Approximate beam instrumentation needs for the MYRRHA linac

	Double injector	Main linac	HEBT	Used for beam tuning and adjust	Used as input for MPS
Beam position monitors	12	52	15	X	tbd
Beam transverse profilers	15	12	15	X	
Emittance-metres	4	-	-	X	
Beam current monitors	6	2	2 to 6	X	X
Faraday cups	8	-	-	X	
Beam energy monitors	2	-	1	X	tbd
Bunch length monitors	4	12	-	X	
Beam loss monitors	4	52	> 6	X	X
Halo monitors and slits	5	-	13	X	X
Beam monitoring on target	-	-	1	X	X

For safety reasons, the MYRRHA proton beam will have to respect stringent specifications, especially in terms of beam stability and reliability. It is, therefore, crucial to be able to switch off the beam as fast as possible when some irregular circumstances are detected, either linked with the accelerator operation (e.g. unexpected beam loss level), with the nuclear core operation (e.g. unexpected high-criticality level), or with personnel safety (e.g. people entering a forbidden zone during operation). Such fast beam shutdowns will be managed by the Machine Protection interlock System (MPS) that will turn off the beam (in typically less than a few tens of micro-seconds) when abnormal conditions are detected. For MYRRHA, the basic mechanism will probably be to cut the beam in the injector section, acting on the chopper of the LEBT line. For redundancy, the RFQ or/and the ion source RF drive can be also cut off. In a second step, if the fault cannot be fixed quickly by the "fast fault-diagnostic" system and/or the compensation schemes mentioned earlier, the Faraday cup of the LEBT will also be inserted, meaning that the beam is stopped for a while.

Instrumentation and especially beam diagnostics will be the main input to the MYRRHA fast MPS. Beam loss monitors detect beam loss that can cause radiation and thermal damage to equipment in the beam line tunnels. Differential current measurements, performed using beam current monitors, and halo monitors are also to be used for redundancy. Other signals like those coming from beam position monitors can also be useful to anticipate a beam loss. In addition, several other interlock inputs, from vacuum systems, power supply systems, RF systems, etc. must also be used to trigger a fast beam shutdown procedure if a strong malfunctioning is detected in a critical component. In addition to the signals coming from the accelerator itself, it is suggested that the MYRRHA user (= reactor) should provide an extrainput signal reporting the status of the reactor. It should be noted that this fast protection system will have to be designed and implemented carefully to avoid MPS spurious signals that would shut off the beam unnecessarily and decrease the reliability performance of the accelerator, which is of prime importance in the MYRRHA case. Consequently, such MPS false alarms are often one of the main reasons for unwanted beam interruptions [31].

Table 3. MYRRHA main proton beam specifications

Proton energy	600 MeV
Peak beam current	0.1 to 4.0 mA
Repetition rate	1 to 250 Hz
Beam duty cycle	10^{-4} to 1
Beam power stability	< ± 2% on a time scale of 100 ms
Beam footprint on reactor window	Circular ∅85 mm
Beam footprint stability	< ± 10% on a time scale of 1s
# of allowed beam trips on reactor longer than 3 sec	10 maximum per 3-month operation period
# of allowed beam trips on reactor longer than 0.1 sec	100 maximum per day
# of allowed beam trips on reactor shorter than 0.1 sec	unlimited

Summary

Table 3 summarises the MYRRHA main proton beam specifications. The successful and reliable production of such a high power and stable beam is a very interesting challenge that requires a huge R&D investment. The present activities performed within the MAX project and at SCK•CEN are mainly dedicated to the general design of the accelerator and to the development of a few main primary components. Considerable efforts will be required in the coming years, not only to push these on-going R&D activities towards an engineering design phase (construction of a full injector test stand, cryomodules prototyping), but also to initiate activities related to beam operation. This concerns especially; better understanding of beam physics at low energy for transients management, fine optimisation of the strategies and procedures for faults compensation, development of a predictive beam simulation code ("virtual machine"), design of a smart control system including efficient "fast fault diagnostic" and "second-class" automated beam restart capabilities, design of a suited machine protection system, development of a set of reliable beam instrumentation diagnostics and a robust near-target imaging system.

References

[1] http://myrrha.sckcen.be/.

[2] http://ipnweb.in2p3.fr/MAX/.

[3] Barbensi, A. et al. (2007), "EFIT, the European Facility for Industrial Transmutation of Minor Actinides", *Proc. Acc'App 2007 Conf.*, Pocatello, US.

[4] "Summary of Working Group Discussion on Accelerators", OECD Nuclear Energy Agency, International Workshops on Utilization and Reliability of High Power Proton Accelerators (HPPA): 3rd Meeting, 12-16 May 2002, Santa Fe, NM, USA, ISBN 92-64-10211-6.

[5] Rimpault, G. et al. (2013), "Accelerator required characteristics for efficient ADS operation", submitted for publication to ANS Nuclear Technology.

[6] Aït Abderrahim, H. et al. (2010), "Accelerator and target technology for accelerator driven transmutation and energy production", DOE white paper on ADS technology.

[7] Vandeplassche, D., Medeiros Romao, L. (2012), "Accelerator Driven Systems", *Proc. IPAC 2012 Conf.*, New Orleans, US.

[8] Biarrotte, J.-L., Mueller, A.C. et al. (2006), "A reference accelerator scheme for ADS applications", *Nucl. Instr. and Meth. in Phys. Res.* A 562.

[9] Burgazzi, L., Pierini, P. (2007), "Reliability studies of a high power proton accelerator", *Reliability Engineering and Systems Safety*, 92-4, 449.

[10] Biarrotte, J.-L., Uriot, D. (2008), "Dynamic compensation of an rf cavity failure in a superconducting linac", *Phys. Rev. ST – Accel. & Beams*, 11, 072803.

[11] Zhang, C. et al. (2010), "Reliability and current-adaptability studies of a 352 MHz, 17 MeV, continuous-wave injector for an accelerator-driven system", *Phys .Rev. ST – Accel. & Beams,* 13, 080101.

[12] Billebaud, A. et al. (2009), "The GUINEVERE Project for Accelerator Driven System Physics", *Proc. Global 2009 conf.,* Paris, France.

[13] http://isolmyrrha.sckcen.be/.

[14] Reidelbach, K. et al. (1994), "Investigations of Space Charge Compensation of Pulsed Ion Beams", *Proc. EPAC 1994 Conf.,* London, England.

[15] Chauvin, N. et al. (2010), "Source and injector design for intense light ion beams including space charge neutralization", *Proc. LINAC 2010 Conf.*, Tsukuba, Japan.

[16] Uriot, D. et al. (2013), "Commissioning of the SPIRAL-2 deuteron injector", *Proc. IPAC 2013 Conf.*, Shangai, China.

[17] Vandeplassche, D. et al. "The R&D@UCL program in support of the MYRRHA linear accelerator", *TCADS-2 proceedings*.

[18] Zhang, C. et al. (2012), "Front-end linac design and beam dynamics simulations for MYRRHA", *Proc. LINAC 2012 Conf.*, Tel Aviv, Israel.

[19] Vossberg, M. et al. (2012), "Test RFQ for the MAX project", *Proc. LINAC 2012 Conf.*, Tel Aviv, Israel.

[20] Mäder, D. et al. (2012), "Status of CH cavity and solenoid design of the 17 MeV injector for MYRRHA", *Proc. LINAC 2012 Conf.*, Tel Aviv, Israel.

[21] Biarrotte, J.L. (2012), "Design of the MYRRHA superconducting linac and beam delivery", *Proc. SLHiPP-2 meeting*, Catania, Italy.

[22] El Yakoubi, M. et al. (2013), "Superconducting RF cavities activities for the MAX Project", *TCADS-2 proceedings*.

[23] Biarrotte, J.-L. et al. (2004), "Beam Dynamics Studies for the Fault Tolerance Assessment of the PDS-XADS Linac Design", *Proc. EPAC 2004 Conf.,* Lucerne, Switzerland.

[24] Carneiro, J.-P. et al. (2013), "Approach of a Failure Analysis for the MYRRHA Linac", *TCADS-2 proceedings*.

[25] Galambos, J. et al. (2007), "Operational Experience of a Superconducting Cavity Fault Recovery System at the Spallation Neutron Source", *Proc. HPPA 2007 workshop*, Mol, Belgium.

[26] Bouly, F. (2011), "Etude d'un module accélérateur supraconducteur et de ses systèmes de régulation pour le projet MYRRHA", PhD thesis, Université Paris Sud.

[27] Pitigoï, A. (2013), "Reliability model of SNS linac", *TCADS-2 proceedings*.

[28] Saugnac, H. et al. (2011), "High-energy beam line design of the 600 MeV 4 mA proton linac for the MYRRHA facility", *Proc. IPAC 2011 Conf.,* San Sebastian, Spain.

[29] Thomsen, K. (2009), "VIMOS beam monitoring for SINQ", *Proc. of the DIPAC'2009 workshop*, Basel, Switzerland.

[30] Blokland, W. (2010), "SNS target imaging system software and analysis", *Proc. of the BIW'2010 workshop*, Santa Fe, US.

[31] Kim, S.-H. et al. (2010), "High power operational experience at Spallation Neutron Source (SNS)", *Proc. TCADS-1 workshop*, Karlsruhe, Germany.

The R&D@UCL Programme in support of the MYRRHA linear accelerator

R. Salemme[1*], D. Vandeplassche[1], L. Medeiros Romão[1], J.-P. Carneiro[1], J.-L. Biarrotte[2], M. Baylac[3], D. Uriot[4], H. Podlech[5]
[1]Centre d'Étude de l'énergie Nucléaire (SCK•CEN), Mol, Belgium
[2]Institut de Physique Nucléaire d'Orsay (IPNO/CNRS/IN2P3), Orsay, France
[3]Laboratoire de Physique Subatomique et de Cosmologie, Grenoble, France
[4]Commissariat à l'Énergie Atomique et aux énergies alternatives (CEA), Saclay, France
[5]Institut für Angewandte Physik (IAP), Goethe Universität, Frankfurt am Main, Germany

Abstract

The MYRRHA project, currently proposed by the SCK•CEN, aims to demonstrate the feasibility and operability of a safe and efficient transmuter, constituted of a subcritical core fed by an external neutron source obtained by a high power proton accelerator. The outstanding challenge of the MYRRHA accelerator is the design requirement of Mean Time Between Failures (MTBF), set at 250 hours. The current R&D programme is divided into three lines of investigation. The second R&D line, named RFQ@UCL, is devoted to injector engineering design and subsequent construction, including prototyping and feedback to design. This activity is led by SCK•CEN in collaboration with the Cyclotron Resources Center (CRC), at Louvain-la-Neuve, Belgium, the CNRS/IN2P3 laboratories IPN Orsay (IPNO) and LPSC Grenoble and the IAP Frankfurt laboratory. This programme is related to the first R&D line, the FP7 MAX programme.

The principal motivation of the RFQ@UCL programme is the experimental address of the MYRRHA injector design. The first scope is focused on the 4-rod RFQ. After successful construction of a short test section for thermal behaviour investigation conducted by IAP in the framework of MAX, the full-size 4-rod RFQ prototype is expected to be constructed and installed for beam tests. The initial setup includes a commercial ECR proton source, a dedicated LEBT section, a full-size 4-rod RFQ prototype, a diagnostic section and a beam dump. In a later stage, the RFQ@UCL activity could be extended towards the subsequent higher beam energy structures of the injector. Such an initial injector will evaluate the choice of RFQ itself, and furthermore, this test platform is capable of exploring many other critical issues in the injector design.

Introduction

Accelerator-driven systems are playing an important role in the future energy production scenarios including Gen-IV nuclear reactors, as they are potential and promising candidates for transmutation purposes [1]. The introduction of the Partitioning and Transmutation (P&T) technique in the nuclear waste reprocessing cycle is currently being studied to allow isolation of long living radioisotopes and their subsequent transformation in much shorter lifetime isotopes via neutron irradiation. This method would significantly alleviate the burden upon the geological disposal of high-level nuclear waste. However, the road towards an industrial transmutation prototype still features many R&D steps. The MYRRHA project [2], currently proposed by the SCK•CEN aims to demonstrate the feasibility and operability of a safe and efficient transmuter, comprising a subcritical core fed by an external neutron source obtained by a high power proton accelerator.

This paper gives a description of part of the R&D focused on the linear accelerator that may be used for the MYRRHA project in its ADS configuration. The MYRRHA reactor, with a thermal power of approximately 80 MW_{th} in the ADS mode will be cooled by liquid Pb-Bi eutectic (LBE). Given these parameters, the subcritical core of such an ADS requires an intense external neutron source to deliver a continuous fission power. The spallation mechanism is considered for obtaining a source of fast neutrons through an external high energy and high intensity proton beam. The subcritical core geometry of MYRRHA is optimised for an impinging proton beam energy of 600 MeV, where the Pb-Bi coolant is also used as the heavy target for the spallation reaction. At this energy, the neutron yield obtained by spallation on lead is around 15 per incoming proton. The requested maximum beam intensity has been calculated by Monte-Carlo simulations and varies between 2.5 and 4 mA depending on the burn-up of the nuclear fuel, delivered up to 2.4 MW beam above the core in continuous wave mode, through a beam window. Table 1 summarises the main characteristics of the required beam.

Table 1. MYRRHA beam characteristics

Accelerated particle	Protons
Beam energy	600 MeV
Beam current	4 mA
Time structure	CW, with 200 μs holes at 250 Hz repetition rate for sub-criticality monitoring
Beam delivery to the reactor	Vertically from above through an achromatic beam line
Beam stability	Energy ±1%; Current ±2%; Position and size ±10%
Beam shape on target	Circular ϕ=80 mm, flat or donut shaped power density, by AC scanning magnets
MTBF	> 250 h, a failure being a beam trip longer than 3 s

These current beam specifications set the MYRRHA accelerator in the high power proton machines category. In the particle accelerators, state-of-the-art machines have been developed and constructed (ISIS, SNS) or are under development (ESS, SPL, SPIRAL-2, J-PARC, IFMIF). While the specificity and difficulty of the Continuous Wave (CW) nature of the beam delivery of MYRRHA is acknowledged, the really outstanding challenge is the design requirement set on the Mean Time Between Failures (MTBF). In the MYRRHA operational context, the beam is considered to fail if its delivery to the subcritical core is interrupted during a time period that lasts longer than three seconds. Since the MYRRHA

cycle will take 3 months and during such a cycle it is expected to have not more than 10 beam failures, the quoted MTBF is then set at 250 hours. Shorter beam trips are tolerated at a virtually unlimited occurrence frequency. This demanding reliability requirement package is strongly related to the thermal shocks which a beam interruption causes in an ADS, adversely affecting structural materials of the reactor and possibly causing safety issues. A high available proton beam is required for long operability of the plant [3].The allowed beam trip frequency of the whole accelerator is thus significantly lower than observed on today's reported achievements of comparable accelerators [4], therefore the issue of reliability is considered to be the main challenge. This issue concerns all R&D activities related to the MYRRHA accelerator.

The accelerator for MYRRHA is now being developed in a strongly collaborative mode, exploiting the very extensive know-how present in the European accelerator community. The R&D activities have, to a large extent, been organised as subsequent European Framework Programme projects. A dedicated R&D programme based on three lines of investigation is on-going. In order to support bilateral agreements for common R&D activities, Memories of Understanding (MoU) are stipulated with research institutes. Finally, partnerships based on a commercial agreement, with research institutes or selected industrial companies, will allow realising prototypes in a highly interactive mode.

The accelerator choices around reliability

The general philosophy to reach a high natural MTBF on the MYRRHA accelerator is identified in the *fault tolerance* capability, achieved only if a single failed element does not automatically imply a global failure [5]. Such a fault tolerance can only be effective if it is accompanied by a realistic switching time (fault detection time plus reconfiguration time: in MYRRHA this time is necessarily three seconds) and a Mean Time To Repair (MTTR) shorter than the MTBF of the failing element or chain. The fault tolerance concept is addressed by design, following three general principles to accomplish the reliability goal: redundancy, with a maximum of the serial version, use of components far from their limits and repairability. For economic reasons, the parallel redundancy scenario should be avoided. The serial redundancy scheme (replacing a missing element's functionality by retuning adjacent elements with equivalent functionalities) may be accomplished if foreseen during the design phase. However, this strategy implies a high degree of modularity of the accelerating and focusing structures.

Since the MYRRHA accelerator is a high power proton accelerator with strongly enhanced reliability operating in CW mode, and in agreement with several high power accelerator projects [6-8], the technical solution of a superconducting linac has been adopted [9]. The compatibility of this choice with the three abovementioned reliability principles is clear: the architecture of a superconducting linac, consisting of a sequence of nearly identical and modular RF cavities, complies perfectly with the serial redundancy scheme, in addition, a superconducting linac can handle a beam current of 4 mA with performances of the superconducting RF cavity very far from present limits.

The linac consists of two clearly distinct sections:

- A medium and high energy section, highly modular, based on individual, independently controlled cavities. In this section, the serial redundancy may be applied successfully to obtain a strong fault tolerance [10]. The function of a faulty cavity may typically be taken over by four adjacent cavities.
- A low-energy section (or injector), in which the modularity and fault tolerance principles are not applicable. In this section, the beam optics is frozen by design and the accelerating structures are mainly based on multi-cell cavities. Here, redundancy has to be applied in its parallel form, thus two complete injectors are foreseen. The transition energy between the two sections is fixed at 17 MeV. At

this energy, a fast dual input switching magnet will be installed to merge the injector lines.

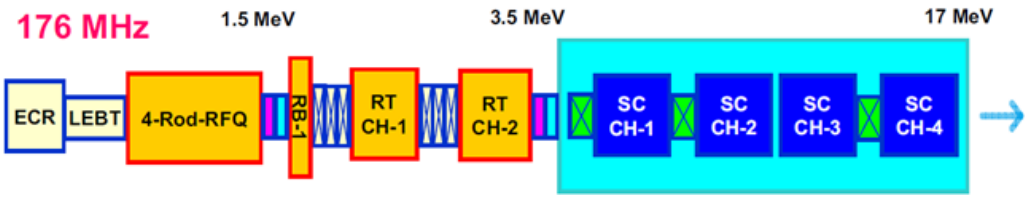
In this paper, only the injector is described. For the whole superconducting linac design choices, please refer to [11].

Injector

The injector part (0 ÷ 17 MeV) is based on some rather unconventional solutions. In this section, the serial redundancy mechanism is not achievable because of the frozen beam optics and the fast evolution of the beam parameters along the line, precluding modularity. In order to preserve the fault tolerance capability of the linac, a full parallel redundancy scheme has been implemented in the MYRRHA injector, implying the installation of two identical accelerating sections up to 17 MeV (one being operational, the other in hot-standby). The injecting sections have been designed in view of optimal efficiency, considering that this section will be doubled for reliability. Each injector consists of an ECR proton source followed by the Low Energy Beam Transport (LEBT) line, a Radio Frequency Quadrupole (RFQ), two room temperature CH-cavities and four superconducting CH-cavities [12].

The principal architect of this section is the Institute for Applied Physics (IAP) in Frankfurt, Germany. A 352.2 MHz version of the injector was developed in the framework of the FP6 EUROTRANS project, in which a common accelerator layout was envisaged for the ADS demonstrator (i.e. MYRRHA) and for the industrial transmuter prototype (called EFIT). In the framework of the FP7, the EUROTRANS programme was developed and followed by the MYRRHA Accelerator eXperiment (MAX) R&D programme, started in 2011. The MAX programme continues the R&D studies on the accelerator candidate for ADS purposes, delivering an updated and consolidated design of a real machine including prototyping and demonstration. Focusing the requirements only on an ADS demonstrator, i.e. MYRRHA, the potential benefits of a 176.1 MHz injector were investigated [13], achieving an optimised reliability and economic efficiency but at the cost of a reduced maximum beam current capability. The expected benefits are: a lower input energy of the copper CH-DTL, therefore a shorter RFQ, reduced power density in the copper structures, a lower input energy of the RFQ, thus a reduced electrostatic potential on the ion source, the possibility to consider a 4-rod RFQ instead of a 4-vane version, yielding relaxed tolerances, easier adjustments and significant savings. A pre-study of this 176.1 MHz scheme confirmed all these benefits (in particular the input and output energies of the 4-rod RFQ at 30 keV and 1.5 MeV, respectively) and added the possibility of reducing the inter-electrode voltage in the 4-rod RFQ for a Kilpatrick factor of 1.2. Figure 1 shows the schematic layout of the 176.1 MHz injector design. This scheme is now considered as the preferred one for the MYRRHA double injector, and it will be the object of a dedicated R&D programme.

Figure 1. The 17 MeV, 176.1MHz, injector of the MYRRHA accelerator



Each of these 2 injectors mainly consists of these elements:

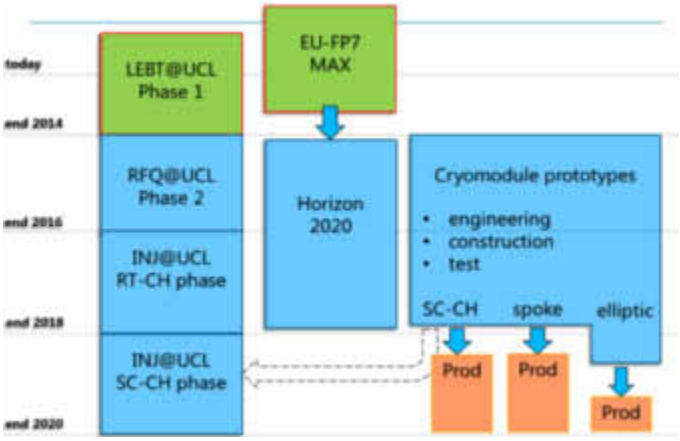
- the Electron Cyclotron Resonance (ECR) type ion source, for optimal longevity, delivering a moderate 30 keV proton beam;

- the Low Energy Beam Transport (LEBT) line, for low energy beam characterisation, manipulation, and appropriate matching into the next element;
- the 4-rod Radio Frequency Quadrupole (RFQ), focusing, bunching and accelerating the beam up to 1.5 MeV;
- two copper multi-cell CH-DTL structures, bringing the beam up to 3.5 MeV;
- four superconducting CH-DTL structures for the acceleration up to 17 MeV; The rationale of this solution is to extend the advantages of the superconducting RF to the lowest possible energy.

R&D on the MYRRHA accelerator

A conceptual design of an ADS-type high power proton linac has been initiated by the EURATOM Framework Programmes (EU FP5 PDS-XADS and FP6 EUROTRANS projects [14] [15]), in which the fundamental choices regarding the accelerator for MYRRHA were adopted. The current R&D activity period, in which accelerator reliability will actually be the most important issue, is focused on the following topics: advanced beam dynamics and error studies, reliability modelling studies, optimised injector design, prototype cryomodules operation.

Figure 2. Scheme of the R&D activities foreseen in view of the linac for MYRRHA



The R&D programme related to the MYRRHA linac is divided into three lines of investigation, which have linac reliability as a common subject. They are combined in a coherent scheme presented in Figure 2. The on-going FP7 MAX project is continuing the R&D studies on the accelerator candidate for the ADS demonstrator with the goal of delivering an updated and consolidated design of a real superconducting linac to be adopted in the MYRRHA project. This R&D line is led by IPN Orsay in collaboration with a large number of research institutions and industrial companies. Developments, studies and experiments on accelerator test sections are performed to increase the level of confidence of the MYRRHA accelerator design. In addition to these activities, studies and simulations on general accelerator design and reliability issues are being carried out. The work has been divided into four main work packages, including:

- global design coherence;
- injector design;
- main linac design;
- system optimisation.

The second R&D line, RFQ@UCL, is devoted to the injector engineering design and subsequent construction including prototyping and feedback to design. The principal motivation of this R&D programme is to address the MYRRHA injector design gaining experience from a tangible prototype. On the other hand, the Injector@UCL is a tool for relevant reliability-oriented experiments, which implies experience, education, and innovation in this field. This activity is led by SCK•CEN in close collaboration with the Cyclotron Resources Center (CRC), at Louvain-la-Neuve, Belgium. CRC is part of the Catholic University of Louvain, UCL. Obviously, this programme is closely related to the MAX programme. The third R&D line addresses cryomodules prototyping and operation. Cryomodules prototyping is envisaged for the superconducting CH, spoke, elliptical cavities. The goal is to provide a solid engineering design and then construction, operational tests and feedback to design in view of the final industrial procurement for the MYRRHA accelerator construction. This activity should be co-ordinated by SCK•CEN after 2014 and executed by the respective principal architects (namely research institutes).

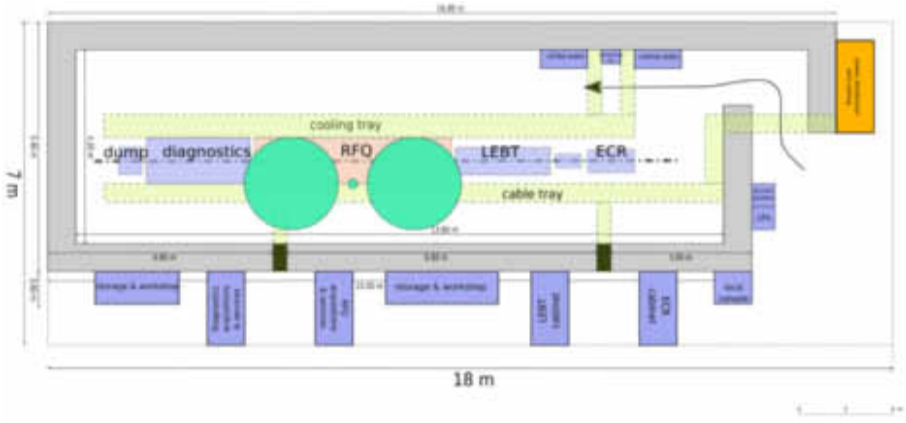
The R&D@UCL programme

This experimental programme, under the name of RFQ@UCL, is executed in collaboration with the Cyclotron Resources Center (CRC), at Louvain-la-Neuve, Belgium, where the experimental test line will be located. On the other hand, the programme is based on bilateral collaboration agreements with the CNRS/IN2P3 laboratories IPN Orsay (IPNO) and LPSC Grenoble and with the IAP Frankfurt laboratory. Moreover, the RFQ@UCL programme is heavily interacting with and relying on the European FP7 MAX programme. The construction of the Injector@UCL, up to final 17 MeV energy and including beam diagnostics development, has recently been supported by the MYRRHA accelerator 1st International Design Review held in Bruxelles in November 2012. Figure 3 shows the overview of the foreseen experimental set-up.

The installation layout

All experimental equipment will be installed in a shielded area specifically built in the experimental hall at UCL/CRC. For safety purposes, the area will be enclosed by concrete blocks conveniently arranged to form a bunker. The set-up includes a limited space in the CRC pump room, where the cooling system machinery will be installed and a remote workspace in the CRC control room.

Figure 3. General layout of the experimental set-up of RFQ@UCL R&D programme



The round structures represent the 160 kW Solid State RF amplifier to be installed on top of the bunker.

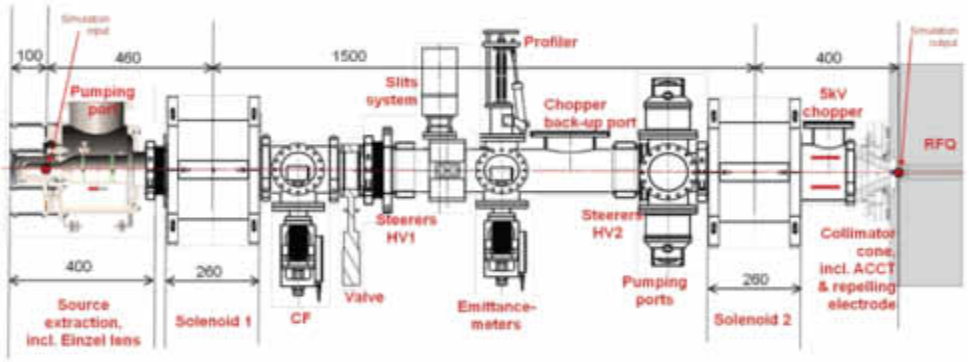
A large proportion of the injector equipment requires dedicated cooling and electrical power supply (the RFQ only requires 160 kW of continuous RF power, where the corresponding amplifier has a wall plug power of around 350 kVA). The electrical distribution is accomplished by means of two electrical cabinets, to be installed in the experiment hall and in the pump room, respectively. Each major piece of the experimental equipment will then correspond to a dedicated cabinet, housing its specific power distribution, power converters, controls and acquisitions. At this stage, a high degree of reliability of all the adopted solutions is definitely important. It should be noted that the set-up concerns an experimental activity, a high flexibility with respect to control and interlocks is compulsory.

Like the electrical distribution system, the cooling system will involve two locations: the thermal hydraulic machinery (pumps, heat exchangers, chiller) will be installed in the pump room, while the dedicated distributions to the cooling end users will be installed in the experimental hall. The cooling system should provide three distinct supplies: the cooling air circuit, the chilled (demineralised) water circuit, the moderate temperature (demineralised) water circuit. These three circuits dissipate into a general cooling loop belonging to CRC, directly (air circuit) or through heat exchangers (chilled and normal water). The last loop exchanges its heat with the water from the CRC cooling tower. The total cooling capacity is expected to be 725 kW.

The R&D test stand

The principal motivation of this R&D programme is the experimental address of the MYRRHA injector design. The first scope is focused on the 4-rod RFQ. After a successful construction and assessment of a short section (400 mm) for thermal behaviour investigation conducted by IAP in the framework of MAX, the full-size 4-rod RFQ prototype is expected to be constructed and installed for beam tests. This test stand will include a commercial ECR proton source and a dedicated LEBT section placed before the RFQ, followed by a diagnostic section and a beam dump.

Figure 4. Preliminary layout of the first experimental set-up of the RFQ@UCL R&D programme, including the ECR proton source, the LEBT and the RFQ interface sections



In a later stage, the RFQ@UCL activity could be eventually extended towards the subsequent higher beam energy structures of the injector, adding copper CH-type accelerating cavities to the existing set-up for long reliability runs. A full injector comprising SC structures will, however, need a dedicated cryogenic plant, currently missing at CRC.

The proton source has been commercially procured from Pantechnik, France. Pantechnik design choices include an ECR 2.45 GHz proton source with a specific magnetic configuration. A tapered axial RF injection is adopted. The source will be delivered with its own control and power supply system. In Table 2 the source design requirements are listed.

Table 2. Injector's proton source design requirements

Voltage	30 kV (40 kV capable)
Beam current	20 mA DC
RF	2.45 GHz, 1200 W
Transverse emittance @ 5 mA	0.1 π·mm·mrad RMS norm.
Magnetic system	Permanent magnets
Autonomous control system	NI CompactRIO
Beam diagnostics devices incl.	Faraday cup, allison scanner
	incl. provisions for reliability/reparability

The LEBT design and engineering has been provided by LPSC Grenoble, under a bilateral agreement signed between CNRS and SCK•CEN. The design for beam dynamics simulations and error analysis has been supported by IPNO. The aim of the LEBT transport line is to efficiently inject the proton beam inside the RFQ by providing at the RFQ entrance a centered beam with matched transverse emittances, lower or equal to the RFQ design value, which is 0.2 π·mm·mrad RMS normalised. The choice of a classical short magnetic LEBT layout, inspired from similar injection lines, was validated in October 2011. The overall length of the line, from the plasma chamber extraction hole to the RFQ entrance (inner flange), is around 2500 mm long. The beam focusing is demanded to multiple magnetic solenoids. The first magnetic solenoid is located as close as possible to the source extraction chamber in order to minimise the beam size at the entrance. This magnet includes additional coils for dipole corrections (horizontal and vertical). A Faraday cup system is then installed and will be used for ion source tuning and safety aspects. The line follows with a vacuum gate valve and a series of ports dedicated to: a collimating system to reshape and clean the beam, a set of locations for beam instrumentation, like secondary emission 2D profiler and beam emittance-meter(s), dedicated ports for pumping and gas injection, a second vacuum gate valve. One of these ports should be designed to be able to host the beam chopper in a back-up location. The overall distance between the two solenoid centres has been set at 1500 mm. This second magnet should be located as close as possible to the RFQ entrance (maximum 400 mm from the last solenoid's center) in order to focus the beam inside the RFQ within nominal specifications.

Finally, the space available between the last solenoid and the RFQ entrance (240 mm long) needs to host the following elements:

- An electrostatic beam chopper. It is required to give a precise time structure to the beam delivery towards the MYRRHA reactor. It has a critical role in the machine protection mechanism. For reactor subcritical monitoring, 200 μs/250 Hz beam interruptions will be implemented. The adoption of an extraction kicker magnet in the HEBT, at 600 MeV, will make available 190 μs/250 Hz beam pulses for an ISOL facility. This chopper is very similar to the solution adopted in SPIRAL-2 [16] with shorter electrodes and reduced plate-to-plate total voltage (about 5 kV). The capability to operate it with an extremely variable duty cycle is the real challenge and will imply specific design solutions of the driving system.
- An RFQ injection collimator, to intercept the beam deviated by the upstream chopper and a large portion of the pollutant particles (H_2^+, H_3^+) that are not properly focused in the RFQ. The critical issue is the high peak power density deposited by the proton beam on the collimator surface, which must be safely evacuated by water cooling. In order to reduce it, a conical shape might be adopted.
- A beam current monitor (probably a short ACCT current transformer), should be located as close as possible to the RFQ flange in order to accurately monitor RFQ transmission efficiency. Such a transformer will require an electrical insulation at

the end of the line. A particular ACCT integration directly inside the RFQ flange is under discussion.

- A negative electrode should also be located close to the RFQ flange. This will serve as an electron repeller, keeping good space-charge compensation conditions in the area [17].

The design of this RFQ interface section is on-going at SCK•CEN in collaboration with UCL/CRC. The engineering design of the LEBT line, its subsequent production and the installation in UCL/CRC Louvain-la-Neuve will follow during the next 2 years.

Such an initial injector will evaluate the choice of RFQ itself, and furthermore, it will be an efficient test platform for a large number of related critical issues. Currently, interest is focused on:

- the adoption of a high power, modular, Solid State RF amplifier at 176.1 MHz;
- interceptive and non-interceptive diagnostic devices for high intensity CW beams; A full set of diagnostic devices is to be tested. Given the properties of the beam in this section (low energy but high current), it is envisaged that the following parameters will be monitored: beam current (interceptive methods by Faraday cups, non-interceptive by BCTs), beam position, beam profiles, emittances, longitudinal bunch properties. The diagnostic equipment set-up is currently under discussion.
- a robust and comprehensive control system, based on the 3-tier approach of typical large machines control systems, adopted in physics research; The candidate architecture is EPICS. The RFQ@UCL is capable of being a significant representation of the final MYRRHA accelerator control system and of acting as a test platform, where architectural choices and on-line beam simulations at small scale can be tested.
- the location of the beam chopper in the LEBT of the injector is under assessment; The beam chopper location in the LEBT is a particular issue: in its reference configuration it should be as close as possible to the RFQ in order to minimise the effects of the Space Charge Compensation (SCC) transients that are related to the compensation recovery speed and the distance travelled while restoring SCC during chopping transients.
- space charge compensation efficiency and global behaviour in the LEBT, both during steady-state and transients, including the gas injection techniques assessment;
- full experimental characterisation of the low-energy beam, allowing an optimal initial beam configuration at the entrance of the RFQ.

Long reliability runs will allow triggering reliability issues coming both from design and operation, optimising and consolidating the design choices. Feedback to design and in-depth analysis can contribute to improving the final injector project. Operational experience can be gained and training of the accelerator team within SCK•CEN can be obtained. Finally, this installation will acquire a solid educational role.

Conclusion

The set-up at UCL/CRC addresses important design choices of the future MYRRHA superconducting Linac. The initial set-up includes a commercial ECR proton source, a dedicated LEBT section, a full-size 4-rod RFQ prototype, a diagnostic section and a beam dump. The CW operability of a 4-rod RFQ will be carefully investigated including beam characterisation, RFQ matching assessment and transmission efficiency measurements.

This test platform is also capable of exploring many other critical issues in the injector design. The experimental programme includes beam characterisation and RFQ matching, space charge assessment, test of different diagnostic equipment performed in long reliability runs in order to trigger possible critical issues. The set-up will also be a control system test platform. The RFQ@UCL programme is an essential part of the engineering activities and the full development cycle of the future MYRRHA injector. It addresses the engineering design, prototyping, production, tests and in-depth analysis. This activity ensures the translation of the design into engineering solutions that will allow achieving the reliability and quality requirements. The study and evaluation of risks arising from the design and prototyping provide feedback and eventually a complete package of consolidated solutions for the final MYRRHA injector.

References

[1] Aït Abderrahim, H. et al. (2010), "Accelerator and Target Technology for Accelerator Driven Transmutation and Energy Production", *DOE sponsored White Paper on Technology for Accelerator Driven Systems*, FERMILAB-FN-0907-DI, LA-UR-10-06754.

[2] Aït Abderrahim, H. (2011), "MYRRHA an Innovative and Unique Research Facility", AccApp'11, p. 1, Knoxville, US.

[3] Rimpault, G. et al. (2012), "The issue of Beam Trips of the accelerator for efficient ADS operation", *Nuclear Technology*.

[4] Galambos, J., Koseki, T., Seidel, M. (2008), "Hadron Beams 2008", Nashville, Tennessee, CPL04, p. 489.

[5] Burgazzi, L., Pierini, P. (2007), "Reliability studies of a high-power proton accelerator for accelerator-driven system applications for nuclear waste transmutation", *Reliability Engineering and Systems Safety*, p. 449

[6] Rej, D.J. (2001), "High-power LINAC for the Spallation Neutron Source", *Pulsed Power Plasma Science, IEEE Conference Record*.

[7] Lindroos, M., Oyon, C., Peggs, S. (2009), "The ESS Superconducting Linear Accelerator", FROBAU02, *Proc. SRF2009*, p. 918, Berlin, Germany.

[8] Cornell, J.C. (2009), Final Report of the EURISOL Design Study, published by GANIL, France.

[9] Vandeplassche, D., Biarrotte, J.-L., Klein, H., Podlech, H. (2011), "The MYRRHA linear accelerator", *Proc. IPAC 2011*, WEPS090, p. 2718, San Sebastian, Spain.

[10] Biarrotte, J.-L., Uriot, D. "Dynamic compensation of an RF cavity failure in a superconducting linac", *Phys. Rev. ST Accel. Beams 11*, 072803.

[11] Vandeplassche, D., Biarrotte, J.-L., Podlech, H., Klein, H. (2011), "The MYRRHA linear accelerator", *AccApp11 conference*, Knoxville, US.

[12] Podlech, H., Amberg, M., Klein, H., Mäder, D., Ratzinger, U., Schempp, A., Tiede, R., Vossberg, M., Zhang, C. (2011), "General layout of the 17 MeV injector for MYRRHA", *Proc. IPAC 2011*, WEPS039, p. 2574, San Sebastian, Spain.

[13] Zhang, C. Klein, H., Mäder, D., Podlech, H., Ratzinger, U., Schempp, A., Tiede, R. "New strategies and approached for the injector development", EUROTRANS to MAX *Proc. IPAC 2011*, WEPS043, San Sebastian, Spain.

[14] Giraud, B. (2004), "Principal Concepts of XADS designs in the 5th FP", ICRS 10 RPS, Madeira Island.

[15] Knebel, J.U. (2010), "The EUROTRANS Project: Partitioning and transmutation research in Europe", *Technology and Components of Accelerator-driven-Systems,* Karlsruhe (TCADS), p. 43.

[16] Caruso, A. et al. (2011), "The LEBT chopper for the SPIRAL2 project", *IPAC 2011*, TUPS082, p.1732, San Sebastian, Spain.

[17] Chauvin, N. et al. (2010), "Source and injector design for intense light ion beams including space charge neutralization", *Proceedings of Linear Accelerator Conference LINAC2010,* TH302, Tsukuba, Japan.

Superconducting RF cavity activities for the MAX Project

Marouan El Yakoubi[1], Hervé Saugnac[1], Emmanuel Rampenoux[1], Jean Luc Biarrotte[1], Frédéric Bouly[2], Rocco Paparella[3], Paulo Perini[3]
[1]CNRS/IPN Orsay, France, [2]CERN, Switzerland, [3]INFN, Italy

Abstract

Within the framework of the MAX Project associated with the detailed study of the MYRRHA Facility linac, two tasks relating to the design of superconducting accelerating components are under progress. Cryogenic tests, in a cryomodule configuration of a 700 MHz, beta = 0.47, elliptical RF superconducting cavity are performed with the aim of evaluating and improving the reliability of the different components (RF cavity, power coupler, cold tuning system and the cryogenic features). The other task addresses the first superconducting linac section cryomodule. It is composed of two 350 MHz, beta = 0.5 spoke type cavities cooled at 2 K. This paper presents the results on the elliptical cavity and the status of the spoke cryomodule design.

Introduction

The proton superconducting linac for MYRRHA (600 MeV, 5 mA) consists of 4 sections. The low beta (0.37) section from ~17 MeV to ~100 MeV is comprised of cryomodules housing two single spoke cavities. A beta = 0.47, from ~ 100 MeV to ~ 200 MeV, and a beta = 0.65 from ~ 200 MeV to ~ 600 MeV, sections are comprised of cryomodules housing 4 elliptical cavities.

Within the framework of the European project EUROTRANS, several components for the elliptical cavities section have been designed and built for R&D purposes. Tests on these components (cold tuning system, beta 0.65 cavity, power coupler) are performed in a cryomodule, like configuration, in a dedicated cryogenic test stand at IPN Orsay. These tests, currently performed within the framework of the MAX project, are focused on the reliability aspects, which are a major issue of the MHYRRA accelerator. In addition, a detailed design of the spoke cryomodule of the low beta section is in progress.

Spoke cryomodule design

The detailed design of the Spoke (beta=0.37, 352.2 MHz) cryomodule started within the framework of MAX in January 2012 and was to be achieved in January 2014. It concerns the complete definition of the cryostat, the cavities, and the auxiliary components (cold tuning system, magnetic shielding, power coupler), the procedure and the tooling for the assembly.

Cavity design

The RF design has been fixed using CST MicroWave Studio 2012 on an around 100 00 tetrahedral mesh model. The optimisation was obtained by playing on a dozen of

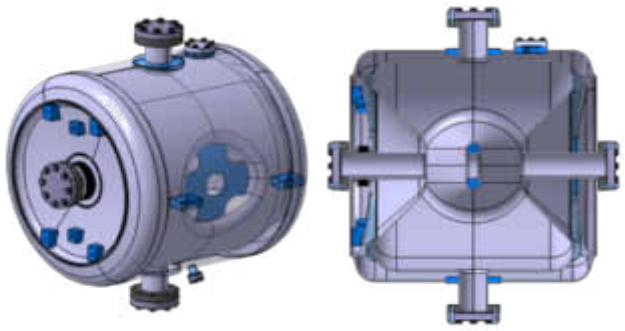
geometrical parameters taking into account manufacturing constrains. The goal for the MYRRHA Linac, set to E_{pk}/E_{acc}< 4,4 and B_{pk}/E_{acc}< 8,3 is achieved (see Table 1).

Table 1. Cavity (beta = 0.37, 352 MHz) main parameters

Optimised parameters		Optimised parameters	
$E_{acc\ normal\ operation}$; $E_{acc\ fault\ tolerance}$	6,2; 8,2 MeV/m	L_{acc}=optimal beta x c x f [m]	0,315
E_{pk}/E_{acc}	4,29	Tuning sensitivity [kHz/mm]	156
B_{pk}/E_{acc} [mT/MV/m]	7,32	Sensitivity to tressure [Hz/mbar]	7,6 < S_P< 14
G [Ohm]	109	Lorentz force factor [Hz/(MV/m)^2]	-6 < K_L< -5,28
r/Q [Ohm]	217	Approximated bandwidth	150 Hz
Qo @ 2K for Rres=20 nΩ	$5{,}2.10^9$	$\beta_{optimal}$	0,37

A study, made by the ACS Company, shows that for our 352 MHz Spoke cavity, an operating temperature of 2 K is more efficient in terms of electrical power consumption. It also leads to a better stabilisation of the cavity helium bath pressure.

Figure 1. Spoke cavity with its helium vessel



The mechanical design optimisation has been performed using ANSYS FEM software for the mechanical and the mechanical/electromagnetic coupled simulations. The thickness is 3 mm both for the cavity walls, made of the niobium with RRR>200, and for the helium vessel, made of titanium grade 2. The low sensitivity to pressure (see Table 1) implies that the cold tuning system, which may be a weak part in terms of reliability, will have small operating time, which corresponds to the high constraints on reliability required by the MYRRHA accelerator.

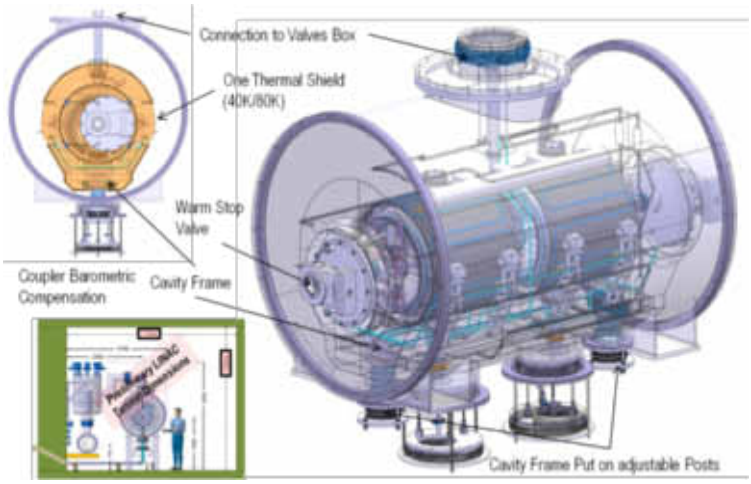
Cryostat

For the MYHHRA Linac, fine cryomodule segmentation was chosen in order to be able to apply fault tolerance scenarios in case of failure for any reasons (RF, vacuum, cryogenics) of a single spoke cryomodule. Hence, there will be only one separate valves box per cryomodule. The cryostat will have a single thermal shield cooled with gaseous helium at 4 bars, from 40 K to 80 K. Multi layers insulation (30 layers on thermal shield, 10 on cavity) will provide thermal radiation insulation. Thermal intercepts, between 5 K to 10 K, for the power couplers and the cavity supporting frame, will be performed by a circuitry fed by supercritical helium at 3 bars. The cavities and the magnetic shields will be cooled down from 300 K to 5 K using a dedicated loop with liquid helium at 1.2 bars. A

phase separator of around 5 litres, placed on the top of the cavity string, allows maintaining the cavities at 2 K with small pressure fluctuations. Preliminary evaluations of the cryogenic static losses, < 3W@2K, <10W@5/10K, < 90W@40/80K, satisfy the cryoplant specifications.

The two cavity string is maintained on a simple frame put on two posts fixed to the cryostat vacuum vessel. The cavities are able to slide on the frame which can slide itself on one of the posts. An invar rod fixed to the fix part of the frame limits and controls the longitudinal displacement of the two cavities, to, respectively, 0.1 mm and 0,4 mm. The cavities will vertically go down from less than 1 mm during cool-down. This possible misalignment can be adjusted by anticipating this displacement during warm temperature assembly or, as the posts can be adjusted, by performing a new alignment after cool-down. The vacuum vessel diameter is 1200 mm and the length between the cryostat warm valves is 2200 mm. The cryogenic connection line is situated at the top of the vacuum vessel. All the cryogenic valves and subcooling heat exchanger are implemented in a dedicated valve box fixed on the linac tunnel close to the cryomodule.

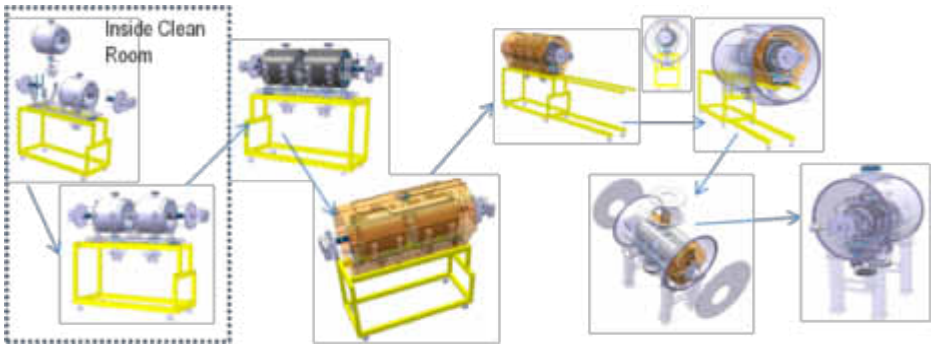
Figure 2. Cryomodule overview



Cryomodule assembly

The cavities, the power couplers and the warm stop valves are assembled on the cavity frame inside an Iso 4 Clean Room. The rest of the cold mass (magnetic shielding, cold tuning system, thermal shield, MLI, sensors) are then assembled outside the clean room. The cold mass is inserted inside the vacuum vessel, off-axis, due to the 300 mm length between the cavity and the warm window block of the power coupler. The remaining parts of the vacuum vessel, the cryogenic connections and the power couplers' compensation systems are finally assembled.

Figure 3. Spoke cryomodule assembly sequence



Auxiliary components

The power coupler with only one warm window (SNS type) is designed for 20 kW CW and 50 Ohm. The specifications for the spoke section of the MYHRRA linac are 10 kW average with a maximum of 16 kW for fault tolerance recovery (adjacent cavities operating at higher power to compensate cavity failure). The external conductor is fitted to the cavity bottom with a CF 63 flange. The distance between 2 K and 300 K is around 300 mm. Two heat intercepts, at 50 K and 5 K respectively, are sufficient to reach the thermal loss specifications. A barometric compensating system, placed outside the cryomodule, reduces the pressure induced inside the cavity when evacuating the vacuum vessel.

The Cold Tuning System (CEA "Soleil" type) is identical to the one designed at IPN Orsay for the ESS spoke cavities. For this cavity, it allows a slow coarse tuning of around 150 kHz at 2 K. Piezo-electrical actuators allow a fast tuning for micro phonics compensations on a fine range of around 300 Hz. Further studies should be performed on how to decrease the time in which the cavity can be totally detuned, around 15 kHz (around 100 bandwidths) in less than 2 seconds, which is a constraint given by the fault tolerance concept.

704 MHz prototypical test bench

The aim is to demonstrate the possibility to implement the RF fault-tolerance concept foreseen for the MYHRRA accelerator, on a prototypical cryomodule. A prototype test cryomodule, operating at 2 K, together with its associated valve box, has been developed and built. This programme started within the framework of EUROTRANS in collaboration with INFN Milano and IPN Orsay and is in progress within the framework of the MAX project dedicated to the design of the MYRRHA accelerator.

Experimental site

An experimental site has been built at IPN Orsay to do cryogenic and high RF power tests. The cryogenic installation developed from 2007, allows the cool-down of a thermal shield at 80 K using liquid nitrogen and has a complete helium feeding and recovery system. The super fluid helium operation is made using a warm pumping group composed of a primary pump of 1600 m^3/h and a roots pump of 4000 m^3/h. First, cryogenic tests on the prototypical cryomodule show that the maximum operating power of the whole system (cryostat, valves box, pumping line and pumping group) is, as expected, around 40 W@1.9 K. A cryogenic upgrade, by adding a second pumping group to increase the available power at 2 K, is currently in progress.

The RF power installation allows supplying the power coupler during the cryogenic tests and the couplers conditioning at 300 K. The RF power source is constituted by a first solid-state stage operating at up to 1 kW at 704.4 MHz, feeding a second amplifier stage

performed by an Inductive Output Tube (I.O.T.), manufactured by the THALES Company, able to provide a maximum power of 80 W in CW operation. The test bench features a RF conditioning cavity for two 704 MHz couplers, diagnostics (vacuum, RF power, cooling water flow, multiplication current), hardware safety systems (Coupler and I.O.T. "security box"), monitoring software, data acquisition system and circulator.

Figure 4. Experimental pit at IPN Orsay



Prototypical cryomodule

The prototypical cryomodule houses one 704 MHz, beta=0.47 elliptical designed by INFN Milano, a Cold Tuning System (INFN Blade-Type Tuner) with piezo-electrical actuators for fast frequency tuning and a power coupler with a warm window (SNS Type) developed by IPN Orsay. The cryostat has been designed by INFN Milano and the cryogenic valve box by IPN Orsay. Several cryogenic tests have been performed and show expected performances for most of the components (cold tuning system, cryostat and valve box) and the RF control system. A RF characteristic (see Figure 5) of the cavity has been measured and showed good results $Q_0 > 1\ 10^{10}$ at 8 MV/m above the requirements for MYRRHA (Red Star in Figure 5). A full power test with a cavity equipped with its power coupler is to be completed before the end of 2013.

Figure 5. Prototypical cryomodule

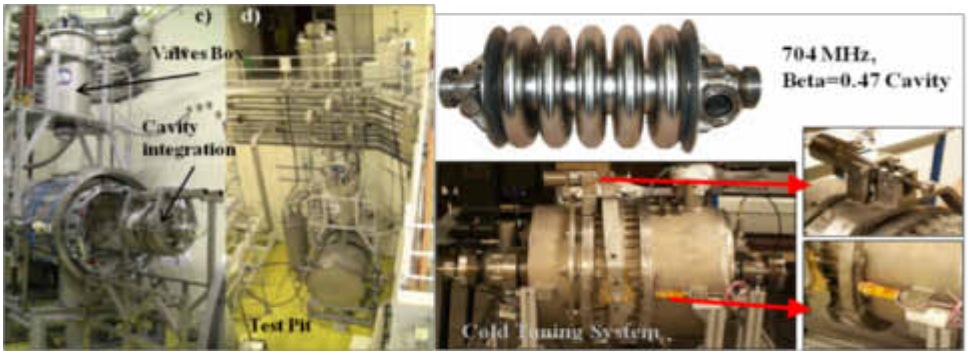
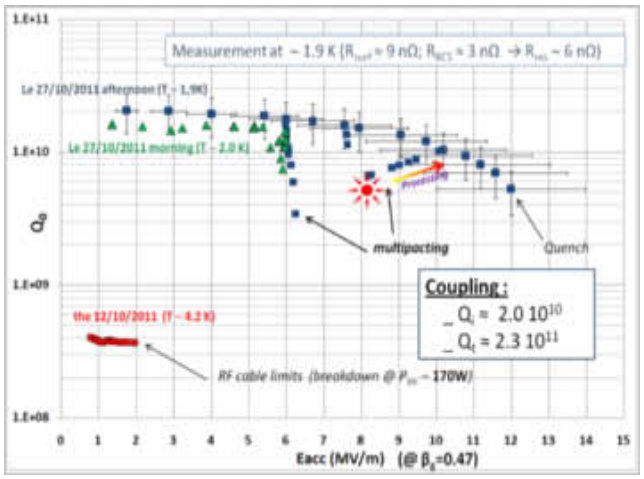


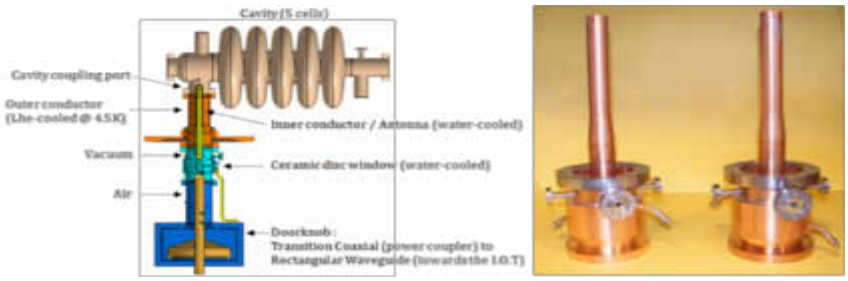
Figure 6. 704 MHz, Beta=0.47, measured RF characteristics



Power coupler

The MAX power coupler is made of three parts, as shown in Figure 7.

Figure 7. 704 MHz power coupler



The RF power coupler's central part is composed of a coaxial window, associated with an antenna which allows transferring handing all the RF power to the cavity due to a capacitive coupling. Its 50 Ohm matching is performed by a chokes' system, composed of a ceramic disc in alumina and brazed, on the one hand, on the terminal conductor and on the other hand, on the external conductor of the window. The power coupler's window itself adopts a coaxial geometry where the tightness between cavity's vacuum and waveguide's air is accomplished through a ceramic disc, which is made of 97% of alumina. The frequency under operation of the window is around 704.4 MHz with a RF "peak" power of 150 kW and of 80 kW in travelling CW mode. The outer conductor of the power coupler makes the connection between the RF window and the TRASCO superconducting cavity and should handle the temperature gradient between the 300 K of the window to the 2 K of the cavity's port. Finally, a rectangular waveguide (WR1150) to the coaxial transition (called doorknob transition) allows transmitting the RF power from the RF source (I.O.T. delivering 80 kW) to the power coupler.

Two complete couplers have been fabricated by the SCT company, located at Tarbes in France, and have been checked at IPN Orsay in May 2009 (Figure 7).

Power coupler conditioning set-up

The conditioning cavity, the power coupler and the I.O.T. associated with the high power DC supply are the central part of the test bench. The following components are articulated:

- diagnostics such as measures of vacuum, RF power, water flow and multipacting current;
- hardware safety systems (Coupler and I.O.T. "securities box");
- monitoring software of the power couplers conditioning;
- data acquisition system;
- RF power components (WR1130, doorknobs, RF circulator, 1 kW RF pre-amplifier).

Power coupler conditioning has been designed to be carried out in a travelling wave. In this case, the RF power is transmitted from the RF source (Thales I.O.T.) to an RF high power 50Ω load through the two power couplers mounted on a 704.4 MHz resonant cavity. The input coupler is connected to the RF power waveguides (WR1130) and the power coupler located at the cavity's output is connected to the RF power load. The RF power line is composed of rectangular waveguides elements of WR1130 type. The connection between the coupler and the RF power line was carried out by the doorknob.

During this first conditioning campaign, the conditioning programme worked in "normal" mode. From 17 kW RF power, the vacuum level is recovered to 1, 62.10^{-07} mbar.l.s^{-1} of 30 kW RF power. The RF power transmission has created a warm-up of the conditioning test bench which involved degassing of the walls of elements subjected to high vacuum and thus degraded the vacuum level.

This conditioning allowed the validation ofthe conditioning test bench mount and the associated facilities which which seems promising for the second conditioning campaign whose RF power to be reached is 80 kW.

Figure 8. Coupler conditioning bench layout

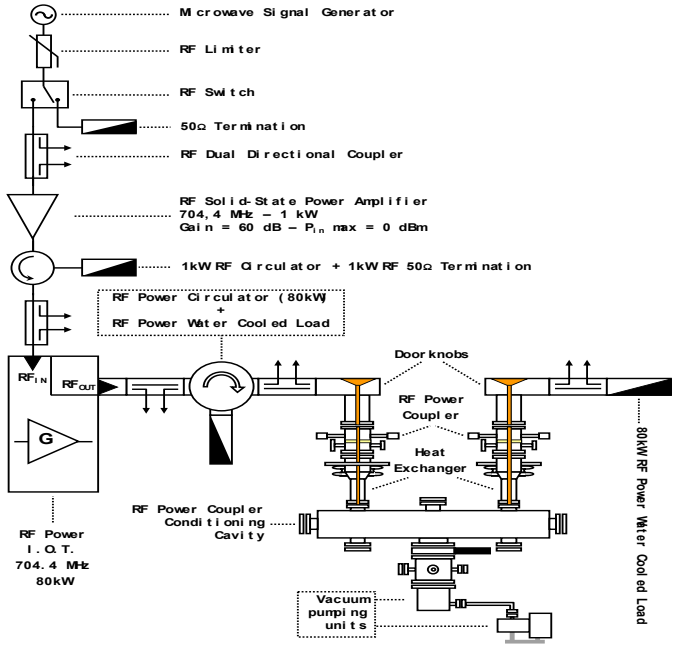
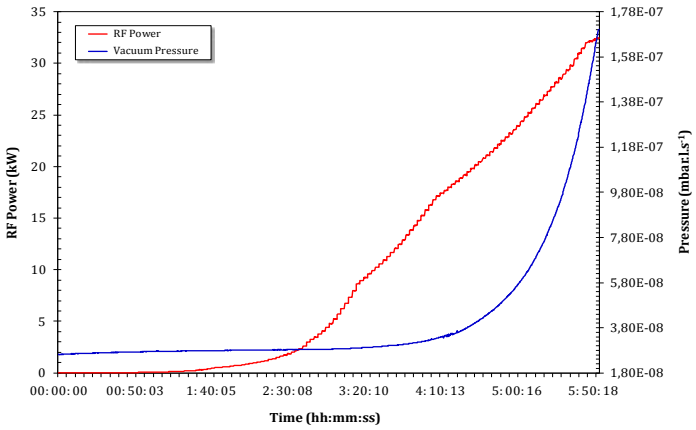


Figure 9. 30 kW RF power conditioning couplers in CW operation mode



Future work

During the last RF conditioning campaign, a failure of a power coupler ceramic window occurred. Analysis is underway to understand the cause of this failure. A new coupler was manufactured and is currently under preparation. Its RF conditioning was planned for June 2013. A new cryogenic test of the prototypical cryomodule with full RF power was expected in September 2013. The experimental assessment of the main steps of the fault recovery procedure can then start.

The detailed design and the final mechanical and thermal optimisations of the spoke cryomodule are underway. Detailed drawings for the definition of a prototype cryomodule manufacturing were expected to be achieved in 2013.

Reliability model of SNS linac (spallation neutron source-ORNL)

Adrian Pitigoi, Pedro Fernandez
Empresarios Agrupados, Spain

Abstract

A reliability model of SNS LINAC has been developed using risk spectrum reliability analysis software and the analysis of the accelerator system's reliability has been performed. The analysis results have been evaluated by comparing them with the SNS operational data. This paper presents the main results and conclusions focusing on the definition of design weaknesses and provides recommendations to improve reliability of the MYRRHA linear accelerator.

Introduction

The collaborative MAX (MYRRHA Accelerator eXperiment research and development programme) Project launched in February 2011 and co-funded by the European Commission under the Seventh EURATOM Framework programme for Nuclear Research and Training Activities (2007-2011), followed from the recommendations of the European Union's Strategic Energy Technology Plan for the development and deployment of sustainable nuclear fission technologies in Europe.

MAX participates in addressing the issue of high-level long-lived radioactive waste transmutation by pursuing the development of the high-power proton accelerator as specified by the MYRRHA accelerator-driven system (ADS) demonstrator project in Belgium.

The main goal of the MAX Project is to deliver an updated consolidated reference layout of the MYRRHA linear accelerator with sufficient detail and an adequate level of confidence to initiate its engineering design and subsequent construction phase in 2015.

In this context, the MAX team aims to develop an accurate reliability model of the MYRRHA accelerator (Task 4.4), using the methodology applied for nuclear power plants. For this purpose, a reliability model of an existing accelerator has been developed as part of the Task 4.2 MAX project activities. The reliability model development is described and the results of the performed analysis are presented in this paper.

Paper contents

The MAX Task 4.2 activities performed are presented in the paper:

- compiling and processing data needed for developing the model and performing the reliability study;
- development of a detailed reliability model of the SNS using a risk spectrum fault tree;

- performing reliability analysis of the SNS linac, the major critical issues related to the accelerator reliability have been identified,
- compiling and processing SNS logbook data available on the SNS website (recorded during the period October 2011-June 2012) for evaluation of the SNS risk spectrum analysis results.

Theoretical results from the model were compared with the operational data records (real operation data). It was concluded that the RS model can be considered a trustworthy tool to further build the model for evaluation of the MAX linac reliability.

As a result of performing the SNS system's reliability analysis, the systems and components with the strongest impact on overall reliability are identified. This paper presents the conclusions and recommendations for increasing the reliability of the MYRRHA linear accelerator and for design optimisation.

MAX Task 4.2 – Objective

It is essential to develop a reliability model and to provide a feedback on actual reliability performance of an existing accelerator in order to develop a more accurate MAX reliability model and to guide the MYRRHA accelerator engineering design.

One of the most important goals of the MAX project WP4 is therefore to perform a detailed reliability analysis of an existing accelerator, using the methodology applied in the current nuclear power plants. The goal of this reliability analysis is to draft preliminary conclusions and recommendations in order to maximise the reliability/availability and safety of the MYRRHA accelerator.

In view of these goals, the Spallation Neutron Source (SNS – Oak Ridge National Laboratory) was selected within MAX Task 4.2 for reliability modelling using risk spectrum in order to provide feedback on actual SNS accelerator reliability performance as a reliability modelling tool for Task 4.4 of the MAX project.

A model of the full MYRRHA linac will have to be built based on its existing design and taking into account all support systems, smart control strategies, fast beam shutdown and accelerator/reactor interface aspects.

Input data needed for modelling and reliability study

SNS design information and reliability data have been collected, organised and processed to be used as input data to develop the SNS reliability model and to reach the objectives of Task 4.2. The data obtained from different sources could be grouped as follows:

- SNS design data;
- SNS systems and functions data;
- SNS reliability data;
- SNS operating status.

The input data sources are:

- SNS design and technical parameters (SNS public information http://neutrons.ornl.gov/facilities/SNS/);
- SNS reliability data: SNS RAMI and BlockSim models data;
- SNS operation dat: logbook data (http://status.sns.ornl.gov/beam.jsp).

SNS risk spectrum reliability model development

A detailed risk spectrum fault tree model has been developed using the methodology currently applied for nuclear power plants taking into account the available SNS design

information. The developed SNS risk spectrum model has been quantified using the reliability data obtained from the BlockSim model (failures data – MTTF and repair times data - MTTR).The risk spectrum model results have been evaluated with respect to the SNS logbook operational data (accelerator trip failures and overall availability) recorded during the period October 2011-June 2012.

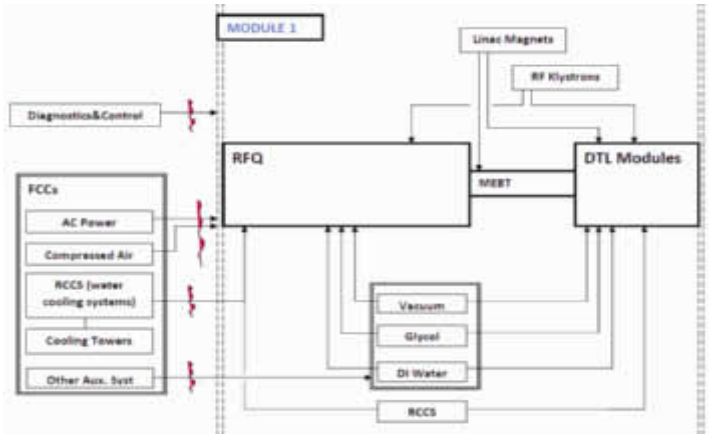
The following scenarios have been considered as the basis for developing the risk spectrum model of the SNS accelerator:

- Some of the SNS systems and components (i.e. stripper foil, ring and RTBT) have been considered as not relevant to the objectives defined for the MAX linac project, which is why these parts were not included in the reliability model.
- The "continuously monitored repairable component" - risk spectrum type 1 reliability model has been considered to model the failure behaviour of all SNS linac components. The risk spectrum type 1 reliability model is used to model a component failure which is detected immediately and which can be repaired.
- "Mean unavailability". This type of calculation is used to obtain the unavailability values of the basic events, the long-term average unavailability Q is calculated for each basic event.

The fault tree developed for SNS linac is a graphical representation of the functional structure of SNS systems, describing undesired events ("failures") and their causes. The fault tree is built using gates, basic events and house events. Generally, a fault tree can be subdivided into several fault tree pages, which are bound together using transfer gates. The level of detail for basic events was established corresponding to the availability of reliability data and the level of detail of the design information.

As a first step in the modelling of the SNS accelerator (linac), a "control volume" (Module 1) has been defined, consisting of the following SNS parts: RFQ, MEBT and DTL (DTL represents the first accelerating part of SNS linac).

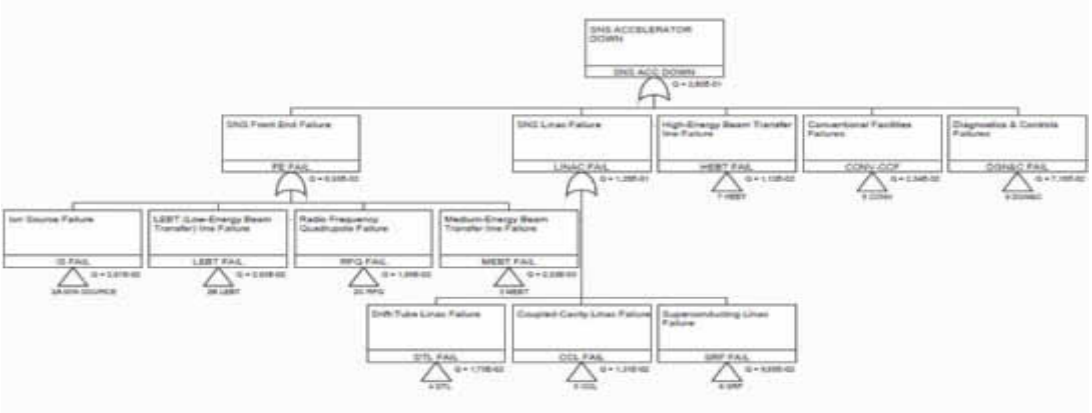
Figure 1. Module 1 functional block diagram



It was necessary to model parts of the technological systems (auxiliary systems) within Module 1, as they are important for RFQ-DTL functioning, i.e. the cooling systems (Glycol-DI Water, and RCCS for RFQ-DTL) and the vacuum systems. As a second step, all linac systems have been modelled and integrated into the SNS linac model, including LEBT, CCL, SCL, and HEBT. The rest of the auxiliary systems has also been modelled and integrated (compressed air, AC power, vacuum, cooling towers, RCCS general distribution, CHL, etc.).

Inputs (in terms of failures) from the auxiliary systems have been considered, some are included in the main linac systems fault trees, while some others function as CCFs in developing the fault tree of the "conventional facilities" event.

Figure 2. First level of the SNS RS model – SNS main fault tree structure



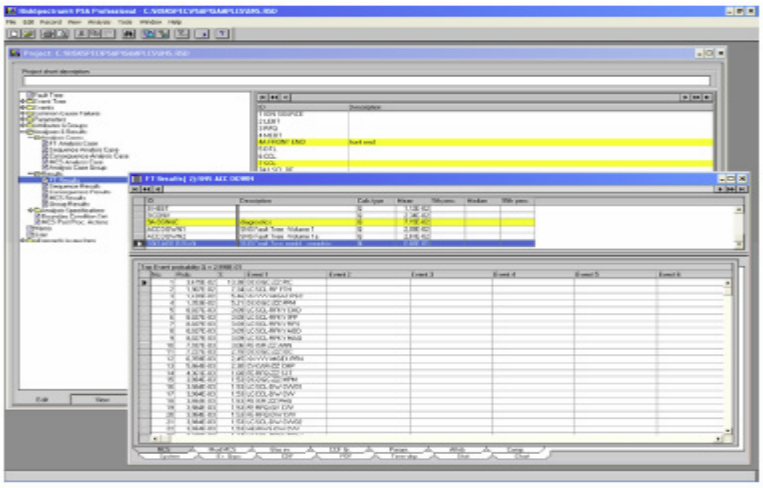
SNS linac reliability analysis

RS Model – MCS analysis

The SNS linac fault tree is a graphical representation of a Boolean expression. This Boolean expression can be converted by using Boolean algebra laws into a minimal cut set (MCS) representation.

The goal of the minimal cut set (MCS) analysis is to generate the minimal cut-sets of the fault tree and to perform a point-estimate quantification of the top event. The minimal cut-set (MCS) is that combination of events which causes the top event to occur. The term "minimal" means that if any of these events is removed from the set, the top event no longer occurs. The MCSs of the top event (SNS ACC DOWN) analysis case are presented below.

Figure 3. SNS ACC DOWN analysis case – minimal cut-sets list



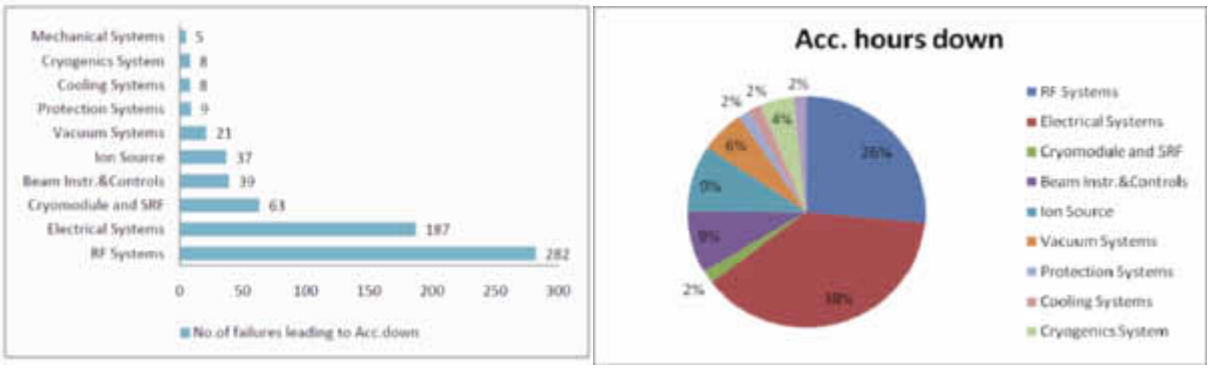
An MCS analysis has been performed for the complete SNS linac model as well as for different parts of the accelerator with the following conclusions:

- As the main result for the top event (SNS ACC DOWN) analysis case, the complete model running analysis has indicated a mean unavailability value of Q = 2.60E-01 = 0.26. Thus, Q = 26%, which results in a mean availability value of A = 1 - Q = 73% (the limit availability).
- The MCS analysis results indicate a wide range of failure modes (failures affect relatively all types of components.
- The linac (DTL-CCL-SCL) represents the system most affected by failures in terms of unavailability (Q=1.25E-01; A=87.5%).
- The highest values of unavailability are as follows:
  - SCL (Q=9.85E-02; A=90%);
  - DGN and C (Q=7.15E-02; A=93%);
  - Front-End (Q=6.93E-02; A=93%).
- The most affected part is the SCL, especially due to the malfunctioning of the SCL RF system (radiofrequency system of the superconducting linac) for which Q=6.33E-02 and A=94% (due to power supplies failures and klystron failures). The SCL usually fails as a consequence of cavities, cooling and vacuum malfunctions.
- The most affected parts of the front-end are the LEBT (Q=2.83E-02; A=97%) and MEBT (Q= 2.82E-02; A=97%), more specifically the magnets and the vacuum systems.

SNS reliability considerations (operating experience)

Reviewing the accelerator trips failure data from SNS logbook records from past operation experience, it has been concluded that the RF system and electrical system failures are the most frequent, while the failures in the electrical systems represent the most important contribution to total accelerator downtime (see Figure 4) in agreement with the conclusions from the SNS RS model runs.

Figure 4. Frequency of accelerator trip failures (by systems) and accelerator downtime contribution (by systems)



The pie chart above shows the distribution of breakdown hours by system. Accelerator trips caused by failures of components in the electrical systems represent 38% of the total accelerator downtime over the studied period. The second largest contribution is from the RF systems (26%), which are also the systems more often involved in failures leading to short accelerator trips (up to 0.2 hours).

According to the SCL risk spectrum analysis results, SCL-HPRF (Superconducting Linac – High Power Radiofrequency) and HVCM (High Voltage Converter Modulator) are the most affected subsystems of the SNS linac as far as failures leading to accelerator

trips are concerned. SCL-HPRF is affected by frequent short failures, while HVCM is affected by long duration trips.

Figure 5. RF system failures

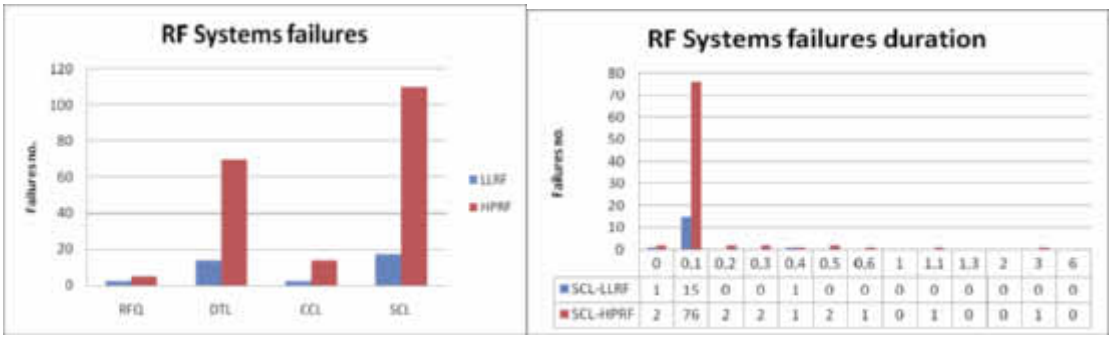
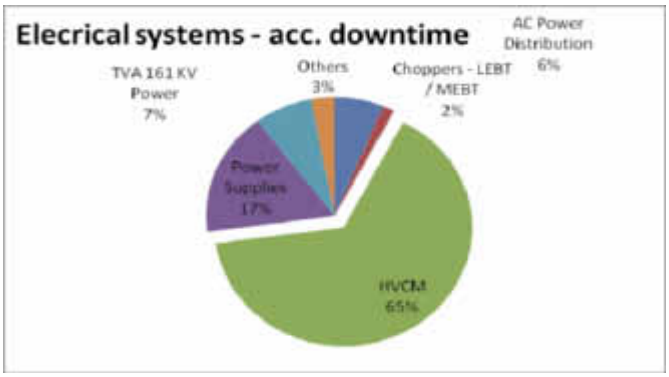
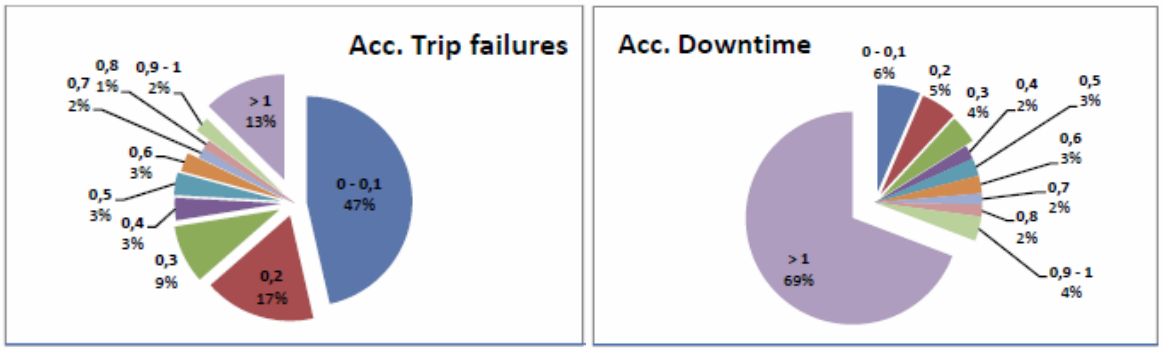


Figure 6. Electrical subsystems contribution to the accelerator downtime



In addressing all linac systems, beam interruptions of between 0 and six minutes (0 - 0.1 hours) represent 47 % of beam trips, i.e., 327 failures from the total of 705 failures recorded over the studied period of time. Failures whose duration exceed 1 hour represent 13% of the total. The latter contributes most to the total downtime for the same period, accounting for 308 hours, which represent 70% of the total (445 hours).

Figure 7. Statistics of accelerator trips by duration (hour fractions): a) failure frequency, b) contribution to the total downtime



The SNS RS model results have been evaluated compared with the above statistics and taking into account the assumptions formulated for the model development and the model limitations mentioned in Section 3.

Given the consistency of the SNS design information database and due to the conservatism of the reliability data used for model quantifying and to the fact that the human factor has not been taken into account (neither have improved operational reliability or the improvements of the maintenance programme), it can be concluded that the overall availability of the SNS linac (A=73%) resulting from the RS model is confirmed by the availability figures of the SNS from the first years of SNS operation.

The availability results obtained by MCS analysis run separately for the different SNS linac parts (IS, RFQ, MEBT, DTL, CCL, SCL, HEBT), have agreed very well with the SNS logbook availability records, although the global result is A=73%. This difference is attributable to the fact that the MTTF and MTTR values used for model quantification may be too conservative, and to assumptions and constraints of the model. The MTTF and MTTR data used represent a data mix from SNS registers including previous experience. Reliability input data used do not result from the statistical interpretation of logbook data over the entire operation period, which explains the differences between the values compared.

It should be noted that the results from the model agree substantially with what is indicated by the operational data, despite the model limitations and the fact that some parts are not considered and other parts are not developed in detail. As a consequence, the RS model developed for SNS linac is validated by the site operation data (data registered in the SNS logbook).

Conclusion

- The reliability results show that the most affected SNS linac parts/systems are:
  - SCL, front-end systems (IS, LEBT, MEBT), diagnostics and controls;
  - RF systems (especially the SCL RF system);
  - power supplies and PS controllers;

These results are in line with the records in the SNS logbook:

- The reliability issue that needs to be enforced in the linac design is the redundancy of the systems, subsystems and components most affected by failures.
- For compensation purposes, there is a need for intelligent fail-over redundancy implementation in controllers.
- Enough diagnostics has to be implemented to allow reliable functioning of the redundant solutions and to ensure the compensation function.

Acknowledgements

G. Dodson and J. Galambos (SNS) are acknowledged for their contribution to the SNS Reliability Study.

References

[1] Biarotte, J.-L., Vandeplassche, D. (2011), “MAX Project Presentation”, Deliv. No. 5.1, FP7 MAX project.

[2] Brucker, R. (2009), “Reliability Analysis of the XT-ADS Accelerator”, Doc. No. 092-148-FZ-000001, FP6 Eurotrans.

[3] http://neutrons.ornl.gov/facilities/SNS/.
http://neutrons.ornl.gov/facilities/SNS/works.shtml.

[4] http://www.fes.lbl.gov/.

[5] Hardekopf, R. (2001), "Linac Physics, Diagnostics, and Commissioning" (Including MEBT Chopper) – DCD WBS 1.4.5-doc. No. SNS-104050000-DC0001-R00.

[6] Keller, R. et al. (2000), "Status of the SNS Front-End systems", Front-End Systems Team - E.O. Lawrence Berkeley National Laboratory, Berkeley, CA, EPAC.

[7] Keller, R. et al. "Progress with the SNS Front-End systems", LBNL-47317.

[8] Lynch, M., Rees, D., Reass, B., Regan, A. (2000), "Linac RF System" – DCD WBS 1.4.1, doc. No. SNS-104010000-DC0001-R00.

[9] Hardy, L. (2002), "Accelerator Reliability – Availability", *Proceeding of EPAC 2002*, Paris.

[10] "Accelerator Reliability Workshop", *Proceedings of ARW 2011*, South Africa.

[11] Dodson, G. (2011), "SNS Reliability Program" - SNS Research Accelerator Division, *Proceedings of ARW 2011*, Cape Town.

[12] www.neutrons.ornl.gov/facilities/SNS/status.shtml; www. status.sns.ornl.gov/beam.jsp, www.status.sns.ornl.gov/logbook.jsp, www.status.sns.ornl.gov/availability. Jsp.

[13] Risk Spectrum – PSA User Manuals.

[14] Popova, I.I., Gallimeier, F.X. "Full scale radiation dose analyses for the SNS accelerator system", Oak Ridge National Laboratory, US.

[15] http://www.weibull.com.

Approach of a failure analysis for the MYRRHA linac

J.-P. Carneiro[1], L. Medeiros-Romão[1], R. Salemme[1], D. Vandeplassche[1], J.-L. Biarotte[2], Frédéric Bouly[2], D. Uriot[3]
[1]SCK•CEN, Mol, Belgium, [2]CNRS/IPN Orsay, France, [3]CEA Saclay, France

Abstract

The MYRRHA project currently under development at SCK•CEN (Mol, Belgium) is a subcritical research reactor that requires a 600 MeV proton accelerator as a driver. This linac is expected to produce a beam power of 1.5 MW onto a spallation target for the reactor to deliver a thermal power around 70 MW. Thermomechanical considerations of the spallation target set stringent requirements on the beam trip rate which should not exceed 40 trips/year for interruptions longer than three seconds. This paper presents a first approach of developing a method that allows rematching the beam online in the MYRRHA linac upon the failure of accelerator components.

Introduction

About 2500 tonnes of nuclear wastes are produced every year in Europe by the 145 nuclear reactors currently under operation. Some of this material (mainly minor actinides) remains radioactive for thousands if not millions of years [1]. The MYRRHA project currently under development at Mol, Belgium, is an accelerator-driven system expected to be operational in 2023 with the primary purpose to study the feasibility of efficiently transmuting such nuclear waste products into isotopes with much shorter lifetimes (about three orders of magnitude shorter). After transmutation, the nuclear wastes would then be stored underground, 300 to 1000 meters deep, for a period ranging from a few hundred to a few thousand years.

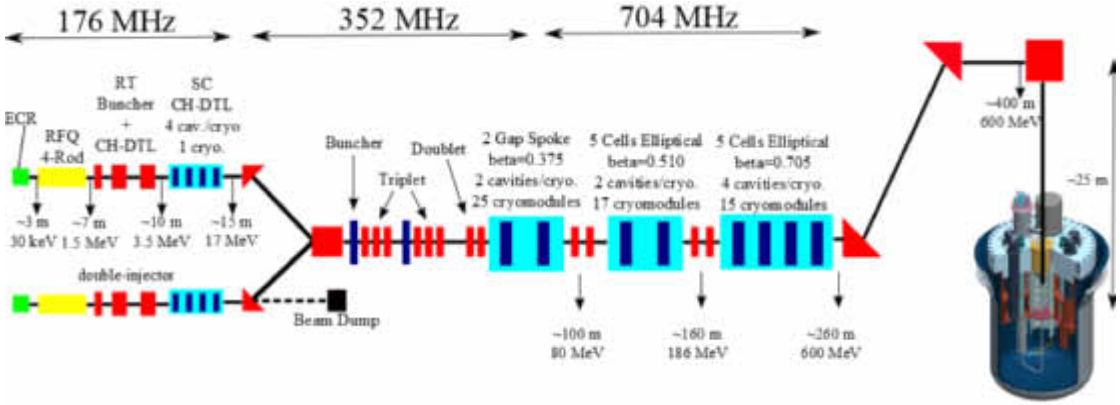
Liquid Pb-Bi eutectic (LBE) alloy has been selected as a coolant and neutron spallation source for the development of the MYRRHA reactor. The reactor is expected to have a thermal power of ~70 MW and may be operated in both critical and subcritical modes. In the latter case, the core is fed by spallation neutrons obtained from a 600 MeV superconducting proton linac beam hitting the LBE coolant/target with an average current of 4 mA. The accelerator providing this beam needs to be compatible with the steady state character of the reactor operation and as a consequence the beam has to be delivered in CW mode (with 200 μs empty gaps at 1 Hz repetition, for subcritical monitoring).

The major issue that needs to be taken into account during the design and the operation of the MYRRHA linac concerns the acceptable rate of unwanted beam interruption, commonly called beam trips. A recent study performed by AREVA and reported in [2] shows that, due to thermal stresses on structural materials (beam window, inner barrel, reactor vessel), no more than 10 beam trips longer than three seconds should take place in the linac per operational period of three months. This paper presents a strategic approach during the design of the linac and in its expected operation to fulfill this stringent requirement.

Layout of the MYRRHA linac

Figure 1 shows the schematic layout of the MYRRHA linac and the transport line to the reactor.

Figure 1. Overview of the MYRRHA linac and reactor



The 30 keV proton beam from the ECR source is bunched and accelerated by a 4-rod Radio-Frequency Quadrupole (RFQ) to an energy of 1.5 MeV with an average current of 4 mA. Downstream the RFQ, a buncher and 2 cooper multicell CH-DTL cavities further accelerate the beam to 3.5 MeV.

At this energy, the transition from room-temperature (RT) to superconducting (SC) structures takes place with the beam accelerated to 17 MeV by 4 SC CH-DTL cavities. The front-end of the linac (RFQ, buncher, RT and SC CH-DTL) operates at a frequency of 176 MHz. In the linac front-end, between the RFQ and the SC CH-DTL cavities, transverse focusing is achieved using RT quadrupole triplets and in the cryomodule hosting the 4 SC CH-DTL cavities using SC solenoid magnets.

At the exit of the dual-injector, two dipoles direct the selected beam into the SC main linac for final acceleration to 600 MeV. To boost the beam from 17 MeV to 80 MeV, SC 2-gap spoke resonators (β=0.375) operating at 352 MHz are used. Further acceleration to 600 MeV is provided by 2 types of 5-cells elliptical cavities (β=0.510 and β=0.705) operating at 704 MHz. The matching from the injector to the main LINAC is performed by 2 bunchers and 2 RT quadrupole triplets. In the 352 MHz and 704 MHz sections, RT quadrupole doublets located between the cryomodules are selected as focusing elements. At the end of the SC linac, the beam is vertically bent in the transport line by two 45° dipoles and reaches a height of ~25 m before injection into the nuclear reactor by a 90° dipole, as presented in Figure 1. The total length of the linac and the transport line to the reactor is ~400 m.

Approach towards a very high availability of the MYRRHA linac

The challenging aspect of the MYRRHA linac consists in its very high availability. It is required that the number of beam interruption longer than three seconds remains under 10 during a three-month operation period of the MYRRHA reactor. The corresponding Mean Time Between Failure (MTBF) is expected to be higher than 250 hours and the linac availability close to 100%.

As of today, the typical availability of superconducting proton linacs in operation like the Spallation Neutron Source (SNS) at Oak Ridge National Laboratory is reported to be slightly above 90% [3]. Some other accelerators like the ProjectX hydrogen ion linac currently under development at Fermilab must demonstrate that it can meet the

requirement of 90% availability [4] for a 1 mA beam in CW operation at 3 GeV which turns to be well within reach taking into account the reported availability of the SNS linac.

The technology to build multi-GeV proton superconduting linacs with average currents of few mA and operating with availability in the order of 90% is available today. The strategic approach taken towards the very high required availability of the MYRRHA linac concerns not only the design of the linac but also its operation and this approach is summarised in the 4 principles below:

- element redundancy;
- use of linac components far from their limits;
- design of the linac following the fault-tolerance concept [5];
- operation of the linac under the virtual accelerator concept [6].

Element redundancy

Figure 1 presents the example of element redundancy. A dual-injector is foreseen in the MYRRHA linac to maximise the reliability of its front-end. The beam is expected to be injected in the linac from one injector, while the second injector is on stand-by mode with all elements operating at nominal power. With the dipole magnet turned off at the end of the second injector, the beam is directed into a beam bump. If abnormal beam losses are detected in the first injector, the Machine Protection System (MPS) stops the beam in both injectors using the LEBT choppers (typically in less than 0.1 msec). Once the beam is stopped, attempts are made to recover, if possible, the faulty component. If recovery fails, the beam is resumed in the second injector and sent to the main linac (in typically one or two seconds) by changing the polarity of the injector dipoles.

The linac components and their ancillary equipment need to be selected with the highest MTBF value and some of these components (like power converters, RF generators or quadrupole power supplies) may need to be doubled in the linac.

Use of linac components far from their limits

The three types of cavities in the main superconducting linac are to operate at a derated value, about 30% lower than the nominal values at which these cavities could safely operate. This safety margin is considered primarily for fault-compensation procedures.

The chosen rules for the operation of the MYRRHA superconducting cavities are the following:

- The RF field at the inner surface of the SC cavities is always kept below 35 MV/m and the peak magnetic field below 60 mT.
- The corresponding maximum accelerating field (given at optimal beta and normalised to the length of the cavities) is then 8.3 MV/m (for the beta=0.375 spoke), 10.7 MV/m (for the beta=0.51 elliptical) and 14.3 MV/m (for the beta=0.705 elliptical).
- The derated operating points are then obtained removing 30%, leading to 6.4 MV/m (for the beta=0.375 spoke), 8.2 MV/m (for the beta=0.51 elliptical) and 11 MV/m (for the beta=0.705 elliptical).

The SNS (beta=0.61) elliptical cavities are reported in [7] to operate with an average accelerating gradient in the order of 12-13 MV/m, which is lower than the derated accelerating field for the MYRRHA elliptical cavities. Therefore, the above-mentioned derated operating fields for the cavities of the main linac seem well within reach.

Following the same idea, the magnetic field of the pole is always kept below 0.3 T in all the linac quadrupoles, giving some comfortable (~30%) room for gradients increase if needed. Also, the RF power amplifiers are derated by ~40%.

Design of the linac following the fault tolerance concept

The main superconducting linac has been designed based on the fault tolerance concept. The philosophy behind this concept [5] is that if an element fails during the operation of the linac, proper compensation and re-matching can be achieved with the neighbouring elements and beam operation under nominal conditions can be resumed after a short (<3 sec) beam interruption.

Namely, the fault tolerance procedure is expected as follows [8]:

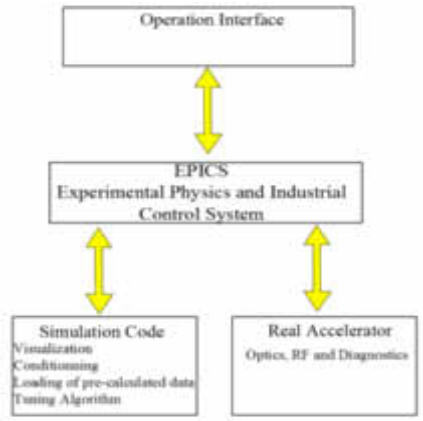
- If abnormal beam losses are detected along the linac then the MPS stops the beam in the injector using the LEBT chopper.
- The origin of the fault is analysed. If the fault cannot be cured, the fault-recovery procedure is initiated. In the case of a faulty cavity, the 4 nearest neighbouring cavities are used for compensation, while the faulty cavity is being detuned. If a quadrupole is faulty, the whole doublet is switched off and the 4 neighbouring quadrupoles are used for compensation.
- New values for cavity phases and fields and/or quadrupole settings need to come either from a predefined table or from a predictive and fast "online" beam dynamics calculation.
- The beam is resumed in the linac, first with very short pulses to check the behaviour of the lattice, then with full power for nominal beam operation.

The machine control system of the MYRRHA linac will need to work very fast to ensure the detection and compensation of any failure in the accelerator in less than three seconds. A beam dynamics code will need to be associated with the machine control system to accurately predict the new matching set points in the event of any accelerator element failure. The association of the beam dynamics code to an accelerator control system is often mentioned in the literature as a "virtual accelerator".

Virtual accelerator concept: Architecture and examples

Figure 2 presents the structure of a virtual accelerator based on the EPICS control system.The virtual accelerator includes a beam dynamics simulation code that is able to run in parallel with the real accelerator. In this configuration, it is possible with the virtual accelerator to visualise the operation of a real accelerator and control some new accelerator set points from a dryrun before implementing these set points on the real accelerator. It is also possible during the operation of the real accelerator to load some pre-calculated data set points to compensate for a component failure. Ultimately the simulation code would be able to find, through a tuning algorithm, a new optic to bring the accelerator back onto nominal operation in every fault configuration.

Figure 2. Structure of a virtual accelerator based on EPICS



In 2006, a first test of a virtual accelerator was performed at CEA-Saclay [6], using the code TRACEWIN [9] to optimise the transmission of the SILHI proton injector. While after several days of manual optimisation, the transmission achieved 79%, using the virtual accelerator, it reached 87% within half an hour. More recently, this TRACEWIN based virtual accelerator was successfully used for the conditioning of the SPIRAL2 injector with heavy ions at Grenoble and proton/deuteron at Saclay.

A virtual accelerator based on the code TRACK [10] was also proposed in 2008 in [11]. Since the beginning of 2013, a special interface [12] has been developed at ANL to connect the ATLAS LINAC control system to the code TRACK. The interface is now capable of producing TRACK inputs from the actual element settings (read directly from the control system) and the reverse is under development. Finally, the operation and optimisation of the ATLAS LINAC will be possible through the TRACK based virtual accelerator.

Beam dynamics aspect of the fault tolerance design

It is generally accepted that the fault-recovery procedure cannot be applied at low energies (below 10 MeV). This is the actual main reason for the choice as input energy of 17 MeV for the main linac. It is also important to point out that once the proper compensation and re-matching is found by the beam dynamics code, the new lattice needs to be tolerant to typical accelerator misalignments and jitter. In other words, this new lattice should be able to correct typical errors with losses that need to be below 1 W/m, the threshold taken as a reference to insure "hands-on" maintenance on the linac [13].

The main superconducting linac i.e. from the injector exit (17 MeV, upstream of the dipoles) up to the end of the last cryomodule (600 MeV) has been designed with the code TRACEWIN and the corresponding baseline lattice has been translated as TRACK input for sensitivity studies. First, the behaviour of the baseline lattice of the MYRRHA linac will be presented in the presence of typical errors and correctors and then three fault tolerance cases (failure of the first spoke cryomodule, failure of the first doublet and failure of the first quad of the first doublet) will be studied.

Baseline design with errors and correctors

Static transverse misalignment error of quadrupoles and cavities and dynamic RF jitter (field and amplitude) have been implemented into the beam dynamics code TRACK. The transverse misalignments δ_{xy} are setup in the code such that the element ends are randomly misaligned (with a uniform distribution) horizontally and vertically by the same value which does not exceed the maximum input δ_{xy}. Concerning the dynamic RF jitter, TRACK generates Gaussian distributions truncated at 3 sigma. The TRACK

correction algorithm aims to steer the beam so that the transverse displacements measured by the BPM's are minimised.

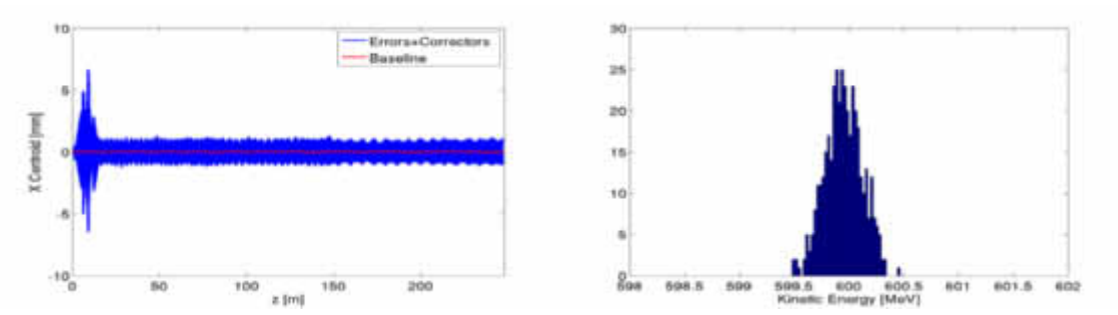
Figure 3(a) presents TRACK beam dynamics simulations of the beam centroid in the main superconducting linac with transverse misalignment of cavities and quadrupoles of δ_{xy} = 500 μm, RF dynamic jitter of 0.2° and 0.2% and quad roll of 5 mrad around the z-axis. A set of 400 randomly generated error runs were performed with TRACK using $5 \cdot 10^4$ macroparticles with 3D space charge routine. These 400 randomly generated error runs were corrected using 1 corrector (acting in both the horizontal and vertical plane) and 1 BPM per triplets (located downstream the second injector dipole) and per doublet (located between the main linac cryomodules). The corrector maximum strength is set to 5 mrad and the resolution and the offset in position of the BPM's are 30 μm and 1 mm. As depicted in Figure 2 (a), after correction the beam centroid motion keeps below 1 mm along the main superconduting linac and no losses due to element misalignments and RF field jitter are observed. This study confirms that the actual baseline design of the MYRRHA superconducting linac is tolerant to typical errors.

Noteworthy in Figure 3(b) is the corresponding energy distribution at the end of the linac, which shows that with an RF jitter of 0.2° and 0.2% the energy distribution keeps well below +/- 1 MeV, as recommended, during the design phase of the transport line from the linac to the reactor. Studies have shown that an RF jitter of 0.5° and 0.5% does bring some of the 400 seeds at an energy exceeding the threshold of +/- 1 MeV.

Fault tolerance design: Failure of the first cryomodule

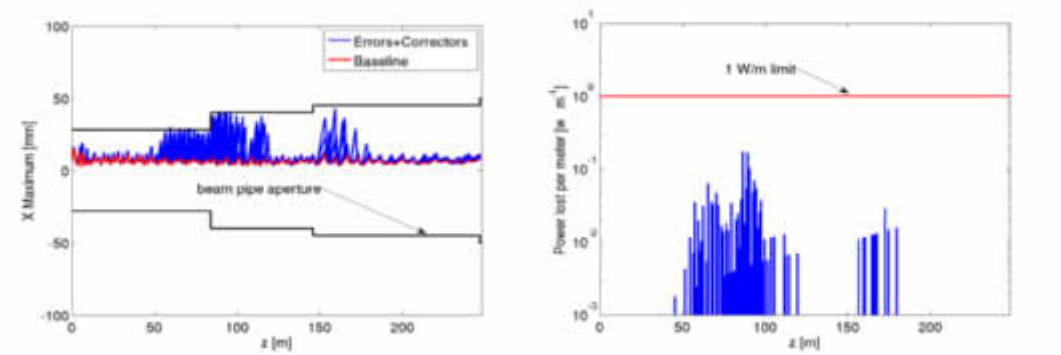
In the event of the failure of the first cryomodule, the code TRACEWIN has been used to find a new optic taking the phases and the fields of the two downstream bunchers and two upstream cryomodules (4 cavities) for matching. During the matching procedure, it was not specified to recover the energy due to the loss of the first cryomodule (slightly lower than 1 MeV). The new optic found by TRACEWIN has been converted into TRACK for typical error and corrector studies following analysis performed with the baseline design lattice. Figure 4(a) shows that some of the 400 TRACK runs are not fully corrected with macroparticles having a maximum excursion larger than the beam pipe aperture radius, leading to losses, as depicted in Figure 4(b). The losses present a maximum of ~0.1 W/m at the intersection between the spoke cavity section and the β=0.501 elliptical cavity section and therefore are acceptable, being by one order of magnitude lower than the 1 W/m threshold. As a result, this study shows that the actual design of the MYRRHA main superconducting linac is able to operate in the event of the failure of its first cryomodule.

Figure 3. (a) TRACK simulations of corrected horizontal beam centroid motion along the linac for static transverse misalignments of 500 microns (quadrupoles and cavities), dynamic RF jitter of 0.2/0.2% and quad roll of 5 mrad along the z-axis (b) corresponding energy distribution at the end of the linac



(a) (b)

Figure 4. Figure 5: TRACK simulations of the fault-recovery of the first cryomodule with errors and correctors



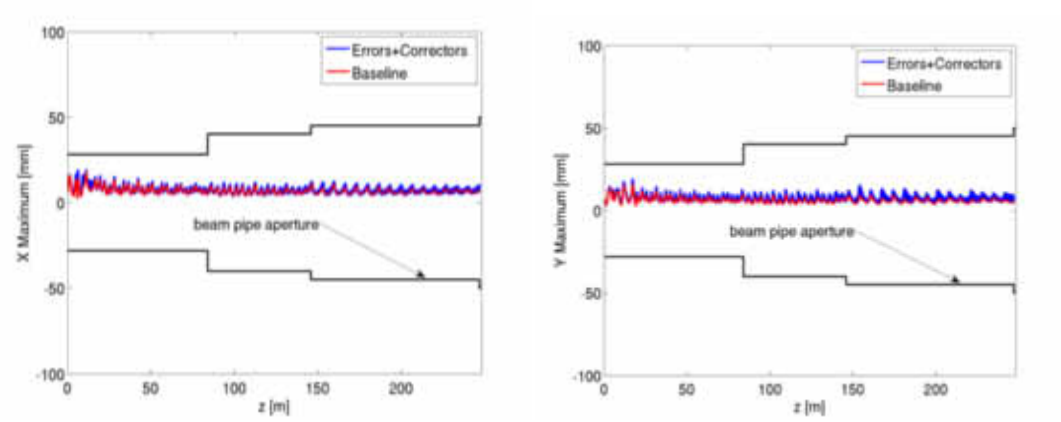
(a) (b)

(a) Maximum horizontal beam excursion along the linac, (b) corresponding average power lost per metre along the linac.

Fault tolerance design: Failure of the first doublet

The behaviour of the baseline lattice has been studied in the event of the failure of the first quadrupole doublet, located upstream the first cryomodule. A new optic was found using TRACEWIN and the two upstream triplets together with the two downstream doublets for matching. Figures 5(a) and 5(b) present the maximum horizontal and vertical beam excursion along the linac in the presence of typical errors and correctors, as previously discussed. These figures show that the re-matched lattice is tolerant to errors with all the 400 seeds computed by TRACK being properly corrected, insuring a maximum beam excursion well below the beam pipe aperture radius (by at least a factor of 2). These studies confirm that the operation of the MYRRHA main superconducting linac is possible even in cases of failure of its first doublet.

Figure 5. Maximum (a) horizontal and (b) vertical beam excursion along the linac after fault-recovery of the first quadrupole doublet with errors and correctors



(a) (b)

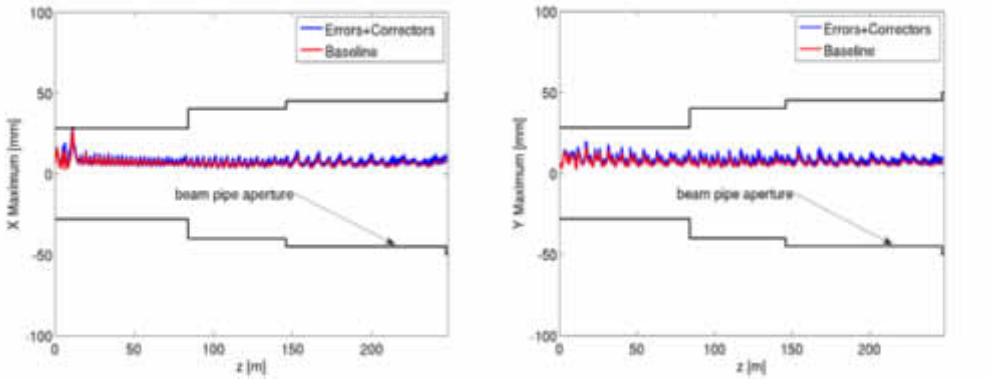
From TRACK.

Fault tolerance design: Failure of the first quadrupole of the first doublet

In the event of a failure of the first quadrupole of the first doublet, TRACEWIN was in charge of finding a new optic, taking into account the upstream two triplets, the remaining quadrupole of the doublet and the downstream doublet for matching. TRACK simulations of the corresponding new TRACEWIN lattice including the usual errors and correctors are presented in Figures 6(a) and 6(b) for the maximum horizontal and vertical beam excursion along the linac. Figure 6(a) shows that, at the location of the failed quadrupole, the beam presents a strong asymmetry in the horizontal plane while this asymmetry is not present in the vertical plane, as shown in Figure 6(b). For some of the 400 runs, the maximum beam excursion in the horizontal plane at this location goes slightly above the beam pipe aperture radius in the presence of errors leading to some limited losses (<0.05 W/m).

The study of the failure of the first quadrupole or the first doublet indicates that a new matching can be found using the remaining quadrupole of the doublet, the two upstream triplets and the downstream doublet. This new lattice presents some limited losses when tested with errors, jitters and correctors. Nevertheless, the results presented in Figures 5(a) and 5(b) suggest that it might be preferable, in the event of one quadrupole failure, to switch off the entire doublet to keep the beam symmetric. In this configuration, the re-matched lattice computed by TRACEWIN shows no losses in the presence of typical errors and correctors.

Figure 6. Maximum (a) horizontal and (b) vertical beam excursion along the linac after fault-recovery of the first quadrupole of the first doublet with errors and correctors



(a) (b)

From TRACK.

Fault-recovery procedure and virtual accelerator control system

The fault-recovery procedure needs to take place within three seconds which is the maximum allowable beam interruption in the MYRRHA linac. Such a short time to resume nomimal beam operation in the linac after an element failure implies the coupling of the accelerator control system to a beam dynamics code. This virtual accelerator will then be in charge of the linac operation and ideally the beam dynamics code will find a re-matched lattice for any failure scenarios. Obviously, this re-matched lattice would need to be tolerant to the typical accelerator misalignments and RF jitter with losses below the 1 W/m treshold once the nominal operation is resumed.

Some promising results have been obtained on optimising injectors using the virtual accelerator concept with TRACEWIN or TRACK at Saclay and ANL. Significant R&D is still necessary to have these codes perform an automatic lattice matching to compensate for

any element failure in a full LINAC. Furthermore, this automatic matching procedure will need to be very fast to cope with the 3-second allowable beam time interruption. Also, the interaction between the beam dynamics code and the real accelerator through the accelerator control system will need to be very efficient, with some R&D needed in auxiliary systems like the cavity tuners and LLRF digital, as mentioned in [8].

Conclusion

The actual state-of-the-art in the design and operation of multi-GeV superconduting proton linacs with few mA of average current guarantees an availability of about 90%, as measured at the Oak Ridge Spallation Neutron Source linac or expected in the ProjectX linac currently under development at Fermilab. The challenging aspect of the MYRRHA linac is its requested reliability with no more than 10 beam trips longer than three seconds that should take place per operational period of three months, leading to an availability close to 100%. This very high availability needs to be incorporated into the design of the linac.

The three underlying principles in the design of the MYRRHA linac are elements redundancy (like the dual-injector), elements operation at derated values (like cavities operating at about 30% from their nominal operating points) and the fault tolerance concept, which allows the failure of a beamline component to be compensated by its neighbouring elements. Studies presented in this document show that in the event of a failure of the first cryomodule or the first quadrupole doublet the linac can resume nominal operation with a re-matched lattice. Since the fault tolerance procedure is expected to work more efficiently at higher energies (due to lower space charge effects) we can extrapolate from our studies that the MYRRHA linac is expected to operate with the failure of any cryomodule or quadrupole doublet in the main linac.

A virtual accelerator-based control system is mandatory for the operation of the MYRRHA linac to ensure the very fast implementation (<3 seconds) of the fault tolerance procedure. The virtual accelerator uses a beam dynamics code (like TRACEWIN or TRACK) to compute the model of the real accelerator in operation and interacts with this later through the accelerator control command. The beam dynamics code could, for instance, upload some pre-defined matched lattices in the event of element failures or it could ideally find some new optimal set points for every fault configuration. Such virtual accelerator-based control command has been successfully tested at Saclay (using TRACEWIN) on the SILHI injector or the SPIRAL2 injector and at ANL (using TRACK) on the ATLAS linac. Significant R&D is still needed to expand the concept of the virtual accelerator to a full linac like MYRRHA.

References

[1] Biarrotte, J.-L. (2012), “L'accélérateur ADS pour le projet MYRRHA, un prototype d’accélérateur pour bruler des déchets nucléaires”, Orsay, France.

[2] Vandeplassche, D., Medeiros-Romão, L. (2012), “Accelerator Driven Systems”, *IPAC12*, New Orleans, Louisiana, US.

[3] Dodson, G. (2011), “The SNS reliability program”, *Accelerator Reliability Workshop*, Cape Town, South Africa.

[4] Bhattacharyya, S. (2012), “Reliability Modeling Method for Proton Accelerator”, *IPAC12*, New Olreans, Louisiana, US.

[5] Biarrotte, J.-L., Uriot, D. (2008), “Dynamic compensation of an RF cavity failure in a superconducting linac”, *PRST-AB,* vol. 11, no. 072803.

[6] Uriot, D., Duperrier, R. (2006), “Accélérateur virtuel: Concept, implémentation et premier test”, CEA/DSM/DAPNIA/SACM/LEDA, Saclay, France.

[7] Kim, S.-H. (2008), "SNS superconducting linac operational experience and upgrade path", *LINAC08*, Victoria, BC, Canada.

[8] Biarrotte, J.-L. (2013), "MAX Deliverable Number 1.2", Brussels, Belgium.

[9] Uriot, D. TRACEWIN web site, http://irfu.cea.fr/Sacm/logiciels/index3.php.

[10] Aseev, V., Ostroumov, P., Lessner E., Mustapha, B. (2005), "TRACK: The new beam dynamics code", *PAC05*, Knoxville, Tennessee, US.

[11] Mustapha, B., Ostroumov, P., Xu, J. (2008), "Towards a Model Driven Accelerator With Petascale Computing", *LINAC08*, Victoria, BC, Canada.

[12] Dickerson, C. (2013), Private communication.

[13] Alonso, J. (2000), "Beam Loss Working Group Report", *FERMILAB-Conf-00/185*, Lake Geneva.

MYRRHA cryogenic system study on performances and reliability requirements*

Tomas Junquera[1], Nicolas R. Chevalier[1], Jean-Pierre Thermeau[2], Luis Medeiros Romão[3], Dirk Vandeplassche[3]
[1]Accelerators and Cryogenic Systems, France, [2]Institut de Physique Nucléaire, France
[3]SCK•CEN, Belgium

Abstract

A preliminary design for a cryogenic system as required by an ADS accelerator has been proposed in previous studies developed within different Euratom Programmes (i.e. EUROTRANS). Currently, within the FP7 MAX programme, a more detailed study, adapted to the MYRRHA project, is being developed. Following the last updates and optimisations of the superconducting linac design, a more precise evaluation of the cryogenic requirements has been performed. In particular, operation temperature, thermal losses, and required cryogenic power have been evaluated. A preliminary architecture of the cryogenic system including all its major components, as well as the principles for the cryogenic fluids distribution has been proposed. A detailed study on the reliability aspects has also been initiated. Preliminary proposals for the technical buildings, their dimensions and layout in respect of the connexions with the accelerator tunnel have been proposed. Several similar size cryogenic systems, currently in operation, have been studied, in particular the LHC. The industrial feasibility and reliability of the main components is a major concern for the final design of the MYRRHA system.

*Work supported by the EU, FP7 MAX contract number 269565.

Introduction

Following initial proposals (PDS-XADS and EUROTRANS projects), detailed analysis and further optimisations have converged in a linac architecture which has been extensively discussed and compared with both existing linac and other more recently proposed projects. Initial proposals on the SC linac operation (heat loads, temperature levels) and cryogenic systems adapted to ADS were developed in the EUROTRANS programme [1]. This analysis resulted in several recommendations and an industrial feasibility analysis.

More recently, within the framework of the MAX project (FP7, end of 2011 – beginning of 2014) one of the main goals was to develop, with much higher level of details, the cryogenic technology that could guarantee a reliable operation of the MYRRHA accelerator. First, the analysis of the optimal operating temperature was developed. It concerns mostly the intermediate-energy sections of the accelerator that could operate either at 4 K (normal liquid helium) or 2 K (superfluid helium). Following this analysis and a more precise evaluation of thermal loads, a preliminary description of the MYRRHA cryogenic system was presented, including its main components (cold boxes, transfer lines and ancillary systems), and practical solutions were proposed to be implemented depending on the section of the accelerator. This proposal was based on the following criteria:

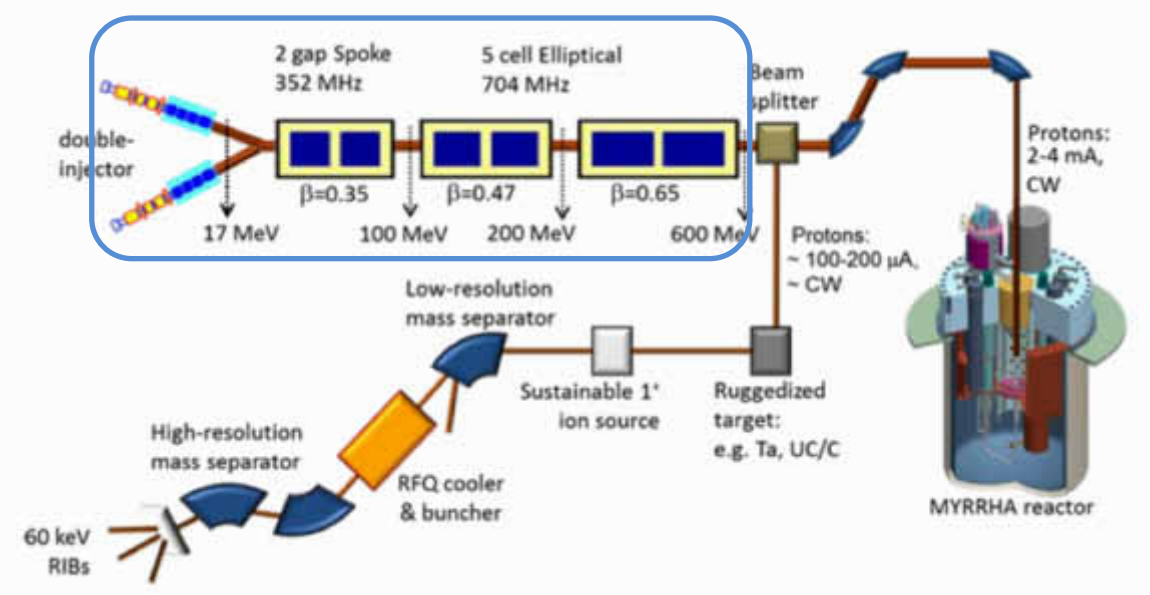
- complexity and reliability of the system;
- associated investment and operation costs;
- upgrading capabilities.

All these aspects were presented and discussed at the MYRRHA Accelerator 1st International Design Review held in Brussels in November 2012. A panel of accelerator experts evaluated this proposal and advised on the cryogenic system optimisation.

Cryogenic heat loads of the MYRRHA SC linac

Figure 1 presents the MYRRHA project in its last updated configuration.

Figure 1. MYRRHA project: Driver linear accelerator, subcritical reactor and ISOL Facility



The linear accelerator (linac) is one of the critical components in this project and it represents a major technological challenge: to deliver a high energy proton beam at high intensity in a continuous wave mode (CW). Only a solution based on Superconducting (SC) Cavities can offer the required feasibility and performances. Several design changes have been recently introduced into the SC linac, like injector frequency modification (352 MHz→176 MHz), a new design of SC – Crossbar H mode (CH) cavities, adopting a new modularity (6 cavities in 3 cryomodules for each injector), and, finally, slight changes on the modularity of the SC spoke (350 MHz) and elliptical (700 MHz) sections in order to optimise the "fault tolerance" architecture as needed for reliability enhancement. Table 1 presents the current status of cavities, their different types and their composition.

Table 1. MYRRHA linac SC cavities

Sections	Injector (SC – CH)	Spoke	Elliptical
Energy	3 – 17 MeV	17 – 100 MeV	100 – 600 MeV
nb. of cavities	6 (each injector)	48 (beta 0.35)	34 (beta 0.47) 60 (beta 0.65)
nb. of cryomodules	3 (each injector)	24	17 (beta 0.47) 15 (beta 0.65)
			

Cryogenic parameters of the MYRRHA SC linac

Cryogenic temperature

An important choice is the operation temperature of the SC linac. Given the RF surface losses on the elliptical cavity walls, operated at 704 MHz frequency (94 cavities over a total number of 154 cavities in the SC linac), these cavities must operate at 2 K in order to reach the accelerating fields with reasonable heat loads and RF power. The spoke cavities, operated at a lower frequency (352 MHz), could eventually be operated at 4 K, but a detailed analysis [2], comparing the two possibilities (2 K or 4 K) concluded with an overall SC linac operation at 2 K. An efficiency analysis shows that the electrical power required to operate the cryogenic system was very similar to the two options. He bath stability at 2 K is also an additional advantage for stable spoke cavity operation.

Heat loads

Nowadays the MYRRHA linac is one of the first linac's where the SC cavities cover almost 100% of the total accelerating range (between 3 MeV and 600 MeV), as compared with similar SC linacs like SNS (SC linac starting at 185 MeV) and the proposal for ESS (SC linac starting at 78 MeV). In addition, due to the beam operation in CW mode, the dynamic cryogenic losses are largely dominant compared to other SC linacs, which must operate in pulsed mode with beam duty cycle of only 5%.

The evaluation of heat loads for the different cavity types has been recently updated (see Table 2).

Table 2. Summary of heat loads@2 K

	CH 176 MHz	Spoke 350 MHz	Elliptic 700 MHz β=0.47	Elliptic700 MHz β=0.65
Number of cavities	12	48	34	60
Static + Dynamic includ. couplers	200 W@2 K	680 W@2 K	635@2 K	1360@2 K
Total (W)	Static (1015 W) + Dynamic (1860 W) = 2875 W@2 K			

This evaluation considers the two major loads contributions:

- The heat loads are associated with the RF couplers. These devices connecting directly the RF amplifiers to the cavities through short coaxial lines need sophisticated cooling systems to reduce the thermal conductive losses that can be introduced at the low temperature level. This is obtained either by heat intercepts of the outer conductor at intermediate temperature levels, or by extracting the RF generated heat by heat exchange (double wall) using cold LHe supplied at 5 K.
- The cavity static losses (related to conductive and radiative induced losses in the absence of RF driving power) are associated with the thermal and mechanical design of the cryomodule, in particular thermal shields, cavity supports, heat intercepts, etc. Based on preliminary studies and extrapolations from similar projects, the following static loads were proposed: 5 W/m at 2 K and 40 W/m for the 40 K intermediate temperature level.

Cryogenic refrigerator capacity

In addition to the heat loads at 2 K presented in Table 2, cryogenic refrigeration should also be supplied at intermediate temperature levels for cooling of the thermal shields at 40 K (total heat load of 15.2 KW), and the RF couplers' outer conductor (equivalent load of 500 W at 5 K).

Table 3 presents the final cryogenic budget at the different temperature levels, including two important specifications:

- Equivalent overall refrigeration capacity at 4.5 K. To ease the evaluation of cryogenic refrigeration requirements, the given loads at various temperature levels are all expressed as an equivalent load at 4.5 K. This is roughly estimated using the Carnot coefficient at the different levels of temperature. This approach allows a simple criterion of comparison with other installations in terms of size, capital cost, and operational demand.
- Overcapacity to take into account uncertainties in the heat loads estimations and to enhance cool-down speed and eventual additional equipment. The philosophy of the LHC cryogenics design has been adopted: an uncertainty factor (=1.25) for cavities defects in production and preparation and refrigeration power margin (=1.5) for cryogenic safe operation.

An overall margin of 1.875 is proposed for the MYRRHA cryogenic heat load at 2 K, and 1.5 for the heat loads at 5 K and 40 K.

Table 3. MYRRHA cryogenic refrigerator specifications

Function	T (K)	Heat load (kW)	Overcapacity	Factor (equiv. 4.5 K)	Cryo capacity (kW)@4.5 K
Cavities	**2.1**	**2.875**	(x 1.875) **= 5.3**	**2.16**	**11.5**
Coupler	**5**	**0.5**	(x 1.5) **= 0.75**	**~ 1**	**0.75**
Thermal shield	**40**	**15.2**	(x 1.5) **= 22.8**	**1/6.5**	**3.5**
	Total equiv @4.5 K				**15.75 KW**

The size of the cryogenic plant, in terms of electrical power needed to operate the system, can be estimated, taking into account the practical efficiencies of the main components, in particular the room-temperature compressors. This is represented by the C.O.P. (coefficient of performance), which gives the refrigerator efficiency with respect to an ideal carnot cycle. In large cryoplants (i.e. LHC) the measured COP is around 230 W/W (for a MYRRHA cryoplant of 15 KW equivalent at 4.5 K, it corresponds to 3.5 MW of electrical input power). Compared to an ideal Carnot coefficient of 65.6 W/W, it represents an efficiency of 28.5%.

MYRRHA cryogenic refrigeration system

Figure 2 shows the main components of the cryogenic plant proposed for MYRRHA:

- liquid and gas storage;
- room temperature compressors with purifiers and oil removing systems;
- 4.5 K cold box, including all heat exchangers and turbine expanders;
- 2 K cold box including cold compressors;
- cryomodules (cavities) with associated cryogenic interfaces (heat exchangers and valves).

This scheme is based on two main principles:

- The distributed subcooling heat exchanger scheme. The main cold box produces supercritical He (i.e. 4.5 – 5 K, 3 bars) for cavities and couplers. Each cryomodule will be associated with a cryogenic interface (valve box) incorporating the subcooling heat exchanger to reduce the temperature and the Joule-Thomson valve to expand and obtain the nominal He bath at 2.1 K and 30 mbar.
- A “mixed compression cycle” as adopted by LHC [3] (Figure 3), the 2 K cold box, with the cold compressors and heat exchangers, recovers the low pressure cold gases from the cryomodules. One or two stages of room temperature compressors can be added in order to optimise the efficiency and dynamic range of the system. In this case the pressurised He gas reaches the main cold box at an intermediate temperature level.

Figure 2. Components of the MYRRHA cryogenic system

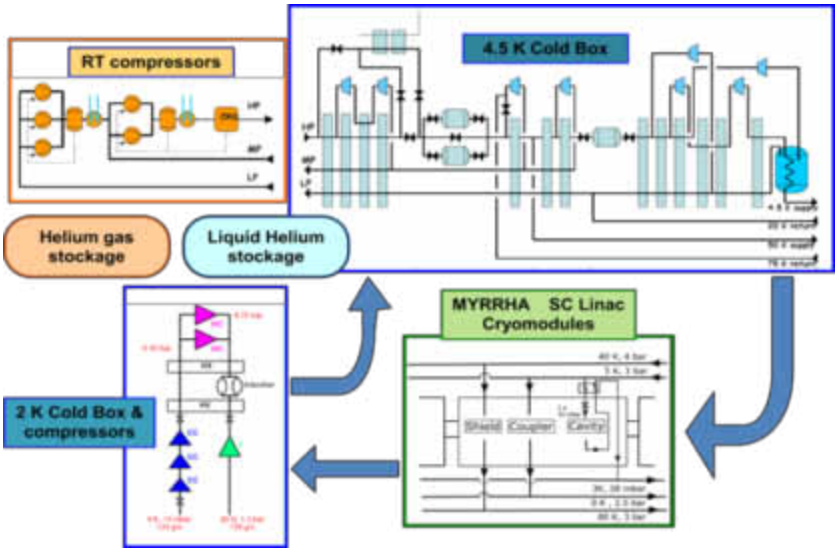
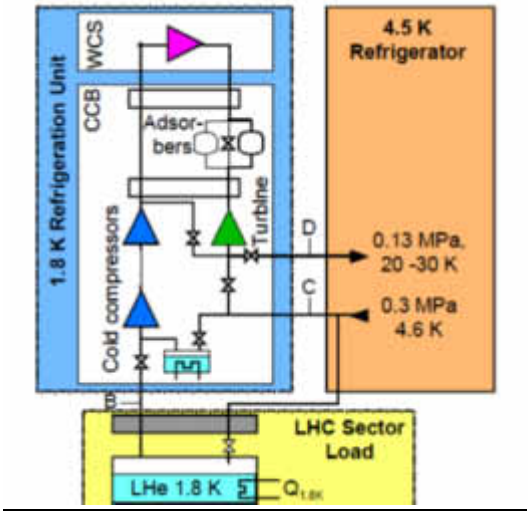


Figure 3. LHC cryogenic refrigerator unit



For MYRRHA, the overall power at 2 K was computed to be 5.4 kW, i.e., roughly twice that of one LHC refrigerator. One important issue will be to determine whether this higher mass flow can still be handled by the cold compressors designed for the LHC or whether a redesign of these components will be necessary.

In the LHC, the 1.8 K boxes are installed underground at - 100 meters, close to the accelerator tunnel. The proposed installation of MYRRHA with a linac tunnel installed at the ground level and closer to the cryogenic buildings could lead to an integration of both cold boxes (4.5 K and 2 K). This is one major aspect of the cryogenic system of MYRRHA that would need further development.

Similar cryogenic refrigerators for SC accelerators linacs can be considered as references for the MYRRHA design: the LHC (one unit) [3] with an equivalent cryogenic power of 18 KW at 4.5 K, and the SNS [4], with an equivalent cryogenic power of 10 KW at

4.5 K. Both operate at superfluid He temperatures (1.8-2 K) with a refrigeration capacity close to the MYRRHA proposal. Following the experience of LHC and SNS, all the new projects (like ESS and XFEL) propose now a distributed subcooling design, together with a centralised cold compressor station.

MYRRHA cryogenic system implementation

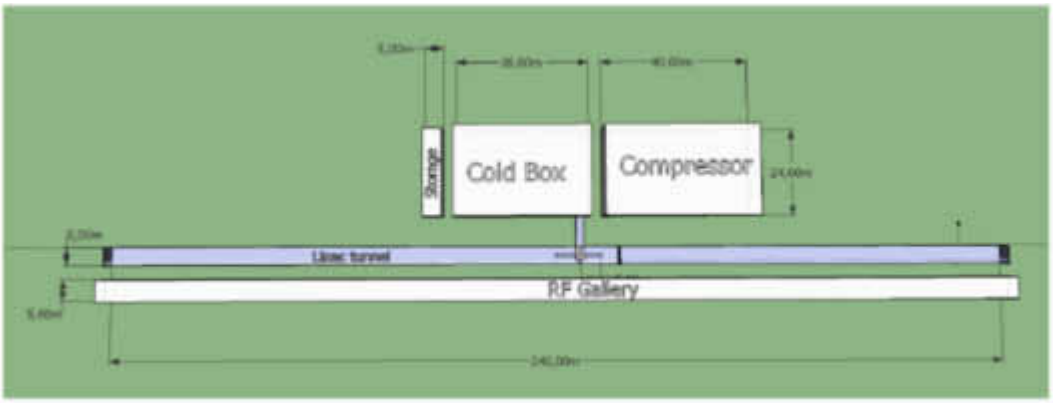
Buildings

Based on building sizes of both LHC and SNS cryogenic systems, a preliminary proposal has been presented: Two main buildings are necessary for the installation of the cryogenic refrigeration systems and also some outdoor surfaces to install gas and liquid helium storage reservoirs.

- compressor building: 40 x 24 m², with adequate sonic insulation;
- cold boxes building: 36 x 24 m² including 4.5 K and 2 K cold boxes

Close to these two buildings, there is a dedicated outdoor surface for helium liquid and gas storage of 5x20 m². A storage capacity of 7000 L of liquid He (~ reservoir of 2.5 m in diameter and 3 m long) and 200 000 L of gas (20 metres long, 3 m in diameter) at 20 bar was estimated.

Figure 4. Preliminary design of MYRRHA cryogenic buildings and the linac tunnel



The cryogenic plant should ideally be located as close as possible to the linac to minimise thermal and load losses in pipes. The heat load centre of gravity is located at 140 m from the injector, close to the geometrical centre point of the linac (120 m) or the beginning of the high β elliptical section (132 m). One advantage of placing the cryogenic plant in the middle of the linac is that the travel length and the mass flow in each segment is divided by two compared to a scheme where the plant is placed at one end. This reduces load losses and the pipe diameters of the transfer lines.

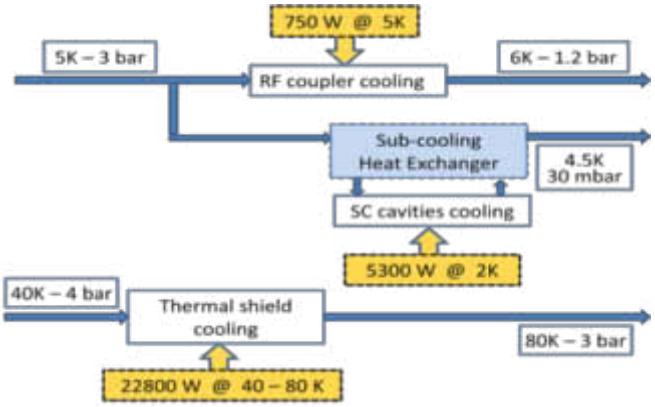
Helium distribution

Figure 5 shows the cryogenic fluids supply requirements:

- For thermal shield cooling, 40 K supercritical helium at ~4 bar will be provided. It will be returned at a temperature of approximately 80 K and ~3 bar (to account for load losses.
- For coupler cooling, supercritical helium will be provided at ~5 K and approximately 3 bar.

- Cavity cool-down requires a dedicated circuit within the interconnecting box associated with each cryomodule. The cavities are first cooled with helium vapours, then partially filled with liquid helium at 4.5 K. The 2 K cavity refrigeration requires an expansion of He through a Joule-Thomson (JT) valve to about ~30 mbar. It is therefore necessary to subcool the He gas to a temperature of about 2.2 K in a counter current heat-exchanger before the JT expansion. Each interconnecting box must integrate this heat exchanger and the associated JT valve.

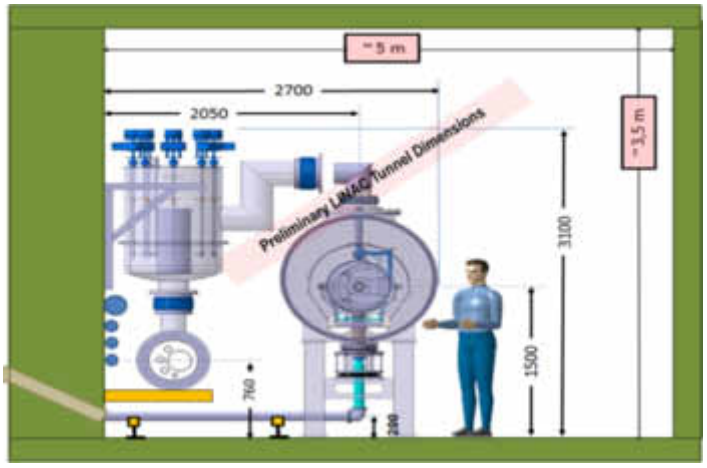
Figure 5. Cryogenic fluids distribution and heat loads



Cavities and couplers need a supply of 4.5 K at 3 bar with a mass flow of 160 g/s and a pipe diameter of 40 mm, thermal shields need a supply of 40 K at 4 bars with a mass flow of 40 g/s and a pipe diameter of 45 mm. Low pressure He gas at 30 mbar requires a large pipe diameter of 240 mm. All the 5 pipes (supply and return) are grouped in a unique composed transfer line, vacuum insulated with a total maximum diameter of 400 mm.

Figure 6 presents the preliminary view of the MYRRHA SC linac tunnel. It includes a spoke cryomodule, the cryogenic transfer line, and the interface valve box associated with each cryomodule.

Figure 6. Preliminary design of the MYRRHA linac tunnel



Reliability aspects of the MYRRHA cryogenic system

Studies developed during the EUROTRANS Project, gave a first estimate of reliability performances, and in the MAX Project, more ambitious reliability modelling and enhancement proposals are currently underway. Following the detailed analysis of fatigue and risks of the subcritical reactor (window, fuel assemblies and structures), the foreseen goal is to operate a 600 MeV-2.5 mA beam with less than 10 beam trips, of duration higher than three seconds, for a three-month period. This is equivalent to a MTBF (mean time between failures) greater than 250 hours. This goal must be compared to currently running high-power accelerators which operate with MTBF for only a few hours.

In order to improve the reliability performances of MYRRHA, several major improvements are proposed:

- redundancy of the injector sections (up to 17 MeV) with two complete injectors in parallel;
- a SC linac with cavities operating at reasonably low accelerating gradients, to fulfill a "fault tolerance" scheme which can accept a certain number of cavities trips, recovering a nominal beam in a very short time;
- use of solid state RF amplifiers, which can offer an internal failure acceptance, allowing avoidance of RF trips and their consequences on nominal beam operation.

Concerning the MYRRHA cryogenic systems, it is difficult to imagine redundancies on the main components for such a large refrigerator. Nevertheless, their reliability performances need an in-depth analysis together with a more detailed failure mode study. In a first approach it can be stated that a cryogenic system does not induce fast transients on the SC linac operation. Unlike a large SC circular machines (synchrotrons), where a local magnetic field trip could trigger loss of beam, in a SC linac, an accident at the refrigerator level which imposes a stop on He nominal flow, can allow enough time to reduce the beam power on the target and perform a safe beam stop. The liquid helium in the transfer lines, interconnecting boxes, and reservoirs of each cavity, could offer a minimum refrigeration capacity for a safe stop. Of course, it will result in a stop procedure of the subcritical reactor, reducing its availability, but without a risk of fatigue on the mechanical structures induced by fast thermal transients. This possibility must be analysed in detail in order to provide an estimate of time constants and possible strategy to stop the beam in a safe way.

Reliability of large cryogenic refrigerators used for accelerators

Within the FP7-MAX activities, a special in-depth study has been performed on the cryogenic system reliability of three large accelerators: HERA synchrotron in DESY, in operation during 15 years (1992-2007) [5], SNS [6] with a SC linac very similar to the MYRRHA linac, started in 2006, and LHC [7] with a refrigerator unit size comparable to that proposed for MYRRHA, started in 2009.

The HERA synchrotron refrigeration plant is composed of three units with a refrigeration capacity of 6.4 KW@4.5 K each. During this period the availability of the refrigeration plant was 99%. Failure statistics of cryogenic components show a total number of 200 events (more than 1000 hours of downtime), with the main causes related to:

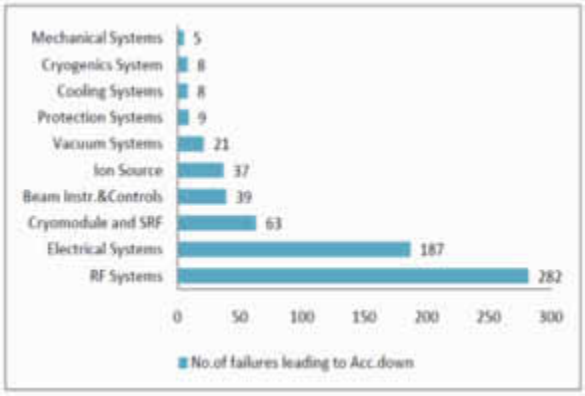
- the process control system; with failures on hardware (power supplies, multiplexers, PLC) and software errors, and some hardware failures are partly due to radiation damage;
- the compressors stations, on average three times a year, a compressor-station caused an emergency stop of the refrigeration plant;

- power outages lead to technical breakdowns of the plant, in average 2.5 power outages per year, mostly short breaks due to thunderstorms;
- other failures such as cooling water and compressed air cause discontinuation of the cryogenic supply, but with an average of one failure per every three years, the HERA technical group (Linde-DESY) concludes that a cryogenic plant availability of 99% can be reached if periodical maintenance and replacement of critical components is carried out.

The SNS SC linac is composed of 23 cryomodules with 81 SC elliptical cavities. Beam loss events from 2007 to 2011, induced by failure occurrences in the cryomodules, represent a total of 85 events. Many failures are related to sensors (pressure and vacuum), associated electronics due to radiation damage, mechanical parts within the cryomodules, ceramic feedthroughs, some bad welding, RF cables and connectors. It can be concluded that after 6 years of improvement, in 2011, only one beam trip (related to SC linac) per day is observed. The general availability has significantly increased in this period from 65% to 86%.

Modelling of the SNS failure modes and analysis of operation, using the logbook data for recent operation periods was performed within the FP7 – MAX Project [8]. A detailed risk spectrum fault tree model (currently applied for nuclear power plants) was developed. Figure 7 presents the failure statistics.

Figure 7. SNS failures statistics (period October 2011 – June 2012)



The SNS availability improvements after the commissioning phase were impressive, increasing from 65.7% availability in 2007 to 91% in 2011. Cryomodules and cryogenics systems related failures induce only 6% of accelerator downtime.

The LHC operation is extensively analysed due to the considerable amount of data concerning cryogenic system reliability. The LHC system was designed such that, to a certain amount, underperformance of one of the refrigerators (in total eight surrounding the collider ring) could be compensated by an adjacent refrigerator. Several major failure causes have been identified:

- compressor station related failures are the most critical (vibrations, friction), as they completely forestall refrigerator operation;
- turbine failures only reduce helium supply by a small percentage;
- other component faults cited are: oil pumps, compressors shaft seals, and control valves of turbine bearings;
- impurity problems are cited as one of the recurrent failure causes, repair times due to clogging problems can be considerable (a complete regeneration is sometimes necessary);

- a more insidious cause of LHC cryosystem shutdown has been controller malfunction due to neutron irradiation coming from residual radioactivity of the beam.

Detailed analyses of LHC operation were published in 2011 and 2012 [9] [10]. In 2011, the machine operated for 269 days, delivering 63 days of stable beams (23.4%). Downtime due to failures was 73 days, and cryogenics systems (both technical stops and failures) contributed for 48 days. Considering only the failures (26 days) the cryogenics availability was 90%. In 2012, the machine operated for 257 days, delivering 73 days of stable beams (28.4%). Downtime due to failures was 67 days, due to cryogenics failures 15 days, with a final cryogenics availability of 95%. LHC cryogenic systems have achieved high availabilty. The availability of a single refrigerator is 99%. On average, one refrigerator can be run for 8-9 weeks without interruption. This figure is close to the three-month irradiation period for MYRRHA.

MYRRHA cryogenic system requirements and reliability improvements

Following the analysis and the recommendations, a number of common cryogenic system failures can be identified. The requirements to guarantee good cryogenic system availability can be summarised as follows:

- Mean Time Between Maintenance (MTBM) should be > 8 000 hous.
- Valves, heat exchangers and turbines are particularly sensitive elements to impurities (dust, oil, gases). Improvements are necessary to keep a minimal level in these components.
- Redundancy studies for all elements containing moving/vibrating parts (turbines, compressors, including their respective bearings and seal shafts) are necessary.
- Periodic maintenance is mandatory: oil checks, control of screw compressors every 10 000-15 000 hours, vibration surveillance programme, etc.
- Special control and maintenance of utilities equipment (supply of cooling water, compressed air and electrical supply) is necessary.
- Periodic vacuum checks to identify leakage appearance such as insulation vacuum of transfer lines and distribution boxes are necessary.
- Easily exchangeable cold compressors are required.

If an appropriate level of redundancy is implemented and the precautions listed above are taken into consideration, high levels of availability of the cryogenic systems (99%) can be achieved. This high availability can be achieved after one or two years of cryogenic system operation ("learning curve").

References

[1] Biarrotte, J.-L. et al. (2010), "Accelerator reference design for the MYRRHA European ADS demonstrator", *Proceedings 15th Int. Linear Accelerator Conf.*, Tsukuba, Japan.

[2] Chevalier, N. (2012), "Cryogenic installation for MHYRRA", *SLHIPP Meeting*, Catania (Italy), https://indico.esss.lu.se/indico/conferenceDisplay.py?confId=13.

[3] Clauder, S. (2006), "Design, construction, installation and first commissioning results of the lhc cryogenic system" (CERN), EPAC, Edinburgh, Scotland.

[4] Arenius, D. et al. (2004), "Cryogenic System for the Spallation Neutron Source", CEC vol.49.

[5] Clausen, J.J. et al. (2007), "Summary and results of the cryoplant operation for HERA Linde Document", http://www.lindekryotechnik.ch/public/fachberichte/hera.pdf.

[6] Arenius, D. et al. (2004), "Maintenance and Reliability Design Aspects of the SNS 2K Refrigeration System", Cryo 2004 Operations Workshop, JLAB, US.

[7] Claudet, S. (2011), "LHC Cryogenics, the approach towards availability/reliability", (CERN) ARW, Cape Town, South Africa.

[8] Pitigoi, A.E. (2013), "Reliability modelling activities, MAX Linac (Myrrha Project)", *SLHIPP Meeting*, Louvain la Neuve, Belgium.

[9] Pojer, M. et al. (2012), "Machine Availability at the LHC", *Proceedings of the IPAC 2012*, New Orleans, US.

[10] Macpherson, A.L. (2012), "LHC availability and performance in 2012", (CERN), *LHC Beam Operation Workshop, Evia*n, France.

Operation of the accelerator driving the VENUS-F core for the low power ADS experiments GUINEVERE and FREYA at SCK•CEN

M. Baylac[1], A.Billebaud[1], P.Boge[1], D.Bondoux[1], J.Bouvier[1], T. Cabanel[1], S. Chabod[1], G.Dargaud[1], E.Froidefond[1], M.Heusch[1], A. Kochetkov[2], E. Labussière[1], F.-R. Lecolley[3], J.-L. Lecouey[3], G. Lehaut[3], N. Marie[3], J. Mertens[2], R. Micoud[1], F. Van Gestel[2], C. Van Grieken[2], B. Van Houdt[2], G. Vittiglio[2]
[1]LPSC, UJF/CNRS-IN2P3/INPG, Grenoble, France,
[2]SCK•CEN, Mol, Belgium,
[3]LPC Caen, ENSICAEN/Université de Caen/ CNRS, France

Abstract

GUINEVERE and FREYA are European projects devoted to experimental studies of accelerator-driven system feasibility. They are mainly dedicated to on-line reactivity monitoring, subcriticality determination and operational procedures. An experimental reactor of SCK•CEN (Belgium) modified into a fast lead core, VENUS-F, is coupled to a versatile accelerator-driven neutron source developed by CNRS/IN2P3 (France) driving the reactor in different modes. A deuteron beam is provided by an electrostatic accelerator with a time structure driven solely by the ion source. The deuteron ions are accelerated (220 keV) onto a tritiated target located at the centre of the reactor core, creating neutrons by T(d,n) 4 He reactions. This paper describes the design and commissioning of the facility and reports on the operation of the accelerator coupled to the reactor.

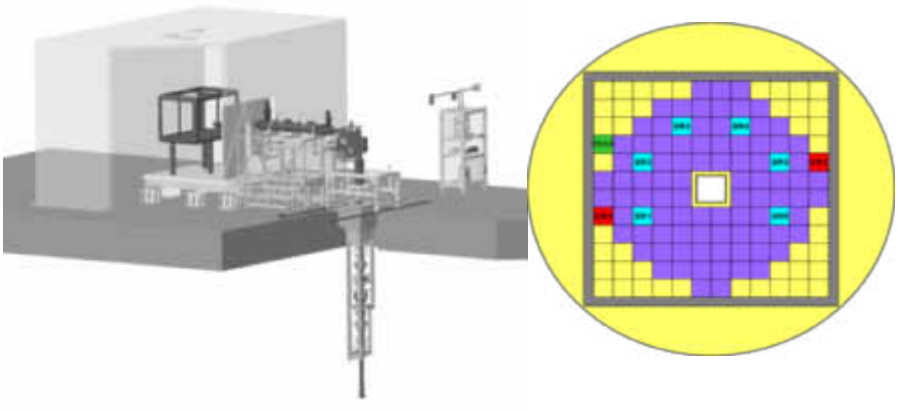
Introduction

The Generator of Uninterrupted Intense NEutrons at the lead VEnus Reactor (GUINEVERE) project was launched in December 2006 within the IP-EUROTRANS (FP6) to be continued with the FP7 Project Fast Reactor Experiments for hYbrid Applications (FREYA). These projects are based on a low-power experimental facility representing an accelerator-driven system (ADS) demonstrator. They aim to investigate the on-line monitoring of the reactivity and its absolute measurement, which are major safety issues, in addition to the operational procedures of an ADS, including core loading, system start-ups and shutdowns [1]. The facility consists of the VENUS-F nuclear core at SCK•CEN (Belgium) coupled to an external accelerator-driven neutron source. The GENEPI-3C accelerator, developed by CNRS/IN2P3 (France) operates both in pulsed and continuous beam modes, the latter being more representative of a powerful system. The low-power coupling of VENUS-F and GENEPI-3C thus provides a unique facility in Europe for fast subcritical reactor physics investigations.

Subcritical reactor core

For the subcritical experiments, the VENUS-F reactor is loaded with 93 square fuel assemblies (FA) arranged in a cylindrical geometry (~800 mm in diameter, 600 mm in height). The outer section of a FA is 80 mm. The FA are composed of 30% ^{235}U enriched metallic uranium and solid lead rodlets acting as a fast system coolant. The core is surrounded by axial and radial lead reflectors [1]. The 4 central FA's are missing in order to place an insertion channel inside the terminal section of the accelerator beam line (Figure. 1). A small lead buffer fills the gap between the target tube shaft and the central hole. The reactor is equipped with six safety rods and two control rods. Rods are located as close as possible to the center without interfering with the vertical structure of the accelerator.

Figure 1. GENEPI-3C accelerator layout (left) showing the terminal section of the beam line which is inserted into the central region of the core (right) in a subcritical configuration (SC1 displayed)



Accelerator facility

The generator of neutrons pulsed and Intense-3C (GENEPI-3C) drives the subcritical lead core VENUS-F. GENEPI-3C is an electrostatic accelerator generating deuteron beams onto a tritium target located at the core center, creating 14 MeV neutrons by T(d,n)^{4}He reactions. This versatile accelerator-driven neutron source designed, constructed and operated by CNRS/IN2P3 (France), is fully described in [2]. Only main features are described here. This electrostatic accelerator produces alternatively short and intense deuteron pulses with adjustable repetition rate, continuous (DC) beam or DC beam with adjustable programmable interruptions to accommodate the experimental physics programme. Table 1 summarises the accelerator specifications.

Table 1. Specifications of the GENEPI-3C accelerator

Pulsed mode	DC interrupted mode
Peak current: 40 mA	Mean current: 160 µA to 1 mA
Repetition rate: 10 Hz to 5 kHz	Beam interruption rate: 0.1 to 100 Hz
Pulse width: ~0.7 µs (FWHM)	Beam interruption duration: ~20 µs to 10 ms
Reproducibility: 1% pulse to pulse	Transition time on/off: ~1 µs

A duoplasmatron ion source generates the deuteron beam with the different required time structures and intensities. The main differences between the pulsed and DC (including DC interrupted) beam modes concern source efficiency and beam transport. The ion source, with its extraction and focusing electrodes lies within a high voltage platform and connects directly to the 220 kV accelerating structure. The first (horizontal) beam line section connects to a dipole magnet performing the magnetic separation of the beam out of the source and bending the D+ beam down towards the target located at the core centre via a ~6 m long vertical beam line (see Figure 1). This 90° bend magnet is supported by a mobile frame, translating it away to grant access to the vertical beam line. Beam transport is ensured using 12 electrostatic quadrupoles and 4 magnetic steerers. The accelerator is designed to enable the vertical section of the beam line to be easily craned out of the reactor bunker for maintenance operations, target changes and core loading.

The neutron production target consists of a thin layer of TiT (12 Ci) deposited on a copper disk mounted at the end of the vertical beam line. The beam size on target is tuned to match approximately the 40 mm diameter of the active layer. Beam current, as well as temperature, is measured continuously on the target. A compact cooling system is implemented to dissipate the beam power (up to 250 W) with compressed air only. It consists of 4 air pipes feeding a diffuser with nozzles facing the back side of the target, the target back being designed with pin fins to increase the heat exchange surface.

Two detectors determine neutron production rates during accelerator operation. A silicon detector (API) provides an absolute measurement of the neutron production rate via the associated alpha particle detection. This silicon detector is sitting within the beam pipe under vacuum approximately 1 m away from the target under direct solid angle. A proton recoil telescope is installed on top of the dipole magnet, in the target line of sight at a distance ~7 m. It provides a direct monitoring of the 14 MeV neutrons after their conversion into protons detected in triple coincidence in layers of silicon detectors.

The driving software of the accelerator is a laboratory developed system compiled with LabWindows which uses the DIM protocol for communication. It interacts with custom hardware containing embedded software and operates a graphical user interface running on various PC's. The local intelligence of each command control module is based on SOPC (System On Programmable Chip). All of the 17 modules are identical (therefore interchangeable) and self-configurating. The system is organised with a distributed architecture centered on the PC. Data transmission is accomplished via ethernet 100 MHz links.

Accelerator commissioning, coupling and operation

Commissioning

The accelerator was fully assembled and tested at LPSC (France) with dummy targets made of solid copper disks before being shipped to SCK•CEN. Infrastructure at LPSC was adapted to provide an exact mock-up of the VENUS site. The machine was tested in different stages along with its design and construction between December 2008 and August 2009. During the accelerator commissioning, all components were tested (ion source and HV platform, magnet, quadrupoles, steerers, command-control system), beam transport and characterisation was performed in the different beam modes as were partial beam line motions (magnet translation and vertical line craning). The machine was dismantled (16 tonnes of equipment) and transferred to Mol (Belgium) over a distance of ~800 km, in September 2009.

The machine was re-assembled in the newly built accelerator room (February 2010). Full motion and guiding of the vertical beam line was tested at SCK•CEN. After adjustment of the guiding structures at the upper and lower level of the accelerator, the vertical line was craned down within the reactor bunker until full insertion in the central

channel of the reactor. All cables remained connected and followed the beam line motions during this displacement (see Figure 2). The compactness of the core yielded to a very dense accelerator and reactor interface holding an accelerator target, a cooling system and a current measurement as well as reactor fission chambers (see Figure 3). After insertion of the vertical line, the accelerator was prepared for operation by a three-step process: translating horizontally the dipole support frame above the vertical line, connecting the two vacuum line sections upstream (H) and downstream (V) of the dipole and connecting the primary pump located on the magnet frame to the turbo pumps of the V line.

The accelerator commissioning was performed on a dummy target with an unloaded core (no fuel assemblies). It had to progress step by step along with nuclear safety authorisations, which turned out to be extremely time consuming. First, the safety interlock module was validated to ensure safe machine operation. The module collects signals related to access control, high voltage, beam line vacuum, beam current, target cooling, dipole cooling and tritium release. Any faulty signal breaks the safety loop open and drops the very high voltage (240 kV), thus stopping the beam. Beam was transported through the machine with settings very similar to those determined at LPSC, attesting good machine reproducibility in both modes.

Special attention was paid to the validation of the target cooling system because of the potential tritium contamination which could be caused by a target meltdown. Temperatures measured on the back of the target were found to be 20° lower than on the target side under beam impact. Test runs were performed in DC beam where the current was ramped gradually up to 1.3 mA to ensure safety margins, abruptly turned off and restored multiple times. Extensive tests were performed to ensure that a high current DC beam, accidently tuned down to small dimensions, can be handled by the target cooling system. No temperature higher than 60° on the target side under beam impact has ever been recorded. Once approved by the nuclear safety authorities, a brand new tritium target was installed and both neutron detectors were commissioned. High-energy neutron (~14 MeV) rates were measured in both beam modes and proved to be in good agreement with neutron production expectations for a new target:

- Pulsed mode : ~ 1.15 x 10^6 n per pulse for f=10-5000 Hz;
- DC mode : ~ 10^8 $n.s^{-1}.\mu A^{-1}$ for I ~20-1100 µA (see Figure 4).

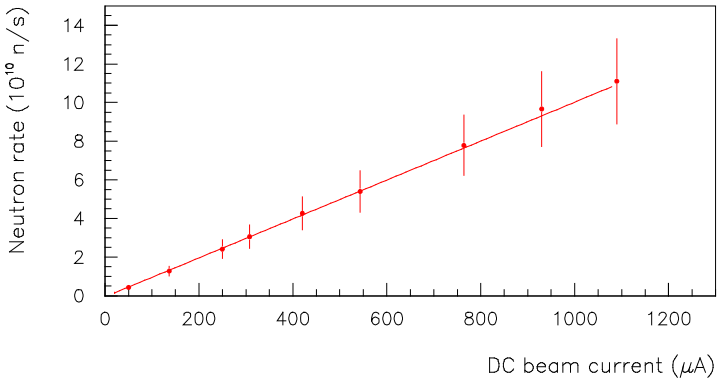
Figure 2. Upper level of the accelerator during beam line handling: The vertical line is being inserted in the reactor bunker while the magnet is retracted



Figure 3. Vertical beam line inserted in the reactor core: (left) full beam line over the bunker height (right) and close-up of the reactor top level showing the top of the thimble atop the fuel assemblies



Figure 4. Neutron rate versus beam current in DC mode measured by the API silicon detector [3]



Once the commissioning of the accelerator was fully completed, the overall commissioning report was transmitted to the safety authorities (September 2010) and the facility was prepared for critical mode: the dipole magnet was rolled away, the vertical beam line was disconnected and stored on its dedicated support structure.

After nuclear safety approval (January 2011), the reactor core was loaded. Core certification was achieved and the experimental programme in critical mode was performed until summer. The authorisation for the reactor and accelerator coupling was finally granted in September 2011 after an overall waiting period of one year.

First accelerator-reactor coupling

The first coupling was reached on 12 October 2011. The accelerator was started in pulsed mode at 200 Hz of repetition rate. The neutron flux as a function of time was recorded in the reactor by 6 monitors for the reactor and 10 detectors for the physics experiments [4]. The reactor rods lifting sequence was initiated: the six safety rods were lifted one by one requiring about 25 minutes, then the two control rods were lifted simultaneously during

~ 5 minutes to their reference height (here 479.3 mm). This sequence is identical for all VENUS-F reactor start-ups.

As the rods are out of the core, it was verified that the reactor power is driven by the accelerator: a core power ~1 W was measured at 200 Hz and increased according to the accelerator repetition rate increase.

Accelerator operation

After the initial coupling, a commissioning phase followed, which aimed to test the different beam modes in the coupled configuration, adjusting the start-up procedures, the detector efficiencies, the piloting and data acquisition software. Since April 2012, the accelerator has been operated for the experimental physics programme within the FP6 IP-EUROTRANS GUINEVERE project and is to be continued within the FP7 FREYA project [5]. The beam mode is determined by the physics requirements: data is mainly taken using pulsed and DC interrupted beam, with some runs in purely DC mode.

During the coupling commissioning phase, the first run period was devoted to pulsed beam (October-November 2011). Operating the duoplasmatron ion source in pulsed mode and transporting short high charge bunches is well acquired as this mode was extensively produced on the first two GENEPI machines. It generates no operational difficulty and the beam production is fairly reliable. However, the pulse peak current is limited to ~25 mA compared to the measured 40 mA of the previous machines. This is due to the mechanical reduction of the hole of the pierced ion source anode, implemented to optimise the beam extraction in DC mode. But this current limit remains acceptable for the physics programme.

Initially, the DC operation (November 2011) was problematic because of a very strong limitation on the beam current imposed by some fission chambers' pile-up in the reactor due to the high neutron source strength with a fresh TiT target. A beam current of 70-100 µA was requested on target whereas the ion source was not suited for such a low D+ current production. Similarly, the initial run in DC interrupted mode was complicated since tuning of the programmable interruptions is difficult at such low currents.

Once fission chambers were reshuffled within the core to adapt their detection efficiencies to the experimental conditions, standard operation of the ion source could be restored to transport hundreds of µA on the target, leading to better machine performances.

The following experimental programme, undergoing the 3 beam modes, corresponds to about 10 months of data taking. Producing DC interrupted beam remains problematic, because this beam mode was commissioned for the first time at SCK•CEN, while operating issues were discovered in the field and during the data taking. Numerous high voltage discharges occur during beam delivery: some remain internal to the region of the source holding extraction and focusing electrodes, others create electric arcs outside the high voltage platform. While some are not harmful to beam delivery, a number of discharges cause accidental beam trips which are detrimental to the experimental programme (see Section 5). The accelerator room is equipped with a ventilation system, constantly renewing the air. Air is taken directly outside the building without treatment or regulation. During machine operation, humidity was measured up to 70% and temperature was measured up to 28°C in the accelerator room. As a result, these poor conditions may cause some high voltage discharges.

In 2013, maintenance work was performed to improve electromagnetic compatibility within the high voltage head and harden the electronics driving the time structure of the source. We expect a reduction of electric discharges during the spring run.

When operating GENEPI-3C, the main issue is the fast ageing of the ion source. Previous experience of duoplasmatrons operated in pulsed mode (low power) only at

Cadarache or Grenoble, showed that a single ion source filament could last ~1.5 years. However, the filament chamber, holding the filament itself and its shield, on the source at SCK•CEN suffers faster ageing. In cases of sole filament depletion, an exchange and restart can be performed within ~ one week. In cases of additional filament shield destruction, an overall cleaning of the ion source is required, leading to a longer downtime. Investigations are currently underway to understand this premature ageing process. Meanwhile, the filament chamber is now replaced preventively at approximately every long downtime. The type of heat treatment of the shield material (tantalum) is under study. Post mortem analysis showed that all damaged shields were made out of sintered metal. The newly installed filament is protected by an annealed tantalum shield with higher strength, allowing a longer lifetime of the ion source in the coming run.

Beam current

The command-control provides measurements of the current intercepted by the target and the collimator. In order to prevent secondary electron yield under beam impact, a positive bias voltage of 200 V is applied to the target (and to its collimator).

In pulsed mode, the current measurement module determines the peak (I_{peak}) and average ($I_{average}$) current, the repetition rate (f) and the bunch width (T_{pulse}). To first order, the average current corresponds to $I_{average} = I_{peak} \times f \times T_{pulse}$. Figure 5 (left) displays an example of the averaged time profile of the bunch. A preliminary analysis was performed and the results showed that the bunch width was around 550 ns (FWHM) and remained stable: $\sigma(T_{pulse})/ T_{pulse} < 1\%$

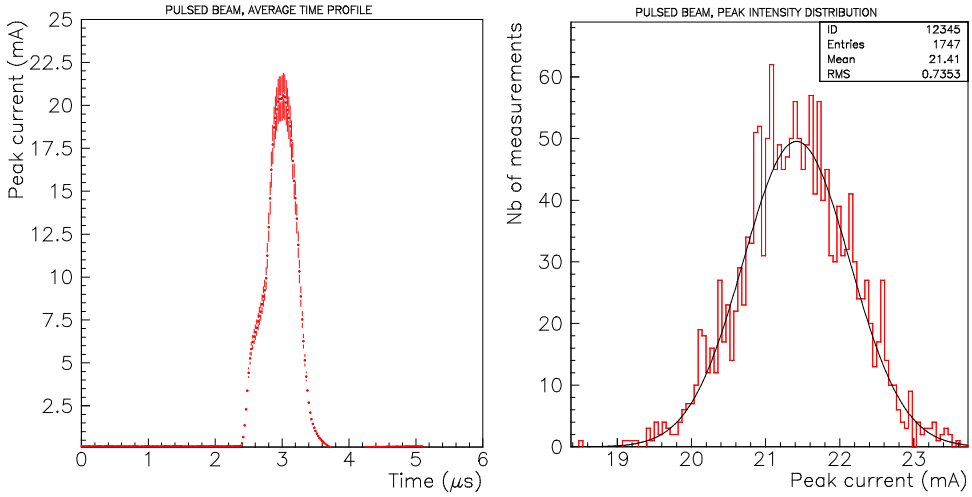
- the stability of the pulse frequency is excellent: $\sigma(f)/f < 10^{-5}$.

A full analysis of all accelerator data runs is still to be performed but so far, it seems that the specifications of the beam in pulsed mode are mostly met, except for the current stability and intensity in pulsed mode [6]. Over the months of data taking, the peak amplitude was measured 20-25 mA, mainly accounting for fluctuations and for a slow current decrease observed daily over the few hours of operation. This decrease detected independently of the beam mode, remains under investigation.

In DC mode, the module measures the current ($I_{average} = I_{peak}$). In DC interrupted mode, the module additionally determines the duration and frequency of beam interruptions. Figure 6 displays the time profile of the beam at ignition after the interruption (left) and at the interruption generation (right). The transition time from “beam on” to “beam off” is on the order of 1 µs, as stated in the beam specifications. Typical settings used for the physics programme are as follows:

- $I_{average}$ = 200-400 µA;
- interruption duration = 300 µs;
- interruption frequency = 200 Hz.

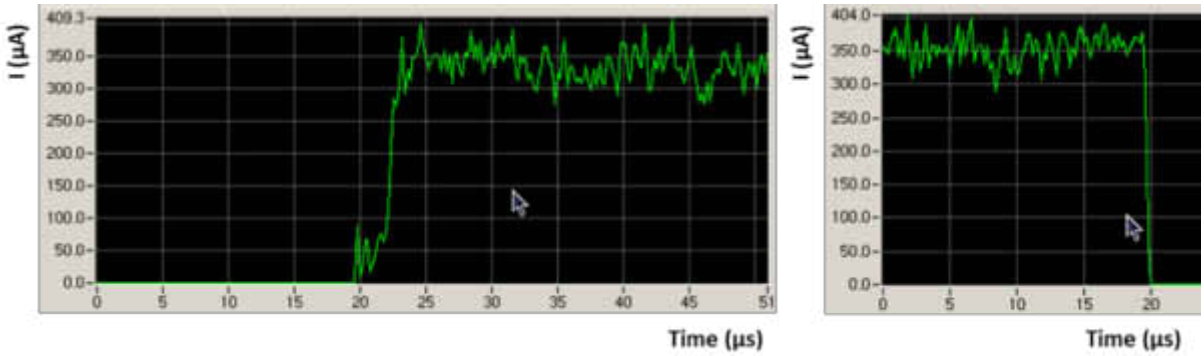
Figure 5. Time profile of pulsed beam on target (time referenced to internal electronics clock) averaged over 10 seconds (left) and peak amplitude distribution over ~5 hours (right)



Under these conditions, the beam operation was fairly stable, apart from the high voltage discharges described in the previous paragraph.

The charge integrated on target is recorded daily. A good day of running can generate a charge as high as ~ 5 C, corresponding to ~7.5 hours of beam.

Figure 6. Time profile of the beam ignition and (left) halt of the DC interrupted beam measured on target referenced to an internal clock (right)



Accelerator and reactor interactions

As explained in Section 4, some accidental beam interruptions occur due to high voltage discharges. These unwanted beam trips create time consuming halts of the data taking and are thus very harmful to the experimental physics programme. When the beam is lost on the target, the neutron production drops within tens of microseconds. If the interruption is long enough, the neutron depletion affects the reactor monitors count rates. When the beam is restored on the target, the monitors detect a sudden increase. If the neutron multiplication rate is so high that it exceeds a limit imposed for reactor safety (related to the reactor doubling time), then reactor emergency shutdown is triggered; the safety rods drop by gravity (reactor SCRAM). Nearly, no accidental beam interruptions can be recovered by the accelerator pilot fast enough to prevent the reactor SCRAM. Similarly, the beam current increase (pulse frequency in pulsed mode or average intensity in DC or DC interrupted mode) must be ramped slow enough not to exceed the safety threshold.

Restarting the coupled system requires about half an hour. Typically, the facility is operated eight hours a day. Therefore, the number of daily (or weekly) SCRAMS dramatically impacts the physics programme and is the leading cause of facility downtime. The number of SCRAMS strongly depends on the beam mode (see paragraph IV, c). Records were analysed over a year of operation, the numbers range from 0 reactor SCRAM per week, up to six reactor SCRAMS per week, mostly when operating higher beam power. Given the upgrades aiming at improving the electromagnetic compatibility of the machine (see paragraph IV c), we expect reduced SCRAM rates during the coming run.

For an effective operation of the coupled facility, an excellent communication level is required between the accelerator and the reactor team for:

- long-term planning to optimise facility downtimes (maintenance, upgrades) and running periods;
- weekly/daily planning for preparation of running conditions, problem solving, optimum scheduling of reactor and accelerator safety checks, site access.

Maintenance work such as ion source exchange or vacuum equipment replacement is now conducted jointly by the CNRS and the SCK•CEN. At the VENUS Facility, the accelerator and reactor control rooms were constructed on top of each other to foster exchanges. The accelerator was driven in the accelerator room from a PC, but the machine command-control system is fully functional from another PC installed in the reactor room. The acquisition system operates a data recording of the machine (accelerator parameters), of the physics experiment (neutron rates) and of the most relevant reactor data (heights of the safety and control rods, current and period of the 6 reactor neutron flux monitors, core temperatures). Two electronic logbooks centralising manual entries dedicated to the machine and the physics are accessible on and off site. Reactor pilots are being trained to operate the machine and will eventually operate the whole facility, reactor and accelerator.

Summary and outlook

The GUINEVERE and the FREYA projects are devoted to ADS reactivity on-line monitoring. The experimental facility gathers a versatile neutron source consisting of an electrostatic deuteron accelerator at 240 keV, GENEPI-3C, generating neutrons from impact on a tritium target and a fast subcritical core VENUS-F. After the machine commissioning on the SCK•CEN site and a long interaction with the safety authorities, the first coupling of the accelerator to the reactor was reached quickly and efficiently. While some improvements remain to be performed on the beam current (stability and intensity), the machine specifications are largely met. The experimental programme has progressed [5] and yielded the first physics results [4]. The main operational constraint is the facility downtime generated by reactor SCRAMS caused by severe electric discharges. After the first year of coupled operation, several improvements of the machine have been implemented to minimise these discharges and we expect enhanced machine reliability during the coming run.

The analysis of the recorded data set of the accelerator coupled to the reactor is being carried out. In spite of the discrepancies of accelerator structures between such a mock-up machine and a high power proton driver for an ADS demonstrator facility, valuable feedback from the coupled operation can be provided to ADS projects, such as MYRRHA [7].

Acknowledgements

This work was partially supported by the Sixth and Seventh Framework Programmes of the European Commission (EURATOM) through the EUROTRANS-IP contract # FI6W-CT-

2005-516520 and FREYA contract # 269665, MAX contract #269565 and the French PACEN programme of CNRS.

References

[1] Billebaud, A. et al. (2009), "The GUINEVERE Project for Accelerator Driven System Physics", *Proc. of the Global 2009 conference*, Paris, France, 6-11 September 2009.

[2] Baylac, M. et al. (2011), "A versatile neutron source for the low power ADS GUINEVERE", *Proc. of the International Topical Meeting on Nuclear Research Applications and Utilization of Accelerators (AccApp '11)*, Knoxville, TN (US), 3-7 April, 2011.

[3] GUINEVERE safety studies, SCK•CEN internal report, (2011).

[4] Chabod, S., Lehaut, G. et al. TCADS-2 proceedings.

[5] Kochetkov, A. et al. TCADS-2 proceedings.

[6] Billebaud, A., Baeten, P. "Cahier des charges de la source de neutrons de GENEPI-3C en mode continu", internal LPSC report, GUI-SPE-1.1-0001-LPSC.

[7] http://myrrha.sckcen.be/.

Session III: Simulation, Safety and Data

Chair: Y. Gohar

Nuclear data for safe operation and waste transmutation: ANDES and CHANDA

Enrique M. Gonzalez
on behalf of the ANDES collaboration
Centro de Investigaciones Energéticas MedioAmbientales y Tecnológicas, Spain

Abstract

Nuclear research within the Seventh Framework Programme (FP7 and FP7+2) of EURATOM has devoted a significant fraction of its efforts to the development of advanced nuclear fuel cycles and reactor concepts, mainly fast reactors, aiming to improve long-term sustainability by reduction of the final wastes, optimal use of natural resources and the improvement of safety in the present and future nuclear installations. The new design needs more accurate basic nuclear data for isotopes, like minor actinides, potentially playing an important role in the operation, fuel concept, safety or final wastes of those reactors and fuel cycles. Four projects, ANDES, ERINDA, EUFRAT and CHANDA, supported by EURATOM within FP7 and FP7+2, have gathered most of the European Nuclear Data community to respond to those needs efficiently and in a co-ordinated way. This paper summarises the objectives, and the main achievements of ANDES and the preparation for CHANDA.

ANDES has developed new experimental methods, performed new measurements, validations and evaluations of cross-sections and other nuclear data. This paper summarises the objectives and the results in the middle of the ANDES project. CHANDA, started in December 2013, will combine similar types of activities with co-ordination and facilitation of the access of experimental teams to the existing European experimental facilities.

Introduction

Nuclear research within the Seventh Framework Programme (FP7 and FP7+2) of EURATOM has devoted a significant fraction of its efforts to the development of advanced nuclear fuel cycles and reactor concepts, mainly fast reactors, aiming to improve long-term sustainability by the reduction of the final wastes, optimal use of natural resources and improvement of safety in the present and future nuclear installations. The new design needs more accurate basic nuclear data for isotopes, like minor actinides, potentially playing an important role in the operation, fuel concept, safety or final wastes of those reactors and fuel cycles. Four projects, ANDES, ERINDA, EUFRAT and CHANDA, supported by EURATOM within FP7 and FP7+2, have gathered most of the European Nuclear Data community to respond to those needs efficiently and in a co-ordinated way. This paper summarises the objectives, and the main achievements of ANDES and the preparations for CHANDA.

Accurate and detailed simulation is a fundamental tool for the design of new nuclear reactors and fuel cycle facilities and for the optimisation of existing nuclear installations and of the fuel cycle as a whole. Simulations are used regularly to identify the limits for safe operation, optimise performance, interpret sensors data as diagnostic or description tools, and evaluate the limits of the validity of experimental demonstrations and other applications. Simulation codes and computing systems are able to describe with great detail the models of the individual phenomenology of process taken place in the nuclear system, inducing only moderate or small biases in the predictions. However, the uncertainties on the basic nuclear data induce uncertainties on the predictions of those codes. Clear needs to reduce these uncertainties had been identified in relation with the simulation of advanced fuel cycles and advanced reactors for improved nuclear sustainability, including waste transmutation. New needs already identified include new isotopes, energy ranges and phenomena. More recently, the Fukushima accident has focused nuclear R&D on safety, and in particular on improving the prediction capabilities for nuclear installations in accidental and beyond design conditions, rising extraordinary challenges to safety simulation systems, including also the basic nuclear data to be used. In addition, it will also be mandatory to be able to make a robust and complete determination of the global uncertainties of these simulations, and this will require a much better evaluation of the uncertainties of the basic nuclear data.

It is important to note that to prepare and maintain reliable nuclear data bases, all the steps of the nuclear cycle have to be correctly covered and improved, including: measurement, evaluation, validation and dissemination, not forgetting in each step to provide the reference value but also the data uncertainties and covariances.

Within the mentioned four EURATOM programmes, ERINDA and EUFRAT are mainly co-ordinating and facilitating the access of experimental teams to the existing experimental facilities for nuclear data measurements and validation. On the other hand, ANDES has developed new experimental methods, performed new measurements, validations and evaluations of cross-sections and other nuclear data. CHANDA, started in December 2013, will combine both activities.

ERINDA, European Research Infrastructures for Nuclear Data Applications, has provided a convenient platform to integrate all scientific efforts needed for high-quality nuclear data measurements in support of waste transmutation studies and design studies for Gen-IV systems. ERINDA has offered the nuclear data research infrastructures of 13 partners (HZDR, IRMM, CERN, CENBG, IPNO, UU-TSL, PTB, NPI, IKI, IFIN-HH, NPL, FRANZ and CEA) from all over Europe to experimental teams making new nuclear data measurements. ERINDA has also provided an efficient framework to support the facilities and the experimental groups, helping to select high-quality experiments and to direct them to the most suitable infrastructure.

EUFRAT, European Facility for Innovative Reactor and Transmutation Neutron Data, facilitates the access of outside users to the facilities of the Nuclear Physics unit at JRC-IRMM and promotes a coherent use of the measurement infrastructure in order to meet high-priority neutron data requests. EUFRAT focused measurements on the international neutron data needs for innovative nuclear systems, particularly to obtain new or more accurate neutron cross-section data for fission-reactor technology, fission-reactor and fuel-cycle safety, high burn-up fuels, nuclear-waste transmutation and innovative reactor systems.

ANDES

The ANDES FP7-EURATOM project addresses the nuclear data needs associated with the new reactors and new fuel cycles supported by the Sustainable Nuclear Energy Technological Platform, SNETP, in its strategic research agenda and in the European Sustainable Nuclear Industrial Initiative, ESNII, a proposal taking into account the priority lists for nuclear data from NEA/OECD, FP6-EURATOM projects EUROTRANS-NUDATRA and CANDIDE. The ANDES collaboration, which started its activities in May 2010, includes 20 research centres and universities.

ANDES combines a reduced group of selected differential measurements, the improvement in uncertainties and covariances within the evaluation process and the validation of present and new data libraries using integral experiments, to bring most critical nuclear data to the level of accuracies required by the new reactors and system promoted by ESNII and the SNETP. In addition, a specific work package is dedicated to improving the prediction capabilities of high-energy transport codes for the design of an accelerator-driven subcritical system, ADS, developing better models and performing a few selected measurements. All these activities are co-ordinated with the main actors for nuclear data dissemination such as the NEA and the IAEA.

For the measurements of low and medium energies for advanced reactor systems, a combination of the best world facilities is being used in ANDES, including IRMM neutron sources, both the e- linear and the Van de Graaff accelerators, the n_TOF spallation facility at CERN, the Jÿvaskÿla cyclotron and the IGISOL facility, the CNRS/Orsay accelerators and the GANIL accelerator complex. ANDES is focusing these measurements on:

- high-accuracy measurements of neutron inelastic scattering cross-sections of ^{238}U and isotopes of structural materials and inert fuel matrix;
- high-accuracy measurements of neutron total and capture cross-sections of ^{238}U and ^{241}Am;
- high-accuracy measurements of fission cross-sections several of which are Pu isotopes and minor actinides, including fission yields by surrogate neutrons and inverse kinematics;
- decay data measurements for reactor kinetics and decay heat of relevant fission fragments.

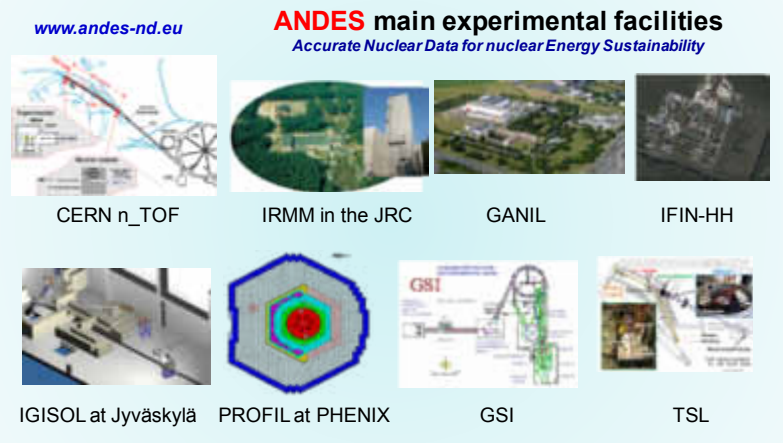
To improve and asses the absolute accuracy of the results from computer simulations, the ANDES collaboration decided to improve the existing tools for nuclear data evaluation with an estimation of the data uncertainties and correlations. A similar effort is being made to prepare simulation programmes to use covariance information. To demonstrate the performance of these tools, the covariance matrices of one major and one minor actinide are being evaluated.

Integral experiments provide very relevant information for the evaluation and validation of nuclear data. For these purposes, ANDES has selected data coming from the following facilities: MUSE, GUINEVERE, PROFIL, ZPPR10A, SNEAK-7A and -7B, and the collection of international criticality benchmarks. Each of these experiments provides specific complementary information.

To provide useful data for the ESNII ADS demonstration facility, the main objective for ANDES in the high energy range is model validation and optimisation in the 150-600 MeV energy field.

In parallel with these technical activities, ANDES is contributing to improving the knowledge and training of young professionals in nuclear science and technology by promoting PhD work within ANDES and organising a dedicated training school. Finally, to accelerate the dissemination of the new measured or evaluated nuclear data ANDES has established a close co-operation with the NEA and the IAEA, the two agencies co-ordinating the distribution of nuclear data.

Figure 1. Main ANDES experimental facilities



Progress of the ANDES Project

By now, ANDES has already made very important progress in the experiments measuring, with high accuracy, very relevant cross-sections of critical isotopes, whose analysis is now in progress or completed and many of which have been presented at international conferences. More than 20 contributions were presented at the recent ND2013 conference (Nuclear Data 2013) based or directly related to the ANDES project. Improvements have been made in the programmes developed for covariance and uncertainties management through the whole nuclear data cycle from measurement to analysis, evaluation and utilisation in standard codes for reactor and fuel cycles calculations. These tools are also being applied to analysing available integral experiments and the collaboration within ANDES is helping to acquire a fast convergence on the methods and tools used by different teams, particularly those using Monte Carlo simulations. Finally, new results on high energy measurements and the interpretation of the recent international benchmarks have allowed identifying some weak points in the high-energy models that are being corrected for their next releases.

In particular, the new measurements already performed within the ANDES project include new data of high accuracy for the cross-sections of inelastic scattering and capture in ^{238}U, capture in ^{241}Am, inelastic scattering in sodium and fission in ^{240,242}Pu(n,f), ^{243}Am(n,f) and ^{245}Cm(n,f). The experiments for ^{238}U and ^{241}Am capture have been performed in two different facilities to further reduce the systematic uncertainties and achieve even better accuracy.

Significant progress has also been achieved in the development of tools for covariance preparation and utilisation in reactor and fuel cycle calculations. One of the most relevant results has been the upgrade of the ACAB code, which is now able to use nearly all available sources of data, uncertainties or covariance information for the simulation and analysis of fuel cycles calculations. Also, the impressive progress on the GENEUS full Bayesian evaluation tool strongly enhances the robustness and mathematical correctness and self-consistency of the nuclear data evaluation, including covariance determinations. The code has also been extended to be able to handle most relevant isotopes (including actinides and structural materials) and most relevant reactions (including fission).

Within ANDES, significant efforts are devoted to precisely define, implement and validate a methodology that allows evaluating uncertainties, sensitivities and extracting feedback for the nuclear data from integral experiments using Monte Carlo simulations. This methodology complements the more standard tools based on deterministic codes. The first demonstrations of the different ANDES teams, for example using the ISCBEP data bank benchmarks and the total MC methods, are already showing the large potential value of the Monte Carlo methodology but also the associated requirements of computing power and storage space. A large number of simulations are being performed with different tools by several institutions both for the validation of the new tools using simple criticality benchmarks and for the evaluation of selected integral experiments.

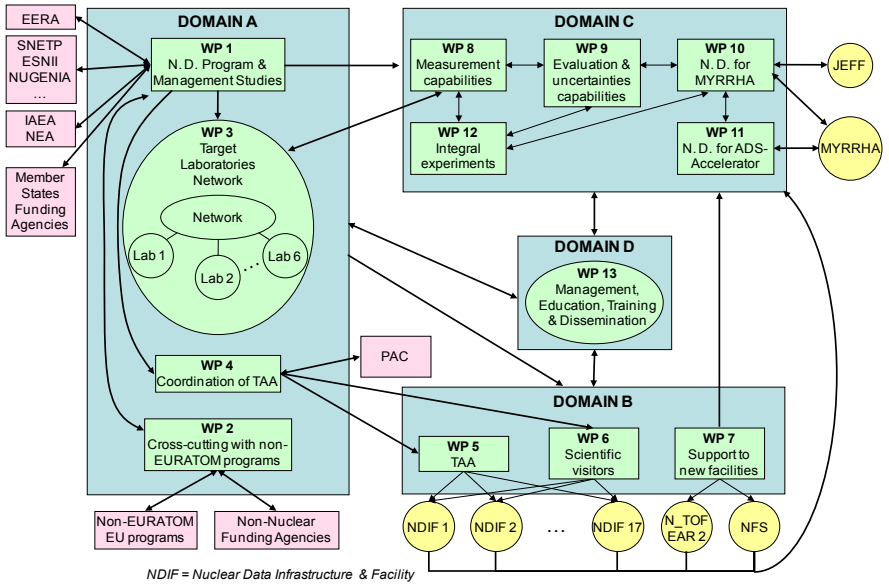
For the high-energy range, the modelling activities have achieved important progress by analysing the results from the international benchmark and using this information to identify components of the models to be improved. In fact, some of these improvements are already being implemented and tested and will be incorporated in future versions of the standard Monte Carlo neutronic simulation codes. The high-energy experiments have also progressed, with an early completion of the measurement of neutron-induced light ion cross-sections at 175 MeV on Fe, Bi and U. The MEGAPIE analysis which is being performed is helping to validate the high-energy models in a direct integral way.

CHANDA

The Fukushima accident has focused nuclear R&D on safety, and, in particular, on improving prediction capabilities for nuclear installations in accidental and beyond design conditions, setting extraordinary challenges to safety simulation systems, also including the basic nuclear data to be used. CHANDA, Solving Challenges in Nuclear Data for the Safety of European Nuclear Facilities, is a project, started in December 2013, will combine the efforts of 35 institutions and the types of activities of ANDES, ERINDA and EUFRAT to develop the capabilities that should allow solving those challenges and to prepare a sustainable framework to maintain those capabilities.

The project is organised in 13 work packages integrating all aspects of the nuclear data preparation and validation cycle, but also co-ordinating with other international players in the field and preparing a structure for the nuclear data R&D co-ordination that can become sustainable for the development of long research programmes. Figure 2 presents the scheme of the CHANDA activities and its work packages.

Figure 2. CHANDA: Activities and connections to other organisations



The CHANDA proposed activities include:

- global co-ordination of nuclear data programmes and capabilities;
- co-ordination of cross-cutting activities with programmes beyond EURATOM in Horizon 2020;
- co-ordination of actions for the development of a network for nuclear target preparation and characterisation;
- calls for proposals of transnational access to the consortium facilities and their evaluation;
- support of experiments at consortium facilities, and scientific support of experiments;
- support of Neutrons For Science and the short path n_TOF experimental area equipment;
- development and validation of new measurement capabilities and methodologies;
- development and validation of new nuclear data evaluation and application capabilities;
- development of nuclear data for Myrrha reactor safety analyses;
- development of a methodology for uncertainty assessment and minimisation in ADS target and accelerator safety analyses;
- development and validation of new integral experiments;
- management, education and training.

A special mention is due to the support of the development of the Neutrons For Science, NFS, and the short path n_TOF experimental area, which will provide the complementarity of one of the most intense neutron sources for average flux (NFS) with one of the most intense sources for instantaneous flux (n_TOF short path). The combination of these high intensity sources, with improved sample preparation capabilities, improved detection systems, improved evaluation and dissemination tools

to be developed within CHANDA will allow remodelling the limits of possible measurements and the size of the smaller samples that can be analysed to solve some of the remaining nuclear data challenges for the safe operation of present reactors and the development of more sustainable ones.

Accelerator-driven system design concept for disposing of spent nuclear fuels

Yousry Gohar, Yan Cao, Roger Kellogg, Elia Merzari
Nuclear Engineering Division, Argonne National Laboratory, US

Abstract

The growth of the nuclear energy production, as a carbon free energy source, is tied to the problem of disposing the current spent nuclear fuel (SNF) inventories and closing the future nuclear fuel cycles. The USA SNF is expected to reach ~70,000 metric tonnes by 2015 from the present operating nuclear plants. A significant increase in this inventory is forecasted from the planned increase in the deployment of new nuclear power plants. The transuranics content of the 2015 US SNF inventory is ~700 MT, which has about ~115 MT of minor actinides (MA). These transuranics are responsible for a significant fraction of the SNF radiotoxicity. Accelerator-driven systems utilising proton accelerators with neutron spallation targets and subcritical blankets can be utilised for transmuting these transuranics, simultaneously generating carbon free energy, and significantly reducing the capacity of the required geological repository storage facility for the spent nuclear fuels. The required number of these systems is a function of the accelerator power, the system operating life time and system availability, and the blanket fuel composition.

The proposed system is intended to: a) transmute/fission the MA, which eliminates the long-term radiotoxicity of the US SNF, b) generates carbon free energy, and c) significantly reduces the geological repository storage requirements per metric tonne of the SNF. A fraction of the SNF plutonium will be used with the SNF MA to reduce the disposition cost and to accelerate the disposition time. The other fraction of the SNF plutonium can be used as a MOX fuel in the current/future thermal power reactors and a starting fuel for future fast power reactors. The uranium of the spent nuclear fuel can be recycled for use in future nuclear power plants. The short-term fission products decay to reach the radiotoxicity level of the natural uranium ore in ~300 years.

This paper shows that only four to five accelerator-driven systems operating for <33 full power years can dispose of the US SNF inventory expected by 2015. Each system consists of a proton accelerator with a neutron spallation target and a subcritical assembly. The accelerator beam parameters are 1 GeV protons and ~25 MW beam power, which produce ~3 GW_t in the subcritical assembly. This paper presents the design concept and the system analyses.

Introduction

The disposal of the US spent nuclear fuel (SNF) inventory using accelerator-driven systems (ADS) is examined. The ADS technical assessment [1] confirmed the potential of this approach. In this study, several requirements are adopted to minimise the required R&D, the infrastructure, and the total cost. The requirements are to: a) avoid multi-processing steps for the spent nuclear fuel, b) avoid long-term technological developments such as new nuclear fuel materials or designs, c) minimise the required number of units for disposing the US spent nuclear inventory, and d) use the current technologies with minimum extrapolation as much as possible.

At present, the US SNF is growing by ~2,000 metric tonnes per year from the current operating nuclear power plants to reach about 70,000 metric tonnes by 2015. This SNF inventory contains ~1% transuranics (~700 MT), which has about ~115 MT of minor actinides (MA). The proposed system is intended to: a) transmute/fission the MA, which eliminates the long-term radiotoxicity of the SNF, b) generates carbon free energy, and c) significantly reduces the geological repository storage requirements per metric tonne of the SNF. A fraction of the SNF plutonium will be used with the SNF MA to reduce the disposition cost and to accelerate the disposition time. The other fraction of the SNF plutonium can be used as a MOX fuel in the current/future thermal power reactors and a starting fuel for future fast power reactors. The uranium of the spent nuclear fuel can be recycled for use in future nuclear power plants. The short-term fission products decay to reach the radiotoxicity level of the natural uranium ore in ~300 years.

This paper presents that only four accelerator-driven systems operating for <33 full power years can dispose of the US SNF inventory [2] expected by 2015. Each system consists of a proton accelerator with a neutron spallation target and a subcritical assembly. The accelerator beam parameters are 1 GeV protons and ~25 MW beam power, which produce 3 GW_t in the subcritical assembly. This paper highlights the concept and the system analyses.

Accelerator-driven system

The system has a CW proton accelerator beam to generate a continuous neutron source for driving the subcritical assembly. The analysis shows that the required proton beam power for the 3 GW_t subcritical system with K_{eff} of 0.98 is 25 MW from 1 GeV protons. Figure 1 shows the beam power requirements as a function of the proton energy with lead-bismuth eutectic target for 3-GW_{th} system. The parameters are almost optimum for such a system. Increasing the proton energy above 1 GeV has a small impact on the required beam power but it has a negative impact on the target and the subcritical assembly designs. As the proton energy increases, the target length, and the subcritical assembly height increase. Such changes increase the neutron leakage, which increase the required proton beam power. In addition, the required shielding thickness increases as the proton energy increases to attenuate the high-energy neutrons.

Liquid metal target [3] is selected because it has several design advantages: a) liquid material does not suffer from radiation damage or thermal stresses, b) physical properties of the liquid material do not change during operation, c) heat removal is much easier and efficient, d) liquid target has simple mechanical design, which improves its performance, including the neutron yield per proton, and e) liquid target relaxes the accelerator reliability design requirements. The target assembly is located at the centre of the subcritical assembly to maximise the utilisation of the spallation neutrons. Figure 2 shows the liquid metal (lead or lead-bismuth eutectic) target design configuration. The target assembly is located at the centre of the subcritical assembly to maximise the utilisation of the spallation neutrons. Because of the high power density in the target material, the target has its coolant loop, which is independent of the subcritical assembly coolant loop.

Subcritical assemblies with solid fuel materials have been considered in the past in order to utilise the gained experience from the operating fission power reactors. However, this choice requires the development of new fuel designs with transuranic materials. A long and expensive R&D programme is required to develop such a fuel form and its fabrication process, to carry out fuel irradiation experiments, and to perform post-irradiation examination of the fuel materials. In addition, the fuel irradiation and testing require a fast irradiation facility, which is not available in the United States at this time. Numerous fuel reprocessing cycles will be needed to extract the unutilised transuranics from the solid spent nuclear. These processing plants do not exist in the US. In addition to the cost, the use of the solid fuel forms will result in much longer time to dispose of the minor actinides. These issues have led to the consideration of mobile fuel.

Mobile fuel forms with transuranic materials without uranium are considered in this work to avoid the issues of the solid fuel forms and to eliminate the minor actinides and the long-lived fission products of the spent nuclear fuels. Liquid metal (liquid lead or lead-bismuth eutectic) is the fuel carrier material. Transuranics are mixed or micro-particles suspended in the fuel carrier material. The use of the mobile fuel concept results in a closed material cycle, which reduces the proliferation risk. The liquid carrier has the fission products mixed with the transuranics all the time. A significant fraction of the long-lived fission products, from the SNF and the MA disposal, are transmuted during the power generation process without extra steps. The continuous feed of the transuranics/long-lived fission products during the operation reduces the radioactive waste and the required geological storage capacity.

In addition, the use of mobile fuel forms: a) eliminate the minor actinides without the need for extra fuel processing steps, b) relax some of the reliability requirements for the accelerators, c) remove fission gases during operation, d) reduce the required R&D to qualify the fuel, the deployment time, and the total cost, e) maintain a fast neutron spectrum, which results in efficient neutron utilisation, good neutron economy in the presence of fission products, and lower probabilities for generating higher actinides, f) achieve the transuranics elimination objective, and g) permit controlling the output power by adjusting the fuel material concentration in the fuel carrier without changing the proton beam power. A thermal-hydraulics performance confirmation for the selected carrier with the selected fuel material form is required. This confirmation can be carried out in the laboratory without the need for a neutron source or an irradiation experiment.

Subcritical assembly parameters and performance

The fuel carrier chemistry defines the upper limit of the transuranic concentration as a function of the operating temperature. In defining the system parameters, a transuranics concentration range was considered but the upper value is lower than the chemistry limit. The system is designed for an effective neutron multiplication factor (K_{eff}) of 0.98, which provides adequate operational safety margin. In order to reach this neutron multiplication factor, a small fraction of the SNF plutonium is mixed with the minor actinides. Different transuranics concentrations are considered with different plutonium fractions to achieve a K_{eff} of 0.98. Figure 3 shows K_{eff} and the ADS power from 25 MW/1GeV proton beam and 7% actinides concentration in the lead-bismuth eutectic as a function of the plutonium concentration. Table 1 summarises the obtained subcritical assembly parameters.

Detailed burn-up analyses for the subcritical assembly were performed using MCB5 computer programme [4] with ENDF/B-VII nuclear data. In the analyses, the composition of the mobile fuel carrier is adjusted every three months, four times per year, to adjust the neutron multiplication to the original value of 0.98. Of course, the time interval of the three months can be changed to continuous feed or any time interval as needed to maintain constant output power and neutron multiplication values within a specific range. The transuranics consumption rate is 1.2 metric tonne per full power year. Figure 4

shows the sample of the results for lead-bismuth eutectic fuel carrier with 5% actinides (35.7% plutonium concentration), 7% actinides (27.2% plutonium concentration), and 10% actinides (20% plutonium concentration) during 10 years of operation. The corresponding long-lived fission product transmutation is shown in Figure 5.

Figure 1. Lead-bismuth target design configuration

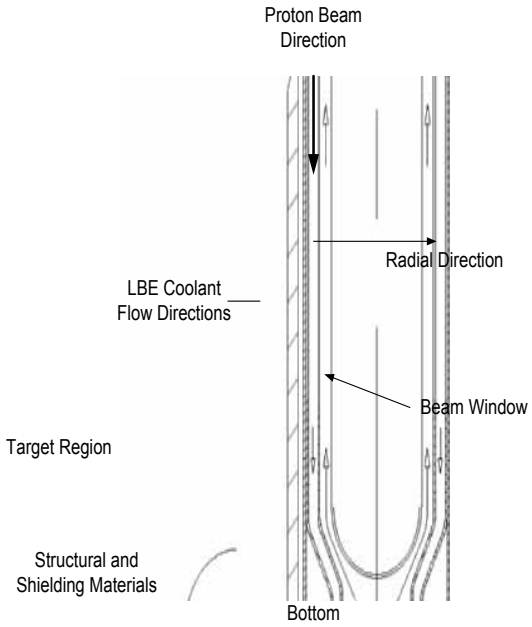


Figure 2. Beam power requirements as a function of the proton energy with lead-bismuth eutectic target for 3 GW_{th} system

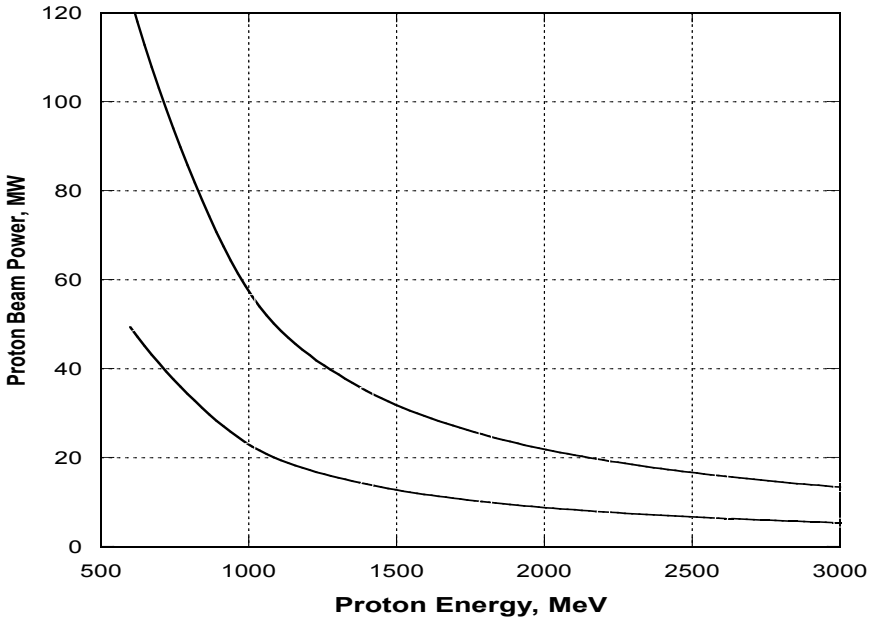


Figure 3. K_{eff} and ADS power from 25 MW/1GeV proton beam and 7% actinides concentration in the lead-bismuth eutectic as a function of the plutonium concentration

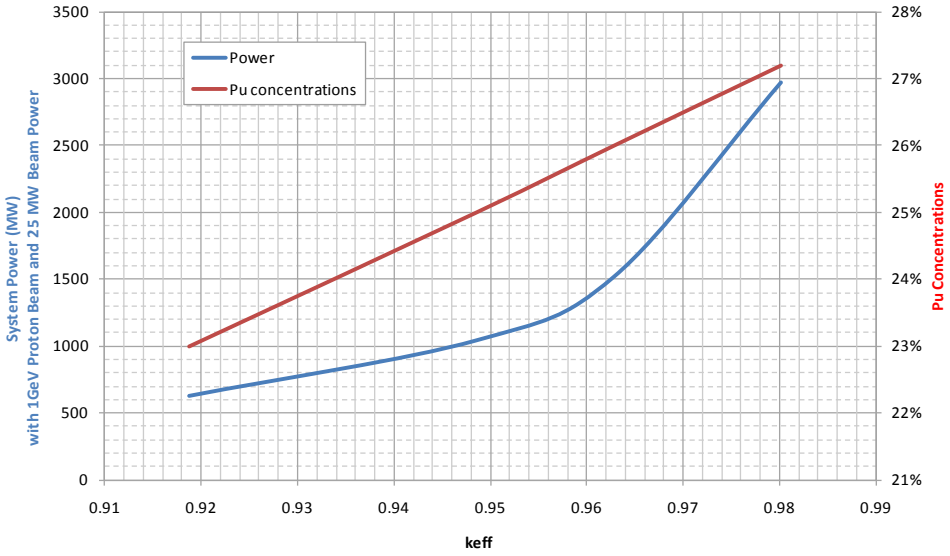


Figure 4. K_{eff} at each fuel burn-up time step for the ADS system with 5% (35.7% Pu), 7% (27.2% Pu) or 10% (20% Pu) actinides concentration in the lead-bismuth eutectic

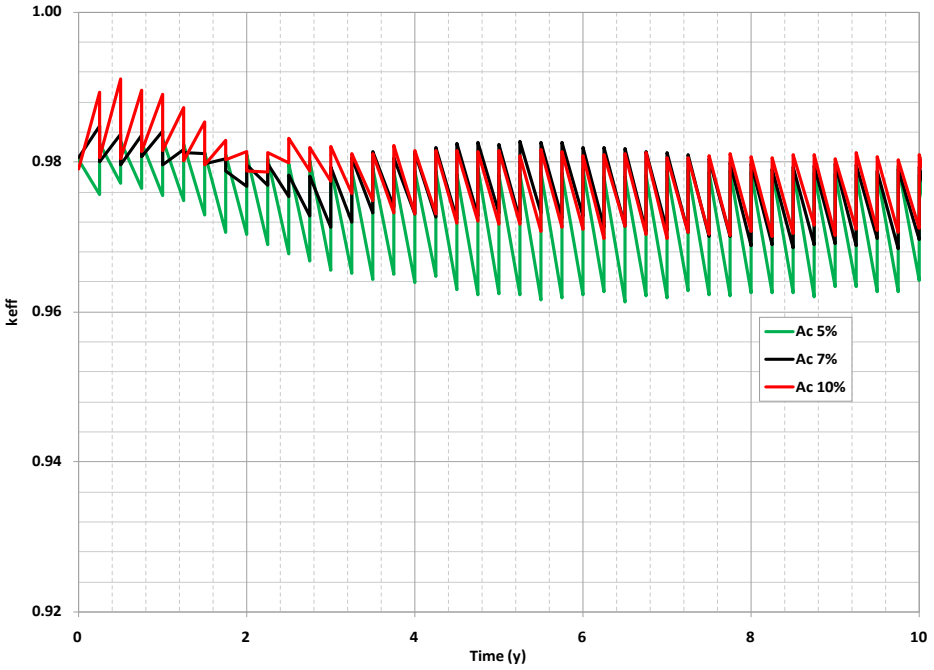


Figure 5. Long-lived fission product transmutation during the first 10 years of ADS operation with 7% actinides (27.2% Pu) in the lead-bismuth eutectic

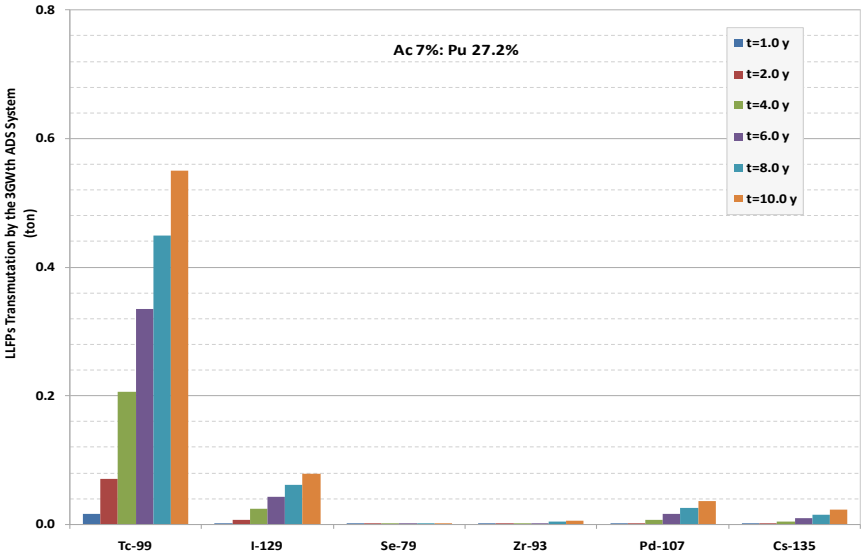


Table 1. Subcritical assembly parameters

Target	
Proton beam parameters	25 MW/1 GeV
Target material	Liquid Pb or Pb-Bi eutectic
Proton beam radius	19.5 cm
Target length	70 cm
Target radius including manifolds	35 cm
Subcritical assembly	
Outer radius	150 cm
Height	300 cm
Fuel carrier/coolant	Pb or Pb-Bi Eutectic
Transuranic concentrations	5 to 10%
Plutonium concentration for the three transuranic concentrations	36 to 20%

Conclusion

This paper proposes an approach to dispose of the 70,000 metric tonnes of the expected US spent nuclear inventory expected by the year 2015. It is based on the use of four to five accelerator-driven subcritical systems. Each has an output thermal power of 3 GW, operates for <33 full power years with an effective neutron multiplication factor of 0.98, and uses a 25 MW beam with 1 GeV protons. A mobile fuel carrier concept for the transuranics is adopted for the subcritical assembly.

According to the MCB5 burn-up simulations, the subcritical assembly with different actinide concentrations consumes about 1.2 metric tonnes of transuranic per year. For the 7% actinide concentration in the liquid metal fuel carrier, the four ADS will consume the minor actinides of the 70,000 metric tonnes in less than 33 full power years and burn about 35 metric tonnes of the spent nuclear fuel plutonium. In addition, a significant fraction of the long-lived fission products will be transmuted at the same time.

Acknowledgements

Argonne National Laboratory's work was supported (or funded) by the U.S. DOE, Office of Science, under Contract No. DE-AC02-06CH11357.

References

[1] Aït Abderrahim, H., Galambos, J., Gohar, Y., Henderson, S., Lawrence, G., McManamy, T., Mueller, A.C., Nagaitsev, S., Nolen, J., Pitcher, E., Rimmer, R., Sheffield, R., Todosow, M. "Accelerator and Target Technology for Accelerator Driven Transmutation and Energy Production", www.science.doe.gov/hep/files/pdfs/ADSWhitePaperFinal.pdf.

[2] DOE Office of Civilian Radioactive Waste Management (1999), "Draft Environmental Impact Statement for a Geologic Repository – Appendix A: Inventory and Characteristics of Spent Nuclear Fuel, High-Level Radioactive Waste, and Other Materials", ODE/EIS-0250D.

[3] Gohar, Y., Finck, P.J., Krajtl, L., Herceg, J.E., Pointer, W.D., Saiveau, J., Sofu, T., Hanson, A.L., Todosow, M., Koploy, M., Jijatovic, P. (2002), "Lead-Bismuth Target Design for the Subcritical Multiplier (SCM) of the Accelerator Driven Test Facility (ADTF)", ANL/TD/02-01, Argonne National Laboratory, US.

[4] Cetnar, J., Gudowski, W., Wallenius, J. "User Manual for Monte-Carlo Continuous Energy Burnup (MCB) Code – Version 1C".

A high-power ADS concept

Nicolas Thiolliere, Baptiste Mouginot, Arnaud Cadiou, Fanny Courtin, Amélie Pector
Subatech, EMN-IN2P3/CNRS-Université, Nantes, France

Abstract

Minor actinide transmutation induced by subcritical reactors is limited by the thermal power of ADS. Transmutation scenarios involving the French nuclear fleet have led to a high number of ADS and large inventories of minor actinides in the nuclear cycle. Increasing the specific and the thermal power by ADS may recover the weaknesses mentioned above. This paper presents a high-power ADS theoretical concept, up to 2 GW_{th}, based on an annular spallation target irradiated by a rotating proton beam. Liquid lead-bismuth coolant circulates in the core and composes the spallation target, too. The subcritical core is divided into an inner core, in which the spatial energy deposition is uniform, and an outer core. A detailed neutronics and thermal-hydraulics study has been performed with the code MURE (MCNP Utility for Reactor Evolution) based on the Monte-Carlo transport codes MCNP or MCNPX. The composition at the beginning of the cycle is a mixture of plutonium and minor actinide oxide coming from a PWR (pressurised water reactor) filled with MOX fuel. ADS initial reactivity is adjusted with an MgO inert matrix which also improves the fuel thermal conductivity. High-power ADS static parameters at the beginning of the cycle such as spatial energy deposition or pin temperature profile are precisely calculated. A complete core and assembly evolution during an irradiation cycle has been performed and provides masses balance.

Introduction and motivations

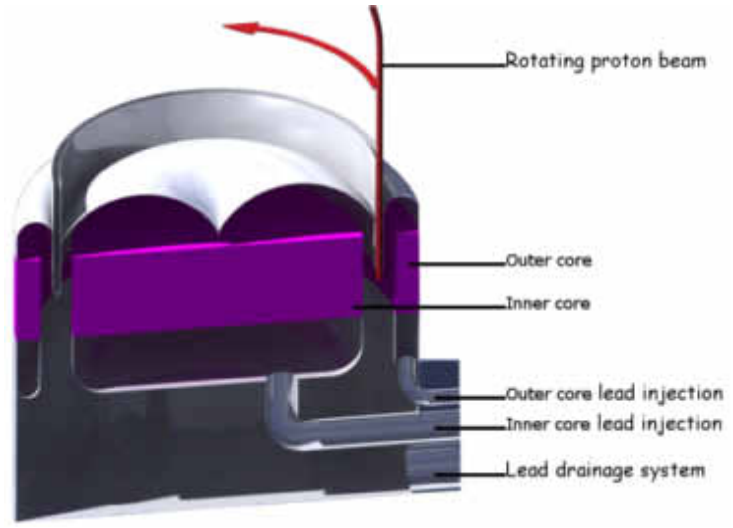
MA (minor actinide) transmutation induced by subcritical reactors is limited by the thermal power of ADS. The European industrial scale reference concept is the EFIT (European Facility for Industrial Transmutation) [1], characterised by a 384 MW thermal power. Scenarios involving the EFIT concept dedicated to the minor actinide transmutation generated by the French nuclear fleet have led to a high number of ADS and large inventories of minor actinides in the nuclear cycle [2].

A standard ADS is composed by three elementary components: a high energy and intensity proton beam, a spallation target and a subcritical core. The neutron flux induced by a spallation target in a homogeneous medium decreases rapidly with the target radial distance. This leads to a subcritical core size and thermal power limitation. Among different techniques to expand the core size and the thermal power, we could mention the following points:

- setting several fissile enrichment zones to compensate the neutron flux decrease;
- disposing several spallation targets in the subcritical core;
- considering an annular spallation inside an inner and outer subcritical core.

A three-target concept has been studied in a previous work [3] at Subatech laboratory. The neutron radial distribution in such a system was not fully optimised, which made the concept difficult to simulate. This work presents a concept based on an annular spallation target irradiated by a rotating proton beam. The BLAST (Burner concept with Liquid Annular Spallation Target) concept is currently being developed to investigate the capacity of the ADS thermal power to increase up to 2 GW_{th}. The subcritical core is designed using neutronics and thermal-hydraulics calculations performed by the MURE [4] software (MCNP Utility for Reactor Evolution) developed by the CNRS.

Figure 1. BLAST concept schematic view



The reference concept is a liquid lead cooled reactor with an annular spallation target disposed inside a subcritical core divided into two cores. The fuel is composed of a mixture of plutonium and minor actinide oxide diluted with an MgO inert matrix. There are numerous benefits to having an annular spallation target producing the neutron flux. On the one hand, a flattened power density distribution can be obtained in the inner core and on the other hand, the cylindrical symmetry highly simplifies simulations.

The BLAST concept principle

Figure 2 shows the current concept geometry. A high frequency rotating magnetic field deflects a 1 GeV proton beam and generates a cylindrical beam. The annular proton beam is guided to the spallation target window. The core is cooled with liquid lead that circulates in three channels. Two channels are dedicated to the inner and the outer core cooling systems. The third channel fills the proton beam interaction zone that constitutes the spallation target with liquid lead.

Table 1. HN (Heavy Nucleus) isotopic vector at the beginning of the cycle

	Isotope	Fraction (%)
Pu molar fraction		27
M.A. molar fraction		73
Pu vector	^{238}Pu	4.8
	^{239}Pu	40.2
	^{240}Pu	27.1
	^{241}Pu	14.4
	^{242}Pu	13.6
M.A. vector	^{237}Np	3.7
	^{241}Am	44.8
	^{243}Am	30.2
	^{244}Cm	17.7
	^{245}Cm	3.6

Assembly geometry is based on a 1200 MW lead pool-type fast reactor design [5]. An 11×11 square array of pin lattice fills the assembly, including 7 positions dedicated to the structural support rods. The assembly side length is 15.2 cm. Assemblies have metallic sidewalls so that the coolant circulates axially. The pin is a 7.9 mm diameter disk with a 2 mm middle hole filled with helium to enable thermal expansion. The fuel is composed of a mixture of heavy nuclides dioxide fuel and MgO inert matrix. The pin cladding is a 9.6 mm diameter cylinder made of T15-15 stainless steel. The height of the subcritical core has been set to 110 cm.

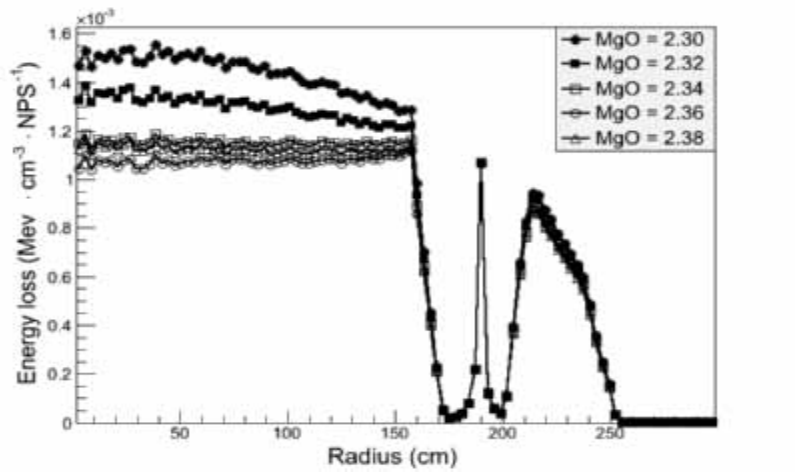
The inner core radius is optimised to obtain a constant spatial deposited power. The distribution inside the core depends mainly on the k_{eff} value. Two configurations have been tested with k_{eff}=0.95 and k_{eff}=0.97. A homogeneous core has been simulated with MCNPX in order to easily change inner core radius R_i. Spatial deposited power is then calculated for wide-ranging radiuses. Plane spatial energy loss is found for a 160 cm and a 120 cm radius, respectively in the core at k_{eff}=0.97 and 0.95. Throughout this document, the focus is on the k_{eff} = 0.97 configuration for which 373 and 236 assemblies, respectively, filled the inner and the outer core. The outer core consists of two assembly rows to prevent the sharp neutron flux from decreasing with the spallation target radial distance.

The heavy nuclide composition at BOC (Beginning of Cycle) is very important regarding the neutronic parameters. The isotopic vector is calculated from a scenario that takes into account an electrogen stratum filled with MOX fuel [6]. Plutonium and MA vectors from the spent MOX compose the ADS heavy nuclides vector at BOC. This fuel is cooled five years after a burn-up of 56 GWd/tonne. The minor actinide molar fraction is estimated to have a constant reactivity as long as possible with a neutron flux close to $4 \bullet 10^{15} cm^{-2} \bullet s^{-1}$. The MgO amount is adjusted to reach k_{eff} = 0.97. Table 1 provides the isotopic vectors at BOC for the considered scenario.

Simulation results

The BLAST concept has been designed with the Monte-Carlo codes MCNP5 [7] and MCNPX2.7.0 [8]. The latter is used every time spallation reaction simulation is needed. MCNP(X) geometry, thermal-hydraulic/neutronic coupling calculations and evolution under irradiation have been performed with the code MURE.

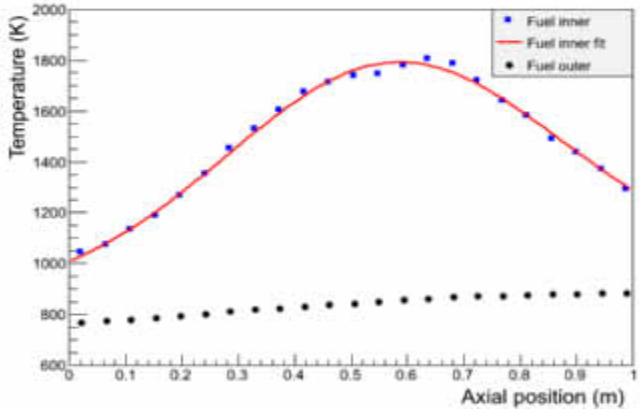
Figure 2. Energy deposition according to the radial distance



A three-dimension cylindrical mesh has been defined in order to calculate energy loss spatial distribution DE (r,θ,z) in the ADS. The radial distance r to the z-axis is divided into 100 bins. The angle θ relative to a rotation about the z-axis is integrated into the whole space as the z-axis itself. Figure 2 presents the energy loss according to r for k_{eff} ~ 0.97 configuration. A small variation on the MgO amount around the reference value (i.e. N_{MgO} = 2.32), thus k_{eff} value, has been imposed. The inner core energy loss distribution, between r=0 and r=160 cm, is uniform for a number of MgO equal to 2.34 (k_{eff}=0.97067±0.00176), 2.36 (k_{eff}=0.96682±0.00157) and 2.38 (k_{eff}=0.96629±0.00168). Around r=190 cm, the spallation target contribution appears. For r higher than 200 cm, the outer core energy loss is low and suggests that the MgO concentration can be adjusted in this part of the core.

A MURE class named BATH [9] (Basic approach of Thermal Hydraulics) manages temperature calculation with a 2D RZ precision from heat and mass transfer equation resolution. Temperature profiles in the liquid lead, the cladding and the fuel pin have been extracted according to the pin thermal power. The liquid lead speed has been set to 2 $m \bullet s^{-1}$ and the entrance temperature in the core is 703 K. The highest temperature allowed in the pin is 1800 K [10] and is reached for a pin thermal power P_{PinMax} = 36 kW. Figure 3 presents the pin temperature profile. The hot spot temperature is obtained by fitting the data set close to 1790 K under the highest allowed temperature.

Figure 3. Fuel inner and outer temperature profile according to Z-axis at 36 kW/pin



A MCNPX calculation provides the energy loss E_i (in eV) in the inner core by one incident proton in all the fuel pins. The inner core spatial distribution of the deposited energy is constant. If N_p is the number of fuel pins that fill the inner core, the proton beam intensity that leads to the maximum allowed pin thermal power is thus given by:

$$I_{max} = \frac{N_p \cdot P_{PinMax}}{E_i}$$

Simulation results lead to the maximum intensity, I_{max} = (138 ± 3) mA, keeping the fuel maximum temperature lower than 1800 K. Uncertainty comes from MCNP statistical error.

From the maximum intensity and the total energy loss in the inner and outer core per incident proton, the relation between the beam intensity (in mA) and the thermal power (in MW) is:

$$P_{th} \simeq 16.4 \cdot I$$

The maximum thermal power for this ADS configuration is close to 2.3 GW_{th}. The inner core represents 72% of the total thermal power. It should be noted that thermal power is clearly limited by the intensity supplied by the beam.

Void coefficient has been calculated for two cases. A 10% variation imposed on the coolant density leads to the positive void coefficient α_t ~1200 pcm/(g•cm^{-3}). The coefficient calculated from the normal condition and the complete loss of coolant leads to a negative void coefficient α_t ~ –1700 pcm/(g•cm^{-3}). Statistical uncertainty provided by MCNP leads to negligible void coefficient error. This calculation related to ADS safety as well as other safety calculations will be performed in the near future. Also, more complete studies should be carried out to prove technical feasibility.

Evolution under irradiation

ADS k_{eff} and inventory evolution have been calculated using the code MURE during an irradiation time set to 5 years. Figure 4 represents the multiplication factor evolution for different ratios between the amounts of minor actinides and plutonium. The k_{eff} value for 72% and 73% of MA simulations ranges between 0.965 and 0.975 with respect to subcriticality behaviour until 4 irradiation years. To understand the k_{eff} evolution, a complete neutron balance has been calculated at each evolution step according to the following formula:

$$G_i = N_i \int \left(\sigma_{fi}(E)\nu_i(E) + 2\sigma_{ni}(E)\right)\phi(E)dE - N_i \int \sigma_{ai}(E)\phi(E)dE$$

G_i represents the neutron balance for the nuclide i, as the difference between neutron creation by fission or (n,2n) reaction (represented by their cross-sections σ_{fi} and σ_{ni}) and absorption (represented by the cross-section σ_{ai}) by fission, capture or (n,2n). N_i is the nuclide i amount; ν the number of neutrons emitted by fission and ϕ is the neutron flux.

Figure 4. Core k_{eff} evolution for MA and heavy nuclides ratios from 70% to 74%

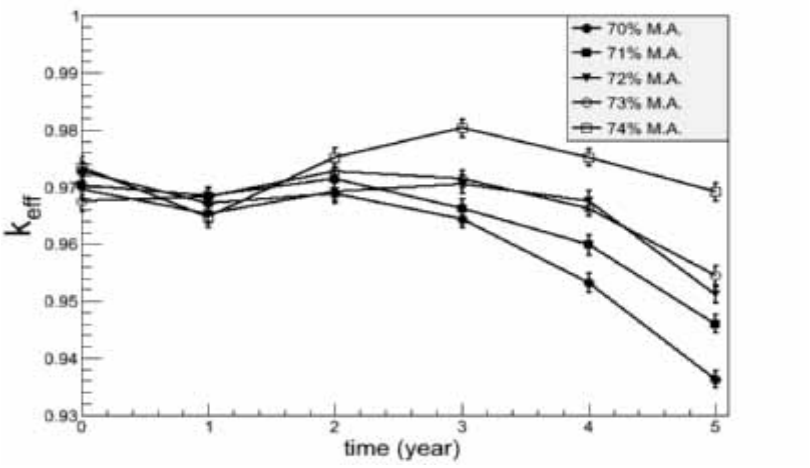
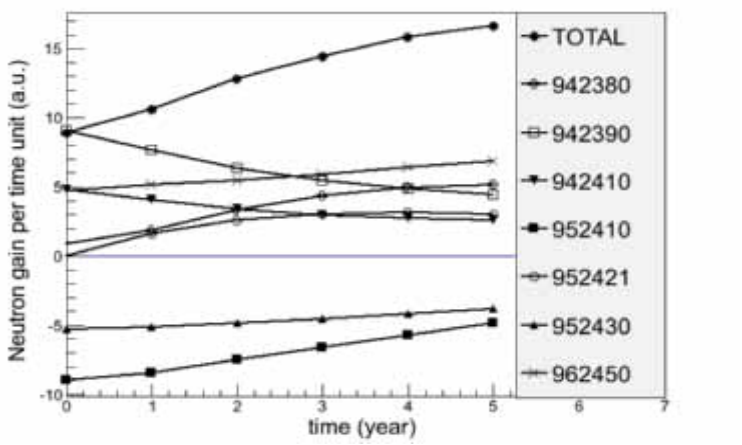


Figure 5 shows the main contributors to the neutron balance among heavy nuclides for the simulation performed with 73% of MA. The neutron absorption due to fission product generation during irradiation is compensated by the total neutron gain increase. Except for ^{239}Pu and ^{241}Pu, individual isotopic neutron balance evolution increases. The consequence of this fact is that reactivity is maintained during irradiation. ^{241}Am and ^{243}Am have a negative neutron balance, which explains their fertile behaviour. Nevertheless, its consumption contributes to increasing total neutron balance. ^{238}Pu production is the main contributor to the neutron gain increase. ^{242m}Am and ^{245}Cm production under irradiation also contribute significantly to the increase in reactivity.

Figure 6 shows the minor actinide and plutonium mass one-cycle evolution in the whole core.

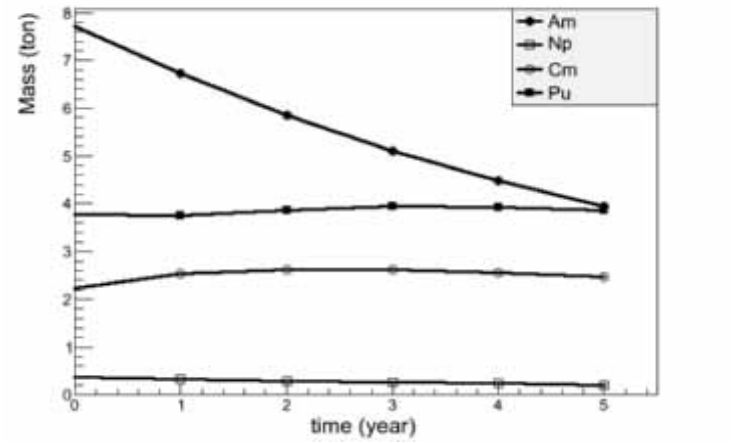
Americium is highly transmuted since 3.8 tonnes are consumed during the five irradiation years. This corresponds to 754 kg/year and means that 49% of the initial mass has been transmuted. ^{241}Am and ^{243}Am have a similar behaviour. Neptunium evolution is fully represented by ^{237}Np isotope and behaves like americium while 44% of the initial mass has been transmuted. Curium is created mainly from neutronic capture on americium, while 12% of the initial mass is generated during the irradiation. The most important isotope contribution is the ^{244}Cm and its mass balance is close to equilibrium. ^{242}Cm increases strongly but its 163-day half-life means it will decay significantly during the cooling time following irradiation. Plutonium is close to equilibrium since only 2.4% of the initial mass is generated. ^{238}Pu is the main increase contributor while other even isotopes ^{240}Pu and ^{242}Pu also increase weakly. ^{239}Pu and ^{241}Pu decrease by fission or neutronic capture. To summarise, plutonium irradiation in the ADS fast neutron flux leads to a change in the isotopic vector by converting odd to even isotopes. The full core evolution mass balance during a five-year evolution indicates that such an ADS can transmute around 730 kg/year with an initial minor actinide mass close to 10 tonnes. This transmutation efficiency could be improved by increasing the neutron flux into the outer core with an MgO amount modification.

Figure 5. Neutron gain per arbitrary time unit evolution for main contributors



The notation ZZAAAI references isotopes. The balance has been calculated in the inner core only.

Figure 6. Minor actinide and plutonium one-cycle mass evolution in an assembly



Conclusion

Increasing subcritical systems' thermal power is an important issue in improving ADS transmutation capacity. Subatech laboratory is involved in the high-thermal power ADS concept design by numerical simulations since 2009. A key issue is to design a concept with a radial power distribution constant in a significant part of the core. A 1.5 GW_{th} three-spallation target concept was studied in this framework between 2009 and 2012. The neutron flux remains significantly higher close to the spallation targets.

An inner lead cooled subcritical core surrounded by an annular liquid lead spallation target composes the new ADS concept design. A high frequency rotating magnetic field generates an annular proton beam, which limits the spallation target window deposited power. An outer core disposed outside the target benefits from a lower neutron flux. Calculations showed that radial deposited power is uniform inside the inner core for a radius close to 160 cm and a k_{eff} ~ 0.97. The maximum thermal power leading to an acceptable fuel temperature is around 2.3 GW_{th}. The relation between the intensity I in mA and the thermal power P_{th} in MW is given by P_{th} ~ 16.4 I. The thermal power relation with intensity shows that such an ADS concept is limited by the proton beam capacity. In these scenario studies, a hypothesis can be made on proton beam intensity and the

concept thermal power can be deduced from the relation defined above. It can be concluded that a stable 1 GeV proton beam with an intensity greater than 100 mA will not be available for several decades.

Reactivity evolution depends on the ratio between the amounts of minor actinides and plutonium. The reactivity of a fuel in which the minor actinides represent around 73% of the heavy nuclides' total number varies slightly over 4 irradiation years. Minor actinides have, in this case, a fertile behaviour that compensates absorption due to the fission product generation. Mass balance has been calculated in the designed high-power ADS concept and shows that 730 kg/year is transmuted with initial minor actinide mass close to 10 tonnes. Adjusting the MgO amount can create a neutron flux increase inside the outer core. In this case, the transmutation efficiency would improve.

This work is a small step towards a high-power ADS theoretical concept. It is necessary to perform additional calculations. Safety aspects, such as dpa on structure, or corrosion by lead during prolonged irradiation cycles will have to be assessed. Also, more complete studies should be carried out to prove technical feasibility.

References

[1] De Bruyn, D., Larmignat, S., Hune, A.W., Mansani, L., Rimpault, G., Artioli, C. (2010), "Accelerator Driven Systems for Transmutation: Main Design Achievements of the XT-ADS and EFIT Systems within the FP6 IP-EUROTRANS Integrated Project", *International Congress on Advances in Nuclear Power Plants (ICAPP'10)*, San Diego (California, US), paper (Vol. 10112, pp. 1808-1816).

[2] Direction de l'Energie Nucléaire, CEA (2012), "Bilan des recherches conduites sur la séparation-transmutation des éléments radioactifs à vie longue et sur le développement de réacteurs nucléaires de nouvelle génération", Tome 2 Séparation-transmutation des éléments radioactifs à vie longue.

[3] Clavel, J.B. (2012), "Étude de systèmes et scénarios électronucléaires double strate de transmutation des actinides mineurs en ADS", PhD thesis, Ecole des Mines de Nantes, France.

[4] Meplan, O. et al. (2009), "MURE, MCNP Utility for Reactor Evolution : couples Monte Carlo transport with fuel burnup calculations", *Computer Program Services of OECD/NEA*.

[5] Adamov, E.,* Orlov, V., Filin, A. et al. (1997), "The next generation of fast reactors", *Nuclear Engineering and Design* 173 (1997) 143-150.

[6] OECD/NEA (2007), "Management of Recyclable Fissile and Fertile Materials", NEA #6107 (ISBN: 9789264032552).

[7] Briesmeister, J.F. (2000), "MCNP - A General Monte Carlo N-Particle Transport Code", version 4C, Los Alamos National Laboratory, US.

[8] Pelowitz, D.B. (2005), MCNPX user's manual, version 2.5.0.

[9] Capellan Nicolas, et al. (2009), "3D coupling of Monte Carlo neutronics and thermal-hydraulics calculations as a simulation tool for innovative reactor concepts", *Global, 2009,* Paper 9274.

[10] Haas, D. et al. (2007), "Cermet fuel behavior and properties in ADS reactors", *International Conference on Emerging Nuclear Energy Systems*, Istanbul.

CLASS: Core Library for Advanced Scenario Simulations

Baptiste Mouginot, Nicolas Thiolliere
Subatech Laboratory, EMN, Université de Nantes, CNRS, France

Abstract

The nuclear reactor simulation community has to perform complex electronuclear scenario simulations. To avoid constraints coming from the existing powerful scenario software such as COSI, VISION or FAMILY, the open source Core Library for Advanced Scenario Simulation (CLASS) has been developed.

The main asset of CLASS is its ability to include any type of reactor, whether the system is innovative or standard. A reactor is fully described by its evolution database which should contain a set of different validated fuel compositions in order to simulate transitional scenarios. CLASS aims to be a useful tool to study scenarios involving Generation-IV reactors as well as innovative fuel cycles, like the thorium cycle.

In addition to all standard key objects required by an electronuclear scenario simulation (the isotopic vector, the reactor, the fuel storage and the fabrication units), CLASS also integrates two new specific modules: fresh fuel evolution and recycled fuel fabrication. The first module, dealing with fresh fuel evolution, is implemented in CLASS by solving Bateman equations built from a database induced cross-sections. The second module, which incorporates the fabrication of recycled fuel to CLASS, can be defined by user priorities and/or algorithms. By default, it uses a "linear Pu equivalent"method [1], which allows predicting, from the isotopic composition, the maximum burn-up accessible for a set type of fuel.

This paper presents the basis of the CLASS scenario, the fuel method applied to a MOX fuel and an evolution module benchmark based on the French electronuclear fleet from 1977 to 2012. Results of the CLASS calculation were compared with the inventory made and published by the ANDRA organisation in 2012 [2].

Introduction

The nuclear reactor simulation community has to perform complex electronuclear scenario simulations. To avoid constraints coming from the existing powerful scenario software such as COSI, VISION or FAMILY, the open source Core Library for Advance Scenario Simulation (CLASS) has been developed. The main asset of CLASS is its ability to include any type of reactor, whether the system is innovative or standard.

CLASS principle

As all electronuclear scenario software, CLASS includes the entire set of key elements to describe an electronuclear fleet, from the reactor to the storage of used fuel, including the fuel reprocessing facility.

The main element of the CLASS library is the reactor. It is described by its power (in W), its mass (in tonne), its fuel type (UOX/MOX/…) and the final burn-up (in GWj/tonne)

of the used fuel. The cycle time of the fuel is calculated from the couple power/BU_{MAX} through the well-known relation Equation (1):

$$BU_{MAX} = \frac{P * CycleTime}{HeavyMetalMass} \quad (1)$$

It is also possible to set another couple of the triplet (BU/Power/CycleTime), depending on the user choices.

At the end of the irradiation, the spent fuel is sent to a cooling facility, from where it will be sent to the storage, at the end of a cooling time (five years by default). In storage, all output fuels from any reactor are stored individually. During all the cooling and storage time, the decay of all radioisotopes present in the fuel is taken into account. In addition to all the key parameters, a database is included to describe the evolution of the fuel during the irradiation.

There are currently two separate types of reactors. The most basic one corresponds to a reactor always filled with the same fresh fuel. This reactor type is used, for instance, to manage PWR reactor filled with uranium oxide (UOX) fuel.

The complex part comes from the other type of reactors, which reprocess fuels. Here, the composition of the used fuel in stock does not depend only on the final burn-up in the reactor, but also on the time spent in storage due to the decay of all radioactive isotopes. Thus, the composition of each reactor refill changes at each cycle. In order to simulate the evolution of the reprocessed fuel, CLASS needs two additional modules: the first one builds the reprocessed fuel with the correct properties in terms of reactivity (k_{eff} evolution) and mass, and the other one describes the irradiated fuel evolution.

At the end of the cycle, the used fuel is sent to the cooling facility. At the end of the cooling (usually five years) the fuel is either sent to a intermediate storage facility (to await reprocessing), or to final storage. During all this time (cooling, storage, waste), radioactive nucleus decays are taken into account.

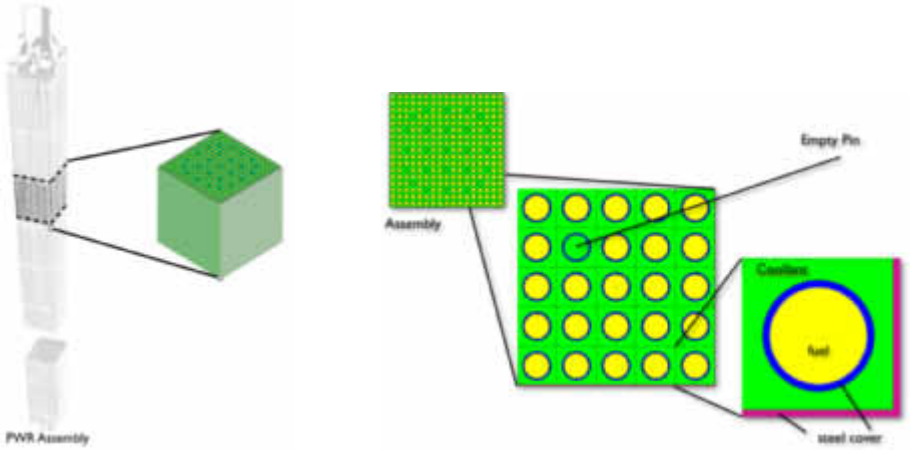
Database, fuel reprocessing and evolution

The following part describes the procedure used to perform all the simulations with the MURE software, and the processing scheme of the two modules mentioned previously: the computation of the reprocessed fuel and the determination of the evolution of the build fuel during irradiation.

Fresh fuel simulation

To compute the new fuel evolution database, the MURE software developed at CNRS has been used. This software allows the evolution from MCNP calculation, which determines at each time step (set by users) the system static parameters (mean cross-section, flux, k_{eff}). For the present example, to avoid full core geometry complexity, cubic assembly simulation was performed (see Figure 1) assuming that the fuel evolution in a cubic assembly with total reflecting surfaces is close to the core evolution.

Figure 1. Schematic representation of the simulated "cubic" assembly



In the present case, a constant power of 2.8 GW_{th} was used for the entire reactor. The simulation was set to perform a new MCNP calculation every quarter of a year. The UOX fuel standard burn-up in France ranges from 33 to 46 GWd/tonnes depending on the fuel campaign, so the irradiation time was set to 5 years, which corresponds to a burn-up of about 75 GWd/tonnes to reach the correct burn-up.

For each simulated composition, a CLASS database (called EvolutiveProduct) was generated, containing all the useful physical parameters (as the effective neutron multiplication factor, k_{eff}, the flux φ, nuclei quantities and fission, capture and (n, 2n) mean cross-sections). Figure 2 shows these parameters stored as an ASCII matrix.

Figure 2 presents the format of the CLASS EvolutiveProduct. The database can be generated by only formatting it in the right ASCII format.

Figure 2. Representation CLASS evolutive product in matrix form

$$\begin{pmatrix} k_{eff} \\ \phi \\ zai_1 \\ \dots \\ zai_i \\ \dots \\ zai_m \\ \sigma_{Fission,zai_1} \\ \dots \\ \sigma_{Fission,zai_m} \\ \sigma_{Capture,zai_1} \\ \dots \\ \sigma_{Capture,zai_m} \\ \sigma_{(n,2n),zai_1} \\ \dots \\ \sigma_{(n,2n),zai_m} \end{pmatrix} \begin{pmatrix} t_1 & \dots & t_j & \dots & t_n \\ k_{eff,1} & \dots & k_{eff,j} & \dots & k_{eff,n} \\ \phi 1 & \dots & \phi j & \dots & \phi n \\ Q_{1,1} & \dots & Q_{1,j} & \dots & Q_{1,n} \\ \dots & & \dots & & \dots \\ Q_{i,1} & \dots & Q_{i,j} & \dots & Q_{i,n} \\ \dots & & \dots & & \dots \\ Q_{m,1} & \dots & Q_{m,j} & \dots & Q_{m,n} \\ \sigma_{Fission,1,1} & \dots & \sigma_{Fission,1,j} & \dots & \sigma_{Fission,1,n} \\ \dots & & \dots & & \dots \\ \sigma_{Fission,m,1} & \dots & \sigma_{Fission,m,j} & \dots & \sigma_{Fission,m,n} \\ \sigma_{Capture,1,1} & \dots & \sigma_{Capture,1,j} & \dots & \sigma_{Capture,1,n} \\ \dots & & \dots & & \dots \\ \sigma_{Capture,m,1} & \dots & \sigma_{Capture,m,j} & \dots & \sigma_{Capture,m,n} \\ \sigma_{(n,2n),1,1} & \dots & \sigma_{(n,2n),1,j} & \dots & \sigma_{(n,2n),1,n} \\ \dots & & \dots & & \dots \\ \sigma_{(n,2n),m,1} & \dots & \sigma_{(n,2n),m,j} & \dots & \sigma_{(n,2n),m,n} \end{pmatrix}$$

Recycling fuel process

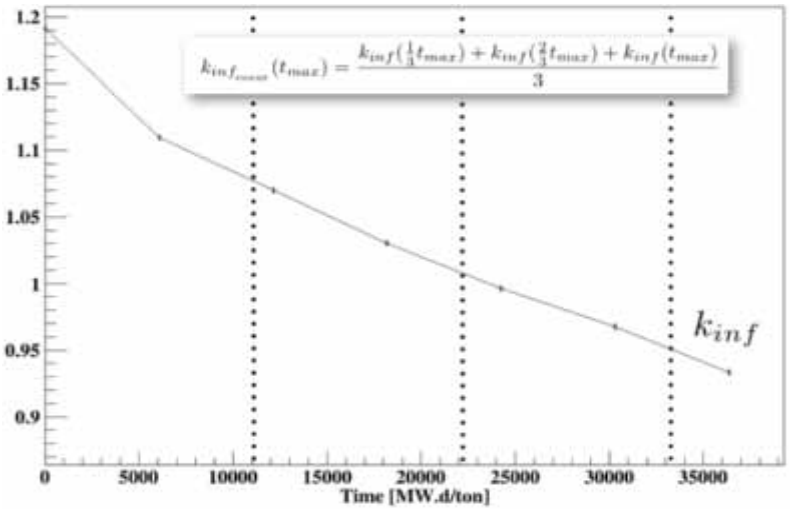
Both modules dedicated to recycled fuel reprocessing rely on a large number of realistic fuel composition evolutions. In order to create them, a random composition of the fuel is first generated within a realistic range (see Table 1) and then its evolution is simulated inside the cubic assembly described previously. The remaining composition is filled with depleted uranium at 3% of ^{235}U.

Table 1. Range of the random composition generation

Isotopes	% Maximum of the final composition	% Minimum of the final composition
^{238}Pu	0.03	0.09
^{239}Pu	1.7	4.8
^{240}Pu	0.65	2.00
^{241}Pu	0.00	0.72
^{242}Pu	0.15	0.45
Depleted U	Remaining	

For each generated fuel, the corresponding maximal burn-up has also been determined. The main limitation for a radioactive fuel is its reactivity, expressed by the effective neutron multiplication factor k_{eff}. In the following work, the maximal burn-up is defined where the mean value (for one-fourth core reloads) of the infinite neutron multiplication factor is equal to 1.06, as illustrated in Figure 3.

Figure 3. Evolution of the k_{inf} as a function of the burn-up and determination of the maximal burn-up



Each different random composition evolution and associated maximal burn-up comprised a database, all databases are stored in the data bank.

Recycled fuel fabrication

To build the proper reprocess fuel, it is necessary to determine the maximal burn-up that each composition can reach. For a set range of burn-ups, the α parameter is adjusted with the "linear Pu equivalent" method [2], which leads to the formula Equation (2):

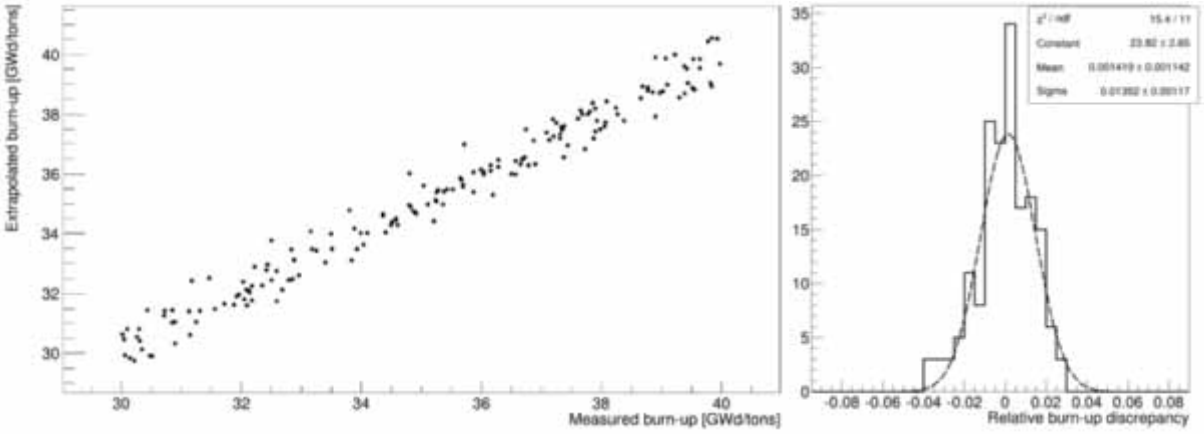
$$BU_{max} = \sum_i \alpha_i n_i + \alpha_0 \qquad (2)$$

where n_i represents the isotopic fraction of the isotope i before irradiation.

In Figure 4, the formula dispersion can be observed; 1% error is obtained on the estimated burn-up ranging between 30 and 40 GWd/tonnes. The accuracy of the result

could be improved by reducing the considered burn-up range, but it would be computationally intensive.

Figure 4. Dispersion on the burn-up estimation, on the left extrapolated burn-up versus measured one in [GWd/tonnes] and on the right, the relative discrepancy between them



Once the maximal burn-up is estimated for any reprocessed fuel composition, a reprocessed fuel can be built for a reactor set by Equation (3):

$$\begin{cases} BU_{\max} = \sum_i \alpha_i n_i + \alpha_0 \\ M_{reactor} = M_{Pu} + M_{depletedU} \end{cases} \quad (3)$$

In the previous equation, $M_{reactor}$ represents the mass in the reactor using the built fuel, M_{Pu} the mass of plutonium extracted from the recycled stock (composed of used UOX fuel) and $M_{depletedU}$ the mass of depleted uranium needed to build the proper fuel in terms of the maximal burn-up and total mass, and BU_{max} the maximal burn-up reached by the fuel inside the reactor set. From Equation (3), the fraction of the stock required and the amount of depleted uranium needed to build a reprocessed fuel can be determined. If more than the tested stock is required to build the fuel (fraction>1), all the plutonium isotopes of this stock are used and the remaining portion is taken in the next stock.

This way, this built fuel is able to reach the maximal burn-up of the specific reactor that should be filled. The next step is to determine how the composition of this fuel could evolve inside the reactor through irradiation.

Recycled fuel evolution

In order to determine the evolution of the reprocessed fuel composition, the data bank of the fuel evolution (described previously), from which the closest fuel composition is extracted, was sed. Thus, a reference database was defined for the specific reprocessed fuel composition.

Using the cross-sections, σ_i, and flux, φ_i, given by the reference database, and the well-known Bateman equation [Equation (4)], the evolution of the built fuel is calculated after renormalisation of the flux. At each time step, the cross-sections and the flux are updated from the reference database (and the flux renormalised), until the end of the evolution. This module performs the evolution only for the main actinide isotopes.

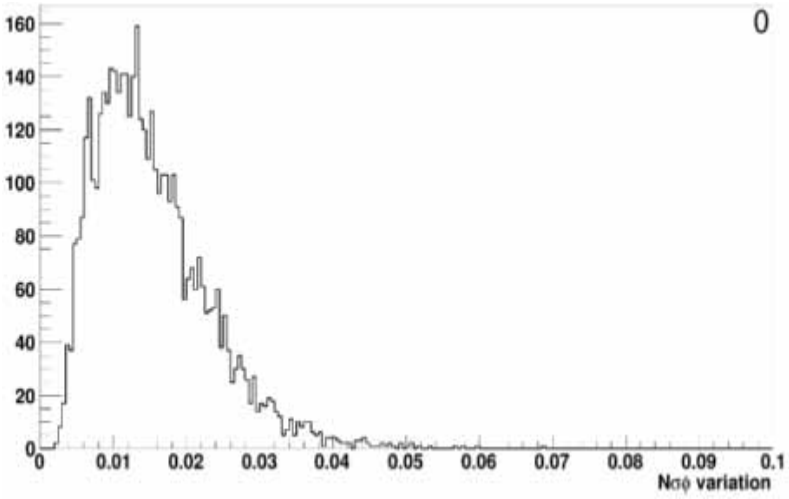
$$\frac{dN}{dt} = -\lambda_i N_i - \sigma_i \varphi N_i + \sum_{j \neq i} \lambda_{j \to i} N_j + \sum_{j \neq i} \sigma_{j \to i} \varphi N_i, \forall i \quad (4)$$

An on-going study allows estimating the error associated with this method. This study consists of reconstructing the evolution of each random composition fuel using Equation 4 from all the other databases in the data bank. So far only one parameter has been studied; the relative differences in reaction rate, "nσφ variation", Equation (5):

$$(n\sigma\varphi \text{ variation}) = \frac{\sum_i \left| (n_i\sigma_i\varphi)_{estimated} - (n_i\sigma_i\varphi)_{simulated} \right|}{\sum_i (n_i\sigma_i\varphi)_{simulated}} \quad (5),$$

where the estimated parameter corresponds to the calculation through previously described method, the simulated parameter corresponds to the simulation, n is the quantity of isotope i, σ the cross-section for a set reaction, and φ the renormalised flux (the sum is made on all isotopes present in the fuel and on the fission, capture and (n, 2n) reactions).

Figure 5. Dispersion of the relative reaction rate differences at first time step



In Figure 4, the dispersion of the "nσφ variation" is about 1% (in Figure 4, each point of the distribution corresponds to the relative difference for one randomly generated fuel), which seems reasonable. As shown in Figures 5-6, this dispersion exponentially increases with time and decreases with the number of random fuel composition initially generated, following a well-known tendency in $\frac{1}{\sqrt{n}}$.

Figure 6. Evolution of the mean of relative reaction rate dispersion as a function of the time step, each curve represents the number of random fuel composition simulated

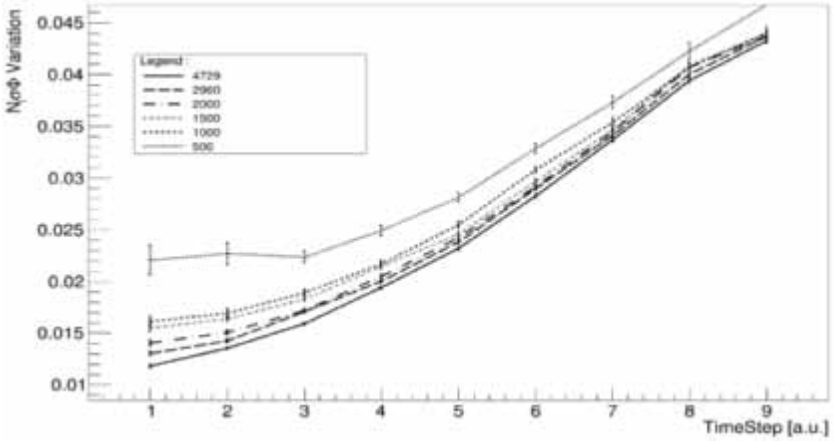
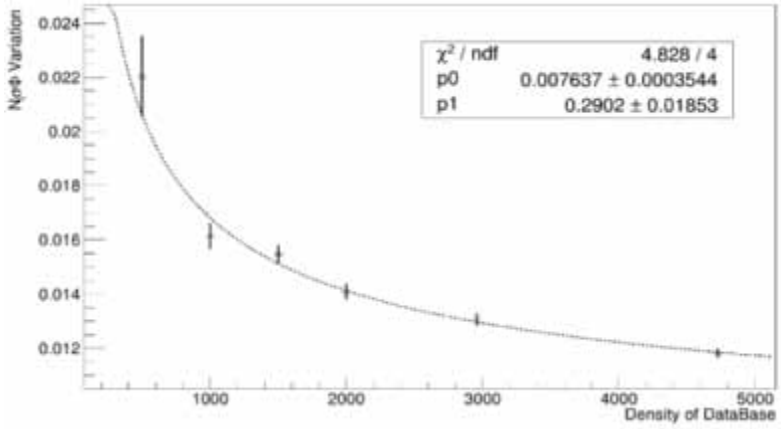


Figure 7. Evolution of the mean of relative reaction rate dispersion as a function of the number of random fuel composition simulated



On-going studies are being performed in order to improve this result. There are two main ideas: one is to improve the flux management in the evolution module and the other is to test different algorithms to determine the distance between two isotopic vectors. Flux management is necessary in order to conserve a constant power. Indeed, it would be better to renormalise the flux many times between two time steps. Finally, the definition of distance between two isotopic vectors is a crucial aspect, because the evolution method is very sensitive to it. To define this distance, different algorithms will be examined.

CLASS application: French electronuclear fleet 1978-2011

In the present study, the CLASS software has been used to reproduce the evolution of the French electronuclear fleet from 1978 until 2011. The Pressurised Water Reactors (PWR) installed after 1978 are considered here, but the Uranium Naturel Graphite Gas (UNGG) reactors used before are not. Only the stocks produced by the French reactors are taken into account.

The French fleet

Six different types of PWR constitute the French electronuclear fleet: the CP0, CP1 and CP2, the P4 and P'4, and the N4. In order to simplify the description of the fleet and because their characteristics are close, we will consider that the CP1 and CP2 are identical, as are the P4 and P'4, and are, respectively, called CPY and P4. Table 2 shows the characteristics in terms of enrichment, burn-up and loading plan for all the considered campaigns.

In order to simplify the realisation of the scenario, the different loading plans have not been taken into account. We are assuming that all the fuels inside the reactor are removed at the end of the cycle, and that the reactor is completely refilled at the beginning of the new cycle. Consequently, the cycle corresponding to a loading plan by a third and by a quarter, respectively, lasts 3 and 4 years. This can fluctuate a little, depending on the reactor and the campaign.

Table 2. Characteristics of the different fuel campaigns

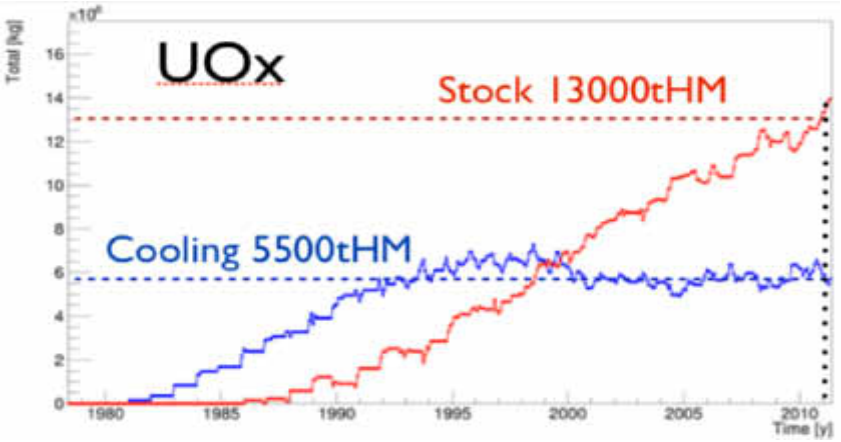
Campaign	^{235}U Enrichment	Pu quantity	Burn-up max	Cycle time (day equiv. full Px)	Loading plan
Standard 1450	3.4 %	None	43	258	1/4
Standard 1300	3.1 %	None	33	300	1/3
Standard 900	3.25 %	None	33	298	1/3
Garance	3.7 %	None	42	275	1/4
Cyclades	4.2 %	None	42	355	1/3
Gemmes	4.0 %	None	43	395	1/3
MOX 16%	Equiv. 3.7 %	7%	35	280	1/3
MOW "low"	Equiv. 3.25 %	5.3%	36	290	1/3

The used fuel stock

Throughout the process from reactor to storage, the CLASS software allows us to follow the composition of each fuel in each facility of the fleet. The aim of this work is to present the total inventory in stock and in cooling for UOX and MOX. This information is also provided by the ANDRA organism [3].

For UOX used fuels, the ANDRA reported 12 006 tonnes of heavy metal in stock, including cooling, versus 18 500 tonnes of heavy metal predicted by CLASS (see Figure 8). The large difference is easily explained by the presence of 56 tonnes of plutonium already separated from used UOX fuel, which corresponds to about 5600 tonnes of heavy metal before separation. However, CLASS still overestimates the amount of UOX fuel in the fleet by about 1000 tonnes. This could be explained by the large tendency of the PWR operator to always use the fuel at maximum burn-up, adding about 20 days' equivalent full power at the normal irradiation of the fuel.

Figure 8. Evolution of the total amount of UOX used fuel in stock and cooling, in tonnes of heavy metal



For the MOX fuel, the predictions are in good agreement: 1250 tonnes is predicted by CLASS versus 1287 tonnes for ANDRA. Overall, CLASS is performing well in estimating the total amount of fuel in the fleet, these results are the first step towards the validation of the CLASS software. A detailed benchmark will be performed in the coming years, including a comparison with the COSI software developed by CEA. In this comparison, the isotopic evolution of the different fuels will be analysed.

Conclusion

In the present work, the current status of the CLASS software is detailed and illustrated with a simple example. The main working scheme is explained through the example of the French fleet. The basic capacities of the CLASS software are verified, nevertheless, a detailed analysis and a precise benchmark are still required.

CLASS is a young software (about 1 year's development), but it has got off to a promising start. Many further developments and analyses are already in progress, and other will come in order to make CLASS, some precise software for electronuclear scenario simulation. During the upcoming year, precise comparisons with different items of scenario software such as COSI will be performed on transitional scenarios. This benchmark will allow validating the CLASS software.

Future improvements will also concern the development of a standard method for data bank generation. Priority will be given to the generation of a sodium fast reactor MOX and Multi MOX data bank and one for ADS in order to consider the management of minor actinides and eventually plutonium in "end game" scenarios.

As mentioned previously, on-going analyses will also study different aspects of the definition of distances between two isotopic vectors and their influence on the evolution module. The evolution modules will also be extended to the entire nuclear chart.

Acknowledgements

The authors would like to thank the young collaboration team involved in CLASS, for their enthusiasm, discussions and ideas present and future, which have been and will be the fuel of CLASS's development.

References

[1] Meplan, O. et al. (2009), "MCNP Utility for Reactor Evolution: Couples Monte Carlo transport with fuel burnup calculations", *MURE, Computer Program Services of OECD/NEA*.

[2] Kepisty, G., David, S. (1970), "Performance of Pu/Th fuels in PWR, analysis of the fissile material effiency for future reactors", *Internship report, Institut de Physique Nucléaire d'Orsay* – CNRS.

[3] Inventaire national 2012, Rapport de synthèse, ANDRA.

Transient analysis for lead-bismuth-cooled accelerator-driven system proposed by JAEA

Takanori Sugawara, Kenji Nishihara, Kazufumi Tsujimoto
Japan Atomic Energy Agency, Japan

Abstract

It is supposed that an Accelerator-driven System (ADS) is safer than conventional critical reactors since an ADS is driven by the external neutron source in the subcritical state. In this study, the transient analyses for the lead-bismuth cooled ADS proposed by JAEA were performed using the SIMMER-III and RELAP5/mod3.2 codes to investigate the possibility of core damage.

In this research, three accidents; the protected loss of heat sink, the protected overcooling and the unprotected blockage accident were considered as typical ADS accidents. Through these calculations, it was confirmed that all calculation results, except for the protected loss of heat sink, fulfilled the no-damage criteria. In the protected loss of heat sink, the cladding tube temperature reached its melting temperature after 18-21 hours, although the calculation condition was very conservative. These results have led to requirements to design a safety system of the ADS to decrease the frequencies of accidents.

Introduction

The Japan Atomic Energy Agency (JAEA) has performed research and development of an Accelerator-driven System (ADS) to reduce the burden for the conditioning and disposal of high-level radioactive waste. The proposed ADS is a lead-bismuth eutectic (LBE) cooled tank type ADS, which consists of a high intensity proton accelerator with 1.5 GeV beam energy and a subcritical core with 800 MW thermal power [1, 2]. It can transmute 250 kg minor actinide (MA) per year.

It is supposed that the ADS is safer than critical reactors since an ADS is operated in a subcritical state. The advantages of the subcritical system are:

- the shutdown is easy (just to stop the supply of spallation neutrons by the shutdown of the accelerator);
- a possibility of a critical accident is smaller than the critical reactors.

The advantages of using the LBE as a coolant are the following:

- there is little possibility of a void generation by boiling due to the high boiling point of the LBE (1670°C);
- the LBE is inactive against the water, unlike sodium.

On the other hand, it is very important to control oxygen concentration in the LBE to protect corrosion and the generation of lead oxide. Preventing the LBE from overcooling is also important in an LBE-cooled system. It is supposed that the lead oxide or frozen LBE

will be one of the causes of a flow blockage at a fuel assembly, a heat exchanger tube or other components.

In the previous study, a preliminary investigation of safety was performed by Level 1 PSA (probabilistic safety assessment) with the consideration of such characteristics of the LBE-cooled ADS [3]. The previous study showed that the probabilities of the two cases, beam window breakage (BWB) and protected loss of heat sink (PLOHS) were more than 10^{-6} [reactor year]. For other events, such as beam overpower (BOP) and unprotected loss of flow (ULOF), Level 1 PSA showed that the frequencies of these events were less than 10^{-6} [reactor year]. Here, "protected" and "unprotected" mean a success and a failure of the beam-shutdown, respectively. In addition, the previous study showed that there was little possibility of core damage in BWB, BOP and ULOF through the transient analysis.

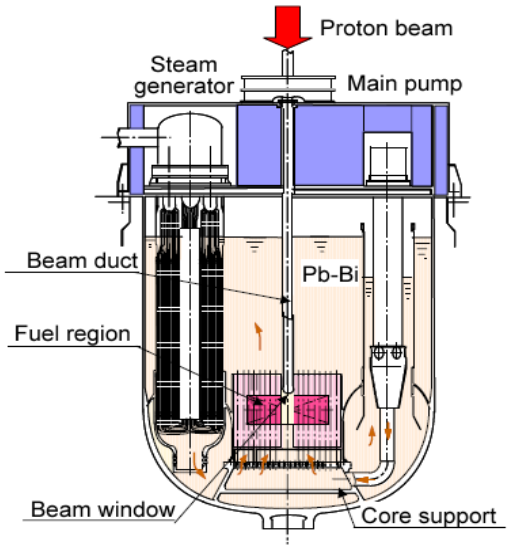
This study aims to analyse transients of other typical accidents for the ADS based on past assessments. Two calculation codes, the SIMMER-III [4] and the RELAP5/mod3.2 codes [5], are employed for the analyses. Throughout these analyses, the possibility of the core damage in the ADS is discussed.

Calculation condition

Calculation code

The SIMMER-III code is an advanced safety analysis code, which has been developed to investigate postulated core disruptive accidents in fast reactors [4]. The SIMMER-III code is a two-dimensional three-velocity field, multi-phase, multi-component, eulerian fluid dynamics codes coupled with a structure model and a space-, time- and energy-dependent neutron kinetics model. The latest version of the SIMMER-III code is available to analyse the LBE-cooled ADS by adding features to treat the subcritical state with the external neutron source and physical properties for the LBE [6]. However, it is unable to treat a heat generation by the spallation reaction in the target region. Hence, heat generation in the target region was ignored in the SIMMER-III calculation. It is appropriate to analyse a short-range (a few seconds, for example) transient.

Figure 1. Conceptual diagram of ADS



The RELAP5/mod3.2 (RELAP5 in the following) code is a thermal hydraulic computer code, which has been developed to predict the behaviour of nuclear plants during transient and accidental conditions [5]. The code models the coupled behaviour of the reactor coolant system, the core for loss of coolant accidents and operational transients such as anticipated transient without scram and loss of flow. The module to use the LBE as a coolant was prepared and employed in this study. The code models the whole flow of the system including a secondary cooling system but no eutronic model is available. It is adequate to calculate a long-range (several hours, for example) transient.

Table 1. Main parameters of ADS

Plant	Thermal power	800 MWt
	Coolant	LBE
	Inlet temperature	300°C
	Coolant velocity	2.0 m/sec
	Upper limitation of k_{eff}	0.97
	Operation period	600 EFPDs*
Fuel assembly	Type	Duct-less and hexagonal
	Number of fuel assemblies	84
	Pitch	233.9 mm
	Width	232.9 mm
	Number of fuel pins per assembly	391
	Number of tie rods per assembly	6
Fuel	Composition	(MA+Pu)N+ZrN
	Pu enrichment (inner/outer)	15.1/21.3 wt%
	ZrN ratio (inner/outer)	49.7/49.7 wt%
	Pin outer diameter	7.65 mm
	Thickness of cladding tube	0.5 mm
	Pin pitch	11.48 mm
	Active height	1000 mm

*Effective full power days

Calculation model

The calculation was performed for the ADS proposed by JAEA [7]. Table 1 summarises the main parameters of the ADS and Figure 1 presents a conceptual diagram of the ADS. The reactor vessel contains a beam duct, a subcritical core, a steam generator (SG) and a primary pump. A primary reactor auxiliary cooling system (PRACS) is prepared to remove decay heat. However, in this study, the PRACS was not considered for the treatment of the most severe case.

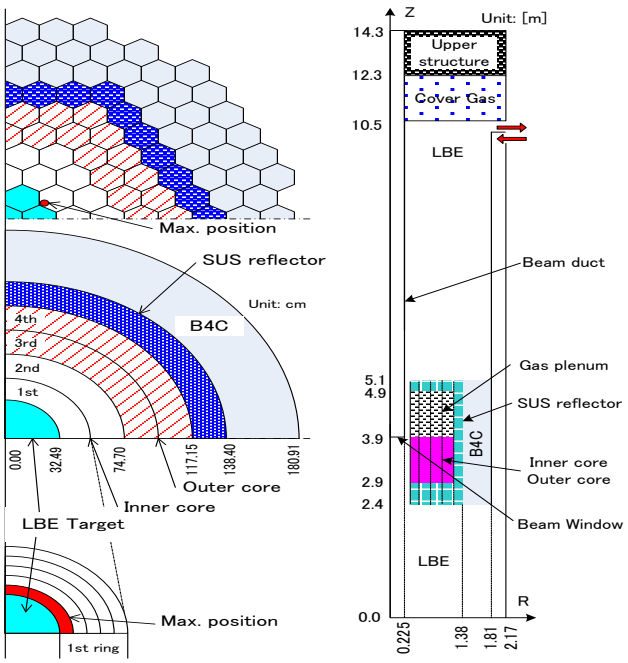
As described above, the LBE is used as both the spallation target and the coolant. A nitride fuel of plutonium and MA is cladded by T91 steel as a fuel pin. The fuel pins are assembled as a ductless hexagonal fuel assembly (FA), then these 84 FAs are loaded into the subcritical core.

SIMMER-III

Since the SIMMER-III code is unable to treat a hexagonal model, the subcritical core was simulated by an RZ calculation model, as shown in Figure 2. The subcritical core consists of 84 FAs that are divided into four rings. The inner most one is named the first ring, the next one is the second ring. These zones were used in the investigation of a multi-zoned ADS [7], and in this study, a two-zoned model, which has two different types of plutonium enrichment is employed.

When the subcriticality is large, the importance of the fission reaction near the spallation target increases. This means that the cladding tube temperature at the nearest position from the spallation target reaches maximum value at this moment. The power distribution in the second EOC (End of Cycle) was the most severe state since the subcriticality in the second EOC was the largest during the ADS operation [7]. Based on this result, a neutronic calculation model in the second EOC state was employed.

Figure 2. RZ calculation model for SIMMER-III



RELAP5

Figure 3 shows the calculation model used in the RELAP5 calculation. In this calculation model, the subcritical core consists of three components, the spallation target, first ring and other rings (second-fourth), hence, the most important point of this analysis is to confirm the cladding tube temperature at the first ring. Thus, the calculation model is simplified for other FA rings. The heat structure of the RELAP5 input is given to the spallation target, each FA ring and the SG. For other components, the adiabatic assumption is considered, so the heat removal from the reactor vessel is ignored, for example. For the heat distribution in the subcritical core, the calculation

result by the SIMMER-III code provides the same cladding tube temperature. In the SG, the heat balance is adjusted to keep the LBE temperature at the inlet of the core at 300°C.

Figure 3. Calculation model for RELAP5 calculation

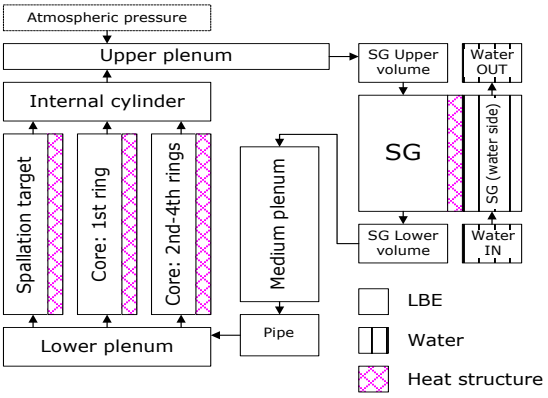


Table 2 summarises the parameters for the RELAP5 calculation model. Some parameters shown in Table 1 are also employed in the RELAP5 calculation. The pressure in the SG is 6.0 MPa and the water mass flowrate is 870 kg/s. A detailed design of the primary pump for the ADS has not been performed yet and Table 2 shows the parameters of the primary pump [8]. The decay heat calculated by the ORIGEN-II code [9] in second EOC condition was used in that case.

Table 2. Parameters for RELAP5 calculation model

SG	LBE inlet temperature	400°C
	LBE outlet temperature	300°C
	Water inlet temperature	243.8°C
	Water outlet temperature	275.4°C
	Pressure in SG	6.0 MPa
	Water mass flow rate	870 kg/s
Pump	Pump head	4.5 m
	NPSH*1	2.5 m
	Inertia moment*2	12 000 kg m^2
	Rated torque*2	40 000 N m
Coolant	Mass flow rate	56 900 kg/s
	Total amount of LBE	8240 t

*1: Net positive suction head.

*2: Provisional value.

Calculation case

In the previous study [3], Level 1 PSA was used to quantify the frequency of an abnormal event. As a result, the frequencies of beam window breakage (BWB) and protected loss of heat sink (PLOHS) were larger than the criteria (10^{-6} [reactor year]), which were employed in the feasibility study of fast reactors [10]. The transient of BWB was calculated by the SIMMER-III code and the result showed that there was no possibility of the core damage by BWB because the LBE flowed into the beam duct and the external neutron source decreased.

The frequencies of other events, such as Beam Overpower (BOP) and Unprotected Loss of Flow (ULOF), were less than those of the criteria. However, the transient analyses for these two events were also performed in the previous study because BOP was the inherent event of ADS and ULOF was reported as one of the most severe events for ADS [11]. The calculation results indicated that there was very little possibility of core damage by BOP and ULOF although there was the possibility of the creep rapture of the cladding tube.

Table 3. Calculation cases and codes

	Previous study*	SIMMER-III	RELAP5
BWB	O		
PLOHS	-	-	O
POVC	-	-	O
BOP	O		
ULOF	O		
UBA	-	O	-

*The case has already been calculated in the previous study [3]. Therefore, the case is not treated in this study.

Based on previous results, this study aims to calculate three events: PLOHS, protected overcooling (POVC) and unprotected blockage accident (UBA), as a typical accident of ADS. For PLOHS, the frequency was larger than that of the criteria, 10^{-6} [reactor year], so it is necessary to confirm the possibility of core damage. For POVC, it is supposed that there is no possibility of core damage by the overcooling of the LBE. However, it is an inherent issue for the LBE-cooled system and will be a cause for a flow blockage at the FA, the heat exchanger tube or other components. Thus, it is important to understand a boundary condition for a temperature of a secondary system. For UBA, which is an accident of the flow channel block in a fuel assembly without the beam-shutdown, it was pointed out that UBA has an effect leading to core damage in the LBE-cooled system [11]. UBA was also selected as a calculation case in this study.

Table 3 summarises the calculation cases and codes to be used in each calculation case. It was considered that the time range of transient analysis would be long for PLOHS. It was also supposed that the SG model was necessary to model a loss of heat sink. Therefore, the RELAP5 code was employed for PLOHS. In the case of POVC, it was reasonable to use the SG model to change the LBE inlet temperature. Hence, the RELAP5 code was used for the POVC calculation. For UBA, it was necessary to model the FA to represent a blockage of the flow. It was considered that both calculation codes were able to treat the blockage of the flow, but the RELAP5 code was unable to treat the ductless FA. Hence, the SIMMER-III code was employed for UBA.

Figure 4. Change of water flow rate at SG in PLOHS

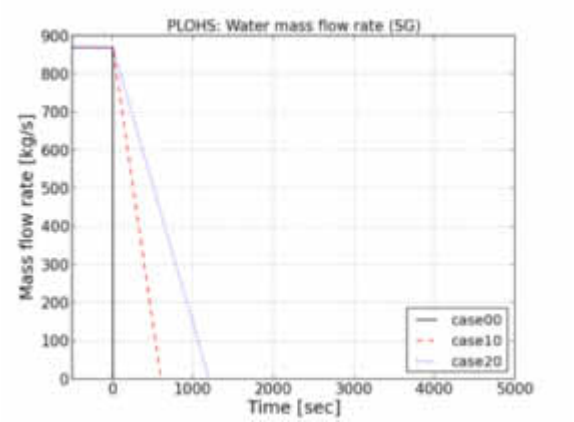
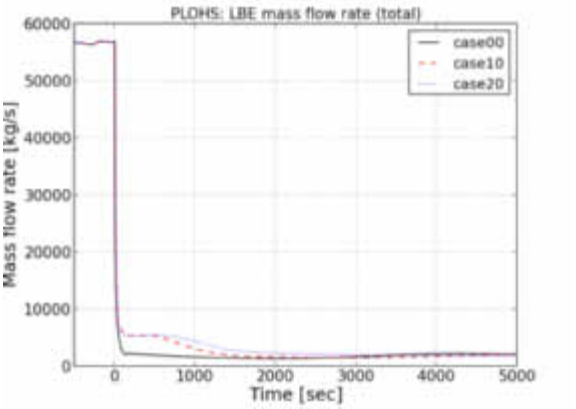


Figure 5. Change of LBE flow rate in PLOHS



In this study, the following criteria were used to judge core damage, namely, the fuel and cladding tube temperatures should be less than those melting temperatures, 2781°C and 1320°C, respectively. If the temperatures exceed those, it is deemed that the core has been damaged.

Calculation result

Protected loss of heat sink (PLOHS)

The calculation of PLOHS was carried out by the RELAP5 code. The loss of heat sink was expressed as a decrease of the water mass flow rate in the SG. Three calculation cases were performed in this study. In each calculation case, the time during which the water mass flow rate reached zero was changed as 0 minutes, 10 minutes and 20 minutes (case00, case10 and case20, respectively). Case00 was the hypothetical case to see the most severe result. A linear decrease was assumed for the water mass flow rate. Figure 4 shows the change of the water flow rate for each case. When the water flow rate in the SG began to decrease, the operation of both the accelerator and the primary pump was stopped. The coolant flow decreased with a flow halving time of about 8 seconds. Figure 5 presents the change of the LBE flow rate in the core region. When the primary pump was stopped, the LBE mass flow rate decreased immediately, but a natural convection by the decay heat was generated. The mass flow rate by the natural convection was about 3.5% of the nominal value.

Figure 6 presents the changes of the cladding tube temperature at the first ring for each calculation case. When the accelerator was shut down, the temperature decreased rapidly (small window in Figure 6). After the rapid decrease, the temperature decreased moderately in case10 and case20 until about 600 seconds and 1000 seconds, respectively, because the water was supplied to the SG in that time. Then, the temperature increased moderately due to the loss of heat sink. The times which the cladding tube temperature reached at 1320°C were 65,000 seconds (18h), 71,800 seconds (20h) and 75,200 seconds (21h) in case00, case10 and case20, respectively. These results exceeded the damage criteria, so there was a possibility of the core being damaged by the loss of heat sink, although the PRACS was ignored. On the other hand, these results indicate that there is 18 hours at minimum to manage the accident when PLOHS would occur.

Figure 6. Change of cladding tube temperature at first ring in PLOHS

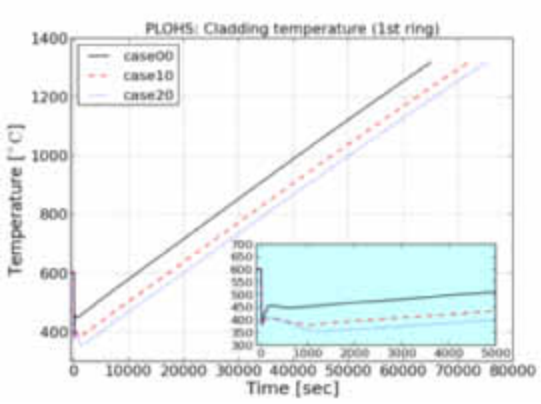
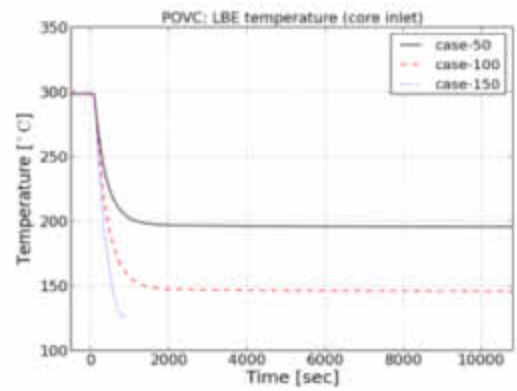


Figure 7. Change of LBE temperature at the core inlet in POVC



Protected overcooling (POVC)

The transient of POVC was calculated by the RELAP5 code. In this calculation, a water inlet temperature at the SG was decreased -50°C, -100°C and -150°C (case-50, case-100 and case-150, respectively) within 200 seconds and it was expected that the LBE temperature would converge to 193.8°C, 143.8°C and 93.8°C since the water inlet temperature in the normal operation was 243.8°C. This means that the LBE will freeze in case-150 because the melting point of the LBE is about 124°C. One of the purposes of calculating POVC was to confirm the time until the LBE froze.

Figure 7 plots the LBE temperatures at the core inlet in POVC. It was confirmed that the LBE temperature decreased to the SG water inlet temperature in each case. In case-

150, the LBE temperature reached at its melting point at about 900 seconds (15 minutes). Since the adiabatic condition was assumed for the reactor vessel, this time would be shorter with the consideration of heat release from the reactor vessel. It is necessary to detect the decrease of the water inlet temperature at the SG during 15 minutes, at least, to avoid freezing of the LBE by overcooling.

Unprotected blockage accident (UBA)

The calculation of UBA was performed by the SIMMER-III code. A full blockage at the first ring was supposed. This assumption is extremely conservative because the first ring corresponds to 12FAs, so it makes no sense that the flow of the 12 FAs is blocked at the same time. However, the calculation was carried out as one of the most severe cases. Three calculation cases, case-bottom, case-middle and case-top, were considered by changing a blockage position for z-direction. Figure 8 shows the blockage positions for three cases and an LBE flow vector in the core region before and after the blockage. In this figure, blue and black colours represent the LBE and steel, respectively, and grey colour corresponds to fuel particle. Before the blockage (steady state in Figure 8), the LBE flowed from bottom to top at the first and second rings (Radial 3 and 4 in Figure 8) and the vector looked slightly towards the right. After the blockage at the first ring, it was observed that the LBE velocity decreased but the flow was maintained by a cross-flow in all cases. The vector at the first and second rings looked towards the left. It can be noted that the flow at the second ring moved into the first ring when the blockage occurred.

Figure 8. LBE flow vector in the FA region before and after the blockage

Figure 9 presents the cladding tube temperature distributions at the first ring for each case. The horizontal axis in Figure 9 corresponds to the z-axis shown in Figure 2. When the bottom of the first ring was blocked, the cladding tube temperature increased with a maximum temperature less than 700°C. In case-top, the cladding tube temperature near a top region (z=360-390cm) increased, however, the value was much smaller than the melting point of the cladding tube. In case-middle, it was found that the cladding tube temperature near the blockage position increased significantly. The value reached 1260°C

at z=345cm, and the values decreased as the z-position increased by the increase of the cross-flow from the second ring. Although creep damage of the cladding tube might have occured, this result fulfilled the no-damage criteria.

Figure 10 presents the transients of the cladding tube temperature at z=345 cm in UBA. In this figure, the calculation result with wrapper tube (FA with duct) is added as case-duct. In case-duct, the duct was added to each FA region in the calculation model and the temperature condition was adjusted to that steady state by changing the flow rate. The bottom of FA was blocked in case-duct. It was observed that the cladding tube temperature increased immediately and reached 1260°C after 5 seconds in case-middle. It was found that the cladding tube temperature reached the melting point at two seconds after the blockage in case-duct. This means that UBA has an impact leading to core damage in the LBE-cooled system, as described in [11]. However, the present results indicated that UBA would not be a serious accident if the ductless FA was employed.

Figure 9. Cladding tube temperature distributions in UBA

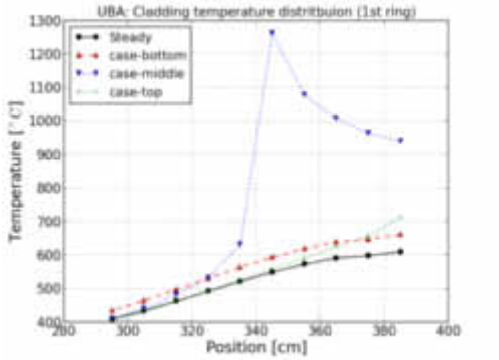
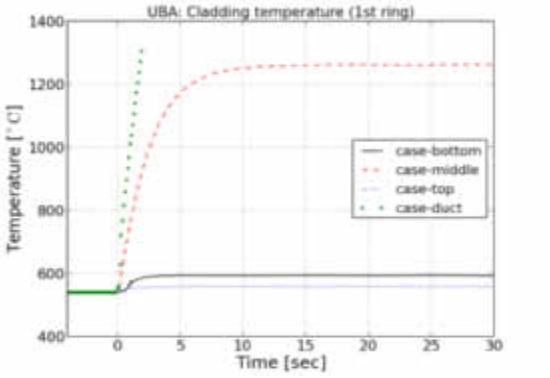


Figure 10. Cladding tube temperature transients at z=345cm in UBA



Conclusion

The transient analyses for the LBE-cooled ADS were performed using the SIMMER-III and RELAP5 codes to investigate the possibility of core damage. Based on the previous study, three cases were calculated as typical accidents of the ADS.

In the case of PLOHS, the cladding tube temperature decreased immediately after the shutdown of the accelerator. After the shutdown, the temperature increased moderately by the loss of heat sink and the cladding tube temperature reached 1320°C after 18 hours, 20 hours and 21 hours in case-00, case-10 and case-20, respectively. These calculation

results showed that there was a possibility of core damage by PLOHS, although the calculation condition was very conservative (adiabatic assumption for the reactor vessel and no PRACS). In the case of POVC, it was confirmed that the LBE temperature decreased to the water inlet temperature at the SG. In case-150, the LBE temperature reached its melting point at 15 minutes. Although there was no possibility of core damage by POVC, it was necessary to detect the decrease of the water inlet temperature at the SG during 15 minutes to avoid freezing of the LBE by overcooling. Obviously, it is important to design the secondary coolant system to maintain the water inlet temperature at the SG above the LBE melting point.

In the case of UBA, it was found that the flow at the first ring, which was blocked, was maintained by the cross-flow because the ductless FA was assumed to be used in the ADS design. In case-middle, the cladding tube temperature reached 1260°C, and it was supposed that the creep damage of the cladding tube might be possible. However, all results fulfilled the no-damage criteria, although a very conservative calculation condition was employed. These transient analyses indicated that there was a possibility of the core being damaged by the loss of heat sink in the ADS investigated in this study, if the PRACS were out of order. As a next step, it is required to design a safety system of the ADS to decrease the frequencies of accidents.

References

[1] Tsujimoto, K. et al. (2004), "Neutronics Design for Lead-Bismuth Cooled Accelerator-Driven System for Transmutation of Minor Actinide", *J. Nucl. Sci. and Technol.*, 41 [1], 21-36.

[2] Oigawa, H. et al. (2011), "Role of ADS in the back-end of the fuel cycle strategies and associated design activities: the case of Japan", *J. Nucl. Mater.,* 415 [3], 229-236.

[3] Sugawara, T. et al. (2010), "Investigation of safety for Accelerator Driven System", *Proc. of 1st International Workshop on Technology and Components of Accelerator-Driven System (TCADS-1*), Karlsruhe, Germany.

[4] Tobita, Y., Kondo, Sa., Yamano, H. et al. (2006), "The Development of SIMMER-III, An Advanced Computer Program for LMFR Safety Analysis, and Its Application to Sodium Experiments", *Nuclear Technol.*, 153, pp. 245-255.

[5] The RELAP5 Development Team (1995), "RELAP5/Mod 3.2 Code Manual", NUREG/CR-5535 Report, Vol. 1-5, Idaho National Engineering Laboratory, US.

[6] Maschek, W. et al. (2000), "SIMMER-III, a code for analyzing transients and accidents in ADS", *Proc. of Topical Meeting on AccApp'00*, Washington, DC, US.

[7] Nishihara, K. et al. (2008), "Neutronics Design of Accelerator-Driven System for Power Flattening and Beam Current Reduction", *J. Nucl. Sci. and Technol.*, 45, *8*, 812-822.

[8] Saito, S. et al. (2006), "Design optimization of ADS plant proposed by JAERI", *Nucl. Instrum. Methods Phys.* Res. A 562, 646–649.

[9] Croff, A.G. (1980), "ORIGEN-2: A Revised and Updated Version of Oak Ridge Isotope Generation and Depletion Code", ORNL-5621, Oak Ridge National Laboratory, US.

[10] JAEA (2006), "Feasibility Study on Commercialized Fast Reactor Cycle Systems Technical Study Report of Phase II – (1) Fast Reactor Plant Systems", *JAEA-Research 2006-042 Japan Atomic Energy Agency,* [In Japanese].

[11] Suzuki, T. et al. (2005), "Transient analyses for accelerator driven system PDS-XADS using the extended SIMMER-III code", *Nucl. Eng. Des.* 235, 2594-2611.

Session IV: Neutron Sources

Chair: B. Grambow

KIPT accelerator-driven system design and performance

Yousry Gohar[1], Igor Bolshinsky[2], Ivan Karnaukhov[3]
[1]Argonne National Laboratory, US, [2]Idaho National Laboratory, US
[3]National Science Center "Kharkov Institute of Physics and Technology", Ukraine

Abstract

Argonne National Laboratory (ANL) of the US is collaborating with the Kharkov Institute of Physics and Technology (KIPT) of Ukraine to develop and construct a neutron source facility. The facility is planned to produce medical isotopes, train young nuclear professionals, support Ukraine's nuclear industry and provide capability to perform reactor physics, material research, and basic science experiments. It consists of a subcritical assembly with low-enriched uranium fuel driven with an electron accelerator. The target design utilises tungsten or natural uranium for neutron production through photonuclear reactions from 100-MeV electrons. The accelerator electron beam power is 100 KW. The neutron source intensity, spectrum, and spatial distribution have been studied as a function of the electron beam parameters to maximise the neutron yield and satisfy different engineering requirements. Physics, thermal-hydraulics, and thermal-stress analyses were performed and iterated to maximise the neutron source strength and to minimise the maximum temperature and the thermal stress in the target materials. The subcritical assembly is designed to obtain the highest possible neutron flux intensity with an effective neutron multiplication factor of <0.98. Different fuel and reflector materials are considered for the subcritical assembly design. The mechanical design of the facility has been developed to maximise its utility and minimise the time for replacing the target, fuel, and irradiation cassettes by using simple and efficient procedures. Shielding analyses were performed to define the dose map around the facility during operation as a function of the heavy concrete shield thickness. Safety, reliability and environmental considerations are included in the facility design. The facility is configured to accommodate future design upgrades and new missions. In addition, it has unique features relative to the other international facilities and it can be used for studying accelerator-driven systems. The facility utilisation study shows that this neutron source facility has excellent capability for producing different medical isotopes. Several horizontal neutron channels are incorporated to perform basic research, including cold neutron source. This paper highlights the design, the performed analyses, and the current status of the facility.

Introduction

For more than five years, Argonne National Laboratory (ANL) of the US has been collaborating with Kharkov Institute of Physics and Technology (KIPT) of Ukraine to develop and construct a neutron source facility [1-28]. The facility has an accelerator-driven subcritical assembly with low-enriched uranium (LEU) fuel. An electron accelerator is utilised for generating neutrons from photonuclear reactions with high mass number material, tungsten or natural uranium to drive the subcritical assembly. The facility will be utilised to produce medical isotopes, train young nuclear professionals, support Ukraine's nuclear industry and provide capability to perform reactor physics, material research and basic science experiments.

Several studies have been performed to develop the facility design and examine the main design parameters to fulfill the above facility objectives. The electron beam target assembly design, the spatial energy deposition in the target materials and the intensity, spectrum and spatial distribution of the neutron source have been studied as a function of the electron beam parameters, target materials, and target configurations. The main objectives are to maximise the neutron production from the 100-KW electron beam power and to fulfill the different engineering design requirements. Target designs have been developed based on these studies and the engineering analyses have been performed including heat transfer, thermal hydraulics, thermal stresses, and material requirements. The target geometrical configuration has been designed to maximise the neutron utilisation in the subcritical assembly and to match the geometry of the fuel assemblies. The neutron flux distribution of the subcritical assembly design has been examined as a function of uranium fuel enrichment, uranium density, reflector material selection, reflector thickness, and target material for k_{eff} of ~0.98. The facility design is configured to maximise its utilisation by using simple and efficient procedures for its operation and maintenance, to ensure safety, reliability, and environmental considerations and to allow future upgrades and new functions. The medical isotope production capability of the facility has been analysed to define the irradiation locations and the sample sizes for about 50 radioactive isotopes. This paper highlights the current facility design, the key results from the design analyses and the current status of the facility.

Main components

The neutron source facility consists of several components, which are integrated for steady-state operation. The main components are the target assembly, the subcritical assembly, the biological shield, and the radial neutron ports. Auxiliary components are also designed to support the operation including cooling loops, fuel loading machine, removable biological shield for accessing the subcritical assembly and the target assembly, and cold neutron source. The main components are presented with their key performance parameters.

Target assembly

Several studies have been carried out to investigate the target design choices and the accelerator beam parameters for a satisfactory design and an acceptable operating performance. The main focus is to maximise the neutron production from the 100 KW beam power. The target design has been configured to operate satisfactorily with 100 MeV electrons. The MCNPX computer program [29] is utilised to determine the neutron source intensity, the neutron spectrum, the spatial neutron distribution, and the spatial energy deposition in the target assembly as a function of the beam parameters, the target materials, and the target design details. The Computational Fluid Dynamics (CFD) software packages STAR-CD [30] and STAR-CCM+ [31] are used for the thermal-hydraulics analyses. The coolant velocity profiles and the spatial temperature distributions in the target assembly have been studied using the spatial energy

deposition distributions obtained from the MCNPX analyses. The NASTRAN [32] structure analysis computer code has been used to calculate the thermal stresses in the target materials using the spatial temperature distributions from the CFD analyses. These analyses have been iterated to satisfy the temperature and the thermal stress limits for a satisfactory operation. Target designs have been developed based on the results of these studies and the engineering practices including nuclear physics, heat transfer, thermal hydraulics, structure, fabrication, and material requirements. Samples from the target studies are summarised in this section.

The electron beam generates x-rays with a continuous energy spectrum (Bremsstrahlung radiation) from the interactions with the target materials. These x-rays are absorbed in a variety of photonuclear reactions in the target materials and neutrons are produced from these reactions. Target materials with a high atomic number are required to maximise the neutron yield. In addition, high melting point, high thermal conductivity, chemical inertness, high radiation damage resistance, and low neutron absorption cross-section are the desirable properties for the target materials. The physics analyses of the possible target materials show that uranium, tungsten, lead, and tantalum produce the highest number of neutrons per electron. The physical properties of the uranium and tungsten materials, their neutron yields, and the operating experience from different accelerator facilities around the world led to their selection to generate neutrons. Tungsten has the highest melting point of all metals (~3422 C). Uranium target material produces the highest neutron yield per electron due to its photo-neutron reactions and the additional neutrons from the photo- and the neutron-fission reactions. The operating lifetime of uranium target is shorter relative to tungsten because of the extra swelling caused by fission gasses.

In order to characterise each target material, several performance parameters were analysed in this study. These parameters include total neutron yield, total energy deposition, neutron spectrum, neutron and energy deposition spatial distributions, and required target length. Each of these parameters has a particular role in defining the target performance and design. A high neutron yield enhances neutron source intensity, which defines the neutron flux level and the total power of the subcritical assembly. The target energy deposition influences the design of the target coolant system and the neutron yield. The neutron spectrum affects the system's effectiveness in performing material characterisations and producing medical isotopes. The spatial neutron distribution from the target determines the target position inside the subcritical assembly and the neutron source utilisation fraction. All these parameters were studied to define the target performance characteristics and the design configuration. The main geometrical parameters of the target designs which resulted from parametric and optimisation studies are shown in Table 1. The calculated neutron yields are 1.88×10^{14} and 3.06×10^{14} neutrons per second (n/s) using 100 KW electron beam power with the tungsten and the uranium target designs, respectively. Figure 1 shows the spatial energy deposition normalised to 2 KW/cm^2 power density on the beam window and the resulting temperature distribution in the tungsten target disks.

Heat transfer and thermal-hydraulics parametric studies were performed to help define the target mechanical configuration, the size of the water coolant channels, and the temperature distribution in the target materials. The 100-KW electron beam with ~2-KW/cm^2 uniform beam power density, the 7.5-m/s water coolant velocity inside the target manifold, and the 4-atm coolant pressure are used. The analyses showed that higher coolant velocity enhanced the target performance. The target material has a square geometry and its axis coincides with the electron beam axis. The flow direction of the water coolant is perpendicular to the target axis. This arrangement results in a stack of disks forming the target design. The water coolant channels between the target disks have a constant thickness of 1.75 mm. The average increase in the water coolant temperature is less than 5°C for the current coolant conditions. Each target disk is cooled from both sides to minimise thermal deformation. The target water coolant channels are

connected in parallel to the input and the output manifolds. The analyses defined the thickness of the different target disks for a subcooled boiling margin of 30 to 40°C. The uranium disks have a 0.7-mm aluminum clad to avoid water coolant contamination with fission products while the tungsten disks are coated with tantalum to improve corrosion resistance.

The results from the MCNPX studies using three-dimensional geometrical models were used for the CFD thermal-hydraulics analyses. The three-dimensional geometrical models account for the target design details. The CFD calculations were performed to define the thickness of each target disk. In these analyses, water velocity distribution was calculated for each coolant channel and spatial temperature profile was calculated for each target disk and each coolant channel using a single geometrical model for the target assembly and the three-dimensional MCNPX energy deposition results. Figure 2 shows the temperature profile in the uranium material for the 100 KW uniform beam using 100-MeV electrons. These temperatures fulfill the adopted temperature design criteria.

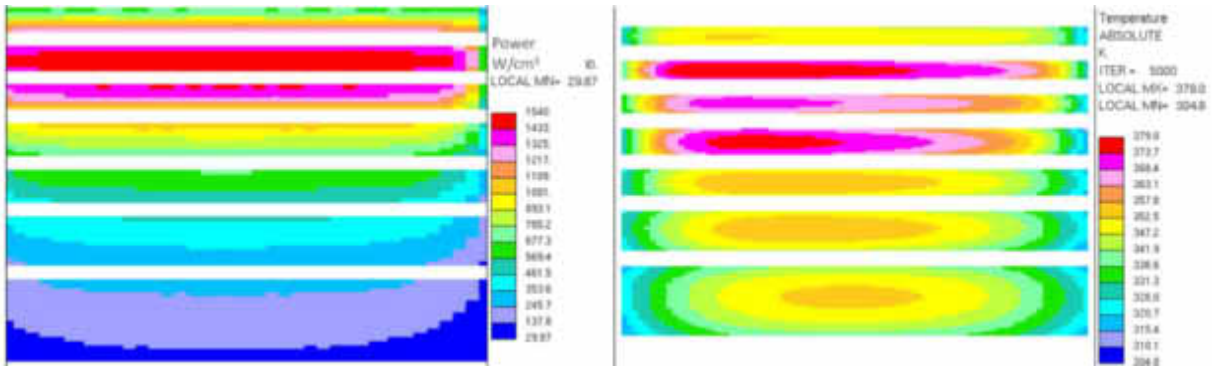
The three-dimensional model and the corresponding temperature profiles of the uranium and the tungsten targets were imported into NASTRAN computer code for thermal stress analyses. The intensity and distribution of the thermal stresses were evaluated for normal operating conditions. In the target design, the disks are allowed to expand in the radial and axial directions to reduce operating stresses. Thermal stress intensity distribution during the normal operation was evaluated. Although thermal stresses are secondary stresses, their maximum values are limited to a fraction of the material yield stress. This is a very conservative approach, leaving a large design margin to account for radiation damage and thermal-cycling effects. These effects are important to define the target operating lifetime. The tungsten target results show the peak thermal stress is less than 100 MPa.

Table 1. Target design parameters

Beam Power:	100 kW
Distribution:	Uniform
Electron Energy:	100 MeV
Beam Size:	64 × 64 mm
Target Plate:	66 × 66 mm
Coolant:	Water
Pressure:	5 atm
Inlet Temperature:	20.0 C
Outlet Temperature:	24.1C

Channel Number	Tungsten Target			Uranium Target		
	Water Channel Thickness mm	Target Plate Thickness mm	Clad Thickness mm	Water Channel Thickness mm	Target Plate Thickness mm	Clad Thickness mm
0	1.0			1.0		
1	1.75	3.0	0.25x2	1.75	3.0	0.7 ×2
2	1.75	3.0	0.25x2	1.75	2.5	0.95 ×2
3	1.75	3.0	0.25x2	1.75	2.5	0.95 ×2
4	1.75	4.0	0.25x2	1.75	2.5	0.95 ×2
5	1.75	4.0	0.25x2	1.75	3.0	0.7 ×2
6	1.75	6.0	0.25x2	1.75	3.0	0.7 ×2
7	1.0	10.0	0.25x2	1.75	4.0	0.7 ×2
8				1.75	5.0	0.7 ×2
9				1.75	7.0	0.7 ×2
10				1.75	10.0	0.7 ×2
11				1.0	14.0	0.7 ×2
Total	12.5	33.0	3.5	19.5	56.5	16.9

Figure 1. Power density distribution (left) and temperature distribution (right) in tungsten target disks



Subcritical assembly

Parametric studies were performed to maximise the neutron flux of the subcritical assembly with an effective neutron multiplication of <0.98. Different fuel designs, uranium enrichments, and reflector materials were considered. The target assembly is placed at the subcritical assembly centre. LEU with <20% ^{235}U and HEU with 90% ^{235}U were analysed with two uranium densities of 1.0 and 2.7 g/cm^3. The analyses focused on the possibility of utilising LEU fuel instead of HEU fuel without penalising the neutron source facility performance. Three-dimensional models of the subcritical assembly, including the detailed target design, were developed to define the subcriticality level and the neutron flux distribution. The target and the fuel assemblies are explicitly modelled without any geometrical approximation or material homogenisation to obtain an accurate performance characterisation. The MCNPX computer code with continuous energy data libraries and S (α,β) thermal data was used for the analyses. Three reflector materials, beryllium, water, and carbon were considered. Parametric analyses were performed to assess the number of fuel assemblies required to get k_{eff} of ~0.98 for different combinations of the reflector and target materials, fuel densities, and fuel enrichments. The corresponding neutron fluxes were also calculated.

The results show that the use of the uranium target requires the smallest number of fuel assemblies to achieve the desirable k_{eff} value. This small number of assemblies is due to the extra neutron multiplication produced from the natural uranium target material. The subcritical configurations with water reflector require a larger number of fuel assemblies as compared to the configurations with beryllium and carbon reflectors, because of the neutron absorption in the water. The very small number of fuel assemblies limits the subcritical assembly flexibility to study different geometrical configurations. In addition, the fuel assembly arrangements with beryllium reflector and uranium target are significantly asymmetric. The fuel design of the Kiev research reactor with low-enriched uranium (LEU) produced higher neutron flux relative to other fuel designs.

In order to compare the performance of the subcritical assembly for irradiation experiments with the LEU and the HEU fuels, the average neutron flux values in different locations were calculated. The results show that no significant difference between the subcritical assemblies with HEU and LEU fuels was observed. However, the HEU subcritical assembly has an extremely small number of fuel assemblies, which limits its utilisation for reactor physics experiments, generates difficulties for reactivity measurements, and calibration procedures. Consequently, it is desirable to use the LEU fuel instead of the HEU fuel to avoid such difficulties.

The calculated neutron spectra in the fuel region of the subcritical assembly show that about half of the neutrons have energies below 100 keV and the other half are in the energy range of 100 keV to 20 MeV. The neutron fraction with energy above 20 MeV is very small but impacts the biological shield design. The use of uranium instead of tungsten as a target material doubles the neutron flux intensity because of the higher neutron yield, as shown from the target analyses. The use of beryllium or carbon reflectors produces higher neutron flux relative to the water reflector. A beryllium-carbon hybrid reflector design is utilised to provide flexibility to change the subcritical assembly configuration since a beryllium assembly can replace a fuel assembly. In addition, the fabrication of high density carbon blocks is difficult and expensive relative to beryllium blocks. A carbon reflector ring is used around the beryllium reflector.

Figure 2 shows the MCNPX geometrical model of the subcritical assembly with uranium target, LEU fuel, and beryllium-carbon reflector while Figure 3 presents the subcritical assembly configurations with tungsten and uranium targets. The main parameters of the two subcritical configurations are listed in Table 1 including the effective neutron multiplication factors, the average neutron flux in the target coolant channel and the first fuel ring, and the energy deposition. Figure 4 shows the energy deposition distribution in the different materials of the subcritical assembly with the uranium target from the 100-KW electron beam. Figure 5 shows the corresponding total neutron flux distributions.

Table 2. Effective neutron multiplication factor, average neutron flux and energy deposition values using beryllium-graphite reflector and 100 kW/100 MeV electron beam

Target	# of FAs	k_{eff}	Average neutron flux (n/cm^2·s)		Target energy deposition (kW)	Subcritical energy deposition (kW)	Reflector energy deposition (kW)	Total energy deposition (kW)
			First fuel ring	Target coolant channel				
W	38	0.95686 ±0.00013	6.281e+12 ±0.26 %	7.873e+12 ±0.23%	85.70 ±0.01%	69.19 ±0.24%	5.84 ±0.13%	160.73
U	37	0.97547 ±0.00012	1.965+13 ±0.26 %	2.470e+13 ±0.25%	90.57 ±0.01%	196.89 ±0.35%	11.57 ±0.19%	299.04

Figure 2. MCNPX geometrical model of the subcritical assembly, X-Y cross-section on the left and X-Z cross-section on the right

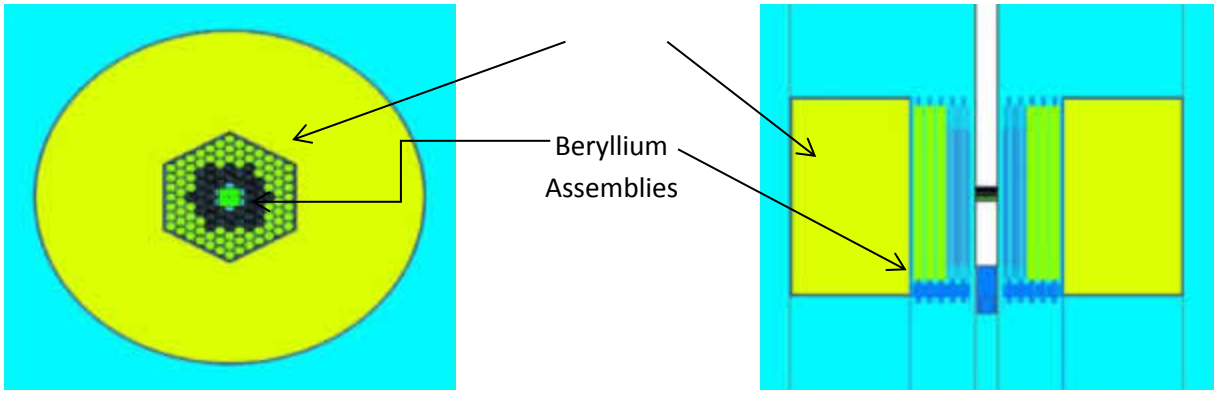
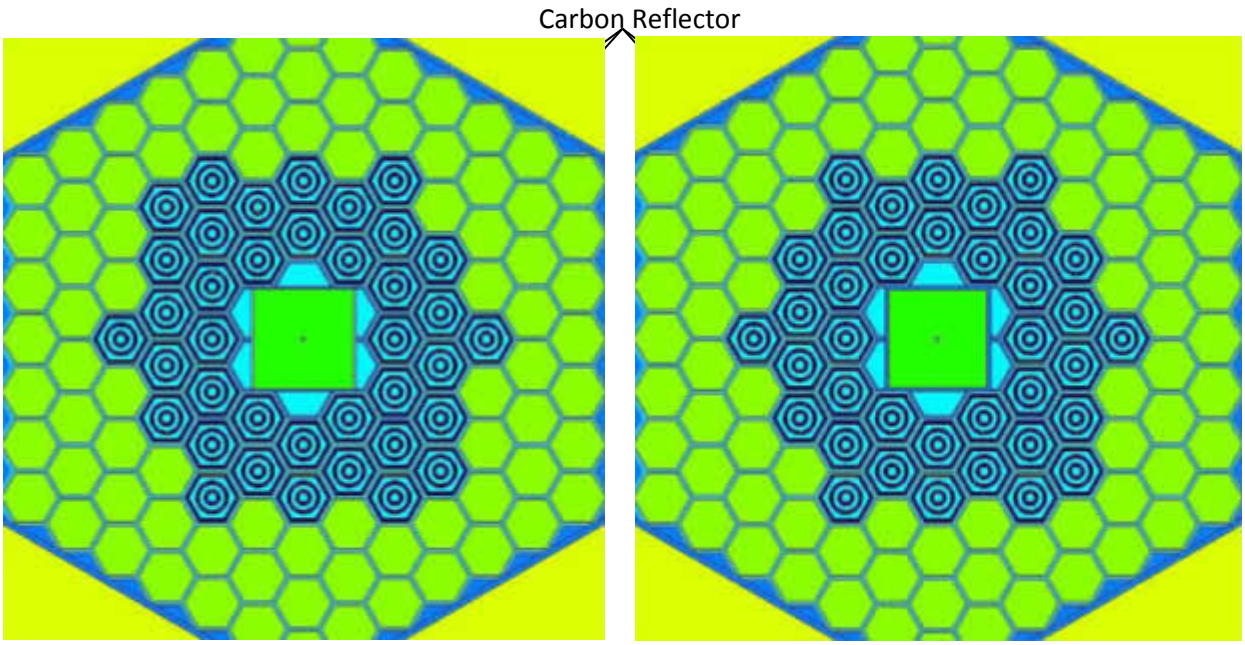


Figure 3. Subcritical assembly configurations with tungsten target on the left and uranium target on the right with beryllium-graphite reflector



Uranium target with 37 fuel assemblies loaded.

Preliminary linac tunnel dimensions.

Figure 4. Subcritical assembly configurations with tungsten target on the left and uranium target on the right with beryllium-graphite reflector

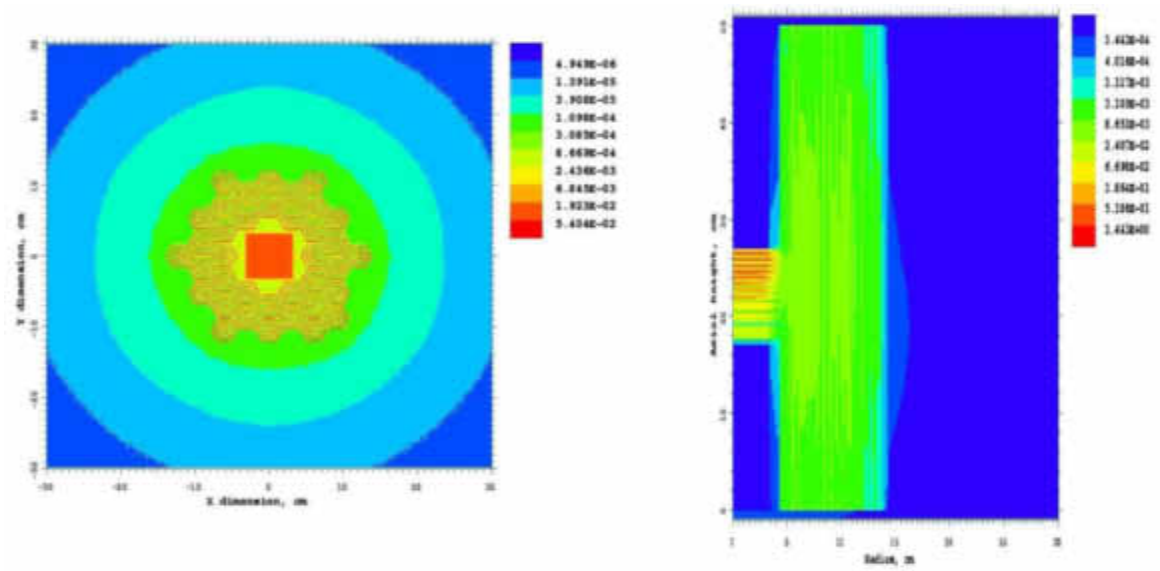
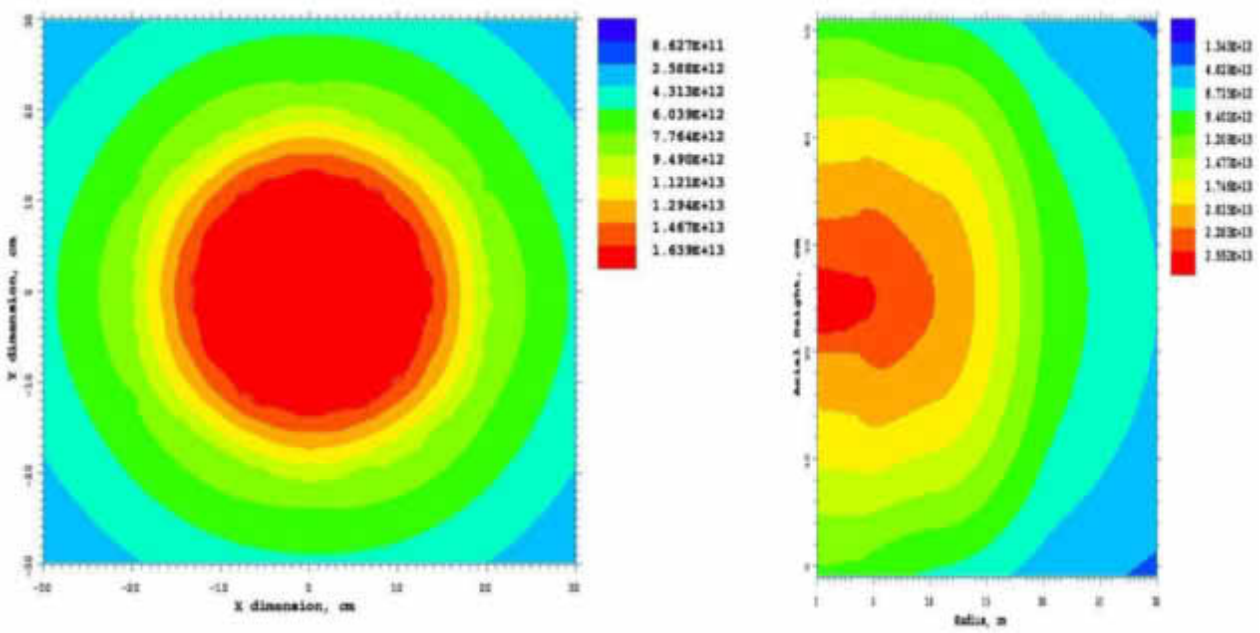


Figure 5. Total neutron flux distributions, X-Y map on the left, and X-Z map on the right for the subcritical assembly configuration with uranium target and 100-KW electron beam power



Biological shield

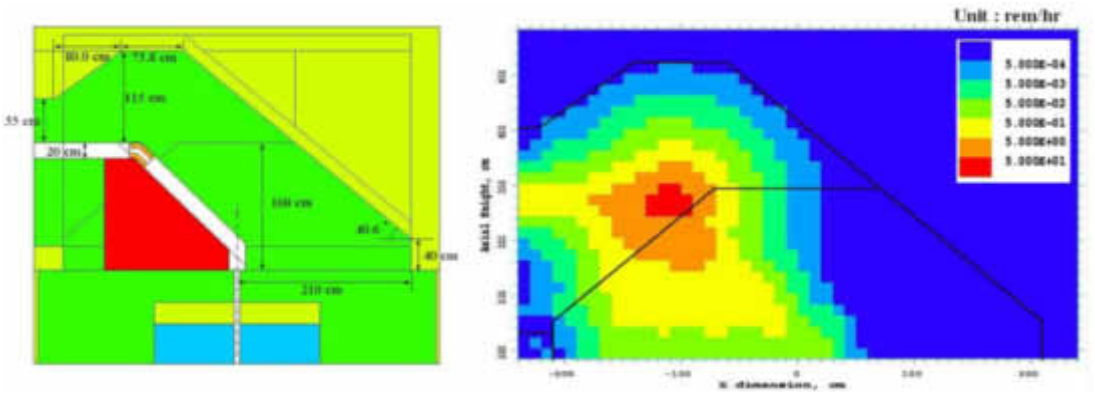
Biological shielding analyses have been performed to define the shield thickness to permit personal access to the subcritical assembly during operation. The shielding design criterion limits the biological dose to <2.5 mrem/hr. Such dose value allows the worker to have 40-hour working week without exceeding the allowable international exposure limit. In the design analyses, this value is reduced by a factor of 5 to account for uncertainties in the nuclear data, the calculational method, and the modelling details. Elaborate three-dimensional models have been developed to perform the shielding analyses with MCNPX starting with the electron beam. The biological shield of the subcritical assembly has two main sections, radial and top sections. The top section includes the top cover of the subcritical assembly and the biological shield of the electron beam.

The parametric shielding results showed that the use of a steel shield zone in front of the heavy concrete has a small impact on the biological dose and the shield thickness. The heavy concrete density is 4.8 g/cm^3 and it is the selected shielding material to reduce the cost and simplify the fabrication. In the radial direction, a shielding thickness of 140 cm is required to reduce the total (neutron and photon) biological dose to 0.5 mrem/hr, as shown in Table 3. On the top of the subcritical assembly, the water coolant in the subcritical assembly pool acts as a shielding material, which reduces the required heavy concrete shield thickness. However, the radiation streaming from the beam tube and the electron beam losses at the bending beam magnet complicate the shielding design in this area. The electron beam losses define the required shield thickness of the top section. Figure 7 shows the calculated dose map and the required shield dimensions at the top section due to 80-W electron beam losses at the first bending magnet.

Table 3. Calculated biological dose values around the subcritical assembly with uranium target during operation with 100-KW beam power and 140 cm of heavy concrete radial shield thickness

Radiation source	Radiation biological dose (mrem/hr)
Neutron	0.206 ± 7.24%
Photon	0.056 ± 4.63%
Total	0.262

Figure 6. Main dimensions of the biological shield top section on the left and the corresponding total biological dose map on the right



Neutron source facility design

The subcritical assembly facility uses proven techniques and practices for its design, operation, and maintenance to enhance its utilisation. The main facility components are the target assembly, the subcritical assembly, the biological shield, and the auxiliary supporting systems. Figure 8 shows a quarter cut isometric view of the subcritical assembly design where the main components are viewed, including the target assembly, the fuel assemblies, the beryllium reflector assemblies, the carbon ring reflector, the fuel machine arm, the storage racks, and the support grid. The loading and unloading of the fuel assemblies, beryllium reflector assemblies, and irradiation cassettes are performed without opening the biological shield. Replacing the target assembly requires opening the top shield sections without removing the top cover of the subcritical assembly.

Figure 8 shows the overview of the neutron source facility. It includes the accelerator building, the subcritical assembly hall, the attached laboratory building, the secondary coolant towers, and the electrical power station to operate the facility. Medical isotopes and material testing glove boxes, water distillation facility, back-up diesel generator units, temporary spent fuel and used target storage pool, and temporary liquid radioactive waste storage are included in the design. At the time of writing this paper, the facility was under construction and the expected start-up date was planned for March 2014.

Figure 7. Quarter cut isometric view of the subcritical assembly design

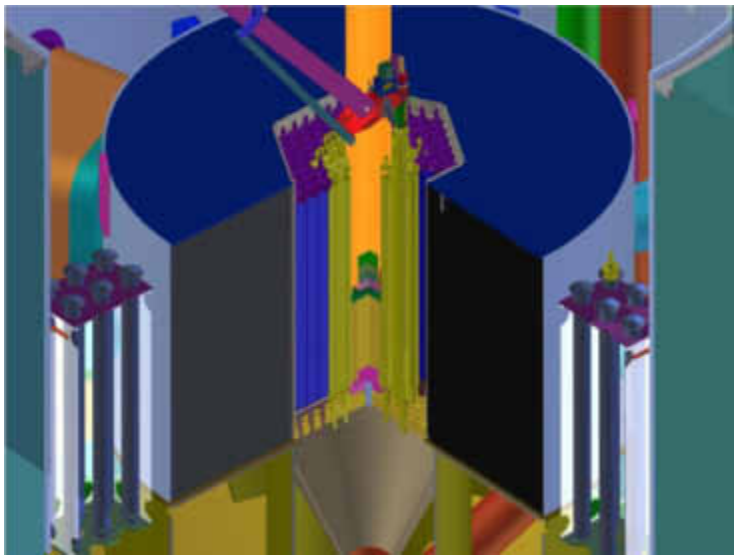


Figure 8. Isometric view of KIPT accelerator-driven system facility



Conclusion

The design of the KIPT accelerator-driven subcritical assembly facility has been successfully developed using 100 KW – 100 MeV electron accelerator within the collaborative activity between ANL and KIPT. The facility is designed with the low-enriched uranium fuel design of the Kiev's Research Reactor. The developed design satisfies the facility objectives and it has flexibility for future upgrades and new functions. It has excellent capabilities to produce medical isotopes, perform basic research using its radial neutron beams, perform physics studies, and train young nuclear scientists. At the time of writing this paper, the facility was under construction and the expected start-up date was palnned for March 2014.

Acknowledgements

Argonne National Laboratory's work was supported by the U.S. Department of Energy, Office of Global Nuclear Material Threat Reduction (NA213), National Nuclear Security Administration of U. S. Department of Energy.

References

[1] Gohar, Y., Bailey, J., Belch, H., Naberezhnev, D., Strons, P., Bolshinsky, I. (2004), "Accelerator-Driven Subcritical Assembly: Concept Development And Analyses", *Proceeding of The RERTR-2004 International Meeting on Reduced Enrichment for Research and Test Reactors*, Vienna, Austria.

[2] Gohar, Y., Bolshinsky, I., Naberezhnev, D.G., Duo, J., Belch, H., Bailey, J. (2005), "Accelerator Driven Subcritical Facility: Conceptual Design Development", *AccApp05,* 29 August-1 September 2005, Venice, Italy.

[3] Naberezhnev, D.G., Gohar, Y., Bailey, J., Belch, H. (2005), "Physics Analyses of Accelerator Driven Subcritical Assembly", *AccApp05,* 29 August-September 1 2005, Venice, Italy.

[4] Gohar, Y., Bolshinsky, I., Naberezhnev, D., Duo, J., Belch, H., Bailey, J. (2006), "Accelerator Driven Subcritical Facility: Conceptual Design Development"*, Nuclear Instruments and Methods in Physics Research A,* Volume 562, Page 870-874.

[5] Naberezhnev, D.G., Gohar, Y., Bailey, J., Belch, H. (2006), "Physics Analyses of Accelerator Driven Subcritical Assembly", *Nuclear Instruments and Methods in Physics Research* A, Volume 562, Page 841-844.

[6] Gohar, Y., Bolshinsky, I., Belch, H., Naberezhnev, D., Sofu, T., Talamo, A., Zhong, Z. (2007), "Accelerator Driven Subcritical Facility Design Concept", *the 8th International Topical Meeting on Nuclear Applications and Utilization of Accelerators (AccApp07),* Pocatello, Idaho, US.

[7] Talamo, A., Gohar, Y., Naberezhnev, D. (2007), "MCNPX Analysis Of The Medical Isotope Production In The Kharkov Electron Driven Subcritical Facility", *the 8th International Topical Meeting on Nuclear Applications and Utilization of Accelerators (AccApp07)*, Pocatello, Idaho, US.

[8] Sofu, T., Gohar, Y., Belch, H., Zhong, Z., Naberezhnev, D. (2007), "Neutronic, Thermal-Hydraulic, And Structural Analyses of The Electron Target For An Accelerator-Driven Subcritical System", *the 8th International Topical Meeting on Nuclear Applications and Utilization of Accelerators (AccApp07),* Pocatello, Idaho, US.

[9] Gohar, Y., Bolshinsky, I., Belch, H., Sofu, T., Talamo, A., Zhong, Z. (2007), "Design and Analyses of KIPT Electron Accelerator Driven Subcritical Assembly Facility Concept", *the 20th International Workshop on Charged Particle Accelerators, the Accelerator Driven Subcritical Assemblies Workshop*, Alushta, Ukraine.

[10] Belch, B., Gohar, Y., Sofu, T., Zhong, Z. (2007), "Conceptual Design Configuration for Electron Accelerator Driven Subcritical Assembly", *the 20th International Workshop on Charged Particle Accelerators, the Accelerator Driven Subcritical Assemblies Workshop*, Alushta, Ukraine.

[11] Sofu, T., Gohar, Y., Belch, H., Naberezhnevthe, D. (2007), "Multi-Physics Analysis of an Electron Target for the KIPT Subcritical Assembly", *the 20th International Workshop on Charged Particle Accelerators, the Accelerator Driven Subcritical Assemblies Workshop,* Alushta, Ukraine.

[12] Talamo, A., Gohar, Y. (2008), "Production of Medical Radioactive Isotopes Using KIPT Electron Driven Subcritical Facility", *Applied Radiation and Isotopes* 66, 577–586.

[13] Gohar, Y., Bolshinsky, I., Nekludov, I.M., Karnaukhov, I.M. (2008), "Ukraine Experimental Neutron Source Facility", *the 2nd International Conference on Current Problems in Nuclear Physics and Atomic Energy (NPAE-2008)* Kiev, Ukraine.

[14] Talamo, A., Gohar, Y. (2008), "Medical Isotopes Production Analyses of the Kharkov Electron Driven Subcritical Assembly", *American Nuclear Society Annual Meeting*.

[15] Zhong, Z., Gohar, Y. (2008), "KIPT Accelerator Driven Subcritical Facility Shield Design", *American Nuclear Society Annual Meeting*.

[16] Zhong, Z., Gohar, Y., Naberezhnev, D.G., Duo, J. (2008), "Shielding Analysis and Design of the KIPT Experimental Neutron Source Facility of Ukraine", Argonne National Laboratory Report, ANL-NE-08/23.

[17] Sofu, T., Gohar, Y., Zhong, Z., Belch, H., Naberezhnev, D. (2008), "Target Design Optimization for an Electron Accelerator Driven Subcritical Facility with Circular and Square Beam Profile", Argonne National Laboratory Report, ANL-NE-08/25.

[18] Zhong, Z., Gohar, Y., Kellogg, R. (2008), "Physics Design of a Cold Neutron Source for KIPT Neutron Source Facility", Argonne National Laboratory Report, ANL-08/36.

[19] Zhong, Z., Gohar, Y., Talamo, A. (2009), "Burnup Calculations for KIPT Accelerator Driven Subcritical Facility Using Monte Carlo Computer Codes – MCB and MCNPX", Argonne National Laboratory Report, ANL-09/07.

[20] Zhong, Z., Gohar, Y., Talamo, A. (2009), "MCNPX and MCB Coupled Methodology for the Burnup Calculation of the KIPT Accelerator Driven Subcritical System", *International Conference on Mathematics, Computational Methods and Reactor Physics (M&C 2009),* Saratoga Springs, New York, US.

[21] Zhong, Z., Gohar, Y., Kellogg, R. (2009), "KIPT Cold Neutron Source Physics Analyses", *American Nuclear Society Annual Meeting*.

[22] Gohar, Y. (2009), "Experimental Neutron Source Facility Based on Accelerator Driven System", *Proceeding of the Workshop on Applications of High Intensity Proton Accelerators,* Fermilab, 19-21 October 2009, ISBN-13 978-981-4317-28-3, Chicago, US.

[23] Zhong, Z., Gohar, Y. (2009), "Fuel Cycle Analyses of the KIPT Neutron Source Facility With Low-Enriched Uranium Fuel", *RERTR 2009 – 31st International Meeting on Reduced Enrichment for Research and Test Reactors*, Beijing, China.

[24] Zhong, Z., Gohar, Y., Belch, H., Sofu, T. (2009), "Biological Shield Design and Analysis of KIPT Accelerator Driven Subcritical Facility", *Nuclear Technology*.

[25] Zhong, Z., Gohar, Y., Talamo, A. (2011), "Analysis of Fuel Management in the KIPT Neutron Source Facility", *Annals of Nuclear Energy*.

[26] Zhong, Z., Gohar, Y. (2011), "Shielding design and analyses of KIPT neutron source facility", *Progress in Nuclear Energy,* Volume 53, Issue 1, January 2011.

[27] Zhong, Z., Gohar, Y. (2012), "Use of a Neutron Source File in MCNPX Shielding Calculation for an Electron Accelerator Driven Facility", *PHYSOR 2012 – Advances in Reactor Physics*, 15-20 April 2012, Knoxville, Tennessee, US.

[28] Zhong, Z., Gohar, Y. (2013), "Accelerator Shield Design of KIPT Neutron Source Facility", *International Conference on Mathematics and Computational Methods Applied to Nuclear Science & Engineering (M&C 2013),* 5-9 May 2013, Sun Valley, Idaho, US.

[29] MCNPX Version 2.5.0 User's Manual (LA-CP-05-0369) Los Alamos National Laboratory, (http://mcnpx.lanl.gov/) April 2005.

[30] II.3.2 "User Guide, STAR-CD 4.08", CD-ADAPCO, 2009, Mellville, NY, US.

[31] II.3.3 "User Guide, STAR-CCM+ 5.06", CD-ADAPCO, 2010, Mellville, NY, US.

[32] MSC NASTRAN and MARC User's Manual, (http://www.mscsoftware.com/), MSC Software Corporation, Santa Ana, CA.

A multi-megawatt compact neutron – source for ADS

Karel Samec
CERN, Geneva, Switzerland

Abstract

The development of high-power liquid-metal neutron sources is continuing in Switzerland, in the context of the TIARA FP7 research programme. A design is being proposed which draws on the combined experience from programmes previously conducted in Switzerland such as MEGAPIE and EURISOL. The neutron source is a key component in an accelerator-driven system, or ADS, requiring it to be safe, reliable and capable of absorbing vast amounts of heat from the high-power proton beam in a very small volume so as to provide a dense neutron field to the subcritical blanket.

The current work presents a neutron source concept able to operate safely under beam power levels of several megawatts. Key to the novel design is a conical concave thin-gauge beam window optimised for low stress as well as the implementation of multiple barriers to mitigate the consequences of an eventual failure in any component. In terms of the neutronic performance, the chosen configuration presents minimal neutron losses from the central spallation zone, an important consideration for the neutron economy. The overall design is based on a "matriošk a" concept in which successive components are enclosed within one another, thus allowing rapid assembly and maintenance and at the same time ensuring that the most active components are safely shielded by multiple barriers.

Introduction

In the description of an "Energy Amplifier" or Accelerator-driven System [1], C. Rubbia laid out the plan for a nuclear reactor in which the usual method of controlling a nuclear chain reaction, the proportion of delayed neutrons, would be replaced by a central neutron source. The neutron source surrounded by a subcritical nuclear fuel core would provide the additional neutrons needed to keep the fission process in equilibrium. In a subsequent article [2], presenting an abridged version of the concept, the author summarised the three main components of an ADS as:

- accelerator;
- energy producing tank;
- fuel fabrication and reprocessing.

The "energy producing tank" comprises the subcritical core and the spallation source at its centre. The power of the source envisaged in these early studies was approximately 10 [MW], leading to a thermal power of the reactor of 1.5 [GW]. The power deposition in the window was estimated at 1[kW/cm^3] with a fairly wide proton beam characterised by a Gaussian profile of $2\sigma = 15$ [cm]. The author highlighted the necessity to keep the beam window thickness below 1.5 [mm], in order to keep stresses and temperatures at a safe level.

Since these early proposals were made, tests have been conducted on various neutron spallation source concepts. A test of a liquid metal neutron source under proton beam irradiation was conducted in 2006 with the MEGAPIE experiment at 0.76 [MW] of beam power. The 4-month test showed that the concept was viable [3], although some practical difficulties arose in relation to a faulty heat exchanger. Later in 2009, a more compact liquid metal neutron source EURISOL was designed for operations under a 4 [MW] proton beam [4] and tested at full-scale in representative hydraulic conditions but without beam irradiation [5]. The latter test was successful in validating the design of a very thin concave shaped beam window capable of withstanding a multi-megawatt beam with a very small footprint (2σ = 5[cm]), which could result in very high neutron fluxes in the range of ~10^{15}[n/cm^{2}s].

The neutron spallation source envisaged in the current paper draws on experience gained from both programmes and proposes a solution for designing a safe and compact high-power neutron spallation source.

Lessons learnt from past research programmes

The design proposed draws heavily on the experience obtained recently in the test mentioned above. The MEGAPIE test [3] registered a significant success for a first-of-a-kind megawatt-class spallation source, notably the ability of the safety-critical beam window to withstand very high thermal loads and high dpa (displacement per atom) values. The irradiation over a period of 4 months reached 10 dpa on the window and would have led to a high degree of embrittlement. This point is still being investigated in the post-irradiation part of the MEGAPIE programme. The overall configuration of the MEGAPIE source is that of an elongated cylinder, 4 metres in length impacted by a proton beam from below. This configuration was originally chosen to allow natural convection of the liquid metal in the target as the heat exchangers are situated at the top of the target. However, later on in the development, serious doubts arose as to the coolability of the target window under such natural convection conditions and the idea was dropped. Instead, the flow was driven by an electromagnetic pump, which proved utterly dependable in the test.

A second source of inspiration for the proposed design is the EURISOL liquid metal spallation neutron source, which featured a concave conical beam window, only 0.8 mm thick, as described in [4]. Despite the thinness of the target beam window, the specially developed hyperbolic profile and tapered thickness allowed the source to be tested hydraulically at full power without undergoing any failure [5]. A mass flow rate of 150 kg/s flowed through the central 6 cm diameter guide tube, resulting in speeds as high as 6 m/s in the liquid metal. No beam irradiation was tested, however, the flow rate was high enough to cool and evacuate a beam of 4 MW. The lessons learnt from these two tests are summed up in Table 1 and Figure 1 shows the two designs for comparison.

Figure 1. MEGAPIE source (left in transport cask) and EURISOL source (right on hydraulic test stand)



Table 1. Lessons learnt from testing liquid-metal spallation neutron sources

Relevance to	Lesson learnt
System	Multiple containment strategy is vital.
	Natural circulation is difficult to control.
	Leaks will occur and must not flow into the path of the beam.
	Leak analysis and mitigation strategy must be planned ahead.
	No organic cooling liquid should be used inside a source.
	Design supported by multi-physics codes is reliable.
Component	Calibrated electro-magnetic pumps are reliable.
	Novel concave beam window is effective.
	T91 (316) stainless steel is an appropriate material choice.
Monitoring	Flow-meter instrumentation must be diversified.
	Instrumentation is needed both inside and outside the source.
	Ensure leak detection using diverse sensors.
	Pressure transducers and thermocouples are resilient.

Essential principles of the new proposed design

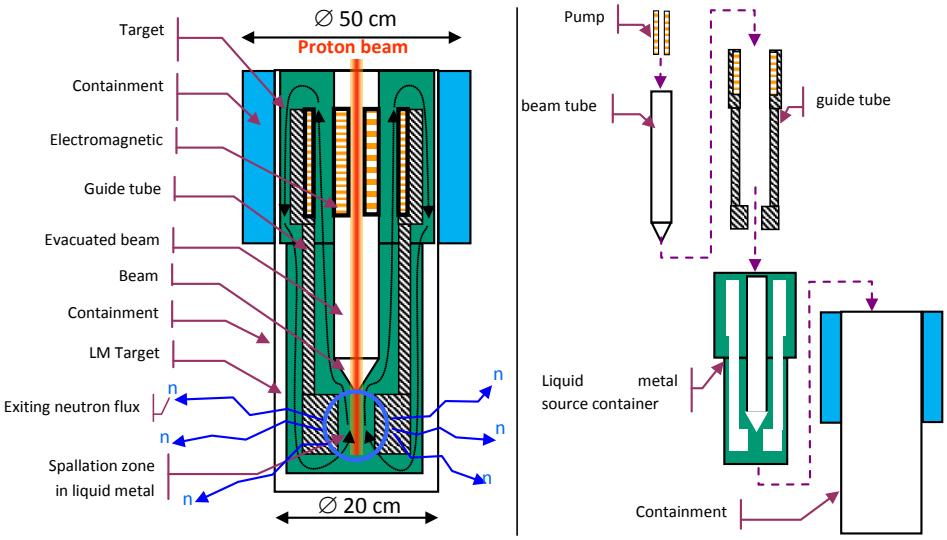
The "matrioška" principle alluded to in the introduction, refers to a system of successive confinements that would mitigate leaks from the central source of radioactivity in the event of an accident. It is also a design concept facilitating rapid assembly or disassembly.

For greater clarity, Figure 2 shows the design principle schematically. The complete actual engineering design is shown fully in the next section. The schematic below gives but an approximate overview of the main advantages of the proposed design, and is completed thereafter with a few details of the engineering aspects.

The source is divided into an upper part which contains a heat exchanger and a pump and a lower part, where the beam impacts the liquid metal, releasing spallation neutrons. This division is the same as in MEGAPIE. However, the new proposed design separates completely the secondary circuit and the pump from the primary circuit located inside the source containment, which is essentially an inert container with no active components. Robustness is thus enhanced since the primary circuit contains the highest activity but it contains no wiring for the pump or direct interface with the secondary fluid as was the case in MEGAPIE.

Maintainability is also addressed by the proposed design by separating each functionality of the source into distinct successive compartmentalised vessels which slide into each other in a vertical position from the top. Using simple guiding techniques, this method is by far the most convenient for precisely interfacing the successive cylindrical vessels within one another.

Figure 2. Proposed high-power neutron source: operation (left), assembly procedure for maintenance (right)



Improvements

Enhanced ability to handle beam trips

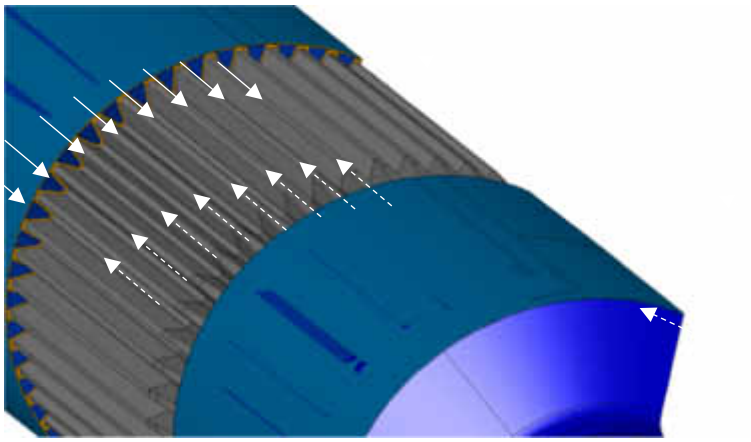
The vertical configuration has been retained in the proposed new design shown in Figure 2, inspired by MEGAPIE. However, unlike MEGAPIE, the proton beam does not come from below the source, instead, it is channelled down a central tube inside the source through a conical concave beam window taken from EURISOL and impacts the liquid metal in the bottom part of the source. Such a configuration allows a gentle coast-down in the event of a pump trip since natural circulation driven by the proton beam impacting the source in the bottom section will continue to cool the window. Hence it is not necessary to immediately switch off the beam in the event of a pump trip, there would be sufficient time to either restart the pump or take corrective action which can terminate operation with an orderly beam shut-down if all else fails.

Conformal ribbed external heat exchanger

The heat exchanger in MEGAPIE has been traced as the source of the graphite contamination which was placed in the containment upon inspection post-irradiation. The heat exchanger placed in the new design offers significant improvements.

The ribbing showed in the figure below creates a considerably larger exchange surface area in a relatively small space. In this manner it is not necessary to increase, by a great amount, the heat transfer coefficient or the temperature gradient between the primary and secondary circuit, which results in a greater flexibility as to the choice of the coolant on the secondary side.

Figure 3. Conformal ribbed external heat exchanger



Primary circulation: dashed arrows in grey ribs , secondary circulation: full arrows in blue ribs.

Hence the secondary circuit employs no organic fluids. Liquid metals such as LBE, gallium or conventional water are all possible due to the presence of a gap between the secondary and primary fluid, which excludes the possibility of an interaction in the event of a vessel rupture on either side. Indeed, the secondary fluid is located in the channels of the heat exchanger, which is a conformal part of the upper inner portion of the containment. It is physically separated from the matching primary side of the heat exchanger situated on the outer upper surface of the source and separated by a gas gap 1 mm thick. Since the two circuits do not share a common wall, like with the steam generators of a conventional Nuclear Power Plant (NPP), it is not possible for activity from the primary circuit to leak into the circuit as this would require multiple failures, an unlikely event (its likelihood being the multiplication of the two likelihoods of either leak).

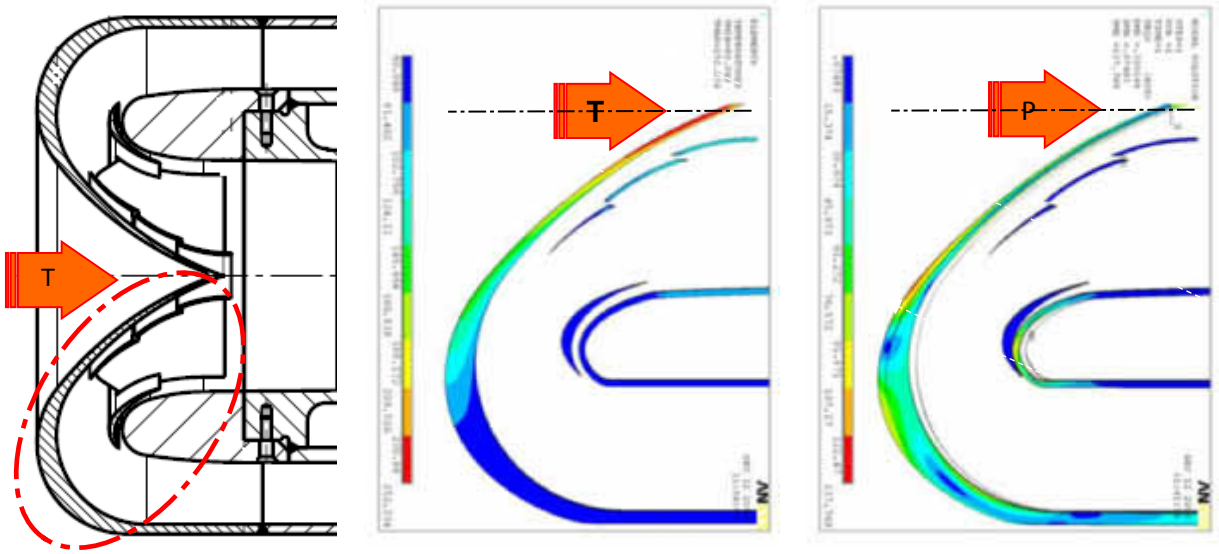
The gas also serves as a leak detector – any pressure change indicating a leak- and as a means of controlling the heat transferred from the primary to the secondary side. It acts as a self-adjusting mechanism since any increase in temperature inside the source will lead to the swelling of the primary surface, which will close the gap and increase heat exchange to the secondary side.

Low stresses due to a concave beam window

The beam window is impacted by the proton beam as it drives through the source into the liquid metal contained inside. Its importance as a barrier is due to the presence of active compounds inside the source and the maintenance of vacuum in the beam tube. The beam tube is a major containment bypass in an ADS facility needing adequate protection. Although some ADS designs purport to do away with a window by envisaging impacting a film of liquid metal with the beam directly, it seems doubtful that abandoning such an important barrier would meet the necessary safety requirements.

Beam window coolability is therefore paramount to its integrity and in the current design this has been achieved by tapering the local thickness down to a minimum of 0.8 mm and adopting a hyperbolic curve for the window profile to give it structural stability against internal pressure. Figure 4 shows a section of the beam window and the corresponding temperature and stress profile under a 25 mm-sigma Gaussian profile proton beam. A larger profile can lead to lower stresses.

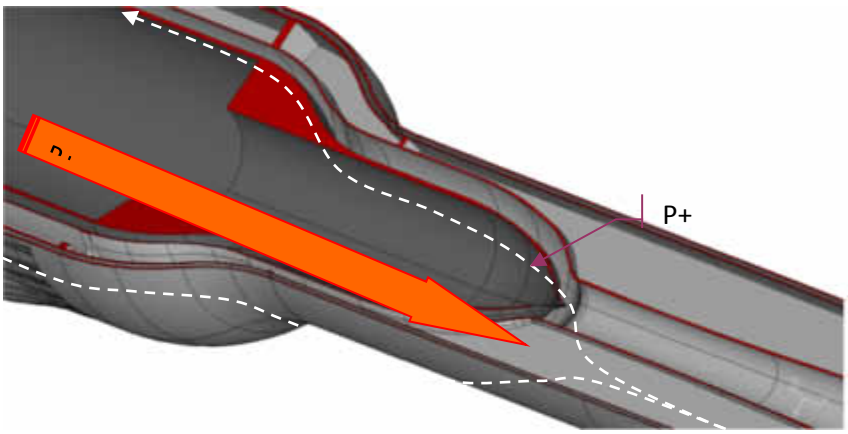
Figure 4. Concave window design (left) 15 cm in diameter, calculation results on an axis-symmetric model of the resulting temperature (centre) and stress (right) from a 4 MW beam with a σ = 2.5 cm



The maximum temperature for a low-temperature liquid metal such as mercury was shown in [4] to reach 250°C. Hence for lead-bismuth eutectic (LBE), the temperature would be approximately 100°C higher or 350°C. In the case of pure lead, the peak temperature in the window would reach 550°C, such temperatures are within the range that is admissible for T91 under irradiation. The stress shown in the left figure is a function of the temperature gradient through the beam window thickness, which does not change significantly according to the liquid metal used. Hence the peak total stress in the beam window, including membrane, bending and secondary thermal stresses reaches a peak of 135 MPa, below the admissible at high dpa, which is approximately 200 MPa at 550°C.

Figure 5 shows the implementation of the concave beam window in the proposed new design. The direction of the flow in this design is towards the pointed concave window whereas in EURISOL it was the opposite. The cooling effect remains the same and thereofore, stresses are also similar.

Figure 5. Concave window implementation in new proposed design



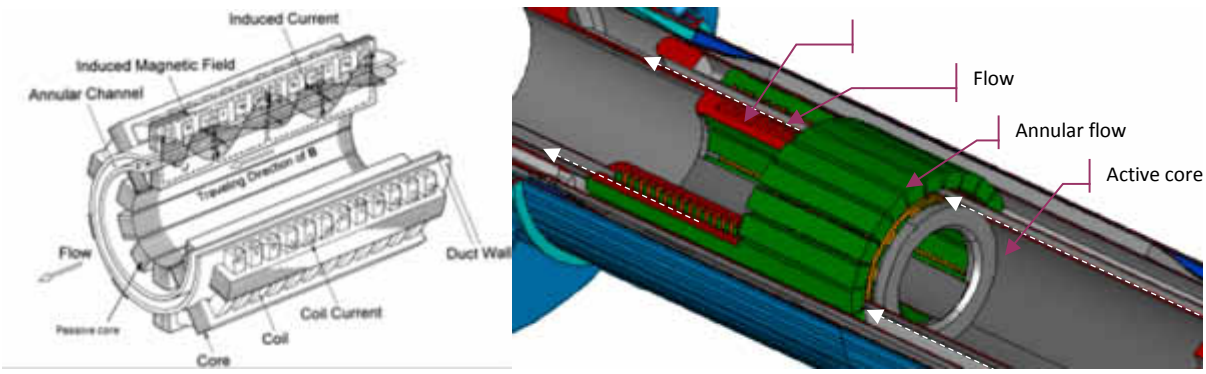
Robustness against beam window failure

An eventual rupture of the beam window due to material fatigue or beam over-focusing would result in a partial flooding of the central tube inside the source, up to 1/2 of the height but would not leak into the beam tube of the accelerator and would not impact any containment and thus cannot result in any bypass of the containment. This is a great advantage compared to MEGAPIE, where any leak of the window would have impacted the containment, which could have ruptured. The entire beam tube would then have been contaminated, thus breaching all containment barriers and releasing activity into the environment. Furthermore, in the new design, progress of such an accident would be arrested. Any flooding of the central tube of the source would not impact the containment which is situated outside the source opposite the beam tube. In order for the beam to impact the containment, it would be necessary to first evaporate the entire liquid metal inventory inside the neutron source container which takes about five minutes if the full power of the beam (4 MW) is left on. This lapse of time is quite sufficient for a series of engineered safety systems to respond to a variety of diversified shutdown signals such as loss of flow inside the source container, overpressure in the containment, overpressure in the source beam tube, multiple temperature exceeds, and activity release inside the target beam tube.

Protection of the pumps

The pumps are of primary importance as the heat of the beam must be evacuated at all times and the window must be adequately cooled. The pump serves as the primary source driving the circulation of liquid metal, although the vertical configuration with the beam impacting the lower end of the source provides natural circulation of the liquid metal, sufficient to protect against pump trip at least for a short time. An electro-magnetic pump (EMP) of the type used in MEGAPIE or the current design consists in an active part with coils, through which circulates an alternating current, as well as a passive core without any wiring. Conventional EMPs (shown on the left in Figure 6) feature an annulus with the liquid metal flowing between two cylinders, an active core situated in the inner-most cylindrical shell and a passive core located on the outermost cylinder. This order has been inversed in the current design (see Figure 6 right), the reason being that by locating the active coils inside the innermost cylinder, it is possible to position these active electrical components outside the liquid metal container of the neutron source, inside the beam tube. Thus, the coils and their wiring cannot be brought into contact with liquid metal and are well protected against short-circuiting. Past EMPs have used a special ceramic coating to guard against this danger, but the coating is neither well-known nor manufactured to well-defined nuclear specifications. It therefore gives a certain advantage to position the active core of the EMPs in the beam tube outside the liquid metal container to offer the best possible protection for the active coils. The passive core, on the other hand, contains no wiring and is less sensitive. It is therefore left in the guide tube, which is immersed in the liquid metal container.

Figure 6. Conventional EMP (left) and new proposed EMP configuration (cut-away right)



Having examined the essential details of the proposed improvements featured most prominently in the new design, the next section gives an overview of the overall design.

Engineering overview

The following figures illustrate how the different details for improving the operation of a neutron source as described above may be brought into a single engineering design. Figure 7 (left) shows the outer containment with the integrated ribbing. Each rib is traversed by secondary cooling fluid, as shown in Figure 3. The source shown in the right figure has a matching ribbed surface set at a distance of 1 mm, thus allowing a very narrow 1 mm gas gap between the two components. The ribs on the source are traversed by primary fluid flowing up from the central spallation zone, to be cooled by releasing heat into the containment ribbed surface.

The piping connected to the upper containment heat exchanger comprises a set of distribution outlets so as to ensure equal supply of cooling to the cooling jacket.

Figure 7. Source section view (top), separate containment with ribbed integrated heat exchanger (bottom left), containment with inlaid source (containment cut-away bottom right)

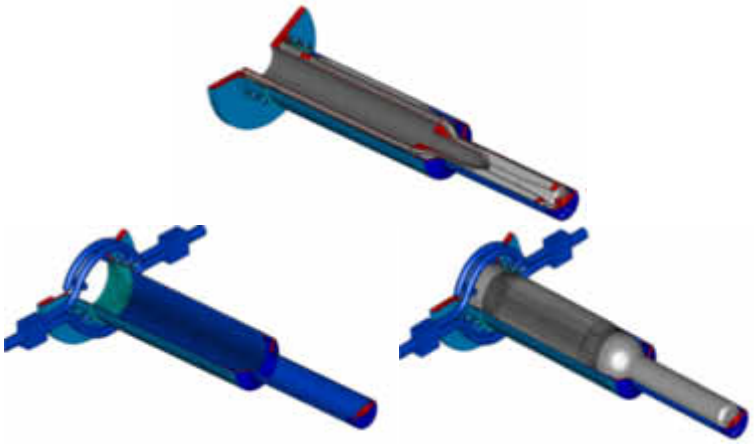
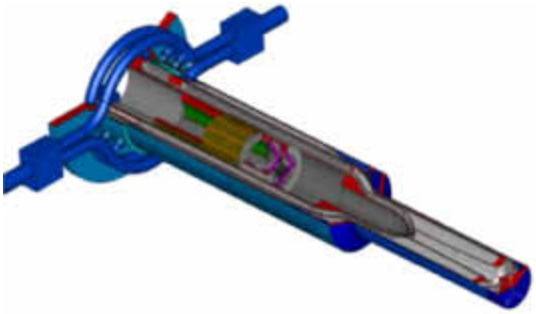


Figure 8 shows the method of placing the pump; the active part of the pump containing the coils is inserted in the beam tube and rests on the inner surface of the annulus containing the driven liquid metal opposite the passive core (see Figure 6 in more detail).

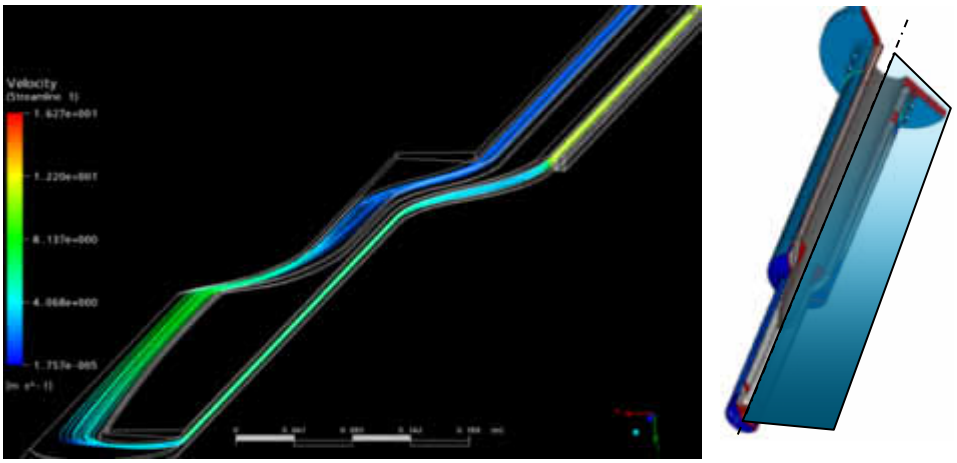
Figure 8. Integration of pump and diagnostics in beam tube



Fluid dynamic analysis

Some preliminary CFD analyses have been performed on a two-dimensional axis-symmetric section model. It shows the overall distribution of velocities in the source; a peak velocity is reached in the primary side of the heat exchanger due to the reduced local section used to enhance heat transfer. The simplifications caused by the axis-symmetry are also partly responsible for this high velocity since it is impossible to reproduce the ribbing in such a model. In the upwards flowing section of the spallation zone, the velocity is approximately 8 m/s, which is compatible with the velocities observed in the EURISOL test. No large-scale recirculation zone has been detected in this first simple CFD model.

Figure 9. Flow calculated with CFD for a two-dimensional model of the source



Conclusion

The design proposed in the current work will fulfill most operational requirements for a high-power target at 4 MW. Higher power ratings may be reached by changing the beam profile, essentially widening it and using either a chopped parabolic or rectangular profile in lieu of a 25 mm sigma Gaussian, as was retained above, a conservative assumption.

Many safety aspects dealing with the integrity of the containment, the retention of successive barriers, passive heat evacuation and coast-down times of the pumps have been optimised to ease operational use. A vertical stacking of all the components gives the operator greater flexibility in maintaining the source as each separate component can be easily extracted from the assembly and dispatched to an overhaul facility while a new replacement part is inserted in its place. Since the different components have been ordered according to their degree of exposition to irradiation, it may be expected that scheduling replacements can easily be optimised as the likely mean time between failures can be more easily predicted than if the components contained heterogeneous exposed parts.

Finally, the overall configuration of the proposed neutron spallation source offers advantages in terms of the neutron economy. The central spallation zone can be located deep inside a subcritical core, enhancing the production fission potential from the spallation source neutrons. The elongated shape of the source also reduces gamma exposition by minimising possible leakage of direct radiation.

Acknowledgements

The research leading to these results has received funding from the European Commission under the FP7-INFRASTRUCTURES-2010-1/INFRA-2010-2.2.11 project TIARA (CNI-PP), Grant agreement no 261905.

References

[1] Rubbia, C. et al. (1995), "Conceptual design of a fast neutron operated high power energy amplifier", CERN Internal Note CERN-AT-95-44 ET.

[2] Rubbia, C. (1996), "The energy amplifier; a description for the non-specialists", CERN/ET/Internal Note 96-01.

[3] Wagner, W., Groeschel, F., Thomsen, K., Heyck, H. (2008), "MEGAPIE at SINQ – the first liquid metal target driven by a megawatt class proton beam", *J. Nucl. Mater*, Vol 377, pp 12-16.

[4] Samec, K., Milenkovic, R., Demetjevs, S., Ashrafi-Nik, M., Kalt, A. (2009), "Design of a compact high power neutron source", *Nuclear Instruments and Methods in Physics Research Section A*, Vol.606, Issue 3, pp. 281-290.

[5] Samec, K., Milenkovic, R., Blumenfeld, L., Dementjevs, S., Kharoua, C., Kadi, Y. (2011), "Measurement and analysis of turbulent liquid metal flow in a high-power spallation neutron source–EURISOL", *Nuclear Instruments and Methods in Physics Research, A*, Volume 638, issue 1, pp. 1-10.

Thermal hydraulic numerical investigation of the heavy liquid metal free surface of MYRRHA spallation target experimental

A. Batta, A. Class
Karlsruhe Institute of Technology, Germany

Abstract

Accelerator-driven systems (ADS) are extensively investigated for the transmutation of high-level nuclear waste within many worldwide research programmes. The first advanced design of ADS is currently being built in SCK•CEN MOL-Belgium (Multi-purpose hybrid research reactor for high-tech applications (MYRRHA)). Many European research programmes support the design of MYRRHA. In the framework of the EU project Thermal Hydraulics of Innovative nuclear Systems (THINS), a free surface experiment is performed at the Karlsruhe Liquid Metal Laboratory (KALLA) of Karlsruhe Institute of Technology (KIT). The experiment investigates the free surface design of the MYRRHA target. The KALLA free surface lead-bismuth eutectic (LBE) liquid metal experiment is a full-scale model of the concentric MYRRHA target. The design of the target is combined with CFD simulations using a volume of fluid method accounting for mass transfer across the free surface. The used model is verified with water experimental results obtained at the University Catholic of Louvain (UCL) within the Integrated Project EUROpean Research Programme for the TRANSmutation of High Level Nuclear Waste in Accelerator-driven System (EUROTRANS). The design of the target enables a high fluid velocity and a stable surface at the beam entry. In the current work, we present numerical results of Star- CD simulations employing a high-resolution interface-capturing scheme in conjunction with the cavitation model for the nominal operation conditions. Thermal hydraulic of the target is considered for the nominal flow rate and nominal heat load. Results show that the target has a very stable free surface configuration for the considered flow rate and heat load.

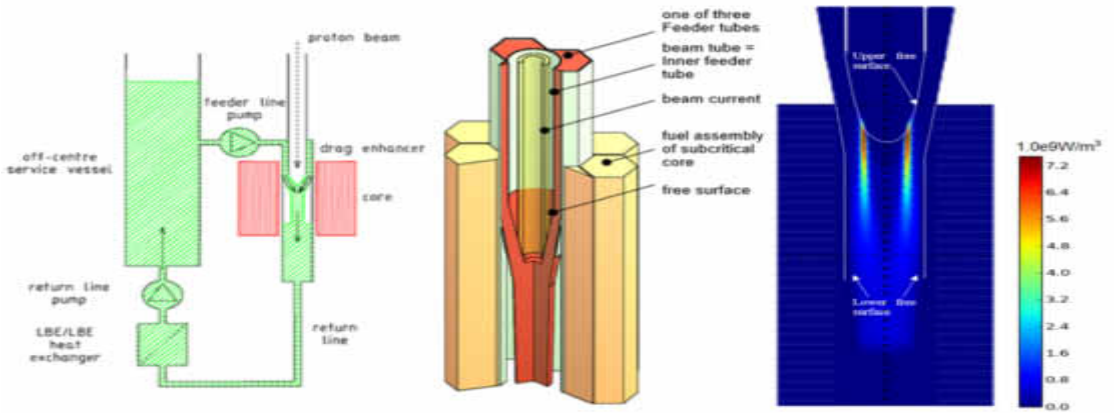
Introduction

Thermal hydraulic studies of free surface with Heavy Liquid Metals (HLM) has become more important for innovative nuclear reactors design. In some of the reactors, the HLM can be used as a coolant. In accelerator-driven systems (ADS) it can be used as a coolant and a target. According to previous studies performed in the Integrated Project EUROpean Research Programme for the TRANSmutation of High Level Nuclear Waste in Accelerator-driven Systems (EUROTRANS), the first advanced design of a 50 to 100 MW_{th} experimental facility demonstrated the technical feasibility of the transmutation in an accelerator-driven system (XT-ADS) [1]. In SCK•CEN MOL-Belgium, the first advanced design of ADS system is currently designed. Preparation for the construction of a Multi-purpose hybrid research reactor for high-tech applications (MYRRHA) is under development. Several European research programmes support the design of MYRRHA. The Thermal-Hydraulics of the Innovative Nuclear Systems (THINS) project is one of these programmes. It is devoted to important cross-cutting thermal-hydraulic issues encountered in various innovative nuclear systems, such as advanced reactor core thermal-hydraulics, single

phase mixed convection and turbulence, specific multiphase flow, and code coupling and qualification. Another objective of THINS is to achieve optimum usage of available European resources in experimental facilities, numerical tools and expertise [2]. Within THINS, Karlsruhe Liquid Metal Laboratory (KALLA) is testing the performance of a free surface target. A full-scale model of the concentric MYRRHA target is investigated for a range of operation conditions. A thermal analysis of the target is performed by CFD. The first design of the target was tested for water, which is easier to treat and characterise than the LBE target. The design of the water experiment was based on CFD simulations using a volume of fluid method accounting for mass transfer across the free surface [3-6]. The results of water target experiment were used for the variation and validation of the used model. This was established within the FP6 EUROTRANS where a water experiment was designed and run at the University Catholic of Louvain (UCL). The experience gained from the water experiment is used for the design of the KALLA LBE free surface target. The schematics of the spallation loop is shown in Figure 1-a. It shows the target integrated in the core. It also shows the LBE loop and the proton beam hitting the free surface of the target. According to the MYRRHA target design, the LBE free surface target replaces three fuel assemblies of the core, as shown in Figure 1-b. The LBE flows through three feeder tubes downstream to form a hollow flow with two free surfaces: one facing the proton beam and the other one designated as the lower free surface, as shown in Figure 1-c, which depicts the nominal volumetric heat source due to spallation reactions.

Figure 1. Illustration of, a) schematics of the spallation loop, [3], b) illustration of target inserted into reactor core [3] c) typical beam characteristics

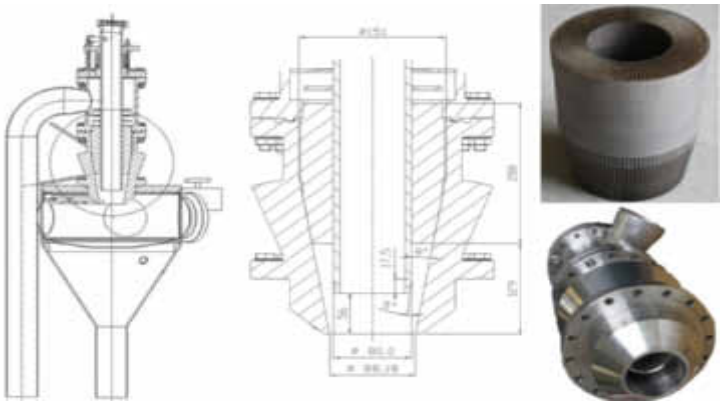
a b c



According to the design specification, the proton beam travels in a vacuum to hit the upper free surface. This requires that potential cavitation in the feeder nozzle of the target be suppressed by fins which raise the pressure in the feeder. A small injection angle at the feeder nozzle outflow was optimised to minimise the size of recirculation flow in the thermally highly loaded zones [7]. The high heat load within the limited space available for the target makes the design a challenging task. Several iterations were needed to come to a final target design. Many details about target design activities can be found in [8-10]. The axi-symmetric design was considered to allow fast analysis for better fundamental understanding. The final target design represents a more complex 3-feeder configuration [4]. The final design v0.10LBE studied in [8] was built in KALLA after some modifications introduced due to space limitation and available pump capacity. Due to the previously mentioned limitations, a shorter feeder is selected to enable higher mass flow rate (expected flow rate is lower than nominal, pump limitations). Beam pipe is slightly modified at the tip and outer radius. The axial position of the beam pipe is adjustable since larger acceleration lowers the risk of cavitation in cases of small flow rate. Due to

shortening the feeder to 200 mm, the number of fins is increased from 100 to 122 fins. Figure 2 shows the target mock-up construction and photographs of the target and the drag limiter. The current design of the target enables a high fluid velocity and a stable surface at the beam entry. This was studied in [10] for a wide range around nominal flow rate. In what follows, Figure 1-c shows the numerical results of the thermalhydraulic behaviour of the target for nominal flow (11 l/s) condition and the nominal heat load.

Figure 2. Blue print of MYRRHA mock-up, photograph of the target and the drag limiter with 122 fins



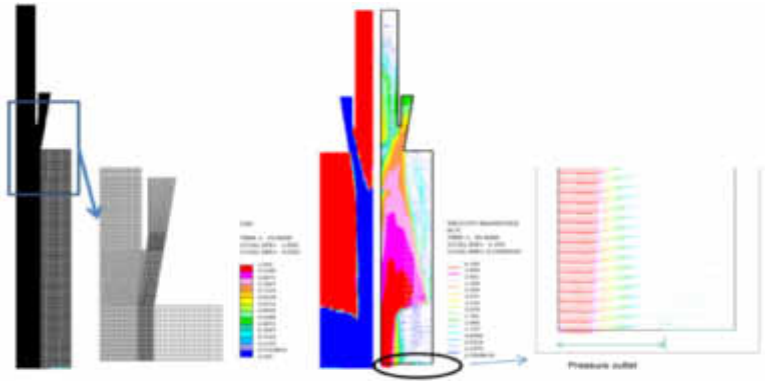
Numerical study

For the study of the mock-up target illustrated in Figure 2, an axi-symmetrically domain of 5° is considered. 10 900 mesh cells, k-ε model, fluid properties at 593 K, and the CFD code Star-CD version 4.16 are used. Cavitation model is used with unsteady computations, time step of 0.001 seconds. The results converge to a near steady-state position of the free surface. The feeder part is not considered in these simulations, where another study for flow rates above 5 l/s has proven that the used number of fins in the drag limiter is sufficient to rule out cavitation in the feeder [10]. The tested power provided in Figure 1-c is 900 kW. This corresponds to a heat source of 12.5 kW considered in the domain. In order to reduce the computational time constant fluid properties are also used for the thermal study. The heat source results in average heating of 56.7°C. The proposed heat source shown in Figure 1-c is calculated by SCK as a volumetric heat source as a function of local cartesian position by assuming fixed free surface position.

Isothermal hydraulic study of the target

The hydraulic behaviour of the KALLA-LBE target shown in Figure 2 is tested by using the previously described model. Different flow cases are studied, where the nominal flow and other lower flow cases are considered. In the analysis, the mesh illustrated in Figure 3 is used, where the flow in the feeder is not considered. The axi-symmetrical domain permits uniform inlet flow in the circumferential direction, where flow rates of 11.0 l/s, 8.08 l/s, 7.00 l/s and 5.88 l/s are studied. Details of the hydraulic study and a preliminary comparison with the obtained experimental results are in [10]. Figure 3 shows contours of volume fraction of LBE and the velocity of the fluid in the target for nominal flow conditions. A pressure outlet condition was applied at the outlet, as illustrated in Figure 3. This allows some additional flow to enter the domain from the outlet. The very small amount re-entering the computational domain can be predicted from the velocity vectors, as shown in Figure 3. Since the outlet is selected far downstream of the target region, the outflow conditions do not influence the results in the spallation zone. The hydraulic study of [10] shows that a stable free surface is generated for the tested flow rates. When lowering the flow rate, the position of the small recirculation zone on the axis of the conical free surface is also lowered. For flow rates of 11.0 l /s and 8.08 l /s, the radius of the recirculation zone area is about 1/3 of the beam tube radius.

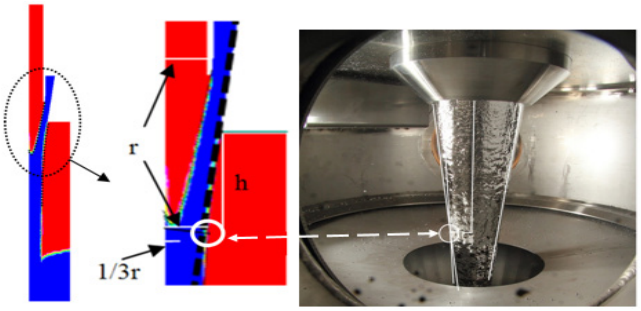
Figure 3. Illustration of the used computation mesh, computed vapour volume fraction, (CAV, red vapour and blue is liquid LBE), velocity magnitude and velocity vectors in the outlet region, nominal flow, 11 l/s



Measurements from the first experimental campaign are reported in [11]. These results were obtained by a digital camera, which was installed at the height of the nozzle exit to monitor the heavy liquid metal jet during start-up phase and in operational mode. A second digital camera was mounted on top of the target to observe the free surface area through the proton beam tube. Figure 4 presents a schema for comparison between experimental and numerical results. On the left side the outer contour of the LBE flow (blue) can be compared to the experimentally obtained average outer contour as illustrated.

It should be noted that the position *h* of the recirculation zone approximately coincides with the position of the slope "discontinuity" of the outer contour of the jet, as highlighted by the white circle shown in Figure 4 (right) [10]. The predicted size of the recirculation zone 1/3 *r* proves that the heat deposited in the target is outside of the recirculation zone (referring to heat deposition profile in Figure 1c). Consequently, overheating in the circulation zone is not expected. At this stage, the obtained instantaneous experimental photographs are compared to time-averaged numerical results. Calibration and extensive averaging are scheduled for the second measurement campaign. Preliminary experimental results verify the numerically obtained hydraulic results, where stable surface in a wide range of operating conditions starting from 35% of the nominal flow rate was observed [10].

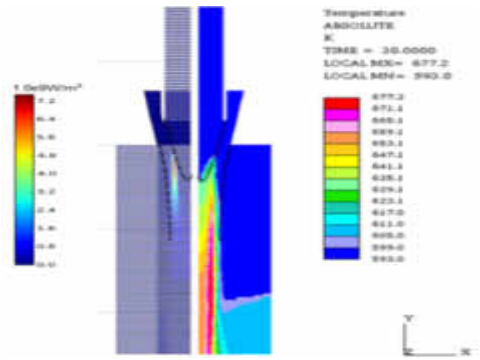
Figure 4. Comparison of flow rate effect on the HLM vapour volume fraction (VVF) domains, (red is vapour, blue is liquid) and right is a side view onto the target nozzle in stable operation mode at 4.6 l/s [11]



Thermal hydraulic study of the target

The nominal flow case corresponding to a 3 mA proton beam is selected for the thermal hydraulic study of the target. The heat source presented in Figure 1-c was used in this study. It was calculated for a fixed position of the free surface. However, a small oscillation in the position of the upper free surface was observed in the calculation. The calculated oscillation of the free surface is very small compared to the height of a computation cell at the interface. However, this results in a proportional change of the mass fraction of the liquid in the boundary cell. Consequently, it results in an unpredicted very high boundary temperature at the free surface for the case if the boundary cell has a smaller mass than used for the calculation of the heat source. This is due to the big difference in density between vapour and liquid. For an even more accurate calculation, a heat source needs to be introduced, which is a function of time and free surface position. This will add some numerical complexity to the investigated problem. Accordingly, the heat generated in interface cells between LBE liquid and vapour is not considered accurate in this initial study. Figure 5 shows the used heat source and the resulting temperature contours. The results show that the generated heat is removed effectively without overheating. The highest temperature values are downstream of the free surface. As expected, the circulation zone did not adversely influence the heat removal. Note that the heat source is a function of the vertical distance from the free surface, with its maximum close to the surface. Since the flow is almost aligned with the vertical direction, a fluid particle is substantially heated near the surface and then subjected to weaker heating as it is transported downward. Therefore, the maximum temperature is reached far away from the circulation region and the free surface. The computed flow thus leads to stable heat removal in the target for the nominal flow rate considered.

Figure 5. Nominal heat source and computed temperature contours, 11 l/s



Conclusion

Our thermohydraulic study considers the mock-up of the windowless target for MYRRHA at nominal flow conditions and shows that the selected design results in stable concentric flow forming a small recirculation zone in the centre. The size of the recirculation zone is about 1/3 of the beam tube radius for flow cases around nominal, 8- 11.0 l/s. The beam is circularly swept around the centre region, so that direct heating of the recirculation zone is omitted. This provides stable heat removal from the target for all flow rates considered. In our simulation, the heat source profile is provided time-independently. For accurate surface temperature predictions, the heat source would have to be provided as a function of the free surface position, which slightly fluctuates in our calculation. In the current study, the heat source in the interface cells is deactivated. Our simulations show that the maximum temperature is reached far from the recirculation zone. Overall, the heat can be successfully removed from the target so that only moderate temperature is reached.

Acknowledgements

This work has been supported by FP7 Thermal-Hydraulics of Innovative Nuclear Systems (THINS), Grant 249337 and the AREVA nuclear professional school.

References

[1] Annex I, "EUROpean Research Programme for the TRANSmutation of High Level Nuclear Waste in an Accelerator Driven System", Project acronym: EUROTRANS, Contract no. FI6W-CT-2004-516520, (2005).

[2] Annex I – "Description of Work for THINS project", Seventh framework programme of EURATOM for nuclear research and training activities (2007-2011), theme: nuclear fission and radiation protection, collaborative project "large-scale integrating project", no. 249337.

[3] Dierckx, M. (2009), "Target area design options for the XT-ADS spallation loop", restricted contract report SCK•CEN-R-4649, Mol, Belgium, European 6th Framework Programme EUROTRANS, (2009).

[4] Guertin, A. et al. (2010), "XT-ADS windowless spallation target design and corresponding R&D topics", *1st Internat. Workshop on Technology and Components of Accelerator-driven Systems (ADS)*, Karlsruhe, 15-17 March 2010.

[5] Class, A.G, et al. (2011), "XT-ADS windowless spallation target thermohydraulic design and experimental setup", *Journal of Nuclear Materials*, 415, S.378-384.

[6] Batta, A., Class, A.G., Dierckx M., Schuurmans, P., Van Tichelen, K., Jeanmart H., Roelofs, F. (2009), "Hydraulic Design of the Windowless XT-ADS Spallation Target" HeLiMeRT in Europe; SCK•CEN, Mol, Belgium.

[7] Batta, A. et al. (2010), "Comparative Experimental and Numerical Analysis of the Hydraulic Behaviour of Free-Surface Flow in the Water Experiment of the XT-ADS Windowless Spallation Target", *Proceedings of ICAPP '10*, San Diego, CA, US.

[8] Batta, A., Class, A.G. (2010), "XT-ADS windowless target high resolution interface capturing simulations, *8th International Topical Meeting on Nuclear Thermal-Hydraulics, Operation and Safety (NUTHOS-8)*, Shanghai, China.

[9] Batta, A., Class, A.G. (2009), "Hydraulic Analysis of the Heavy Liquid Metal Free Surface in the Windowless XT-ADS Spallation Target", *Proc. NURETH13*.

[10] Batta, A. et al. (2013), "Numerical and experimental hydraulic analysis of the heavy liquid metal free surface of MYRRHA spallation target experiment", *2nd THINS Cluster Workshop* Stockholm, KTH, 5-7 February 2013.

[11] Litfin, K. et al. (2012), "Investigation of a heavy liquid metal free surface target experiment", *Proc. of the 20th Internat.Conf.on Nuclear Engineering Collocated with the ASME 2012 Power Conf.*, Anaheim, Calif.

A flexible testing facility for high-power targets T-MIF

Yoann Fusco[1], Masoud Behzad[2], Karel Samec[1], Yacine Kadi[1,2]
[1]CERN, Geneva, Switzerland
[2]Sungkyunkwan University, Republic of Korea

Abstract

Building on recent experience in the field of applied physics, the TIARA work package (No. 9) focuses on target applications for accelerators in Europe. A roadmap for target development has been derived from major achievements in the EU-FP6 and EU-FP7 programmes such as the MEGAPIE and EURISOL experiments. The TIARA management board concluded that a worthwhile continuation of such projects would be in the development of a flexible material irradiation facility which would be easily transportable and could be installed in different laboratories. The power is limited to 100 kW in a very compact arrangement so as to obtain the best neutron economy from a moderate beam power, which is more likely to be found in laboratories across Europe. The challenges posed by such a compact design and accompanying calculations are presented in the current work.

Introduction

A dedicated material test irradiation facility is being proposed that evolved from prior work funded by the EU FP7 programme, the EURISOL design study, which examined the feasibility of an advanced isotope production facility. The neutron source in EURISOL was the subject of intense design work and was subsequently tested at full power in a hydraulic test, an experience which can be relied on for the current work since the design allowed the passage of a dense proton beam able to generate high neutron fluxes and hence high displacement per atom damage in material or dpas.

As currently envisaged in [1], the testing station will allow critical issues concerning materials under irradiation to be addressed, such as the impact of proton beam irradiation, neutron irradiation, liquid metal corrosion and temperature. The material samples to be investigated in such a facility will be subjected to tensile stress, either constant or cyclical. The facility may also be used for sensor development under irradiation and isotope production, albeit centred on medical applications instead of the exotic nuclei aimed for in the EURISOL design study.

Another aspect of the facility is to aim for greater compatibility with visiting laboratories. The recent spate of projects comprising neutron sources is promising; they have, however, been one-off designs tailored to a specific accelerator infrastructure. The goal of the current work is to propose a facility that is sufficiently versatile so that it may be transported and used in different laboratories.

Specifications

Focusing on testing materials and sensors under irradiated conditions led to the selection of a key set of parameters defining the most promising design. A survey of compatible installations, the parameters of the circuits and a beam were chosen as follows:

Table 1. Parameters defining the T-MIF Facility [1]

Particles	Protons
Kinetic energy	200 MeV - 1 GeV
Beam shape	Elliptical cross-section σ_x / σ_y = 1 / 3-6 Parabolic density distribution
Current	< 500 μA
Power	< 100 kW in beam (70 kW thermal)
Primary circuit and spallation source	Lead or LBE < 15 liter inventory
Secondary circuit	Gallium < 50 liter inventory
Cold source-open inventory	Air or water
Saturation radioactivity in primary	~ 20 - 30 TBq/kg
Decay heat in primary	~ 1 - 2 W/kg
Neutron flux density	~ 10^{13} n/cm^2 s

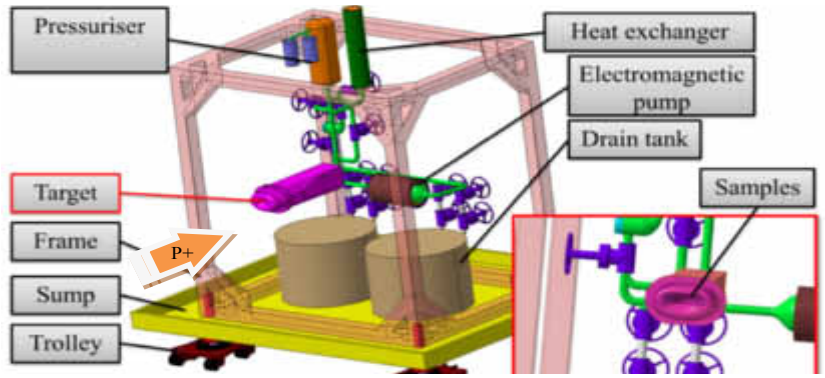
The cross-section of the beam deposition profile is elliptical, as can be seen in Table 1. With such a profile it is possible to impact a fair length of a tensile stress specimen edge-on and thus obtain high dpas homogeneously distributed on the sample without needing to oscillate the beam to "paint" the specimen with particles. The latter method was attempted in the LISOR programme and led to a containment failure leaking radioactive liquid metal to the outside.

Essential characteristics of the new proposed design

The general aspect of the proposed irradiation facility is a cube, 2 metres deep and comprising within it all the necessary systems (see Figure 1). The interface to the laboratory is limited to the coolant connections, the secondary circuit, the electric energy supply and the signals from the instrumentation.

The liquid metal target placed in the centre of the facility contains the samples which are subjected to a proton beam (arrow marked P+), creating irradiation damage directly through protons or indirectly through neutrons created by spallation of the surrounding liquid metal by the incoming protons.

Figure 1. Overall view of the proposed T-MIF Facility



Note that the figure reflects the current design status and is not complete.

Flow control

The liquid metal in the target is re-circulated by an electromagnetic pump (EMP) with an annular design in which a pulsating electromagnetic field created by coils drives the liquid metal with an efficiency of 5-7%. The low efficiency of the chosen pump design is compensated for by the absence of any moving parts, an important consideration in the primary circuit. Unlike most EMP designs, the stator is located inside the inner diameter of the annulus and the coils are located on the outer diameter. Thus, there is no penetration of the EMP coil wires through the liquid metal and all the active parts of the pump are easily accessible. The stator consists in stacks of ferritic steel plates and, therefore, has no wired connections.

The pump is used to drive the liquid metal through a heat exchanger located at the top of the facility, the position of which was chosen to encourage natural circulation. Since there is a 1 metre difference between the heat source (target) and the cold source (heat exchanger) and a temperature difference of 300°C, a positive pressure difference entraining the flow from the target to the heat exchanger exits:

$$\Delta P = g \cdot \rho \cdot \beta_{Vol} \cdot \Delta T \cdot L = 9.81 \cdot 10'550 \cdot 0.00012 \cdot 300 \cdot 1 = 3'725 \left[Pa\right]$$

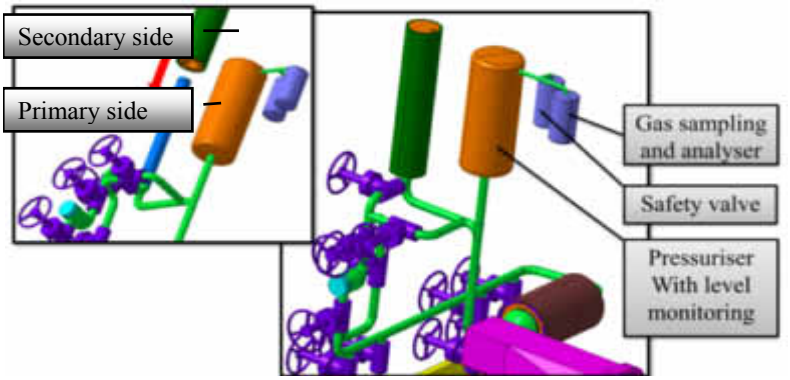
The pressure difference is relatively small, but high enough to lengthen the coast-down time of the liquid metal over the beam entrance window on the target in the event of a beam trip. This aspect has an important positive safety implication.

Pressure control

The pressure inside the target may be varied as it will influence the dissolution of oxygen in the target. It can also vary over short time periods if the beam intensity varies. Therefore, it is necessary to provide the loop with a simple means of controlling internal pressure.

The pressuriser situated at the top of the installation (see Figure 2) is controlled by the release of nitrogen gas into the top of the pressuriser, which is half filled with liquid metal. All gaseous spallation products thus accumulate at the top and lead to a gradual rise in pressure. Release of excess pressure is either gradual through controlled release of these radioactive gases to a series of decay gas bottles or sudden in accident cases, through a series of pressure relief valves and burst disks. The pressuriser will also be provided with gaseous analytical instrumentation capable of measuring activity and gas composition such as a gas chromatograph.

Figure 2. Details of the pressuriser



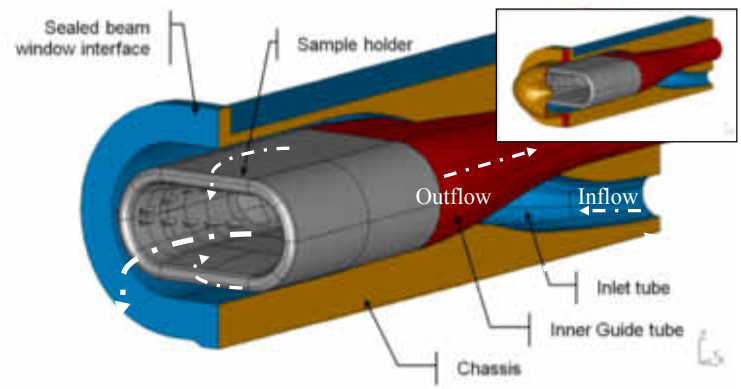
The heat exchanger is made up of two separate parts which allow the primary and secondary circuit to separate cleanly (see following paragraphs). This will enhance maintainability and resistance to accidental leaks in the primary circuit.

Target station

The target station at the heart of the facility allows the testing of either material samples or instrumentation under conditions representative of high-power neutron spallation targets. The design (see Figure 3) of the target is based upon the EURISOL target. The same beam window design is used, albeit stretched horizontally to adopt an elliptical section which is compatible with the shape of the beam used to irradiate the samples (see Figure 5). The sample holder located on the guide tube (in grey below) has an inner surface which contains receptacles for loading mechanisms for testing samples (see Figure 5). Note that the sample holder can be exchanged for another design. It is simply bolted in place by a series of captured bolts that can be unscrewed by a robot, allowing rapid exchange.

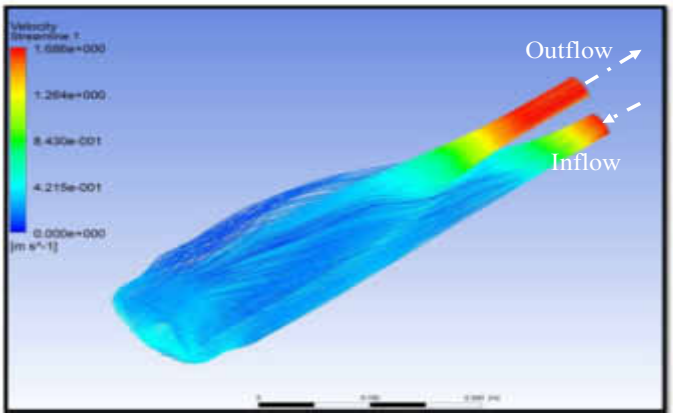
From a hydraulic point of view, the advantages of this configuration lie in the low pressure loss at high flow rates, as was demonstrated in the hydraulic test of the EURISOL target [4]. This improves the economics of the project by allowing the selection of a smaller pump with lower specifications and decreasing the sizing of all the connecting piping.

Figure 3. Details of the target [1]



As illustrated in Figure 4, the inflow is divided equally over the guide tube and wets the conical surface of the window at a speed of about 1 m/s. The flow rate in this calculation is only half the full speed at full power. With 2 m/s over the window, there is sufficient cooling to evacuate the projected 100 kW of the given past calculations on the EURISOL converter target.

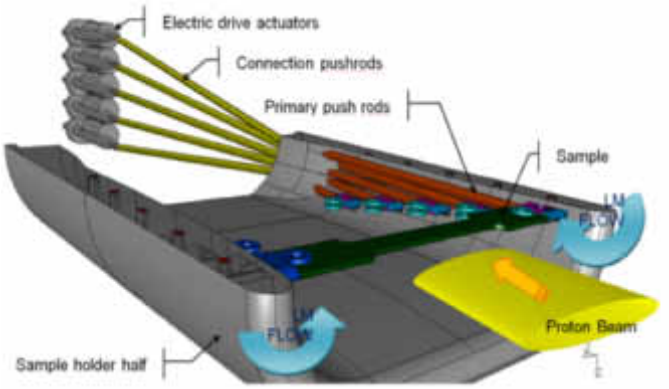
Figure 4. Flow inside the target [2]



Sample testing

The samples are held in place by a series of rocker arms which transform the compression load form pusher roads into a tension load by inversion around a pivot. The pusher roads transfer a compressive load coming from external electric drive actuators. A compressive load is seen as intrinsically more robust in this design as it allows the sample holder connection to be simplified. Thus, the pusher rod interfaces are in compression and need no connection clips.

Figure 5. Sample loading inside the target [1]



The sample holder is essentially a flattened tube split in the middle and opens like a clam-shell, allowing access to the sample loading mechanism and the samples. As can be seen in the figure, the flattened elliptical beam, which is 1 cm across, fully envelopes the sample thickness of 1 mm, which ensures a homogeneous distribution of dpa in the sample. Thus the effect of proton damage on a loaded sample under the simultaneous action of liquid metal and temperature may be investigated. The load can be cyclical or constant.

Heat exchanger

The design is based on the concept of a central pin which sends a flow of primary fluid down a very narrow annulus. The secondary fluid surrounds the annulus with a spiral flow. The two fluids are contained in their own vessel and do not share a common wall. In contrast, each part is separated by a gas gap which provides robustness against leaks and a method of detecting leaks.

As explained in the introduction, the heat exchanger allows primary and secondary side to be detached (lower left in Figure 6) along with all the assorted cabling and connection for data acquisition or the power supply to the electric drive actuators needed on the target.

The heat transferred in the heat exchanger is estimated according to the latest CFD calculation shown in Figure 7 to reach 130 kW, above the specifications already set out for the design (see Table 2). The additional margin gives some scope for optimising the gas gap and the nature of the gas contained therein which have not yet been determined.

Figure 6. Principles of the heat exchanger [1]/[2]

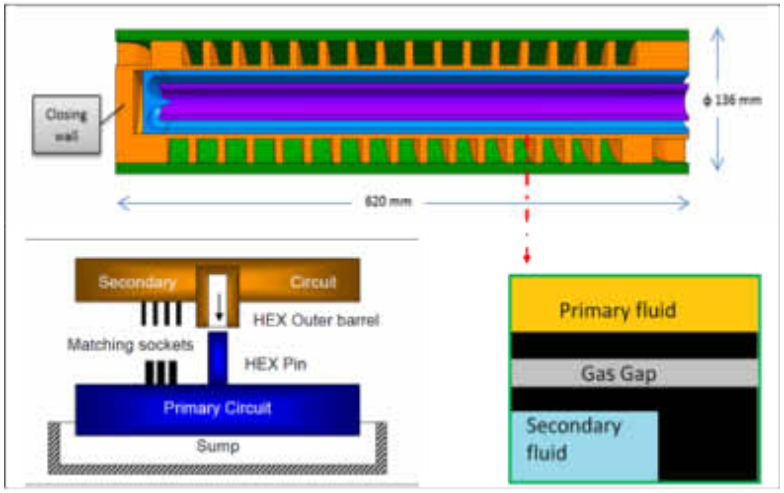
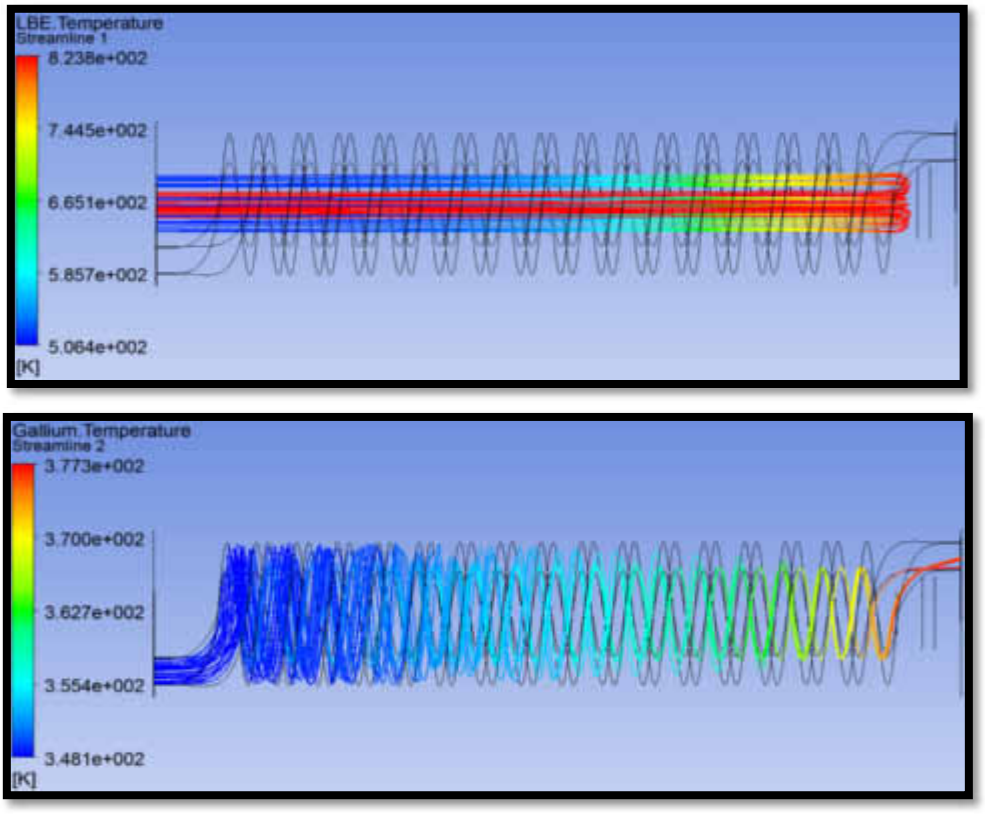


Table 2. Heat exchanger characteristics

Power exchanged	>100 kW
Primary side fluid	Lead or LBE or mercury 550°C/250 °C
Secondary side fluid	Gallium 100°C/75°C
Specific requirements	Leak-resistant Leak detection Able to disconnect primary/secondary Gravity-fed in case of pump trip Minimal inventory primary-side
Pressure	12 Bar

Figure 7. Flow on primary side (top) and secondary side (bottom) of the heat exchanger [2]



Conclusion

An irradiation target is being proposed which should allow significant progress in the field of materials and sensors used in highly irradiated environments. Given the current focus on ever-higher power for scientific instruments, the interest in new forms of nuclear energy, both for fission and fusion, there is a need to investigate designs such as T-MIF.

These aspects relate to the neutronic performance in particular, as an estimate of the dpas caused by protons and neutrons for different positions of the samples is required in order to assess the performance of the proposed concept.

A final report, which is an EU deliverable report, was expected in 2013, and recapitulates the design aspects and includes further analysis in the field of neutronics and thermal-hydraulics.

Acknowledgements

The research leading to these results has received funding from the European Commission under the FP7-INFRASTRUCTURES-2010-1/INFRA-2010-2.2.11 project TIARA (CNI-PP), Grant agreement no 261905.

This research was also supported by WCU (World Class University) programme through the National Research Foundation of Korea funded by the Ministry of Education, Science and Technology (R31-2008-10029).

References

[1] Samec, K. (2013), "Preliminary design report for a high-power Material Irradiation Facility T-MIF", TIARA Deliverable DSIF – Milestone MS34, FP7-Infrastructures-2010-1/INFRA-2010-2.2.11 project TIARA, 25 February 2013.

[2] Fusco, Y., Behzad, M. "CERN internal reports on the target and heat exchanger thermal-hydraulics in the context of the TIARA initiative".

[3] Samec, K., Milenkovic, R., Demetjevs, S., Ashrafi-Nik, M., Kalt, A. (2009), "Design of a compact high power neutron source", *Nuclear Instruments and Methods in Physics Research Section A,* Vol.606, Issue 3, pp. 281-290.

[4] Samec, K., Milenkovic, R., Blumenfeld, L., Dementjevs, S., Kharoua, C., Kadi, Y. (2011), "Measurement and analysis of turbulent liquid metal flow in a high-power spallation neutron source–EURISOL", *Nuclear Instruments and Methods in Physics Research, A,* Volume 638, issue 1, pp. 1-10.

Numerical analysis of the feasibility of a beam window for TEF target

Hironari Obayashi, Hayanori Takei, Hiroki Iwamoto, Toshinobu Sasa
Japan Atomic Energy Agency, Japan

Abstract

The Japan Atomic Energy Agency (JAEA) has been researching and developing an accelerator-driven system (ADS) as a dedicated system for the transmutation of long-lived radioactive nuclides. The ADS proposed by JAEA is a tank-type subcritical reactor with a thermal power of 800 MW_{th} which uses lead-bismuth eutectic (LBE) alloy as a target material and a coolant, driven by a 30 MW superconducting proton linac. In the various R&D activities for ADS, the construction of the Transmutation Experimental Facility (TEF) is planned within the framework of the J-PARC project as a preceding step before the construction of the demonstrative ADS. In the development of the TEF, the estimation of the thermal-fluid properties of the flowing LBE is an important issue. The LBE has the tendency to cause corrosion/erosion to the structural materials. The beam window of ADS, which separates the proton accelerator and the LBE subcritical core vessel, is exposed to the high-temperature environment induced by the incidence of proton beam. Therefore, the feasibility of the beam window is the most important factor for the realisation of TEF. The objective of this study is to evaluate the feasibility of a designed beam window of TEF target by the numerical analysis with a three-dimensional model. The analysis was performed by considering (1) the current density and shape of the incident beam, (2) the thermal-fluid behaviour of LBE around the beam window as a function of the flow rate and inlet temperature, (3) the material and the thickness of the beam window, (4) the structural strength of the beam window. In the reference case, the current density and the profile of the proton beam were 20 $\mu A/cm^2$ and a Gaussian shape, respectively. The flow rate of LBE and temperature at the inlet were 1 l/sec and 350°C. The material of a beam window was SUS316 stainless steel 2 mm thick. In this reference case, the maximum velocity of LBE and the maximum temperature located at the top of the beam window were about 1.2 m/sec and 477°C. By increasing the flow rate of LBE up to 4L/sec, the maximum temperature of a beam window was reduced to around 420°C. The maximum shear stress was 194 MPa, which was observed at the centre on the outside surface of a beam window. The analysed stress in the reference case was lower than the tolerance level of the stress strength of the material, and hence the feasibility of a designed beam window was confirmed.

Introduction

The Japan Atomic Energy Agency (JAEA) has been researching and developing an accelerator-driven system (ADS) as a dedicated system for the transmutation of long-lived radioactive nuclides. The ADS proposed by JAEA is a tank-type subcritical reactor with a thermal power of 800 MW_{th} which uses the lead-bismuth eutectic (LBE) alloy as a target material and a coolant, driven by a 30 MW superconducting proton linac. In the various R&D activities for ADS, the construction of the Transmutation Experimental Facility (TEF) is planned within the framework of the J-PARC project as a preceding step before the construction of a demonstrative ADS. In this R&D, TEF is considered for the experimental investigation of the feasibility of the beam window, the structural materials, and to investigate the operation properties of the target system. This system consists of a proton accelerator and LBE spallation target, like the actual ADS. Figure 1 shows the schematic illustration of TEF in J-PARC [1]. The beam window of ADS, which separates the proton accelerator and the LBE subcritical reactor vessel, is exposed to the high-temperature environment induced by the incidence of the proton beam. The structural materials are damaged by irradiation due to the corrosiveness of LBE. These factors make it more difficult to conduct the design and development of TEF. Therefore, the feasibility of the beam window is the most important factor for the realisation of TEF. In particlar, to understand the LBE flow around the beam window is a requisite for the detailed design of TEF because the flow behaviour is closely related to not only thermal-fluid characteristics but also erosion/corrosion. The objective of this study is to evaluate the feasibility of a designed beam window of TEF target by the numerical analysis with a three-dimensional model. This analysis was performed by considering the current density and the shape of the incident beam in the target region, and the thermal-fluid behaviour of LBE around the beam window as a function of changing the flow rate and inlet temperature of LBE, and the material and thickness and the structural strength of the beam window.

Analysis conditions

Present design of the TEF target system and the analysis model

A beam window which has a concave shape was used for this analysis. The prototype design of the beam window for TEF target system is shown in Figure 2. The material of the beam window would be type 316 stainless steel or T91 steel. The curvature of the concave section was 79.5 mm. The concave section was connected to the other curved surface with a curvature of 32 mm to the opposite direction in the terminal part, and finally, it was connected to the straight tube. In this analysis, the thickness of the beam window was set to 3 or 2 mm. This design has the coaxially arranged annular and tube type channels. The inner diameter of the outside and the inside tube was set to 150 mm and 105 mm, respectively. The gap between the two coaxial tubes was 19.5 mm. The total length of the analysis region was 600 mm. The irradiation sample holder, which was shown on the right of Figure 2, was installed in the front side of inner tube. There were eight irradiation specimens, which were arranged every 4 mm in the horizontal direction. In this situation, the specimen of both ends acts as the side wall of the sample holder. The size of each specimen was 40×145×2 mm. The rectification lattice having the aperture of the plural squares type was installed at the front-end of the sample holder. The size of the rectification lattice was 52×52×5 mm, and the size of the square aperture was 4×4 mm. A slit of 2 mm in width was arranged along the side of the rectification lattice to cool off the side wall of the sample holder by flowing LBE.

Figure 1. Schematic illustration of the Transmutation Experimental Facility (TEF)

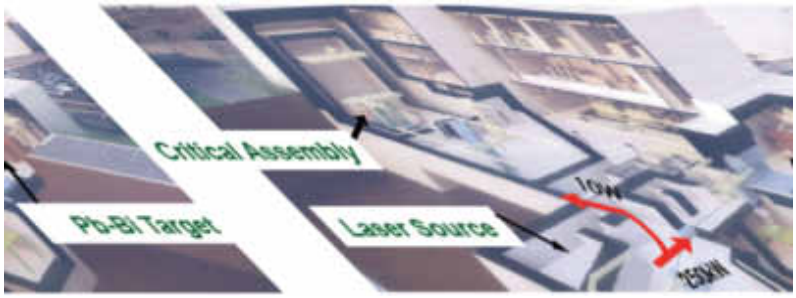
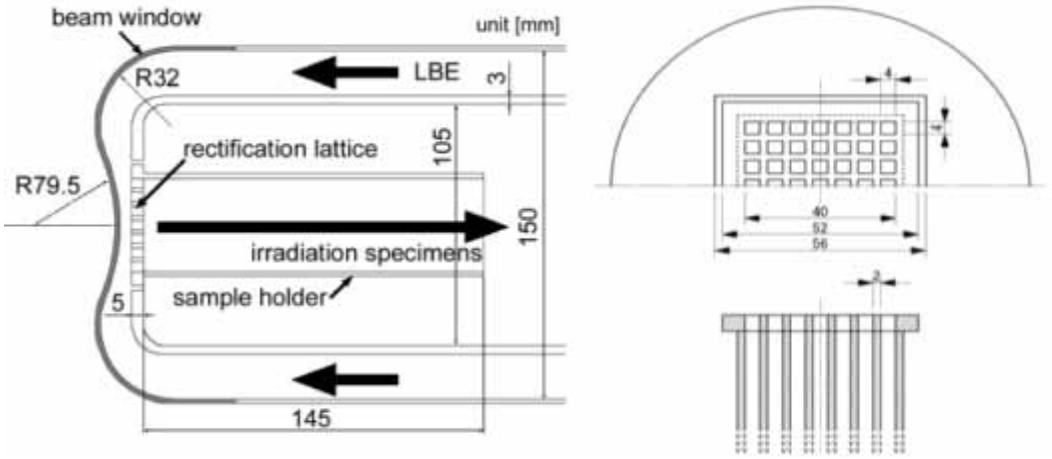


Figure 2. Prototype design of beam window for TEF target system



Proton beam profile

In the condition of the incident beam for the TEF target system, the beam current density was expressed by the following equation:

$$I(r) = \frac{A}{2\pi\sigma^2}\exp(-\frac{r^2}{2\sigma^2}), \qquad (1)$$

where, $I(r)$ and A represent beam current density and beam current, respectively. Table 1 summarises the condition of the proton beam profile used for the verification of the feasibility of the TEF target system. The material of the target system was type 316 stainless steel or T91 steel. Figure 3 shows a heat generation density at the beam window with a different beam profile. Figure 4 shows the examples of head deposition distribution in the TEF spallation target. These were analysed by PHITS code [2] by keeping the beam current as 625 μA, which would be the maximum beam current during the TEF operation. The Gaussian profile was set to the reference case in JAEA's beam window studies [3]. As shown in Figure 3, two types of profiles, Gaussian and flat, have different beam shapes by changing the density of the beam current for the direction of the beam diameter.

Table 1. Conditions of proton beam profile

	Parameters			
	Case 1	Case 2	Case 3	Case 4
Energy	400 MeV			
Beam current	625 μA			
Power	250 kW			
Beam shape	Gaussian			Flat top
Current density	20 μA/cm^2	40 μA/cm^2	60 μA/cm^2	20 μA/cm^2

Figure 3. Heat generation density profile of the incident beam

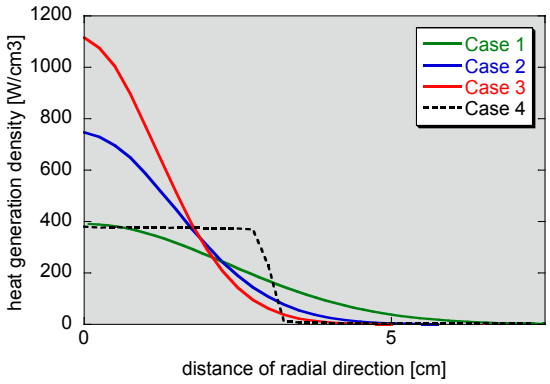
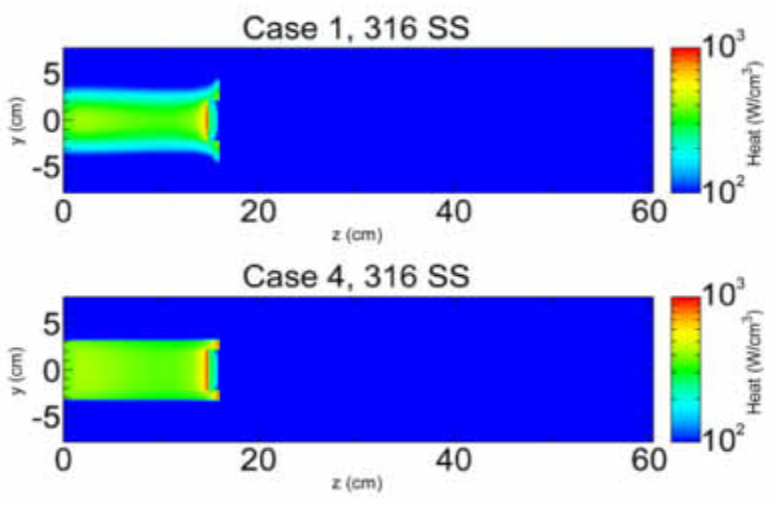


Figure 4. Examples of heat deposition distribution in the TEF target

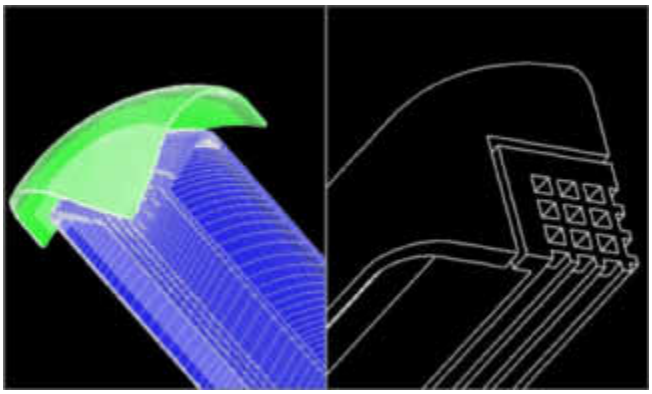


Analysis methods and conditions

It is obvious that the beam window is exposed to the severe environment, which is caused by the flowing LBE and the incident of proton beam. The temperature profile of the beam window greatly catches the influence of the temperature profile of the flowing LBE around the beam window. To secure the soundness of the window structure, it is necessary to prevent the immoderate temperature difference in the local region. Furthermore, because the flowing LBE is used not only for the window but also for the cooling of irradiation specimens, its temperature profile affects the irradiation temperature of each specimen. Therefore, it is important that (1) the temperature profile of structural materials and LBE should be predicted by the thermal-fluid analysis and (2) the verification of the feasibility of the beam window and other problems should be predicted previously by the structural analysis. Also, it is necessary to decide the operative condition that the soundness of the TEF target system would be secured by these analysis results.

The thermal-fluid behaviour of LBE in the TEF target was calculated by the STAR-CD with a detailed three-dimensional model. The model used for this analysis is shown in Figure 5. In this calculation model, a hexahedral element was used and the total number of the elements was about 220,000. First, LBE flowed through the annular region towards the centre of the beam window and flowed in the inner tube after a rectification lattice and an irradiation sample. In a default condition, the flow rate at the inlet of the annulus region was 1 *l*/sec, and this was equivalent to the flow velocity of 0.125 m/sec. In the actual target system, because LBE would be driven uniformly by the electromagnetic pump (EMP), the inlet velocity was set in a uniform velocity condition. Therefore, the k-ε model for high *Re* number type was used for a turbulence model. Each condition of heat generation given by the incident proton beam (see Figure 5) was used for the CFD analysis. The internal pressure to the inside of the beam window was set to 0.3 MPa in consideration of the flowing LBE and the cover gas. Release of the radiant heat on the outer wall of the beam window and the border of the atmosphere was considered. In this analysis, embrittlement of the structural materials by the irradiation was not considered. Based on the results provided by the CFD analysis, the analysis to verify the feasibility of the beam window was performed by the ABAQUS code.

Figure 5. CFD analysis model of tetra metric type



Analysis results

Velocity profile and temperature profile

This section introduces the CFD analysis result of the present conceptual design in order to investigate the thermal-fluid behaviour of LBE. In this paper, the result of the inlet LBE temperature of 350°C is introduced. This condition is the prioritised temperature condition that should be clarified in the development of the TEF target system. The result, which uses type 316 stainless steel as the structural material of a beam window and the other components, is introduced.

The flow rates were set to 1, 2, and 4 *l*/sec. In each flow rate, a similar tendency was confirmed as for the overall LBE flow. The dead region was formed in the centre region of the inside of the beam window, and the scale was hardly changed even if the inlet flow rate was increased. The maximum velocity of the LBE flow was confirmed at the region that passed a rectification lattice, and it was approximately 1.2 m/sec in the case of the inlet flow rate of 1 *l*/sec. Where the flow rate was set to 4 *l*/sec, this maximum velocity was reached approximately at 4.8 m/sec. As the flowing velocity was too fast in this condition, vibration of the target vessel by the LBE flow and acceleration of erosion/corrosion could arise. An additional analysis by changing the gravity direction was performed; however, the deflection of LBE flow was not observed in this operation condition.

Figure 6. Velocity profile by changing the inlet flow rate

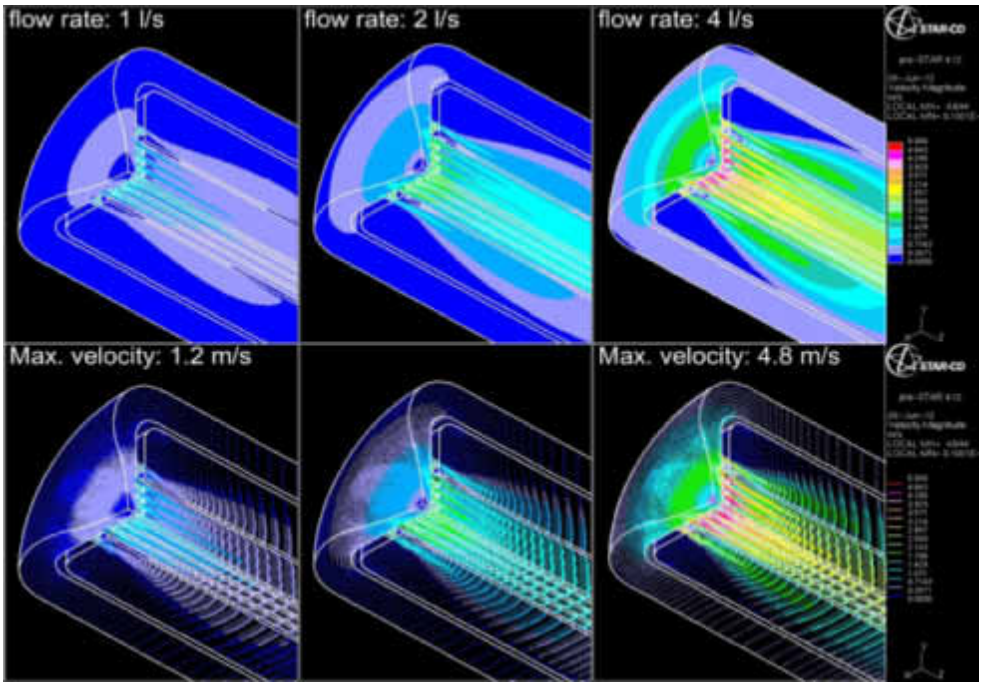


Figure 7. Temperature profile of beam window by changing thickness

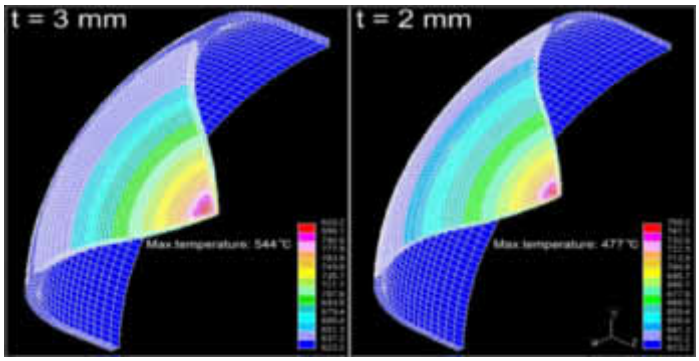
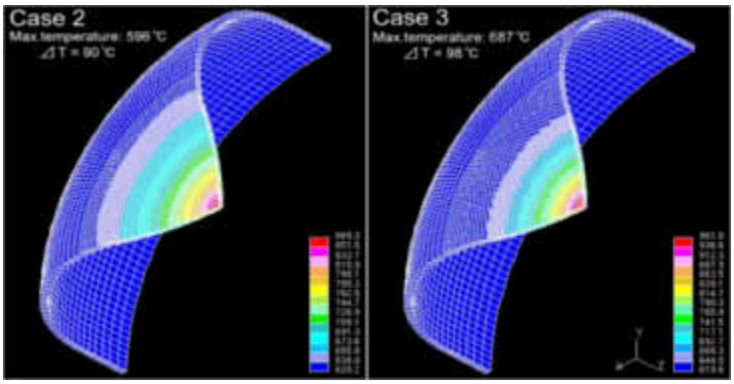
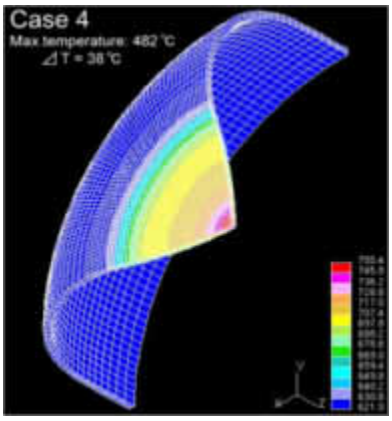


Figure 8. Temperature profile by changing current density of proton beam



An example of the analysis result is shown in Figure 7. This result was the temperature profile on the beam window by changing the thickness of the beam window from 2 mm to 3 mm. The flow rate of LBE was 1 l/sec, and the proton beam profile was Case 1. The maximum temperature of 554°C was observed at the centre of the outside surface of the beam window due to the formation of the dead region of the LBE flow in the case of a 3 mm thick beam window. In the case of 2 mm thick window, peak temperature reaches 477°C. In this condition, it was confirmed that the maximum temperature was reduced to 12% by decreasing the thickness of the window. The temperature difference of the outside and the inside was 65°C and 37°C in the case of 3 mm window and 2 mm window, respectively. From these results, it was clear that a condition of 2 mm was reasonable. The result of the condition that changed the current density of the proton beam is shown in Figure 8. The flow rate was 1 l/sec, and the thickness of the beam window was 2 mm. In the conditions of Case 2 and Case 3, in which the beam current density was increased, the maximum temperature reached more than 500°C. The temperature differences also increased in both conditions, it was confirmed that this was a severe condition in the structural soundness of the beam window. As one method to realise a uniform exposure dose for each specimen, the beam of the flat top type has been considered. The temperature profile of Case 4 is shown in Figure 9. The flow rate was 1 l/sec, and the thickness of the beam window was 2 mm. The current density of the proton beam was 20 $\mu A/cm^2$, which was the same condition as Case 1. The maximum temperature was 482°C and the temperature difference was 38°C.

Figure 9. Temperature profile of Case 4



As a result of these analyses, the following conditions are reasonable for the TEF operation; (1) the flow rate of LBE is 1 l/sec, (2) the thickness of the beam window is 2 mm, and (3) the proton beam which has a Gaussian shape with the current density of 20 μA/cm^2. These conditions were set as a reference case for the realisation of TEF and thermal-stress analyses of the beam window were carried out.

Thermal stress analysis

The temperature and thermal stress for the steady-state was estimated using the ABAQUS code, the computational code for the finite element method. In the ABAQUS code, the beam window was modelled as the cylinder-slab geometry. The model consisted of 1,896 4-node axial-symmetric elements. For the estimation, the numerical results of the STAR-CD were converted to the temperature of each node. Figure 10 shows the analysis results under the reference condition. This figure is the contour plot of the stress strength (Tresca stress) in the in the cross-section of the beam window along the direction of the beam-axis, which is taken upwards in the vertical direction. The stress strength reached the maximum value of 190 MPa on the outer surface of the beam window.

Next, the stress strength obtained by steady-state analysis was divided into primary general membrane stress (P_m), primary bending stress (P_b) and secondary thermal-load stress (Q) to estimate the structural integrity of the beam window. At this time, P_m and P_b were calculated only from the inner pressure of the beam window. On the other hand, P_m+P_b+Q was calculated from both the inner pressure and the temperature distribution of the beam window. The results are tabulated in Table 2. These stresses should fulfill the following Equations 2-4 [4]:

$$P_m \leq S_m, \tag{2}$$

$$P_m + P_b \leq 1.5 S_m, \tag{3}$$

$$P_m + P_b + Q \leq 3 S_m. \tag{4}$$

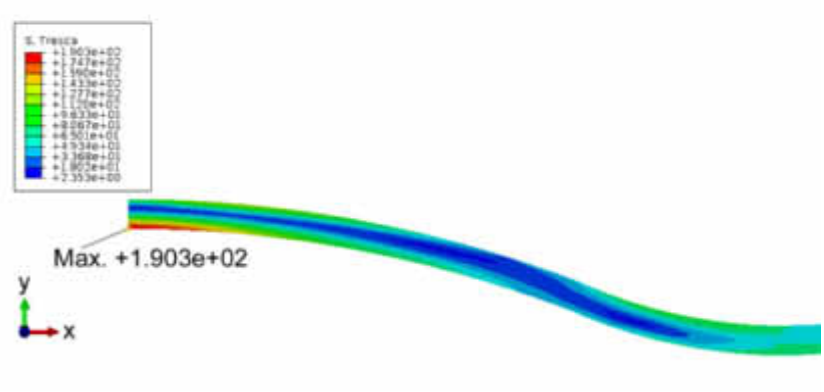
Here, S_m is time-independent design stress strength, and we adopted values for the maximum temperature at the centre of the wall thickness of the beam window (470°C).

Table 2 tabulates the evaluated values obtained in the left-hand side of Equations 2-4 and the acceptable values in the right-hand side. These stresses were lower than the tolerance level of the stress strength of the material because the feasibility of a designed beam window was confirmed.

Table 2. Comparison of the evaluated and acceptable values for each equation

Equation	Evaluated values	Acceptable values
(2)	44 MPa	98 MPa
(3)	73 MPa	147 MPa
(4)	190 MPa	294 MPa

Figure 10. Contour plot of the stress strength of the beam window



Conclusion

The reference case that was a first target condition in the development of TEF was decided by the thermal-fluid analysis result and it was shown that the soundness of the beam window was established in this condition by a result of stress analysis. In the near future, the following analyses will be performed, (a) the optimisation of a beam shape and the configuration of the flow channel, (b) the inlet LBE condition including the deflection of the LBE flow, and (c) the change in cooling performance for the beam window by the additional bypass jet flow.

References

[1] Sasa, T. et al. (2005), "Conceptual Study of Transmutation Experimental Facility (2) Study on ADS Target Test Facility", *JAERI-Tech 2005-021* [In Japanese].

[2] Niita, K. et al. (2010), "PHITS: Particle and Heavy Ion Transport code System, Version 2.23", JAEA-Data/Code 2010-022.

[3] Sugawara, T., Suzuki, K., Nishihara, K. et al. (2008), "Investigation of Beam Window Structure for Accelerator Driven System -Simplified Overall Integrity Assessment and Detailed Assessment on Buckling", JAEA-Research 2008-026, Japan Atomic Energy Agency, [in Japanese].

[4] Tsujimoto, K., Nishihara, K., Takei, H. et al. (2010), "Feasibility Study for Transmutation System Using Lead-Bismuth Cooled Accelerator-Driven System", JAEA-Research 2010-012, Japan Atomic Energy Agency, [in Japanese].

Parameters promoting liquid metal embrittlement of the T91 steel in lead-bismuth eutectic alloy

Ingrid Proriol Serre, Changqing Ye, Jean-Bernard Vogt
Université Lille 1, Unité Matériaux et Transformations, France

Abstract

The use of liquid lead-bismuth eutectic (LBE) as a spallation target and a coolant in accelerator-driven systems raises the question of the reliability of structural materials, such as T91 martensitic steel in terms of liquid metal assisted damage and corrosion. In this study, the mechanical behaviour of the T91 martensitic steel was examined in liquid lead-bismuth eutectic (LBE) and in inert atmosphere. Several conditions showed the most sensitive embrittling factor. The Small Punch Test technique was employed using smooth specimens.

In this standard heat treatment, T91 appeared in general as a ductile material, and became brittle in the considered conditions if the test was performed in LBE. It turns out that the loading rate appeared as a critical parameter for the occurrence of LME of the T91 steel in LBE. Loading the T91 very slowly instead of rapidly in oxygen saturated LBE resulted in brittle fracture. Furthermore, low-oxygen content in LBE and an increase in temperature promote this LME.

Introduction

The use of liquid lead-bismuth eutectic (LBE) as a spallation target and a coolant in accelerator-driven systems raises the question of the reliability of structural materials, T91 martensitic steel and 316L austenitic stainless steel in terms of liquid metal assisted damage and of corrosion. Previous studies have analysed the corrosion resistance and the mechanical properties of the T91 steel in LBE [1] [2]. The corrosion phenomena depend on the oxygen content in the LBE bath: a) oxidation when the oxygen concentration is high enough to permit the magnetite formation according to thermodynamic equilibrium and b) dissolution of the metal substrate when the oxygen concentration is too low [3]. The fatigue resistance of the T91 steel decreases in an LBE bath saturated in oxygen compared with the fatigue resistance in air. LBE assists the propagation of the first short cracks by preventing the nucleation and propagation of other cracks. Thus, the grain boundary resistance to crystallographic growth vanishes when LBE is in contact and allows easy extension of the crack into the bulk [4]. Some studies aimed to analyse the coupling effect between corrosion degradation and mechanical damage for these steels have been conducted in two successive stages: pre-immersion in an LBE bath at controlled oxygen content without mechanical loading followed by a mechanical test in saturated oxygen LBE. Pre-immersion has a negative impact on the monotonic resistance, the creep properties and the fatigue resistance of the T91 according to the oxygen content in the LBE bath of the pre-immersion and the loading conditions. LBE can be considered as a source of “microcracks” when the dissolution process occurs and a promoter of crack growth [5].

One of the major criteria used to evaluate the compatibility of the structural materials with the presence of a liquid metal is the risk of Liquid Metal Embrittlement (LME). Liquid metal embrittlement refers to a loss of ductility of an otherwise ductile material when stressed in contact with a liquid metal [6] [7]. In this case, the liquid metal induces a ductile to brittle transition in the mechanical behaviour of the material. Some studies showed a risk of LME of the T91 steel by the LBE saturated in oxygen. Then, LME was associated to a hardening of the microstructure of the T91 steel or to the nature of the oxide layer. In high-strength materials (T91 steel as quenched, tempered at 600°C or 500°C), a ductile to brittle transition is induced by LBE, confirmed by the observation of brittle fracture [8] [9]. In relative high-strength materials (tempered at 650°C and 700°C), LBE promotes a decrease in the mechanical properties and a reduction of the ductility of materials, with a mixed ductile and brittle fracture. For the standard heat treatment (tempered at 750°C), no effect of the LBE has been observed for the following conditions: LBE saturated in oxygen, T91 steel with its native oxide layer, strain rate around 5.10^{-3} s^{-1}. The absence of the native oxide layer or the presence of a Fe_2O_3 layer promotes the LME of the T91 steel in his standard heat treatment [10].

The objective of the present paper is to study whether other factors (velocity, temperature, oxygen content in LBE) promote the embrittlement in LBE of the T91 steel in standard heat treatment. The Small Punch Test (SPT) has been employed as a mechanical test. Indeed, even if first it was developed to study irradiated materials because it requires small amounts of materials, it later proved very sensitive to evidence liquid metal embrittlement.

Material and experiment

The material studied in this investigation is the T91 martensitic steel supplied in the form of rolled plate. Its chemical composition is given in Table 1. The standard heat treatment of the steel is normalised at 1050°C for 1h followed by air cooling and subsequent tempering for 1h at 750°C. The microstructure observed after etching with Villela's reagent is martensitic with a prior austenitic grain size of 20 µm. The Vickers hardness (Hv_{10}) of the steel is 278 Hv.

Table 1. Chemical composition of T91 steel

Element	C	Cr	Mo	Nb	V	Si	Mn	Ni	Fe
wt%	0.11	8.80	1.00	0.07	0.25	0.41	0.38	0.17	Bal

Small Punch Tests (SPT) were performed in air, in an argon/hydrogen gas mixture environment, in an oxygen saturated LBE (44 wt% Pb and 56 wt% Bi) bath and in a purified low-oxygen LBE bath. The SPT consists of a disk specimen holder, a pushing rod and a ball. The specimen holder includes a lower die and an upper die, which is also used as the tank for the liquid metal. The load is transferred onto the specimen by means of a pushing rod and a 2.5 mm diameter tungsten carbide ball in contact with the lower surface of the disk specimen. In this way, the puncher being under the specimen, the upper surface of the specimen is in contact with the liquid metal and is submitted to tensile loading. SPT specimens with dimensions of 10×10×0.5 mm were mechanically polished with SiC paper up to 1200 grade, and then polished step by step with a suspension liquid to 1 µm. The thickness of the specimen was controlled around 500±10 µm. SPT were performed using an INSTRON electronic mechanical machine which can control the experimental cross-head displacement velocities of 0.0005 mm/min, 0.005 mm/min, 0.05 mm/min and 0.5 mm/min. A heat ring surrounded the set-up with the specimen and the liquid metal. The temperature was controlled by a thermocouple placed

3 mm away from the specimen to perform tests at different temperatures: from 200°C to 450°C. Other details concerning the SPT set up can be found in [8] [11].

To perform SPT in a low-oxygen LBE (purified LBE), a purification unit was designed. It consisted in filling the LBE bath with a mixture of argon/hydrogen gas which allowed decreasing the oxygen content up to 10^{-8} wt% at 450°C. Then the purified LBE was transferred to the SPT set-up installed in a test cell made of stainless steel, where the atmosphere was controlled. Indeed, to protect the purified LBE from oxidation, the cell interior atmosphere was controlled due to a purification unit in order to remove water vapour and oxygen. This was based on flux sweeping by argon and argon/hydrogen, and on the use of reactive filters. The oxygen content and the water content in the cell interior are lowered as low as 0.1 ppm and 10 ppm, respectively.

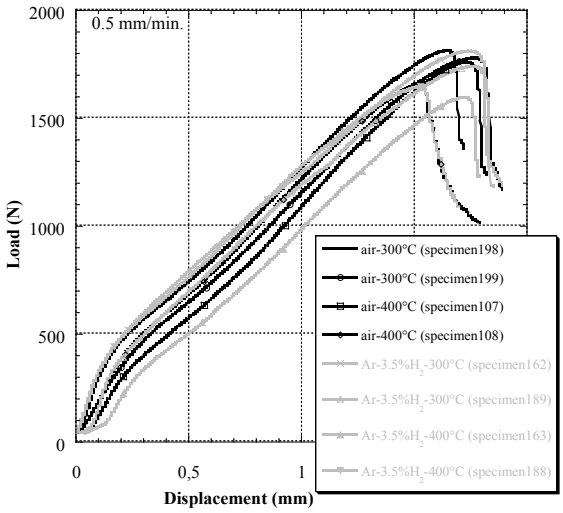
After SPT, the fracture surfaces were analysed by a scanning electron microscope (SEM). Prior to the SEM examination, some samples tested in LBE were cleaned in a solution containing CH_3COOH, H_2O_2 and C_2H_5OH at a ratio of 1:1:1 to remove the LBE.

Results

Influence of the protective Ar-3.5% H_2 gas on the testing cell

The removal of the oxygen from LBE and the cleaning of the test cell were achieved by using a mixture of argon/hydrogen. Then, SPT at 300°C in air and in Ar-3.5% H_2 gas (see Figure 1) were performed to confirm that the gas mixture (Ar-3.5% H_2) did not have any effect on the mechanical response of the T91 steel in the absence of liquid metal. In the two environments, the SPT curves showed the ductile behaviour of the T91 steel, which was confirmed by the observation of a large plastic deformation of the sample, of a circular crack, and of the presence of dimples on the fracture surfaces. No effect of Ar-3.5% H_2 was observed. This result also showed that the presence of hydrogen in the protective gas in the testing cell had no effect on the mechanical response of the T91 steel.

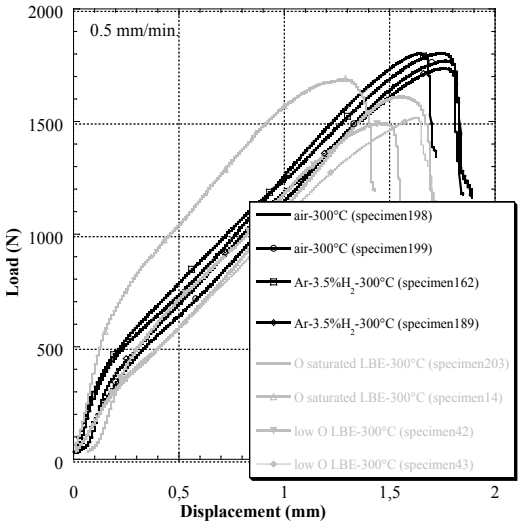
Figure 1. Load-displacement curves of the T91 steel tested in air and in Ar-3.5% H_2 gas, at 300°C and 400°C, at 0.5 mm/min



Influence of the temperature and of the oxygen content

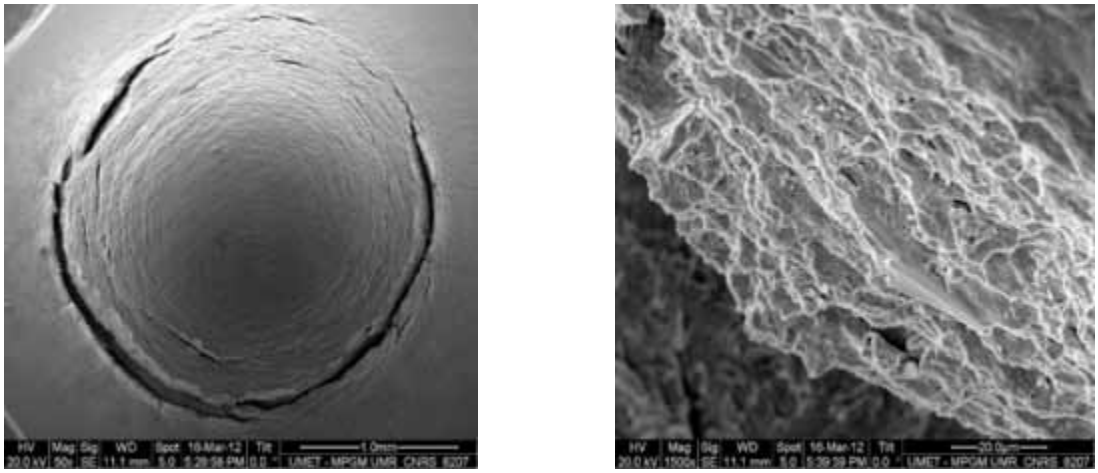
SPT were performed at a displacement speed of 0.5 mm/min, at different temperatures (200, 250, 300 and 400°C), in air, in Ar-3.5% H_2 gas, in oxygen saturated LBE, and in liquid LBE purified by Ar-3.5% H_2.

Figure 2. Load-displacement curves of the T91 steel tested in air, in Ar-3.5% H_2 gas, in oxygen saturated LBE, in low oxygen LBE, at 300°C and at 0.5 mm/min



As for 300°C, for all the studied temperatures, all the curves exhibited a ductile behaviour of the T91 steel (see Figure 2). The SEM observations of the specimens showed the ductility of the fracture (see Figure 3).

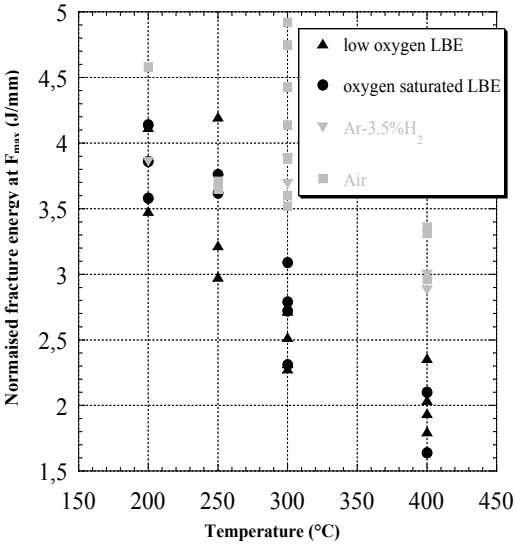
Figure 3. Fracture surface of the T91 tested in oxygen saturated LBE at 200°C, at 0.5 mm/min



The fracture energy at the maximum load F_{max} corresponds to the area under the load versus displacement curve. It was normalised by the thickness of the sample. This normalised energy represents the energy necessary for the elastic and plastic deformations of the sample and for the formation of cracks which are sufficient to

promote the damage of the sample. The graph in Figure 4 shows the evolution of the normalised fracture energy at F_{max} according to the temperature and the environment.

Figure 4. Normalised fracture energy at F_{max} according to the temperature and the environment (SPT at 0.5 mm/min)

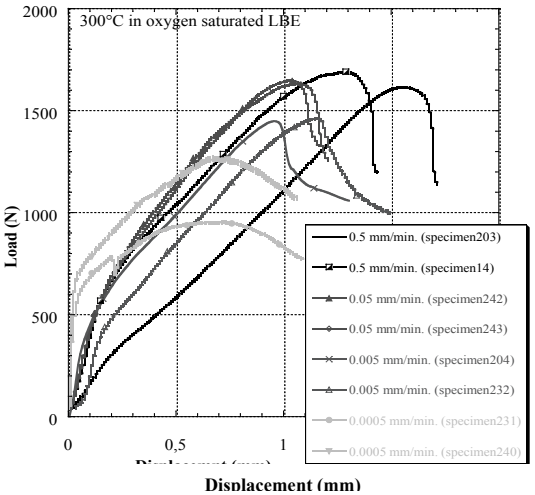


The small decrease of the fracture energy in the presence of the LBE does not involve LME, but only some earlier damage in LBE without transition in fracture mode. This effect seems to increase with temperature. On the other hand, in the studied conditions of strain rate and temperature, no effect of the oxygen content on LBE was observed.

Influence of the strain rate

In order to analyse the role of loading rate or strain rate, tests were performed in oxygen-saturated LBE at 300°C at different displacement velocities: 0.5 mm/min, 0.05 mm/min, 0.005 mm/min and 0.0005 mm/min. SPT curves are reported in Figure 5.

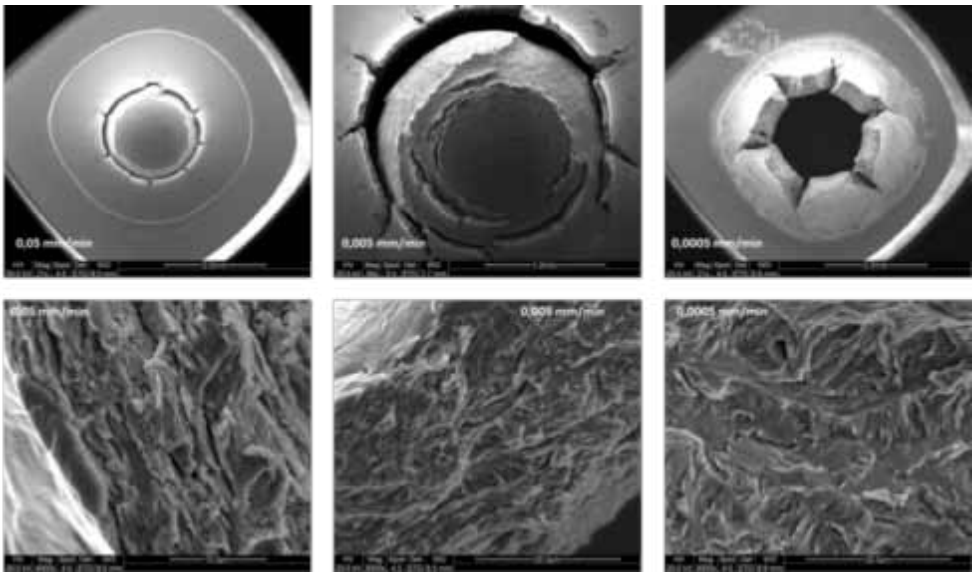
Figure 5. Load-displacements curves of the T91 steel tested in oxygen-saturated LBE, at 300°C and for different loading rates



SPT curves showed a strong dependence on displacement speed. First, for the lowest displacement speed, the maximum load is strongly reduced as compared to the other tests performed at high speed by a factor of two third. Second, the displacement at maximum load is decreased in the same way.

The analysis of the fracture surfaces also highlighted an effect of the displacement velocity (see Figure 6).

Figure 6. Fracture surfaces of the T91 steel tested in oxygen saturated LBE at 300°C



All the SPT specimens exhibited circular and radial cracks but the decrease in the displacement velocity promoted radial cracking. For the lowest displacement velocity, the number of radial cracks is greatly reduced as compared to the other tests and the radial cracks are also much longer. In addition, transgranular brittle fracture was observed. At 0.005 mm/min, the brittle fracture was observed only near the surface of the specimen in contact with the liquid metal. In the case of the lowest strain rate (0.0005 mm/min), the fracture was brittle.

Figure 7 presents the evolution of the normalised fracture at F_{max} according to the displacement rate and the oxygen content in LBE. The lower the displacement speed is, more sensitive the T91 steel of the presence of the liquid metal is. Furthermore, low-oxygen content in LBE promotes this LME.

Figure 7. Normalised fracture energy at F_{max} according to the temperature and the environment (SPT at 0.5 mm/min)

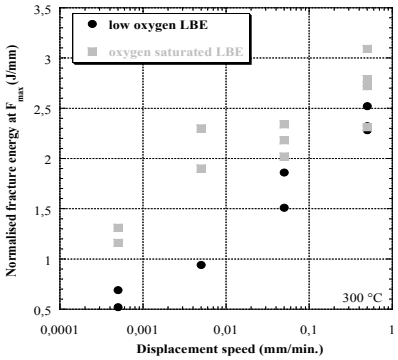
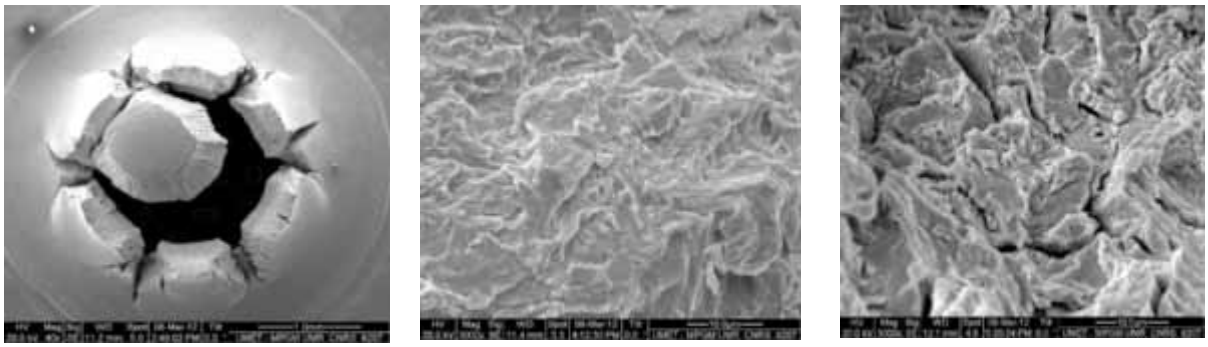


Figure 8. Fracture surface of the T91 steel tested in low oxygen LBE at 300°C and at 0.005 mm/min



Indeed, at 0.005 mm/min, the T91 steel is more sensitive to LBE if the oxygen content of the liquid metal is low. While the steel is essentially ductile in the presence of oxygen saturated LBE, the facture surface (see Figure 8) is brittle in the presence of low-oxygen LBE. The fracture is transgranular, but some intergranular fractures were observed.

Discussion

The present investigation shows that T91 steel is a ductile material but its ductility can be reduced by several factors, resulting in a ductile to brittle transition. Weakening effects of LBE on T91 steel properties have been reported. Basically, two groups of experiments that have pointed out the harmful effect of LBE can be distinguished depending on whether smooth or notched specimens have been employed. By using notched specimens, a reduction in toughness and/or acceleration in crack growth by LBE has been reported on T91 steel [12-15]. On smooth specimens, occurrence of the LBE effect on the ductility of T91 required modification of the microstructure by changing the tempering temperature in the heat treatment of the steel or by decreasing the oxygen content in the LBE bath [8] [11] [16] [17]. A key factor which is systematically presented as a condition is the possibility of wetting. In general, oxidation avoids wetting and brittleness [11].

The present investigation, which employed smooth specimens, tends to show that the situation is not as clear as expected. Indeed, changing the saturated oxygen LBE bath for the low-oxygen LBE, it was not possible to modify much the behaviour of the T91 in a temperature range between 200°C and 400°C when it was deformed at 0.5 mm/min. Indeed, when the steel is in contact with the purified LBE, the native oxide is not affected and the liquid metal could act only at the non-oxidised slip bands surfaces. It should be noted that the reduction was in mechanical resistance in the T91 tempered at 750°C in the low-oxygen LBE bath if deformed at a low displacement velocity (0.005mm/min and 0.0005 mm/min) and in oxygen-saturated LBE at 0.0005 mm/min. The decrease in the displacement velocity resulted not only in a decrease in the maximum load but also in a decrease in the displacement value at maximum load. In the present study, the duration of immersion of the T91 steel in LBE varies from a few minutes to a few hours from the investigated displacement velocity range. This contrasts very much with Hojna' results, where localised conditions for the occurrence of LME required pre-exposure for 1000 hours at 500°C and oxygen less than 10^{-6} wt%. No corrosion effect such as dissolution occurred. Thus, the effect of displacement speed can be related to the rate of adsorbed atoms of the liquid metal at fresh surfaces and the entrance of these atoms into the bulk at favourable sites such lath boundaries. In this way, the surface energy of such an interface could be decreased if a critical number of adsorbed atoms is reached due to the increased duration of contact with the liquid metal. This investigation leads us to believe that the low-oxygen LBE does not modify the wetting conditions, e.g. by removing the oxide layer. However, the low-oxygen content should promote the adsorption effect and

further entry in the material along interfaces from fresh deformation bands since their oxidation is disfavoured. The embrittlement of the T91 steel in oxygen-saturated LBE at very low strain rate tends to confirm this hypothesis.

Conclusion

The mechanical behaviour of the T91 steel has been studied by taking into account various parameters in order to identify the most effective ones that promote liquid embrittlement by LBE. The T91 steel is not very sensitive to LME by LBE even for low-oxygen LBE at high displacement speed. A decrease in the displacement spped leads to a ductile to brittle transition of the T91 steel deformed in oxygen-saturated LBE. Low-oxygen content in LBE and an increase in temperature promote liquid metal embrittlement.

Acknowledgements

The authors wish to acknowledge the financial support of the French CNRS GdR GEDEPEON. Ing. J. Golek and D. Creton are acknowledged for their assistance in the experimental work.

References

[1] Soler Crespo, L. (2007), "Handbook on lead–bismuth eutectic alloy and lead properties, materials compatibility, thermal-hydraulics and technologies", *Chapter 6: Compatibility of Structural Materials with LBE and Pb: Standardisation of Data Corrosion Mechanism and Rate*, *OECD/NEA*.

[2] Gorse, D. (2007), "Handbook on lead–bismuth eutectic alloy and lead properties, materials compatibility, thermal-hydraulics and technologies", *Chapter 7, Effect of LBE and Lead on Mechanical Properties of Structural Materials, OECD/NEA*.

[3] Martinelli, L., Dufreno, T., Jaakou, K., Rusanov, A., Balbaud-Célérier, F. (2008), *J. Nucl. Mater*. 376.282.

[4] Verleene, A., Vogt, J.-B., Serre, I., Legris, A. (2006), *Int. J. Fatigue* 28.843.

[5] Vogt, J.-B., Verleene, A., Serre, I., Balbaud-Célérier, F., Martinelli, L., Terlain, A. (2007), *Eng. Fail. Anal*. 24.1185.

[6] Fernandes, P.J.L., Jones, D.R.H. (1997), *Int. Mater. Rev*. 42.251.

[7] Joseph, B., Picat, M., Barbier, F. (1999), *Eur. Phys*. J. 5.19.

[8] Serre, I., Vogt, J.-B. (2008), *J. Nucl. Mater*. 376.330.

[9] Long, B., Tong, Z., Groschel, F., Dai, Y. (2008), *J. Nucl. Mater*. 377.219.

[10] Auger, T., Serre, I., Lorang, G., Hamouche, Z., Gorse, D., Vogt, J.-B. (2008), *J. Nucl. Mater*. 376.336.

[11] Serre, I., Vogt, J.-B. (2007), *Nucl. Eng. Des*. 237.677.

[12] Long, I., Dai, Y. (2008), *J. Nucl. Mater*. 376.341.

[13] Hojna, A., di Gabriele, F. (2011), *J. Nucl. Mater*. 413.

[14] Auger, T., Gorse, D., Hamouche-Hadjem, Z., van den Bosch, J., Coen, G., Almazouzi, A., Hojna, A., Dalikova, K., di Gabriele, F., Serrano, M., Gessi, A., Agostini, P., Vogt, J.-B., Serre, I. (2011), *J. Nuclear Materials* 415.293.

[15] Coen, G., van den Bosch, J., Almazouzi, A., Degrieck, J. (2010), *J. Nucl. Mater*. 398.122.

[16] van den Bosch, J., Sapundjiev, D., Almazouzi, A. (2006), *J. Nucl. Mater*. 356.237.

[17] van den Bosch, J., Bosch, R.W., Sapundjiev, D., Almazouzi, A. (2008), *J. Nucl. Mater*. 376.322.

[18] Nicaise, G., Legris, A., Vogt, J.-B., Foct, F. (2001), *J. Nucl. Mater*. 296.256.

Conceptual design studies for the liquid metal spallation target META:LIC

J.R. Fetzer[1*], A.G. Class[1], C. Fazio[2], S. Gordeev[3]
[1]Institute for Nuclear and Energy Technologies (IKET), Germany
[2]Nuclear Safety Research Programme (NUKLEAR), Germany
[3]Institute for Neutron Physics and Reactor Technology (INR), Germany
Karlsruhe Institute for Technology (KIT), Germany

Abstract

A re-evaluation of various target concepts was decided by the target station concept selection group during the design update phase of the European Spallation Source (ESS) in order to include new target concepts in their selection process. During this phase, the META:LIC (Megawatt Target: Lead bIsmuth Cooled) concept was invented and developed based on an analysis of existing and new liquid metal targets. Within two years of design and R&D activities, the META:LIC concept reached the level of proof of principle and was selected as comparative target solution for assessment purposes for ESS. Both a window target option for the start of operation and a windowless target option with extended lifetime are foreseen. The present work describes the META:LIC target concept that has LBE (lead-bismuth eutectic) as a spallation material and a primary coolant. Emphasis has been placed on the target module. Thermo-hydraulic simulations for both options are presented, as well as design measures to mitigate pulsed proton beam induced phenomena.

Introduction

The European Spallation Source is a European initiative to build the world's most powerful spallation neutron source in Lund, Sweden. In the 2003 ESS report [6] an extensive feasibility study, including a complete design proposal is provided. The concept is based on directing high-power protons on heavy atoms, which are fragmented in the process yielding free neutrons. The protons provided by an ion source are accelerated to high power by the linear accelerator. This proton beam then hits the spallation target, which represents the subject of our current work. Fast neutrons from the spallation reaction are moderated to fairly low energies in a cold an ultra-cold moderator. Reflectors surrounding the target and moderators enhance the neutron flux. The target monolith ensures safe enclosure of activated structures and materials.

Within ESS, several high-power spallation target design options have been investigated. Among them a helium-cooled solid tungsten rotating target, named RoTHeTa [13], has been selected as the reference option and a water-cooled solid target, as well as the LBE target, as comparative solutions [13]. The above-mentioned META:LIC target is the LBE comparative solution. META:LIC is being currently developed by the Karlsruhe Institute of Technology (KIT) supported by the Helmholtz Zentrum Dresden-Rossendorf (HZDR), Forschungszentrum Jülich (FZJ), Institute of Physics at the University

of Latvia (IPUL) and the Paul Scherrer Institute (PSI). Table 1 shows the relevant beam proton beam parameters for the target design.

Table 1. Relevant beam parameters considered for the META:LIC target design

Average beam power	5 MW
Beam energy	2.5 GeV
Average beam current	2 mA
Pulse length	2.86 ms
Pulse repetition rate	14 Hz
Parabolic beam profile	160 mm x 60 mm

The design motivation of META:LIC is descibed in the following sections. Next, the conceptual design is described with a focus on the two target module options, the window and the windowless option. For each target module a preliminary thermo-hydraulic analysis is presented.

META:LIC design motivation

The META:LIC target design is based on the experience and lessons learnt from previous liquid metal target designs such as the target for the MYRRHA research reactor [14], MEGAPIE [3] [9], NuSTAR [8], SNS [10] and JSNS [11]. The design of the above-mentioned targets, in particular the design of the liquid metal flow was taken into account for the development of META:LIC in order to incorporate the previous experience [14-15]. In particular, the analysed flow characteristics are the angle between the coolant flow and the proton beam, the necessity of flow conditioning upstream of the spallation zone and sensitivity with respect to the outflow. In addition, the flow configuration ensuring window cooling and the pressure inside the target compared to ambient conditions were studied. The resulting design guidelines for the META:LIC concept are hereafter summarised:

- the beam direction has been kept almost coaxial to the LBE flow;
- stagnation points have been avoided;
- flow limiter has been avoided;
- complex flow conditioning has been avoided mainly to allow for an analytical pre-design;
- decoupling of the outflow has been kept.

Concerning the selection of the liquid metal as a spallation material, several options have been available as e.g. mercury, LBE etc. However, liquid lead-bismuth eutectic (LBE) has been selected as the preferred spallation material since considerable experience is available for this liquid metal in Europe. Indeed, the licensing, operation, on-going post-irradiation analysis and decommissioning of the high-power LBE cooled target MEGAPIE (a window target concept) are demonstrated at PSI. Moreover, an extensive database of LBE is summarised in the handbook on LBE published by the OECD/NEA [4].

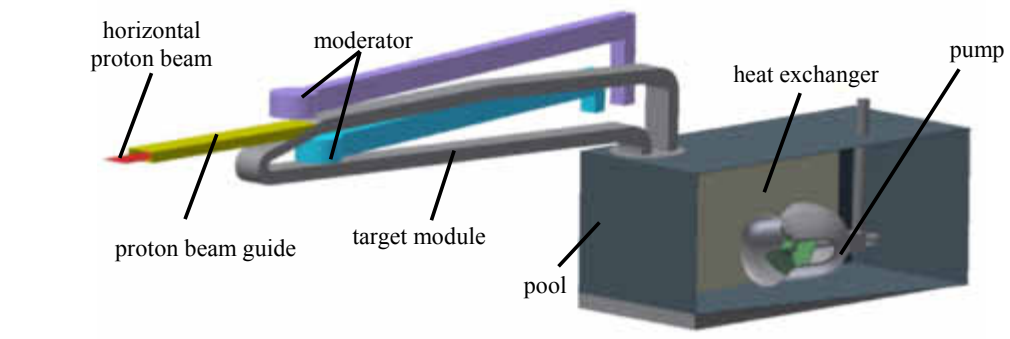
Conceptual design

As mentioned before, the META:LIC target is a liquid metal target in which LBE is both a target material and a primary coolant. Figure 1 shows the conceptual design of the modular target systems. The displayed concept is valid for both the window and the

windowless target systems. The target system has three separately replaceable modules: a target module (window/windowless), a pump module and a heat exchanger module. These three modules are connected to a LBE pool. In particular, the heat exchanger and pump are submerged in the pool and the target module (either the window or the windowless option) is attached to the pool. A containment which safely encloses the whole system is foreseen, however, it is not shown in Figure 1. In order to replace the individual modules, the whole META:LIC target system is moved on a trolley into the hot cells where the containment can be opened. The anticipated trolley system is similar to the arrangements at SNS [1] and JSNS [2].

The decision to develop two target module variants is related to the possibility to handle at the start-up phase, a known concept, namely the window target module and to implement in a later stage the window target option with an extended lifetime and for higher proton beam power.

Figure 1. Modular META:LIC concept including target module, pump module, heat exchanger module, LBE pool, proton beam, proton beam guide and two moderators



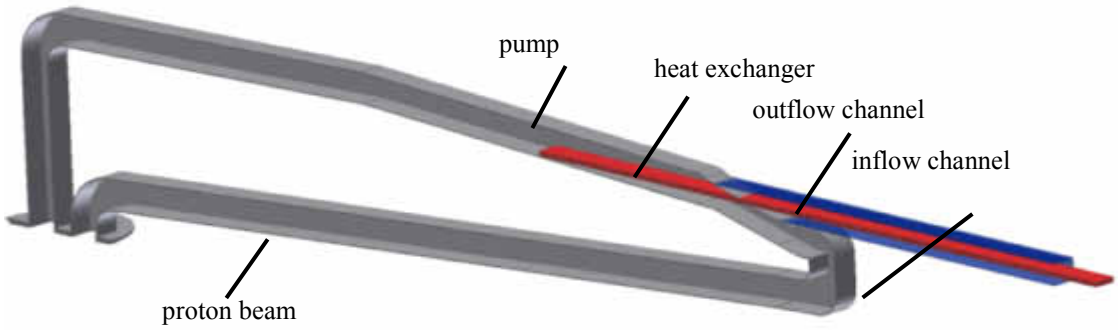
Window target module

Figure 2 depicts the window option of the target module which is double walled. The window target module consists of a proton beam guide with a safety window (not shown), an inflow *channel* leading to a nozzle producing a uniform block velocity profile, a *U-bend* with an expansion chamber and spoiler enforcing flow detachment to counteract the effects of the thermal expansion in the LBE due to the pulsed proton beam, and an *outflow duct*. The flow is pumped upwards into the inclined inflow channel (±3 degree angle), then accelerated by the nozzle producing an extremely stable and uniform block velocity profile that does not suffer instabilities. Next, the LBE flows through the proton beam interaction zone which is inclined relative to the horizontal plane by 15 degrees. The LBE returns to the pool through a U-bend and an outflow duct. A horizontal proton beam enters the liquid metal through a solid wall approximately 1.5 mm thick. The small inclination angle of the proton beam interaction zone provides an almost coaxial LBE flow and proton beam. This results in a fairly uniform heating of the coolant so that a minimal coolant flow rate can be established. Due to the inclination of the proton beam interaction zone, the flow component perpendicular to the proton beam transports the fluid across the beam in a fairly short time. This is advantageous for pulsed beams, as successive beam pulses interact with fluid that was not subjected to the beam previously. Since the window of the target module does not count as a safety barrier, a double-walled proton beam guide welded to the target module and a double-walled target station beam entrance window acting as safety barriers are proposed. In the gap between the walls, a cover gas system is implemented for the monitoring of leakage.

The pulsed nature of the ESS proton beam results in water hammer phenomena in the window target module. Indeed, the energy deposition due to a proton pulse leads to a

temperature rise in the material within a short timescale. Due to inertia of the surrounding LBE the thermal expansion of the target material within the spallation zone is suppressed. This results in an initial pressure rise and thus a pressure wave. Potentially this leads to high stresses on the target container material. Cavitation damage can occur when the pressure wave is reflected, leading to negative pressures. The time-scale of the ESS pulse is such that the target material can respond through an appreciable expansion during the pulse. For normal operation conditions, preliminary calculations of the pressure transients for the META:LIC window option indicate moderate peak pressures up to 10 bars at the container material. Potentially critical are sudden events like beam trips. Starting with normal operation conditions the pressures in the window region will significantly decrease due to the inertia of the liquid metal flow and the deficient thermal expansion when the beam is suddenly cut off. Once the flow field conforms to the beam-off conditions, the pressure will increase during the first pulses, when the beam starts again. There is insufficient stress relaxation during the first pulses following a beam trip and deformations so that stresses will be accumulated for several pulses [7].

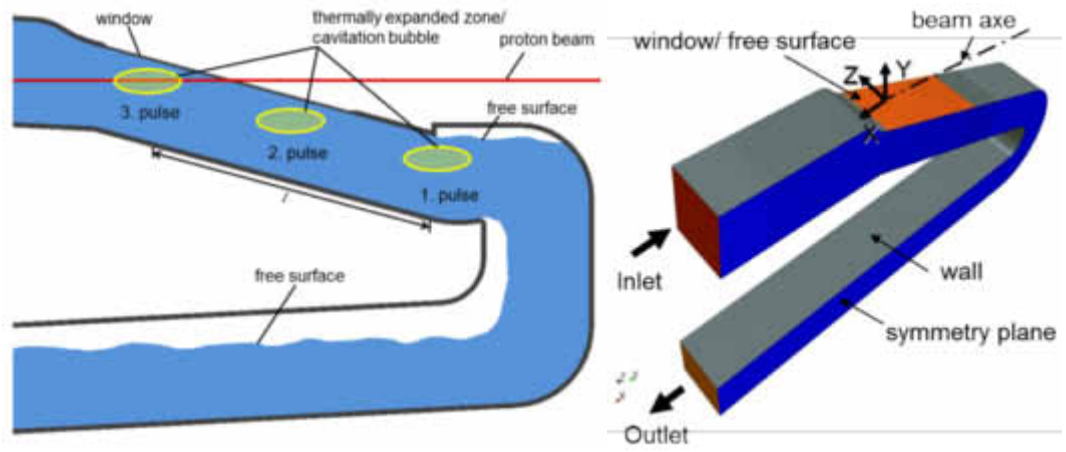
Figure 2. Window target module including proton beam and proton beam guide



The META:LIC window option incorporates design measures to limit the effects of cavitation and high stresses that can occur on the container material during transients. These design measures include an expansion chamber in the U-bend and a spoiler enforcing flow detachment. This results in two internal free surfaces, (i) in the outflow channel and (ii) in the expansion chamber. Moreover, the free surfaces in an effective manner decouple flow in the beam interaction zone from conditions in the outflow duct.

Figure 3 (left) schematically shows how the integrated free surfaces achieved by the described design modifications interact with transients due to unsteady events (e.g. in the case of a sudden beam trip). Starting with steady-state operation conditions the fluid pressure in the window region will decrease due to the inertia of the liquid metal flow and the absence of thermal expansion when the beam is suddenly cut off. This sudden change in volume is compensated by deformations of the container in the window region and probably cavitation within the fluid. Once the flow field conforms to the beam-off conditions the pressure will increase during the first pulses when the beam starts again and the sudden thermal expansion is compensated by deformations of the container in the window region. Figure 3 (left) depicts the approximate locations of the thermally expanded volume /cavitation bubbles for a time scale, corresponding to three successive pulses. The thermally expanded zone/cavitation zone is transported downstream with the bulk velocity to the free surface in the expansion volume chamber zone within 2-3 pulses. When the thermally expanded zone/cavitation zone reaches the free surface, they are neutralised. With this design modification wall stresses due to compensation of a missing thermal expansion during a beam trip or the starting thermal expansion after a beam trip are accumulated for 2-3 pulses until saturation is reached.

Figure 3. META:LIC design with internal free surfaces (left) and geometry and boundary conditions for window/windowless target module thermo hydraulic simulations (right)



Window target: feasibility of expansion volumes

The feasibility of the expansion volume and the transient behaviour of the target module have been investigated with two and three dimensional isothermal, transient CFD simulations with the open source CFD tool OpenFOAM Version 2.1. The utilised OpenFOAM solver is InterFoam, which uses a volume of fluid (VOF) approach to simulate two fluids. The two simulated fluids are air at 525 K (phase 0) and liquid LBE at 525 K (phase 1). The material properties of LBE are taken from [4]. The numerical grid used for the three-dimensional case consists of approximately 1.8 million hexahedral elements and for the two-dimensional case of 102 000 hexahedral elements. At the wall boundaries, a no-slip condition is applied. Turbulence is modelled with the high Reynolds number k-ω SST model. For both simulations, an inflow velocity of 1.5 m/s in x-direction and a vanishing pressure at the outlet have been assumed. The initial and boundary conditions for both calculations are displayed in Figure 4.

Figure 4. Initial and boundary conditions 3d (left) and 2d (right) VOF simulation

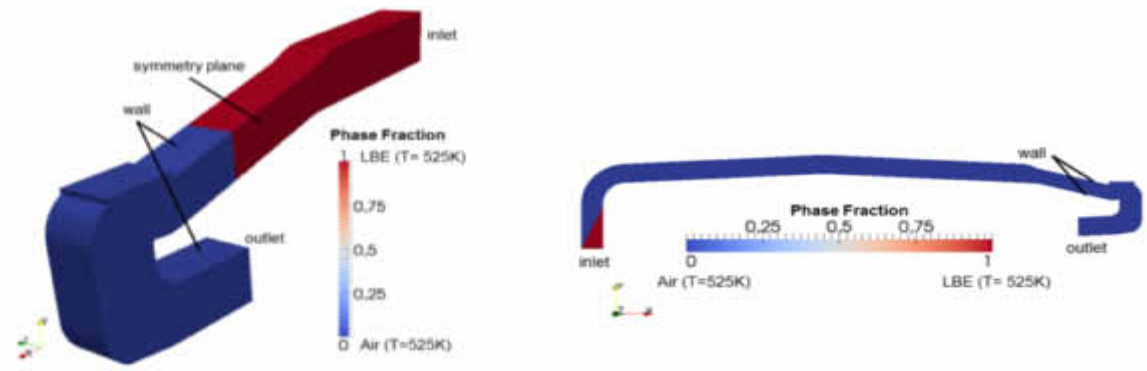
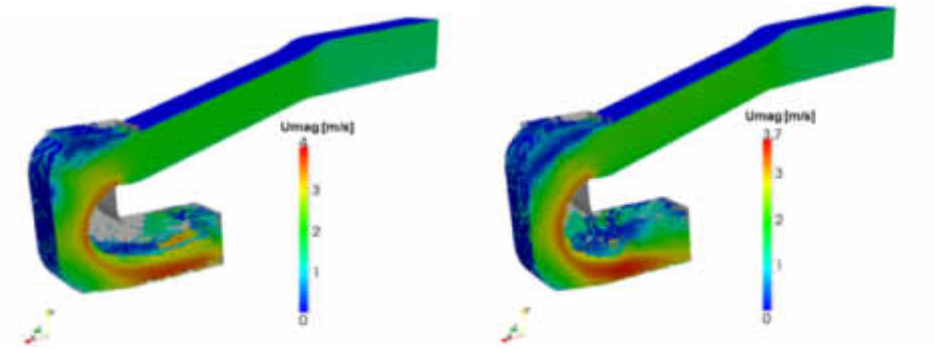


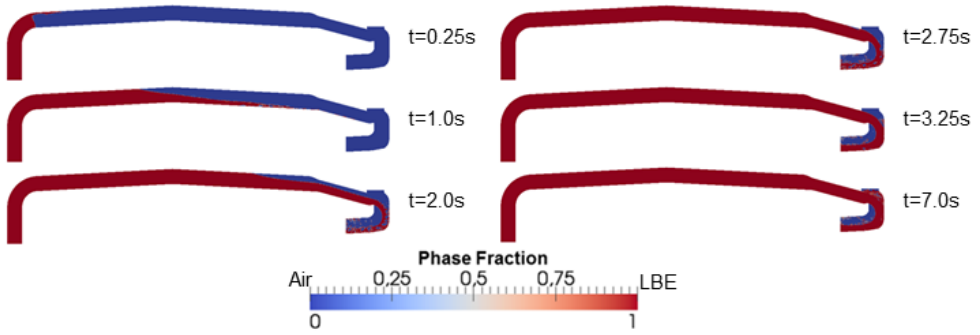
Figure 5 displays the resulting distribution of the velocity magnitude of the LBE phase at t=1.5s (left) and t=3.0s (right). The two figures confirm that the internal free surfaces are formed at the desired locations. The computed flow velocities range between 1 and 4 m/s. However, it can be anticipated that the corrosion limit of the proposed structure material (T91) at the critical locations, i.e. at thin walls, might not be exceeded. Less can be said about erosion limits, since these seem to be dependent on the formation of vortices or similar phenomena. The two figures also show that non-wetted walls are subjected to splashes, so that these structures can possibly be cooled from the inside alone. Splashing can be supported by design if needed.

Figure 5. LBE velocity magnitude distribution in m/s for t=1.5 (left) and t=3.0s (right)



The filling process of the META:LIC target module is simulated with a two-dimensional simulation and shown in Figure 6. In this figure, the filling process of the target module is displayed by the VOF phase fraction for representative time steps. The two-dimensional calculation illustrates that a start-up transient with nominal flow rate establishes the desired flow configuration in META:LIC, with free surfaces at desired locations. A start-up transient with half the nominal flow rate yields a partially filled target module, i.e. an inappropriate flow configuration.

Figure 6. Filling process of the META:LIC target indicated by the VOF PhaseFraction



Window target: thermo-hydraulic analysis

A thermohydraulic analysis of the window target module has been conducted using the commercially available programme package Star-CCM+. The geometry for the simulation as well as the applied boundary patches are shown in Figure 3 (right). It is to be noted that the thermohydraulic results obtained here are for an earlier window target layout. However, since the design modifications occurred outside the beam interaction zone, the obtained results can be applied to the latest design as described in the previous section. A mesh of about 10^6 polyhedral cells has been used for the simulation. For the turbulent flow modelling, the k-ε high Reynolds number model is chosen, since it features a reasonable physical representation of the problem at a reasonable

computational time. Standard wall functions are applied. A second order UPWIND discretisation scheme has been used for momentum, turbulent kinetic energy, turbulent dissipation rate and energy. The test section is modelled, assuming non-slip boundary conditions at each wall.

Figure 7. Energy deposition in LBE (left) and heat deposition in time (right)

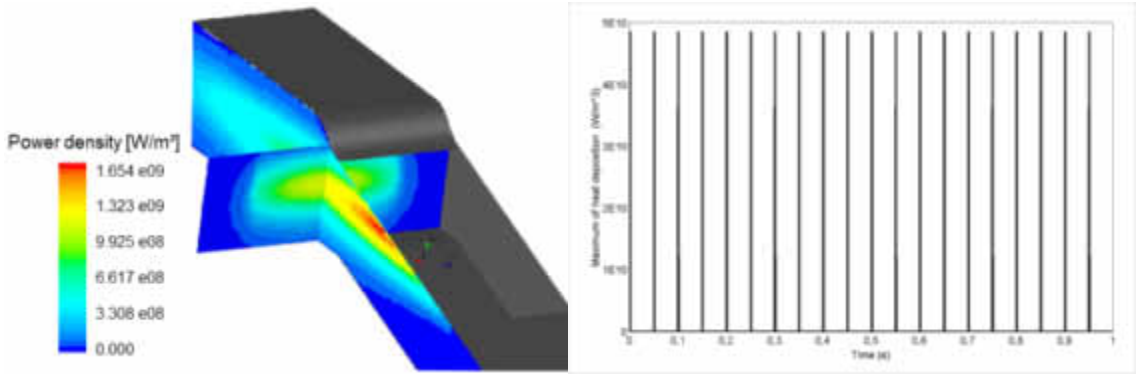


Figure 8. Mean temperature distribution LBE (left) and structure material (right)

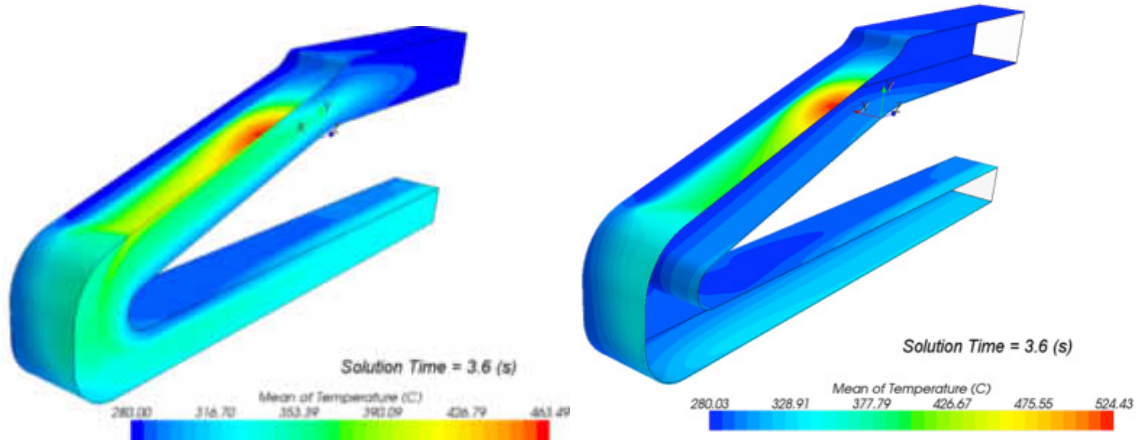
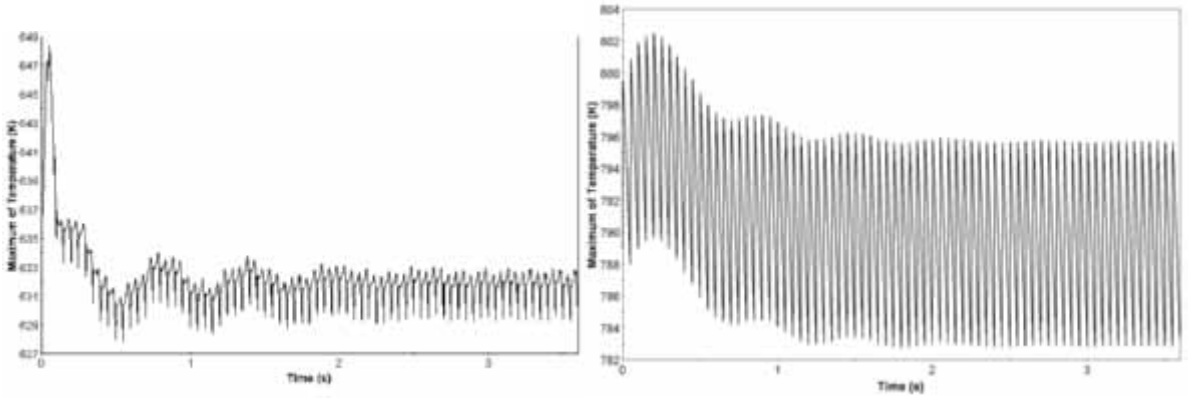


Figure 9. Maximum temperature as a function of time LBE (left) and structure material (right)



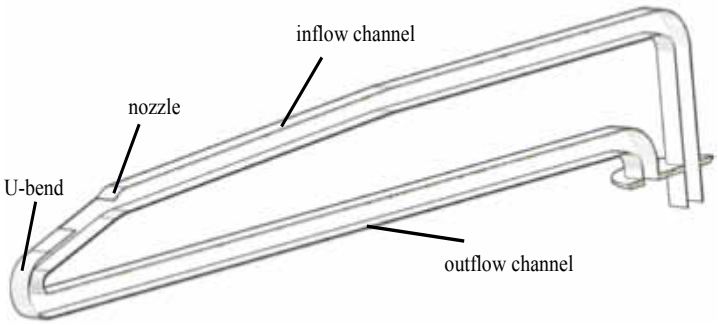
At the inlet a uniform velocity profile is assumed. At the outlet a pressure condition is taken applying an absolute pressure of 1 Pa. The unsteady calculation with the time step of $2 \cdot 10^{-4}$s was carried out with a total calculation time of 3.6 seconds. The thermo-mechanical properties of the structural material (Steel T91) are taken from [5]. The proton beam is modelled as a heat source assuming long pulses of 2 ms and a repetition rate of f=20 Hz. Figure 7 depicts the maximum heat deposition as a function of time and the energy release within the LBE. These proton beam parameters differ from the baseline parameters given in Table 1. The local maximum in time average power density is similar and therefore the effect on time-averaged stationary temperatures is small. However, lower beam pulse repetition rate will signigicantly increase the energy deposition and temperature increments per pulse and corresponding cyclic thermal stresses still need to be investigated.

The proton beam enters the liquid metal through a 1.5 mm thick window made of structural material. The flow velocity in the irradiated area is approximately 2 m/s. Figure 8 displays the mean temperature distribution in the fluid and target structure. The maximum temperatures in LBE and in the target structure as a function of time are given in Figure 9. With the assumed conditions, all computed temperatures are within the temperature range allowed for the proposed structure material. Thermal stresses are yet to be computed. They might be acceptable for the indentified temperature cycling.

Windowless target module

Figure 10 shows the windowless target module. As previously indicated, the windowless target module mainly differs from the window target by the fact that the window is removed and a free surface flow is established. Moreover, no design measures need to be implemented to mitigate the water hammer phenomena induced by the pulsed proton beam, since the proton beam-induced high pressure and cavitation zones are neutralised at the free surface. In general, the windowless target option can potentially provide a larger margin for proton beam power upgrades with respect to the window option since all related performance aspects of the window material are not applicable here.

Figure 10. Windowless target module



In the windowless target design, the proton beam is directed on a free surface so that no solid structures are subjected to the proton beam. Since the proton beam will interact with any material within its path the beam must be guided through a vacuum environment before hitting the target. In general, targets are enclosed in a safety shroud to safely enclose the activated inventory in case of an accident, thus limiting mitigation of the activated material. In the case of the windowless target module, the free surface is a natural boundary between the LBE and a vacuum. Since this natural boundary cannot be counted as a safety barrier, the role of the safety shroud becomes more pronounced. As a safety barrier for this target concept, a double-walled beam guide welded to the target module and a double-walled beam entrance window are proposed. In the gap between the walls, a cover gas system is installed in order to implement leak detection.

Potential splashing from the free surface can be collected in the beam guide and returned to the pool. Vapour condensation is achieved by cooling appropriate sections of the beam guide. This ensures that the target station beam entrance window is protected from direct contact with LBE, allowing the use of low cross-section aluminum alloys.

Windowless target: thermo-hydraulic analysis

One of the major concerns in the windowless configuration is flow stability of the free surface. To simulate the interface, the volume of fluid technique (VOF) applying a fixed eulerian mesh is used as a surface-tracking method. This technique is designed for the interface position prediction of two or more immiscible fluids. The discretisation of the transport equation is realised by an explicit time scheme. For the solution of the differential equations, the Courant number is less than 0.5. The time step for the VOF calculation is refined based on the maximum courant number near the free surface. The thermal-hydraulic analysis of the turbulent flow behaviour is conducted for 2 m/s. Star-CCM+ is used for the simulation. Figure 3 (right) displays the simulated geometry including the applied boundary patches. A mesh of 106 polyhedral cells has been used for the simulations. The two-phase flow problem is solved assuming liquid LBE and vacuum environment, here approximated by air at 1 Pa. The used heat source in the liquid phase is displayed in Figure 7. It should be noted that all other numerical parameters are described in the section: "Window target: thermo-hydraulic analysis".

Figure 11. Development of the free surface flow (left), temperature distribution for inlet flow velocity 2 m/s (right)

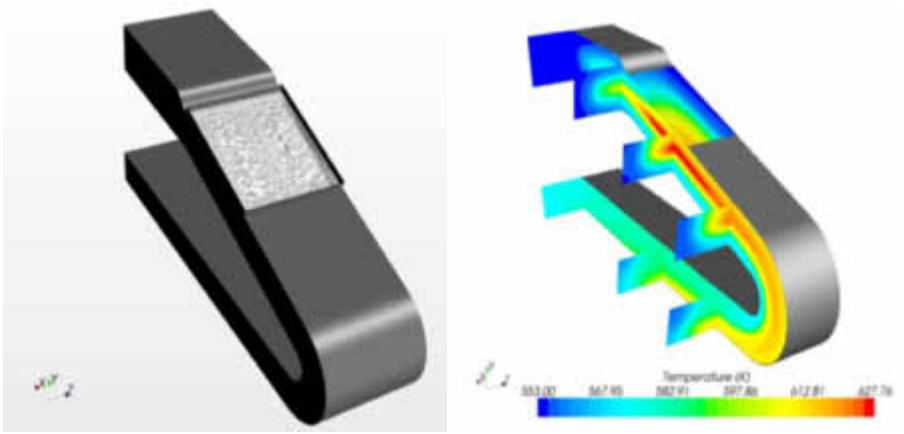


Figure 11 shows that the computed maximal temperature of the LBE in the heat deposition area is between 356°C and 435°C. To detect potential flow instabilities, an unsteady formulation of the VOF calculations is used. These simulations demonstrate the advantageous development of a rather smooth free surface. Some longitudinal standing waves near the side walls are visible, which originate from nozzle corners at their outlet. Figure 11 confirms that they do not propagate towards the beam centreline. Large waves or surface structures caused by effects such as the boundary layer relaxation at the nozzle outlet or the transport of turbulence towards the free surface are not detected. Analytical estimates on the potential height of these types of instabilities indicate that the expected wave amplitude will not exceed 1 mm for the flow conditions assumed. It should be emphasised that the present study has only a preliminary character and does not intend to analyse instability phenomena to their full extent. Moreover, the "flow catcher" needs to be designed yet.

Conclusion

The META:LIC concept exploits the experience of high-power liquid metal spallation sources and accelerator-driven systems. This allowed freezing the nozzle design at an early stage of the project yet keeping the possibility for flow modifications. For the window target option, adequate window cooling has been shown by thermo-hydraulic simulations without reaching flow corrosion relevant velocities. Furthermore, both the effects of propagating pressure waves and cavitation are of major concern for liquid metal window targets subjected to a pulsed proton beam. These are addressed for the META:LIC window option by design measures. Design measures include an expansion volume and result in internal free surfaces. The feasibility of internal free surfaces is proven by VOF simulations. In addition, VOF simulations demonstrate that for the widowless target module a stable free surface flow can be established. In conclusion, the modular META:LIC concept represents an innovative target solution which fits the boundary conditions of ESS. Many of the innovative target design ideas realised within META:LIC can be adapted to ADS targets, e.g. better beam trip performance.

References

[1] McManamy, T., Crabtree, A., Lousteau, D., deVore, J., Jacobs, L., Rennich, M. (2008), "Overview of the SNS target system testing and initial beam operation experience", *J. Nucl. Mater.* 377, 1-11.

[2] Futakawa M. et al. (2009), "Developement of the Hg target in the J-PARC neutron source", *Nuclear Instruments and Methods in Physics Research* A, 600(1):18-21.

[3] Fazio C. et al. (2008), "The MEGAPIE-TEST project: Supporting research and lessons learned in first-of-a-kind spallation target technology", *Nuclear engineering and design*, 238(6):14711495.

[4] Fazio C. et al. (2007), "Handbook on Lead-bismuth Eutectic Alloy and Lead Properties, Materials Compatibility, Thermal-hydraulics and Technologies", technical report ISBN 978-92-64-99002-9, OECD/NEA.

[5] Fokkens J.H. (1998), "HCPB submodule design", Material parameters, technical report ECN Nuclear research.

[6] Bauer G.S. et al. (2003), ESS 2003 Report-Vol. 3 update, technical report, Forschungszentrum Jülich.

[7] Fetzer J.R. et al. (2012), "Dedicated design measures to counteract the effects of pressure waves in the liquid metal target META:LIC", *Proceedings of 11th International Workshop on Spallation Materials,* Gent Belgium.

[8] Gordeev S. et al. (2007), "Liquid-lithium target development for the Super FRS fragment separator at FAIR", Fluid dynamic aspects, *Proceedings of 3rd High-Power Targetry Workshop,* Bad Zurzach, Switzerland.

[9] Bauer G.S. et al. (2001), "MEGAPIE, a 1 MW pilot experiment for a liquid metal spallation target", *J. Nucl. Mater.*, 238(1):17-33.

[10] Mansur L.K. et al. (2001), "R&D for the Spallation Neutron Source mercury target", *J. Nucl. Mater.*, 296(1-3):1-16.

[11] Futakawa M. et al. (2009), "Developement of the Hg target in the J-PARC neuton source", *Nuclear Instruments and Methods in Physics Research* A, 600(1):18-21.

[12] Class A.G. and et al. (2011), "XT-ADS Windowless spallation target thermohydraulic design experimental setup", *J. Nucl. Mater.*, 415(3):378-384.

[13] ESS Target Division (2012), Technical Design Report, Technical Report EDMS 1259002, ESS AB.

[14] Class A.G. et al. (2012), "Conceptual design studies for the liquid metal target META:LIC", *Proceedings of 11th International Workshop on Spallation Materials*, Gent Belgium.

[15] META:LIC KIT Report (2013).

Special Session: In Memoriam Horst Klein

Chair: A.C. Mueller

Horst Klein - Scientist, Teacher, Leader and Friend

Horst Stoecker[1], A. C. Mueller[2]
[1]Goethe-Universität Frankfurt and FIAS, Germany
[2]National Institute for Nuclear and Particle Physics, France

In memoriam Horst Klein

Our colleague and friend, Prof. em., Dr.phil.nat Horst Klein passed away on 12 December 2012. During his final years as a scientist, Horst was a particularly active member of the community performing research and development for the "technology and components of accelerator-driven systems". As members of the international advisory committees to TCADS-1 (Karlsruhe, 2010) and TCADS-2, we all have benefited from Horst's outstanding expertise. The present contribution is to honour his memory and legacy as a Scientist, Teacher, Leader and Friend.

Horst first came to Goethe University, Frankfurt am Main, as a young man, in the 1950s to study physics.

As early as during his undergraduate work there he caught the attention of his teacher, and later mentor and friend, Daenzer. Daenzer's Institut für Angewandte Physik was the place were Horst flourished soon.

IAP was then - and is till today – a wonderful place where senior scientists fostered the scientific independence of ambitious young colleagues, urging them to learn, to try, to seek, to find – to do their own research and practice teaching, at the board and in the laboratory, in an extraordinarily delightful collegial atmosphere.

After a few years, Daenzer was convinced that Horst could be the right person to succeed him as Head of the Institute – and asked him to help shape the future of the accelerator group there – and Horst did just that, with great enthusiasm, energy and a wonderful attention to the other young people in the group.

When Horst accepted an offer for a Professorship in Karlsruhe and engaged in novel interesting accelerator projects, his colleagues in Frankfurt immediately started to think about ways to lure him back to his alma mater.

A few years later, the faculty in Frankfurt announced a key professorship in accelerator physics at IAP. Horst's mentors and colleagues, who had shaped his scientific taste, were successful in luring him back – Horst accepted the offer to take over what is now "his" Institute at Goethe University to strengthen accelerator science and applied science at the faculty.

Over the years, Horst built a large world, leading accelerator institute, as witnessed by many of his own scientific achievements, and by the large flock of excellent students and collaborators, who are now located all over the world. They will now continue his scientific legacy and his ambitious spirit for physics, accelerator science and ever new applications.

He was also famous for his way of influencing the University President's and Senate's strategy. Horst was highly respected by all faculties and fractions in the convent and in the senate as one who, in his quiet way, was deeply involved in shaping Goethe's research programme for about four decades. Famous, his strawberry tarts – plus coffee – meetings were also popular, where he usually gained support for his points of view and convinced many of us to go ahead, stand up for the good of the university and engage in duties and institutional responsibilities. With coffee, strawberry cake and whipped cream, he also persuaded one of us (HS) to run for the Presidium as ViP in 2000, and then, to leave the Presidium at Goethe to take on the directorate at GSI and the Helmholtz-Presidium as ViP in 2007.

Horst was one of the founding fathers of GSI, the former Gesellschaft fuer Schwerionenforschung GmbH, now GSI Helmholtzzentrum fuer Schwerionenforschung GmbH.

Relying on its unique linear accelerator, this national research center for Heavy Ion Research was driven from the middle sixties by the "gang of six"[1] at the Hessian Universities, plus Mainz and Heidelberg, to become a reality in 1974, and developed into an international focal point for our science: heavy ion-driven nuclear structure, superheavy element research, nuclear astrophysics, hadron physics, relativistic heavy ion physics, atomic physics, biomedical- and material science applications, plasma physics and heavy ion driven fusion, etc.

Today, GSI is also the mother-laboratory for the outstanding international "Facility for Antiproton and Ion Research in Europe", FAIR, under construction adjacent to the GSI premises, with 2500 founding scientists from over 40 countries and a dozen or so shareholding partner countries, which have invested about one and a half billion euros and tremendous manpower for the construction of this world's largest fundamental science project of this decade.

Many of the staff at GSI are alumni of Goethe University, and many members, youngs researchers and seniors alike, of our accelerator group hold an IAP master diploma or hold PhD degrees from Horst's Institute. Also at CERN, at Brookhaven, Fermi Lab, RIKEN, the MYRRHA project R&D, Lanzhou. We find today both people and accelerator components, which originated in Horst's IAP group.

In the past ten years, while Horst was very keen to check the shaping of the FAIR projet and guided many students and collaborators to participate in it, most of his own research was focused on the development of linear accelerators of the highest possible intensities and reliabilities for nuclear energy applications, both in fusion, and in fission for accelerator-driven systems. Horst led IAP participation to the relevant EURATOM contracts, like PDS-XADS (FP5), EUROTRANS (FP6), MAX (FP7) to name just a few. The collaboration for the recently started EURATOM project MARISA, to which Horst's contribution for its preparation was instrumental, will now have to continue without its elder statesman.

As an intellectual leader in heavy ion accelerator science for more than half a century, Horst shaped this field of science, mentored more than a hundred Diploma and PhD students. He will be sorely missed.

[1] The Hessians Klein, Greiner and Schopper from Frankfurt, Walcher senior from Marburg, Brix and Beck from Darmstadt, as well as Schmelzer and Boehne from Heidelberg, and Hermann from Mainz.



Horst and Rudolf Bock, and their first ladies, receiving the honorary award “senior professor” from the Frankfurter Förderverein für die Physikalische Grundlagenforschung in 2011.

The FAIR proton linac

O. Kester
GSI and Goethe-Universität, Germany

Abstract

FAIR – the Facility for Antiproton and Ion Research in Europe – constructed at GSI Helmholtzzentrum für Schwerionenforschung GmbH in Darmstadt comprises an international centre of heavy ion accelerators that will drive heavy ion and antimatter research [1]. FAIR will provide worldwide unique accelerator and experimental facilities, allowing a large variety of fore-front research in physics and applied science. FAIR will deliver antiproton and ion beams of unprecedented intensities and qualities. The main part of the FAIR facility is a sophisticated accelerator system, which delivers beams to different experiments of the FAIR experimental collaborations – APPA, NuSTAR, CBM and PANDA – in parallel. The accelerated primary beams will then be employed to create new, highly exotic particles in a series of experimental programmes.

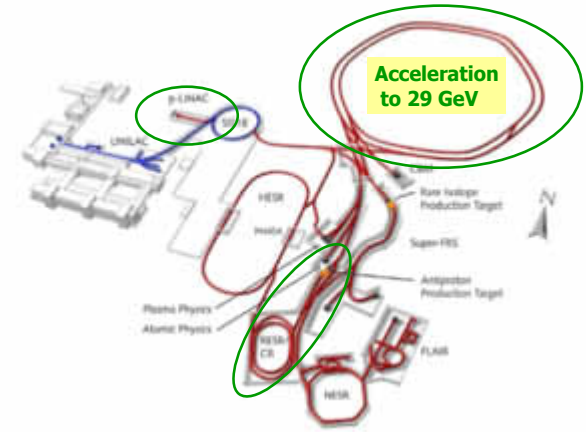
Introduction

In the PANDA experiment, collision of the antiproton beam with the internal hydrogen gas-target will be possible. In order to generate the required intensity of antiproton beams, the proton beam intensity must be driven to $2*10^{12}$ per spill. Those intensities cannot be delivered by the existing UNILAC but a high intensity proton linac injector is required for the SIS18. A significant part of the experimental programme at FAIR is dedicated to antiproton physics and for some experiments up to $7{\cdot}10^{10}$ cooled antiprotons per hour are required. Taking into account the pbar production and cooling rate, this is equivalent to a primary beam of $2{\cdot}10^{16}$ protons/h to be provided by the chain of accelerators comprising the proton linac and the two synchrotrons SIS18 and SIS100 (see Figure 1).

The driver accelerator of FAIR is the fast ramping, superconducting heavy ion synchrotron – SIS100 – that allows the acceleration of the most intense beams of stable elements from protons (30 GeV) to uranium (10 AGeV). SIS100 is installed in a 20 m deep tunnel, which is designed for the installation of the SIS300 synchrotron in a later stage of the project. The CBM – Plasma- and Biomat-experiments are directly supplied with primary beams from the SIS100. Two target stations for the generation of secondary beams (antiprotons and RIBs) allow the conversion of primary ions. The intensities of secondary beams will increase by a factor of 1,000-10,000 as compared to currently available beams. With beams of antiprotons, a variety of experiments is planned at FAIR. Antiprotons are produced in high-energy collisions of nuclei. The common technique uses a set of 10 cm long nickel rods, which are bombarded with proton beams. SIS100 will deliver proton beams with 29 GeV to the target. At 29 GeV beam energy, one out of ten-thousand protons will produce an antiproton. About 10^8 antiprotons per spill are

expected and injected into the collector ring (CR) for beam preparation via stochastic cooling. The maximum rate of cooled pbars is limited by the stochastic cooling power since the cooling time scale is proportional to the number of hot pbars for a sufficiently high signal-to-noise ratio. Typical cooling times in the case of a non-ideal signal-to-noise ratio are about five seconds. During the stochastic cooling process in the CR, the SIS100 can be used to accelerate ion species different from protons.

Figure 1. Overview of the FAIR Facility and the steps required for the production and accumulation of antiprotons

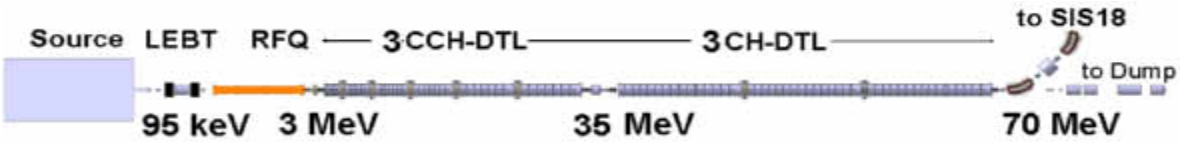


The FAIR proton linac design

For the high-intensity proton beams, as required for antiproton production, a dedicated 325 MHz proton linac delivering 35 mA and 70 MeV protons is needed [2]. The structure and elements of the p-linac are depicted in Figure 2. The FAIR proton injector has to provide at least 35 mA at the final energy with a repetition rate of 4 Hz. A 2.45 GHz ECR source generating 100 mA of 95 keV protons is employed, followed by a Radio-Frequency Quadrupole (RFQ). The subsequent Low-Energy Beam Transport (LEBT) is based on two-solenoid magnetic focusing and provides the required separation of H^{3+}, H^{2+}, and H_2 fractions from the proton beam. At present, a 4-rod RFQ and a ladder-RFQ are under investigation at the University of Frankfurt. The RFQ beam dynamics layout is based on the New-Four-Section-Procedure which drops the constant-focusing strength scheme [3].

At 3 MeV, the beam is accelerated by three coupled crossed-bar (CH) resonators to 36 MeV where a dedicated section for beam diagnostics is installed [4]. The remaining three CH-resonators perform the final acceleration to 70 MeV where the beam enters the transfer channel towards the SIS 18. Although at SIS18 injection a current of 35 mA is required, a maximum design current of 70 mA for the linac was chosen. If the stochastic cooling power is increased in future, the accelerator chain will demand higher proton linac currents.

Figure 2. Overview of the 70 MeV p- linac of FAIR

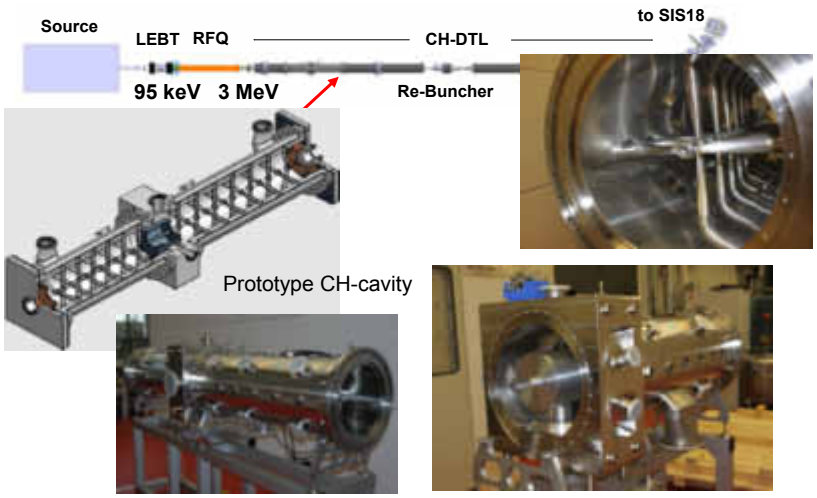


Modern H-type cavities offer highest shunt impedances of resonant structures of heavy ion linacs at low beam energies < 20 MeV/u and enable the acceleration of intense proton and ion beams. One example is the interdigital H-type structure. The crossed-bar

H-cavities extend these properties to high energies even beyond 100 MeV/u. Compared to conventional Alvarez cavities, these crossed-bar (CH) cavities feature much higher shunt impedance at low energies. The design of the proton linac is based on those cavities. As usual for H-mode structures, the beam dynamics lattice is derived from the KONUS beam dynamics [5].

Three coupled CH-DTL perform the first stage of acceleration to the energy of 36 MeV. At this energy, space charge effects are of reduced importance and KONUS offers the possibility to build long lens free sections. The coupled structures consist of two CH-DTL connected through a single cell resonator. This intertank section oscillates in the Alvarez mode and the large drift tube houses an electromagnetic quadrupole triplet. The radius of the single cell resonator has to be adjusted so that the resonance frequency of this unit matches the adjacent CH cavities. The first coupled CH has been fabricated (see Figure 3) and low level RF-tuning has been performed with respect to frequency and field flatness. The low-energy part consists of 13 gaps, followed by the coupling cell and by the 14 gap high energy part. The whole cavity has an inner length of about 2.8 m and an inner diameter of about 360 mm. For all structures, the power consumption is expected to be lower than 1 MW, although it is expected to feed the structures with a 3.0 MW-class klystrons.

Figure 3. Prototype cavity of the 325 MHz CH-structures of the FAIR p- linac



The KONUS design has been optimised in order to fulfill the transverse acceptance requirements of the SIS18 of about 5 mm mrad at 70 MeV injection energy. The injection into the synchrotron is planned by a multiturn injection scheme. The horizontal acceptance of the SIS 18 will be filled by a 35 mA within a normalised brilliance of 16.5 mA/µm, while a momentum spread of less than 1% is required. The maximum repetition rate is fixed at 4 Hz.

To determine the beam brilliance and the beam losses due to alignment errors, an error analysis has been performed. The error study comprises the DTL section, i.e. after the end plate of the RFQ. With this analysis mechanical tolerances and the design robustness against random errors can be determined. The errors include quadrupole rotation, translation, and variations of operational parameters such as voltage and phase oscillations of the amplifiers. The simulations show that the present design is robust against errors. At present, only three pairs of XY steerers are planned along the linac, one pair after the RFQ and two pairs at the end of the diagnostics sections. The design, mechanical integration, and data acquisition of the phase probe and BPMs in the p-linac are challenging. These four-button BPMs are partially to be integrated into the end drift tubes of the CH-cavities. Special care must be taken for the suppression of primary RF

leeking into the drift tube that houses the BPM. Therefore, a ferrite shield is expected to reduce this effect.

References

[1] FAIR, Baseline Technical Report (2006), www.faircenter.de/Publikationen.171.0.html?&L=1.

[2] Technical Design Report (2008), "Proton Linac", www.edms.cern.ch/document/994418/1.

[3] Zhang, C. (2009), *Nucl. Intrum. and Meth.* A 609. p.95.

[4] Clemente, G. et al. (2011), PRST-AB 14.110101.

[5] Ratzinger, U., Tiede, R. (1998), *Nucl. Instr. and Meth.* A 415, p. 229-235.

Linac strategies for the lower beam energies

Ulrich Ratzinger
IAP, Goethe-University Frankfurt, Germany

Abstract

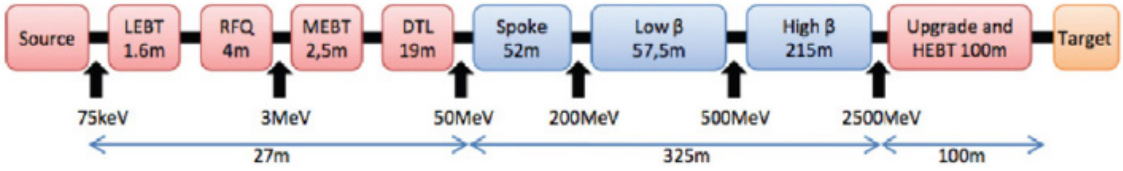
Linear accelerator capabilities are improved steadily to fulfill the demands on driver beams for new beam facilities. At high beam energies above 200 AMeV and towards $\beta \rightarrow 1$, well-established concepts exist for both room temperature (r.t.) and superconducting (s.c.) linacs, while for low and medium beam energies many different solutions have been developed and realised to meet specifications for individual cases. However, there is still no low - and medium - energy standard concept for "long" linacs. This paper mentions a main limitation of present technology, namely field emission already at modest surface fields and, as a result, limited acceleration rate. Moreover, current cavity developments and trends are discussed.

Introduction

Proton beam currents up to 100 mA and at duty factors up to cw operation have been demonstrated successfully at low-energy test stands – up to a few MeV beam energy [1]. At present, the most powerful linac in routine operation is the spallation neutron source SNS in Oak Ridge, Tennessee. It accelerates negatively charged hydrogen ions H^- to beam energies around 940 MeV approaching the 1 MW level of averaged beam power at pulse lengths around 1 ms and beam currents around 30 mA. One main limitation in beam loss reduction is the intra – beam scattering of ions where the weakly bound additional electron is easily lost followed by particle loss and activation of the accelerator equipment [2]. Upgrades to 3 MW beam power levels seem feasible. There is the 590 MeV sector cyclotrons at the Paul Scherrer Institute PSI, Villigen, Suisse, which holds the beam power record with a 1.4 MW beam, 2.4 mA, cw operation [3]. This case shows some potential for an upgrade in beam power.

The 6 MW European Spallation Source ESS has been under investigation for many years and will be realised in the forthcoming years in Lund, Sweden. This facility will be driven by a 2.5 GeV proton beam. The layout of the proposed linac is shown in Figure 1. An averaged voltage gain of 7 MV/m along the linac results in a total length of 357 m. This relatively high averaged value is due to the most efficient high beta section.

Figure 1. Layout scheme of the 2.5 GeV driver linac for ESS [4]



Acceleration by linacs starts with an electrostatic beam extraction from ion sources followed by a main acceleration along RF cavities. While at low beam energies the voltage gain is typically at the 1 MV/m level, it is seriously increased at the high energy end. Another parameter to increase the voltage gain is a reduced duty factor; this is true for room temperature as well as for superconducting structures.

Transverse beam focusing along linacs is provided by magnetic quadrupoles. Only at low-energy sections are magnetic solenoid focusing and electrostatic focusing used alternatively. The quadrupole focusing lattice along the linac is FODO along Alvarez – type DTL's and doublet or triplet channels with magnet free drift tube sections between lenses in most other cases. It has been demonstrated in many cases that the separated function linacs mentioned last achieve considerably higher effective acceleration fields.

One severe disadvantage of linacs is the great extension along the beam axis, which often causes problems during the acquisition of a suited building site.

Another important issue is the RF amplifier costs. Linacs offer the fastest acceleration but with the disadvantage that every gap voltage is exploited only once per beam particle.

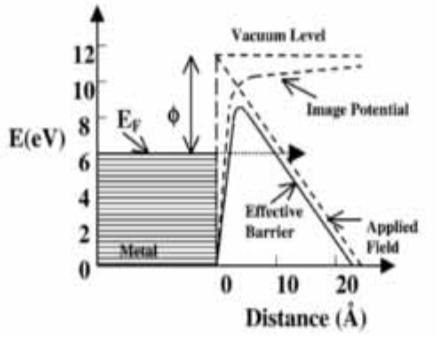
This article presents the following topics:

- higher acceleration fields;
- accelerator cavities;
- linac front end concepts;

Field emission

A typical behaviour of cavities is an increase in cavity power losses over-proportionally to the square of the voltage amplitude beyond a certain field level. This effect is due to "field emission" between cavity surface spots. There is a great variety of effects in detail, differing also between r.t. and s.c. cavities [5]. The local field emission current density is predicted by the Fowler –Nordheim equation:

Figure 2. Fowler-Nordheim equation and sketch of the effective surface potential



$d\,[\ln (I_F/E^{2.5})/d\,(1/E) = -k/\beta$;

I_F= *outflow channel* E=*inflow channel;*

$K=f(\Phi)$, *field emission current;*

β=*electric field;*

$E_F=\beta \cdot E$;

$E=E_{surf}$ *material dependent*

In this case, I_F is the current from an added sum of cavity surfaces exposed to the maximum surface field E. The enhancement factor β indicates by which factor the calculated field at a given cavity operation level has to be increased to explain the measured field emission current. In experiments β is derived from data points in the so-called Fowler-Nordheim plot, which allows directly evaluating the value 1/β. Figures 3 and 4 show some results from measurements at r.t. and s.c. H – type cavities. It should be noted that β typically varies in the range from 100 to several hundred. There should still be a potential for improvements with respect to effective voltage gains.

Figure 3. The 19 gap, 359 MHz s.c.CH – cavity, quality factor Q over acceleration field (left), Fowler-Nordheim – plots after two separate BCP treatments (centre), and 3D – sketch of the cavity (right)

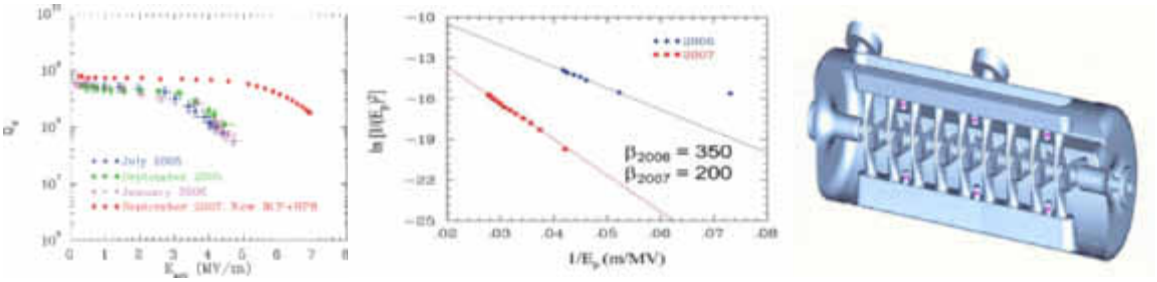
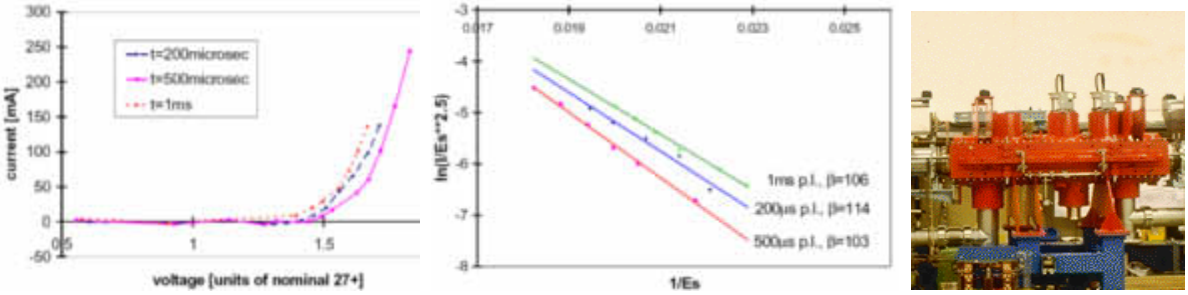


Figure 4. Results from measurements on the r.t. CERN Linac3 IH2-cavity at field gain levels up to 10.7 MV/m and at peak surface field levels up to 54 MV/m /6/: dark current dependence at field level, Fowler – Nordheim-Plot, photo from the 1.5 m long IH2 cavity



The Kilpatrick criterium gives additional orientation for the layout of cavity parameters: It predicts a maximum for the surface fields at a given RF frequency before sparking occurs:

$$f = 1.64\,E^2 \cdot e^{\frac{-8.5}{E}} \quad ; \qquad E\,/\,MV\,/\,m \quad ; \quad f\,/\,MHz$$

Table 1 predicts the maximum surface field levels from the Kilpatrick – criterium at RF frequencies:

	f / MHz	*E* / MV/m	
	7.5	5	GSI-HSI, 36 MHz too pessimistic
	70	10	
Fit to experiments	429	20	
	2122	40	DESY-Tesla, 1.3 GHz SLAC
	9438	80	
	15063	100	
	22001	120	too optimistic CERN CLIC-TF
	30250	140	

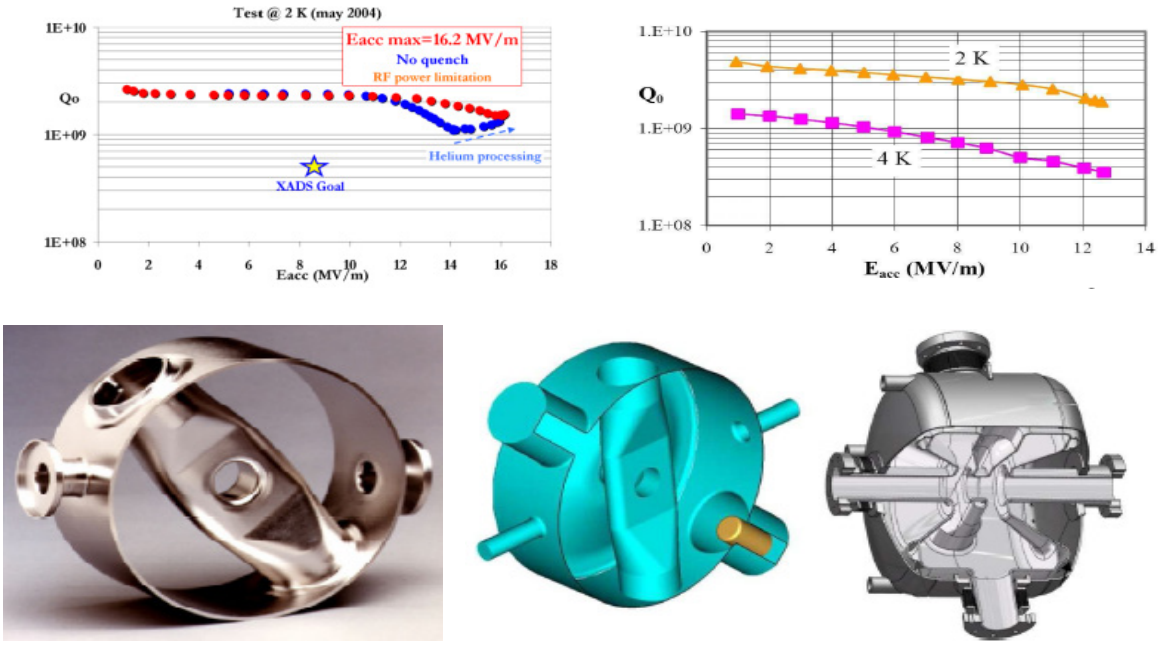
A comparison with experiments shows that this criterion for frequencies below 300 MHz is too pessimistic while it is too optimistic for frequencies above 10 GHz.

Many studies about surface treatment and about sparking limits have been performed during the last decades but there is still no breakthrough towards surface preparation techniques resulting in field enhancement factors β closer to one.

However, progress was achieved with respect to maximum operable field levels in superconducting cavities. In that case, the critical magnetic field level sets another barrier, and this limit has been nearly achieved in the case of superconducting bulk niobium elliptical cavities for a relativistic β=1. They reach 40 MV/m voltage gain.

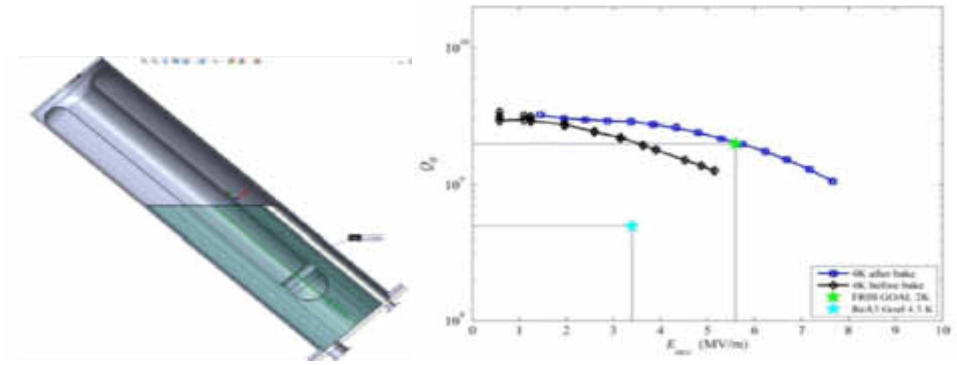
Figures 5 and 6 show results from prototyping work on superconducting cavities for lower beam velocity [7] [8].

Figure 5. Single spoke cavity development: performance of the 352 MHz, β = 0.35 cavity from IPN Orsay (top left) and of the 350 MHz, β = 0.175 cavity at LANL, Los Alamos (top right), from [7]



Below from left to right: First single spoke (LANL, 1991), 350 MHz (LANL), 352 MHz (IPN Orsay).

Figure 6. Quarter wave resonator development for FRIB and achieved performance, 80.5 MHz, β= 0.08 [8]



Effective voltage gain

Room temperature structures at low beam energies improved a lot with respect to acceleration gradients after applying multi-cell H-type structures. One example is shown in Figure 7. This 217 MHz IH – type cavity follows the "Combined Zero Degree Beam dynamics" KONUS and is in use at medical facilities for cancer treatment by carbon beams in several places now [9]. The effective shunt impedance is as high as 125 MΩ/m, resulting in 830 kW thermal losses.

Figure 7. 19.8 MV, 217 MHz IH-cavity accelerating C4+ ions from 400 AkeV to 7 AMeV within an outer tank length of 3.8 m



It contains 3 quadrupole triplet lenses for transverse focusing.

In a next step, a CH – cavity is under development at IAP [10] to reach even higher acceleration fields (see Figure 8 and Table 2). This stainless steel cavity will be operated at 325 MHz, there will be tests on two different galvanic copperplating techniques (shining against mat surface). The geometry was optimised for a high shunt impedance and at the same time for maximum local field maxima below 100 MV/m.

Figure 8. High-field test cavity, 325 MHz

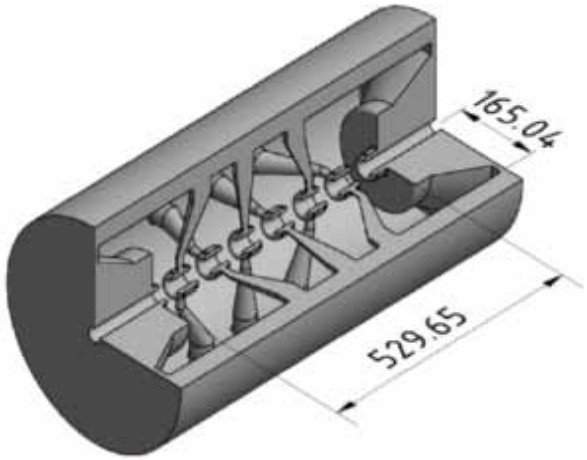


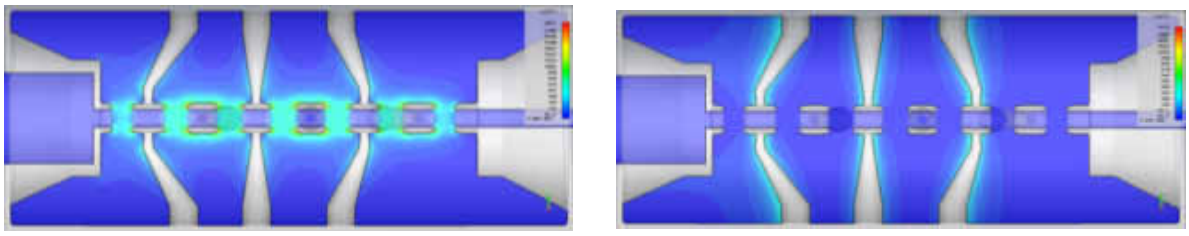
Table 2. The main CH – cavity parameters for the high – field prototype cavity

Number of gaps	7
Frequency (MHz)	325.2
Voltage gain (MV)	6
Eff. Accel. length (mm)	529.6
Eff. Accel. field (MV/m)	11.2

Power loss (MW)	1.58
Q_0 – value	13500
Effective shunt impedance (M Ω/m)	57.3
Beam aperture (mm)	27

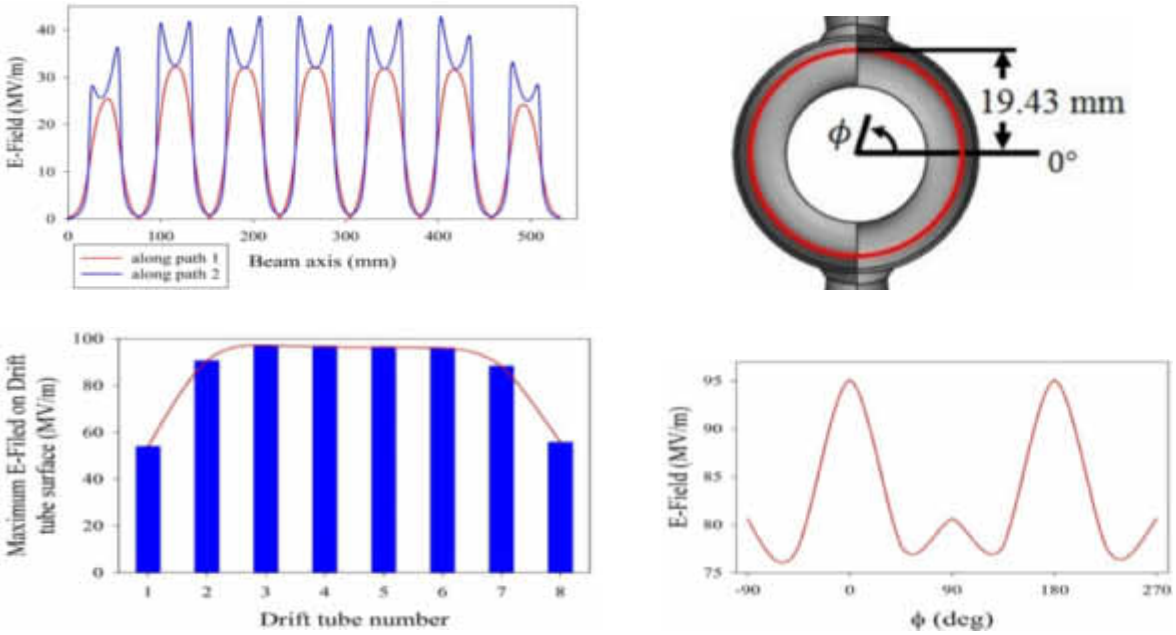
Maximum electric field levels appear locally on the drift tubes at a radius of 19.43 mm. Maximum field spots are up to 97 MV at the envisaged amplitude level. Figure 9 shows the electric and magnetic field distributions, respectively.

Figure 9. Electric (left) and magnetic field levels in the cross-sectional area



A first CH – type proton linac is under development for the FAIR Facility at GSI Darmstadt [11]. It will provide 70 MeV protons at beam currents up to 70 mA for synchrotron injection. The CH – section has a length of only about 20 m.

Figure 10. Electric field levels along the beam axis (path 1) and along the aperture radius (path 2) (upper left), indication of a path on the drift tube surfaces, containing the maximum field spot (upper right) and showing a variation along Φ with two maxima at 0 (lower left) and at 180 deg (lower right)



Amplifier technology

Solid state amplifiers have been increased rapidly, their maximum RF power levels at frequencies being attractive for ion acceleration. At the same time the investment costs per watt are sinking. This trend might influence future accelerators in such a way that room temperature structures could become attractive again in some large linac projects, where pulsed beam operation is acceptable and pulsed beam current levels can be handled [12].

Transverse focusing

After reaching a certain beam energy the transverse beam focusing is achieved by quadrupole doublets or quadrupole triplets located in intertank sections between cavities. At lower beam energies several techniques are applied: at superconducting linacs superconducting solenoids can be integrated into a long cryostat containing cavities and lenses. This technique was applied successfully at ATLAS, ANL, Argonne for the first time, and later at the TRIUMF- ISAC Facility. At ALPI, INFN, Legnaro and at SPIRAL2, GANIL, Caen (under construction) room temperature quadrupole doublets between s.c. cavities provide the transverse focusing. In the latter case, an easy control of the transverse lens position is guaranteed, while lens integration into the cryostat reduces the drift between cavities, providing better longitudinal beam acceptance.

At Alvarez – type DTL's every drift tube is equipped with a magnetic quadrupole. Recently, also permanent magnetic quadrupoles are used to save in transverse space and by that reducing the outer drift tube diameter. This technique was used at the SNS DTL front end and will now be applied at the CERN Linac 4 and probably at the ESS Alvarez – type DTL section in Lund, Sweden.

In IH – type linacs quadrupole triplet lenses are integrated between slim drift tubes for acceleration at the low energy end to minimise the drift between neighboured acceleration sections. Moreover, this technique allows matching the RF power requirement of the first cavity to the available amplifier power class, reducing investment costs for traditional tube-driven amplifier systems. The following lenses are mounted on the intertank sections between the cavities.

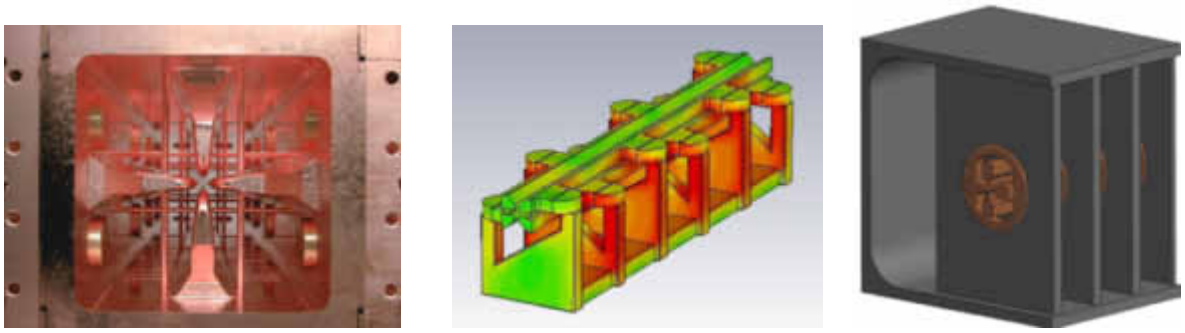
RFQ development

The RF ion linac begins with an RFQ, providing a high acceptance for low energetic beams – down to several 10 keV for protons and down to several AkeV for heavy ions (the ion source needs only electrostatic voltages on the 30 kV to 100 kV level typically). The RFQ forms the bunch structure and accelerates the beam to energies of some 100 AkeV for heavy ions and to some MeV for protons. For 30 years, RFQs have been used in most ion beam facilities as the first element of the RF linac.

Two types of RFQ resonators are in use – the 4 Vane Cavity and the 4-Rod- type resonator (see Figure 11). For proton acceleration, at frequencies around and beyond 300 MHz the 4 – Vane cavity is mostly used. For ion acceleration, at frequencies up to 220 MHz 4-Rod-RFQs are commonly chosen.

Studies about 4-Rod RFQs for higher frequencies have not been successful so far. At IAP, a new attempt was made to develop a 325 MHz RFQ of the 4 –Rod type, namely the "ladder – RFQ". This geometry should allow achieving reasonable transverse dimensions at high frequencies [13]. Figure 11 shows the design concept.

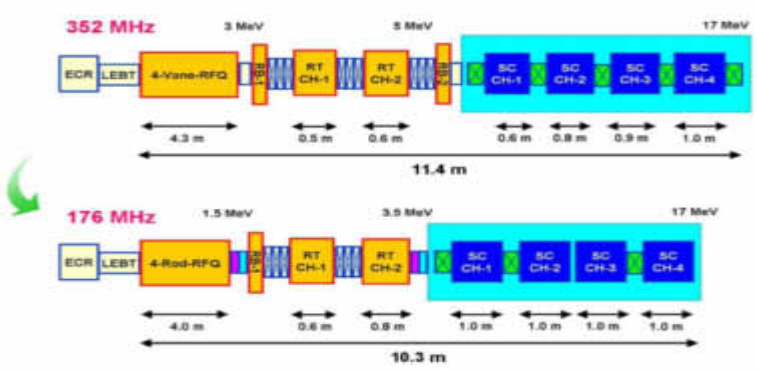
Figure 11. 402.5 MHz SNS 4-Vane RFQ (left), 176 MHz 4-Rod-RFQ and 325 MHz ladder type 4-Rod RFQ (right)



MYRRHA front-end design

The ADS project MYRRHA in Mol, Belgium needs a very safe linac layout with very restricted rules for beam delivery failures [14]. To secure these needs, the front end is doubled up to energies of 17 MeV. Both lines will be in operation and only one will deliver beams to the main linac. If a fault occurs in this line the second one can immediately overtake the duty. Both lines have to achieve as much independence from each other as possible with respect to supplying systems. Figure 12 shows two versions discussed for the front end: one is operated at 352 MHz, the main linac frequency, the other one uses 176 MHz. A warm section is followed by a superconducting CH – section in both cases. The subharmonic frequency is feasible at the relatively low beam current foreseen at this facility. It allows a classical 4-Rod RFQ design and a low transition energy to the more efficient DTL – section.

Figure 12. Conceptual design options for the MYRRHA front end



Focusing is provided by quadrupole triplets along the room temperature section and afterwards by superconducting solenoids, integrated in the cryostat.

References

[1] Schulte, M.E. et al. (2001), "Characterization of the Proton Beam from the 6.7 MeV LEDA RFQ", *Proc. of the 2001 PAC Conf.*, Chicago, p. 591.

[2] Galambos, J. et al. (2012), "Increased Understanding of Beam Losses from the SNS Linac Proton Experiment", *Proc. of the LINAC 2012 Conf.*, Tel-Aviv, p.115.

[3] Seidel, M. (2010), "Towards the 2 MW Cyclotron and Latest Developments at PSI", *Proc. of the 2010 Cyclotron Conf.*, Lanzhou, p. 275.

[4] Danared, H. et al. (2011), "Layout of the ESS Linac", *Proc. of the 2011 IPAC Conf.*, San Sebastian, p. 2631.

[5] Padamsee, H., Knobloch, J. (2007), "RF Superconductivity for Accelerators", Wiley-VCH.

[6] Broere, J. et al. (1998), "High Power Conditioning of the 202 MHz IH Tank2 at the CERN Linac3", *Proc. of the 1998 LINAC Conf.*, Chicago, p. 771.

[7] Kelly, M. (2006), "Superconducting Spoke Cavities", *Proc. of the Int. Conf. on Hadrons and Beams*, HB, Tsukuba, p.337.

[8] Popielarski, L. et al. (2012), "Process developments for S.C. RF Low Beta Resonators for the ReA3 Linac and for FRIB", *Proc. of the LINAC 2012 Conf.*, Tel-Aviv, p.342.

[9] Maier, M. et al. (2007), "Commissioning of the Linac for the Heidelberg Heavy Ion Cancer Therapy Centre (HIT)", *Proc. of the PAC 2007 Conf.*, Albuquerque, p. 2734.

[10] Almomani, A. et al. (2013), "High Gradient Room Temperature Cavity Development for 10 – 100 AMeV Beams", *Proc. of the IPAC 2013 Conf.*, Shanghai, p. 3787.

[11] Brodhage, R. et al. (2013), "First Coupled CH Power Cavity for the FAIR Proton Injector", *Proc. of the IPAC 2013 Conf.*, Shanghai, p. 3791.

[12] Ratzinger, U. et al. (2012), "A Pulsed Front-End for ADS Applications", *Proc. of the LINAC 2012 Conf.*, Tel-Aviv, p. 855.

[13] Brodhage, R. et al. (2013), "Design Study of a High Frequency Proton Ladder RFQ", *Proc. of the IPAC 2013 Conf.*, Shanghai, p. 3788.

[14] Biarotte, J.-L. et al. TCADS-2 Proceedings.

Recent developments of the MYRRHA Project

P. Baeten, D. De Bruyn, R. Fernandez, G. Van den Eynde, H. Aït Abderrahim
Studie Centrum voor Kernenergie-Centre d'Etude de l'Energie Nucléaire (SCK•CEN), Belgium

Abstract

MYRRHA (Multi-purpose hYbrid Research Reactor for High-tech Applications) is a multi-purpose research facility currently being developed at SCK•CEN. MYRRHA is based on the ADS (Accelerator-driven System) concept where a proton accelerator, a spallation target and a subcritical reactor are coupled. MYRRHA will demonstrate the ADS full concept by coupling these three components at a reasonable power level to allow operation feedback.

As a flexible irradiation facility, the MYRRHA research facility will be able to work in both critical and subcritical modes. In this way, MYRRHA will allow fuel developments for innovative reactor systems, material developments for GEN-IV and fusion reactors, and radioisotope production for medical and industrial applications. MYRRHA will be cooled by lead-bismuth eutectic and will play an important role in the development of the Pb-alloys technology needed for the LFR (Lead Fast Reactor) GEN-IV concept.

MYRRHA will also contribute to the study of partitioning and transmutation of high-level waste. Transmutation of minor actinides can be completed in an efficient way in fast neutron spectrum facilities, so both critical reactors and subcritical ADS are potential candidates as dedicated transmutation systems. However, critical reactors heavily loaded with fuel containing large amounts of MA pose reactivity control problems, and thus safety problems. A subcritical ADS operates in a flexible and safe manner, even with a core loading containing a high amount of MA, leading to a high transmutation rate.

The MYRRHA design has progressed through various framework programmes (FP) of the European Commission in the context of Partitioning and Transmutation. The XT-ADS version was a short-term, small-scale (57 MW_{th}) experimental facility, and has been developed within the EUROTRANS project in the FP6 (2005-2010). The most recent version FASTEF is a further upgrade of XT-ADS, still conceived as a flexible irradiation facility, now able to work in both subcritical and critical modes. FASTEF has been developed within the CDT project in FP7 (2009-2012). The MYRRHA design has now entered into the Front End Engineering Phase, covering the period 2012-2014. The engineering company which will handle this phase is currently being selected.

This paper presents the most recent developments in the design of the MYRRHA Facility.

Introduction

Since its creation in 1952, the Belgian Nuclear Research Centre (SCK•CEN) at Mol has always been heavily involved in the conception, design, realisation and operation of large nuclear infrastructures. It has even played a pioneering role in such type of infrastructures in Europe and worldwide. SCK•CEN has successfully operated these facilities at all times due to the high degree of qualification and competence of its personnel and by inserting these facilities in European and international research networks, contributing to the development of crucial aspects of nuclear energy at an international level.

One of the flagships of the nuclear infrastructure of SCK•CEN is the BR2 reactor, a flexible irradiation facility known as a multi-purpose materials testing reactor (MTR). This reactor has been in operation since 1962 and has proven to be an excellent research tool, which has produced remarkable results for the international nuclear energy community in various fields such as material research for fission and fusion reactors, fuel research, reactor safety, reactor technology and for the production of radioisotopes for medical and industrial applications. BR2 has been refurbished twice, consisting of the replacement of the beryllium matrix and considerable safety improvements at the beginning of the 1980s and 1990s.

The BR2 reactor is now licensed for operation until 2016 with a potential extension for another ten-year period until 2026. The SCK•CEN at Mol has been working for several years at the pre- and conceptual design of a multi-purpose flexible irradiation facility, which can replace BR2 and is innovative to support long-term oriented research projects ensuring the future of our research centre. This facility, called MYRRHA (Multi-purpose hYbrid Research Reactor for High-tech Applications), has been designed as a multi-purpose accelerator-driven system (ADS) for R&D applications, and consists of a proton accelerator delivering its beam to a spallation target which, in turn, couples to a subcritical fast core, cooled with lead-bismuth eutectic (LBE).

MYRRHA is able to work both in subcritical (ADS) and in critical modes. To determine the characteristics of this multi-purpose flexible irradiation facility, an analysis of the present day needs of the international community has been conducted in particular in the European Union, and as a result, MYRRHA should target the following applications:

- to demonstrate the full ADS concept by coupling the three components (accelerator, spallation target and subcritical reactor) at a reasonable power level to allow operation feedback and scalability to an industrial demonstrator;
- to allow the study of the efficient technological transmutation of high-level nuclear waste, in particular minor actinides that would require high fast flux intensity ($\Phi_{>0.75MeV} = 10^{15}$ n/cm^2.s);
- to be operated as a flexible fast spectrum irradiation facility allowing for:
  - fuel developments for innovative reactor systems, which need irradiation rigs with a representative flux spectrum, a representative irradiation temperature and high total flux levels ($\Phi_{tot} = 5{\cdot}10^{14}$ to 10^{15} n/cm^2.s); the main target will be Gen-IV systems which require fast spectrum conditions;
  - material developments for Gen-IV systems, which need large irradiation volumes (3000 cm^3) with high uniform fast flux level ($\Phi_{>1\,MeV} = \sim 5{\cdot}10^{14}$ n/cm^2.s) in various irradiation positions, representative irradiation temperature and representative neutron spectrum conditions; the main target will be fast spectrum Gen-IV systems;
  - material developments for fusion reactors which also need large irradiation volumes (3000 cm^3) with high fast flux level ($\Phi_{>1\,MeV} = \sim 5{\cdot}10^{14}$ n/cm^2.s) with low

gradients, a representative and controlled irradiation temperature and a representative ratio appm He/dpa(Fe)[1] = 10;

- radioisotope production for medical and industrial applications by:
  - holding a back-up role for classical medical radioisotopes;
  - focusing on R&D and production of radioisotopes requiring very high thermal flux levels ($\Phi_{thermal}$ = 2 to $3 \cdot 10^{15}$ n/cm^2.s) due to double capture reactions;
- industrial applications, such as Si-doping which needs a thermal flux level depending on the desired irradiation time: for a flux level $\Phi_{thermal} = 10^{13}$ n/cm^2.s, an irradiation time in the order of days is needed and for a flux level of $\Phi_{thermal} = 10^{14}$ n/cm^2.s, an irradiation time in the order of hours is needed to obtain the required specifications.

MYRRHA developed from the ADONIS Project (1995 – 1997), which was the first project at SCK•CEN where the coupling between an accelerator, a spallation target and a subcritical core was studied. ADONIS was a small irradiation facility, having the production of ^{99}Mo as its single objective. In 1998, the *ad-hoc* scientific advisory committee recommended extending the purpose of the ADONIS machine to become a material testing reactor for material and fuel research, to study the feasibility of transmutation of minor actinides and to demonstrate the principle of the ADS at a reasonable power scale. Since 1998, the project has been called MYRRHA.

In 2005 MYRRHA consisted of a proton accelerator delivering 350 MeV * 5 mA to a windowless spallation target coupled to a subcritical fast core of 50 MWth. This 2005 version is the "MYRRHA – draft 2" design [1]. The different versions of MYRRHA have been included in successive collaborative projects of the European Commission in its framework programmes. The 2005 design was used as a starting base within the FP6 EUROTRANS integrated project [2], which resulted in the XT-ADS (Experimental Demonstration of the Technical Feasibility of Transmutation in an Accelerator-driven System) design [3], where a linear proton accelerator delivers a 600 MeV * 3.2 mA beam into the spallation target. The reactor power of XT-ADS was 57 MWth.

The XT-ADS design was taken as a starting point for the work performed in the FP7 CDT project, which resulted in the MYRRHA-FASTEF (MYRRHA Fast Spectrum Transmutation Experimental Facility) design [4-5]. The current design of MYRRHA-FASTEF is described in more detail in this paper.

The MYRRHA accelerator

The accelerator is the driver of MYRRHA since it provides the high energy protons that are used in the spallation target to create primary neutrons, which, in turn, feed the subcritical core. In the current design of MYRRHA, the machine must be able to provide a proton beam with an energy of 600 MeV and an average beam current of 3.2 mA. The beam is delivered in continuous wave (CW) mode. Once a second, the beam is shut off for 200 μs so that accurate on-line measurements and monitoring of the subcriticality of the reactor can take place. The beam is delivered to the core from above through a beam window.

Accelerator reliability is a crucial issue for the operation of an ADS. A high reliability is expressed by a long Mean Time Between Failure (MTBF), which is commonly obtained by a combination of over-design and redundancy. On top of these two strategies, fault tolerance in the high-energy section of the linac (above 17 MeV) must be implemented to

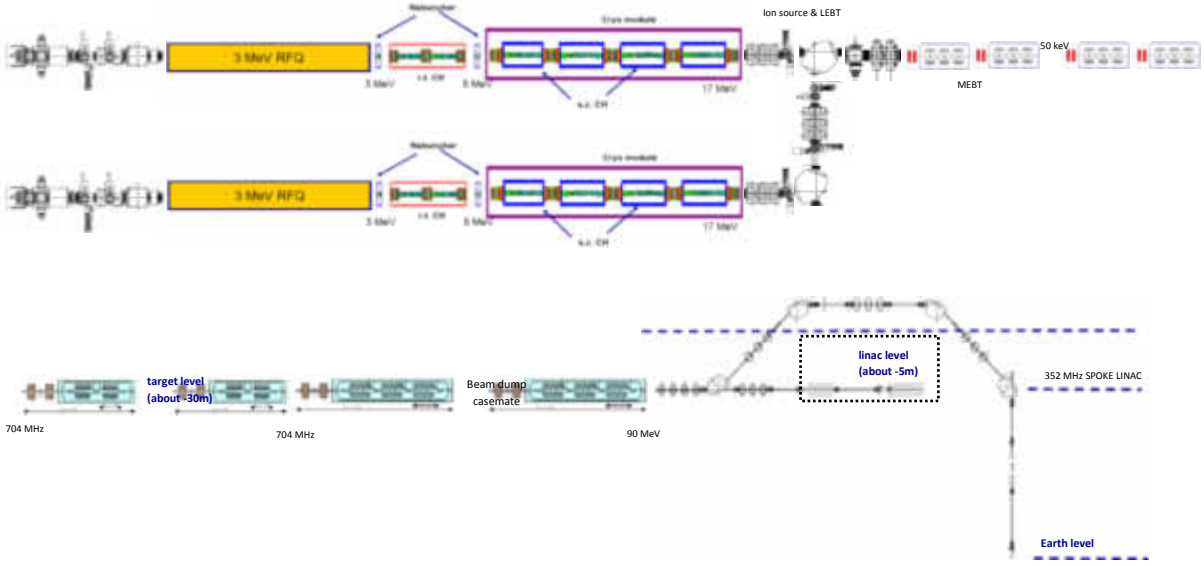
[1] appm He/dpa = atomic parts per million helium per displacement per atom

obtain the required MTBF. Fault tolerance will allow the accelerator to recover the beam within a beam trip duration tolerance after failure of a single cavity. In the MYRRHA case, the beam trip duration tolerance is three seconds. Within an operational period of MYRRHA of three months, the number of allowed beam trips exceeding three seconds must remain under 10, shorter beam trips are allowed without limitations. The combination of redundancy and fault tolerance should allow obtaining a MTBF value in excess of 250 hours to meet the required number of beam trips per operation cycle of three months.

At present, proton accelerators with megawatt level beam power in CW mode only exist in two basic concepts: sector-focused cyclotrons and linear accelerators (linacs). Cyclotrons are an attractive option with respect to construction costs, but they do not have any modularity, which means that a fault tolerance scheme cannot be implemented. Also, an upgrade of its beam energy is not a realistic option. A linear accelerator, especially if made superconducting, has the potential for implementing a fault tolerance scheme and offers a high modularity, resulting in the possibility to recover the beam within a short time and increasing the beam energy.

A basic layout of the MYRRHA accelerator, aiming at maximising its efficiency, its reliability (or MTBF) and its modularity, is provided in Figure 1.

Figure 1. A schematic layout of the reference design of the MYRRHA accelerator



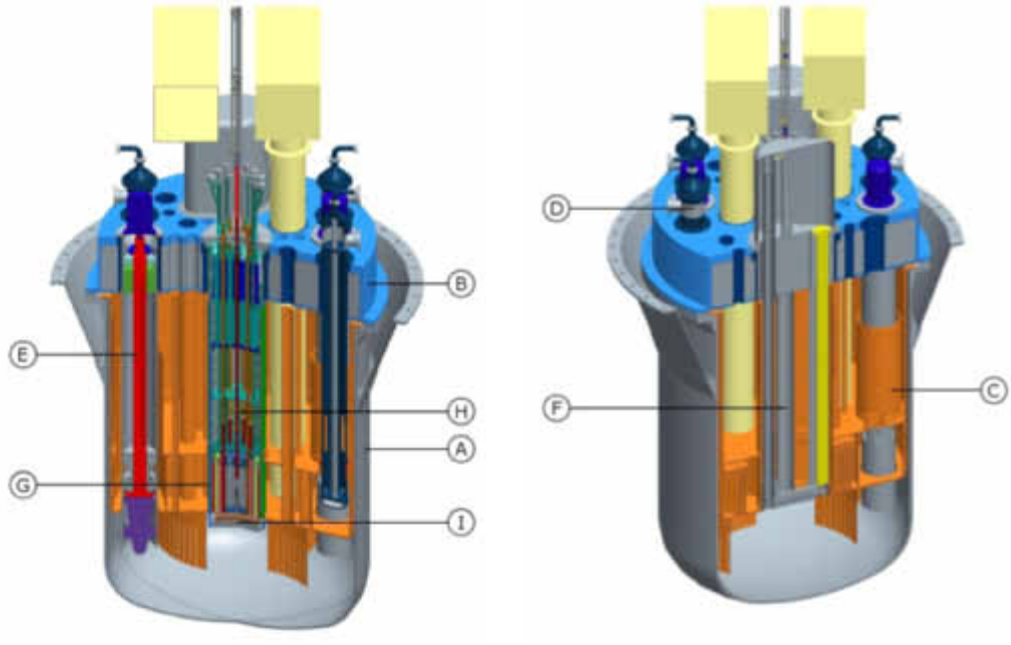
MYRRHA core and primary system

The main components or systems of the current MYRRHA-FASTEF design are of the same MYRRHA/XT-ADS type, as defined within the EUROTRANS project, with only increased size. The primary and secondary systems have been designed to evacuate a maximum core power of 100 MW_{th}. All the MYRRHA-FASTEF components are optimised for the extensive use of the remote handling system during components replacement, inspection and handling.

Since MYRRHA-FASTEF is a pool-type ADS, the reactor vessel houses all the primary systems. In previous designs of MYRRHA, an outer vessel served as secondary containment in case the reactor vessel leaks or breaks. In the current design, the reactor pit implements this function, improving the capabilities of the reactor vault air cooling system. The vessel is closed by the reactor cover which supports all the in-vessel components. A diaphragm inside the vessel functions to separate the hot and cold lead-

bismuth eutectic (LBE), to support the In-Vessel Fuel Storage (IVFS) and to provide a pressure separation. The core is held in place by the core support structure consisting of a core barrel and a core support plate. Figure 2 shows a section of the MYRRHA-FASTEF reactor showing its main internal components.

Figure 2. Section of the MYRRHA-FASTEF reactor showing its main internal components



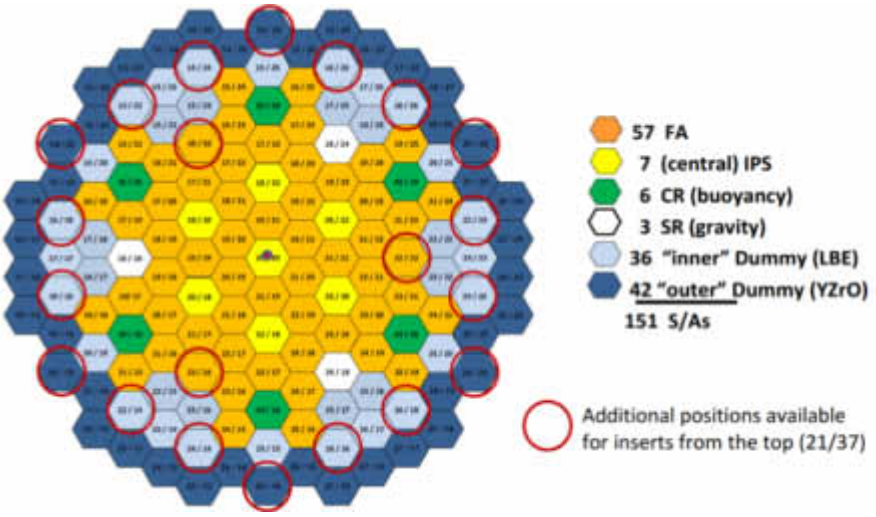
A. Reactor vessel
B. Reactor cover
C. Diaphragm
D. Primary heat exchanger
E. Primary pump
F. In-vessel fuel handling machine
G. Core
H. Above core structure
I. Core restraint system

At the present state of the design, the reactor core (see Figure 3) consists of mixed oxide (MOX) fuel pins, typical of fast reactors. A major change with respect to the previous version of the core is the switch from a windowless loop-type spallation target to a window beam tube-type spallation target. The previous version needed three central hexagons to house the spallation target while the present day design only needs one central hexagon. To better accommodate this central target, the fuel assemblies' size is a little bit increased as compared to the MYRRHA/XT-ADS design. Consequently, the In-Pile test Sections (IPS), which will be located in dedicated FAs positions, are larger in diameter, giving more flexibility to experiments. Thirty-seven positions can be occupied by IPSs or by the spallation target (the central one of the core in subcritical configuration) or by control and shutdown rods (in the core critical configuration). This gives a large flexibility in the choice of the more suitable position (neutron flux) for each experiment.

The requested high fast flux intensity has been obtained by optimising the core configuration geometry (fuel rod diameter and pitch) and maximising power density. For the first core loadings, 15-15Ti will be used as a cladding material instead of T91, which will be qualified progressively further on during MYRRHA operation for a later use. The

use of lead-bismuth eutectic (LBE) as a coolant permits lowering the core inlet operating temperature (down to 270°C), decreasing the risk of corrosion and allowing an increase in the core ΔT. This, together with the adoption of reliable and passive shutdown systems, will permit meeting the high fast flux intensity target.

Figure 3. Cut in the MYRRHA-FASTEF core showing the central target, the different types of fuel assemblies and dummy components



As depicted in the figure, showing a critical core layout (with 7 central IPS) at the equilibrium of the fuel cycle, 37 positions are available for Multi-Functional Channels (MFC) that can host indifferently:

- fuel assembly and dummy, loaded from the bottom (in all the 151 positions);
- IPS, control and scram rods, loaded from the top.

In subcritical mode, the accelerator (as described in the previous section) is the driver of the system. It provides the high-energy protons that are used in the spallation target to create neutrons which, in their turn, feed the subcritical core. The accelerator is able to provide a proton beam with energies of 600 MeV and a maximum current of 4 mA.

In subcritical mode, the spallation target assembly, located in the central position of the core, brings the proton beam via the beam tube into the central core region. The spallation heat deposit is dissipated to the reactor primary circuit. The spallation module guarantees the barrier between the reactor LBE and the reactor hall and ensures optimal conditions for the spallation reaction. The spallation module assembly is conceived of as an IPS and is easily removable or replaceable.

Unlike the critical layout, in ADS mode the six control rods (buoyancy driven in LBE) and the three scram rods (gravity driven in LBE) will be replaced by absorbing devices to be adopted only during refuelling. Due to the (aimed and reached) flexibility, such absorbing devices will be implemented by adopting the control rods, but they will be controlled manually only by the operator.

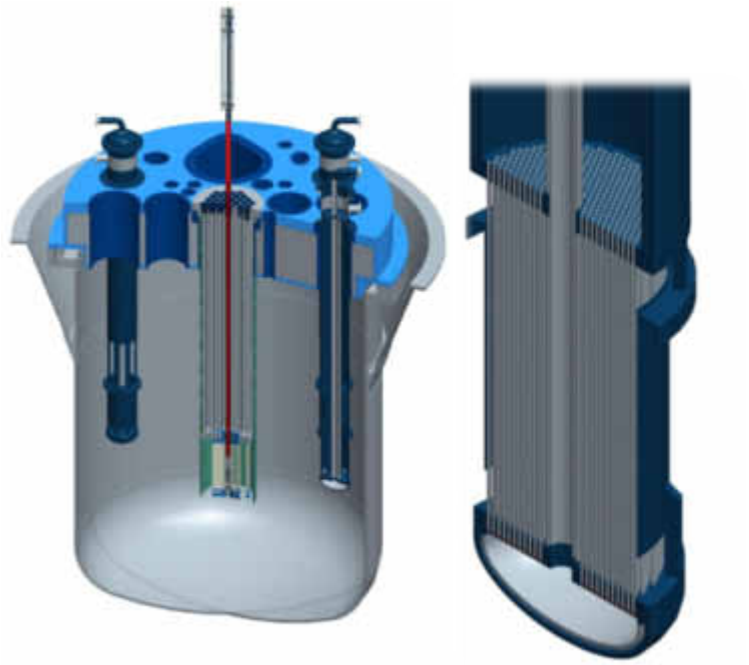
The primary, secondary and tertiary cooling systems were designed to evacuate a maximum thermal core power of 110 MW. The 10 MW more than the nominal core power account for the power deposited by the protons, for the power of in-vessel fuel and for the power deposited in the structures by γ-heating. The average coolant temperature increase in the core in nominal conditions is 140°C with a coolant velocity of 2 m/s. The primary cooling system consists of two pumps and four primary heat exchangers (PHX).

The primary pumps will deliver the LBE to the core with a mass flow rate of 15-15Ti 4750 kg/s (453 l/s per pump). The working pressure of the pump is 300 kPa. The pump will be fixed at the top of the reactor cover, which is supposed to be the only supporting and guiding element of the pump assembly.

The secondary cooling system is a water cooling system while the tertiary system is an air cooling system. These systems function in active mode during normal operation and in passive mode in emergency conditions for decay heat removal.

The main thermal connection between the primary and secondary cooling systems is provided by the primary heat exchangers (see Figure 4). These heat exchangers are shell and tube, single-pass and counter-current heat exchangers. Pressurised water at 200°C is used as a secondary coolant, flowing through the feed-water pipe in the centre of the PHX to the lower dome. All the walls separating the LBE and water plena (feed-water tube, lower dome and upper annular space) are double-walled to avoid pre-heating of the secondary coolant and to prevent water leaking in the LBE in case of tube rupture.

Figure 4. Heat exchangers



In the case of loss of the primary flow (primary pumps failure), the primary heat exchangers are not able to extract the full heat power. In such cases, the beam must be shut off in the subcritical case and the shutdown rods inserted in the critical case. Decay heat removal (DHR) is achieved by natural convection. Ultimate DHR is performed through the reactor vessel cooling system (RVACS, reactor vessel air cooling system) by natural convection.

The interference of the core with the proton beam, the fact that the room located directly above the core will be occupied by a great deal of instrumentation and IPS penetrations, and core compactness results in insufficient space for fuel handling to (un)load the core from above. Since the very first design of MYRRHA, fuel handling has been performed from underneath the core. Fuel assemblies are kept by buoyancy under the core support plate.

Two fuel handling machines are used, located at opposite sides of the core. Each machine covers one side of the core. The use of two machines provides sufficient range to cover the necessary fuel storage positions without the need of an increase for the reactor vessel when only one fuel-handling machine is used. Each machine is based on the well-known fast reactor technology of the "rotating plug" concept using SCARA (Selective Compliant Assembly Robot Arm) robots. To extract or insert the fuel assemblies, the robot arm can move up or down for about two meters. A gripper and guide arm is used to handle the FAs: the gripper locks the FA and the guide has two functions, namely to hold the FA in the vertical orientation and to ensure neighboring FAs are not disturbed when a FA is extracted from the core. An ultrasonic (US) sensor is used to uniquely identify the FAs.

Figure 5. The in-vessel fuel handling machine



The in-vessel fuel handling machine will also perform in-vessel inspection and recovery of an unconstrained FA. Incremental single-point scanning of the diaphragm can be performed by a US sensor mounted at the gripper of the IVFHM. The baffle under the diaphragm is crucial for the strategy as it limits the work area where inspection and recovery are needed. It also eliminates the need of additional recovery and inspection manipulators, prevents items from migrating into the space between the diaphragm and the reactor cover, and permits side scanning.

Conclusion

SCK•CEN is proposing to replace its ageing flagship facility, the Material Testing Reactor BR2, by a new flexible irradiation facility, MYRRHA. Considering the international and European needs, MYRRHA is conceived as a flexible fast spectrum irradiation facility able to work in both subcritical and critical modes.

MYRRHA is expected to be in full operation by 2024 and it will be able to operate in both operation modes: subcritical and critical. In subcritical mode, it will demonstrate ADS technology and the efficient demonstration of MA in subcritical mode. As a fast spectrum irradiation facility, it will address fuel research for innovative reactor systems, material research for Gen-IV systems and for fusion reactors, radioisotope production for medical and industrial applications and industrial applications, such as Si-doping.

The MYRRHA design has now, with the latest FASTEF version, entered into the Front End Engineering Phase covering the period 2012-2014. The engineering company which will handle this phase is currently being selected. At the end of this phase, the purpose is to have progressed in such a way in the design of the facility that the specifications for the different procurement packages of the facility can be written, to have adequately addressed the remaining R&D issues, to have obtained the licensability agreement from the Belgian Safety Authorities and to have formed the international members' consortium for MYRRHA.

Acknowledgements

The XT ADS design work has been performed under the Integrated Project EUROTRANS (Ref. FI6W-CT-2004-516520) co-funded by the European Union in its Sixth Framework Programme. The FASTEF design work has been performed under the Collaborative Project CDT (Ref. FP7-232527) co-funded by the European Union in its Seventh Framework Programme. Acknowledgement is due to all the colleagues of the participant institutes for their contributions in many different topics related to the XT ADS and FASTEF design and operation.

References

[1] Aït Abderrahim, H., de Bruyn, D. et al. (2007), MYRRHA Project – Technical Description, SCK•CEN Report reference AND/HAA/DDB/3900.B043000/85/07-17bis.

[2] EU Integrated Project EUROTRANS, contract nr. FI6W-CT-2004-516520.

[3] de Bruyn, D., Larmignat, S., Woaye Hune, A., Mansani, L., Rimpault, G., Artioli, C. (2010), "Accelerator Driven Systems for Transmutation: Main Design Achievements of the XT-ADS and EFIT systems" within the FP6 IP-EUROTRANS Integrated Project, *International Congress on Advances in Nuclear Power Plants (ICAPP'10)*, 13-17 June 2010, American Nuclear Society, San Diego, California, US.

[4] de Bruyn, D., Fernandez, R., Mansani, L., Woaye-Hune, A., Sarotto, M., Bubelis, E. (2012), "The Fast-spectrum Transmutation Experimental Facility FASTEF: Main Design Achievements (Part 1: Core and Primary System)" within the FP7-CDT Collaborative Project of the European Commission, *International Congress on Advances in Nuclear Power Plants (ICAPP '12)*, 24-28 June 24-2012, American Nuclear Society, Chicago, Illinois, US.

[5] de Bruyn, D., Engelen, J., Ortega A., Perezagua Aguado, M. (2012), "The Fast-spectrum Transmutation Experimental Facility FASTEF: Main Design Achievements (Part 2: Reactor Building Design and Plant Layout)" within the FP7-CDT Collaborative Project of the European Commission, *International Congress on Advances in Nuclear Power Plants (ICAPP'12)*, 24-28 June 2012, American Nuclear Society, Chicago, Illinois, US.

Annex 1: Scientific Advisory Committee

Chair

Alex C. Mueller (CNRS, France)

Scientific Secretary

Simone Massara (OECD/NEA)

Committee Members

Pierre D'Hondt (SCK•CEN, Belgium)

Bernd Grambow (CNRS, France

Concetta Fazio (KIT, Germany)

Marco Napolitano (INFN, Italy)

Minoru Takahashi (Tokyo Institute of Technology, Japan)

Kazufumi Tsujimoto (JAEA, Japan)

Mike Seidel (PSI, Switzerland)

John D. Galambos (ORNL, US)

Yousry Gohar (ANL, US)

Richard Sheffield (LANL, US)

† Horst Klein (University of Frankfurt, Germany)

Annex 2: List of participants

BELGIUM

D'HONDT, Pierre
SCK•CEN
Deputy Director-General
Boeretang 200
B-2400 Mol
Tel: +32 14 33 25 95
Eml: pierre.dhondt@sckcen.be

KOCHETKOV, Anatoly
SCK•CEN
Research Reactors Operation
Boeretang 200
B-2400 Mol
Tel: +32 14 33 21 93
Eml: akochetk@sckcen.be

MEDEIROS ROMAO, Luis
SCK•CEN
Boeretang 200
B-2400 Mol
Tel: +32495586805
Eml: lmromao@sckcen.be

SALEMME, Roberto
SCK•CEN
B-1348 Louvain-la-Neuve
Tel: +32(0)10473231
Eml: rsalemme@sckcen.be

VAN DEN EYNDE, Gert
SCK•CEN,
Institute for Advanced Nuclear Systems
Nuclear Systems Physics, Boeretang 200
B-2400 Mol
Tel: +32 14 33 22 30
Eml: gvdeynde@sckcen.be

VANDEPLASSCHE, Dirk
SCK•CEN
IBA, Chemin du Cyclotron 3
B-1348 Louvain-la-Neuve
Tel: +32 (10) 475849
Eml: dvandepl@sckcen.be

FRANCE

ARNAUD, Cadiou
Laboratoire SUBATECH
CNRS/IN2P3 École des Mines
4, Rue Alfred Kastler
F-44307 Nantes
Tel: +33251858509
Eml: arnaud.cadiou@subatech.in2p3.f

BAYLAC, Maud
CNRS/IN2P3
53, Avenue des Martyrs
F-38026 Grenoble
Tel: +33476284112
Eml: baylac@lpsc.in2p3.fr

BELLOT, Gaëtan
IRSN
DRPH/SER/UETP
BP 17
F-92265 Fontenay-aux-Roses
Tel: +33 6 4343 5422
Eml: gaetan.bellot@irsn.fr

BIARROTTE, Jean-Luc
CNRS/IN2P3
IPN Orsay,
F-91406 Orsay, France
Tel: +33 1 69 15 79 30
Eml: biarrott@ipno.in2p3.fr

BILLEBAUD, Annick
Reacteurs Hybrides
LPSC
Institut des Sciences Nucleaires
53, avenue des Martyres
F-38026 Grenoble
Tel: +33 (0)4 76 28 40 57
Eml: billebaud@lpsc.in2p3.fr

CHABOD, Sebastien
Lab. de Phys. Subatomique et de Cosmologi
53, Rue des Martyrs
F-38026 Grenoble
Tel:
Eml: chabod@lpsc.in2p3.fr

CLAVEL, Jean-Baptiste
IRSN, 31, Avenue de la Division Leclerc
F-92260 Fontenay-aux-Roses
Tel: +33 1 58 35 72 92
Eml: jean-baptiste.clavel@irsn.fr

COURTIN, Fanny
CNRS/IN2P3 École des Mines
4, Rue Alfred Kastler
F-44307 Nantes
Tel: +33 0661095442
Eml: courtin@subatech.in2p3.fr

DAVID, Sylvain
CNRS/IN2P3
Institut de Physique Nucleaire,
Bat. 100,
15, Rue Clemenceau,
F-91406 Orsay
Tel: +33(0)1 69 15 6952
Eml: sdavid@ipno.in2p3.fr

EL YAKOUBI, Marouan
CNRS Institut de Physique Nucléaire
Division Accélérateurs
F-91406 Orsay
Tel: +331 69 15 65 31
Eml: marouan@ipno.in2p3.fr

FALLOT, Muriel
Laboratoire SUBATECH
CNRS/IN2P3 École des Mines
4, Rue Alfred Kastler
F-44307 Nantes
Tel: +33 251858415
Eml: fallot@subatech.in2p3.fr

FROIDEFOND, Emmanuel
53, Rue des Martyrs
F-38026 Grenoble
Tel: +33 4 76 28 40 32
Eml: froidefond@lpsc.in2p3.fr

GRAMBOW, Bernd
École de Mines de Nantes
Laboratoire SUBATECH
4, Rue Alfred Kastler
F-44307 Nantes
Tel: +33 02 51 85 84 70
Eml: grambow@subatech.in2p3.fr

JUNQUERA, Thomas
Institut de Physique Nucléaire
F-91406 Orsay
Tel: +33 01 69 15 51 65
Eml: tomas.junquera@acsfrance.com

LECOLLEY, François-René
LPC Caen
6, Bd du Marechal Juin
F-14050 Caen
Tel: +33 + (33) 231 452 545
Eml: fr.lecolley@lpccaen.in2p3.fr

LECOUEY, Jean Luc
ENSICAEN / LSC
6, Bd du Marechal Juin
F-14050 Caen
Tel: +33 02 31 45 29 65
Eml: lecouey@lpccaen.in2p3.fr

LEFEVRE, Frederic
Laboratoire SUBATECH
4, rue Alfred Kastler
F-44307 Nantes
Tel: +33 (0) 2 51 85 84 08
Eml: frederic.lefevre@cern.ch

LEHAUT, Grégory
6, Bd Marechal Juin
F-14050 Caen
Tel:
Eml: lehaut@lpccaen.in2p3.fr

LE SCORNET, Jean-Claude
Institut de Physique Nucléaire
F-91400 Orsay
Tel: +33 0243954627
Eml: jeanclaude.lescornet@acsfrance

MARIE-NOURRY, Nathalie A.
ENSICAEN
Laboratoire de Physique Corpusculaire
ISMRA - 6, Bd. du Maréchal Juin
F-14050 Caen
Tel: +33 2 31 45 25 16
Eml: marie@lpccaen.in2p2.fr

MOUGINOT, Baptiste
Laboratoire SUBATECH
UMR 6457
4, Rue Alfred Kastler
La Chantrerie BP 20722
F-44307 Nantes
Tel: +33 (0) 2 51 85 85 64
Eml: baptiste.mouginot@subatech.in2

MUELLER, Alex
CNRS
Institut National de Physique Nucléaire
et de Physique des Particules,
F-75794 Paris
Tel: +33 1 69 15 62 40
Eml: mueller@ipno.in2p3.fr

PRORIOL SERRE, Ingrid
Bat C6 UMR 8205
Cité scientifique
Université de Lille
F-59655 Villeneuve d'Ascq
Tel: +33 (0) 3 20 43 66 06
Eml: ingrid.proriol-serre@univ-lill

SAUGNAC, Hervé
CNRS Institut de Physique Nucléaire
Division Accélérateurs
F-91400 Orsay
Tel: +33 1 69 15 81 36
Eml: saugnac@ipno.in2p3.fr

TAKIBAYEV, Alan
DSM/IRFU/SENAC
CEA Saclay
F-91191 Gif-sur-Yvette
Tel:
Eml: alan.takibayev@esss.se

THIOLLIERE, Nicolas
Laboratoire SUBATECH
Ecole des Mines
4, Rue Alfred Kastler
F-44307 Nantes
Tel: +33 (0)2 51 85 86 42
Eml: nicolas.thiolliere@subatech.in

VOGT, Jean-Bernard
University of Lille 1
Cité Scientifique
F-59650 Villeneuve d'Ascq
Tel: +33 3 20 43 40 35
Eml: jean-bernard.vogt@univ-lille1.

XAVIER, Doligez
IPN, 15, Rue Georges Clemenceau
F-91406 Orsay
Tel: +33 1 69 15 51 96
Eml: doligez@ipno.in2p3.fr

ZAKARI-ISSOUFOU, Abdoul-aziz
Laboratoire SUBATECH
4, Rue Alfred Kastler
F-44307 Nantes
Tel: +33 0251858421
Eml: zakari@subatech.in2p3.fr

GERMANY

BATTA, Abdalla
KIT IKET
Hermann von Helmholtz Platz 1
D-76344 Eggenstein-Leopoldshafen
Tel: +49 7247 82 2464
Eml: abdalla.batta@kit.edu

FETZER, Jana R.
KIT IKET
Institute for Nuclear and Energy Technology
D-76344 Eggenstein-Leopoldshafen
Tel: +49 721 608-23445
Eml: jana.fetzer@kit.edu

GABRIELLI, Fabrizio
KIT
Karlsruhe Institute of Technology
Hermann-von-Helholtplatz, 1
D-76344 Eggenstein-Leopoldshafen
Tel: +49 721 608 22491
Eml: fabrizio.gabrielli@kit.edu

KESTER, Oliver
GSI Darmstadt
Planckstrasse 1
Institut für Angewandte Physik
Goethe-Universität Frankfurt
Tel:
Eml: o.kester@gsi.de

PACIO, Julio
KIT
Hermann-von-Helmholtz Platz 1
D-76344
Eggenstein-Leopoldshafen
Tel: +49 72160826902
Eml: julio.pacio@kit.edu

PEKELER, Michael
RI Research Instruments GmbH
Director,
Friedrich-Ebert-Strasse 1
D-51429 Bergisch Gladbach
Tel: +49 2204 7062 2565
Eml: michael.pekeler@research-instr

RATZINGER, Ulrich
Goethe-Universität
Max-von-Laue-Str.1
D-60431 Frankfurt/Main
Tel: +49 0049-69-798-47404
Eml: u.ratzinger@iap.uni-frankfurt.

STOECKER, Horst
GSI
Planckstr. 1
D-64291 Darmstadt
Tel: +49 00496159712648
Eml: stoecker@gsi.de

ITALY

RICCO, Giovanni
University of Genoa
via Dodecaneso 33
I-16146 Genova
Tel:
Eml: ricco@ge.infn.it

RIPANI, Marco
INFN
Via Dodecaneso 33
I-16146 Genova

Tel: +39 0103536458
Eml: ripani@ge.infn.it

JAPAN

HASHIMOTO, Kengo
KinkI University
Atomic Energy Research Institute,
3-4-1, Kowakae
HIGASHI-OSAKA
577-8502, Japan

Tel: +81667212332
Eml: kengoh@pp.iij4u.or.jp

OBAYASHI, Hironari
JAEA
2-4, Shirane, Shirakata,
Tokai-mura, Ibaraki-ken,
Japan

Tel: +81 29 282 6256
Eml: obayashi.hironari@jaea.go.jp

PYEON, Cheol Ho
Kyoto University
Research Reactor Institute
2-1010 Asashiro-nishi
Kumatori-cho, Sennan-gun
Osaka 590-0494, Japan

Tel: +81 724 51 2356
Eml: pyeon@rri.kyoto-u.ac.jp

SAKON, Atsushi
Kinki University
3-4-1, Kowakae
HIGASHI-OSAKA
Japan

Tel: +81667212332
Eml: atsushi0223@hotmail.com

SUGAWARA, Takanori
JAEA
Shirakata-shirane 2-4,
Tokai, Ibaraki,
Japan 319-1195

Tel: +81 29 282 5058
Eml: sugawara.takanori@jaea.go.jp

TSUJIMOTO, Kazufumi
Research Group for Nuclear Transmutation
Nuclear Science & Engineering Center,
Japan Atomic Energy Agency (JAEA)
2-4 Shirane Shirakata, Tokai-mura,
Ibaraki 319-1195

Tel: +81 29 282 6436
Eml: tsujimoto.kazufumi@jaea.go.jp

RUSSIAN FEDERATION

BOGDANOV, Aleksey
St.Petersburg
Moskovskoye Shosse, 44.

Tel: +79046330975
Eml: foyd1@rambler.ru

KHORASANOV, Georgii
IPPE
1 Bondarenko square
Obninsk
Kaluga region
249033 Russian Federation
Tel: +7 48439 98505
Eml: khorasan@ippe.ru

SPAIN

GONZALEZ-ROMERO, Enrique Miguel
CIEMAT
Director of the Nuclear Fission Division
Department of Energy of CIEMAT
Avenida Complutense, 22
ES-28040 Madrid
Tel: +34 91 346 6120
Eml: enrique.gonzalez@ciemat.es

MARTINEZ-VAL, Jose Maria
Univ. Politécnica de Madrid
Director
Fundación para el Fomento
de la Innovación Industrial - UP Madrid
José Gutiérrez Abascal 2
Tel: +34 91 336 30 78
Eml: mval@etsii.upm.es

PITIGOI, Adrian
EA
Magallanes 3
ES-28015 Madrid
Tel: +34 91 309 80 00
Eml: aph@empre.es

SWITZERLAND

FUSCO, Yoann
CERN
Route de Meyrin
CH-1211 Genève
Tel: +41 0041227675249
Eml: yoann.fusco@cern.ch

SAMEC, Karel
Mech. Eng. ETH Zürich, Nucl. Eng. INSTN 1
Postbox: M17610
CERN
CH-1211 Genève
Tel: +41 56 460 8539
Eml: karel.samec@cern.ch

SEIDEL, Mike
Paul Scherrer Institute
5232 Villigen PSI
Tel: +41 563103378
Eml: mike.seidel@psi.ch

WOHLMUTHER, Michael
Paul Scherrer Institute
WMHA/C40
5232 Villigen PSI
Tel: +41 56 310 3052
Eml: michael.wohlmuther@psi.ch

UNITED STATES

GOHAR, Yousry
Argonne National Laboratory
9700 South Cass Avenue
Argonne, Illinois 60439
Tel: +1 630 252 4816
Eml: gohar@anl.gov

MCINTYRE, Peter
Texas A&M
Dept. of Physics
College Station, TX 777843
Tel: +1 979 255 5531
Eml: mcintyre@physics.tamu.edu

INTERNATIONAL ORGANISATIONS

HAAS, Didier
European Commission
Joint Research Centre,
Corporate Services
8, Square de Meeus,
1040 Brussels
Tel: +32 2 299 2642
Eml: didier.haas@ec.europa.eu

CORNET, Stéphanie
OECD/NEA
12 Boulevard des Iles
92130 Issy-les-Moulineaux
Tel: +33 (0) 1 45 24 10 82
Eml: stephanie.cornet@oecd.org

MASSARA, Simone
OECD/NEA
12 Boulevard des Iles
92130 Issy-les-Moulineaux
Tel: +33 (0) 1 45 24 10 85
Eml: simone.massara@oecd.org

KADI, Yacine
European Organization for
Nuclear Research
Emerging Energy Technologies
SL Division
CH-1211 Genève
Tel: +41 22 7679569
Eml: yacine.kadi@cern.ch